

processes

Study of Biodegradation and Bioremediation

Edited by

Ewa Kaczorek and Wojciech Smułek

Printed Edition of the Special Issue Published in *Processes*

Study of Biodegradation and Bioremediation

Study of Biodegradation and Bioremediation

Editors

Ewa Kaczorek

Wojciech Smułek

MDPI • Basel • Beijing • Wuhan • Barcelona • Belgrade • Manchester • Tokyo • Cluj • Tianjin



Editors

Ewa Kaczorek
Poznan University of
Technology
Poland

Wojciech Smułek
Poznan University of
Technology
Poland

Editorial Office

MDPI
St. Alban-Anlage 66
4052 Basel, Switzerland

This is a reprint of articles from the Special Issue published online in the open access journal *Processes* (ISSN 2227-9717) (available at: https://www.mdpi.com/journal/processes/special_issues/biodegradation_bioremediation).

For citation purposes, cite each article independently as indicated on the article page online and as indicated below:

LastName, A.A.; LastName, B.B.; LastName, C.C. Article Title. <i>Journal Name</i> Year , Volume Number, Page Range.
--

ISBN 978-3-0365-2900-4 (Hbk)

ISBN 978-3-0365-2901-1 (PDF)

Cover image courtesy of Wojciech Smułek

© 2022 by the authors. Articles in this book are Open Access and distributed under the Creative Commons Attribution (CC BY) license, which allows users to download, copy and build upon published articles, as long as the author and publisher are properly credited, which ensures maximum dissemination and a wider impact of our publications.

The book as a whole is distributed by MDPI under the terms and conditions of the Creative Commons license CC BY-NC-ND.

Contents

About the Editors	vii
Ewa Kaczorek and Wojciech Smułek Special Issue “Study of Biodegradation and Bioremediation” Reprinted from: <i>Processes</i> 2021 , <i>9</i> , 1130, doi:10.3390/pr9071130	1
Argyro Tsipa, Konstantina Stylianou, Maria Papalli, Erato Papageorgiou, Loucas Kyriakou, Ioannis Rigopoulos, Ioannis Ioannou and Eftychia Pinakoulaki Iron-Stimulated Production and Antimicrobial Potential of a Novel Biosurfactant Produced by a Drilling Waste-Degrading <i>Pseudomonas citronellolis</i> Strain Reprinted from: <i>Processes</i> 2021 , <i>9</i> , 686, doi:10.3390/pr9040686	5
Yinka Titilawo, Wiya L. Masudi, Jacob T. Olawale, Lerato M. Sekhohola-Dlamini and A. Keith Cowan Coal-Degrading Bacteria Display Characteristics Typical of Plant Growth Promoting Rhizobacteria Reprinted from: <i>Processes</i> 2020 , <i>8</i> , 1111, doi:10.3390/pr8091111	25
Guillermo Bravo, Paulina Vega-Celedón, Juan Carlos Gentina and Michael Seeger Effects of Mercury II on <i>Cupriavidus metallidurans</i> Strain MSR33 during Mercury Bioremediation under Aerobic and Anaerobic Conditions Reprinted from: <i>Processes</i> 8 , <i>8</i> , 893, doi:10.3390/pr8080893	41
Agnieszka Kołodziejczak-Radzimska and Teofil Jesionowski A Novel Cysteine-Functionalized M_xO_y Material as Support for Laccase Immobilization and a Potential Application in Decolorization of Alizarin Red S Reprinted from: <i>Processes</i> 2020 , <i>8</i> , 885, doi:10.3390/pr8080885	55
Cevat Yaman Performance and Kinetics of Bioaugmentation, Biostimulation, and Natural Attenuation Processes for Bioremediation of Crude Oil-Contaminated Soils Reprinted from: <i>Processes</i> 2020 , <i>8</i> , 883, doi:10.3390/pr8080883	73
Juan Francisco García-Martín, Amanda Teixeira Badaró, Douglas Fernandes Barbin and Paloma Álvarez-Mateos Identification of Copper in Stems and Roots of <i>Jatropha curcas</i> L. by Hyperspectral Imaging Reprinted from: <i>Processes</i> 2020 , <i>8</i> , 823, doi:10.3390/pr8070823	87
Luong N. Nguyen, Minh T. Vu, Md Abu Hasan Johir, Nirenkumar Pathak, Jakub Zdarta, Teofil Jesionowski, Galilee U. Semblante, Faisal I. Hai, Hong Khanh Dieu Nguyen and Long D. Nghiem A Novel Approach in Crude Enzyme Laccase Production and Application in Emerging Contaminant Bioremediation Reprinted from: <i>Processes</i> 2020 , <i>8</i> , 648, doi:10.3390/pr8060648	97
Sobia Ashraf, Muhammad Naveed, Muhammad Afzal, Sana Ashraf, Sajid Rashid Ahmad, Khadeeja Rehman, Zahir Ahmad Zahir and Avelino Núñez-Delgado Evaluation of Toxicity on <i>Ctenopharyngodon idella</i> Due to Tannery Effluent Remediated by Constructed Wetland Technology Reprinted from: <i>Processes</i> 2020 , <i>8</i> , 612, doi:10.3390/pr8050612	109

Kateřina Malachov, enek Novotny, Grażyna Adamus, Nadia Lotti, Zuzana Rybkov, Michelina Soccio, Pavlna řlosarikov, Vincent Verney and Fabio Fava Ability of <i>Trichoderma hamatum</i> Isolated from Plastics-Polluted Environments to Attack Petroleum-Based, Synthetic Polymer Films Reprinted from: <i>Processes</i> 2020 , <i>8</i> , 467, doi:10.3390/pr8040467	125
Wojciech Smulek, Amanda Pacholak and Ewa Kaczorek Modification of the Bacterial Cell Wall—Is the Bioavailability Important in Creosote Biodegradation? Reprinted from: <i>Processes</i> 2020 , <i>8</i> , 147, doi:10.3390/pr8020147	139
Li Liu, Yang Li and Shisuo Fan Preparation of KOH and H ₃ PO ₄ Modified Biochar and Its Application in Methylene Blue Removal from Aqueous Solution Reprinted from: <i>Processes</i> 2019 , <i>7</i> , 891, doi:10.3390/pr7120891	149
Edgar Vazquez-Nunez, Carlos Eduardo Molina-Guerrero, Julin Mario Pena-Castro, Fabin Fernandez-Luqueno and Ma. Guadalupe de la Rosa-lvarez Use of Nanotechnology for the Bioremediation of Contaminants: A Review Reprinted from: <i>Processes</i> 2020 , <i>8</i> , 826, doi:10.3390/pr8070826	169
Abhilash Kumar Tripathi, Aditi David, Tanvi Govil, Shailabh Rauniyar, Navanietha Krishnaraj Rathinam, Kian Mau Goh and Rajesh Kumar Sani Environmental Remediation of Antineoplastic Drugs: Present Status, Challenges, and Future Directions Reprinted from: <i>Processes</i> 2020 , <i>8</i> , 747, doi:10.3390/pr8070747	187

About the Editors

Ewa Kaczorek Graduate of the Faculty of Chemical Technology at Poznan University of Technology. Since 2016, she has served Vice Dean for Student Affairs and, since 2020, as Dean of the Faculty of Chemical Technology at Poznan University of Technology. She is the Deputy Chairman of the Committee on Chemical Sciences of the Polish Academy of Sciences (Poznań Regional Section) and Chairman of the Organizing Committee of the National Symposium on Bioorganic, Organic and Biomaterials Chemistry held every two years at the Faculty of Chemical Technology. During the 2017 scientific and organizational internship to Chongqing Jiaotong University (China), she was a visiting professor at School of Ocean and River Engineering. She is a member of the Polish Chemical Society and Polish Society of Microbiologists, as well as a member of the Editorial Board of "Journal of Chemistry".

Wojciech Smulek Graduate of doctoral studies at the Faculty of Chemical Technology of Poznan University of Technology. When preparing his doctoral thesis, he completed an internship at the Institute of Natural Resources and Agrobiology in Seville. He is a member of the Polish Chemical Society and the Polish Society of Microbiologists.

Editorial

Special Issue “Study of Biodegradation and Bioremediation”

Ewa Kaczorek * and Wojciech Smulek *

Institute of Chemical Technology and Engineering, Faculty of Chemical Technology,
Poznan University of Technology, Berdychowo 4, 60-965 Poznan, Poland

* Correspondence: ewa.kaczorek@put.poznan.pl (E.K.); wojciech.smulek@put.poznan.pl (W.S.)

It is with great pleasure that we present to you the output of the Special Issue Study of Biodegradation and Bioremediation. We are extremely pleased that despite the difficult time of the pandemic, many researchers from all over the world wanted to include their research in our Special Issue.

With regret, it has to be said that despite several regulations and great care for storage and transport safety, there is still the possibility of uncontrolled release of petroleum products, substrates in chemical synthesis, drugs, dyes, etc. Moreover, the currently used solid waste and sewage water management methods do not allow for the effective removal of both persistent contaminants and pharmaceuticals. Ecological disasters, frequently occurring in large sizes and regular waste management, show how important it is to have some appropriate techniques that are helpful in rapid remediation of the environment. The biodegradation of pollutants depends on various factors, such as their chemical structure, physicochemical properties, or bioavailability for microorganisms. Therefore, there is a need to develop new effective bioremediation processes and extensive and deep studies on biodegradation processes conducted by microorganisms.

What is more, a comprehensive and multifaceted look at the phenomena accompanying biological degradation is very important. Work on effective conduct of biodegradation and bioremediation processes has been going on for decades. However, in recent years, new analytical techniques and an intensively developed interdisciplinary perspective on these issues have yielded many valuable results. These have become the core of the articles forming this Special Issue.

We would now like to introduce the publications included in this collection briefly. To begin, we would like to clearly emphasize that neither the order of the mentioned articles nor the amount of text devoted to them proves the value of these publications. In our opinion, each of them is an important and valuable contribution to the development of our knowledge and carries significant application meaning. The first group of articles deal with the removal of petroleum hydrocarbons from the environment.

Yaman’s article “Performance and Kinetics of Bioaugmentation, Biostimulation, and Natural Attenuation Processes for Bioremediation of Crude Oil-Contaminated Soils” [1] considered the effectiveness of bioaugmentation and biostimulation in hydrocarbon removal in his paper. In his pilot study, the author noted that the TPH degradation in the crude oil contaminated soil was improved by bioaugmentation with genus *Alcanivorax* and biostimulation with nitrogen and phosphorus. On the other hand, Smulek et al. focused on the bioavailability of pollutants to cells as a limiting factor for the biodegradation process [2]. Their paper “Modification of the Bacterial Cell Wall-Is the Bioavailability Important in Creosote Biodegradation?” is a significant study showing the complexity of changes occurring on the cell surface and inside cell membranes that are caused by contact of bacteria with PAHs.

The paper by Malachov et al. “Ability of *Trichoderma hamatum* Isolated from Plastics-Polluted Environments to Attack Petroleum-Based, Synthetic Polymer Films” provides a link between the problem of hydrocarbon contamination and environmental plastic pollution [3]. The results presented here add a great deal to knowledge on the biodegradation of

Citation: Kaczorek, E.; Smulek, W. Special Issue “Study of Biodegradation and Bioremediation”. *Processes* **2021**, *9*, 1130. <https://doi.org/10.3390/pr9071130>

Received: 28 June 2021

Accepted: 28 June 2021

Published: 29 June 2021

Publisher’s Note: MDPI stays neutral with regard to jurisdictional claims in published maps and institutional affiliations.



Copyright: © 2021 by the authors. Licensee MDPI, Basel, Switzerland. This article is an open access article distributed under the terms and conditions of the Creative Commons Attribution (CC BY) license (<https://creativecommons.org/licenses/by/4.0/>).

plastics by different consortia of microorganisms. Contamination of the environment by heavy metals is a particularly difficult challenge due to their extreme toxicity and bioaccumulation in living organisms. It is, therefore, worthwhile to look at new possibilities for removing heavy metals from soils and waters.

The combination of phytoremediation and microbial remediation was addressed by Garcia-Martin et al. In their paper, "Identification of Copper in Stems and Roots of *Jatropha curcas* L. by Hyperspectral Imaging." They studied these issues based on an extensive statistical analysis of hyperspectral images in the visible/near-infrared [4]. Moreover, Tsipa et al., in their article "Iron-Stimulated Production and Antimicrobial Potential of a Novel Biosurfactant Produced by a Drilling Waste-Degrading *Pseudomonas citronellolis* Strain," showed the high potential of a peptide biosurfactant produced by a strain of the genus *Pseudomonas* [5]. Thus, these researchers confirm that hydrocarbon-contaminated sites can also become a source of bacterial strains capable of producing valuable compounds from a pharmaceutical and cosmetic perspective.

There is a trend of looking at contaminated sites as a source of interesting microorganisms, including extremophilic ones. As such, the publication "Coal-Degrading Bacteria Display Characteristics Typical of Plant Growth Promoting Rhizobacteria" by Titilawo et al. determines the genetic relatedness of coal-degrading bacterial strains isolated from the rhizosphere of grasses growing on coal discard dumps and from diesel-contaminated sites [6].

Another equally interesting Special Issue thread is research on effective heavy metal remediation. Bravo et al. published a paper, "Effects of Mercury II on *Cupriavidus metallidurans* Strain MSR33 during Mercury Bioremediation under Aerobic and Anaerobic Conditions." Their research indicates that the *C. metallidurans* strain MSR33 they tested may be useful for mercury bioremediation in polluted water under aerobic and anaerobic conditions [7].

The global production of dyes is still increasing, which affects their dispersion in the environment. This problem was addressed by Liu et al. [8]. Their article "Preparation of KOH and H₃PO₄ Modified Biochar and Its Application in Methylene Blue Removal from Aqueous Solution," touches upon the problem of using bio-based materials for methylene blue water treatment. The research of Kolodziejczak-Radzimska and Jesionowski in the article "A Novel Cysteine-Functionalized MxOy Material as Support for Laccase Immobilization and a Potential Application in Decolorization of Alizarin Red S," is significant, as well [9]. These researchers used immobilized laccase to remove alizarin dye, highlighting key technological aspects, including the importance of proper carrier selection in the immobilization process. These studies are referenced in the paper by Nguyen et al. "A Novel Approach in Crude Enzyme Laccase Production and Application in Emerging Contaminant Bioremediation," describing the potential of an enzymatic membrane reactor for the oxidation and removal of emerging contaminants (ECs), such as pesticides, pharmaceuticals and steroid hormones [10].

Also of interest are the results of Ashraf et al. ("Evaluation of Toxicity on *Ctenopharyngodon idella* Due to Tannery Effluent Remediated by Constructed Wetland Technology"), who highlighted the problem that is tannery effluent water. The specific composition of pollutants poses a problem for aquatic microorganisms, however the use of constructed wetlands is a promising option to reduce pollutant emissions [11]. Last but not least, two review papers round out the Special Issue. Vázquez-Núñez et al., in their swim article "Use of Nanotechnology for the Bioremediation of Contaminants: A Review," provides a broad perspective on using state-of-the-art nanotechnology in bioremediation processes while highlighting the complexity of interactions between microorganisms, nanomaterials, and environmental contaminants [12].

Our collection also could not miss the issues related to environmental contamination with drugs. This topic was taken up by Tripathi et al., who presented the publication "Environmental Remediation of Antineoplastic Drugs: Present Status, Challenges, and

Future Directions” [13]. Although they focused on a specific group of pharmaceuticals, their observations are relevant to the broader issue of removing bioactive compounds.

In closing, we would like to again thank all the authors for their work. Thanks to them, we all gain insight into the latest research on bioremediation and biodegradation processes. We are convinced that this will bring tangible benefits to scientists and society as a whole.

Author Contributions: Writing—original draft preparation, review and editing, E.K. and W.S. Both authors have read and agreed to the published version of the manuscript.

Conflicts of Interest: The authors declare no conflict of interest.

References

1. Yaman, C. Performance and Kinetics of Bioaugmentation, Biostimulation, and Natural Attenuation Processes for Bioremediation of Crude Oil-Contaminated Soils. *Processes* **2020**, *8*, 883. [[CrossRef](#)]
2. Smulek, W.; Pacholak, A.; Kaczorek, E. Modification of the Bacterial Cell Wall—Is the Bioavailability Important in Creosote Biodegradation? *Processes* **2020**, *8*, 147. [[CrossRef](#)]
3. Malachová, K.; Novotný, Č.; Adamus, G.; Lotti, N.; Rybková, Z.; Soccio, M.; Šlosarčíková, P.; Verney, V.; Fava, F. Ability of *Trichoderma hamatum* Isolated from Plastics-Polluted Environments to Attack Petroleum-Based, Synthetic Polymer Films. *Processes* **2020**, *8*, 467. [[CrossRef](#)]
4. García-Martín, J.F.; Badaró, A.T.; Barbin, D.F.; Álvarez-Mateos, P. Identification of Copper in Stems and Roots of *Jatropha curcas* L. by Hyperspectral Imaging. *Processes* **2020**, *8*, 823. [[CrossRef](#)]
5. Tsipa, A.; Stylianou, K.; Papalli, M.; Papageorgiou, E.; Kyriakou, L.; Rigopoulos, I.; Ioannou, I.; Pinakoulaki, E. Iron-Stimulated Production and Antimicrobial Potential of a Novel Biosurfactant Produced by a Drilling Waste-Degrading *Pseudomonas citronellolis* Strain. *Processes* **2021**, *9*, 686. [[CrossRef](#)]
6. Titilawo, Y.; Masudi, W.L.; Olawale, J.T.; Sekhohola-Dlamini, L.M.; Cowan, A.K. Coal-Degrading Bacteria Display Characteristics Typical of Plant Growth Promoting Rhizobacteria. *Processes* **2020**, *8*, 1111. [[CrossRef](#)]
7. Bravo, G.; Vega-Celedón, P.; Gentina, J.C.; Seeger, M. Effects of Mercury II on *Cupriavidus metallidurans* Strain MSR33 during Mercury Bioremediation under Aerobic and Anaerobic Conditions. *Processes* **2020**, *8*, 893. [[CrossRef](#)]
8. Liu, L.; Li, Y.; Fan, S. Preparation of KOH and H₃PO₄ Modified Biochar and Its Application in Methylene Blue Removal from Aqueous Solution. *Processes* **2019**, *7*, 891. [[CrossRef](#)]
9. Kołodziejczak-Radzimska, A.; Jesionowski, T. A Novel Cysteine-Functionalized M_xO_y Material as Support for Laccase Immobilization and a Potential Application in Decolorization of Alizarin Red S. *Processes* **2020**, *8*, 885. [[CrossRef](#)]
10. Nguyen, L.N.; Vu, M.T.; Johir, M.A.H.; Pathak, N.; Zarta, J.; Jesionowski, T.; Semblante, G.U.; Hai, F.I.; Khanh Dieu Nguyen, H.; Nghiem, L.D. A Novel Approach in Crude Enzyme Laccase Production and Application in Emerging Contaminant Bioremediation. *Processes* **2020**, *8*, 648. [[CrossRef](#)]
11. Ashraf, S.; Naveed, M.; Afzal, M.; Ashraf, S.; Ahmad, S.R.; Rehman, K.; Zahir, Z.A.; Núñez-Delgado, A. Evaluation of Toxicity on *Ctenopharyngodon idella* Due to Tannery Effluent Remediated by Constructed Wetland Technology. *Processes* **2020**, *8*, 612. [[CrossRef](#)]
12. Vázquez-Núñez, E.; Molina-Guerrero, C.E.; Peña-Castro, J.M.; Fernández-Luqueño, F.; de la Rosa-Álvarez, M.G. Use of Nanotechnology for the Bioremediation of Contaminants: A Review. *Processes* **2020**, *8*, 826. [[CrossRef](#)]
13. Tripathi, A.K.; David, A.; Govil, T.; Rauniyar, S.; Rathinam, N.K.; Goh, K.M.; Sani, R.K. Environmental Remediation of Antineoplastic Drugs: Present Status, Challenges, and Future Directions. *Processes* **2020**, *8*, 747. [[CrossRef](#)]

Article

Iron-Stimulated Production and Antimicrobial Potential of a Novel Biosurfactant Produced by a Drilling Waste-Degrading *Pseudomonas citronellolis* Strain

Argyro Tsipa ^{1,2,*}, Konstantina Stylianou ¹, Maria Papalli ¹, Erato Papageorgiou ³, Loucas Kyriakou ¹, Ioannis Rigopoulos ¹, Ioannis Ioannou ¹ and Eftychia Pinakoulaki ³

¹ Department of Civil and Environmental Engineering, University of Cyprus, 75 Kallipoleos, Nicosia 1678, Cyprus; stylianou.k@hotmail.com (K.S.); papalli.maria@ucy.ac.cy (M.P.); kyriakou.loucas@ucy.ac.cy (L.K.); rigopoulos.ioannis@ucy.ac.cy (I.R.); ioannis@ucy.ac.cy (I.I.)

² Nireas International Water Research Centre, University of Cyprus, Nicosia 1678, Cyprus

³ Department of Chemistry, University of Cyprus, Nicosia 1678, Cyprus; papageorgiou.erato@ucy.ac.cy (E.P.); effie@ucy.ac.cy (E.P.)

* Correspondence: tsipa.argo@ucy.ac.cy

Citation: Tsipa, A.; Stylianou, K.; Papalli, M.; Papageorgiou, E.; Kyriakou, L.; Rigopoulos, I.; Ioannou, I.; Pinakoulaki, E. Iron-Stimulated Production and Antimicrobial Potential of a Novel Biosurfactant Produced by a Drilling Waste-Degrading *Pseudomonas citronellolis* Strain. *Processes* **2021**, *9*, 686. <https://doi.org/10.3390/pr9040686>

Academic Editors: Ewa Kaczorek and Wojciech Smulek

Received: 20 March 2021

Accepted: 12 April 2021

Published: 14 April 2021

Publisher's Note: MDPI stays neutral with regard to jurisdictional claims in published maps and institutional affiliations.



Copyright: © 2021 by the authors. Licensee MDPI, Basel, Switzerland. This article is an open access article distributed under the terms and conditions of the Creative Commons Attribution (CC BY) license (<https://creativecommons.org/licenses/by/4.0/>).

Abstract: A *Pseudomonas citronellolis* strain was isolated from drilling waste (DW). This strain utilizes DW as the sole energy and carbon source to produce biosurfactants (BSs). The BS produced was thermally stable, amorphous and includes a peptide structure. FeSO₄, FeCl₃ and Fe(NO₃)₃ were supplemented at various concentration levels to assess possible enhancement of BS production and DW biodegradation. The limit concentration of Fe compounds between the increase in BS formation and microbial toxicity was 0.1 mM. FeCl₃ enhanced DW biodegradation and more than doubled the BS formation yield, determining an optimization strategy for BS production. The BS was then partially purified and used against several Gram-negative and positive multi-drug resistant bacteria (such as *Klebsiella pneumoniae*, *Pseudomonas aeruginosa*, *Escherichia coli* spp, *Acinetobacter baumannii*, *Enterococcus faecalis* spp, *Streptococcus pneumoniae*, *Staphylococcus aureus*, *Salmonella enterica*). The minimum inhibitory concentration was defined at a range of 0.25 to 10 mg/mL. The antimicrobial properties of the partially purified BS established its effectiveness and suggested a down-stream processing cost reduction, as no additional purification steps were necessary. The study could lead to a sustainable low-cost bioprocess towards a circular bioeconomy because waste, a non-expensive substrate, is used; while the BS holds great potential as a novel compound with antibiotic and disinfectant-like action, following toxicity testing with human cells.

Keywords: biosurfactant; drilling waste; iron-stimulation; characterization; antimicrobial properties

1. Introduction

Surfactants, which are surface active agents, are classified into two main categories: synthetic surfactants and biosurfactants. Synthetic surfactants are produced by organic chemical reactions, whereas biosurfactants are produced by biological processes of microorganisms [1]. Biosurfactants (BS) are amphiphilic molecules possessing a hydrophilic and a hydrophobic moiety [2]. BSs production has been attracting increased attention due to their low toxicity, high biodegradability, better environmental compatibility, higher selectivity, high foaming capacity, stable activity at extreme pH, salinity and temperature, and compatibility with human skin [3,4], when compared to their synthetic counterparts. Given the different types of BS-producing microbial species and BS chemical structures, microbial surfactants are separated into four main categories: (1) glycolipids, (2) phospholipids, (3) polymeric surfactants, and (4) lipoproteins and lipopeptides [5].

Due to their exceptional properties, BSs are being increasingly used in various fields including: pharmaceutical and food industries as emulsifiers; surfactants in laundry products by detergent-producing industries; biological control agents in heavy oil spill

mobilization for the control of oil pollution, for cleaning of oil sludge at storage facilities, as well as in the bioremediation of oil contaminated soil and (microbial) enhanced oil recovery ((M)EOR) [6]. Interestingly, several BSs also exhibit antibacterial, antifungal, anticancer and antiviral activities, which render them appropriate candidate molecules for applications in combating many infections, viruses and diseases [7,8].

Even though interest in BS research and development is increasing, these compounds are not yet industrially and financially feasible, as opposed to synthetic surfactants. One of the main reasons for this is their high production cost, which is almost 50 times that of synthetic surfactants [9]. Nevertheless, the cost can be reduced by optimizing the medium composition through statistical methods, optimizing culture conditions, using high yield BS-producing strains [10], strain improvement, or by using alternative inexpensive substrates, such as agricultural and drilling waste and wastewater. The latter is important to the overall economy of the process, as it accounts for up to 50% of the final production cost and may also lead to a reduction in expenses as regards to waste treatment [11], thereby leading to circular economy and sustainability. Therefore, low-cost or underutilized substrates, such as industrial waste, can be utilized to address this issue [12].

The safe disposal of drilling waste (DW) poses important waste management and environmental problems to the oil and gas (O & G) industry, mainly due to the vast quantities generated and the high content of contaminants. DW is the second largest volume of waste, behind produced water, generated by the O & G industry [13]. It mainly consists of hydrocarbons, leading to contamination of the natural resources. Bioremediation by biodegradation is considered as one of the primary mechanisms for the elimination of hydrocarbon pollutants from the environment. The potential for DW bioremediation may efficiently contribute to effective waste management in the O & G industry. Furthermore, oil-related waste bioconversion to high added-value compounds, such as BSs, is an environmentally compatible and sustainable solution, enhancing the biodegradation process itself, while substantially reducing the production costs of BSs [14]. Well-known BSs used to enhance biodegradation of oil-contaminated sites and oil recovery are rhamnolipids from *Pseudomonas* spp. [15], sophorolipids from *Candida* spp. [16] and surfactins from *Bacillus* spp. [17].

Microorganisms are greatly affected by the growth conditions that prevail around them [18]. Different carbon and nitrogen sources, along with variations at pH and temperature, have resulted in increased yields of BSs [2]. In addition, metal supplementation was reported to be one of the critical factors required for the enhanced production of BSs [19]. Among the metal ions, Fe is the key microelement for BS production in several microorganisms, which also plays a key role in microbial metabolism [20].

Considering all the above, in the current study, a BS-producing microorganism, called *Pseudomonas citronellolis*, was isolated from DW. BS production by *P. citronellolis* will be exploited by degrading drill cutting fluid (DCF), a constituent of DW, and by supplementing different Fe compounds at different concentration levels. The BS will be characterized in principal and its antimicrobial potential will be tested against several Gram-negative and positive bacteria. To the best of author's knowledge, this is the first collection of data on antimicrobial activity of BSs extracted from a *P. citronellolis* strain against a wide number of bacterial pathogens.

2. Materials and Methods

2.1. Microbial Enrichment Experiments

The microorganism was isolated using 0.5% (v/v) drill cutting fluid (DCF), provided by Innovating Environmental Solutions Center (IESC Ltd., Limassol, Cyprus), 5% (w/v) activated sludge coming from the municipal wastewater treatment plant of Limassol (Cyprus) as an inoculum, 10 times concentrated (10×) M9 minimal medium (i.e., 33.91 g Na₂HPO₄, 15 g KH₂PO₄, 15 g NaCl, 5 g NH₄Cl in 0.5 L dH₂O) [21] and 500 times concentrated (500×) MgSO₄ (12.0372 g in 100 mL dH₂O). Microbial enrichments were grown in a total volume of 50 mL in a 250 mL Erlenmeyer flask. In the flask, 10% of the volume was M9 minimal

medium and 0.02% MgSO_4 . The total incubation period lasted 21 days, at a temperature of 30 °C. Within the 21 days, 10% (*v/v*) of the inoculum was transferred every 7 days to a freshly prepared media, which contained M9 minimal medium, MgSO_4 and 0.5% (*v/v*) DCF. Following the total incubation period, 300 μL of the microbial enrichment was spread to a Petri dish containing agar with 10% M9 minimal medium, 0.02% MgSO_4 and 0.5% (*v/v*) DCF. The Petri dish was incubated at 30 °C for 48 h. Following that, the culture of the Petri dish was spread to a new Petri dish, following the same procedure, until single colonies were observed. The process was repeated three times. Single colonies were then grown in liquid media containing 10% M9 minimal medium, 0.02% MgSO_4 and 0.5% (*v/v*) DCF in a total volume of 50 mL in a 250 mL Erlenmeyer flask for 24 h in triplicates. Microbial culture aliquots were separated and stored in 25% (*v/v*) glycerol at -80 °C. Following that, the microbial cultures were centrifuged at 4000 rpm, the supernatant was discarded, and the biomass was proceeded for total DNA extraction.

2.2. Microorganism Identification and Homology

Total DNA was extracted from 100 mL microbial cultures using the DNeasy Kit (Qiagen, Düsseldorf, Germany), following the manufacturer's instructions. For identification of the microbial culture, de novo sequencing was performed (Macrogen Ltd., Amsterdam, the Netherlands). A draft genome sequence was generated by performing the following steps: (i) DNA PCR-Free Library construction (Illumina TruSeq), (ii) 150 bp PE sequencing run-2Gb data (illumina NovaSeq), (iii) de novo assembly, (iv) genome annotation. The nearest relative strains were identified by Basic Local Alignment Search Tool (BLAST) analysis against the National Center for Biotechnology Information (NCBI).

2.3. Bacterial Culture Conditions

Subcultures of the isolated strain were pre-grown for 24 h at 30 °C and 100 rpm (Shaking Orbital Incubator SI50, Stuart) in M9 minimal medium [21] and MgSO_4 supplemented with 1% (*v/v*) DCF (IESC company, Limassol, Cyprus). Each experiment was conducted in three independent cultures, which were prepared by diluting the 24 h culture in M9 minimal medium and MgSO_4 to an initial optical density (OD) of 0.1 (0.1 L culture volume) at 600 nm (UV-Visible Spectrophotometer, JASCO V-530 PC, Nicosia, Cyprus). In each experiment, 10% of the volume was M9 minimal medium and 0.02% MgSO_4 . The exact recipe of the prepared M9 minimal medium and MgSO_4 is described in Section 2.1. The M9 minimal medium and MgSO_4 were supplemented with 1% (*v/v*) DCF, while varying additions of different Fe forms were further used, depending on the experiment performed (see below). Cultures were prepared using 500 mL conical Erlenmeyer flasks, which were continuously stirred at the same conditions as pre-culture. The flasks were filled with medium up to one-fifth of their volume, to ensure sufficient oxygen availability to the microorganism.

2.4. Effect of Iron Forms and Concentration Level on the Isolated Strain

For every study, the pre-inoculum was prepared with 1% (*v/v*) DCF at M9 minimal media and MgSO_4 and was left for 24 h at 30 °C and 100 rpm. For every experiment, the pre-inoculum was diluted to 0.1 OD. Certain concentrations of Fe of 3 different forms were added to the medium containing DCF. The different Fe compounds used in this study were: FeSO_4 (Scharlau, Barcelona, Spain), $\text{Fe}(\text{NO}_3)_3$ (Carlo Erba, Barcelona, Spain), and FeCl_3 (Carlo Erba, Barcelona, Spain). A control experiment without iron was also performed. To study the effect of iron concentration on biosurfactant production, bacterial growth and chemical oxygen demand (COD) removal, FeSO_4 was added to the microbial cultures with DCF at concentrations of 0.1, 0.2, 0.4 and 0.6 mM. The compounds $\text{Fe}(\text{NO}_3)_3$ and FeCl_3 were added at concentrations of 0.1 and 0.6 mM. In all experiments, the flasks were incubated in triplicate for 24 h at 30 °C and 100 rpm.

2.5. Biosurfactant Isolation, Extraction and Partial-Purification

For the isolation of the BS, a method similar to Suryanti et al. (2013) [22] was followed. In particular, following the completion of each experiment, the cultures were centrifuged for 25 min at 4500 rpm to precipitate and remove the biomass. The BS recovery process initiated from the cell-free supernatants of DCF containing media where the pH was adjusted to 2 using 1M H₂SO₄. The samples were incubated at 4 °C overnight. On the next day, the supernatant was centrifuged for 30 min at 4500 rpm, resulting in the precipitation of the BS, and the supernatant was discarded. A total of 5 mL of a mixture of chloroform:methanol (2:1 v/v) was added to the precipitated BS. The mixture was mixed vigorously, resulting in BS dissolution. The mixture was incubated at 30 °C for 15 min. Following that, the BS solution was centrifuged for 30 min at 4500 rpm, leading to the precipitation of the partially purified BS. The supernatant was discarded, the precipitate was left to dry, and was kept at −20 °C.

2.6. Analytical Methods: Chemical Oxygen Demand (COD)

Following the completion of each experiment, the cultures were centrifuged for 25 min at 4500 rpm to precipitate and remove the biomass. A total of 1 mL of the supernatant was collected and diluted in 4 mL of distilled H₂O (×5 dilution). The method for the determination of COD was based on instructions by a kit (Supelco, Inc, Sigma-Aldrich, St. Louis, MI, USA) with COD range between 500 to 10,000 mg/L. The sample was diluted to fall within the kit COD range. The method agrees with the DIN ISO 15,705 and is similar to EPA410.4, APHA 5220D, and ASTM D1252-06 B. The kit provides the cell which contains sulfuric solution of potassium dichromate and silver sulfate as catalyst. Kit instructions for sample preparation, incubation and COD quantification were followed. Briefly, 1 mL of the diluted sample was added to the cell. The cell was vigorously mixed and then heated at 148 °C in a pre-heated thermoreactor (CR 3200, WTW, Xylem Analytics, Weilheim, Germany) for 120 min. Following complete cooling of the cell down to room temperature, the COD concentration was measured in a photometer (Spectroquant pharo 100, Merck Millipore, Darmstadt, Germany). The control for the COD measurement contained the medium and 1% (v/v) DCF.

2.7. Antimicrobial Activity

2.7.1. Bacterial Strains Tested

The antimicrobial activity of the studied biosurfactant was tested against Gram-negative and Gram-positive multi-drug resistant bacteria purchased from Leibniz Institute DSMZ-German Collection of Microorganisms and Cell Cultures GmbH (Germany). All the purchased microorganisms were grown in the relevant culture conditions recommended by the company. Furthermore, the antimicrobial activity was tested against an *Escherichia coli* strain and *Enterococcus faecalis* strain, isolated from the municipal wastewater treatment of Limassol (Cyprus). These two strains, in the present study, were called *Escherichia coli* resistant and *Enterococcus faecalis* resistant.

The Gram-negative bacteria purchased were: *Klebsiella pneumoniae* (DSM 681), *Pseudomonas aeruginosa* (DSM 19880), *Escherichia coli* (DSM 17076), *Acinetobacter baumannii* (DSM 24110). The Gram-positive bacteria were: *Enterococcus faecalis* (DSM 20409), *Streptococcus pneumoniae* (DSM 11865), *Staphylococcus aureus* (DSM 799), *Salmonella enterica* (DSM 26655).

2.7.2. Preparation of Biosurfactant Solution

The BS was dissolved in 5% (v/v) methanol in distilled H₂O. The pH of the solution was adjusted to 9. The concentration of the biosurfactant in the solution was adjusted to either 1 or 10 mg/mL and serial dilutions in distilled H₂O were prepared to adjust to lower concentrations of the BS, as needed. In particular, 1 mg/mL was diluted to 0.25 and 0.5 mg/mL, whereas 10 mg/mL was diluted to 5 mg/mL to test the minimum inhibitory concentration of the BS, as described in Section 2.7.4 below. The control solution was 5% (v/v) methanol in distilled H₂O with pH 9.

2.7.3. Agar Disc Susceptibility Test

The antimicrobial activity was determined using the standard clear zone inhibition halo method [23]. The susceptibility of the test strains against the BS was tested with the agar disc diffusion test. The method is similar to that used by Das et al. (2008), with a few modifications. For the test, all the bacterial test strains, including the isolated strains, were cultured overnight in sterile trypticase soy broth (TSB) at 37 °C. TSB contains 17 g tryptone (pancreatic digest of casein), 3 g soytone (peptic digest of soybean), 2.5 g glucose (=dextrose), 5 g sodium chloride, 2.5 g dipotassium phosphate per liter of dH₂O at pH 7.3 ± 0.2. The OD of all broth cultures was adjusted to 0.1 equivalents to an inoculum of 1.5 × 10⁸ CFU ml⁻¹ (according to McFarland turbidity standards). Exactly 500 µL of each of the diluted in TSB cultures was used to inoculate agar plates by flooding their surface and spreading them uniformly on plates. The excess liquid broth was allowed to air dry for 15 min under the sterile environment of a biosafety laminar flow cabinet (Esco, Barnsley, UK). The agar disc diffusion was performed, following optimization experiments, on sterile TSB agar (Sigma-Aldrich Ltd, St. Louis, MI, USA) (*K. pneumoniae*, *P. aeruginosa*, *E. coli* resistant, *E. coli*, *A. baumannii*, *S. pneumoniae*), sterile TSB with yeast extract agar (Liofilchem, Roseto degli Abruzzi, Italy) (*E. faecalis* resistant, *E. faecalis*, *S. aureus*) and sterile nutrient agar (Scharlau, Barcelona, Spain) (*S. enterica*) plates. TSB with yeast extract contains 30 g TSB, 3 g yeast extract and 15 g agar per liter of dH₂O. Nutrient agar contains 1 g meat extract, 2 g yeast extract, 5 g peptone, 5 g sodium chloride, 15 g agar per liter of dH₂O. Sterile Whatman filter paper (No. 1) discs of 6 mm diameter, impregnated with 15 µL of the different stock solutions of the BS, were kept aseptically on the surface of these pre-inoculated plates. A disc soaked in the control solution (as described in Section 2.7.2 above) was kept as a negative control. The plates were incubated at 37 °C for 48 h and, after growth, the microbial growth inhibition zones around the discs were measured. All tests were performed in four replicates and the inhibition zone diameter values (mm) were expressed as the mean value ± standard deviation (SD).

2.7.4. Minimum Inhibitory Concentration (MIC) Agar Susceptibility Test

The agar disc diffusion test was carried out to determine the minimum inhibitory concentration (MIC) of the BS against the different tested microorganisms. The plates inoculated with the tested microorganisms were prepared as presented to Section 2.7.3. Sterile Whatman (No. 1) filter paper discs were impregnated with 15 µL of different dilutions of the solution of the partially purified BS. Those discs were then kept aseptically on the surface of the pre-inoculated plates. The plates were incubated at 37 °C for 48 h. The minimum concentration of the BS, which showed a clear zone of inhibition around the applied disc, was considered as their MIC against that particular microorganism. All tests were performed in four replicates and the inhibition zone diameter values (mm) were expressed as the mean value ± standard deviation (SD). A disc soaked in the control solution (as described in Section 2.7.2 above) was kept as a negative control.

2.8. Emulsification Index (E24)

The emulsification index (E24) was determined by adding 2 mL of DCF to the same amount of two different aqueous solutions (5% (*w/v*) and 1% (*w/v*)) of biosurfactant extracted as above. The DCF-biosurfactant solution was vortexed at maximum speed for 2 min and left to stand for 24 h. After that time period, the E24 was calculated as the percentage of height of emulsified layer (mm) divided by the total height of the liquid column (mm) [24] (Equation (1)). The emulsification percentage was determined based in triplicates.

$$E24 = (\text{Height of emulsion layer} / \text{Total height of solution}) \times 100 \quad (1)$$

2.9. Surface Tension

The BS surface tension was estimated based on the method of capillary rise [25–27]. The surface tension was determined based on the *P. citronellolis* isolated strain growth in M9 minimal media and MgSO₄ at 30 °C and pH 7. The biomass was removed and the BS was extracted as described in Section 2.5. Before being stored at −20 °C, the BS was dissolved in water. The density of the BS was 1.78 g/mL. Surface tension was determined using Equation (2), where d is the liquid density, h the height of the capillary, r the capillary radius, γ the surface tension and θ the contact angle. Since the liquid completely wet the capillary walls, the contact angle θ was considered 0°, and $\cos\theta$ was equal to 1.

$$\gamma = (rhdg)/(2\cos\theta) \quad (2)$$

2.10. Fourier Transform Infrared Spectroscopy (FTIR)

The FTIR measurements were performed with a Bruker (Mannheim, Germany) Vertex 70 FTIR-spectrometer. The spectra were recorded in the attenuated total reflectance (ATR) mode by using a Pike Miracle ATR accessory configured with a single reflection ZnSe crystal. The biosurfactant was placed in the ZnSe crystal in powder form and a high-pressure clamp was used to improve contact between the sample and the ATR crystal. A background spectrum was recorded with a clean crystal before each measurement. ATR-FTIR spectra were recorded between 4000 and 600 cm^{−1} at a resolution of 4 cm^{−1}.

2.11. Thermal Gravimetric Analysis (TGA) and Differential Thermal Analysis (DTA)

Simultaneous differential thermal analysis (DTA) and thermogravimetry (TG) on a representative sample of mass 13.61 mg of the extracted BS were undertaken using a Shimadzu (Kyoto, Japan) DTG-60H analyzer. These analyses were carried out from room temperature (ca. 25 °C) to 800 °C, at a heating rate of 5 °C/min, in a flowing dry nitrogen atmosphere (20 mL/min).

2.12. X-ray Diffraction (XRD) Analysis

The X-ray diffraction (XRD) analysis of the extracted BS (mass = 13.61 mg) was also performed using a Bruker (Mannheim, Germany) D8 Advance system with Cu K α radiation ($\lambda = 0.1541$ nm) at 40 kV and 40 mA. The analysis was carried out with continual rotation of the sample and a step of 10°/min within the 10–80° 2 θ angle range. The International Centre for Diffraction Data (ICDD) Powder Diffraction File (PDF) 4 database was used for the qualitative identification of the amino acids.

2.13. Statistical Analysis

For the antimicrobial activity test four technical replicates of each assay (i.e., agar disc susceptibility method and MIC) were performed on the same day with the same solution of the BS which was extracted from each experiment. Each experiment was performed in biological triplicates. The results are stated as mean \pm SD.

3. Results and Discussion

3.1. Identification of the Microorganism, Production of BS and Determination of Surface Tension and Emulsification Index (E24)

DNA sequencing of three different single colonies derived from the isolation experiment showed that each colony was derived from the same microorganism. It is likely that the presence of biocides in the DCF prevented the isolation of more than one microorganism. According to BLAST results, following genome annotation of the draft genome sequence, the top ten (10) hits recognize that the microorganism is *Pseudomonas citronellolis*. The current isolated strain showed a 97–99% homology with *P. citronellolis* P3B5 or SJTE-3 (Table S1, Supplementary Material). Hence, current strain holds the potential to be a novel strain of *P. citronellolis* which, herein, was named *P. citronellolis* 620C. The genomes of both P3B5 and SJTE-3 strains were completely sequenced and both strains have been identi-

fied as hydrocarbon-degrading [28,29]. Furthermore, P3B5 has also been characterized as surfactant-producing using diesel as a substrate [30]. Nevertheless, analysis of the microorganism genome is beyond the scope of the present study.

BS formation is usually demonstrated from the late exponential phase until the end of the stationary phase [31], while the release of cell-bound BS in the medium leads to a decrease in surface tension, even after the stationary phase [32]. In the current study, it was observed that microbial growth, with 1% DCF as a substrate, was reduced at 26 h of culture and the BS was extracted at that time point. The surface tension of water and BS solution were 72.1 mN/m and 32.8 mN/m, respectively. Therefore, BS efficiently reduced the surface tension of water. The surface tension of the BS solution was similar to other studies in the literature, whereby BS was produced by *Pseudomonas* species. For instance, Singh et al. 2016 [31] reported a reduction in surface tension of a BS formed by *P. otitidis* P4 from 71.18 to 33.4 mN/m. Recently, a mixture of biosurfactants formed by *P. syringae* *pv.* *tabaci* reduced the surface tension of water down to 36.89 mN/m [33].

The formation of BS increases the bioavailability and biodegradation of hydrocarbons [34]. An indication of the increased bioavailability is the emulsification index (E24). The E24 using two solutions of BS with 1% (*w/v*) and 5% (*w/v*) BS concentration was 24.8% and 44.6%, respectively. The E24 results did not show high emulsification of the BS, despite the different concentration of BS used. This indicates that the current BS could be a low molecular weight molecule. Low molecular weight biosurfactants are the glycolipids or lipopeptides [35]. For instance, E24 of the glycolipid named rhamnolipid formed by *P. fluorescens* was up to 10% and 49% upon growth on hexadecane and olive oil, respectively [36]. Furthermore, several lipopeptides showed a E24 between 20–31% upon *Pseudomonas* spp growth on hexadecane biodegradation [37]. In another study, among several *P. citronellolis* isolates from hydrocarbon contaminated soil, the E24 ranged between 43.75–70.45% [38], showing low and high emulsification capability. Finally, upon E24 testing of a BS produced by *P. citronellolis* 222A, emulsification was not detected, indicating that the molecular weight of the BS produced by that strain was not high [39].

3.2. Microbial Growth and the Effect of Different Iron Forms

In this study, the effect of different iron forms, at different concentration levels, on the microbial growth of *P. citronellolis* isolate 620C was evaluated. In particular, FeSO_4 , FeCl_3 and $\text{Fe}(\text{NO}_3)_3$ forms were studied based on the results reported by Santos et al. (2008) [40]. In that study, the effect of different iron forms on anthracene and other hydrocarbons degradation, and BS production was demonstrated using *P. citronellolis* and *P. aeruginosa* isolates. In the current study, to demonstrate the level of toxicity of iron forms on *P. citronellolis* 620C, FeSO_4 supplementation was studied at concentration levels of 0.1, 0.2, 0.4 and 0.6 mM (Figure 1A). Santos et al. (2008) reported that the addition of iron forms at a concentration ≥ 0.5 mM was inhibitory for microbial growth. The results were compared to microbial growth without the addition of iron forms. It was observed that the addition of 0.1 mM of FeSO_4 greatly enhanced microbial growth, similarly to Santos et al. 2008 [40] who chose that concentration level for further studies. Furthermore, unlike Santos et al. 2008 [40], the addition of higher than 0.1 mM concentrations of FeSO_4 did not affect the growth of *P. citronellolis* isolate 620C.

Following that, the effect of adding FeCl_3 and $\text{Fe}(\text{NO}_3)_3$ forms was studied. These iron forms were supplemented in the microbial culture at the lowest (i.e., 0.1 mM) and highest (i.e., 0.6 mM) concentration level of FeSO_4 . This was performed to check microbial growth at the concentration level of Fe compounds which promotes microbial growth, according to the previous experiment (i.e., 0.1 mM of FeSO_4) and one above the limit of toxicity, according to Santos et al. (2008), which is 0.6 mM. Microbial growth kinetics were evaluated at regular time points (Figure 1B). The results were compared to microbial growth without the addition of iron forms. It was observed that 0.1 mM of both iron forms significantly enhanced microbial growth, while the addition of 0.6 mM resulted in the inhibition of *P. citronellolis* 620C growth. The latter can be attributed to the toxicity that

may have been caused to the microorganism's metabolism. These results are in accordance to Santos et al. 2008 [40]. Furthermore, the addition of 0.1 mM of the three different iron forms was compared to each other and to the microbial growth without the addition of any iron form (Figure 1C). Among the three iron forms, the addition of FeCl_3 resulted in the highest microbial growth. Overall, when iron was supplemented in the microbial culture at the lowest concentration, microbial growth was significantly increased.

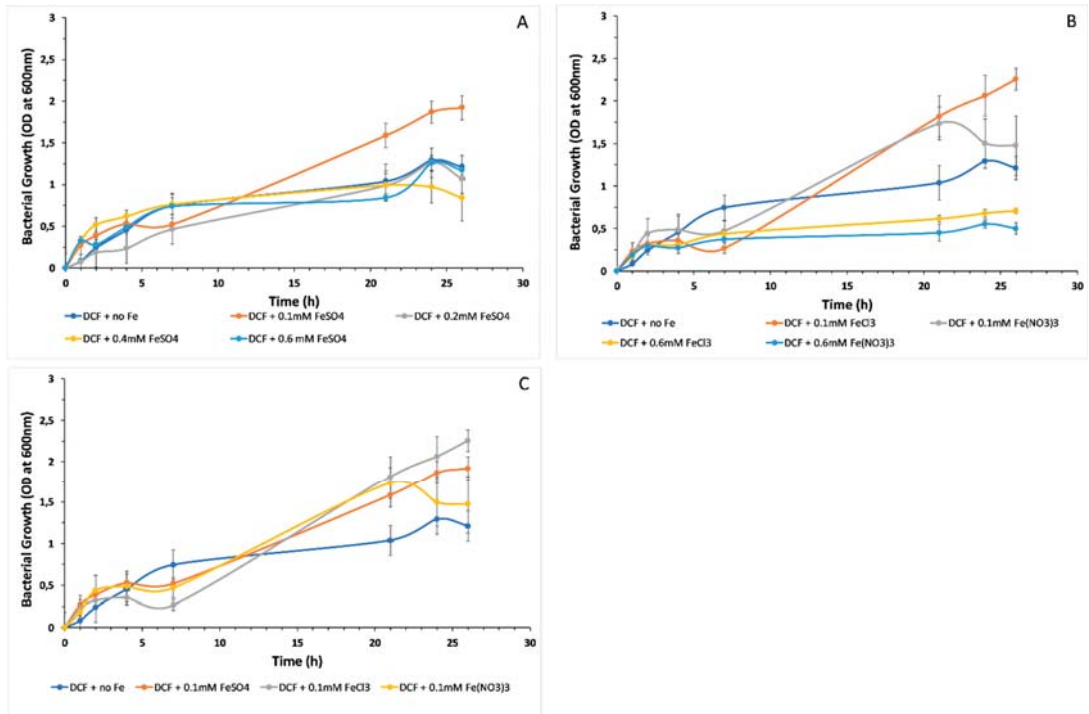


Figure 1. Microbial net growth of *P. citronellolis* 620C with 1% (*v/v*) drill cutting fluid (DCF) as substrate: (A) with and without the supplementation of different concentration levels of FeSO_4 , (B) with and without the addition of high and low concentration level of FeCl_3 and $\text{Fe(NO}_3)_3$, (C) comparison when different 0.1 mM iron forms are supplemented.

Several necessary functions of microbial metabolism are performed due to iron participation, such as the protection of the cells against superoxide radicals, whilst iron is also a key component of cytochromes and contributes to the Krebs cycle [41]. However, the limit between deficiency and toxicity is narrow. For instance, iron can interact with reactive oxygen species, such as hydrogen peroxide and superoxide, forming greatly damaging and reactive hydroxyl radicals. Furthermore, bacteria are highly sensitive in the presence of redox agents upon growth under iron-supplemented conditions [42]. Therefore, low amounts of iron are required.

The presence of oxygen leads to insolubility and low reactivity of Fe, and thus, low bioavailability and higher toxicity [40]. For instance, the predominant form of Fe, ferric iron, which exists in rhizosphere, is highly insoluble. Therefore, it is possible that appropriate concentrations of soluble iron forms can enhance the microbial growth, resulting in increased hydrocarbon biodegradation and, thus, higher microbial growth, as observed in the rhizosphere [43,44].

Consequently, in the present study, the effect of iron forms on microbial growth was more evident when more soluble iron forms were used. Specifically, microbial growth

was further increased when FeCl_3 and $\text{Fe}(\text{NO}_3)_3$ were added to the microbial cultures, compared to FeSO_4 addition. The addition of more soluble forms of iron increases iron availability to the microorganism. FeSO_4 is relatively insoluble in water, therefore, an increase in the concentration of FeSO_4 leads to an increase in insolubility. Thus, the insignificant effect of >0.1 mM concentration of FeSO_4 in the microbial culture may also be attributed to insolubility, which inevitably leads to a lower interaction of Fe with the microbial culture. Another cause of the lower effect of FeSO_4 to the microbial growth could be that this compound may also cause microbial culture acidification [40].

3.3. Biosurfactant Production and the Effect of Different Iron Forms

In the current study, BS production was evaluated upon supplementation of the microbial culture with FeSO_4 at the concentration level of 0.1, 0.2, 0.4 and 0.6 mM (Figure 2A). Santos et al. (2008) reported that the addition of iron forms at concentrations ≥ 0.5 mM was inhibitory for microbial growth and, thus, BS production. The results were compared to BS production without the addition of iron forms. It was observed that the addition of 0.1 mM of FeSO_4 greatly enhanced BS production, in line with the results of Santos et al. 2008 [40]. Specifically, the BS yield was increased by 95%, as shown in Figure 2A. Furthermore, addition of higher concentrations of FeSO_4 led to lower levels of BS production than the control specimen, despite the fact that those concentration levels did not negatively affect the growth of *P. citronellolis* 620C. These results are consistent with those of Santos et al. 2008 [40], suggesting a strong correlation and dependence of iron and BS formation up to a limit where iron is not beneficial for BS formation. Following that, the addition of FeCl_3 and $\text{Fe}(\text{NO}_3)_3$ were supplemented in the microbial culture at the lowest (i.e., 0.1 mM) and highest (i.e., 0.6 mM) concentration levels. It was observed that 0.1 mM of both iron forms greatly increased BS production. In particular, the addition of 0.1 mM of FeCl_3 and $\text{Fe}(\text{NO}_3)_3$ resulted in a 112% and 90% increase, respectively, whereas the addition of 0.6 mM resulted in BS production that was lower than the control specimen (Figure 2B). The results were similar to the microbial growth results and they could be attributed to the toxicity that may have been caused to the microorganism's metabolism, leading to low microbial growth and, thus, limited BS formation. These results are also in accordance to Santos et al. 2008 [40]. BS production was compared upon addition of 0.1 mM of the three different iron forms (Figure 2C). Among the three iron forms, the addition of FeCl_3 resulted in the highest BS formation, which corresponds to the highest microbial growth. Overall, similarly to microbial growth, when iron was supplemented in the microbial culture at the lowest concentration, BS production was significantly increased. The addition of iron forms to the growth medium of *Bacillus subtilis* [45] and *P. citronellolis* strains [40] resulted in overproduction of the relevant BSs. Makkar and Cameotra (2002) also reported that metal ion addition greatly enhanced BS production [46]. Several other studies have also evaluated the positive effect of Fe nanoparticles on BS production [2,18].

Furthermore, in the present study, FeCl_3 addition resulted in the highest BS yield, over-doubling the production. This is in line with Dinkla et al. (2001) [43], who reported the positive effect of FeCl_3 on BS formation upon toluene biodegradation. In another study of the production of BS by marine *Nocardiopsis lucentensis* MSA04 in solid-state cultivation, FeCl_3 was found to be the most suitable metal precursor [47]. Therefore, the addition of more soluble forms of iron at adequate concentrations could be a key strategy for the optimization of BS production.

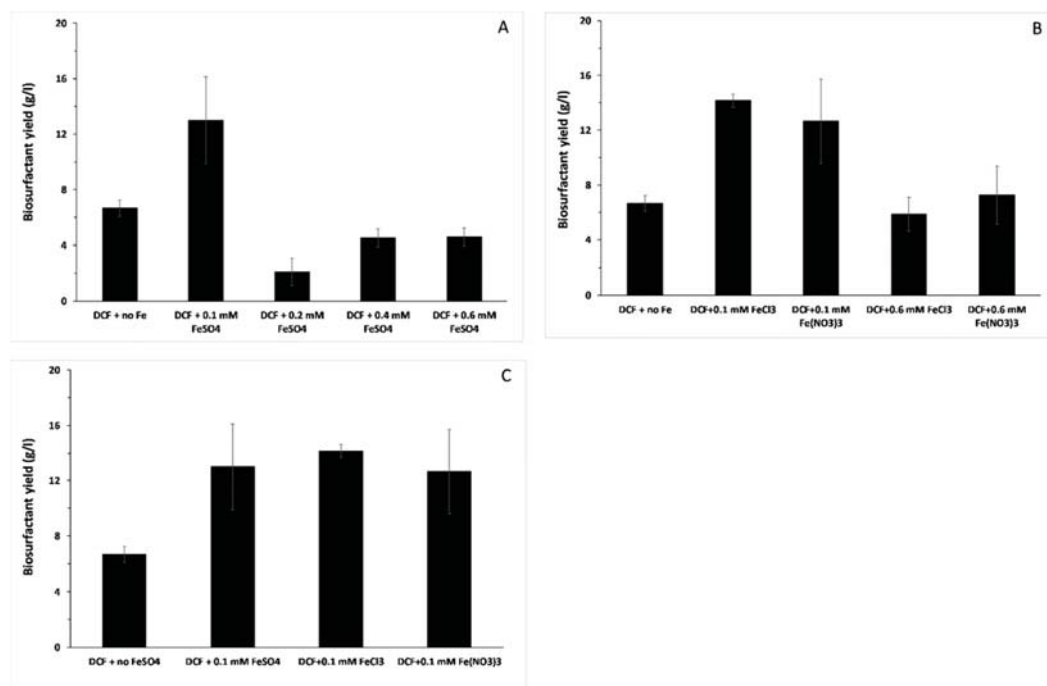


Figure 2. Biosurfactant production by *P. citronellolis* 620C with 1% (*v/v*) DCF as substrate, based on the product yield of the biosurfactant (BS) over drilling waste consumption: (A) with and without supplementation of different concentration levels of FeSO₄, (B) with and without the addition of high and low concentration levels of FeCl₃ and Fe(NO₃)₃, (C) comparison when different 0.1mM iron forms were supplemented.

3.4. COD Removal and the Effect of Different Iron Forms

BSs enhance the bioremediation of oil waste [14]. Therefore, COD was studied to observe the effect of enhanced biodegradation due to BS production. The effect of the addition of the different iron forms was also evaluated through COD measurement. The experimental conditions were similar as those mentioned above (Section 3.2). The FeSO₄ effect on % COD removal of DCF was studied upon the addition of 0.1, 0.2, 0.4 and 0.6 mM (Figure 3A), whereby a slight increase in the % COD removal was observed, compared to the control experiment (i.e., without iron addition). The results followed the microbial growth results, suggesting that FeSO₄ addition does not greatly affect the metabolic pathways related to hydrocarbons and biomass formation activities. Following that, the effect of addition of 0.1 and 0.6 mM FeCl₃ and Fe(NO₃)₃ was studied (Figure 3B), whereby at 0.1 mM, both forms increased the % COD removal, with the effect of FeCl₃ being more pronounced, in agreement with the previous results of the present study. Additionally, at 0.1 mM addition, among the three iron forms, FeCl₃, similarly to the microbial growth and BS production, further enhanced the % COD removal, demonstrating its positive effect in the bioprocess (Figure 3C).

It was noticed that, although the different iron forms resulted in increased % COD removal, compared to the COD removal without the supplementation of iron forms, the removal was not as high as that of the COD removal reported in other studies (e.g., Santos et al., 2008), whereby pure hydrocarbon forms were used, such as anthracene. It is suggested that the higher COD removal observed in the microbial cultures supplemented with iron was due to the higher availability of iron for induction, expression and activity of the enzymes catalyzing hydrocarbon biodegradation, as iron is a key element of oxygenases [48]. Furthermore, at low iron concentration, the direct dependence of the BS on the

presence of iron, which resulted in BS over-production, probably increased hydrocarbon bioavailability to degradation, thus, leading to an increase in the % COD removal.

DCF is a highly toxic waste stream which, unless safely disposed, can lead to an adverse impact on human health and the environment due to its hazardous components and additives [49]. DCF biodegradation is an alternative eco-friendly approach for disposal management which is enhanced by BSs produced during the microbial bioprocess [50]. Therefore, the potential of *P. citronellolis* 620C to be used in a scaled-up bioprocess was examined. The enhancement of DCF biodegradation through the use of the BS-producing *P. citronellolis* 620C was also evaluated at higher than 1% (*v/v*) DCF concentrations (i.e., 5% and 10%) through monitoring of microbial growth kinetics and % COD removal. Despite the toxicity of the DCF (initial COD: 41.000 mg/L), the % COD removal was promising (i.e., 42% and 27.5%, respectively) (Supplementary Material Figure S1).

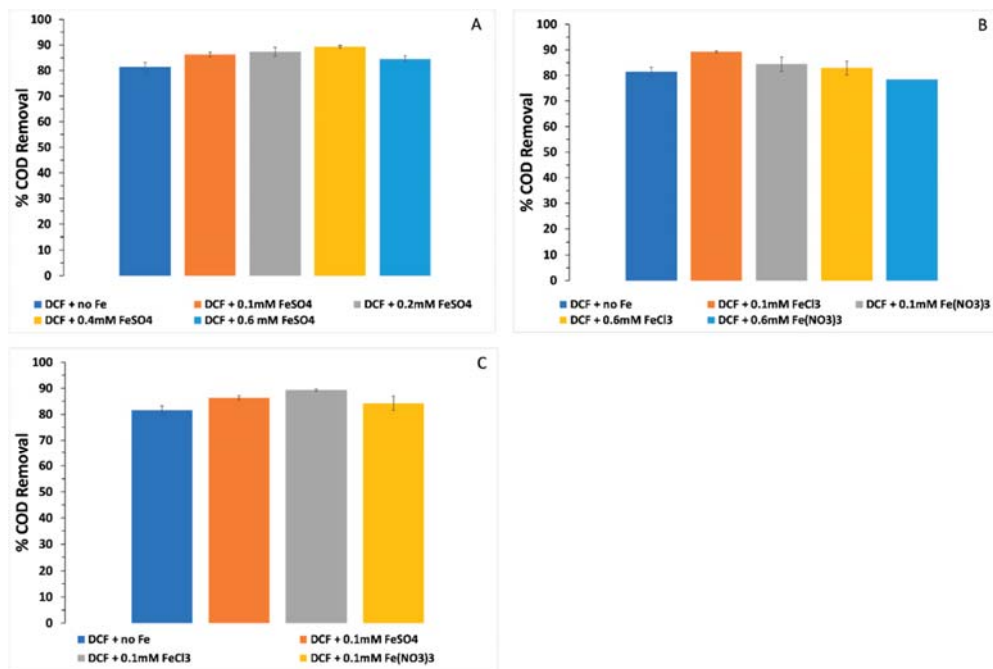


Figure 3. % chemical oxygen demand (COD) removal of DCF in *P. citronellolis* 620C culture with 1% (*v/v*) DCF as substrate: (A) with and without the supplementation of different concentration levels of FeSO₄, (B) with and without the addition of high and low concentration levels of FeCl₃ and Fe(NO₃)₃, (C) comparison when different 0.1 mM iron forms were supplemented.

3.5. Biosurfactant Characterization

3.5.1. FTIR

FTIR spectroscopy is a valuable tool in the identification of the chemical structure of compounds, as FTIR spectra comprise bands that are characteristic for specific chemical bonds. In this work, the ATR-FTIR approach was employed, as it offers the advantage of working with solid or liquid samples with minimal sample preparation prior to spectral measurements. The ATR-FTIR spectra of the powder form of the BS are shown in Figure 4, with traces a and b corresponding to the spectra of the BS produced by the *P. citronellolis* 620C culture in the absence and presence of FeSO₄, respectively. The vibrations detected in the ATR-FTIR spectra are characteristic of a peptide structure [51]. More specifically, the bands at 3275 and 3075 cm⁻¹ were assigned to the amide A and amide B vibrations

(N-H stretch) of the peptide, while contributions from O-H bonds in the 3000–3500 cm^{-1} region cannot be excluded. The peptide backbone, additionally, gave rise to the amide I vibrations (C=O stretch) observed at 1650 and 1625 cm^{-1} , and to the amide II vibration (out-of-phase combination of the NH in plane bend and the CN stretching vibration) identified at 1530 cm^{-1} [51]. Furthermore, peaks originating from the C-H stretch of CH_3 and CH_2 groups were detected at 2960, 2930 and 2870 cm^{-1} , demonstrating the presence of alkyl groups [51,52]. To identify additional functional groups in the BS, the 1300–1000 cm^{-1} region was examined. In this region, bands could be observed at 1225, 1110 and 1050 cm^{-1} . These vibrations were attributed primarily to C-C and C-O(H) bonds and in conjunction with the contribution of O-H bonds in the ~ 3370 cm^{-1} region, they provide an indication of the presence of carbohydrate moieties in the peptide [52,53]. Finally, it should be noted that a shoulder was observed in the amide I band at 1720 cm^{-1} . This band could have originated from the C=O stretch of Glu or Asp carboxylic acid side chains or from lipid ester group; therefore, a lipopeptide structure is also possible [51,54]. Overall, from the analysis of the ATR-FTIR spectra of the BS described herein and considering the similarity of these spectra to the FTIR spectra of biosurfactants produced by lactic acid [52] and marine [55] bacteria, a glycopeptide or lipopeptide structure is proposed. Furthermore, the FTIR spectra of the BS produced in the absence and presence of FeSO_4 were similar, suggesting that Supplementation of the microbial culture with FeSO_4 did not affect the structure of the BS.

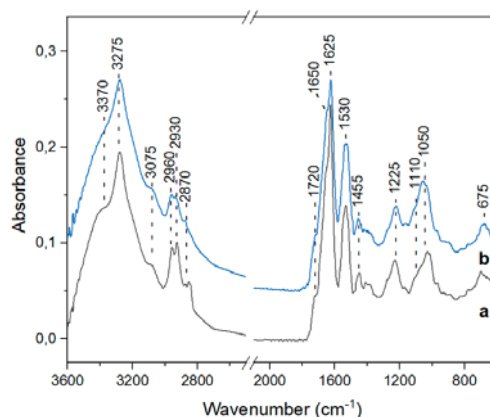


Figure 4. FT-IR analysis of the novel BS extracted and partially purified from *P. citronellolis* isolate 620C culture with 1% DCF as substrate: (a) without and (b) with the supplementation of FeSO_4 .

3.5.2. TGA, DTA and XRD

TGA/DTA, and XRD analyses were performed for the partially purified BS extracted by the microbial culture, where 1% DCF was used as the substrate. The thermal stability of BSs is a key property that is relevant to the applicability of these molecules in industrial and commercial processes [56]. In the first step of TGA (Figure 5A), during the temperature range 27–100 $^{\circ}\text{C}$, the loss of BS weight due to the loss of water and solvent molecules was estimated at 9.73%. Thermal degradation takes place upon mass loss of at least 5% [57]. In the current analysis, following the initial weight loss, 5% loss of BS weight was observed at 196.4 $^{\circ}\text{C}$. This step was followed by a rapid weight loss of 31.22% until 338.1 $^{\circ}\text{C}$, which could be attributed to the degradation of thermolabile content, such as carbohydrates and peptides in the BS. The thermal decomposition at 338.1 $^{\circ}\text{C}$ was confirmed by the exothermic peak of the DTA analysis. These results are similar to those reported by Weiss et al. 2018 [58], where thermal decomposition of several amino acids (i.e., asparagine, glycine, glutamic acid, cysteine, aspartic acid, histidine, arginine and glutamine) was studied, demonstrating decomposition between 200–300 $^{\circ}\text{C}$. The non-thermolabile content

was gradually degraded, resulting in BS weight loss of 27.91 % over the temperature range of 338.1–546.9 °C. This could be attributed to fatty acids, which are commonly decomposed over a temperature of 300 °C [59]. At 546.9 °C, another exothermic peak on the DTA graph was noticed, further confirming the thermal decomposition. As determined from the TGA and DTA graphs, the degradation temperature of BS was found to be 546.9 °C, while complete weight loss took place after 800 °C. Therefore, the BS formed by *P. citronellolis* isolate 620C was determined to be thermostable. A similar TGA graph of a lipoprotein BS, produced by *Bacillus subtilis*, has been established [60].

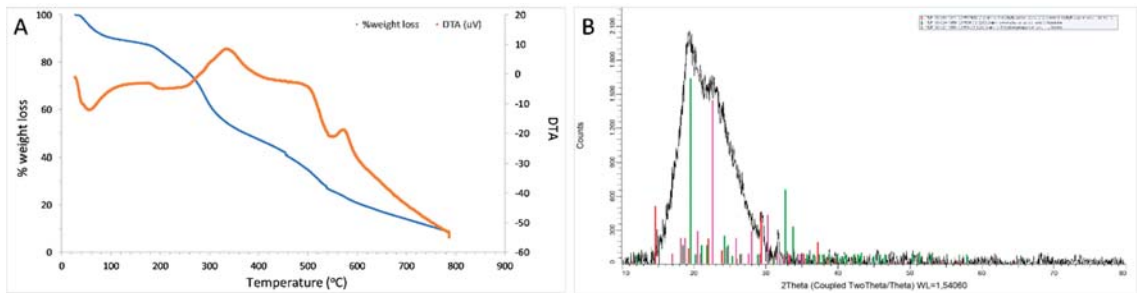


Figure 5. (A) Thermal gravimetric analysis (TGA) and differential thermal analysis (DTA) curves, and (B) XRD analysis of the novel BS extracted and partially purified by *P. citronellolis* isolate 620C culture with 1% DCF as substrate.

The powder XRD pattern (Figure 5B) indicated a highly (57.2%) amorphous BS with crystallinity index (CI_{xrd}) equal to 0.428. XRD was used to qualitatively assess the amino acids in the BS. Peptides are usually detected between 20–30° 2 θ [61]. As confirmed by the FTIR analysis, the structure of the BS formed by the *P. citronellolis* 620C contains amino acids, the building blocks of peptides.

3.6. Antimicrobial Activity of the Biosurfactant

The antimicrobial activity was studied using the solution of the partially purified BS, extracted by the *P. citronellolis* 620C culture with 1% (v/v) DCF. The BS showed antimicrobial activity against all the multi-drug resistant Gram-positive and negative microorganisms tested (Table 1).

Firstly, the antimicrobial activity of the BS was tested at a concentration level of 1 mg/mL (Table 1). This concentration level is commonly used in the agar susceptibility method [62,63]. This BS concentration inhibited the growth of the Gram-negative bacteria *K. pneumoniae*, *P. aeruginosa*, *E. coli* resistant and *E. coli*. In contrast, this level of BS concentration did not inhibit the growth of the Gram-negative *A. baumannii* and all the Gram-positive bacteria (i.e., *E. faecalis* resistant, *E. faecalis*, *S. pneumoniae*, *S. aureus*, *S. enterica*). These pathogens were inhibited at 10 mg/mL BS concentration (Table 1). These results indicate that some bacterial pathogens can be more resistant to antimicrobial agents compared to others. Commonly, the inhibition of BS on growth of bacterial pathogens is studied in a broad concentration range from few µg (e.g., 4.9 µg) [64] to 100 mg/mL [65]. Most probably, this is dependent on the chemical compartments which are contained in a BS, resulting in the antimicrobial activity, purification of the BS tested and the method used which can either be the agar susceptibility method or the micro-broth dilution technique. BSs, such as rhamnolipids at a concentration level of 1.12 mg/mL, caused an inhibition zone similar to that in the present study, against several Gram-negative and -positive bacterial pathogens [63]. The rhamnolipids were isolated and partially purified using a method similar to that of the present study.

Table 1. In Vitro antimicrobial activity of the partially purified biosurfactant against multidrug-resistant pathogenic bacterial strains, using the agar susceptibility method.

	Biosurfactant (mg/mL)	Antimicrobial Zone Diameter (mm)
<i>Klebsiella pneumoniae</i>	1	9.0 ± 0.7
<i>Pseudomonas aeruginosa</i>	1	8.8 ± 0.8
<i>Escherichia coli</i> resistant	1	10.5 ± 1.5
<i>Escherichia coli</i>	1	8.8 ± 0.4
<i>Enterococcus faecalis</i> resistant	10	9.3 ± 2.2
<i>Enterococcus faecalis</i>	10	8.3 ± 1.9
<i>Acinetobacter baumannii</i>	10	7.3 ± 5.3
<i>Streptococcus pneumoniae</i>	10	9.8 ± 1.0
<i>Staphylococcus aureus</i>	10	9.0 ± 0.8
<i>Salmonella enterica</i>	10	9.3 ± 0.5

Antimicrobial properties are more common for glycolipids or lipopeptides [62]. Most of the biosurfactants which possess antimicrobial properties have usually been produced from microorganisms isolated from contaminated and domestic sites [66]. Similarly, *P. citronellolis* 620C was isolated from a tank containing drilling waste.

The antimicrobial activity of BSs relies on the outer membrane of pathogens, which can be disrupted by the hydrophobic domain of the BSs, thus, breaking the structure of microorganisms and disabling pathogen activity. Therefore, the current BS has the potential to act as an alternative natural antibiotic, when tested against human cells. Furthermore, the current BS also has the potential to act as a disinfectant. Disinfectants are chemical means employed to inactivate pathogens, which are not inhibited anymore due to antimicrobial resistance [67]. Thus, further research on the toxicity of the BS to human skin and metabolic pathways is necessary to establish its antibiotic or disinfectant potential.

Although in recent years several studies on the antimicrobial activity of BSs have been performed, such studies are debated. This is because of the diversity of methodologies which have been employed to establish the activity and the different purity levels of the examined BSs. Upon use of the agar susceptibility method, Das et al., 2008a [62] provided a solution of the partially purified BS in methanol. The latter could be the main factor for bacterial pathogens lethality in that study. Furthermore, in other studies, the concentration of the BS used to determine antimicrobial activity was not mentioned, such as that of Ilori et al. (2008) [68]. Over recent years, materials and methods analysis of antimicrobial activity has become more detailed.

It has to be pointed out, that the majority of the studies found by the author exploit the antimicrobial activity of the purified BS acquired through the solvent extraction method described in Section 2.5. Therefore, biological activity can be attributed to the presence of several compounds, which may act synergistically, enabling antimicrobial action. Further purification of the BS may enhance antimicrobial properties. This is achieved through the exhaustive use of solvents and extraction steps [69] which, however, greatly increases the cost of the bioprocess, rendering down-stream processing unattractive. In the present study, the antimicrobial potential of the partially purified BS was examined, without further purification steps, leading to promising results and a promising, less-costly, down-stream processing method of the BS. However, further research on the purity, chemical structure and identification is necessary.

3.7. MIC of the Biosurfactant

The commonly used halo technique, using the agar disc diffusion method, was employed to determine the MIC of the BS (Table 2). The partially purified BS was extracted from the *P. citronellolis* 620C culture using 1% (v/v) DCF. The solution of the BS was able to inhibit bacterial growth in concentrations as low as 0.25 mg/mL. *K. pneumoniae* was affected at such a low BS concentration. *P. aeruginosa*, *E. coli* resistant and *E. coli* were observed to be inhibited at a relatively higher BS concentration (0.5 mg/mL). The BS inhibited

the *E. faecalis* and *S. enterica* at concentrations as low as 5 mg/mL. However, in the agar plate of *E. faecalis*, only one out of four discs impregnated with BS solution showed an inhibition zone, resulting in a high SD (Table 2). Furthermore, *A. baumannii*, *S. pneumoniae* and *S. aureus* were inhibited at relatively higher concentrations of 10 mg/mL. It was noticed that the Gram-positive pathogens were more resilient and insensitive to the BS solution, compared to the Gram-negative strains. Specifically, at least five and in most cases 10 times more BS solution was needed to inhibit these multi-drug resistant bacteria. This could be attributed to their structure, whereby the cell wall is relatively harder to break, compared to that of the Gram-negative bacteria. Interestingly, a higher dose of the BS solution was essential to observe inhibition of the Gram-negative *A. baumannii*, demonstrating the high resistance of the pathogen [70], but also the importance of the antimicrobial activity of the current BS, which can efficiently inhibit the growth of this emerging pathogen. The differences observed in the sensitivity of the pathogens to the BS do not only depend on the composition of the BS. The antimicrobial activity, except of the purity of the BS, may also be influenced by the nutritional and environmental conditions, and adaptation of the bacterial pathogens [71].

Table 2. Minimum inhibitory concentration (MIC) of the partially purified BS against multidrug-resistant pathogenic bacterial strains, using the agar susceptibility method.

Biosurfactant (mg/mL):	Antimicrobial Zone Diameter (mm)					
	10	5	1	0.5	0.25	0.1
<i>Klebsiella pneumoniae</i>	-	-	9.0 ± 0.7	8.0 ± 0.0	7.0 ± 0.0	0.0 ± 0.0
<i>Pseudomonas aeruginosa</i>	-	-	8.8 ± 0.8	8.5 ± 0.6	0.0 ± 0.0	0.0 ± 0.0
<i>Escherichia coli</i> resistant	-	-	10.5 ± 1.5	7.3 ± 0.5	0.0 ± 0.0	0.0 ± 0.0
<i>Escherichia coli</i>	-	-	8.8 ± 0.4	0.0 ± 0.0	0.0 ± 0.0	0.0 ± 0.0
<i>Enterococcus faecalis</i> resistant	9.3 ± 2.2	0.0 ± 0.0	0.0 ± 0.0	-	-	-
<i>Enterococcus faecalis</i>	8.3 ± 1.9	1.8 ± 3.5	0.0 ± 0.0	-	-	-
<i>Acinetobacter baumannii</i>	7.3 ± 5.3	0.0 ± 0.0	0.0 ± 0.0	-	-	-
<i>Streptococcus pneumoniae</i>	9.8 ± 1.0	0.0 ± 0.0	0.0 ± 0.0	-	-	-
<i>Staphylococcus aureus</i>	9.0 ± 0.8	0.0 ± 0.0	0.0 ± 0.0	-	-	-
<i>Salmonella enterica</i>	9.3 ± 0.5	8.3 ± 1.9	0.0 ± 0.0	-	-	-

MIC may be performed for highly pure BSs, such as rhamnolipids, reaching 99% purity [64]. Despite the purity level, the inhibition zone observed against *E. coli*, *S. aureus* and *S. enterica* is similar to that of the current study. The inhibition zone against *E. coli* strains was also similar to other studies such as Onbasli & Aslim (2008) [72].

4. Conclusions

In the current study, (i) a novel BS-producing microorganism was isolated from a waste site, (ii) BS formation was a result of DW biodegradation, (iii) an optimization strategy of BS production was explored through supplementation of iron forms, which led to a great production enhancement upon induction with 0.1 mM. Among FeSO₄, FeCl₃ and Fe(NO₃)₃, addition of FeCl₃ resulted in the highest increase in both BS, microbial growth and DW biodegradation. Use of a waste stream as substrate may result in a significant reduction in the bioprocess cost. The partially purified BS has promising antimicrobial potential against several Gram-negative and -positive multi-drug resistant bacterial pathogens. Hence, as no extra purification steps are necessary, a reduction in down-stream processing costs is possible. Preliminary characterization of the aforementioned BS via a number of analytical methods established its thermostability, low crystallinity and the presence of a peptide structure. The BS hereby produced and studied appears to have great potential in biomedical and environmental biotechnological applications.

Supplementary Materials: The following are available online at <https://www.mdpi.com/article/10.3390/pr9040686/s1>, Figure S1: Bacterial growth and % COD removal upon biodegradation of 5 and 10% (v/v) DCF, Table S1: Top 10 hits of the BLAST results.

Author Contributions: A.T.: conceptualization, methodology, investigation, experimentation, validation, writing original manuscript, reviewing, editing. K.S.: methodology, investigation, experimentation for extraction of the BS, iron forms effect, antimicrobial properties of BS. M.P.: methodology, investigation, experimentation for extraction of the BS, iron forms effect. L.K.: methodology, TGA/DTA analysis. I.R.: methodology, XRD analysis, reviewing and editing of the manuscript. I.I.: methodology, TGA/DTA and XRD analysis, reviewing and editing of the manuscript. E.P. (Erato Papageorgiou): methodology, FTIR analysis. E.P. (Eftychia Pinakoulaki): methodology, FTIR analysis, writing of FTIR results, reviewing and editing of the manuscript. All authors have read and agreed to the published version of the manuscript.

Funding: This research was funded by University of Cyprus, Cyprus. The APC was funded by the Department of Civil and Environmental Engineering, University of Cyprus, Cyprus.

Institutional Review Board Statement: Not applicable.

Informed Consent Statement: Not applicable.

Data Availability Statement: Data available on request due to privacy restrictions. The data presented in this study are available on request from the corresponding author.

Acknowledgments: The corresponding author would like to thank IESC Ltd. (Limassol, Cyprus) for providing the drilling waste. Furthermore, the corresponding author would like to thank researcher Anna Korelidou for providing the multi-drug resistant strains isolated from the municipal wastewater treatment of Limassol and the University of Cyprus for financial support.

Conflicts of Interest: The authors declare no conflict of interest.

References

- Hemlata, B.; Selvin, J.; Tukaram, K. Optimization of iron chelating biosurfactant production by *Stenotrophomonas maltophilia* NBS-11. *Biocatal. Agric. Biotechnol.* **2015**, *4*, 135–143. [[CrossRef](#)]
- Liu, J.; Vipulanandan, C.; Cooper, T.F.; Vipulanandan, G. Effects of Fe nanoparticles on bacterial growth and biosurfactant production. *J. Nanoparticle Res.* **2013**, *15*, 1–13. [[CrossRef](#)]
- Banat, I.M.; Makkar, R.S.; Cameotra, S.S. Potential commercial applications of microbial surfactants. *Appl. Microbiol. Biotechnol.* **2000**, *53*, 495–508. [[CrossRef](#)]
- Naughton, P.; Marchant, R.; Naughton, V.; Banat, I. Microbial biosurfactants: Current trends and applications in agricultural and biomedical industries. *J. Appl. Microbiol.* **2019**, *127*, 12–28. [[CrossRef](#)] [[PubMed](#)]
- Dhiman, R.; Meena, K.R.; Sharma, A.; Kanwar, S.S. Biosurfactants and their Screening Methods Biosurfactants and their Screening Methods. *Res. J. Recent Sci.* **2016**, *5*, 1–6.
- Shekhar, S.; Sundaramanickam, A.; Balasubramanian, T. Biosurfactant Producing Microbes and their Potential Applications: A Review. *Crit. Rev. Environ. Sci. Technol.* **2015**, *45*, 1522–1554. [[CrossRef](#)]
- Markande, A.R.; Patel, D.; Varjani, S. A review on biosurfactants: Properties, applications and current developments. *Bioresour. Technol.* **2021**, *330*, 124963. [[CrossRef](#)] [[PubMed](#)]
- Smith, M.L.; Gandolfi, S.; Coshall, P.M.; Rahman, P.K.S.M. Biosurfactants: A Covid-19 Perspective. *Front. Microbiol.* **2020**, *11*, 1341. [[CrossRef](#)] [[PubMed](#)]
- Franzetti, A.; Gandolfi, I.; Bestetti, G.; Smyth, T.J.P.; Banat, I.M. Production and applications of trehalose lipid biosurfactants. *Eur. J. Lipid Sci. Technol.* **2010**, *112*, 617–627. [[CrossRef](#)]
- Kaskatepe, B.; Yildiz, S. Rhamnolipid Biosurfactants Produced by *Pseudomonas* Species. *Braz. Arch. Biol. Technol.* **2016**, *59*, 1–16. [[CrossRef](#)]
- Jimoh, A.A.; Lin, J. Biosurfactant: A new frontier for greener technology and environmental sustainability. *Ecotoxicol. Environ. Saf.* **2019**, *184*, 109607. [[CrossRef](#)] [[PubMed](#)]
- Santos, D.K.; Rufino, R.D.; Luna, J.M.; Santos, V.A.; Salgueiro, A.A.; Sarubbo, L.A. Synthesis and evaluation of biosurfactant produced by *Candida lipolytica* using animal fat and corn steep liquor. *J. Pet. Sci. Eng.* **2013**, *105*, 43–50. [[CrossRef](#)]
- Onwukwe, S.I.; Nwakaudu, M.S. Drilling Wastes Generation and Management Approach. *Int. J. Environ. Sci. Dev.* **2012**, *3*, 252–257. [[CrossRef](#)]
- Karlapudi, A.P.; Venkateswarulu, T.; Tammineedi, J.; Kanumuri, L.; Ravuru, B.K.; Dirisala, V.R.; Kodali, V.P. Role of biosurfactants in bioremediation of oil pollution—a review. *Petroleum* **2018**, *4*, 241–249. [[CrossRef](#)]
- Yan, P.; Lu, M.; Yang, Q.; Zhang, H.-L.; Zhang, Z.-Z.; Chen, R. Oil recovery from refinery oily sludge using a rhamnolipid biosurfactant-producing *Pseudomonas*. *Bioresour. Technol.* **2012**, *116*, 24–28. [[CrossRef](#)]

16. Elshafie, A.E.; Joshi, S.J.; Al-Wahaibi, Y.M.; Al-Bemani, A.S.; Al-Bahry, S.N.; Al-Maqbali, D.; Banat, I.M. Sophorolipids Production by *Candida bombicola* ATCC 22214 and its Potential Application in Microbial Enhanced Oil Recovery. *Front. Microbiol.* **2015**, *6*, 1324. [\[CrossRef\]](#)
17. Datta, P.; Tiwari, P.; Pandey, L.M. Isolation and characterization of biosurfactant producing and oil degrading *Bacillus subtilis* MG495086 from formation water of Assam oil reservoir and its suitability for enhanced oil recovery. *Bioresour. Technol.* **2018**, *270*, 439–448. [\[CrossRef\]](#)
18. Kiran, G.S.; Nishanth, L.A.; Priyadharshini, S.; Anitha, K.; Selvin, J. Effect of Fe nanoparticle on growth and glycolipid biosurfactant production under solid state culture by marine *Nocardiopsis* MSA13A. *BMC Biotechnol.* **2014**, *14*, 48. [\[CrossRef\]](#) [\[PubMed\]](#)
19. Jimoh, A.A.; Lin, J. Enhancement of *Paenibacillus* sp. D9 Lipopeptide Biosurfactant Production Through the Optimization of Medium Composition and Its Application for Biodegradation of Hydrophobic Pollutants. *Appl. Biochem. Biotechnol.* **2019**, *187*, 724–743. [\[CrossRef\]](#)
20. Haferburg, G.; Kothe, E. Microbes and metals: Interactions in the environment. *J. Basic Microbiol.* **2007**, *47*, 453–467. [\[CrossRef\]](#) [\[PubMed\]](#)
21. Sambrook, J.; Fritsch, E.F.; Maniatis, E. *Molecular Cloning: A Laboratory Manual*; Cold Spring Harbour Press: Cold Spring Harbor, NY, USA, 1989.
22. Suryanti, V.; Marliyani, S.D.; Handayani, D.S.; Ratnaningrum, D. Production and characterization of biosurfactant by *Pseudomonas fluorescens* using cassava flour wastewater as media. *Indones. J. Chem.* **2013**, *13*, 229–235. [\[CrossRef\]](#)
23. De Rienzo, M.A.D.; Stevenson, P.; Marchant, R.; Banat, I.M. Antibacterial properties of biosurfactants against selected Gram-positive and -negative bacteria. *FEMS Microbiol. Lett.* **2016**, *363*, fmv224. [\[CrossRef\]](#) [\[PubMed\]](#)
24. Desai, J.D.; Banat, I.M. Microbial production of surfactants and their commercial potential. *Microbiol. Mol. Biol. Rev.* **1997**, *61*, 47–64. [\[CrossRef\]](#)
25. Huck-Iriart, C.; De-Candia, A.; Rodriguez, J.; Rinaldi, C. Determination of Surface Tension of Surfactant Solutions through Capillary Rise Measurements: An Image-Processing Undergraduate Laboratory Experiment. *J. Chem. Educ.* **2016**, *93*, 1647–1651. [\[CrossRef\]](#)
26. Eldin, A.M.; Kamel, Z.; Hossam, N. Isolation and genetic identification of yeast producing biosurfactants, evaluated by different screening methods. *Microchem. J.* **2019**, *146*, 309–314. [\[CrossRef\]](#)
27. Wang, Q.; Fang, X.; Bai, B.; Liang, X.; Shuler, P.J.; Iii, W.A.G.; Tang, Y. Engineering bacteria for production of rhamnolipid as an agent for enhanced oil recovery. *Biotechnol. Bioeng.* **2007**, *98*, 842–853. [\[CrossRef\]](#) [\[PubMed\]](#)
28. Remus-Emsermann, M.N.; Schmid, M.; Gekenidis, M.-T.; Pelludat, C.; Frey, J.E.; Ahrens, C.H.; Drissner, D. Complete genome sequence of *Pseudomonas citronellolis* P3B5, a candidate for microbial phyllo-remediation of hydrocarbon-contaminated sites. *Stand. Genom. Sci.* **2016**, *11*, 1–12. [\[CrossRef\]](#) [\[PubMed\]](#)
29. Zheng, D.; Wang, X.; Wang, P.; Peng, W.; Ji, N.; Liang, R. Genome Sequence of *Pseudomonas citronellolis* SJTE-3, an Estrogen- and Polycyclic Aromatic Hydrocarbon-Degrading Bacterium. *Genome Announc.* **2016**, *4*, 16–17. [\[CrossRef\]](#) [\[PubMed\]](#)
30. Oso, S.; Walters, M.; Schlechter, R.O.; Remus-Emsermann, M.N.P. Utilisation of hydrocarbons and production of surfactants by bacteria isolated from plant leaf surfaces. *FEMS Microbiol. Lett.* **2019**, *366*, 1–10. [\[CrossRef\]](#)
31. Singh, P.; Tiwary, B.N. Isolation and characterization of glycolipid biosurfactant produced by a *Pseudomonas otitidis* strain isolated from Chirimiri coal mines, India. *Bioresour. Bioprocess.* **2016**, *3*, 42. [\[CrossRef\]](#)
32. Ron, E.Z.; Rosenberg, E. Biosurfactants and oil bioremediation. *Curr. Opin. Biotechnol.* **2002**, *13*, 249–252. [\[CrossRef\]](#)
33. Haidar, C.N.; Pereira, M.M.; Lima, Á.S.; Nerli, B.B.; Malpiedi, L.P. Biosurfactants produced by *Pseudomonas syringae* pv *tabaci*: A versatile mixture with interesting emulsifying properties. *Process. Biochem.* **2020**, *97*, 121–129. [\[CrossRef\]](#)
34. Meliani, A. Enhancement of Hydrocarbons Degradation by Use of *Pseudomonas* Biosurfactants and Biofilms. *J. Pet. Environ. Biotechnol.* **2014**, *05*, 1–7. [\[CrossRef\]](#)
35. Rosenberg, E.; Ron, E.Z. Biosurfactants. In *The Prokaryotes: Applied Bacteriology and Biotechnology*; Rosenberg, E.F., DeLong, S., Lory, E., Stackebrandt, F., Thompson, E., Eds.; Springer: Berlin/Heidelberg, Germany, 2013; pp. 281–294. [\[CrossRef\]](#)
36. Abouseoud, M.; Maachi, R.; Amrane, A.; Boudergua, S.; Nabi, A. Evaluation of different carbon and nitrogen sources in production of biosurfactant by *Pseudomonas fluorescens*. *Desalination* **2008**, *223*, 143–151. [\[CrossRef\]](#)
37. Bak, F.; Bonnichsen, L.; Jørgensen, N.O.G.; Nicolaisen, M.H.; Nybroe, O. The biosurfactant viscosin transiently stimulates n-hexadecane mineralization by a bacterial consortium. *Appl. Microbiol. Biotechnol.* **2015**, *99*, 1475–1483. [\[CrossRef\]](#)
38. Ismail Isa, T.; Ngoshe, I.Y.; Gajere, H.M. Biosurfactant Production by Bacteria Isolated from Hydrocarbon-impacted soil. *Bioremed. Sci. Technol. Res.* **2019**, *6*, 4–8.
39. Jacques, R.J.S.; Santos, E.C.; Haddad, R.; Catharino, R.R.; Eberlin, M.N.; Bento, F.M.; Camargo, F.A.D.O. Mass spectrometry analysis of surface tension reducing substances produced by a pah-degrading *Pseudomonas citronellolis* strain. *Braz. J. Microbiol.* **2008**, *39*, 353–356. [\[CrossRef\]](#)
40. Santos, E.C.; Jacques, R.J.; Bento, F.M.; Peralba, M.D.C.R.; Selbach, P.A.; Sá, E.L.; Camargo, F.A. Anthracene biodegradation and surface activity by an iron-stimulated *Pseudomonas* sp. *Bioresour. Technol.* **2008**, *99*, 2644–2649. [\[CrossRef\]](#)
41. Wei, Y.-H.; Wang, L.-F.; Changy, J.-S.; Kung, S.-S. Identification of induced acidification in iron-enriched cultures of *Bacillus subtilis* during biosurfactant fermentation. *J. Biosci. Bioeng.* **2003**, *96*, 174–178. [\[CrossRef\]](#)

42. Andrews, S.C.; Robinson, A.K.; Rodríguez-Quivones, F. Bacterial iron homeostasis. *FEMS Microbiol. Rev.* **2003**, *27*, 215–237. [[CrossRef](#)]
43. Dinkla, I.J.T.; Gabor, E.M.; Janssen, D.B. Effects of Iron Limitation on the Degradation of Toluene by *Pseudomonas* Strains Carrying the TOL (pWWO) Plasmid. *Appl. Environ. Microbiol.* **2001**, *67*, 3406–3412. [[CrossRef](#)]
44. Dinkla, I.; Janssen, D. Simultaneous Growth on Citrate Reduces the Effects of Iron Limitation during Toluene Degradation in *Pseudomonas*. *Microb. Ecol.* **2003**, *45*, 97–107. [[CrossRef](#)]
45. Wei, Y.-H.; Chu, I.-M. Enhancement of surfactin production in iron-enriched media by *Bacillus subtilis* ATCC 21332. *Enzym. Microb. Technol.* **1998**, *22*, 724–728. [[CrossRef](#)]
46. Makkar, S.C.R. An update on the use of unconventional substrates for biosurfactant production and their new applications. *Appl. Microbiol. Biotechnol.* **2002**, *58*, 428–434. [[CrossRef](#)]
47. Kiran, G.S.; Thomas, T.A.; Selvin, J. Production of a new glycolipid biosurfactant from marine *Nocardioopsis lucentensis* MSA04 in solid-state cultivation. *Colloids Surf. B Biointerfaces* **2010**, *78*, 8–16. [[CrossRef](#)]
48. Dunham, N.P.; Arnold, F.H. Nature's Machinery, Repurposed: Expanding the Repertoire of Iron-Dependent Oxygenases. *ACS Catal.* **2020**, *10*, 12239–12255. [[CrossRef](#)]
49. Ismail, A.R.; Alias, A.H.; Sulaiman, W.R.W.; Jaafar, M.Z.; Ismail, I. Drilling fluid waste management in drilling for oil and gas wells. *Chem. Eng. Trans.* **2017**, *56*, 1351–1356. [[CrossRef](#)]
50. De Almeida, D.G.; Silva, R.D.C.F.S.D.; Luna, J.M.; Rufino, R.D.; Santos, V.A.; Banat, I.M.; Sarubbo, L.A. Biosurfactants: Promising Molecules for Petroleum Biotechnology Advances. *Front. Microbiol.* **2016**, *7*, 1718. [[CrossRef](#)] [[PubMed](#)]
51. Barth, A. Infrared spectroscopy of proteins. *Biochim. Biophys. Acta (BBA) Bioenerg.* **2007**, *1767*, 1073–1101. [[CrossRef](#)] [[PubMed](#)]
52. Moldes, A.B.; Paradelo, R.; Vecino, X.; Cruz, J.M.; Gudiña, E.; Rodrigues, L.; Teixeira, J.A.; Domínguez, J.M.; Barral, M.T. Partial Characterization of Biosurfactant from *Lactobacillus pentosus* and Comparison with Sodium Dodecyl Sulphate for the Bioremediation of Hydrocarbon Contaminated Soil. *BioMed Res. Int.* **2013**, *2013*, 1–6. [[CrossRef](#)] [[PubMed](#)]
53. Derenne, A.; Derfoufi, K.-M.; Cowper, B.; Delporte, C.; Goormaghtigh, E. FTIR spectroscopy as an analytical tool to compare glycosylation in therapeutic monoclonal antibodies. *Anal. Chim. Acta* **2020**, *1112*, 62–71. [[CrossRef](#)] [[PubMed](#)]
54. Krilov, D.; Balarin, M.; Kosovic, M.; Gamulin, O.; Brnjas-Kraljević, J. FT-IR spectroscopy of lipoproteins—A comparative study. *Spectrochim. Acta Part A: Mol. Biomol. Spectrosc.* **2009**, *73*, 701–706. [[CrossRef](#)] [[PubMed](#)]
55. Kiran, G.S.; Priyadharsini, S.; Sajayan, A.; Priyadharsini, G.B.; Poulouse, N.; Selvin, J. Production of Lipopeptide Biosurfactant by a Marine *Nesterenkonia* sp. and Its Application in Food Industry. *Front. Microbiol.* **2017**, *8*, 1138. [[CrossRef](#)] [[PubMed](#)]
56. Chandankere, R.; Yao, J.; Cai, M.; Masakorala, K.; Jain, A.; Choi, M.M. Properties and characterization of biosurfactant in crude oil biodegradation by bacterium *Bacillus methylotrophicus* USTBa. *Fuel* **2014**, *122*, 140–148. [[CrossRef](#)]
57. Kourmentza, C.; Costa, J.; Azevedo, Z.; Servin, C.; Grandfils, C.; De Freitas, V.; Reis, M. *Burkholderia thailandensis* as a microbial cell factory for the bioconversion of used cooking oil to polyhydroxyalkanoates and rhamnolipids. *Bioresour. Technol.* **2018**, *247*, 829–837. [[CrossRef](#)]
58. Weiss, I.M.; Muth, C.; Drumm, R.; Kirchner, H.O.K. Thermal decomposition of the amino acids glycine, cysteine, aspartic acid, asparagine, glutamic acid, glutamine, arginine and histidine. *BMC Biophys.* **2018**, *11*, 1–15. [[CrossRef](#)]
59. Reeves, C.J.; Menezes, P.L.; Jen, T.-C.; Lovell, M.R. The influence of fatty acids on tribological and thermal properties of natural oils as sustainable biolubricants. *Tribol. Int.* **2015**, *90*, 123–134. [[CrossRef](#)]
60. Saranya, P.; Swarnalatha, S.; Sekaran, G. Lipoprotein biosurfactant production from an extreme acidophile using fish oil and its immobilization in nanoporous activated carbon for the removal of Ca²⁺ and Cr³⁺ in aqueous solution. *RSC Adv.* **2014**, *4*, 34144–34155. [[CrossRef](#)]
61. Hutchinson, J.A.; Hamley, I.W.; Torras, J.; Alemán, C.; Seitonen, J.; Ruokolainen, J. Self-Assembly of Lipopeptides Containing Short Peptide Fragments Derived from the Gastrointestinal Hormone PYY3–36: From Micelles to Amyloid Fibrils. *J. Phys. Chem. B* **2019**, *123*, 614–621. [[CrossRef](#)] [[PubMed](#)]
62. Das, P.; Mukherjee, S.; Sen, R. Antimicrobial potential of a lipopeptide biosurfactant derived from a marine *Bacillus circulans*. *J. Appl. Microbiol.* **2008**, *104*, 1675–1684. [[CrossRef](#)]
63. Ndlovu, T.; Rautenbach, M.; Vosloo, J.A.; Khan, S.; Khan, W. Characterisation and antimicrobial activity of biosurfactant extracts produced by *Bacillus amyloliquefaciens* and *Pseudomonas aeruginosa* isolated from a wastewater treatment plant. *AMB Express* **2017**, *7*, 1–19. [[CrossRef](#)] [[PubMed](#)]
64. Ferreira, J.D.F.; Vieira, E.A.; Nitschke, M. The antibacterial activity of rhamnolipid biosurfactant is pH dependent. *Food Res. Int.* **2019**, *116*, 737–744. [[CrossRef](#)]
65. Karlapudi, A.P.; T.C., V.; Srirama, K.; Kota, R.K.; Mikkili, I.; Kodali, V.P. Evaluation of anti-cancer, anti-microbial and anti-biofilm potential of biosurfactant extracted from an *Acinetobacter* M6 strain. *J. King Saud Univ. Sci.* **2020**, *32*, 223–227. [[CrossRef](#)]
66. Das, P.; Mukherjee, S.; Sen, R. Genetic Regulations of the Biosynthesis of Microbial Surfactants: An Overview. *Biotechnol. Genet. Eng. Rev.* **2008**, *25*, 165–186. [[CrossRef](#)] [[PubMed](#)]
67. Singh, A.K.; Sharma, P. Disinfectant-like activity of lipopeptide biosurfactant produced by *Bacillus tequilensis* strain SDS21. *Colloids Surfaces B: Biointerfaces* **2020**, *185*, 110514. [[CrossRef](#)]
68. Ilori, M.O.; Adebusoye, S.A.; Ojo, A.C. Isolation and characterization of hydrocarbon-degrading and biosurfactant-producing yeast strains obtained from a polluted lagoon water. *World J. Microbiol. Biotechnol.* **2008**, *24*, 2539–2545. [[CrossRef](#)]

69. Tang, Y.; Ma, Q.; Du, Y.; Ren, L.; Van Zyl, L.J.; Long, X. Efficient purification of sophorolipids via chemical modifications coupled with extractions and their potential applications as antibacterial agents. *Sep. Purif. Technol.* **2020**, *245*, 116897. [[CrossRef](#)]
70. Howard, A.; O'Donoghue, M.; Feeney, A.; Sleator, R.D. *Acinetobacter baumannii*. *Virulence* **2012**, *3*, 243–250. [[CrossRef](#)]
71. Otzen, D.E. Biosurfactants and surfactants interacting with membranes and proteins: Same but different? *Biochim. Biophys. Acta (BBA) Biomembr.* **2017**, *1859*, 639–649. [[CrossRef](#)]
72. Onbasli, D.; Aslim, B. Determination of antimicrobial activity and production of some metabolites by *Pseudomonas aeruginosa* B1 and B2 in sugar beet molasses. *Afr. J. Biotechnol.* **2008**, *7*, 4614–4619.

Article

Coal-Degrading Bacteria Display Characteristics Typical of Plant Growth Promoting Rhizobacteria

Yinka Titilawo, Wiya L. Masudi, Jacob T. Olawale, Lerato M. Sekhohola-Dlamini and A. Keith Cowan *

Institute for Environmental Biotechnology, Rhodes University, Makhanda (Grahamstown) 6140, South Africa; olayinkatemi@yahoo.co.uk (Y.T.); desamunya@gmail.com (W.L.M.); jaclawale@yahoo.com (J.T.O.); sekholalerato0@gmail.com (L.M.S.-D.)

* Correspondence: a.cowan@ru.ac.za; Tel.: +27-46-603-7050

Received: 16 July 2020; Accepted: 26 August 2020; Published: 7 September 2020

Abstract: Coal mining produces large quantities of discard that is stockpiled in large dumps. This stockpiled material, termed coal discard, poses an environmental threat emphasising the need for appropriate bioremediation. Here, metagenomic analysis of the 16S rRNA from ten coal-degrading strains previously isolated from coal slurry from discard dumps and from the rhizosphere of diesel-contaminated sites was used to establish genetic relatedness to known plant growth-promoting (PGP) bacteria in the NCBI database. Measurement of indole and ammonium production and solubilisation of P and K were used to screen bacteria for PGP characteristics. BLAST analysis revealed $\geq 99\%$ homology of six isolates with reference PGP strains of *Bacillus*, *Escherichia*, *Citrobacter*, *Serratia*, *Exiguobacterium* and *Microbacterium*, while two strains showed 94% and 91% homology with *Proteus*. The most competent PGP strains were *Proteus* strain ECCN 20b, *Proteus* strain ECCN 23b and *Serratia* strain ECCN 24b isolated from diesel-contaminated soil. In response to L-trp supplementation, the concentration of indolic compounds (measured as indole-3-acetic acid) increased. Production of ammonium and solubilisation of insoluble P by these strains was also apparent. Only *Serratia* strain ECCN 24b was capable of solubilising insoluble K. Production of indoles increased following exposure to increasing aliquots of coal discard, suggesting no negative effect of this material on indole production by these coal-degrading bacterial isolates and that these bacteria may indeed possess PGP characteristics.

Keywords: coal discard; diesel-contaminated soil; discard dumps; biodegradation; phylogeny; plant growth-promoting bacteria

1. Introduction

Coal is a hydrophobic, highly porous and heterogeneous sedimentary rock mined for its energy content. It is classified according to the degree of aromaticity and ranked as either lignite, (sub)-bituminous coal or anthracite [1,2]. Physically, it is a material with a hardness scale of up to 3 Mohs for anthracite and classified as naturally recalcitrant [3,4]. Chemically, it is a complex mixture of aromatic, heterocyclic and aliphatic carbonaceous constituents, hence the high calorific value. In South Africa, residual coal and other materials of very low energy content are stockpiled in discard dumps. These discard dumps are numerous and a major source and contributor of pollutants (e.g., particulate matter, heavy metals, acid leachate, etc.) to the surrounding environment including the atmosphere and water bodies and, as a consequence, threaten the environment, human health and quality of life [5,6]. Not surprisingly, there is an urgent need for intervention [7]. Although attempts to stabilise these dumps by cultivation of cover crops does occur once mining is complete [8], a major oversight in developing rehabilitation strategies has been the apparent omission of biotic factors that underpin successful and sustainable revegetation. Recently, it was demonstrated that successful rehabilitation

and vegetation of discard dumps can be achieved by exploiting the mutualism between coal-degrading microorganisms, mycorrhizal fungi and grasses [8].

Coal mining not only visibly disrupts the aesthetics of a landscape but also disrupts all of the soil components including soil horizons, structure, microorganisms and nutrient cycles that are crucial to sustaining a healthy ecosystem [9,10]. While a number of fungi show potential as rehabilitation biocatalysts and degrade coal into a soil-like humic-rich material [11–18], the only candidate enzymes identified and functionally characterised from coal-degrading fungi so far are laccase and esterase. Heterologous expression of *Fusarium oxysporum* laccase in *Pichia pastoris* was shown to depolymerise and liquefy solubilised brown coal with the release of humic and fulvic acids [18]. By comparison, the *Penicillium decumbens* P6 esterase depolymerised lignite resulting in increased formation of low-molecular mass humic acids with lower-percentage aromatic carbon but higher-percentage aliphatic carbon [19].

Bacterial conversion of coal, by comparison, has typically been to derive clean fuels and chemicals by developing environmentally sound energy-saving processes that do not cause secondary pollution [20,21]. While numerous studies on bacterial solubilisation and degradation of coal by different species of bacteria have been forthcoming, the underlying biochemical and molecular mechanisms involved are not yet fully understood [22,23]. Even so, numerous studies have revealed a role for bacteria in the degradative assimilation of petroleum hydrocarbons such as polynuclear aromatic hydrocarbons (PAHs), naphthalene, the monoaromatic hydrocarbons such as toluene and aliphatic hydrocarbons such as the *n*-alkanes [24,25]. These hydrocarbons are well represented in the naturally complex and highly aromatic coal structure and are also readily available in petroleum-contaminated soil environments [7]. Indeed, several recent extensive reviews on the subject have been published [26,27] and the potential for plant–bacteria partnerships in the remediation of hydrocarbon-contaminated soil has been proposed [28,29]. Bacterial conversion and utilisation of coal, though generally influenced by environmental conditions such as temperature and pH, are dependent mainly on the type of coal and microorganism used [29] and similar to fungal biodegradation, the mechanisms seem to involve solubilisation, depolymerisation and degradative assimilation [7]. Bio-solubilisation is by alkaline substances, chelators and/or surfactants, whereas depolymerisation and liquefaction likely entail oxidoreductases such as peroxidases and laccases, and hydrolases [30]. Under aerobic conditions, coal is oxidised by both biotic and abiotic processes to a weathered material rich in humic substances [31]. Under anaerobic conditions, a sequence of primary and secondary bacterial fermenters depolymerise and metabolise coal, providing a diverse range of short-chain organic acids and alcohols [32]. These low-molecular weight organic compounds serve as substrates for other consortia of microorganisms such as acetogens and methanogens [33–36]. In spite of many studies on the coal-degrading potential of bacteria, there remain limitations in phenotypic identification and the identification of other beneficial properties of these bacteria such as plant growth promotion. Modern molecular approaches, including analysis of PCR-amplified 16S rRNA gene sequences, have provided some insight into the identity, characterisation and phylogenetic classification of microorganisms capable of degrading and/or utilising coal [37–39]. To our knowledge, bacterial isolates from South African environments with coal-degrading capability have neither been extensively explored nor characterised genotypically.

An earlier bioprospecting study allowed for selected bacterial isolates with coal biodegradation potential to be characterised [40], but a more detailed biochemical and genetic analysis has yet to be described. Furthermore, screening of these coal-degrading bacteria for plant growth-promoting (PGP) characteristics has not previously been the subject of study. Defined as a class of microorganism that occupy the rhizosphere to promote plant growth, PGP bacteria are from diverse genera, display properties such as phytohormone production, siderophore and phosphate solubilisation activity, ACC deaminase activity and enhance plant productivity [41]. Typical uses are as inoculants for biostimulation, biocontrol and biofertilisation in agriculture and phytoremediation. In light of this background, the present study sought to establish, first, the genetic relatedness of these isolates to the

diverse array of PGP bacteria contained in the established NCBI database and, second, screen these coal-degrading strains for characteristics typically displayed by PGP bacteria. An ability to mineralise phosphate and potassium and to produce ammonium and indoles (including the phytohormone, indole-3-acetic acid) was the criteria used in this study to determine bacterial PGP potential.

2. Materials and Methods

2.1. Bacterial Strains

Bacterial strains used in this study were previously isolated from coal slurry obtained from coal discard dumps at coal mines in Emalaheni (26°0'0" S; 29°10'0" E), Mpumalanga Province, South Africa, and slurries of material from diesel-contaminated sites (at a depth of ~15 cm) collected either from soil at mechanical workshops in Makhanda (33°17'0" S; 26°31'0" E) or from old tractor engines at a farm in the Makana Local Municipality, Eastern Cape Province, South Africa (Table 1). Details of strain isolation, molecular characterisation, coal biodegrading activity and deposit into an international repository are recounted elsewhere [40].

Table 1. Bacterial strains with coal biodegrading activity isolated either from coal slurry (CS) or diesel-contaminated sites (DCS).

Source	Bacterial Isolates and Assigned Strain Number	Identity (%)	Microbial Culture Collection No.	GenBank Accession No.	Length (bp)
CS	<i>Citrobacter</i> strain ECCN 19b	99	MCC0033	KC700328	372
CS	<i>Escherichia</i> strain ECCN 25b	99	MCC0041	KC700329	382
CS	<i>Bacillus</i> strain ECCN 26b	99	MCC0062	KC700330	450
DCS	<i>Bacillus</i> strain ECCN 18b	98	MCC0034	KC620473	560
DCS	<i>Proteus</i> strain ECCN 20b	94	MCC0027	KC620475	553
DCS	<i>Exiguobacterium</i> strain ECCN 21b	99	MCC0016	KC620476	551
DCS	<i>Microbacterium</i> strain ECCN 22b	99	MCC0042	KC620477	543
DCS	<i>Proteus</i> strain ECCN 23b	91	MCC0022	KC620478	439
DCS	<i>Serratia</i> strain ECCN 24b	99	MCC0021	KC620474	525
DCS	<i>Bacillus</i> strain ECCN 41b	99	MCC0039	KC758162	392

2.2. Culture Conditions

Coal-degrading bacterial isolates, listed in Table 1, were resurrected from glycerol stock by culture in nutrient broth (NB; 5 g L⁻¹ peptone, 3 g L⁻¹ yeast extract and 8 g L⁻¹ NaCl) at 30 °C on a rotary shaker (120 rpm) for 72 h. Then, aliquots of NB were transferred to nutrient agar (NA; 5 g L⁻¹ peptone, 3 g L⁻¹ yeast extract and 8 g L⁻¹ NaCl and 15 g L⁻¹ agar) plates and incubated at 30 °C for 24 to 48 h to establish strain purity. Individual but distinct colonies were picked and inoculated into 40 mL of freshly prepared NB, grown at 30 °C, and maintained in log phase.

2.3. Extraction and PCR Amplification of Genomic DNA

Extraction of total DNA was achieved using the ZR Fungal/Bacterial DNA Kit™ (Zymo Research, Irvine, CA, USA) according to the manufacturer's instructions. Target 16S rRNA regions were amplified using DreamTaq™ DNA polymerase (Thermo Scientific™, Thermo Fisher Scientific, Waltham, MA, USA) with the bacterial universal primers 27F (5'-AGAGTTTGATCMTGGCTCAG-3') and 1492R (5'-CGGTTACCTTGTTACGACTT-3') as described by Lane et al. [42] and Turner et al. [43].

Sanger sequencing of the purified PCR products was carried out by Inqaba Biotechnical Industries (Pty) Ltd., Hatfield, South Africa using the PRISM™ Ready Reaction Dye Terminator Cycle sequencing kit using chain termination by the dideoxy-nucleotides methodology and electrophoresed on an ABI PRISM® 3500XL DNA Sequencer (Applied Biosystems, Foster City, CA, USA) following the manufacturer's instructions. Resultant chromatograms were analysed (Chromas version 2.6.6) as outlined in Technelysium [44], followed by pairwise alignment in BioEdit Sequence Alignment Editor, version 7.0.5.3 [45], and the resultant gene sequences compared with those already deposited (<https://www.ncbi.nlm.nih.gov/>).

2.4. Phylogenetic Analysis

Phylogenetic analysis using the 16S rRNA sequences of the nine isolates and 32 reference nucleotide sequences for PGP bacteria from the NCBI GenBank database was conducted. Multiple alignment of nucleotide sequences was achieved using CLUSTALW as implemented in the BioEdit Sequence Alignment Editor. A phylogenetic tree was constructed from the neighbour-joining method using MEGA6 (Molecular Evolutionary Genetics Analysis Version 6.0) after calculating distances via the Jukes–Cantor method [46]. Trees were bootstrapped using 1000 replications.

2.5. Screening for Plant Growth Promoting Characteristics

2.5.1. Ammonium Production

Production of ammonium (NH_4^+) by the coal-degrading bacterial strains was determined using peptone water and Nessler's reagent (HgI_4K_2) as indicator. Peptone water containing 10 g of peptone (Sigma-Aldrich, Millipore Sigma, St. Louis, MO) and 5 g of NaCl was prepared in 1 L distilled water and autoclaved at 121 °C and 1.5 kg cm^{-2} for 15 min. Nessler's reagent was prepared by suspending in 100 mL of distilled water, 10 g of HgCl_2 , 7 g of KI and 16 g of NaOH. The bacterial inoculants were added to flasks containing 40 mL PW and incubated on a rotary shaker at 30 °C for 3 d. After incubation, 4 mL of each culture was harvested by centrifugation ($3920\times g$ for 3 min) and NH_4^+ concentration of the supernatant quantified spectrophotometrically. For colorimetric assay of NH_4^+ , to 2 mL aliquots of supernatant from each sample was added 0.2 mL of Nessler's reagent and colour development allowed to proceed for 5 min. Development of a brown colour was taken as a positive indicator of NH_4^+ . For quantification, 1 mL was transferred to a cuvette and absorbance measured at 430 nm and results interpolated from a standard curve prepared using NH_4Cl [47].

2.5.2. Indole-3-Acetic Acid Production

To determine the ability of the isolated bacterial strains to produce indole-3-acetic acid (IAA), NB was supplemented with L-trp and the concentration of indolic compounds produced by coal-degrading bacterial isolates determined using Salkowski's reagent [48–50].

Aliquots, equivalent to 40 μL of bacterial suspension, were inoculated into NB supplemented with L-trp (at either 0, 0.1, 0.5 and 1 g L^{-1}) and incubated at 30 °C on a rotary shaker (120 rpm) for 72 h. After incubation, 4 mL of each culture was sedimented by centrifugation ($3920\times g$ for 3 min) and the cell-free supernatant used for colorimetric quantification of IAA which was carried out as follows: Two drops of 10 mM of orthophosphoric acid and 4 mL of Salkowski's reagent (50 mL 35% perchloric acid; and, 1.0 mL 0.5 M FeCl_3 solution) were added to 2 mL cell-free supernatant, the mixture incubated at room temperature for 20 min and absorbance measured at 530 nm. The quantity of indolic compounds (expressed as IAA equivalents) was determined by interpolation from a standard curve of authentic IAA (Sigma-Aldrich) and background subtracted to account for any interference from the culture medium.

2.5.3. Solubilisation of Insoluble Phosphate and Potassium

Phosphate and potassium solubilisation activity was initially determined using pour plates of either Pikovskayas agar (PVK) supplemented with tri-calcium phosphate ($\text{Ca}_3(\text{PO}_4)_2$) or Aleksandrow medium (AM) containing AlKO_6Si_2 as the respective substrates. Modified PVK agar was prepared using 0.5 g of yeast extract, 10 g of glucose, 5 g of $\text{Ca}_3(\text{PO}_4)_2$, 0.5 g of $(\text{NH}_4)_2\text{SO}_4$, 0.2 g of KCl, 0.1 g of MgSO_4 , 0.0001 g of $\text{MnSO}_4\cdot\text{H}_2\text{O}$, 0.0001 g of $\text{FeSO}_4\cdot 7\text{H}_2\text{O}$ and 15 g of agar in a total volume of 1 L of distilled water [46]. For the solubilisation of potassium by coal-degrading bacteria, AM was prepared containing 0.5 g of $\text{MgSO}_4\cdot 7\text{H}_2\text{O}$, 0.1 g of CaCO_3 , 2 g of AlKO_6Si_2 , 5 g of glucose, 0.005 g of $\text{FeCl}_3\cdot 6\text{H}_2\text{O}$, 2 g of $\text{Ca}_3(\text{PO}_4)_2$ and 20 g of agar in 1 L of distilled water. An aliquot (5 μL) of bacterial cell suspension was placed at 4 equidistant positions on either PVK or AM plates which were incubated at 30 °C for periods up to 14 d. After incubation, $\text{Ca}_3(\text{PO}_4)_2$ and AlKO_6Si_2 solubilising activity was

determined by observation of clear zones around active bacterial colonies [51,52]. Phosphate and potassium solubilising activity was quantified after inoculation of either liquid PVK or AM, prepared as above but without agar, with equal quantities of bacterial suspension from cells in exponential phase.

Following incubation at 30 °C on a rotary shaker (120 rpm), cell suspensions were sedimented by centrifugation (3920× *g* for 3 min) and the supernatant recovered for analysis. *Ortho*-phosphate concentration was determined spectrophotometrically using a Phosphate Test kit (Merck KGaA, Darmstadt, Germany) after 14 d while potassium concentration was measured after 9 d using sodium tetra-phenylborate as described by Pflaum and Howick [53]. The final concentration of phosphate and or potassium was determined by interpolation from standard curves prepared using *ortho*-phosphate and KCl, respectively.

2.6. Effect of Coal Discard on Production of IAA

Geologically weathered coal was sourced and prepared to yield particles of approximately 0.2–0.5 mm in diameter and sterilised by freeze-thawing using liquid nitrogen as described earlier by Olawale et al. [40]. Aliquots of dry sterilised coal (0–1 g) were added directly to seed cultures prepared from stationary phase cells (i.e., OD₆₀₀ 0.4 after 3 d at 30 °C) of the specified coal-degrading strains. Nutrient broth (40 mL) supplemented with L-trp and incubated at 30 °C on a rotary shaker (120 rpm) for 3 d. Concentration of indolic compounds in solution was determined as described above after background subtraction to account for any coal-derived indoles.

2.7. Statistical Analysis

All data were computed using the statistical function in Sigma Plot version 11 (Systat Software Inc., San Jose, CA, USA). Where necessary, results were analysed by one-way analysis of variance and significant differences between measurements for each treatment were determined (Holm–Sidak method; $p < 0.05$). Data are presented as the mean of at least three determinations ± standard error (SE).

3. Results

3.1. Bacterial Genomes and Their Identification

Partial 16S rRNA genomes of varying lengths ranging from 372 to 560 bp were amplified and sequenced from each of the resurrected coal-degrading bacterial strains previously isolated from coal slurry and diesel-contaminated soil. The ten strains represent seven genera from three families. The most abundant were Bacillaceae and Enterobacteriaceae, each with four strains and one Microbacteriaceae representative. Six isolates showed 99% sequence homology to reference strains that were confirmed as *Exiguobacterium* (KC620476), *Serratia* (KC620474), *Citrobacter* (KC700328), *Bacillus* (KC758162 and KC700330), *Escherichia* (KC700329) and *Microbacterium* (KC620477). One isolate, *Bacillus* (KC620473), showed 98% sequence homology, whereas KC620475 and KC620478 were 94% and 91% homologous to *Proteus*, respectively (Table 1). In this suite of previously identified coal-degrading bacterial strains, the most prevalent genus was *Bacillus*, accounting for 30%. Strains of *Proteus* comprising 20% of the isolates were the next most abundant and were from diesel-contaminated soil. Remaining strains were confirmed to belong to the genera *Escherichia*, *Citrobacter*, *Exiguobacterium*, *Serratia* and *Microbacterium*.

3.2. Nucleotide Sequence and Phylogenetic Analysis

The coal-degrading bacterial isolates were further characterised following phylogenetic analysis of sequence relatedness to PGP reference strain sequences within GenBank. Together with the selected 32 reference sequences from GenBank, our sequences revealed six distinct but associated clusters. Eight (8) sequences clustered individually with their respective PGP bacteria relatives, with virtually all showing 100% bootstrap support at the corresponding major nodes (Figure 1). However, strain ECCN 19b (KC700328) which was from a coal environment, was the stand-out within a major cluster consisting of the genera *Proteus*, *Serratia* and *Citrobacter*. Other sequences from strains within the same

cluster (KC620475 and KC620478) formed a distinct cluster with *Proteus*, and KC620474 clustered distinctly within the *Serratia* clade (Figure 1). Although most clusters in the phylogenetic tree showed high bootstrap values, strain ECCN 25b (KC700329) was excluded from the constructed phylogenetic tree as it did not match closely with any of the available GenBank PGP reference sequences in relation to source.

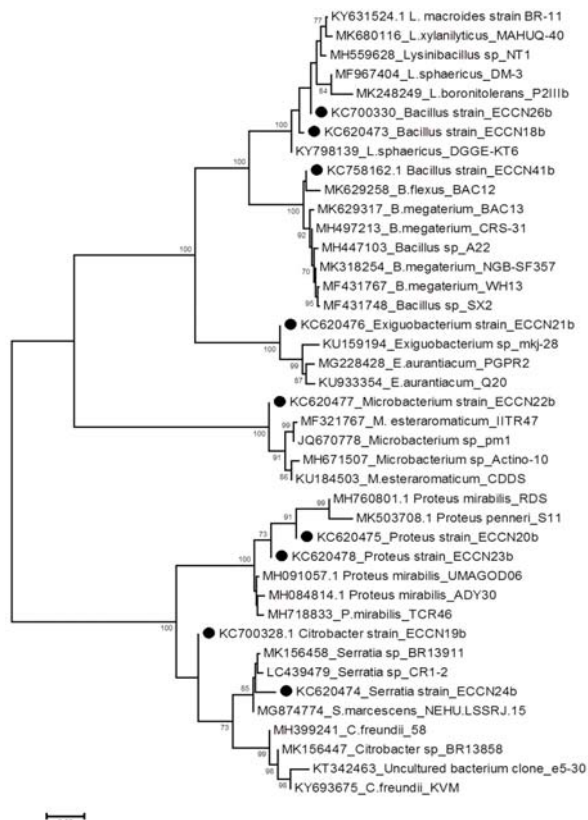


Figure 1. Phylogenetic tree showing relation between coal-degrading bacterial isolates (●) and reference PGP strains contained in the NCBI GenBank database. GenBank accession numbers and the corresponding taxonomic annotations are shown to the right of the strains. Bootstrap values of $\geq 70\%$ are shown at the nodes.

3.3. Plant Growth Promoting Characteristics

Production of ammonium and indolic compounds (measured as IAA equivalents) by the coal-degrading bacterial strains *Citrobacter* ECCN 19b (KC700328), *Proteus* ECCN 20b (KC620475), *Exiguobacterium* ECCN 21b (KC620476), *Microbacterium* ECCN 22b (KC620477), *Proteus* ECCN 23b (KC620478), *Serratia* ECCN 24b (KC620474), *Bacillus* ECCN 26b (KC700330) and *Bacillus* ECCN 41b (KC758162) and solubilisation of P and K were determined spectrophotometrically and the results are shown in Figure 2.

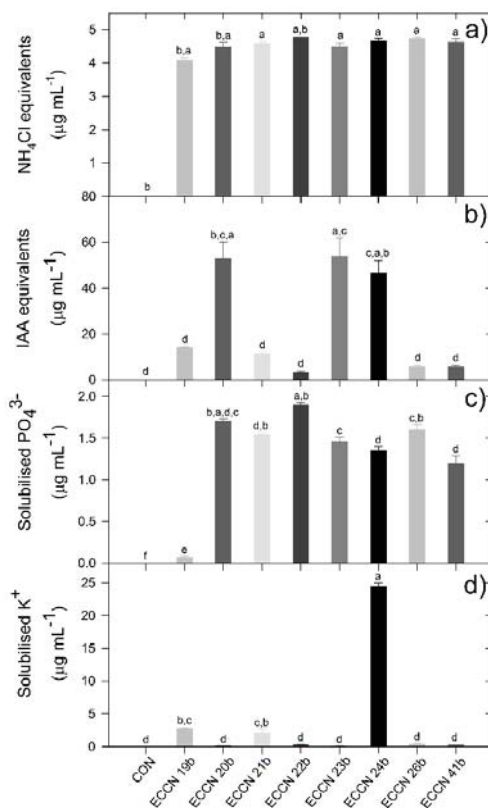


Figure 2. Screening of coal-degrading bacterial isolates for plant growth-promoting characteristics. Estimates of ammonium production (a), indole production (b), phosphate (c) and potassium solubilisation (d) by these bacterial isolates in stationary phase (OD₆₀₀ = 0.4 at 30 °C) were determined spectrophotometrically. Results are expressed as the mean ± S.E. Means denoted by a different letter indicate significant differences relative to a negative control ($p < 0.05$).

Ammonium production appeared to be a common trait of the coal-degrading bacterial strains evaluated for PGP characteristics (Figure 2a). Furthermore, whereas all of the strains produced above background levels of indolic compounds (Figure 2b), *Proteus* ECCN 20b, *Proteus* ECCN 23b and *Serratia* ECCN 24b produced substantial quantities in response to L-trp (0.5 g L⁻¹) supplementation (Figure 2b). Further, while it is accepted that mineral solubilisation can sometimes depend on the medium used [54], results from this study show that while phosphate solubilisation was low for these coal-degrading isolates, only one coal-degrading strain was unable to solubilise Ca₃(PO₄)₂ (Figure 2c). By comparison, *Serratia* strain ECCN 24b, and to a much lesser extent *Citrobacter* strain ECCN 19b and *Exiguobacterium* strain ECCN 21b, were the only coal-degrading bacteria able to solubilise potassium from AlK₆Si₂ (Figure 2d).

Indole-3-acetic acid is a common, naturally occurring plant hormone of the auxin class, is derived from L-trp and is characteristically produced by many different PGP bacterial strains [55]. In an effort to gain further insight into the relationship between IAA production and the PGP potential of these coal-degrading bacterial strains, L-trp-activated IAA production by *Proteus* ECCN 20b, *Proteus* ECCN 23b and *Serratia* ECCN 24b was examined, firstly, in response to increasing concentrations of this indole

precursor and, secondly, following exposure of L-trp-supplemented cultures to increasing amounts of coal discard.

Results in Figure 3 clearly show that by increasing the concentration of L-trp supplied to cultures of *Proteus* ECCN 20b, *Proteus* ECCN 23b and *Serratia* ECCN 24b, production of indolic compounds including IAA, increased. Furthermore, these coal-degrading strains seemed equally competent in terms of indole production in response to activation by L-trp supplementation. Mean medium indolic compound concentration for the three strains increased from a mean minimum of $5.91 \mu\text{g mL}^{-1}$ in the absence of L-trp to a mean maximum of $83.49 \mu\text{g mL}^{-1}$ IAA (equivalents) in response to 1 g L^{-1} L-trp supplementation. The almost linear increase in medium indolic compound concentration ($R^2 = 0.93$), concomitant with increasing concentration of L-trp supplementation, appears to support the operation of an L-trp-dependent pathway for indole/IAA production by these bacterial isolates.

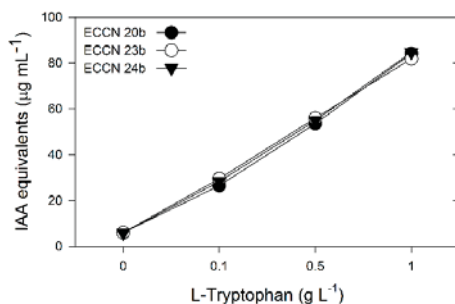


Figure 3. Indolic compound formation by cultures of *Proteus* ECCN 20b, *Proteus* ECCN 23b and *Serratia* ECCN 24b in response to increasing L-trp concentration. Results are from three experiments and expressed as the mean \pm S.E.

In view of the already established coal-biodegrading property of these strains, it was of interest to examine the effect of coal discard on production of indolic compounds by cultures of *Proteus* strain ECCN 20b, *Proteus* strain ECCN 23b and *Serratia* strain ECCN 24b. Increasing quantities of coal discard were supplied to these isolates in liquid culture and the effect on L-trp-supplemented indolic compound accumulation is shown in Figure 4.

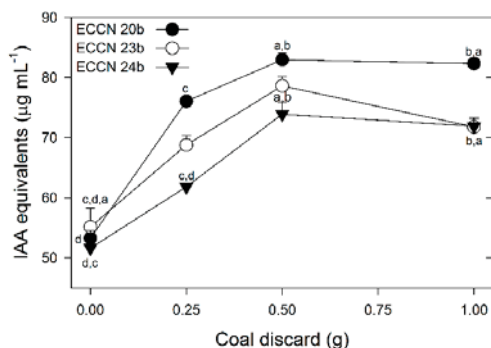


Figure 4. Effect of coal discard on formation of indolic compounds by cultures of *Proteus* ECCN 20b, *Proteus* ECCN 23b and *Serratia* ECCN 24b in response to L-trp supplementation. Results are from three experiments and expressed as the mean \pm S.E. Means denoted by a different letter indicate significant differences within treatments ($p < 0.05$).

Typically, screening for production of IAA by putative PGP bacteria is carried out using an L-trp-supplemented medium [56,57]. Here, too, a L-trp-supplemented medium was used, and results show that in the presence of coal discard, production of indoles was enhanced for all three of the coal-degrading strains tested (Figure 4). In this experiment, coal was added to NB supplemented with L-trp at 0.5 g L⁻¹. In the absence of coal discard, formation of indoles averaged 53.34 µg mL⁻¹ IAA for the three strains tested, an observation that was similar to and corroborated initial screening studies (cf. Figure 2b). For strain ECCN 20b however, indole formation increased to 76.05, 82.96 and 82.33 µg mL⁻¹ IAA in response to addition of 0.25, 0.5 and 1 g of coal discard, respectively (Figure 4). A similar, albeit less dramatic, response was observed for strains ECCN 23b and ECCN 24b. Indeed, coal discard above 0.5 g appeared to slow accumulation of indoles in all bacterial isolates tested. Maximum IAA was thus achieved in response to 0.5 g-added coal discard, while competence for production of indolic compounds by these strains appeared to be ECCN 20b > ECCN 23b > ECCN 24b.

4. Discussion

Molecular ecological studies involve separation of amplicons based on differences in DNA nucleotide sequences and most often the 16S rRNA gene, which can then be analysed from complex environments such as soil [58]. Databases thus generated yield invaluable information about indicator species [59]. To determine the phylogenetic relationship between coal-degrading bacteria isolated earlier [40] and the diverse array of PGP bacteria contained in the NCBI GenBank database, basic bioinformatics was used to determine the genetic relatedness of the 16S rRNA gene sequences while conventional biochemical assays were used to screen for putative PGP characteristics. Strains from seven genera of coal-degrading bacterial isolates utilised in the present study showed ≥ 99% homology with reference gene sequences of PGP bacteria contained in the NCBI GenBank database. A < 1% deviation was attributed to the diversity of ecological niches from where the coal-degrading isolates and reference PGP strains were sourced.

Biochemical screening for traits typically associated with PGP showed that the most competent strains were those sourced from diesel-contaminated soil. These isolates were *Proteus* strain ECCN 20b, *Proteus* strain ECCN 23b and *Serratia* strain ECCN 24b. Interestingly, *Serratia* strain ECCN 24b, either alone or in consort with *Citrobacter* strain ECCN 19b and *Exiguobacterium* strain ECCN 21b, was previously shown to be most effective in coal bioconversion [40]. Furthermore, and in corroboration with results from other studies, *Serratia* strain ECCN 24b was able to solubilise insoluble phosphate [60,61] and potassium [62]. Recent studies have shown that the mineral-solubilising activity for promotion of plant growth is typically associated with the production of organic acids which, for strains of *Serratia* spp., appears to include gluconic and lactic acid [63].

In addition to the liberation of mineral nutrients, production of indolic compounds by *Proteus* strain ECCN 20b, *Proteus* strain ECCN 23b and *Serratia* strain ECCN 24b in L-trp-supplemented medium was substantial relative to the other coal-degrading bacterial isolates screened and increased linearly with an increase in L-trp concentration. Production of the plant hormone IAA and other indoles by bacteria is a long held and accepted view, in particular for microorganisms that inhabit subterranean plant surfaces [64–67]. Indeed, bacterial IAA biosynthesis can be either trp-dependent or independent [68] and results from the present study would seem to support the formation of indolic compounds by *Proteus* strain ECCN 20b, *Proteus* strain ECCN 23b and *Serratia* strain ECCN 24b via L-trp. Coal-degrading isolates that display a weak response to L-trp supplementation may either be non-responsive or produce indole by a trp-independent route. In higher plants like *Arabidopsis thaliana* and *Zea mays*, the major biosynthetic pathway to IAA is not via trp but seems to be from an earlier intermediate such as anthranilate [69]. Further, several studies have confirmed formation by bacteria of methyl anthranilate via chorismite in a single-step conversion of anthranilate to its methyl ester metabolite catalysed by an S-adenosyl-L-methionine (SAM)-dependent methyltransferase [70,71]. Whether a similar pathway operates in the coal-degrading strains that were unresponsive to L-trp supplementation in the present study is currently unknown.

Additionally, exposure of *Proteus* strain ECCN 20b, *Proteus* strain ECCN 23b and *Serratia* strain ECCN 24b to coal discard resulted in an apparent dose-dependent increase in the formation of indolic compounds. While indoles are a component of carbonised coal, e.g., coal tar and coke [72], and pyrolysates of Leonardite humic acids [73], they are not readily liberated from hard coal or coal discard, and in this study were undetectable in samples used to background correct for possible contribution to spectrophotometric quantitation using Salkowski's reagent.

In addition to the well-established PGP properties of *Serratia* spp. [74–77] and their ability to degrade the coal distillation product creosote [78], several promising PGP rhizobacterial strains of *Proteus* spp. have been isolated from the rhizosphere of rice [79–81], wild grass [82], a halophytic glasswort [83,84] and a nematocidal strain of *P. penneri* obtained from cow dung [85]. This genus was also relatively well represented (20%) among the coal-degrading isolates utilised in this study and strains ECCN 20b and ECCN 23b, isolated from diesel-contaminated soil. There are numerous reports of hydrocarbon-degrading strains of *Proteus* spp. from soils [86–88], whereas, to our knowledge, the strains described here represent the first reported *Proteus* isolates with PGP potential capable of degrading coal. While there is reported evidence for isolation of *Proteus* spp. from diverse soil environments including isolates with heavy metals tolerance [89–91] and xenobiotic-degrading capability [92,93], no coal-degrading strains have been documented. However, at least one report indicates that a strain isolated from two different ranks of coal was unable to degrade lignin [94].

5. Conclusions

Our goal in the present study was to determine the genetic relatedness of coal-degrading bacterial strains isolated from the rhizosphere of grasses growing on coal discard dumps and from diesel-contaminated sites to sequences of known PGP isolates contained in the NCBI GenBank database. We then determined the potential functionality of this relatedness by screening for PGP characteristics. Analysis of PCR-amplified 16S rRNA gene sequences from the seven genera of coal-degrading bacteria showed >99% homology to 32 sequences of known PGP strains from the NCBI GenBank database representing three families viz. four strains from each of the Bacillaceae and Enterobacteriaceae and one strain from the Microbacteriaceae. The Gram-negative isolates *Proteus* strain ECCN 20b, *Proteus* strain ECCN 23b and *Serratia* strain ECCN 24b, all from Enterobacteriaceae and isolated from diesel-contaminated soil, were shown to be competent for PGP characteristics using the biochemical parameters described in this study. Thus, while all strains were competent for ammonium and indole compound production, and solubilisation of insoluble phosphate, only *Proteus* strain ECCN 20b, *Proteus* strain ECCN 23b and *Serratia* strain ECCN 24b responded to the L-trp-supplemented medium by substantial accumulation of indolic compounds. Further, for these strains, indole compound accumulation in response to L-trp supplementation was linear with increasing L-trp concentration and not negatively affected in the presence of coal discard. Even so, it remains to be determined whether bioconversion of coal can occur with simultaneous production of indole compounds and in particular the auxin, IAA.

Further screening is therefore needed to expand our knowledge of the suite of PGP properties of the coal-degrading isolates. Using a combination of genome mining and metabolomics, possible target characteristics could include auxin and siderophore production, nitrogen fixation and potential phyto-protective mechanisms. It is also important to determine any direct effect of the isolated PGP coal-degrading bacteria on plant growth and development. A better understanding of the plant–bacteria relation may lead eventually to candidate strains for the development of a biological process with which to treat, stabilise and even rehabilitate disturbed soils.

Author Contributions: Conceptualisation of the work was by A.K.C. and Y.T., methodology by A.K.C. and Y.T. while execution was by Y.T., W.L.M., and J.T.O.; validation, Y.T.; L.M.S.-D.; and W.L.M.; data curation, A.K.C.; writing—original draft preparation, Y.T. and A.K.C.; writing—review and editing, Y.T., A.K.C., L.M.S.-D.; J.T.O.; supervision, A.K.C.; project administration, A.K.C.; funding acquisition, A.K.C. All authors have read and agreed to the published version of the manuscript.

Funding: This research was funded by Anglo Operations (Pty.) Ltd. (Anglo Coal), the National Research Foundation, South Africa (IFR1202220169, Grant No: 80879), and the Technology for Human Resources for Industry Programme (THRIP; TP13070820781, UID 90252).

Acknowledgments: Y.T. is supported by a Rhodes University Post-Doctoral Research Fellowship. W.L.M., and J.T.O. were supported by bursaries from EBRU. The authors are grateful to Rhodes University for additional financial support. Authors acknowledge the earlier bioprospecting work carried out by Lwazikazi Madikiza, Michelle Isaacs, and Gerald Edeki which led to the isolation and characterisation of the coal-degrading bacteria used in this study.

Conflicts of Interest: The authors declare no conflict of interest.

References

1. Fakoussa, R.M.; Hofrichter, M. Biotechnology and microbiology of coal degradation. *Appl. Microbiol. Biotechnol.* **1999**, *52*, 25–40. [[CrossRef](#)] [[PubMed](#)]
2. Machnikowska, H.; Pawelec, K.; Podgórska, A. Microbial degradation of low rank coals. *Fuel Proc. Technol.* **2002**, *77*, 17–23. [[CrossRef](#)]
3. Jiang, F.; Li, Z.; Lv, Z.; Gao, T.; Yang, J.; Qin, Z.; Yuan, H. The biosolubilization of lignite by *Bacillus* sp. Y7 and characterization of the soluble products. *Fuel* **2013**, *103*, 639–645. [[CrossRef](#)]
4. Speight, J.G. Handbook of Coal Analysis. In *Chemical Analysis. A Series of Monographs on Analytical Chemistry and its Applications*, 2nd ed.; Vitha, M.F., Ed.; John Wiley and Sons: Hoboken, NJ, USA, 2015; p. 368.
5. Claassens, S.; Van Rensburg, P.J.; Van Rensburg, L. Soil microbial community structure of coal mine discard under rehabilitation. *Water Air Soil Pollut.* **2006**, *174*, 355–366. [[CrossRef](#)]
6. Truter, W.J.; Rethman, N.F.G.; Potgieter, C.E.; Kruger, R.A. Re-vegetation of cover soils and coal discard material ameliorated with Class F fly ash. In Proceedings of the Collected Abstracts, 2009 World of Coal Ash (WOCA) Conference, Lexington, KY, USA, 4–7 May 2009; Available online: <http://www.flyash.info/2009/110-truter2009.pdf> (accessed on 10 July 2020).
7. Sekhohola, M.L.; Igbinigie, E.E.; Cowan, A.K. Biological degradation and solubilisation of coal. *Biodegradation* **2013**, *24*, 305–318. [[CrossRef](#)]
8. Cowan, A.K.; Lodewijks, H.M.; Sekhohola, L.M.; Edeki, O.G. In situ bioremediation of South African coal discard dumps. In Proceedings of the 11th International Conference on Mine Closure, Perth, Australia, 15–17 March 2016; Fourie, A.B., Tibbett, M., Eds.; Australian Centre for Geomechanics: Perth, Western Australia, 2016; pp. 501–509.
9. Šourková, M.; Frouz, J.; Šantrucková, H. Accumulation of carbon, nitrogen and phosphorus during soil formation on alder spoil heaps after brown-coal mining, near Sokolov (Czech Republic). *Geoderma* **2005**, *124*, 203–214. [[CrossRef](#)]
10. Vindušková, O.; Frouz, J. Soil carbon accumulation after open-cast coal and oil shale mining in Northern Hemisphere: A quantitative review. *Environ. Earth Sci.* **2013**, *69*, 1685–1698. [[CrossRef](#)]
11. Sekhohola, L.M.; Cowan, A.K. Biological conversion of low-grade coal discard to a humic substance-enriched soil-like material. *Int. J. Coal Sci. Technol.* **2017**, *4*, 183–190. [[CrossRef](#)]
12. Ralph, J.P.; Catcheside, D.E.A. Transformations of low rank coal by *Phanerochaete chrysosporium* and other wood-rot fungi. *Fuel Proc. Technol.* **1997**, *52*, 79–93. [[CrossRef](#)]
13. Gotz, K.E.; Fakoussa, R.M. Fungal biosolubilization of Rhenish brown coal monitored by Curie-point pyrolysis/gas chromatography/mass spectrometry using tetraethylammonium hydroxide. *Appl. Microbiol. Biotechnol.* **1999**, *52*, 41–48. [[CrossRef](#)]
14. Gokcay, C.F.; Kolankaya, N.; Dilek, F.B. Microbial solubilization of lignites. *Fuel* **2001**, *80*, 1421–1433. [[CrossRef](#)]
15. Yuan, H.; Yang, J.; Chen, W. Production of alkaline materials, surfactants and enzymes by *Penicillium decumbens* strain P6 in association with lignite degradation/solubilization. *Fuel* **2006**, *85*, 1378–1382. [[CrossRef](#)]
16. Haider, R.; Ghauri, M.A.; SanFilipo, J.R.; Jones, E.J.; Orem, W.H.; Tatu, C.A.; Akhtar, K.; Akhtar, N. Fungal degradation of coal as a pretreatment for methane production. *Fuel* **2013**, *104*, 717–725. [[CrossRef](#)] [[PubMed](#)]
17. Kwiatos, N.; Jędrzejczak-Krzepkowska, M.; Krzemińska, A.; Delavari, A.; Paneth, P.; Bielecki, S. Evolved *Fusarium oxysporum* laccase expressed in *Saccharomyces cerevisiae*. *Sci. Rep.* **2020**, *10*, 3244. [[CrossRef](#)] [[PubMed](#)]
18. Kwiatos, N.; Jędrzejczak-Krzepkowska, M.; Strzelecki, B.; Bielecki, S. Improvement of efficiency of brown coal biosolubilization by novel recombinant *Fusarium oxysporum* laccase. *AMB Express* **2018**, *8*, 133. [[CrossRef](#)] [[PubMed](#)]

19. Yang, Y.; Yang, J.; Li, B.; Wang, E.; Yuan, H. An esterase from *Penicillium decumbens* P6 involved in lignite depolymerization. *Fuel* **2018**, *214*, 416–422. [[CrossRef](#)]
20. Gao, T.G.; Jiang, F.; Yang, J.S.; Li, B.Z.; Yuan, H.L. Biodegradation of Leonardite an alkali-producing bacterial community and characterization of the degraded products. *Appl. Microbiol. Biotechnol.* **2012**, *93*, 2581–2590. [[CrossRef](#)]
21. David, Y.; Baylon, M.G.; Pamidimarri, S.D.V.N.; Baritugo, K.-A.; Chae, C.G.; Kim, Y.J.; Kim, T.W.; Kim, M.-S.; Na, J.G.; Par, S.J. Screening of microorganisms able to degrade low-rank coal in aerobic conditions: Potential coal biosolubilization mediators from coal to biochemicals. *Biotechnol. Bioprocess Eng.* **2017**, *22*, 178–185. [[CrossRef](#)]
22. Akimbekov, N.; Digel, I.; Qiaoa, X.; Tastambeka, K.; Zhubanova, A. Lignite biosolubilization by *Bacillus* sp. RKB 2 and characterization of its products. *Geomicrobiol. J.* **2020**, *37*, 255–261. [[CrossRef](#)]
23. Akimbekov, N.; Digel, I.; Abdieva, G.; Ualieva, P.; Tastambek, K. Lignite biosolubilization and bioconversion by *Bacillus* sp.: The collation of analytical data. *Biofuels* **2020**. [[CrossRef](#)]
24. Lyle, G.; Whyte, L.; Charles, W.G. Biodegradation of petroleum hydrocarbons by psychrotrophic *Pseudomonas* strains possessing both alkane (alk) and naphthalene (nah) catabolic pathways. *Appl. Environ. Microbiol.* **1997**, *63*, 3719–3723.
25. Jiang, B.; Zhou, Z.; Dong, Y.; Tao, W.; Wang, B.; Jiang, J.; Guan, X. Biodegradation of benzene, toluene, ethylbenzene, and *o*-, *m*-, and *p*-xylenes by the newly isolated bacterium *Comamonas* sp. *Appl. Biochem. Biotechnol.* **2015**, *176*, 1700–1708. [[CrossRef](#)] [[PubMed](#)]
26. Truskewycz, A.; Gundry, T.D.; Khudur, L.S.; Kolobaric, A.; Taha, M.; Aburto-Medina, A.; Ball, A.S.; Shahsavari, E. Petroleum hydrocarbon contamination in terrestrial ecosystems—Fate and microbial responses. *Molecules* **2019**, *24*, 3400. [[CrossRef](#)]
27. Lee, Y.; Lee, Y.; Jeon, C.O. Biodegradation of naphthalene, BTEX, and aliphatic hydrocarbons by *Paraburkholderia aromaticivorans* BN5 isolated from petroleum-contaminated soil. *Sci. Rep.* **2019**, *9*, 860. [[CrossRef](#)] [[PubMed](#)]
28. Khan, S.; Afzal, M.; Iqbal, S.; Khan, Q.M. Plant—Bacteria partnerships for the remediation of hydrocarbon contaminated soils. *Chemosphere* **2013**, *90*, 1317–1332. [[CrossRef](#)]
29. Yu, Y.; Zhang, Y.; Zhao, N.; Guo, J.; Xu, W.; Ma, M.; Li, X. Remediation of crude oil-polluted soil by the bacterial rhizosphere community of *Suaeda salsa* revealed by 16S rRNA genes. *Int. J. Environ. Res. Public Health* **2020**, *17*, 1471. [[CrossRef](#)]
30. Silva-Stenico, M.E.; Vengadajellum, C.J.; Janjua, H.A.; Harisson, S.T.L.; Burton, S.G.; Cowan, D.A. Degradation of low rank coal by *Trichoderma atroviride* ES11. *J. Ind. Microbiol. Biotechnol.* **2007**, *34*, 625–631. [[CrossRef](#)]
31. Romanowska, I.; Strzelecki, B.; Bielecki, S. Biosolubilization of Polish brown coal by *Gordonia alkanivorans* S7 and *Bacillus mycoides* NS1020. *Fuel Proc. Technol.* **2015**, *131*, 430–436. [[CrossRef](#)]
32. Valero, N.; Gómez, L.; Pantoja, M.; Ramírez, R. Production of humic substances through coal-solubilizing bacteria. *Braz. J. Microbiol.* **2014**, *45*, 911–918. [[CrossRef](#)]
33. Strapoć, D.; Mastalerz, M.; Dawson, K.; Macalady, J.; Callaghan, A.V.; Wawrik, B.; Turich, C.; Ashby, M. Biogeochemistry of microbial coal-bed methane. *Annu. Rev. Earth Pl. Sci.* **2011**, *39*, 617–656. [[CrossRef](#)]
34. Huang, Z.; Urynowicz, M.A.; Colberg, P.J.S. Bioassay of chemically treated subbituminous coal derivatives using *Pseudomonas putida* F1. *Int. J. Coal Geol.* **2013**, *115*, 97–105. [[CrossRef](#)]
35. Jones, E.J.P.; Voytek, M.A.; Warwick, P.D.; Corum, M.D.; Cohn, A.; Bunnell, J.E.; Clark, A.C.; Orem, W.H. Bioassay for estimating the biogenic methane generating potential of coal samples. *Int. J. Coal Geol.* **2008**, *76*, 138–150. [[CrossRef](#)]
36. Yin, S.; Tao, X.; Shi, K.; Tan, Z. Biosolubilisation of Chinese lignite. *Energy* **2009**, *34*, 775–781. [[CrossRef](#)]
37. Barboza, N.R.; Amorim, S.S.; Santos, P.A.; Reis, F.D.; Cordeiro, M.M.; Guerra-Sá, R.; Leão, V.A. Indirect manganese removal by *Stenotrophomonas* sp. and *Lysinibacillus* sp. isolated from Brazilian mine water. *Biomed. Res. Int.* **2015**, *2015*, 925972. [[CrossRef](#)] [[PubMed](#)]
38. Barboza, N.R.; Morais, M.M.C.A.; Queiroz, P.S.; Amorim, S.S.; Guerra-Sá, R.; Leão, V.A. High manganese tolerance and biooxidation ability of *Serratia marcescens* isolated from manganese mine water in Minas Gerais, Brazil. *Front. Microbiol.* **2017**, *8*, 1946. [[CrossRef](#)] [[PubMed](#)]
39. Ibrahim, H.M.M. Biodegradation of used engine oil by novel strains of *Ochrobactrum anthropi* HM-1 and *Citrobacter freundii* HM-2 isolated from oil-contaminated soil. *3 Biotech.* **2016**, *6*, 226. [[CrossRef](#)]

40. Olawale, J.T.; Edeki, O.G.; Cowan, A.K. Bacterial degradation of coal discard and geologically weathered coal. *Int. J. Coal Sci. Technol.* **2020**, *7*, 405–416. [CrossRef]
41. Santoyo, G.; Moreno-Hagelsieb, G.; del Carmen Orozco-Mosqued, M.; Glick, B.R. Plant growth-promoting bacterial endophytes. *Microbiol. Res.* **2016**, *183*, 92–99. [CrossRef]
42. Lane, D.J. 16S/23S rRNA sequencing. In *Nucleic acid Techniques in Bacterial Systematics*; Stackebrandt, E., Goodfellow, M., Eds.; John Wiley & Sons: New York, NY, USA, 1991; pp. 115–175.
43. Turner, S.J.; Pryer, K.M.; Miao, V.P.M.; Palmer, J.D. Investigating deep phylogenetic relationships among cyanobacteria and plastids by small subunit rRNA sequence analysis. *J. Eukaryot. Microbiol.* **1999**, *46*, 327–338. [CrossRef]
44. Technelysium (Chromas). Available online: <http://www.technelysium.com.au/chromas.html> (accessed on 18 May 2019).
45. Hall, T.A. BioEdit: A user-friendly biological sequence alignment editor and analysis program for Windows 95/98/NT. *Nucl. Acids Symp. Ser.* **1999**, *41*, 95–98.
46. Tamura, K.; Stecher, G.; Peterson, D.; Filipski, K.; Kumar, S. Molecular evolutionary genetic analysis version 6.0. *Mol. Biol. Evol.* **2013**, *30*, 2725–2729. [CrossRef] [PubMed]
47. Jeong, H.; Park, J.; Kim, H. Determination of NH_4^+ in environmental water with interfering substances using the modified Nessler method. *J. Chem.* **2013**, e359217. [CrossRef]
48. Gordon, S.A.; Weber, R.P. Colorimetric estimation of indoleacetic acid. *Plant Physiol.* **1951**, *26*, 192–195. [CrossRef] [PubMed]
49. Glickmann, E.; Dessaux, Y. A critical examination of the specificity of the Salkowski reagent for indolic compounds produced by phytopathogenic bacteria. *Appl. Environ. Microbiol.* **1995**, *61*, 793–796. [CrossRef]
50. Majeed, A.; Abbasi, M.K.; Hameed, S.; Imran, A.; Rahim, N. Isolation and characterization of plant growth-promoting rhizobacteria from wheat rhizosphere and their effect on plant growth promotion. *Front. Microbiol.* **2015**, *6*, 198. [CrossRef]
51. Sharma, S.B.; Sayyed, R.Z.; Trivedi, M.H.; Gobi, T.A. Phosphate solubilising microbes: Sustainable approach for managing phosphorus deficiency in agricultural soils. *SpringerPlus* **2013**, *2*, 587. [CrossRef]
52. Saha, M.; Maurya, B.R.; Meena, V.S.; Bahadur, I.; Kumar, A. Identification and characterisation of potassium solubilising bacteria (KSB) from Indo-Gangetic Plains of India. *Biocatal. Agric. Biotechnol.* **2016**, *7*, 202–209. [CrossRef]
53. Pflaum, R.T.; Howick, L.C. Spectrophotometric determination of potassium with sodium tetraphenyl-borate. *Anal. Chem.* **1956**, *28*, 1542–1544. [CrossRef]
54. Bechtaoui, N.; Raklami, A.; Tahiri, A.-I.; Benidire, L.; El Alaoui, A.; Meddich, A.; Gottfert, M.; Oufdou, K. Characterization of plant growth promoting rhizobacteria and their benefits on growth and phosphate nutrition of faba bean and wheat. *Biol. Open* **2019**, *8*, bio043968. [CrossRef]
55. Patten, C.L.; Blakney, A.J.C.; Coulson, T.J.D. Activity, distribution and function of indole-3-acetic acid biosynthetic pathways in bacteria. *Crit. Rev. Microbiol.* **2013**, *39*, 395–415. [CrossRef]
56. Tien, T.M.; Gaskins, M.H.; Hubbell, D.H. Plant growth substances produced by *Azospirillum brasilense* and their effect on the growth of pearl millet (*Pennisetum americanum* L.). *Appl. Environ. Microbiol.* **1979**, *37*, 1016–1024. [CrossRef] [PubMed]
57. Marappa, N.; Ramachandran, L.; Dharumadurai, D.; Nooruddin, T. Plant growth-promoting active metabolites from *Frankia* spp. of *Actinorhizal Casuarina* spp. *Appl. Biochem. Biotechnol.* **2020**, *191*, 74–91. [CrossRef] [PubMed]
58. Throbäck, I.N.; Enwall, K.; Jarvis, A.; Hallin, S. Reassessing PCR primers targeting nirS, nirK and nosZ genes for community surveys of denitrifying bacteria with DGGE. *FEMS Microbiol. Ecol.* **2004**, *49*, 401–417. [CrossRef] [PubMed]
59. Reynolds, K.A.; Surridge, A.K.J. Ash microbiology: A molecular study. In Proceedings of the Collected Abstracts, 2009 World of Coal Ash (WOCA) Conference, Lexington, KY, USA, 4–7 May 2009; Available online: <http://www.flyash.info/2009/031-surridge2009.pdf> (accessed on 10 July 2020).
60. Chen, Y.P.; Rekha, P.D.; Arun, A.B.; Shen, F.T.; Lai, W.A.; Young, C.C. Phosphate solubilizing bacteria from subtropical soil and their tricalcium phosphate solubilizing abilities. *Appl. Soil Ecol.* **2006**, *34*, 33–41. [CrossRef]

61. Farhat, M.B.; Farhat, A.; Bejar, W.; Kammoun, R.; Bouchaala, K.; Fourati, A.; Antoun, H.; Bejar, S.; Chouayekh, H. Characterization of the mineral phosphate solubilizing activity of *Serratia marcescens* CTM 50650 isolated from the phosphate mine of Gafsa. *Arch. Microbiol.* **2009**, *191*, 815–824. [[CrossRef](#)]
62. Mursyida, E.; Mubarik, N.R.; Tjahjoleksono, A. Selection and identification of phosphate-potassium solubilizing bacteria from the area around the limestone mining in Cirebon Quarry. *Res. J. Microbiol.* **2015**, *10*, 270–279.
63. Borgi, M.A.; Saidi, I.; Moula, A.; Rhimi, S.; Rhimi, M. The attractive *Serratia plymuthica* BMA1 strain with high rock phosphate-solubilizing activity and its effect on the growth and phosphorus uptake by *Vicia faba* L. plants. *Geomicrobiol. J.* **2020**, *37*, 437–445. [[CrossRef](#)]
64. Wichner, S.; Libbert, E. Interactions between plants and epiphytic bacteria regarding their auxin metabolism. I. Detection of IAA-producing epiphytic bacteria and their role in long duration experiments on tryptophan metabolism in plant homogenates. *Physiol. Plant.* **1968**, *21*, 227–241. [[CrossRef](#)]
65. Fett, W.F.; Osman, S.F.; Dunn, M.F. Auxin production by plant-pathogenic Pseudomonads and Xanthomonads. *Appl. Environ. Microbiol.* **1987**, *53*, 1839–1845. [[CrossRef](#)]
66. Patten, C.L.; Glick, B.R. Bacterial biosynthesis of indole-3-acetic acid. *Can. J. Microbiol.* **1996**, *42*, 207–220. [[CrossRef](#)]
67. Zarkan, A.; Liu, J.; Matuszewska, M.; Gaimster, H.; Summer, D.K. Local and universal action: The paradoxes of indole signalling in bacteria. *Trends Microbiol.* **2020**, *28*, 566–577. [[CrossRef](#)] [[PubMed](#)]
68. Duca, D.; Lorv, J.; Patten, C.L.; Rose, D.; Glick, B.R. Indole-3-acetic acid in plant-microbe interactions. *Antonie Van Leeuwenhoek* **2014**, *106*, 85–125. [[CrossRef](#)] [[PubMed](#)]
69. Normanly, J.; Cohen, J.D.; Fink, G.R. *Arabidopsis thaliana* auxotrophs reveal a tryptophan-independent biosynthetic pathway for indole-3-acetic acid. *Proc. Natl. Acad. Sci. USA* **1993**, *90*, 10355–10359. [[CrossRef](#)] [[PubMed](#)]
70. Taupp, M.; Harmsen, D.; Heckel, F.; Schreier, P. Production of natural methyl anthranilate by microbial N-demethylation of N-methyl methyl anthranilate by the topsoil-isolated bacterium *Bacillus megaterium*. *J. Agric. Food Chem.* **2005**, *53*, 9586–9589. [[CrossRef](#)] [[PubMed](#)]
71. Luo, Z.W.; Cho, J.S.; Lee, S.Y. Microbial production of methyl anthranilate, a grape flavor compound. *Proc. Natl. Acad. Sci. USA* **2019**, *116*, 10749–10756. [[CrossRef](#)]
72. Kölling, G. Products of coal (coke, tar, gas) and their analysis. *Pure Appl. Chem.* **1977**, *49*, 1475–1482. [[CrossRef](#)]
73. Stefanova, M.; Gonsalves, L.; Marinov, S.P.; Czech, J.; Carleer, R.; Yperman, J. Reductive pyrolysis of leonardite humic acids. *Bulg. Chem. Commun.* **2014**, *46*, 123–128.
74. Grimont, P.A.D.; Grimont, F. The genus *Serratia*. *Annu. Rev. Microbiol.* **1978**, *32*, 221–248. [[CrossRef](#)]
75. Singh, R.P.; Jha, P.N. The multifarious PGPR *Serratia marcescens* CDP-13 augments induced systemic resistance and enhanced salinity tolerance of wheat (*Triticum aestivum* L.). *PLoS ONE* **2016**, *11*, e0155026. [[CrossRef](#)]
76. Khan, A.R.; Park, G.-S.; Asaf, S.; Hong, S.-J.; Jung, B.K.; Shin, S.-H. Complete genome analysis of *Serratia marcescens* RSC-14: A plant growth-promoting bacterium that alleviates cadmium stress in host plants. *PLoS ONE* **2017**, *12*, e0171534. [[CrossRef](#)]
77. Matteoli, F.P.; Passarelli-Araujo, H.; Reis, R.J.A.; da Rocha, L.O.; de Souza, E.M.; Aravind, L.; Olivares, F.L.; Venancio, T.M. Genome sequencing and assessment of plant growth-promoting properties of a *Serratia marcescens* strain isolated from vermicompost. *BMC Genom.* **2018**, *19*, 750. [[CrossRef](#)] [[PubMed](#)]
78. Smulek, W.; Sydow, M.; Zabielska-Matejuk, J.; Kaczorek, E. Bacteria involved in biodegradation of creosote PAH—A case study of long-term contaminated industrial area. *Ecotox. Environ. Saf.* **2020**, *187*, 109843. [[CrossRef](#)] [[PubMed](#)]
79. Das, A.C.; Mukherjee, D. Soil application of insecticides influences microorganisms and plant nutrients. *Appl. Soil Ecol.* **2000**, *14*, 55–62. [[CrossRef](#)]
80. Das, A.C.; Chakravarty, A.; Sukul, P.; Mukherjee, D. Insecticides: Their effect on microorganisms and persistence in rice soil. *Microbiol. Res.* **1995**, *150*, 187–194. [[CrossRef](#)]
81. Das, A.C.; Chakravarty, A.; Sukul, P.; Mukherjee, D. Influence and persistence of phorate and carbofuran insecticides on microorganisms in rice field. *Chemosphere* **2003**, *53*, 1033–1037. [[CrossRef](#)]
82. Rau, N.; Mishra, V.; Sharma, M.; Das, M.K.; Ahaluwalia, K.; Sharma, R.S. Evaluation of functional diversity in Rhizobacterial taxa of a wild grass (*Saccharum ravennae*) colonizing abandoned fly ash dumps in Delhi urban ecosystem. *Soil Biol. Biochem.* **2009**, *41*, 813–821. [[CrossRef](#)]

83. Yu, S.M.; Lee, Y.H. Plant growth promoting rhizobacterium *Proteus vulgaris* JBLS202 stimulates the seedling growth of Chinese cabbage through indole emission. *Plant Soil* **2013**, *370*, 485–495. [[CrossRef](#)]
84. Bhattacharyya, D.; Garlandin, M.; Lee, Y.H. Volatile indole produced by rhizobacterium *Proteus vulgaris* JBLS202 stimulates growth of *Arabidopsis thaliana* through auxin, cytokinin, and brassinosteroid pathways. *J. Plant Growth Regul.* **2015**, *34*, 158–168. [[CrossRef](#)]
85. Lu, H.; Wang, X.; Zhang, K.; Lu, Y.; Zhou, L.; Li, G. Identification and nematicidal activity of bacteria isolated from cow dung. *Ann. Microbiol.* **2014**, *64*, 407–411. [[CrossRef](#)]
86. Hernandez-Rivera, M.A.; Ojeda-Morales, M.E.; Martinez-Vazquez, J.G.; Villegas-Cornelio, V.M.; Cordova-Bautista, Y. Optimal parameters for in vitro development of the hydrocarbonoclastic microorganism *Proteus* sp. *J. Soil Sci. Plant Nutr.* **2011**, *11*, 29–43. [[CrossRef](#)]
87. Ibrahim, M.L.; Ijah, U.J.J.; Manga, S.B.; Bilbis, L.S.; Umar, S. Production and partial characterization of biosurfactant produced by crude oil degrading bacteria. *Int. Biodeterior. Biodegrad.* **2013**, *81*, 28–34. [[CrossRef](#)]
88. Obayori, O.S.; Salam, L.B.; Oyetibo, G.O.; Idowu, M.; Amund, O.O. Biodegradation potentials of polyaromatic hydrocarbon (pyrene and phenanthrene) by *Proteus mirabilis* isolated from an animal charcoal polluted site. *Biocatal. Agric. Biotechnol.* **2017**, *12*, 78–84. [[CrossRef](#)]
89. Hassen, A.; Saidi, N.; Cherif, M.; Boudabous, A. Resistance of environmental bacteria to heavy metals. *Bioresour. Technol.* **1998**, *64*, 7–15. [[CrossRef](#)]
90. Ge, S.; Dong, X.; Zhou, J.; Ge, S. Comparative evaluations on bio-treatment of hexavalent chromate by resting cells of *Pseudochrobactrum* sp. and *Proteus* sp. in wastewater. *J. Environ. Manag.* **2013**, *126*, 7–12. [[CrossRef](#)] [[PubMed](#)]
91. Islam, F.; Yasmeen, T.; Riaz, M.; Arif, M.S.; Ali, S.; Raza, S.H. *Proteus mirabilis* alleviates zinc toxicity by preventing oxidative stress in maize (*Zea mays*) plants. *Ecotoxicol. Environ. Saf.* **2014**, *110*, 143–152. [[CrossRef](#)]
92. Olukanni, O.D.; Osuntoki, A.A.; Kalyani, D.C.; Gbenle, G.O.; Govindw, S.P. Decolorization and biodegradation of Reactive Blue 13 by *Proteus mirabilis* LAG. *J. Hazard Mater.* **2010**, *184*, 290–298. [[CrossRef](#)]
93. Pino, N.J.; Dominguez, M.C.; Peñuela, G.A. Isolation of a selected microbial consortium capable of degrading methyl parathion and p-nitrophenol from a contaminated soil site. *J. Environ. Sci. Heal. B* **2011**, *46*, 173–180. [[CrossRef](#)]
94. Wang, L.; Nie, Y.; Tang, Y.-Q.; Song, X.-M.; Cao, K.; Sun, L.-Z.; Wang, Z.-J.; Wu, X.-L. Diverse bacteria with lignin degrading potentials isolated from two ranks of coal. *Front. Microbiol.* **2016**, *7*, 1428. [[CrossRef](#)]



© 2020 by the authors. Licensee MDPI, Basel, Switzerland. This article is an open access article distributed under the terms and conditions of the Creative Commons Attribution (CC BY) license (<http://creativecommons.org/licenses/by/4.0/>).

Article

Effects of Mercury II on *Cupriavidus metallidurans* Strain MSR33 during Mercury Bioremediation under Aerobic and Anaerobic Conditions

Guillermo Bravo ¹, Paulina Vega-Celedón ¹, Juan Carlos Gentina ² and Michael Seeger ^{1,*}

¹ Molecular Microbiology and Environmental Biotechnology Laboratory, Department of Chemistry & Center of Biotechnology Daniel Alkalay Lowitt, Universidad Técnica Federico Santa María, Avenida España 1680, Valparaíso 2390123, Chile; bravoc.guillermo@gmail.com (G.B.); pvegacedon@gmail.com (P.V.-C.)

² School of Biochemical Engineering, Pontificia Universidad Católica de Valparaíso, Avenida Brasil 2085, Valparaíso 2362803, Chile; carlos.gentina@pucv.cl

* Correspondence: michael.seeger@gmail.com or michael.seeger@usm.cl; Tel.: +56-322654236

Received: 1 July 2020; Accepted: 23 July 2020; Published: 25 July 2020

Abstract: Mercury is a toxic element that harms organisms and disturbs biogeochemical cycles. Mercury bioremediation is based on the reduction of Hg (II) to Hg (0) by mercury-resistant bacteria. *Cupriavidus metallidurans* MSR33 possesses a broad-spectrum mercury resistance. This study aims to establish the effects of mercury on growth, oxygen uptake, and mercury removal parameters by *C. metallidurans* MSR33 in aqueous solution during aerobic and anaerobic mercury bioremediation. A new culture medium (GBC) was designed. The effects of mercury (II) (20 ppm) on growth parameters, oxygen uptake, and mercury removal were evaluated in GBC medium in a bioreactor (3 L) under aerobiosis. The anaerobic kinetics of mercury removal was evaluated by nitrogen replacement during mercury bioremediation in a bioreactor. Strain MSR33 reached a growth rate of $\mu = 0.43 \text{ h}^{-1}$ in the bioreactor. Mercury inhibited oxygen uptake and bacterial growth; however, this inhibition was reversed after 5 h. Strain MSR33 was able to reduce Hg (II) under aerobic and anaerobic conditions, reaching, at 24 h, a metal removal of 97% and 71%, respectively. Therefore, oxygen was crucial for efficient mercury removal by this bacterium. Strain MSR33 was capable of tolerating the toxic effects of mercury (II) during aerobic bioremediation and recovered its metabolic activity.

Keywords: *Cupriavidus metallidurans*; mercury; bioremediation; aerobic; anaerobic

1. Introduction

Mercury is a highly toxic metal for cells and is distributed in the water, soil, and air, due to human activities including mining and natural cycles [1–4]. Mercury presents in the Earth's crust at concentrations between 20 and 150 ppb [4]. Until 2010, it was estimated that a cumulative total of 1540 (1060–2800) Gg of mercury had been released by human activities, 73% of which were released after 1850 [5]. The main sources of mercury pollution are mining (e.g., gold, copper), the chloralkali industry, sludge deposited in landfills, paints, disinfectants, pharmaceuticals, and seed-coat dressing, which mobilizes mercury into the water, soil, and atmosphere [3–5]. Mercury (II) is a highly toxic specie due to its high affinity to sulfhydryl and thioester groups of proteins, inactivating proteins of living organisms [2,6–9]. Due to its high toxicity, several technologies have been developed for the remediation of mercury. Physicochemical processes are efficient, but expensive at the industrial scale and not applicable in large polluted areas [10,11]. Bioremediation is an eco-friendly and low-cost strategy for the clean-up of polluted environments but is limited to a range of pollutant concentrations that are tolerated by microorganisms [12–18]. Bioremediation is based on the inoculation of microorganisms, especially bacteria and fungi, to mineralize or transform toxic compounds or elements into less toxic forms [12–18].

Mercury bioremediation by metal-resistant bacteria is mainly based on the reduction of Hg (II) to Hg (0) by proteins codified by the *mer* genes and the reducing power NADPH (Figure 1). Elemental mercury, Hg (0), is volatile due to its high vapor pressure and insoluble in water. Mercury removal strategies are based on the volatility and water insolubility of this heavy metal [19]. Diverse bacteria, including *C. metallidurans* strains CH34 and MSR33, *Pseudomonas putida* strains PpY101/pSR134, Spi3, Elb2 and KT2442, *P. stutzeri* strains Ibu8 and OX, *P. aeruginosa* Bro12, *Aeromonas hydrophila*, and *Sphingomonas* sp. SA2, reduce mercury under aerobic conditions [3,10,11,20–24]. Studies of mercury reduction under anaerobic conditions are scarce. *P. stutzeri* OX, *Geobacter bemidjensis* Bem, and *Geobacter sulfurreducens* PCA reduce mercury under anaerobiosis [20,25,26].

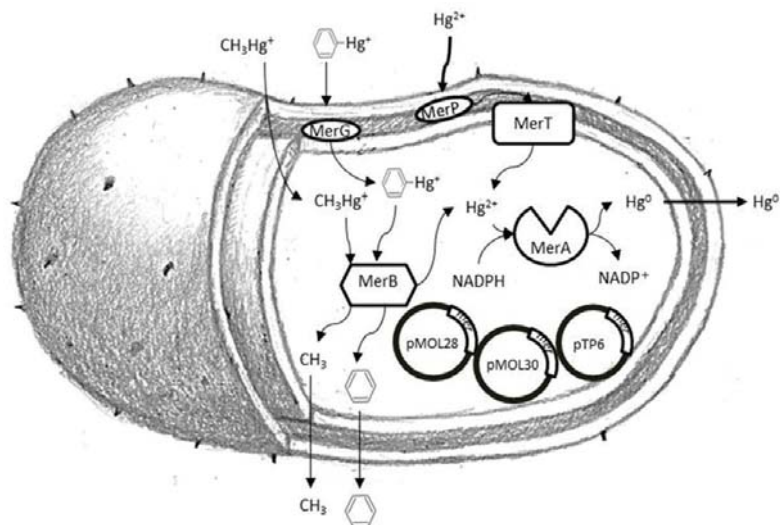


Figure 1. Mercury (II) and organomercurial compounds resistance mechanism of *C. metallidurans* MSR33. Mercury (II) and organomercurial compounds resistance is codified by *mer* genes in the chromosome and the plasmids pMOL30, pMOL28, and pTP6 of strain MSR33. Hg (II) is reduced to Hg (0) by mercuric reductase MerA using reducing power NADPH. MerB catalyzes the protonolysis of the carbon–mercury bond in organomercurials. MerP and MerT are proteins involved in the transport of mercury (II) inside the cell. MerG is a periplasmic protein involved in the importing of phenylmercury. Figure adapted from Rojas et al. [10].

C. metallidurans strains are highly resistant to heavy metals and are able to metabolize toxic organic pollutants such as toluene under aerobic and anaerobic conditions; therefore, specific strains have been applied in bioremediation [27–30]. *C. metallidurans* strain CH34 is a facultative anaerobe and heavy metal multi-resistant bacterium associated to the gold biogeochemical cycle [7,27,28]. Strain MSR33 is a transconjugant strain of wild type *C. metallidurans* CH34 that possesses increased resistance to heavy metals and organomercurial compounds [10,29]. Strain MSR33 exhibits 2.4-fold higher resistance to Hg (II), >16-fold higher resistance to methyl-Hg, and higher resistance to Cd (II), Co (II), and Ni (II) than strain CH34 [10,28,29]. Under aerobic conditions, strain MSR33 possesses a high resistance to mercury II (24 ppm), methyl-Hg (>17 ppm), and is capable of reducing Hg (II) and organomercurial compounds to Hg (0). *C. metallidurans* strain MSR33 has been used for the bioremediation of mercury-polluted aqueous solutions, achieving complete mercury removal in 2 h [10]. Oxygen uptake is a key parameter in bioprocesses such as bioremediation, where oxygen is the final electron acceptor in aerobic respiration. Aerial oxygen is incorporated into the process of mercury bioremediation for the displacement of

gaseous mercury to the oxidizing trap [10,21,23,26]. The effects of mercury on oxygen uptake during the mercury bioremediation process have not been elucidated.

This study aims to establish the effects of mercury on growth, oxygen uptake, and mercury removal parameters by *C. metallidurans* MSR33 in aqueous solution in a bioreactor during aerobic and anaerobic mercury bioremediation. The strain MSR33 showed the ability to reduce mercury (II) under aerobic and anaerobic conditions. However, the presence of oxygen was crucial for efficient mercury removal. *C. metallidurans* MSR33 is capable of tolerating the toxic effects of mercury during mercury bioremediation and recovered its metabolic activity.

2. Materials and Methods

2.1. Chemicals

Succinate, HgCl_2 , H_2SO_4 , NH_4Cl , $\text{NaH}_2\text{PO}_4 \times 2\text{H}_2\text{O}$, KCl , FeSO_4 , HNO_3 , HCl , and NaOH were purchased from Merck (Darmstadt, Germany).

2.2. Culture Medium

A new culture medium for MSR33 strain was designed according to the nutritional requirements of a model microorganism [31]. The nutrient concentrations required in the culture medium were calculated. Theoretical yield ($Y_{x/s}$) for each nutrient was determined. The concentration in excess (100%) of nutrients for 2 g L^{-1} of cellular biomass, except for the carbon and energy sources, was established to cover the theoretical values required by the cell. The components of GBC (Guillermo Bravo Cortés) medium are succinate (4 g L^{-1}) as carbon and energy source, NH_4Cl (1 g L^{-1}) as nitrogen source, $\text{NaHPO}_4 \times 2\text{H}_2\text{O}$ (0.21 g L^{-1}) as phosphorus and sodium sources, FeSO_4 (0.2 g L^{-1}) as iron and sulfur sources, and KCl (0.27 g L^{-1}) as potassium source. The culture medium was adjusted to pH 7 with the addition of HCl (37%) and NaOH (10 M).

2.3. Biomass Determination

The biomass of strain MSR33 was assessed by measuring turbidity at 600 nm and using a curve of turbidity versus dry biomass concentration. For the determination of the cell dry weight, 25 mL of culture broth of strain MSR33 was collected and centrifuged in a Hettich model Rotina 380R centrifuge (Westfalia, Germany) at $3500 \times g$ for 10 min, removing the supernatant, and washing the cells three times with Milli-Q water. Cells were placed in a previously tared aluminum foil and dried in a Memmert oven (Schwabach, Germany) at $60 \text{ }^\circ\text{C}$ for 48 h. The initial and final mass difference was used to calculate the value of dry biomass weight. A correlation curve between turbidity and biomass dry weight was established.

2.4. Succinate Quantification

The succinate degradation was assessed by measuring succinate in GBC broth during the fermentation. The samples (300 μL) were centrifuged at $24,000 \times g$ for 10 min. The supernatant was passed through a $0.22 \mu\text{m}$ syringe filter, and the filtered solution samples (200 μL) were deposited in glass flasks for high performance liquid chromatography (HPLC) analysis. The succinate concentrations were analyzed according to a described protocol [32]. The samples (2 μL) were analyzed in an Agilent model 1260 Infinity Quaternary LC HPLC (Santa Clara, California, USA) equipped with a UV/IR detector using a BioRad Aminex HPX-97H column. The mobile phase was composed of H_2SO_4 (5 mM) with a flow rate of 0.6 mL min^{-1} at $45 \text{ }^\circ\text{C}$.

2.5. Determination of Dissolved Oxygen Concentration

The dissolved oxygen concentration was determined using an oxygen optic sensor PreSens model Fibox 3 (Regensburg, Germany). The calibration of the equipment was carried out according to the manufacturer's specifications. The determination of oxygen uptake rate by strain MSR33 was performed using the dynamic method of Humprey [33]. This method consists of the interruption of air supply during the exponential growth phase of strain MSR33, to reach 10% dissolved oxygen and its later supply to the fermentation. The slope obtained from the fall of oxygen concentration corresponds to the oxygen uptake rate by strain MSR33.

2.6. Mercury Determination

For the determination of Hg in aqueous samples, the AOAC 977.15 methodology was used with modifications [34]. The mercury quantification was carried out by cold vapor atomic absorption spectrometry using an atomic absorption spectrometer Agilent model 240AA series AA1110M032 with a hydride generation module (VGA 77) (Santa Clara, California, USA).

2.7. Kinetics of *C. metallidurans* MSR33 Growth

To increase the cellular biomass of strain MSR33, the growth kinetics were measured at different succinate concentrations (4, 8, and 12 g L⁻¹), increasing the GBC medium concentrations 2 and 3 times. Batch experiments were performed in a stirred-tank bioreactor Applikon Biotechnology model Ez-control (Delft, The Netherlands) of 3 L total volume, equipped with a Rushton type turbine and pH and temperature controllers. MSR33 cells were grown in GBC medium (1 L fermentation volume) with agitation (500 rpm), aeration (air flow of 2 vvm) at pH 7 and 30 °C. Previously, MSR33 cells grown in Luria–Bertani medium until the late exponential phase were harvested and inoculated at 10% v v⁻¹ in the fermentation volume. The specific growth rate (μ), cellular yield ($Y_{x/s}$), cellular productivity (Q_x), and oxygen uptake rate (N_a) of strain MSR33 were assessed.

2.8. Effects of Mercury on Growth and Oxygen Uptake Rate of *C. metallidurans* Strain MSR33

The effects of mercury on growth and oxygen uptake rate of strain MSR33 were studied after the addition of mercury (II) (20 ppm) into the bioreactor during the exponential growth phase on succinate (8 g L⁻¹) as sole carbon and energy source. Reduced mercury, Hg (0), generated by strain MSR33 was removed by air or nitrogen gas stripping and sparged into a solution of HNO₃ (1 M), where Hg (0) was oxidized to Hg (II) [10]. The acidic solution was maintained in the trap for the capture of gaseous mercury.

2.9. Effects of Oxygen Availability on Mercury Reduction

The mercury reduction was assessed in the bioreactor under aerobic and anaerobic conditions. To establish the anaerobic conditions, air supply was replaced by nitrogen gas after strain MSR33 reached a cell mass of 1 g L⁻¹, providing deoxygenation and the displacement of volatile mercury into the oxidizing trap [10,35]. A molecular nitrogen flow of 2 vvm was used. The kinetic evaluation of mercury removal was carried out during the exponential growth phase of strain MSR33 (biomass ~1.3 g cells L⁻¹), by measuring the remaining total mercury concentration in the GBC culture broth.

3. Results

3.1. Culture Medium Design, Kinetics, and Operational Characterization of *C. metallidurans* MSR33 Growth

A new culture medium was designed for higher growth of *C. metallidurans* strain MSR33 (Figure 2). This culture medium was named GBC medium and is composed of succinate, ammonium chloride, phosphate (low concentration), and trace salts. The amount of carbon used for the culture medium was calculated from a carbon mass balance, expecting a theoretical biomass value of 2 g cells L⁻¹

for 4 g L^{-1} succinate. However, the results show a lower biomass value ($1.7 \text{ g cells L}^{-1}$) than the theoretical biomass.

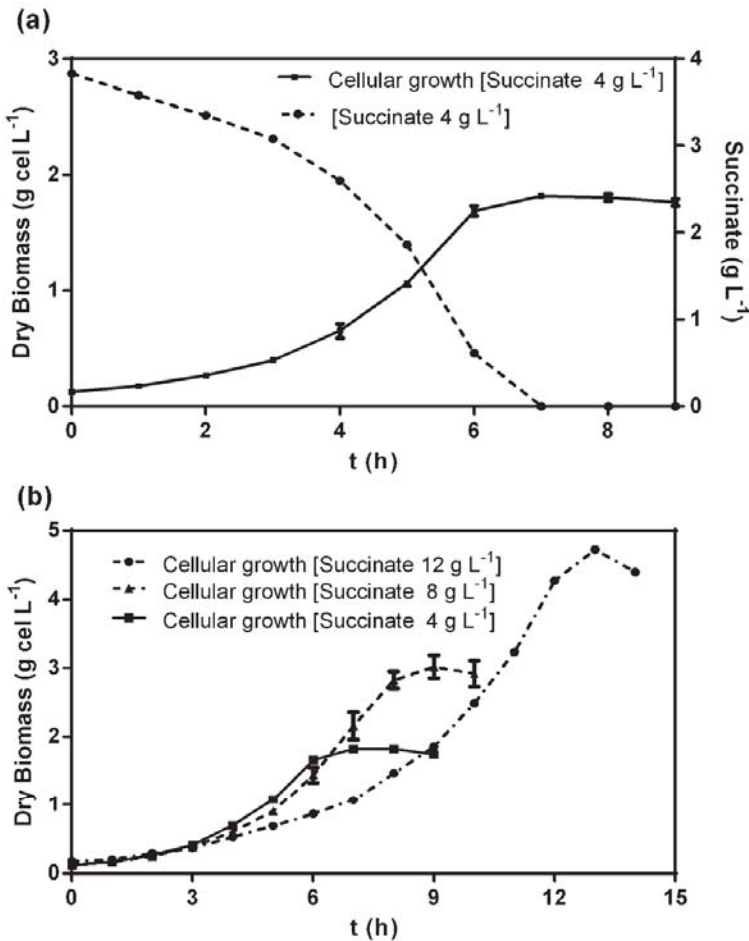


Figure 2. Growth and succinate degradation of *C. metallidurans* MSR33 in GBC medium. (a) Growth of strain MSR33 on succinate 4 g L^{-1} . (b) Effect of increased succinate concentration on the growth kinetics of *C. metallidurans* MSR33. The kinetics was obtained from a batch reactor with aeration (2 vvm), pH 7, $30 \text{ }^\circ\text{C}$ and agitation (500 rpm). The assays were performed in triplicate. Bars indicate the standard deviation.

The kinetic and operational parameters of *C. metallidurans* MSR33 growth in the GBC medium were studied. The results show the dependence on succinate concentration of the growth of strain MSR33 in GBC medium (Figure 2a), validating the use of succinate as the sole carbon and energy source. The kinetics parameters obtained were the specific growth rate (μ) of 0.43 h^{-1} , a doubling time (TD) of 1.61 h , a yield of biomass from the carbon and energy source ($Y_{x/s}$) of $0.41 \text{ g cells g succinate}^{-1}$, an oxygen uptake rate of $120 \text{ ppm oxygen h}^{-1}$, a specific oxygen uptake rate of $60 \text{ mg O}_2 \text{ h}^{-1} \text{ g cell}^{-1}$, and a cellular productivity (Q_x) of $0.24 \text{ g cells L}^{-1} \text{ h}^{-1}$.

To evaluate the kinetic behavior and the final biomass concentration in fermentation with a higher cell density, the carbon, and energy source of the GBC medium (succinate) was used two and three

times concentrated (Figure 2b). When the succinate concentration of the medium GBC was doubled, the strain MSR33 exhibited a similar kinetic pattern and the biomass increased almost two-fold. When three times concentrated succinate was used, the biomass increased almost three-fold, but a delay at the beginning of the exponential phase was observed. Therefore, for mercury bioremediation assays, the GBC medium with the carbon source 2-fold concentrated (succinate 8 g L^{-1}) was selected.

3.2. Effect of Mercury (II) on Bioremediation in Liquid Medium by *C. metallidurans* Strain MSR33

In the first approach, the effect of the addition of mercury to the culture broth on the growth of strain MSR33 was evaluated during 10 h (Figure 3). The addition of mercury (II) (20 ppm) during the exponential phase caused the inhibition of MSR33 growth and the interruption of its oxygen uptake. In contrast, in the absence of mercury (II), the oxygen is consumed during the complete period of cell growth.

In the second set of assays, the effects of mercury (II) (20 ppm) on growth kinetics and oxygen uptake were studied over a period of 26 h (Figure 4). The effects of mercury (II) on cellular growth and respiration were reversible. After a mercury (II) (20 ppm) pulse at the exponential phase, MSR33 cell growth was completely inhibited. However, 5 h after the addition of mercury (II), strain MSR33 reversed the inhibitory effects caused by mercury (II), re-starting the oxygen uptake and cell growth.

3.3. Effect of Oxygen Availability on Mercury (II) Reduction

To determine the effect of oxygen availability on the reduction of mercury (II) (20 ppm) by MSR33 cells, the reduction of mercury (II) under aerobic and anaerobic conditions was compared (Figure 5). Strain MSR33 was able to reduce Hg (II) under aerobic and anaerobic conditions, reaching a mercury removal after 24 h of 96.8% and 71.4%, respectively. The results indicate that the removal of mercury (II) by strain MSR33 after 24 h was higher under aerobic conditions than under anaerobiosis.

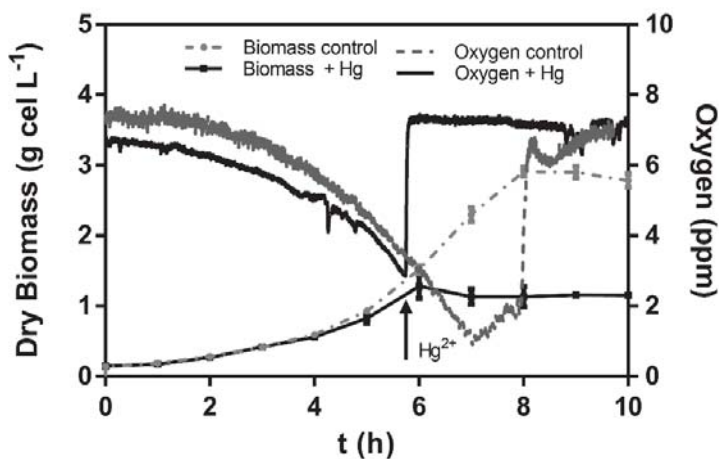


Figure 3. Effects of the addition of mercury (II) on the kinetics of cell growth and oxygen uptake by *C. metallidurans* MSR33. In these assays, Hg (II) (20 ppm) was added during the exponential phase at 6 h of growth onset by *C. metallidurans* MSR33. The assays were performed in duplicate. Bars indicate the standard deviation.

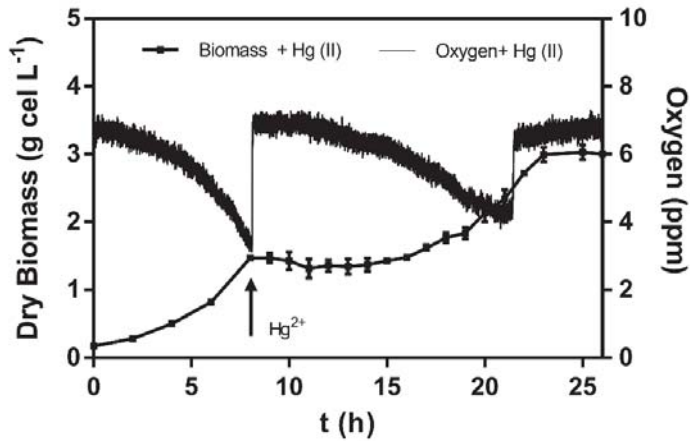


Figure 4. Effect of mercury (II) (20 ppm) on the growth and the respiration of *C. metallidurans* MSR33. In these assays, Hg (II) (20 ppm) was added at the exponential growth phase. The assays were performed in duplicate. Bars indicate the standard deviation.

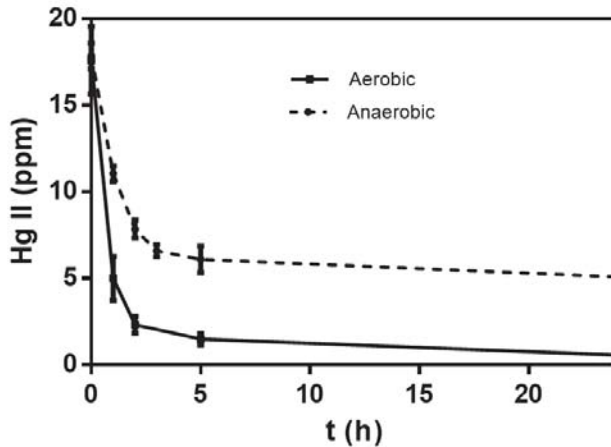


Figure 5. Kinetics of mercury (II) (20 ppm) removal by *C. metallidurans* MSR33 from polluted aqueous solution under aerobic and anaerobic conditions. Hg (II) removal was evaluated during the exponential growth phase ($1.3 \text{ g cells L}^{-1}$), using gas flows (2 vvm) of air and nitrogen gas for aerobic and anaerobic conditions, respectively. The assays were performed in duplicate. Bars indicate the standard deviation.

4. Discussion

This study determined the kinetic parameters of *C. metallidurans* MSR33 growth in a bioreactor (3 L) and the effect of mercury on mercury bioremediation by this strain. The new culture medium GBC for strain MSR33 growth was formulated in this study. Due to the complexing effect of phosphate on mercury, GBC medium was formulated with a low phosphate concentration. The low phosphate Tris-buffered mineral salts (LPTMS) medium has been used previously for *C. metallidurans* growth [10,28,29]. The LPTMS medium requires high concentrations of Tris salts buffer, which is not required for bioreactor cultures with automatic pH control. Succinate concentration was adjusted to energy and growth requirements of strain MSR33. The biomass difference between the theoretical (2 g cells L^{-1}) and the experimental values ($1.7 \text{ g cells L}^{-1}$) may be attributed to factors such as

carbon losses produced by the release of metabolites into the culture and higher maintenance energy requirements (Figure 2a).

The specific growth rate (μ) for *C. metallidurans* strain MSR33 obtained in this study is higher (8 times) than the μ reported previously [10]. Rojas et al. characterized the MSR33 growth in a 200 mL flask, whereas, in the present study, the strain was grown in a bioreactor of 3 L under controlled conditions of pH, agitation, and oxygen supply [10]. In this study, inhibition of MSR33 growth at high concentrations of succinate was observed (Figure 2b), suggesting an inhibition by the substrate. After 7 h of the growth kinetics, this inhibition was reversed. High succinate concentration has been reported to inhibit the succinate dehydrogenase [36], which may explain the initial inhibitory behavior observed with 12 g L⁻¹ succinate. Strain MSR33 grown on succinate showed a lower specific oxygen uptake rate (60 mg O₂ h⁻¹ g cell⁻¹) than *E. coli* NF790 grown on succinate (832 mg O₂ h⁻¹ g cell⁻¹) but within the oxygen uptake range reported by *E. coli* K12 (29–739 mg O₂ h⁻¹ g cell⁻¹) and *Rhodococcus erythropolis* IGTS8 (6.4–137 mg O₂ h⁻¹ g cell⁻¹) [37,38].

In this study, mercury II (20 ppm) inhibited the growth and oxygen uptake of strain MSR33 (Figures 3 and 4). Rojas et al. [10] observed that the addition of Hg II (8 ppm) during the exponential growth phase did not affect MSR33 cell growth. However, Hg II (8 ppm) stopped the growth of wild type strain *C. metallidurans* CH34. The minimum inhibitory concentration (MIC) of Hg (II) described under aerobic conditions for strains CH34 and MSR33 is 10 and 24 ppm, respectively [10,29]. The growth inhibition of strain MSR33 could be associated to the high mercury concentration (20 ppm) used in this study.

At the cellular level, the disruption of the oxygen uptake by mercury addition may be related to its effects on the respiratory chain. Mercury has been reported to alter membranes, reducing membrane transport and potential, affecting the respiratory chain, and producing oxidative stress [6,39]. Specifically, mercury affects sulfhydryl (cysteine) and thioester (methionine) residues of proteins and replaces other metals such as iron in metalloproteins, damaging the respiratory chain functioning at membranes in bacteria and eukaryotes [2,7–9,40]. Rojas et al. reported that Hg (II) (8 ppm) affects the membranes of *C. metallidurans* strain CH34, showing a fuzzy outer membrane [10]. *C. metallidurans* strains CH34 and MSR33 possess outer membrane and periplasmic sulfur-rich proteins such as CopA, CopB, CopC, CopK, and CopJ containing a significant number of methionine and cysteine amino acids, which has been proposed to be oxidized by heavy metals and participate in the reduction of gold (III) ions into Au (0) [7]. Hg (II) increases lipid peroxidation by the increase in H₂O₂ due to Fenton reactions in *Shewanella oneidensis* MR-1 under aerobic conditions, whereas lower lipoperoxidation was observed under anaerobiosis [41]. Mercury decreases the activity of photosystems cytochromes and quinones at the membrane in *Rhodobacter sphaeroides* [42]. Hg (II) decreases oxygen uptake and inhibits the electron transport chain and the oxidative phosphorylation in the mitochondria of fish liver cells [43].

Another factor that may contribute to the disruption of oxygen uptake and inhibition of growth by Hg (II) is the redirection of the NADPH cellular pool, from the synthesis of biomolecules and cell growth to the reduction of mercury and oxidative stress response. The reduction of Hg (II) to Hg (0) by strain MSR33 occurs in the cytosol where the mercury reductase (MerA) reduces Hg (II) into Hg (0) using 2 NADPH molecules [10,44]. The main damage caused by mercury is on the membranes but not in the cytoplasm [41]. The import of mercury (II) and its subsequent reduction are the key processes for detoxification. The exposure to Hg (II) induces the generation of reactive oxygen species (ROS) in bacteria and eukaryotes, which could decrease the NADPH levels in strain MSR33 even more [6,39,41,43]. Under oxidative stress, bacterial growth is arrested, whereas NADPH plays an important role for detoxifying ROS by the regeneration of reduced glutathione and thioredoxin, with a concomitant decrease in the NADPH pool [45,46]. A fast rerouting of the Embden–Meyerhof–Parnas pathway into the pentose phosphate pathway was observed in *E. coli* supplemented with glucose under oxidative stress, increasing the reduction rate of NADP⁺ to NADPH [47]. In our study, succinate was used as the sole carbon and energy source for strain MSR33 growth, suggesting a rerouting pathway for NADPH recycling. The pentose phosphate pathway, isocitrate dehydrogenase, malic enzyme,

and transhydrogenases reactions are probably involved in NADPH pool regeneration in strain MSR33 under these aerobic conditions. On the other hand, higher expression of the *mer* genes under aerobic conditions was observed in *Pseudomonas stutzeri* OX than under anaerobiosis [20]. We postulate that under aerobiosis, mercury (II) in strain MSR33 causes membrane and protein damage that affects the respiratory chain and the oxidative phosphorylation, induces the broad-spectrum *mer* genes, and promotes the redirection of the NADPH reducing power to the mercury-detoxifying and oxidative stress response mechanisms (Figure 6).

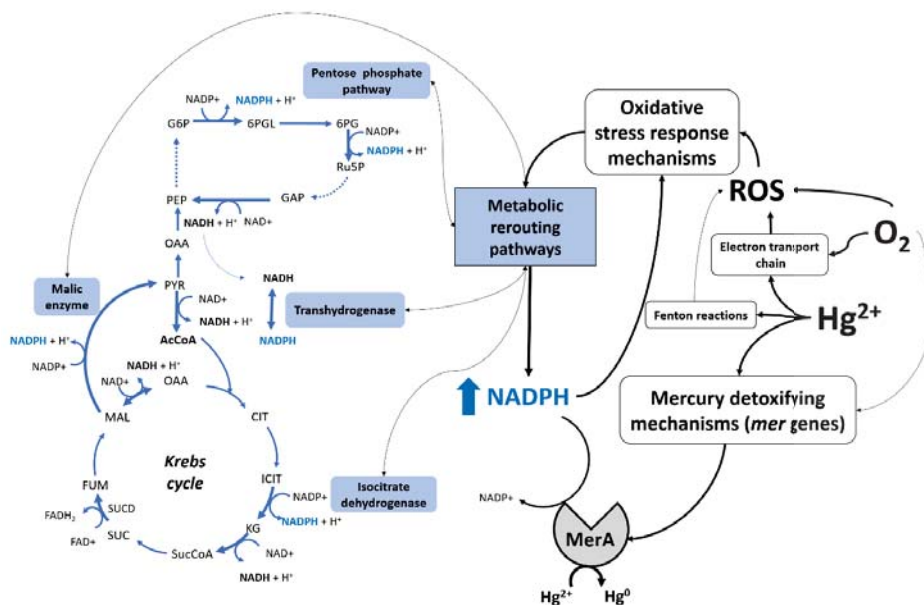


Figure 6. Proposed aerobic mercury detoxifying mechanisms in *C. metallidurans* MSR33. Mercury in presence of oxygen generate reactive oxygen species (ROS) through the electron transport chain and Fenton reactions. ROS activate oxidative stress response mechanisms that induce the rerouting of the metabolism, increasing the NADPH pool (blue letters) through the pentose phosphate pathway, malic enzyme, isocitrate dehydrogenase and transhydrogenase reactions (light blue squares). Mercury under aerobic conditions induces mercury detoxifying mechanisms through the expression of the *mer* genes. The mercuric reductase MerA reduces Hg (II) into Hg (0) using 2 NADPH. The NADPH pool is consumed during mercury reduction and oxidative stress response mechanisms. Abbreviations: SUC, succinate; SUCD, succinate dehydrogenase; FUM, fumarate; MAL, malate; OAA, oxaloacetate; CIT, citrate; ICIT, isocitrate; KG, α -ketoglutarate; SucCoA, succinylCoA; AcCoA, acetylCoA; PYR, pyruvate; PEP, phosphoenolpyruvate; G6P, glucose-6-phosphate; 6PGL, 6-phosphogluconolactone; 6PG, 6-phosphogluconate; Ru5P, Ribulose-5-phosphate; GAP, glyceraldehyde-3-phosphate.

In this study, the capability of strain MSR33 to re-establish the cell growth and the oxygen uptake after an initial inhibition by mercury (II) was observed, increasing the cellular biomass for mercury bioremediation. The response of strain MSR33 is based on the proteins encoded by the *mer* genes in the chromosome and pMOL28, pMOL30, and pTP6 plasmids that are associated with mercury resistance [10,29]. Strain MSR33 is capable of reducing Hg (II) and organomercurial compounds into a less toxic form (Hg 0), which enables detoxifying the environment surrounding the bacterium [26,44]. A high rate of mercury removal was observed after 1 h (Figure 5), indicating high mercury reduction by MSR33 MerA protein. The fast detoxifying response may be based on the mercury resistance genes' redundancy in strain MSR33, which allows the bacterium to restore cell growth and oxygen

uptake after the early inhibitory effects of mercury [10]. Due to the absence of oxygen uptake during exposure to mercury in a liquid medium, the kinetics of mercury removal were determined by strain MSR33 under aerobic conditions through the displacement of gases with an injection of air, and under anaerobic conditions by the injection of gaseous nitrogen (Figure 5). The results indicate that oxygen is required for an efficient removal of mercury, even though mercury inhibits oxygen uptake. Although, during aerobic mercury bioremediation, strain MSR33 stops consuming oxygen during initial mercury exposure, mercury probably induces the mercury reductase activity and the bacterium reroutes its metabolism towards the regeneration of the NADPH pool for the reduction of mercury (II) and to counteract ROS.

In this study, almost complete removal of mercury (II) (20 ppm) by *C. metallidurans* MSR33 was observed under aerobic conditions after 24 h. Rojas et al. [10] observed that strain MSR33 in the presence of thioglycolate reached a complete removal of mercury (II) (20 and 30 ppm) after 2 h in flasks of 250 mL (50 mL aqueous solution) with high aeration (6 vvm). In this study, the mercury removal after 24 h by strain MSR33 under aerobic conditions (97%) is higher than the 79% mercury (3.2 ppm) removal after 6 h by *Sphingobium* sp. SA2 and 88% of mercury (5 ppm) removal after 7 h by *Pseudomonas stutzeri* OX but similar to 92 to 98% mercury (40 ppm) removal after 24 h by *P. putida* PpY101/pSR134 [20,22,48].

Interestingly, the facultative anaerobe strain MSR33 was able to remove 71% Hg (II) (20 ppm) after 24 h under anaerobic conditions. The facultative anaerobe *Pseudomonas stutzeri* OX removes 84% mercury II (5 ppm) after 20 h under anaerobic conditions [20]. Anaerobic mercury reduction associated with methylation and demethylation by anaerobic obligate bacteria has been reported [49,50]. *G. bemidjensis* Bem and *G. sulfurreducens* PCA reduce mercury at low concentrations (1 ppb) under anaerobic conditions [25,26]. Anaerobiosis favors the formation of inorganic mercury sulfide, decreases ROS levels, and significantly reduces the NADPH pool regeneration [45,51]. *P. stutzeri* OX exhibited higher tolerance to Hg (II) under anaerobiosis than under aerobic conditions; anaerobiosis affects Hg (II) transport into the cell and, therefore, also the expression of the *mer* genes [20]. It has been reported that the synthesis of MerA and MerB proteins in *C. metallidurans* MSR33 is strongly induced by mercury [10]. Therefore, a lower mercury reduction under anaerobic conditions by strain MSR33 may be explained by (i) a decreased Hg (II) transport into the cell compared to aerobic conditions, which leads to a lower expression of *mer* genes, and (ii) a lower NADPH pool, which negatively affects the reduction of mercury by MerA in the cytoplasm. However, the higher mercury removal rates during the first hours of mercury exposure under anaerobic conditions could be associated with microaerobic conditions that may be generated inside the reactor by oxygen remnants at the beginning of the anaerobic phase. In this study, mercury (II) removal was performed at concentrations close to the MIC [10]. Mercury concentrations higher than the MIC could irreversibly affect the growth and detoxifying activity of strain MSR33 under aerobic conditions. However, under anaerobic conditions, *C. metallidurans* strain MSR33 may tolerate higher mercury concentration than *P. stutzeri* OX [20].

Mercury inhibits the metabolic activity of *C. metallidurans* MSR33. However, strain MSR33 is capable of tolerating mercury during mercury bioremediation and recovered its metabolic activity. Notably, strain MSR33 is able to remove mercury in solution under anaerobic conditions. Under anaerobic conditions, toluene degradation by *C. metallidurans* CH34 using nitrate as a terminal electron acceptor in bioelectrochemical systems has been reported [30]. The results of our present study confirm the bioremediation capability of *C. metallidurans* strain MSR33 under anaerobic conditions. In this study, nitrate was not included in the composition of the culture medium. Interestingly, facultative anaerobic bacteria including mercury-reducing strains may use fumarate as the electron acceptor, where fumarate reductase catalyzes this final step in anaerobic respiration [46,49,52]. The gene encoding this enzyme was reported in the *C. metallidurans* genome [53], therefore, we propose that fumarate could be the electron acceptor under these anaerobic conditions. Further studies on anaerobic mercury reduction are required to understand the molecular and metabolic mechanisms involved in mercury removal by strain MSR33 under anaerobiosis.

The results of this study indicate that *C. metallidurans* MSR33 is an attractive biocatalyst for mercury bioremediation of polluted water such as mine groundwater and industrial wastewater under aerobic and anaerobic conditions.

5. Conclusions

The defined GBC culture medium was designed in this study for improved growth of strain MSR33, which is limited by succinate as the only carbon and energy source. The MSR33 growth rate in the GBC medium increased up to eight times compared to growth rate values reported by previous studies of this strain.

Mercury inhibited the growth and respiratory rate of strain MSR33 in liquid medium under aerobic conditions. However, the growth and respiration inhibitions were reversed after 5 h. Notably, strain MSR33 was able to remove mercury in a liquid medium under anaerobic conditions but higher removal of mercury was observed under aerobic conditions than under anaerobiosis.

This study suggests that in spite of the fact that mercury (II) harms *C. metallidurans* MSR33 metabolic activity, this strain is able to remove mercury from contaminated water and to recover its metabolic activity after 5 h. Therefore, *C. metallidurans* MSR33 may be useful for mercury bioremediation in polluted water under aerobic and anaerobic conditions.

Author Contributions: G.B., J.C.G., and M.S. conceived and designed the experiments; G.B. and P.V.-C. performed the experiments; G.B., P.V.-C., J.C.G., and M.S. analyzed the data; J.C.G. and M.S. contributed reagents, materials, and analysis tools; G.B., P.V.-C., J.C.G. and M.S. wrote the paper. All authors have read and agreed to the published version of the manuscript.

Funding: This research was funded by PhD Conicyt, PUCV and USM (G.B., P.V.-C.) fellowships, ANID PIA Ring Genomics and Applied Microbiology for Bioremediation and Bioproducts (GAMBIO) ACT172128 Chile (M.S., G.B., P.V.-C.), Fondecup EQM 170914 (M.S., G.B.), Fondecyt 1200756 (M.S., P.V.-C.), PIIC USM (G.B., P.V.-C.), and USM (M.S., P.V.-C., G.B.) grants.

Acknowledgments: Fermentation Laboratory, School of Biochemical Engineering, Pontificia Universidad Católica de Valparaíso.

Conflicts of Interest: The authors declare no conflict of interest.

References

1. Nieboer, E.; Richardson, D.H. The replacement of the nondescript term 'heavy metals' by a biologically and chemically significant classification of metal ions. *Environ. Pollut. Ser. B Chem. Phys.* **1980**, *1*, 3–26. [[CrossRef](#)]
2. Tagliaferro, L.; Officioso, A.; Sorbo, S.; Basile, A.; Manna, C. The protective role of olive oil hydroxytyrosol against oxidative alterations induced by mercury in human erythrocytes. *Food Chem. Toxicol.* **2015**, *82*, 59–63. [[CrossRef](#)] [[PubMed](#)]
3. Yang, L.; Zhang, Y.; Wang, F.; Luo, Z.; Guo, S.; Strähle, U. Toxicity of mercury: Molecular evidence. *Chemosphere* **2020**, *245*, 125586. [[CrossRef](#)] [[PubMed](#)]
4. Patra, M.; Sharma, A. Mercury toxicity in plants. *Bot. Rev.* **2000**, *66*, 379–422. [[CrossRef](#)]
5. Streets, D.G.; Horowitz, H.M.; Jacob, D.J.; Lu, Z.; Levin, L.; Ter Schure, A.F.H.; Sunderland, E.M. Total mercury released to the environment by human activities. *Environ. Sci. Technol.* **2017**, *51*, 5969–5977. [[CrossRef](#)] [[PubMed](#)]
6. Spiller, H.A. Rethinking mercury: The role of selenium in the pathophysiology of mercury toxicity. *Clin. Toxicol.* **2017**, *56*, 313–326. [[CrossRef](#)] [[PubMed](#)]
7. Montero-Silva, F.; Durán, N.; Seeger, M. Synthesis of extracellular gold nanoparticles using *Cupriavidus metallidurans* CH34 cells. *IET Nanobiotechnol.* **2018**, *12*, 40–46. [[CrossRef](#)]
8. Xu, F.F.; Inlay, J.A. Silver(I), mercury (II), cadmium (II), and zinc (II) target exposed enzymic iron-sulfur clusters when they toxify *Escherichia coli*. *Appl. Environ. Microbiol.* **2012**, *78*, 3614–3621. [[CrossRef](#)]
9. Lemire, J.A.; Harrison, J.J.; Turner, R.J. Antimicrobial activity of metals: Mechanisms, molecular targets and applications. *Nat. Rev. Microbiol.* **2013**, *11*, 371–384. [[CrossRef](#)]

10. Rojas, L.A.; Yañez, C.; González, M.; Lobos, S.; Smalla, K.; Seeger, M. Characterization of the metabolically modified heavy metal-resistant *Cupriavidus metallidurans* strain MSR33 generated for mercury bioremediation. *PLoS ONE* **2011**, *6*, e17555. [[CrossRef](#)]
11. McCarthy, D.; Edwards, G.C.; Gustin, M.S.; Care, A.; Miller, M.B.; Sunna, A. An innovative approach to bioremediation of mercury contaminated soils from industrial mining operations. *Chemosphere* **2017**, *184*, 694–699. [[CrossRef](#)] [[PubMed](#)]
12. Hernández, M.; Morgante, V.; Ávila, M.; Villalobos, P.; Millares, P.; González, M.; Seeger, M. Novel s-triazine-degrading bacteria isolated from agricultural soils of central Chile for herbicide bioremediation. *Electron. J. Biotechnol.* **2008**, *11*, 5–6. [[CrossRef](#)]
13. Seeger, M.; Hernández, M.; Mendez, V.; Ponce, B.; Córdova, M.; González, M. Bacterial degradation and bioremediation of chlorinated herbicides and biphenyls. *J. Soil Sci. Plant Nutr.* **2010**, *10*, 320–332. [[CrossRef](#)]
14. Altimira, F.; Yañez, C.; Bravo, G.; González, M.; Rojas, L.A.; Seeger, M. Characterization of copper-resistant bacteria and bacterial communities from copper-polluted agricultural soils of central Chile. *BMC Microbiol.* **2012**, *12*, 193. [[CrossRef](#)] [[PubMed](#)]
15. Romero-Silva, M.J.; Méndez, V.; Agulló, L.; Seeger, M. Genomic and functional analyses of the gentisate and protocatechuate ring-cleavage pathways and related 3-hydroxybenzoate and 4-hydroxybenzoate peripheral pathways in *Burkholderia xenovorans* LB400. *PLoS ONE* **2013**, *8*, e56038. [[CrossRef](#)] [[PubMed](#)]
16. Fuentes, S.; Barra, B.; Caporaso, J.G.; Seeger, M. From rare to dominant: A fine-tuned soil bacterial bloom during petroleum hydrocarbon bioremediation. *Appl. Environ. Microbiol.* **2015**, *82*, 888–896. [[CrossRef](#)]
17. Aguirre, A.; Bernal, P.; Maureira, D.; Ramos, N.; Vásquez, J.; Urrutia, H.; Gentina, J.C.; Aroca, G. Biofiltration of trimethylamine in biotrickling filter inoculated with *Aminobacter aminovorans*. *Electron. J. Biotechnol.* **2018**, *33*, 63–67. [[CrossRef](#)]
18. Orellana, R.; Macaya, C.; Bravo, G.; Dorochesi, F.; Cumsille, A.; Valencia, R.; Rojas, C.; Seeger, M. Living at the frontiers of life: Extremophiles in Chile and their potential for bioremediation. *Front. Microbiol.* **2018**, *9*, 2309. [[CrossRef](#)]
19. Zhang, Z.; Wu, J.; Liu, D. Co₃O₄/g-C₃N₄ hybrids for gas-phase Hg⁰ removal at low temperature. *Processes* **2019**, *7*, 279. [[CrossRef](#)]
20. Schaefer, J.; Letowski, J.; Barkay, T. Mer-mediated resistance and volatilization of Hg (II) under anaerobic conditions. *Geomicrobiol. J.* **2002**, *19*, 87–102. [[CrossRef](#)]
21. Deckwer, W.-D.; Becker, F.U.; Ledakowicz, S.; Wagner-Döbler, I. Microbial removal of ionic mercury in a three-phase fluidized bed reactor. *Environ. Sci. Technol.* **2004**, *38*, 1858–1865. [[CrossRef](#)] [[PubMed](#)]
22. Mahbub, K.; Krishnan, K.; Megharaj, M.; Naidu, R. Bioremediation potential of a highly mercury resistant bacterial strain *Sphingobium* SA2 isolated from contaminated soil. *Chemosphere* **2016**, *144*, 330–337. [[CrossRef](#)] [[PubMed](#)]
23. Dash, H.R.; Basu, S.; Das, S. Evidence of mercury trapping in biofilm-EPS and *mer* operon-based volatilization of inorganic mercury in a marine bacterium *Bacillus cereus* BW-201B. *Arch. Microbiol.* **2016**, *199*, 445–455. [[CrossRef](#)]
24. Wang, X.; He, Z.; Luo, H.; Zhang, M.; Zhang, D.; Pan, X.; Gadd, G.M. Multiple-pathway remediation of mercury contamination by a versatile selenite-reducing bacterium. *Sci. Total Environ.* **2018**, *615*, 615–623. [[CrossRef](#)] [[PubMed](#)]
25. Hu, H.; Lin, H.; Zheng, W.; Tomanicek, S.J.; Johs, A.; Feng, X.; Elias, D.A.; Liang, L.; Gu, B. Oxidation and methylation of dissolved elemental mercury by anaerobic bacteria. *Nat. Geosci.* **2013**, *6*, 751–754. [[CrossRef](#)]
26. Lu, X.; Liu, Y.; Johs, A.; Zhao, L.; Wang, T.; Yang, Z.; Lin, H.; Elias, D.A.; Pierce, E.M.; Liang, L.; et al. Anaerobic mercury methylation and demethylation by *Geobacter bemi* strain Bem. *Environ. Sci. Technol.* **2016**, *50*, 4366–4373. [[CrossRef](#)] [[PubMed](#)]
27. Mergeay, M.; Nies, D.; Schlegel, H.G.; Gerits, J.; Charles, P.; Van Gijsegem, F. *Alcaligenes eutrophus* CH34 is a facultative chemolithotroph with plasmid-bound resistance to heavy metals. *J. Bacteriol.* **1985**, *162*, 328–334. [[CrossRef](#)]
28. Alviz-Gazitua, P.; Fuentes-Alburquenque, S.; Rojas, L.A.; Turner, R.; Guiliani, N.; Seeger, M. The response of *Cupriavidus metallidurans* CH34 to cadmium involves inhibition of the initiation of biofilm formation, decrease in intracellular c-di-GMP levels, and a novel metal regulated phosphodiesterase. *Front. Microbiol.* **2019**, *10*, 1499. [[CrossRef](#)]

29. Millacura, F.A.; Janssen, P.J.; Monsieurs, P.; Janssen, A.; Provoost, A.; Vanhoudt, R.; Rojas, L.A. Unintentional genomic changes endow *Cupriavidus metallidurans* with an augmented heavy-metal resistance. *Genes* **2018**, *9*, 551. [CrossRef]
30. Espinoza-Tofalos, A.; Daghighi, M.; González, M.; Papacchini, M.; Franzetti, A.; Seeger, M. Toluene degradation by *Cupriavidus metallidurans* CH34 in nitrate-reducing conditions and in bioelectrochemical systems. *FEMS Microbiol. Lett.* **2018**, *365*, fny119. [CrossRef]
31. Zhang, J.; Greasham, R. Chemically defined media for commercial fermentations. *Appl. Microbiol. Biotechnol.* **1999**, *51*, 407–421. [CrossRef]
32. Acevedo, A.; Conejeros, R.; Aroca, G. Ethanol production improvement driven by genome-scale metabolic modeling and sensitivity analysis in *Scheffersomyces stipites*. *PLoS ONE* **2017**, *12*, e0180074. [CrossRef] [PubMed]
33. Casas López, J.L.; Rodríguez Porcel, E.M.; Oller Alberola, I.; Ballesteros Martín, M.M.; Sánchez Pérez, J.; Fernández Sevilla, J.M.; Chisti, Y. Simultaneous determination of oxygen consumption rate and volumetric oxygen transfer coefficient in pneumatically agitated bioreactors. *Ind. Eng. Chem. Res.* **2006**, *45*, 1167–1171. [CrossRef]
34. AOAC Official Method 977.15 Mercury in Fish Alternative Flameless Atomic Absorption Spectrophotometric Method First Action 1977 Final Action 1978. Available online: http://www.aocofficialmethod.org/index.php?main_page=product_info&cPath=1&products_id=2383 (accessed on 24 July 2020).
35. Attalah, S.; Waller, P.; Steichen, S.; Gao, S.; Brown, C.; Ogden, K.; Brown, J. Application of deoxygenation-aeration cycling to control the predatory bacterium *Vampirovibrio chlorellavorus* in *Chlorella sorokiniana* cultures. *Algal Res.* **2019**, *39*, 101427. [CrossRef]
36. Cao, Y.; Zhang, R.; Sun, C.; Cheng, T.; Liu, Y.; Xian, M. Fermentative succinate production: An emerging technology to replace the traditional petrochemical processes. *BioMed Res. Int.* **2013**, *2013*, 1–12. [CrossRef]
37. Andersen, K.B.; Von Meyenburg, K. Are growth rates of *Escherichia coli* in batch cultures limited by respiration? *J. Bacteriol.* **1980**, *144*, 114–123. [CrossRef]
38. Garcia-Ochoa, F.; Gomez, E.; Santos, V.E.; Merchuk, J.C. Oxygen uptake rate in microbial processes: An overview. *Biochem. Eng. J.* **2010**, *49*, 289–307. [CrossRef]
39. Belyaeva, E.A.; Sokolova, T.V.; Emelyanova, L.V.; Zakharova, I.O. Mitochondrial electron transport chain in heavy metal-induced neurotoxicity: Effects of cadmium, mercury, and copper. *Sci. World J.* **2012**, *2012*, 136063. [CrossRef]
40. Norambuena, J.; Wang, Y.; Hanson, T.; Boyd, J.M.; Barkay, T. Low-molecular-weight thiols and thioredoxins are important players in Hg (II) resistance in *Thermus thermophilus* HB27. *Appl. Environ. Microbiol.* **2018**, *84*, e01931-17. [CrossRef]
41. Wang, Y.; Robison, T.; Wiatrowski, H. The impact of ionic mercury on antioxidant defenses in two mercury-sensitive anaerobic bacteria. *BioMetals* **2013**, *26*, 1023–1031. [CrossRef]
42. Asztalos, E.; Sipka, G.; Kis, M.; Trotta, M.; Maróti, P. The reaction center is the sensitive target of the mercury (II) ion in intact cells of photosynthetic bacteria. *Photosynth. Res.* **2012**, *112*, 129–140. [CrossRef] [PubMed]
43. Mieiro, C.; Pardal, M.; Duarte, A.C.; Pereira, E.; Palmeira, C. Impairment of mitochondrial energy metabolism of two marine fish by *in vitro* mercuric chloride exposure. *Mar. Pollut. Bull.* **2015**, *97*, 488–493. [CrossRef] [PubMed]
44. Dash, H.R.; Das, S. Bioremediation of mercury and the importance of bacterial *mer* genes. *Int. Biodeterior. Biodegrad.* **2012**, *75*, 207–213. [CrossRef]
45. Shimizu, K.; Matsuoka, Y. Redox rebalance against genetic perturbations and modulation of central carbon metabolism by the oxidative stress regulation. *Biotechnol. Adv.* **2019**, *37*, 107441. [CrossRef] [PubMed]
46. Bergkessel, M.; Basta, D.; Newman, D.K. The physiology of growth arrest: Uniting molecular and environmental microbiology. *Nat. Rev. Microbiol.* **2016**, *14*, 549–562. [CrossRef]
47. Christodoulou, D.; Kuehne, A.; Estermann, A.; Fuhrer, T.; Lang, P.F.; Sauer, U. Reserve flux capacity in the pentose phosphate pathway by NADPH binding is conserved across kingdoms. *iScience* **2019**, *19*, 1133–1144. [CrossRef]
48. Okino, S.; Iwasaki, K.; Yagi, O.; Tanaka, H. Development of a biological mercury removal-recovery system. *Biotechnol. Lett.* **2000**, *22*, 783–788. [CrossRef]
49. Colombo, M.J.; Ha, J.; Reinfelder, J.R.; Barkay, T.; Yee, N. Oxidation of Hg (0) to Hg (II) by diverse anaerobic bacteria. *Chem. Geol.* **2014**, *363*, 334–340. [CrossRef]

50. Ma, M.; Du, H.; Wang, D. Mercury methylation by anaerobic microorganisms: A review. *Crit. Rev. Environ. Sci. Technol.* **2019**, *49*, 1893–1936. [[CrossRef](#)]
51. Ercal, N.; Gurer-Orhan, H.; Aykin-Burns, N. Toxic metals and oxidative stress Part I: Mechanisms involved in metal-induced oxidative damage. *Curr. Top. Med. Chem.* **2001**, *1*, 529–539. [[CrossRef](#)]
52. Maklashina, E.; Berthold, D.A.; Cecchini, G. Anaerobic expression of *Escherichia coli* succinate dehydrogenase: Functional replacement of fumarate reductase in the respiratory chain during anaerobic growth. *J. Bacteriol.* **1998**, *180*, 5989–5996. [[CrossRef](#)] [[PubMed](#)]
53. Janssen, P.J.; Van Houdt, R.; Moors, H.; Monsieurs, P.; Morin, N.; Michaux, A.; Benotmane, M.A.; Leys, N.; Vallaey, T.; Lapidus, A.; et al. The complete genome sequence of *Cupriavidus metallidurans* strain CH34, a master survivalist in harsh and anthropogenic environments. *PLoS ONE* **2010**, *5*, e10433. [[CrossRef](#)] [[PubMed](#)]



© 2020 by the authors. Licensee MDPI, Basel, Switzerland. This article is an open access article distributed under the terms and conditions of the Creative Commons Attribution (CC BY) license (<http://creativecommons.org/licenses/by/4.0/>).

Article

A Novel Cysteine-Functionalized M_xO_y Material as Support for Laccase Immobilization and a Potential Application in Decolorization of Alizarin Red S

Agnieszka Kołodziejczak-Radzimska * and Teofil Jesionowski

Faculty of Chemical Technology, Institute of Technology and Chemical Engineering, Poznan University of Technology, Berdychowo 4, PL-60965 Poznan, Poland; teofil.jesionowski@put.poznan.pl

* Correspondence: agnieszka.kolodziejczak-radzimska@put.poznan.pl

Received: 9 June 2020; Accepted: 20 July 2020; Published: 23 July 2020

Abstract: Immobilization process improves the enzyme properties, like stability, activity, selectivity or specificity. In the study, a novel cysteine-functionalized M_xO_y (ZrO_2 , SiO_2) material was used as a support for the immobilization of laccase from *Trametes versicolor*. The proposed matrix was prepared using a simple sol-gel method. The cysteine was introduced during the synthesis of a sample. Additionally, the obtained supports were modified with glutaraldehyde. The basic properties of the prepared cysteine functionalized ZrO_2 and SiO_2 were determined using spectroscopic, thermal, porous, electrostatic and elemental analysis. Furthermore, the obtained biocatalytic systems were used as catalysts in the oxidation of sulfonic acid. Catalytic and kinetic parameters were determined based on the proposed model reaction. Next, laccase immobilized on ZrO_2 - and SiO_2 -based materials were, for the first time, utilized in the decolorization of Alizarin Red S. In that process, the influence of duration, pH and temperature on the efficiency of decolorization was evaluated. The results show that the proposed biocatalytic systems offer good specific activity (ca. 19 U/mg) and activity retention (ca. 77%). Importantly, they can be successfully used in the decolorization of Alizarin Red S with high efficiency (above 95%).

Keywords: L-cysteine; SiO_2 ; ZrO_2 ; laccase; catalysis; kinetic; decolorization

1. Introduction

The enzyme immobilization is a powerful tool in biocatalyst design, improving protein properties. A proper immobilization can increase stability and activity of enzyme under conditions far from the physiological ones, enzyme selectivity and specificity (using substrates far from the physiological ones), enzyme purity and sensitivity to inhibition, as well as resistance to chemicals. The support properties, the active group presence in the support and enzyme should be considered in immobilization protocol [1].

Cysteine ((R)-2-amino-3-mercaptopropionic acid, *Cys*) is a branched amino acid which contains three functional groups: thiol, amino and carboxyl. The thiol groups can be used to create supports with disulfide bonds. The thiol groups can form stable disulfide bonds; they may bind with metals by coordinate bonding or remain in reduced form [2,3]. Besides, thiol groups play an important role in the synthesis and functionality of metal nanoparticles, because of their high affinity to the particle surface [4]. Additionally, cysteine prevents the aggregation of nanoparticles and enables the attachment of enzymes on the particles' surface. The amino and carboxyl groups present in *Cys* are suitable for the immobilization of enzymes. Furthermore, because of the presence of thiol groups, cysteine is used in the pharmaceutical industry (for drug delivery) and the food industry (as a food additive) [5,6]. Cysteine as a natural antioxidant in several biological processes, including protein synthesis, metabolism, and detoxification. Due to its thiol groups, cysteine can easily be oxidized to

cystine, a dimeric amino acid. This reaction is reversible and allows the control of a wide range of biological activities and protein structures, and, therefore, the determination of cysteine in biological matrices and pharmaceutical preparation is highly important [5]. The cysteine is using in food chemistry as a reducing agent in production of French bread, crackers and cookies. The cysteine is effective in preventing browning of fruit juice during concentration. They also prevent the development of off-flavor in stored orange juice. In addition, in flavor chemistry, cysteine is an important source of sulfur in a variety of aromas [6].

Metal oxides (M_xO_y : SiO_2 , ZrO_2 , ZnO , Fe_2O_3 , Al_2O_3 , etc.) are commonly used as supports for the immobilization of enzymes because of their good thermal and chemical stability, in addition to excellent mechanical resistance [7–10]. These materials are easy to synthesize, which makes them relatively cheap. Moreover, the surface of M_xO_y particles can be modified by various groups, enabling the attachment of enzymes to the surface. The thiol groups present in cysteine have a strong tendency to be adsorbed onto the surfaces of certain metals [11]. According to reports in the literature, cysteine has been used for modifying nanoparticles of gold [12,13], silver [14,15], copper [16] and nickel [17]. Cysteine is also used in the synthesis or modification of nanoparticles which are then used as supports for enzymes. For example, Verma et al. [18] synthesized ZnO using L-cysteine, and then immobilized urease on the cysteine/ZnO nanoparticles. Results have also been reported concerning the modification of silica with cysteine and the use of the obtained material for immobilization of lipase [19]. Magnetic nanoparticles have also been functionalized with Cys and used as a support for xylose reductase [20]. Bezbradica et al. [21] prepared a matrix by chemical activation with cysteine and glutaraldehyde. The proposed support was used to immobilize four different molecules (trypsin, penicillin acylase G, lipase, and *E. coli* BL21 cell extract). In these studies, the immobilization is promoted through a two-step mechanism: in a first step, the enzyme is adsorbed on the support via an anionic exchange mechanism and, then, the covalent immobilization occurs. Immobilization on standard amino support activated with glutaraldehyde is usually via a first ionic exchange, then the covalent bonds may be produced. This is, in fact, a heterofunctional support [22,23]. In most cases, the imine linkage is formulated between glutaraldehyde-activated support and amino groups of enzyme, which should be later reduced to strengthen the linkage. However, most of the proteins are immobilized at neutral pH on glutaraldehyde-activated supports because imine in aqueous medium is unstable and the equilibrium enzyme support is shifted to the dissociated form. According to this, the linkages on glutaraldehyde-activated supports are performed through the reaction with cyclized forms of the glutaraldehyde. This may cause that linkages are more stable than the imines [24,25]. Additionally, the surface of the support functionalized with cysteine is positively and negatively charged. If that surface is activated with glutaraldehyde, the mixed anionic/cationic exchange between enzyme and support takes place [26]. However, it also should be mentioned that, if the support has primary amino groups, and is modified with glutaraldehyde, the covalent bonds can also take place [27,28].

Dyes are organic, colored compounds which are capable of dyeing animal fibers (wool, silk), plant fibers (cotton, flax), leather, etc. The color of organic dyes depends on the presence in the molecule of chromophores (responsible for color formation) and auxochromes (electron donors which also increase the color by improving the solubility and adhesion of the dye to the fiber) [29,30]. Organic dyes are classified as chemical (e.g., nitro, anthraquinone, indigoid) and technical (e.g., acid, basic, vat, and reactive) [31]. Organic dyes are among the most significant contaminants of wastewater, because of their extensive use in numerous industries [32]. Alizarin Red S (ARS) is a 3-substituted derivative of 1,2-dihydroxy-9,10-anthraquinone, which belongs to the group of most durable dyes in textile wastewaters. That dye is water soluble and has application in histological studies to identifying calcium in tissues and vital staining of bone. The ARS can induce structural and functional changes to serum albumins [33]. The research show that ARS are also introduced adverse effects to organisms, such as oxidative damages. Moreover, other experimental show that anthraquinone and its sulfonated derivatives could cause cytotoxicity, genotoxicity and DNA strand breakage [34]. Many methods

are used for the degradation and decolorization of dyes. These methods can be divided into three categories: physical methods (nano-filtration, reverse osmosis, electrodialysis) [35], sorption techniques (photochemical, electrochemical destruction) [36] and biological methods (enzymatic degradation) [37]. Biological methods have low running costs, produce stable and harmless final products, and also require fewer chemicals and less energy than physical and chemical methods. Furthermore, enzymatic degradation complies with the principles of green technology [38]. Immobilized enzymes, especially oxidoreductases (laccases and peroxidases), are used to improve decolorization methods. Many dyes—for example, Acid Blue, Reactive Blue, Remazol Brilliant R, Direct Red etc.—have been decolorized using immobilized laccase. For this purpose, MOFs, bacterial nanocellulose, electrospun fibers and graphene oxide have been utilized as supports for the immobilization of laccase [39–42]. Besides the laccase, the different peroxidases were also successfully used to decolorize organic dye-based wastewaters [43–45].

In this study, we propose a novel cysteine-functionalized M_xO_y material as a support for enzyme immobilization. The materials used are SiO_2 and ZrO_2 , prepared by the sol-gel method. Cysteine was applied in situ, that is, during the sol-gel synthesis. Additionally, the obtained material was activated with glutaraldehyde to improve the attachment of laccase to the material surface. Next, laccase from *Trametes versicolor* (light, brown powder with activity above 0.5 U/mg) was immobilized on the cysteine-functionalized M_xO_y by a simple adsorption method. The research included evaluation of physicochemical properties (Fourier-transform infrared spectroscopy, thermogravimetric, porous structure, zeta potential and elemental analysis) and catalytic properties (relative activity, kinetic parameters, influence of pH, temperature, storage and reuse on enzymatic activity). The obtained biocatalytic system was also tested in the decolorization of an organic dye (Alizarin Red S).

2. Materials and Methods

2.1. Materials

Sol-gel method: tetraethyl orthosilicate (TEOS), zirconium isopropoxide (ZIP), NH_{3aq} (25%), ethanol, isopropanol, L-cysteine (Cys), HCl. Immobilization process: glutaraldehyde (GA), laccase from *Trametes versicolor* (Lac), buffers: acetate (0.1 M; pH = 2–5), phosphate (0.1 M; pH = 6–8) and TRIS (0.1 M; pH = 9–10), Bradford reagent, 2,2-azino-bis(3-ethylbenzothiazoline-6-sulfonic acid) (ABTS). Decolorization of dyes: Alizarin Red S (ARS). All materials were purchased from Sigma-Aldrich® (St. Louis, MO, USA).

2.2. Synthesis of L-Cysteine-Functionalized M_xO_y

The metal oxides (SiO_2 and ZrO_2) were synthesized by a sol-gel method. In the first stage, an appropriate alcohol (ethanol for SiO_2 and isopropanol for ZrO_2) was introduced into a reactor. Next, the organic precursor (TEOS for SiO_2 and ZIP for ZrO_2) and the promotor of hydrolysis (NH_{3aq}) were dosed. Then L-cysteine (10% wt./wt., in 1 M of HCl) was added. The components were mixed for 1 h (at ambient temperature) and left to age for 48 h. The synthesized materials were dried at 105 °C for 12 h. Finally, the obtained powder was washed several times using distilled water and alcohol, and the prepared materials were again dried (12 h, 105 °C). As a result, the systems SiO_2_Cys and ZrO_2_Cys were obtained. The precise information regarding sol-gel synthesis is presented in Table 1.

Table 1. Details information about reagents composition used in sol-gel synthesis of M_xO_y system.

ZrO_2	SiO_2
Isopropanol—250 mL	Ethanol—100 mL
ZIP—60 mL	TEOS—17 mL
NH_{3aq} —30 mL	NH_{3aq} —11 mL

In the next step, SiO_2_Cys and ZrO_2_Cys were activated with glutaraldehyde (5% in pH = 7 buffer) for 24 h. This led to the systems $SiO_2_Cys_GA$ and $ZrO_2_Cys_GA$.

The four kind of supports (SiO₂_Cys; SiO₂_Cys_GA, ZrO₂_Cys and ZrO₂_Cys_GA) were used in the next step of research.

2.3. Immobilization of Laccase from *Trametes Versicolor* and Bradford Analysis

Immobilization of laccase from *Trametes versicolor* was led by adsorption and covalent method. The support (0.5 g of SiO₂_Cys; SiO₂_Cys_GA; ZrO₂_Cys and ZrO₂_Cys_GA) was added to the laccase solution (25 mL of solution with the concentration of 5 mg/mL in 0.1 M buffer at pH = 4). The immobilization process took place for 3 h at 25 °C in an incubator (IKA-Werke, Staufen, Germany). Bradford analysis was used to calculate the quantity of immobilized enzyme [46]. The quantity of immobilized enzyme (mg/g_{support}) is determined from the difference between the initial amount of enzyme and the final laccase concentration in the mixture after immobilization. The calculation was made relative to the mass of the support. The quantity of immobilized laccase (*P*) and immobilization yield (*IY*) were calculated using Equations (1) and (2):

$$P = \frac{(C_0 - C_1) \times V}{m} \quad (1)$$

$$IY = \frac{C_1}{C_0} \times 100 \quad (2)$$

where C₀ and C₁ denote the concentration of the enzyme (mg/mL) in solution before and after immobilization, respectively, V is the volume of solution (mL), and m is the mass of support (g). The following four biocatalytic systems were prepared: SiO₂_Cys_Lac; SiO₂_Cys_GA_Lac; ZrO₂_Cys_Lac and ZrO₂_Cys_GA_Lac.

2.4. Physicochemical Characterization

Spectroscopic, thermogravimetric, porous structure, zeta potential and elemental analysis were applied to characterize the samples obtained during the study.

The pure supports (ZrO₂_Cys, ZrO₂_Cys_GA, SiO₂_Cys and SiO₂_Cys_GA) were evaluated by means of thermal and elemental analysis. Thermogravimetric analysis (TG/DTG) was performed using a Jupiter STA 449F3 thermogravimetric analyzer (Netzsch, Selb, Germany). A sample (ca. 5 mg) was heated in a nitrogen atmosphere in the temperature range 30–1000 °C.

Contents of carbon, nitrogen, hydrogen and sulfur were evaluated to confirm the effectiveness of modification with cysteine. For this purpose, the Vario EL Cube apparatus (Elementar Analysensysteme, Langenselbold, Germany) was used. The analyzed sample (ca. 20 mg) was combusted in an oxygen atmosphere. After passing through a reduction tube, the resulting gases were separated in an adsorption column, and then recorded using a detector. The results are given as averages of three measurements, each accurate to 0.0001%.

Other analyses were used to characterize samples obtained before and after immobilization. Spectroscopic analysis was performed based on FTIR spectra obtained using a Vertex 70 spectrometer (Bruker, Billerica, MA, USA). The analyzed sample had the form of a tablet, made by pressing a mixture of anhydrous KBr (ca. 0.25 g) and 0.001 g of the analyzed material in a special steel ring under a pressure of 10 MPa.

Basic porous structure parameters of prepared samples were determined using an ASAP 2020 instrument (Micromeritics Instrument Co., Norcross, GH, USA). Before the analysis, all samples were degassed (support at 120 °C and biocatalytic system at 70 °C) for 4 h prior to measurement. Next, based on low-temperature N₂ sorption the analysis was carried out. Using the BET (Brunauer–Emmett–Teller) and BJH (Barrett–Joyner–Halenda) methods, the surface area (*A_{BET}*), total pore volume (*V_p*) and mean pore diameter (*S_p*) were assessed. Due to the high accuracy of the instrument used, surface area was determined to an accuracy of 0.1 m²/g, pore volume to 0.01 cm³/g, and pore size to 0.01 nm.

Additionally, the zeta potential and isoelectric point (IEP) were evaluated using the LDV (Laser Doppler Velocimetry) technique, and calculated based on the Henry equation. These parameters were determined using a Zeta Nano ZS equipped with an MPT-2 automatic titration system (Malvern Instruments Ltd., Malvern, Worcester, UK). For the measurement, 0.01 g of the sample was dispersed in 25 mL of sodium chloride solution. Titration was performed with 0.2 M solutions of HCl and NaOH. The standard deviation of the zeta potential measurement was 61.5 mV. The apparatus measures a single zeta potential 30 times at defined pH, and the average value is used as the final result. The standard deviation of the pH value measurement was 0.1.

2.5. Catalytic Properties

The influence of pH, temperature, storage stability and reusability on the catalytic activity of a biocatalytic system is the most important information describing an immobilized enzyme. The influence of temperature was tested in the range 30–70 °C, and the influence of pH in the range 3–7. Storage stability was evaluated after 30 days (the immobilized enzyme was stored in a pH = 4 buffer at 4 °C). Reusability is the most important parameter for an immobilized enzyme; thus, the relative activity was investigated after 10 cycles. For clearer presentation of the data, in these experiments, the highest activity of free and immobilized laccase was defined as 100% activity. All of the above parameters were determined based on the reaction of oxidation of ABTS. In this case, 10 mg of free or immobilized laccase was added to 20 mL of 0.1 mM ABTS. The reaction was carried out for 20 min at 40 °C. Next, the mixture was centrifuged, and the absorbance was measured at $\lambda = 420$ nm (V-750 spectrophotometer, Jasco, Oklahoma City, OK, USA). The required parameters to define the immobilization process were determined [47]. The apparent activity of laccase was defined as the quantity of enzyme which oxidized 1 μ M of ABTS per minute per 1 g of support. The activity retention and specific activity of laccase immobilized on the support were calculated according to Equations (3) and (4):

$$A_R = \frac{A_{S1}}{A_{S0}} \times 100\% \quad (3)$$

$$A_S = \frac{A_{Ap}}{P} \quad (4)$$

where A_R —retention activity (%); A_S —specific activity (U/mg_{enzyme}); A_{S1} —specific activity of immobilized Lac (U/mg); A_{S0} —specific activity of free Lac (U/mg); A_{Ap} —apparent activity (U/g_{support}); P —amount of immobilized Lac (mg/g).

Additionally, the kinetic parameters (K_M , the Michaelis-Menten constant; and V_{max} , the maximum reaction rate) were evaluated based on the above-mentioned ABTS oxidation reaction and calculated using Hanes–Woolf plots. In this process, various concentrations of the ABTS solution (0.005–1.5 M) were used.

All measurements were made in triplicate. Results are presented as mean \pm 3.0 SD.

2.6. Decolorization of Alizarin Red S

A process of decolorization of Alizarin Red S dye was carried out using the four prepared biocatalytic systems. For this purpose, 100 mg of each of the biocatalytic systems was placed in 10 mL of Alizarin Red S dye solution (50 mg/mL; pH = 7). The process was performed at 30 °C for 24 h. The influence of time (0.5, 1, 3, 6, 9, 12, 24 h), temperature (25–70 °C) and the pH of the environment (2–9) on the effect of decolorization of the dye was determined. During these tests, differences in pH in absence of enzyme did not influence dye decolorization. Each experiment was carried out in triplicate, and the results are presented as average values.

After each of the above-mentioned experiments the absorbance of the resulting solution was measured ($\alpha = 464 \text{ nm}$; V-750 spectrophotometer, Jasco, Oklahoma City, OK, USA). The efficiency of decolorization of the dye was calculated based on the value of absorbance and using Equation (5):

$$ED = \frac{C_B - C_A}{C_B} \times 100\% \quad (5)$$

where ED is the efficiency of decolorization of ARS; C_B and C_A are the concentrations of ARS dye before and after the decolorization process, respectively.

3. Results

3.1. Thermogravimetric and Elemental Analysis of Pure Supports (ZrO_2 -Cys, ZrO_2 -Cys_GA, SiO_2 -Cys and SiO_2 -Cys_GA)

The materials used as supports for the immobilization of enzymes should have high thermal stability. Thermogravimetric analysis is one of the methods of evaluating the thermal stability of materials. The TG/DTG curves of pure cysteine show that this material has low thermal stability (Figure 1a,b). Two mass losses are observed: the first at ca. 200 °C related to physically adsorbed water, and the second at ca. 400 °C corresponding to the release of crystallization water. Zirconium and silica oxides offer good thermal stability [48]. As shown in Figure 1, all of the materials prepared in this study have high thermal stability. A mass loss of 20% was observed over the whole analyzed temperature range (30–1000 °C) for ZrO_2 -Cys (Figure 1a). An additional mass loss at 900 °C was observed for the ZrO_2 -Cys_GA system, probably associated with the thermal decomposition of glutaraldehyde. For SiO_2 -Cys and SiO_2 -Cys_GA, the mass loss was smaller than in the case of the zirconium materials. In this case the total mass loss was 10% over the analyzed range of temperatures (30–1000 °C). To summarize these results, it was found that the proposed cysteine-functionalized ZrO_2 or SiO_2 materials are suitable for use as supports in the immobilization of enzymes.

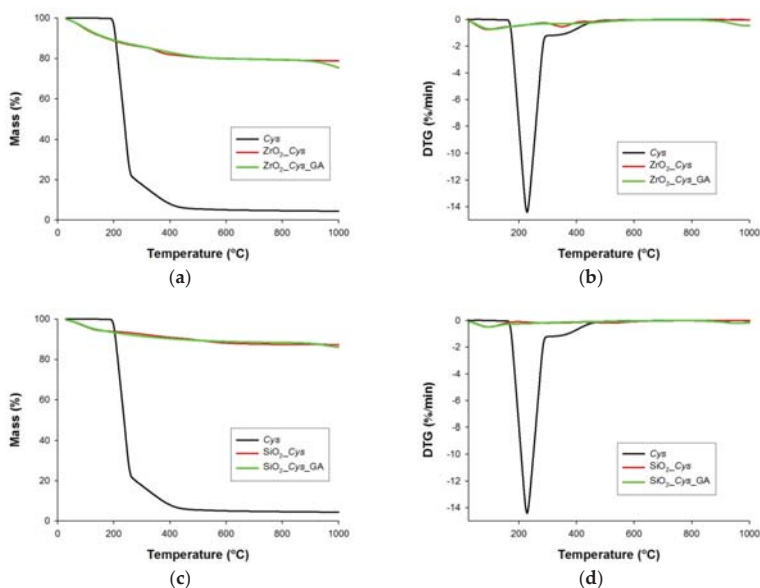


Figure 1. Thermogravimetric curves and their first derivatives (DTG). (a,c) ZrO_2 -Cys and ZrO_2 -Cys_GA; (b,d) SiO_2 -Cys and SiO_2 -Cys_GA.

Moreover, contents of N, C, H and S were determined to confirm the functionalization with cysteine and glutaraldehyde. The results are given in Table 2. To confirm the effectiveness of the modification, the table also provides data for pure ZrO_2 and SiO_2 . An analysis of these data shows that the modification with cysteine and glutaraldehyde was successful. The contents of N, C and S increased for the sample with Cys and GA. The systems ZrO_2_Cys and $ZrO_2_Cys_GA$ have higher contents of nitrogen, carbon and sulfur (N = 0.49%, C = 3.32% and S = 2.18%; N = 0.49%, C = 4.46% and S = 2.14%, respectively) than SiO_2_Cys and $SiO_2_Cys_GA$ (N = 0.07%, C = 1.01% and S = 0.12%; N = 0.09%, C = 1.57% and S = 0.11%, respectively). These results show that functionalization with Cys and GA was more effective for ZrO_2 -based samples.

Table 2. Content of N, C, H and S in the analyzed samples.

Sample Name	N	C	H	S
	(%)			
ZrO_2	0.05	1.09	2.60	0.15
ZrO_2_Cys	0.49	3.32	2.63	2.18
$ZrO_2_Cys_GA$	0.49	4.46	2.61	2.14
SiO_2	0.04	0.15	1.67	0.08
SiO_2_Cys	0.07	1.01	1.68	0.12
$SiO_2_Cys_GA$	0.09	1.57	1.40	0.11

3.2. Spectroscopic, Porous and Zeta Potential Analysis of Samples before and after Immobilization

FTIR analysis is one of the most common methods used to identify the characteristic groups present in samples. In this study, samples were evaluated by this method both before and after immobilization. The FTIR spectra are shown in Figure 2, and the characteristic groups are summarized in Table 3. The amino (N–H; 3215 cm^{-1}), thiol (S–H; 2550 cm^{-1}) and carboxyl (C–O; 1585 cm^{-1}) groups are observed in cysteine (Figure 2a,c). Moreover, ZrO_2_Cys and $ZrO_2_Cys_GA$ contain several groups appearing at $3180\text{--}3650$ (N–H and O–H), 1610 (C–O), under 1000 (Zr–O, Zr–OH and Zr–O–Zr) and 2845 cm^{-1} (C–H; only for the sample with GA) (Figure 2a). Furthermore, N–H (3450 cm^{-1}), C–H (2960 cm^{-1}) and amide I, II and III (1620 , 1480 and 1320 cm^{-1} , respectively) groups are present in the enzyme structure (Figure 2b,d). The systems with laccase immobilized on ZrO_2_Cys and $ZrO_2_Cys_GA$ contain groups characteristic of both the support and free laccase. The most characteristic bands on the FTIR spectrum of $ZrO_2_Cys_Lac$ appear at 1615 , 1492 and 1334 cm^{-1} , corresponding to amide I, II and III, respectively. However, $ZrO_2_Cys_GA_Lac$ contains only amide I and III (1616 and 1328 cm^{-1}). A similar situation is found for the SiO_2 -based materials. Signals for N–H and O–H ($3176\text{--}3578\text{ cm}^{-1}$), C–O (1622 cm^{-1}), Si–O, Si–O–Si ($>1000\text{ cm}^{-1}$) and C–H (2875 cm^{-1}) can be identified on the spectra of SiO_2_Cys and $SiO_2_Cys_GA$. However, the $SiO_2_Cys_Lac$ and $SiO_2_Cys_GA_Lac$ spectra contain, besides the characteristic groups for the support, only a small peak at 1624 cm^{-1} corresponding to the amide I band. Based on the FTIR results, the effectiveness of immobilization of laccase can be partially confirmed. Changes in the range $1650\text{--}1310\text{ cm}^{-1}$ (corresponding to amide I, II and III) confirmed the presence of laccase molecules on the cysteine-functionalized zirconia and silica materials.

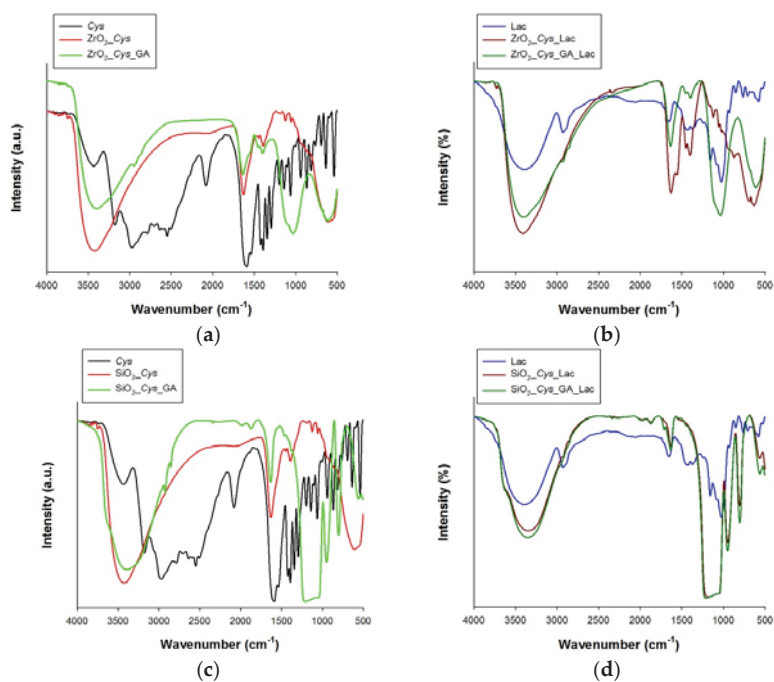


Figure 2. FTIR spectra of samples before (a,c) and after (b,d) immobilization of laccase.

Table 3. Characteristic groups present in cysteine, laccase, and samples before and after immobilization of laccase.

Sample	Characteristic Groups	Wavenumber (cm ⁻¹)
Cys	N-H	3215
	S-H	2550
	C-O	1585
Lac	N-H	3450
	C-H	2960
	Amide I, II and III	1620, 1480 and 1320
ZrO ₂ _Cys	N-H, O-H	3180–3650
	C-O	1610
	Zr-O, Zr-O-Zr	>1000
ZrO ₂ _Cys_GA	C-H	2845
ZrO ₂ _Cys	Amide I, II and III	1615, 1492 and 1334
ZrO ₂ _Cys_GA	Amide I and III	1616 and 1328
SiO ₂ _Cys	N-H, O-H	3176–3578
	C-O	1622
	Si-O, Si-O-Si	>1000
SiO ₂ _Cys_GA	C-H	2875
SiO ₂ _Cys_Lac	Amide I	1624
SiO ₂ _Cys_GA_Lac		

The porosity of materials also plays an important role in enzyme immobilization. A classical method of immobilization is adsorption. Materials may be potential supports if they have a well-developed porous structure. In Table 4, the basic porous parameters (surface area, maximum pore volume and mean pore diameter) are shown. The ZrO₂_Cys and ZrO₂_Cys_GA systems have large surface areas of

295 and 262 m²/g, respectively. After immobilization the surface area decreased, attaining values of 292 m²/g for ZrO₂_Cys_Lac and 146 m²/g for ZrO₂_Cys_GA_Lac. This is probably associated with the attachment of laccase to the support surface and the blocking of pores. The SiO₂-based materials (SiO₂_Cys and SiO₂_Cys_GA) have smaller surface areas (20 and 17 m²/g) than the ZrO₂-based materials. However, the surface area again decreased after immobilization. In this case, the pore diameter was also reduced after immobilization, which may be related to the deposition of laccase inside the pores.

Table 4. Porous parameters of samples before and after immobilization of laccase.

Sample	A_{BET} (m ² /g)	V_p (mL/g)	S_p (nm)
ZrO ₂ _Cys	295	0.032	1.9
ZrO ₂ _Cys_Lac	292	0.034	1.9
ZrO ₂ _Cys_GA	262	0.029	1.9
ZrO ₂ _Cys_GA_Lac	146	0.026	1.9
SiO ₂ _Cys	20	0.018	4.2
SiO ₂ _Cys_Lac	16	0.007	2.1
SiO ₂ _Cys_GA	17	0.006	2
SiO ₂ _Cys_GA_Lac	13	0.006	2.1

In the final part of the physicochemical analysis, the zeta potential (ζ) and isoelectric point (IEP) were determined (Figure 3). Based on the zeta potential values, the electrostatic interactions between the enzyme and support were investigated. The value of ζ for ZrO₂_Cys at all analyzed pH (2–10) is between 40 and –50 mV, with the isoelectric point at 4.57 (Figure 3a). Small changes in the zeta potential are observed after the immobilization of laccase on ZrO₂_Cys (ZrO₂_Cys_Lac), and the isoelectric point of ZrO₂_Cys_Lac occurs at pH = 4.00. Analyzing the zeta potential and isoelectric point values of ZrO₂_Cys_GA (before and after immobilization) no significant changes were observed (Figure 3b). A similar situation was found for the samples based on SiO₂, before and after immobilization of laccase. However, the zeta potential of the proposed biocatalytic systems is more negative. This is associated with the slipping plane, which is slightly stronger after the immobilization of laccase onto cysteine-functionalized ZrO₂ and SiO₂ materials [49,50].

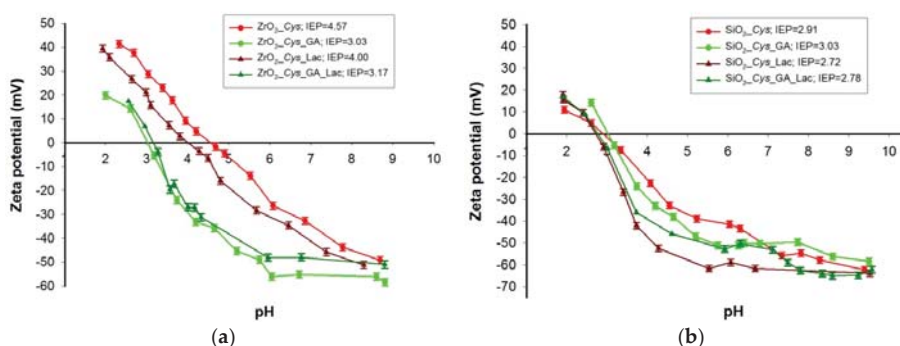


Figure 3. Zeta potential values as a function of pH for samples based on (a) ZrO₂ and (b) SiO₂ before and after immobilization.

Based on the FTIR, BET and potential zeta results, a mechanism for the immobilization of laccase on cysteine-functionalized M_xO_y (activated or not with glutaraldehyde) was proposed and presented in Figure 4. The results from FTIR and zeta potential analysis suggest that the immobilization of laccase on M_xO_y_Cys without glutaraldehyde take place through non-specific forces such as Van der Waals

and electrostatic interactions. Whereas, the activation of $M_xO_y_Cys$ with glutaraldehyde is usually via a first ionic exchange. Then the immobilization by covalent bonds is possible. In addition, the surface of cysteine-functionalized M_xO_y is positively and negatively charged. When that surface is activated with glutaraldehyde, the mixed anion/cationic exchange takes place [26]. On the other hand, the changes in porous structure observed after immobilization suggest that enzyme was adsorbed inside the pores of support.

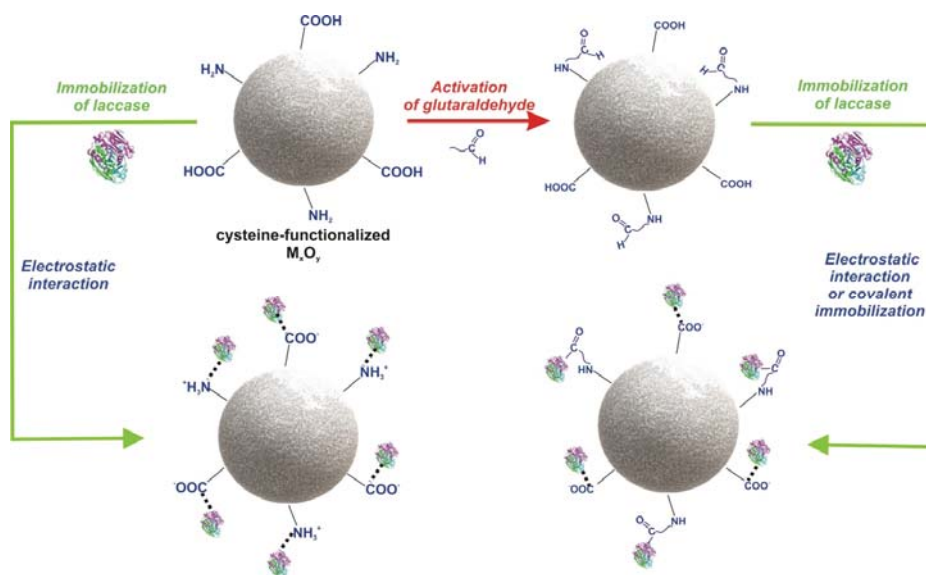


Figure 4. A suggested mechanism of immobilization of laccase onto cysteine-functionalized M_xO_y .

3.3. Catalytic Properties of the Obtained Biocatalytic Systems

Catalytic parameters of the prepared biocatalytic systems are presented in Table 5. These data show that the highest quantity of laccase was immobilized on ZrO_2_Cys (250 mg per 1 g of support), while for the other systems the quantities of immobilized enzyme were smaller (212–225 mg/g). In all cases, the immobilization yield is in the range 94–99%. The activity of biocatalytic systems determines their possible applications. The specific activity of the $ZrO_2_Cys_Lac$ biocatalytic system was found to be 19.3 U/g, compared with 25 U/mg for free laccase. This means that the immobilized laccase ($ZrO_2_Cys_Lac$) retained about 77% of the initial activity. The system $ZrO_2_Cys_GA_Lac$ had slightly lower specific activity (13.5 U/mg) and activity retention (ca. 54%). The activity of laccase immobilized on $ZrO_2_Cys_GA$ is lower than in the case of ZrO_2_Cys , because the modification with glutaraldehyde has an impact on both the enzyme structure and the enzymatic activity. For the other biocatalytic systems, significantly smaller values were obtained (0.6 U/mg and 2.6% for $SiO_2_Cys_Lac$; 7.1 U/mg and 28.5% for $SiO_2_Cys_GA_Lac$). Table 5 also contains kinetic parameters of the obtained biocatalytic systems, which indicate the affinity of laccase to its substrate. The Michaelis constant (K_M) for the laccase immobilized on ZrO_2 -based materials (0.11–0.14 mM) is smaller than the value for free laccase (0.18 mM). Changes are also observed for the maximum retention velocity (V_{max}). The V_{max} values for laccase immobilized on cysteine-functionalized ZrO_2 were higher (0.095 mM/s for $ZrO_2_Cys_Lac$; 0.031 mM/s for $ZrO_2_Cys_GA_Lac$) than the value for free laccase (0.027 mM/s). These results indicate a slightly higher substrate affinity in the case of the immobilized biomolecules. The kinetic parameters of $SiO_2_Cys_Lac$ and $SiO_2_Cys_GA_Lac$ are similar to those of the free enzyme. Similar results were obtained by Qiu et al. [51], which immobilized laccase onto inorganic mesoporous silica and

natural organic polymer like chitosan using functional ionic liquid as bridging agent (SBA-CIL-CS). Kinetic parameters measurement showed that the SBA-CIL-CS-Lac had the outstanding affinity to the substrate.

The values of catalytic properties show that the kinetic parameters are changed after the immobilization process. The changes in kinetic parameters are caused by the transformations of the protein structure and the immobilization methods. Furthermore, a decrease in K_M leads to an increase in the enzyme's affinity to the substrate. This probably occurs when the electric charges on the support and substrate are of different sign [52,53].

Table 5. Catalytic and kinetic parameters describing the biocatalytic systems.

Sample	P (mg/g)	IY (%)	A_S (U/mg)	A_R (%)	K_M (mM)	V_{max} (mM/s)
Free Lac	-	-	25 ± 1.6	-	0.18 ± 0.024	0.027 ± 0.012
ZrO ₂ _Cys_Lac	250 ± 5.6	99.9 ± 0.7	19.3 ± 1.5	77.2 ± 2.8	0.11 ± 0.021	0.095 ± 0.011
ZrO ₂ _Cys_GA_Lac	225 ± 5.4	97.5 ± 0.7	13.5 ± 1.4	53.8 ± 2.5	0.14 ± 0.022	0.031 ± 0.013
SiO ₂ _Cys_Lac	216 ± 5.3	95.6 ± 0.6	0.6 ± 0.3	2.6 ± 0.8	0.17 ± 0.023	0.028 ± 0.010
SiO ₂ _Cys_GA_Lac	212 ± 5.3	94.5 ± 0.6	7.1 ± 1.1	28.5 ± 1.9	0.18 ± 0.022	0.029 ± 0.011

The immobilized enzymes are less sensitive to pH and temperature changes, retain high activity after many days of storage, and can be used in several reaction cycles. Figure 5 shows the influence of pH, temperature, storage stability and reusability on the activity of free and immobilized laccase. All of the biocatalytic systems obtained in this study retain good activity under various chemical and thermal conditions. Furthermore, good activity is retained after a number of days of storage and after several reaction cycles. The ZrO₂_Cys_Lac and ZrO₂_Cys_GA_Lac systems maintain residual activity above 40% at all analyzed pH and temperature values. Furthermore, ZrO₂_Cys_Lac retains high (above 90%) activity after 30 days of storage and after 10 reaction cycles. Laccase immobilized on SiO₂_Cys_GA exhibits slightly lower activity (above 60%) in the same conditions. It preserves about 20–30% of its initial activity at pH = 3–7 and ca. 40% at temperatures of 30–70 °C. Its activity after 30 days of storage and after 10 reaction cycles is only 30–40% and 50–60%, respectively.

Table 6 summarizes the above results together with the results of other studies in which different cysteine-functionalized supports were used to immobilize various enzymes. The table shows that the results obtained using cysteine-functionalized ZrO₂ and SiO₂ materials as supports for laccase are satisfactory compared with the other results. As shown, cysteine has been used to modify Ag, Cu, ZnO and poly(glycidyl methacrylate)-SiO₂, utilized as supports for alkaline phosphatase, urease and lipase, respectively [15,16,18,19]. Upadhyay et al. [15] proposed a cysteine-Ag/AP biocatalytic system, which exhibited a specific activity of 6.31 U/mg and activity retention of 67%, and retained 60% of its initial activity after seven reaction cycles. Kumar et al. [16] and Verma et al. [18] immobilized urease on cysteine-Cu and cysteine-ZnO, respectively. In both cases the activity retention was ca. 72%. Good results were also obtained by Chen et al. [19], who prepared cysteine-poly(glycidyl methacrylate)-SiO₂/Lip biocatalysts with high specific activity (44.1 U/mg) and activity retention (63.3%). That system was also used over eight reaction cycles, retaining 40% of its activity.

Summarizing performed research it has been shown, that the catalytic properties of enzyme in different pH, temperature, storage stability and reusability were improved. The support stabilizes and stiffens the enzyme structure, which consequently protect enzyme against denaturation in extreme pH and temperature conditions. Moreover, the carrier exposes the active sites of the catalyst for easy attachment of substrate molecules and reduce diffusional resistance of the substrates and products. The best catalytic properties were obtained when laccase was immobilized onto ZrO₂_Cys. It can be associated with the properties of that materials, especially well-developed porous structure. Furthermore, the data from elemental analysis showed that the cysteine was successfully introduced into the ZrO₂. The activation with glutaraldehyde causes lowering of catalytic activity. It may be

related with the presence of covalent bonds, which can block active site of enzyme and in consequently reduced enzymatic activity.

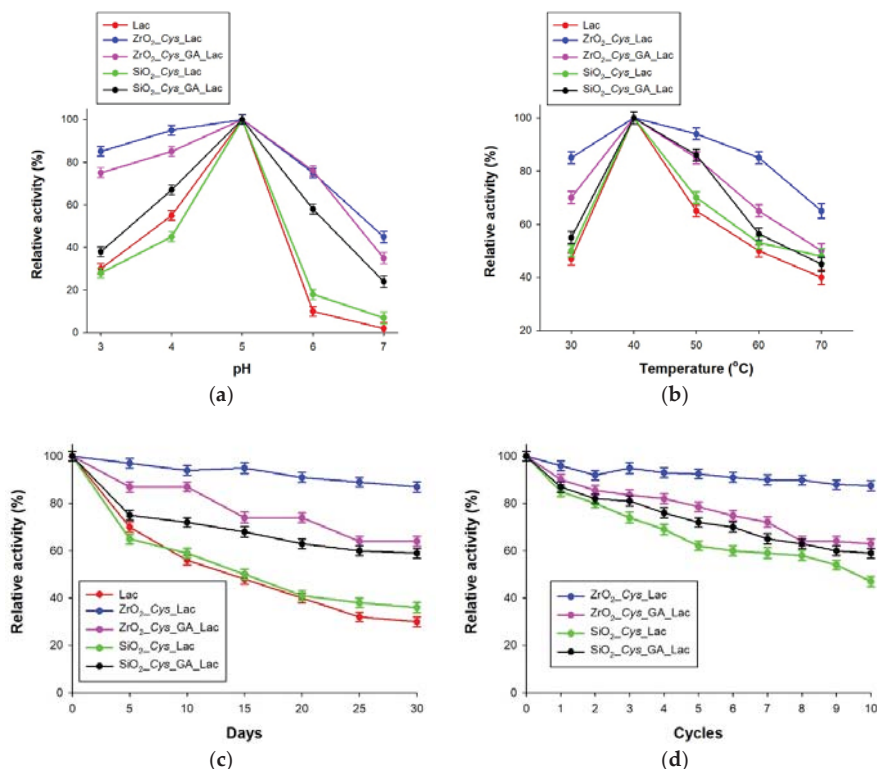


Figure 5. Influence of (a) pH, (b) temperature, (c) storage stability and (d) reusability on relative activity of free and immobilized laccase.

Table 6. Summary of catalytic properties obtained for different enzymes immobilized on cysteine-functionalized materials.

Support	Enzyme	As (U/mg)	A_R (%)	Number of Cycles; Residual Activity (%)	References
cysteine-Ag nanoparticles	alkaline phosphatase (AP)	6.31	67	7; >60	[15]
cysteine-Cu	urease (Ur)	45.8	72.4	10; >80	[16]
cysteine-ZnO	urease (Ur)	3.42	72.5	-	[18]
cysteine-poly(glycidyl methacrylate)-SiO ₂	lipase (Lip)	44.1	63.3	8; >40	[19]
cysteine-ZrO ₂	laccase (Lac)	19.3	77.2	10; >90	This study
cysteine-ZrO ₂ -glutaraldehyde	laccase (Lac)	13.5	53.8	10; >60	This study

3.4. Decolorization of Alizarin Red S

Laccase is an enzyme which is capable of degrading and decolorizing organic dyes from wastewaters. In this study, the obtained biocatalytic systems were used for the decolorization

of Alizarin Red S (ARS) dye. The results are presented in Figure 6, including the effect of time, pH and temperature. As shown in Figure 6a, the ZrO₂-based biocatalytic systems (ZrO₂_Cys_Lac and ZrO₂_Cys_GA_Lac) produced a higher efficiency of decolorization of ARS dye over the analyzed process duration, as compared with the SiO₂-based biocatalytic systems (SiO₂_Cys_Lac and SiO₂_Cys_GA_Lac). The highest decolorization efficiency was achieved after 24 h (95% for ZrO₂_Cys_Lac and 85% for ZrO₂_Cys_GA_Lac), but an efficiency of ca. 90% was already reached after 5 h. After the same time, the efficiency of decolorization of ARS using SiO₂_Cys_Lac and SiO₂_Cys_GA_Lac reached 35% and 20%, respectively. Laccase immobilized on ZrO₂-based materials results in higher decolorization of ARS dye because of the high specific activity and activity retention of these systems. It was observed that Alizarin Red S can be successfully decolorized by immobilizing laccase on ZrO₂-based materials. Furthermore, the efficiency of decolorization of Alizarin Red S in this study was higher than in previous reports where immobilized laccase was used. Zhao et al. [54] immobilized laccase on mesostructured cellular foam silica (MCF), and obtained maximum decolorization of Alizarin Red S equal to 73%. Similarly, Lu et al. [55] used alginate–chitosan microcapsules as a support for laccase. That biocatalytic system was utilized in the decolorization of ARS, and the efficiency of decolorization was measured at 70%.

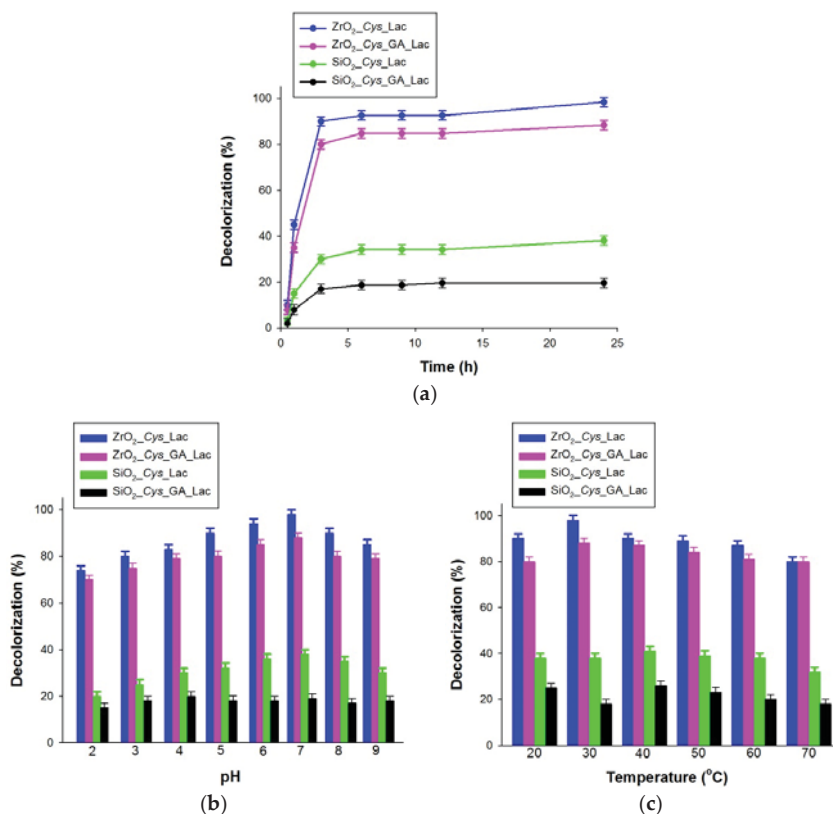


Figure 6. Effect of (a) process duration, (b) pH and (c) temperature on the efficiency of decolorization of Alizarin Red S.

The immobilization process serves to produce biocatalytic systems that can be used in a range of reaction conditions. Therefore, decolorization was carried out under different pH and temperature

conditions (Figure 6b,c). Laccase immobilized on ZrO₂_Cys and ZrO₂_Cys_GA achieved a high efficiency of decolorization (above 70%) in the whole of the analyzed pH and temperature ranges. Laccase immobilized on SiO₂_Cys and SiO₂_Cys_GA resulted in significantly lower efficiency of decolorization of ARS dye, reaching at most 40%. The results indicate that the biocatalytic systems proposed in this study (especially ZrO₂_Cys_Lac and ZrO₂_Cys_Ga_Lac) have potential applications in the decolorization of dyes from wastewaters.

4. Conclusions

The experiments performed in this study showed that large quantities of enzyme were attached to the proposed materials. Cysteine-functionalized ZrO₂ produced a higher immobilization yield and enzymatic activity than cysteine-functionalized SiO₂, which may suggest the superior ability of ZrO₂-based materials to attach to enzymes. Good thermal and electrokinetic stability, a well-developed porous structure and the presence of specific groups enable the use of M_xO_y-based materials for the immobilization of laccase from *Trametes versicolor*. In addition, based on that analysis the catalytic (A_S and A_R) and kinetic (K_M and V_{max}) parameters of the obtained biocatalytic systems were determined based on the oxidation of ABTS. The values of these parameters indicate the higher affinity of immobilized laccase to the substrate compared with the free enzyme. Moreover, laccase immobilized on ZrO₂-based support retains high relative activity over a wide range of pH (>40%) and temperature (>50%), and also after 30 days of storage (>60%) and 10 reaction cycles (>60%). Most importantly, very good results were achieved in the decolorization of Alizarin Red S. In these tests, a high efficiency of decolorization (97%) was obtained. The biocatalytic systems proposed in this study, based on cysteine-functionalized metal oxide, may be used in removing other organic and pharmaceutical pollutants from wastewaters.

Author Contributions: Conceptualization; methodology; validation; writing—original draft preparation—A.K.-R.; writing—review and editing—T.J. All authors have read and agreed to the published version of the manuscript.

Funding: This research was funded by the Ministry of Science and Higher Education, Grant No. 0912/SBAD/2006.

Conflicts of Interest: The authors declare no conflict of interest.

References

- Mateo, C.; Palomo, J.M.; Fernandez-Lorente, G.; Guisan, J.M.; Fernandez-Lafuente, R. Improvement of enzyme activity, stability and selectivity via immobilization techniques. *Enzyme Microb. Technol.* **2007**, *40*, 1451–1463. [\[CrossRef\]](#)
- Aryal, S.; Remant, B.; Dharmaraj, N.; Bhattarai, N.; Kim, C.H.; Kim, H.Y. Spectroscopic identification of SAu interaction in cysteine capped gold nanoparticles. *Spectrochim. Acta A* **2006**, *63*, 160–163. [\[CrossRef\]](#) [\[PubMed\]](#)
- Cai, Z.X.; Yang, H.; Zhang, Y.; Yan, X.P. Preparation, characterization and evaluation of water-soluble L-cysteine-capped-CdS nanoparticles as fluorescence probe for detection of Hg (II) in aqueous solution. *Anal. Chim. Acta* **2006**, *559*, 234–239. [\[CrossRef\]](#)
- Pita, M.; Shleev, S.; Ruzgas, T.; Fernández, V.M.; Yaropolov, A.I.; Gorton, L. Direct heterogeneous electron transfer reactions of fungal laccases at bare and thiol-modified gold electrodes. *Electrochem. Commun.* **2006**, *8*, 747–753. [\[CrossRef\]](#)
- Almeida, J.S.; Meira, L.A.; Teixeira, L.S.G. Indirect determination of cysteine in pharmaceutical formulations by high-resolution continuum source graphite furnace molecular absorption spectrometry. *Microchem. J.* **2018**, *143*, 155–159. [\[CrossRef\]](#)
- Nishiuchi, H.; Kohmura, M.; Wakabayashi, H. A rapid and precise method to determine cysteine content in food materials using 4-(aminosulfonyl)-7-fluoro-2,1,3-benzoxadiazole. *Food Sci. Technol. Res.* **2011**, *17*, 341–346. [\[CrossRef\]](#)
- Zdarta, J.; Meyer, A.S.; Jesionowski, T.; Pinelo, M. A general overview of support materials for enzyme immobilization: Characteristics, properties, practical utility. *Catalysts* **2018**, *8*, 92. [\[CrossRef\]](#)

8. Foresti, M.L.; Valle, G.; Bonetto, R.; Ferreira, M.L.; Briand, L.E. FTIR, SEM and fractal dimension characterization of lipase B from *Candida antarctica* immobilized onto titania at selected conditions. *Appl. Surf. Sci.* **2010**, *256*, 1624–1635. [[CrossRef](#)]
9. Valles, D.; Furtado, S.; Villadoniga, C.; Cantera, A.M.B. Adsorption onto alumina and stabilization of cysteine proteinases from crude extract of solanum granuloso-leprosum fruits. *Process Biochem.* **2011**, *46*, 592–598. [[CrossRef](#)]
10. Yang, Z.; Si, S.; Zhang, C. Study on the activity and stability of urease immobilized onto nanoporous alumina membranes. *Microporous Mesoporous Mater.* **2008**, *111*, 359–366. [[CrossRef](#)]
11. Ataka, K.; Heberle, J. Functional vibrational spectroscopy of a cytochrome c monolayer: SEIDAS probes the interaction with different surface-modified electrodes. *J. Am. Chem. Soc.* **2004**, *126*, 9445–9457. [[CrossRef](#)] [[PubMed](#)]
12. Yang, W.; Justin, R.; Gooding, J.; Brynn, H.D. Characterization of gold electrodes modified with self-assembled monolayers of L-cysteine for the adsorptive stripping analysis of copper. *J. Electroanal. Chem.* **2001**, *516*, 10–16. [[CrossRef](#)]
13. Patil, B.; Kobayashi, Y.; Fujikawa, S.; Okajima, T.; Mao, L.; Ohsaka, T. Direct electrochemistry and intramolecular electron transfer of ascorbate oxidase confined on L-cysteine self-assembled gold electrode. *Bioelectrochemistry* **2014**, *95*, 15–22. [[CrossRef](#)] [[PubMed](#)]
14. Batra, B.; Lata, S.; Devi, R.; Yadav, S.; Pundir, C.S. Fabrication of an amperometric tyramine biosensor based on immobilization of tyramine oxidase on AgNPs/L-Cys-modified Au electrode. *J. Solid State Electrochem.* **2012**, *16*, 3869–3876. [[CrossRef](#)]
15. Upadhyay, L.S.B.; Verma, N. Synthesis and characterization of cysteine functionalized silver nanoparticles for biomolecule immobilization. *Bioprocess Biosyst. Eng.* **2014**, *37*, 2139–2148. [[CrossRef](#)]
16. Kumar, N.; Upadhyay, L.S.B. Enzyme immobilization over polystyrene surface using cysteine functionalized copper nanoparticle as a linker molecule. *Appl. Biochem. Biotechnol.* **2020**, *191*, 1247–1257. [[CrossRef](#)]
17. Sharifia, E.; Shamsa, E.; Salimib, A.; Noorbakhshd, A.; Amini, M.K. Nickel-cysteine nanoparticles: Synthesis, characterization and application for direct electron transfer studies. *Colloids Surf. B Biointerfaces* **2018**, *165*, 135–143. [[CrossRef](#)]
18. Verma, N.; Kumar, N.; Upadhyay, L.S.; Sahu, R.; Dutt, A. Fabrication and characterization of cysteine-functionalized zinc oxide nanoparticles for enzyme immobilization. *Anal. Lett.* **2017**, *50*, 1839–1850. [[CrossRef](#)]
19. Chen, N.; Zhang, C.; Liu, Y.; Dong, X.; Sun, Y. Cysteine-modified poly(glycidyl methacrylate) grafted onto silica nanoparticles: New supports for significantly enhanced performance of immobilized lipase. *Biochem. Eng. J.* **2019**, *145*, 137–144. [[CrossRef](#)]
20. Muthukumar, H.; Malla, S.; Matheswaran, M.; Gummadi, S.N. Immobilization of xylose reductase enzyme on cysteine-functionalized *Murraya koenigii* mediated magnetite nanoparticles. *Mater. Lett.* **2020**, *261*, 127125. [[CrossRef](#)]
21. Bezbradica, D.I.; Mateo, C.; Guisan, J.M. Novel support for enzyme immobilization prepared by chemical activation with cysteine and glutaraldehyde. *J. Mol. Catal. B Enzym.* **2014**, *102*, 218–224. [[CrossRef](#)]
22. Monsan, P. Optimization of glutaraldehyde activation of a support for enzyme immobilization. *J. Mol. Catal.* **1975**, *3*, 371–384. [[CrossRef](#)]
23. Siara, E.H.; Arana-Pena, S.; Barbosa, O.; Zidoune, M.N.; Fernandez-Lafuente, R. Solid phase chemical modification of agarose glyoxyl-ficin: Improving activity and stability properties by amination and modification with glutaraldehyde. *Process Biochem.* **2018**, *73*, 109–116. [[CrossRef](#)]
24. Braham, S.A.; Hussain, F.; Morellon-Sterling, R.; Kamal, S.; Kornecki, J.F.; Barbosa, O.; Kati, D.E.; Fernandez-Lafuente, R. Cooperativity of covalent attachment and ion exchange on alcalase immobilization using glutaraldehyde chemistry: Enzyme stabilization and improved proteolytic activity. *Biotechnol. Prog.* **2019**, *35*, e2768. [[CrossRef](#)]
25. Barbosa, O.; Ortiz, C.; Berenguer-Murcia, A.; Torres, R.; Rodrigues, R.C.; Fernandez-Lafuente, R. Strategies for one-step immobilization-purification of enzyme as industrial biocatalysts. *Biotechnol. Adv.* **2015**, *33*, 435–456. [[CrossRef](#)]

26. Fuentes, M.; Batalla, P.; Grazu, V.; Pessela, B.C.C.; Mateo, C.; Montes, T.; Hermoso, J.A.; Guisan, J.M.; Fernandez-Lafuente, R. Mixed ion exchange supports as useful ion exchangers for protein purification: Purification of Penicillin G Acylase from *Escherichia coli*. *Biomacromolecules* **2007**, *8*, 703–707. [[CrossRef](#)]
27. Barbosa, O.; Ortiz, C.; Berenguer-Murcia, A.; Torres, R.; Rodrigues, R.C.; Fernandez-Lafuente, R. Glutaraldehyde in bio-catalysts design: A useful crosslinker and a versatile tool in enzyme immobilization. *RSC Adv.* **2014**, *4*, 1583–1600. [[CrossRef](#)]
28. Lopez-Gallego, F.; Betancor, L.; Mateo, C.; Hidalgo, A.; Alonso-Morales, N.; Dellamora-Ortiz, G.; Guisan, J.M.; Fernandez-Lafuente, R. Enzyme Stabilization by Glutaraldehyde Crosslinking of Adsorbed Proteins on Aminated Supports. *J. Biotechnol.* **2005**, *119*, 70–75. [[CrossRef](#)]
29. Hasanpour, M.; Hatamib, M. Photocatalytic performance of aerogels for organic dyes removal from wastewaters: Review study. *J. Mol. Liq.* **2020**, *309*, 113094. [[CrossRef](#)]
30. Gupta, V.K. Application of low-cost adsorbents for dye removal—A review. *J. Environ. Manag.* **2009**, *90*, 2313–2342. [[CrossRef](#)]
31. Pereira, L.; Alves, M. Dyes—Environmental Impact and Remediation. In *Environmental Protection Strategies for Sustainable Development*; Springer: Dordrecht, The Netherlands, 2012; pp. 111–162.
32. Salata, R.; Siwinska-Stefanska, K.; Sokołowska, J. Comparative degradation of C. I. Acid Green 25 and C. I. Basic Blue 9 by electrochemical, photoelectrochemical and photocatalytic oxidation methods. *Int. J. Electrochem. Sci.* **2019**, *14*, 792–814. [[CrossRef](#)]
33. Ciesielczyk, F.; Bartzak, P.; Zdarta, J.; Jesionowski, T. Active MgO-SiO₂ hybrid material for organic dye removal: A mechanism and interaction study of the adsorption of C.I. Acid Blue 29 and C.I. Basic Blue 9. *J. Environ. Manag.* **2017**, *204*, 123–135. [[CrossRef](#)] [[PubMed](#)]
34. Hu, S.; Yuan, D.; Liu, Y.; Lining, Z.; Guo, H.; Niu, Q.; Zong, W.; Liu, R. The toxic effects of alizarin red S on catalase at the molecular level. *RSC Adv.* **2019**, *9*, 33368–33377. [[CrossRef](#)]
35. Yang, Z.S.; Zhang, D.P.; Long, H.Y.; Zhao, G.C. Voltammetric Behavior of the Alizarin Red S Interaction with DNA and Damage to DNA. *Electroanalysis* **2007**, *19*, 2577–2582. [[CrossRef](#)]
36. Siwinska-Stefanska, K.; Kubiak, A.; Piasecki, A.; Goscianska, J.; Nowaczyk, G.; Jurga, S.; Jesionowski, T. TiO₂-ZnO binary oxide systems: Comprehensive characterization and tests of photocatalytic activity. *Materials* **2018**, *11*, 841. [[CrossRef](#)] [[PubMed](#)]
37. Anteck, K.; Zdarta, J.; Siwinska-Stefanska, K.; Sztuk, G.; Jankowska, E.; Oleskowicz-Popiel, P.; Jesionowski, T. Synergistic degradation of dye wastewaters using binary or ternary oxide systems with immobilized laccase. *Catalysts* **2018**, *8*, 402. [[CrossRef](#)]
38. Yagub, M.T.; Sen, T.K.; Afroze, S.; Ang, H.M. Dye and its removal from aqueous solution by adsorption: A review. *Adv. Colloid Interface Sci.* **2014**, *209*, 172–184. [[CrossRef](#)]
39. Mahmoodi, N.M.; Abdi, J. Metal-organic framework as a platform of the enzyme to prepare novel environmentally friendly nanobiocatalyst for degrading pollutant in water. *J. Ind. Eng. Chem.* **2019**, *80*, 606–613. [[CrossRef](#)]
40. Yuan, H.; Chen, L.; Cao, Z.; Hong, F.F. Enhanced decolorization efficiency of textile dye Reactive Blue 19 in a horizontal rotating reactor using strips of BNC-immobilized laccase: Optimization of conditions and comparison of decolorization efficiency. *Biochem. Eng. J.* **2020**, *156*, 107501. [[CrossRef](#)]
41. Jankowska, K.; Zdarta, J.; Grzywaczyk, A.; Kijeńska-Gawronska, E.; Biadasz, A.; Jesionowski, T. Electrospun poly(methyl methacrylate)/polyaniline fibres as a support for laccase immobilisation and use in dye decolorisation. *Environment. Res.* **2020**, *184*, 109332. [[CrossRef](#)]
42. Kashfi, S.; Borghei, S.M.; Mahmoodi, N.M. Covalently immobilized laccase onto graphene oxide nanosheets: Preparation, characterization, and biodegradation of azo dyes in colored wastewater. *J. Mol. Liq.* **2019**, *276*, 153–162. [[CrossRef](#)]
43. Shaheen, R.; Asgher, M.; Hussain, F.; Bhatti, H.N. Immobilized lignin peroxidase from *Ganoderma lucidum* IBL-05 with improved dye decolorization and cytotoxicity reduction properties. *Int. J. Biol. Macromol.* **2017**, *103*, 57–64. [[CrossRef](#)] [[PubMed](#)]
44. Sun, H.; Jin, X.; Jiang, F.; Zhang, R. Immobilization of horseradish peroxidase on ZnO nanowires/macroporous SiO₂ composites for the complete decolorization of anthraquinone dyes. *Biotechnol. Appl. Biochem.* **2018**, *65*, 220–229. [[CrossRef](#)] [[PubMed](#)]

45. Jin, X.; Li, S.; Long, N.; Zhang, R. A robust and stable nano-biocatalyst by co-immobilization of chloroperoxidase and horseradish peroxidase for the decolorization of azo dyes. *J. Chem. Technol. Biotechnol.* **2018**, *93*, 489–497. [[CrossRef](#)]
46. Bradford, M.M. A rapid and sensitive method for the quantitation of microgram quantities of protein utilizing the principle of protein-dye binding. *Anal. Biochem.* **1976**, *72*, 248–254. [[CrossRef](#)]
47. Boudrant, J.; Woodley, J.M.; Fernandez-Lafuente, R. Parameters necessary to define an immobilized enzyme preparation. *Process Biochem.* **2020**, *90*, 66–80. [[CrossRef](#)]
48. Liu, D.M.; Dong, C. Recent advances in nano-carrier immobilized enzymes and their applications. *Process Biochem.* **2020**, *92*, 464–475. [[CrossRef](#)]
49. Wisniewska, M.; Ostolska, I.; Szewczuk-Karpisz, K.; Chibowski, S.; Terpiłowski, K.; Gunko, V.M.; Zarko, V.I. Investigation of the polyvinyl alcohol stabilization mechanism and adsorption properties on the surface of ternary mixed nanooxide AST 50 (Al₂O₃–SiO₂–TiO₂). *J. Nanopart. Res.* **2015**, *17*, 1–14. [[CrossRef](#)]
50. Szewczuk-Karpisz, K.; Wisniewska, M. Lysozyme as a flocculant inducing agent improving the silica removal from aqueous solutions—a turbidimetric study. *J. Environ. Manag.* **2018**, *226*, 187–193. [[CrossRef](#)]
51. Qiu, X.; Qin, J.; Xu, M.; Kang, L.; Hu, Y. Organic-inorganic nanocomposites fabricated via functional ionic liquid as the bridging agent for Laccase immobilization and its application in 2,4-dichlorophenol removal. *Colloid. Surf. B Biointerfaces* **2019**, *179*, 260–269. [[CrossRef](#)]
52. Zivkovic, L.T.I.; Zivkovic, L.S.; Babich, B.M.; Kokunesoski, M.J.; Jokic, B.M.; Karadzic, I.M. Immobilization of *Candida rugosa* lipase by adsorption onto biosafe meso/macroporous silica and zirconia. *Biochem. Eng. J.* **2015**, *93*, 73–83. [[CrossRef](#)]
53. Amirkhani, L.; Moghaddas, J.; Jafarizadeh-Malmiri, H. *Candida rugosa* lipase immobilization on magnetic silica aerogel nanodispersion. *RSC Adv.* **2016**, *6*, 12676–12687. [[CrossRef](#)]
54. Zhao, M.; Wang, Y.; Liu, Z.; Cui, D.; Bian, X. Properties of immobilized laccase on mesostructured cellular foam silica and its use in dye decolorization. *J. Macromol. Sci. Part A* **2011**, *48*, 447–453. [[CrossRef](#)]
55. Lu, L.; Zhao, M.; Wang, Y. Immobilization of laccase by alginate–chitosan microcapsules and its use in dye decolorization. *World J. Microbiol. Biotechnol.* **2007**, *23*, 159–166. [[CrossRef](#)]



© 2020 by the authors. Licensee MDPI, Basel, Switzerland. This article is an open access article distributed under the terms and conditions of the Creative Commons Attribution (CC BY) license (<http://creativecommons.org/licenses/by/4.0/>).

Article

Performance and Kinetics of Bioaugmentation, Biostimulation, and Natural Attenuation Processes for Bioremediation of Crude Oil-Contaminated Soils

Cevat Yaman

Environmental Engineering, College of Engineering, Imam Abdulrahman Bin Faisal University, Dammam 34212, Saudi Arabia; cyaman@iau.edu.sa; Tel.: +96-65-50-24-59-37

Received: 11 June 2020; Accepted: 21 July 2020; Published: 22 July 2020

Abstract: Bioremediation of contaminated sites is usually limited due to the inadequate availability of nutrients and microorganisms. This study was conducted to assess the impact of bioaugmentation (BA) and biostimulation (BS) on petroleum hydrocarbon degradation efficiency. In addition, treatment performance and kinetics of different remediation processes were investigated. For this purpose, four tanks containing oil-contaminated soils were tested. Tank 1 was operated as the natural attenuation process. Then, a microbial inoculum and nutrients were added to tank 2 to promote BA and BS. In tank 3, only the BA process was adopted, whereas in tank 4, only the BS process was adopted. After 63 days of operation, the total petroleum hydrocarbon (TPH) in tank 2 was reduced from 1674 to 430 mg/kg, with 74% reduction. Tank 1, tank 3, and tank 4 indicated TPH reductions of 35%, 41%, and 66%, respectively. Microbiological analysis of the inoculum indicated that *Alcanivorax* was the dominant bacterium. The population of TPH degrader bacteria in tank 2 soil was two orders of magnitude higher than in the control tank. Reaction rate data were fitted with a first-order reaction rate model. The Monod kinetic constants, maximum specific growth rate (μ_{max}), and substrate concentration at half-velocity constant (K_s) were also estimated. This study showed that the TPH removal efficiency in the combined BA and BS process was higher than in other processes tested. The populations of TPH degrading microorganisms in soil tanks were positively related to TPH removal efficiency during bioremediation of petroleum-contaminated soils.

Keywords: bioaugmentation; bioremediation; biostimulation; crude oil; first-order reaction rate model; Monod model; natural attenuation

1. Introduction

Petroleum contamination in subsurface environments has become a serious global environmental hazard. Some of the main sources of this contamination are crude oil, refineries, and underground storage tanks (UST). Additionally, some of the chemicals in fossil fuels tend to remain in the environment for a long period of time. These persistent contaminants have several health risks to humans, animals, and other living organisms. When hydrocarbon-containing contaminants spill on land, degradation by indigenous microorganisms progresses slowly due to inadequate nutrients and microorganism populations [1]. Bioremediation is recognized as a cost-effective treatment technology for oil-contaminated soils [2]. For instance, bioaugmentation (BA) and biostimulation (BS) are the two main bioremediation technologies commonly used for soil clean-up [3–8]. Bioaugmentation works by introduction of exogenous microbial population to the contaminated environment [9–11]. Contaminated soils are inoculated with specially cultivated microorganisms with capabilities for the degradation of certain contaminants. The term biostimulation is used to describe the addition of essential electron acceptors such as nutrients to enhance the microbial growth [12–14]. On the other hand, natural attenuation (NA) can include chemical reactions, volatilization, adsorption, and

biodegradation. Microorganisms responsible for degrading petroleum products are defined as either eukaryotic or prokaryotic organisms [15]. Several research studies have been conducted on the treatment of hydrocarbons by various microorganisms [3–6,16–18]. Some of the microorganisms that are effective on the biodegradation of petroleum hydrocarbons are the microorganisms from genera *Pseudomonas*, *Acinetobacter*, *Flavobacterium*, *Achromobacter*, *Rhodococcus*, *Mycobacterium*, *Bacillus*, *Alcaligenes*, *Aspergillus*, *Mucor*, *Penicillium*, and *Candida* [3,16,18].

This study was conducted to find a quick solution to soil contamination due to the leakages of crude oil from transmission pipelines, oil refineries, and underground storage tanks (USTs). Even a small crack on a UST or a pipe along the oil transmission pipelines causes leakages to natural soil and nearby surface waters. It is very common that several incidences of oil leakages occur every year. When these incidences occur, a remediation team reacts to the incident very fast before it spreads, and recovers the contaminated soil and treats them *ex situ* before final disposal. Generally, these contaminated soils are either incinerated or landfilled at hazardous waste landfills. However, the bioremediation and recovery of these contaminated soils should be preferred to prevent the loss of fertile soils. Therefore, rapid *ex situ* or *in situ* disposal of these soils is very crucial. This can be achieved by coupling different technologies. In this study, addition of a microbial inoculum (bioaugmentation) along with nitrogen, phosphorous, and potassium (NPK) nutrients (biostimulation) were performed in simulated soil tanks to treat the contaminated soil. The overall aims of this study were (1) to assess the efficiency of bioaugmentation with TPH-degrading bacteria *Alcanivorax* and biostimulation with addition of nutrients nitrogen and phosphorus, for TPH degradation and (2) to investigate the relationship between TPH degradation efficiency and microbial community in petroleum-contaminated soil. The specific objectives of this study were (1) to investigate the crude oil biodegradation efficiency in a freshly contaminated soil by combined bioaugmentation and biostimulation processes, bioaugmentation process alone, biostimulation process alone, and by natural attenuation; (2) to investigate the treatment time needed for each process; (3) to determine the changes in the number of hydrocarbon degraders for each process during the treatment; and (4) to determine the kinetic parameters for the treatment processes.

2. Materials and Methods

For each treatment process (BA+BS, BA, BS, and NA), experimental analysis included 3 replicates and were repeated 3 times.

2.1. Soil Sampling

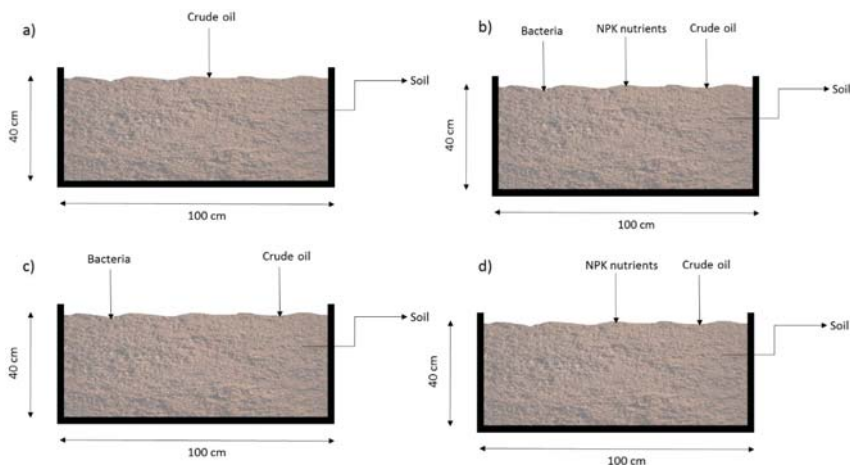
A clean soil sample was obtained from a site where there was no previous history of contamination. Before loading the tanks, the soil sample was grinded and large particles were removed. Then, it was air-dried at room temperature for 48 h. The volume of clean soil sample for each process, tank 1 (NA), tank 2 (BA+BS), tank 3 (BA), and tank 4 (BS), was 0.4 m³.

2.2. Configuration of the Tanks

Simulated bioremediation tanks were designed and constructed for the remediation of soil by natural attenuation, bioaugmentation + biostimulation, bioaugmentation, and biostimulation (Table 1). Tanks were made of high-density polyethylene (HDPE). TPH was degraded in tank 1 under natural attenuation condition (control tank). On the other hand, TPH in tanks 2, 3, and 4 was degraded under the conditions of bioaugmentation and biostimulation (microbial inoculum and nutrients addition), bioaugmentation (microbial inoculum addition only), and biostimulation (nutrient addition only), respectively. The schematics of the pilot-scale bioremediation tanks were depicted in Figure 1. The dimensions of the tanks were 100 cm × 100 cm × 40 cm, with a volume of 0.4 m³.

Table 1. Configuration of the treatment tanks.

	Microbial Inoculum Addition (Bioaugmentation)	Nutrients Addition (Biostimulation) (%20 N, %10 P, %10 K)	Crude Oil Addition
Tank 1 (NA)	No	No	Yes
Tank 2 (BS + BA)	Yes	Yes	Yes
Tank 3 (BA)	Yes	No	Yes
Tank 4 (BS)	No	Yes	Yes

**Figure 1.** Schematics of soil treatment tanks (a) Natural attenuation (NA), (b) Biostimulation + Bioaugmentation (BS+BA), (c) Bioaugmentation (BA), (d) Biostimulation (BS).

2.3. Loading of the Tanks

Clean soil samples were placed in the tanks and mixed thoroughly by a shovel for homogenization. Afterwards, the soil samples were contaminated by adding 1 L of crude oil to each tank. Clean tap water was added to the tanks to sustain minimum of 20% water content. Then, the soil samples in all tanks were mixed again for homogenization.

2.4. Natural Attenuation (Tank 1)

Tank 1 was operated as a natural attenuation process for comparison with other tanks; therefore, no nutrients or microbial inoculum was added. However, 1 L of crude oil was added to tank 1 to contaminate the soil. Natural attenuation treatment is defined as a natural process where no specific remediation technology is used for the contaminated soil.

2.5. Bioaugmentation + Biostimulation (Tank 2)

Analysis of the contaminated soil indicated a C:N:P ratio of 10,000:0.0107:0.0027, which was very high as the soil contained low N and P concentrations. The amount of nutrient addition to tank 2 was calculated by using the C:N:P ratio, which was determined by calculating the mass concentration of the crude oil added. Alexander [19] suggested that a C:N:P ratio of 100:10:2 is optimal for the remediation of soil contaminated by petroleum hydrocarbon. Zhang, Cheng [20] and Alavi, Mesdaghinia [21] reported that a C:N:P ratio of 100:5:1 is also considered optimal. In this study, the C:N:P ratio of 100:5:1 was used as a reference value. This C:N:P ratio was reached by adding appropriate amounts of NH_4Cl and KH_2PO_4 to tank 2. Since 1 L of crude oil was added to each tank, 50 g of N was added to satisfy the C:N ratio of 100:5. Since the fertilizer nutrient contains 20% N, 250 g of NH_4Cl was added to reach

the 50 g of N. Therefore, the initial N addition was 50 g, or 250 g of N NH_4Cl that contains 50 g of N. Based on the C:N:P ratio of 100:5:1, 10 g of P was needed, which is equal to 100 g of KH_2PO_4 (%10 of K). The density of the soil used in the tanks was $1200 \text{ kg}\cdot\text{m}^{-3}$, which is equal to 480 kg of soil in each tank.

In bioremediation processes, microorganisms convert organic compounds such as crude oil into non-toxic substances such as CO_2 and H_2O . Any given bacteria can occur naturally and require essential nutrients. In most cases, naturally occurring microorganisms (indigenous microorganisms) are not in sufficient numbers for complete degradation. Thus, there exists an opportunity to enhance and accelerate the natural degradation by the introduction of additional microorganisms and nutrients. When mixed with water and applied as a slurry to contaminated soil, microorganisms break down the molecular structures of the targeted hydrocarbons by utilizing their mass as a source of energy. Because of the high degree of interface between bacteria and the hydrocarbon, the rate of degradation tends to be quite rapid at first, but gradually diminishes as the more biodegradable hydrocarbon is consumed.

The microbial inoculum used in this study was manufactured as a combination of naturally occurring species. Microbiological analysis of the inoculum indicated that *Alcanivorax* was the dominant bacterium. The bacteria/enzyme mixture used in this study is a combination of naturally occurring species and was manufactured in the U.S. The product contains dried mixed natural bacteria and enzymes combined in a mixture with micro-nutrients. Only naturally occurring, non-genetically modified microorganisms were included in the product. In the making of the product, further efforts were made to identify both the strains of microorganisms and the energy sources. The product is in the form of a free-flowing powder and is activated by the introduction of water. Based on the amounts of crude oil and fertilizers added, 50 g of microbial inoculum was added to 10 L of clean tap water and stirred to solubilize the product. This amount was determined according to the specifications provided by the manufacturer. The slurry then sat for 30 min to make sure that the microorganisms in the product were activated. Then, the slurry was sprayed over the surface of the soil in tank 2, while mixing the soil to make sure that the product was mixed homogeneously with the soil.

2.6. Bioaugmentation (Tank 3)

Tank 3 (BA) was operated to measure the effects of bioaugmentation process on TPH removal rates and the number of TPH degrader bacteria, and then compared the results with tank 2 (BA+BS), tank 4 (BS), and tank 1 (NA). The amount of microbial inoculum addition to tank 3 was calculated exactly the same as it was calculated for tank 2. Nutrient addition was not carried out in tank 3, thus, only microbial inoculum addition was evaluated.

2.7. Biostimulation (Tank 4)

Tank 4 (BS) was operated to measure the effects of biostimulation process on TPH removal rates and the number of TPH degrader bacteria in the tanks, and then compared the results with other tanks. The amount of nutrient addition to tank 4 was calculated exactly the same as it was calculated for tank 2. Microbial inoculum addition was not carried out in tank 4.

2.8. Oxygen Supply and Moisture Content

Aeration through mixing the contaminated soil serves as a highly effective catalyst to speed up the degradation process. The product of microbial inoculum contains facultative strains; thus, they use either dissolved or chemically combined oxygen. Surely, they operate more effectively with dissolved oxygen because they can obtain more oxygen from it. Straight chained hydrocarbon molecules are broken down faster than those cross-linked and branched chained molecules. However, it takes longer to be broken down for many of the cyclic compounds. Therefore, aeration was done in tank 2, tank 3, and tank 4 by daily mixing to provide adequate oxygen to the system. Tank 1 was not aerated since it was used as a control.

All bacteria, either commercially produced or indigenous, need an aqueous environment for growth. For this reason, optimum moisture content must be maintained during the treatment program.

Desired moisture content in all tanks was accomplished by wetting of the soils with clean tap water. By doing this, soil moisture content of at least 25% was maintained. Simultaneous mixing was performed during wetting of the soil to make sure that the water was mixed homogenously with the contaminated soil.

2.9. Soil Analyses

2.9.1. TPH Analysis

TPH was measured based on the carbon number of between C10 and C40 (diesel and oil range). Samples were collected from the tanks at the start of experiments, and every week further on for 63 days. The United States Environmental Protection Agency (USEPA) [22] sampling method 5035A was used to reduce the amount of disturbance during collecting of soil samples. Due to their chemical structure, petroleum compounds are vulnerable to sampling, transport, and analysis. The EPA method 5035A reduces the volatilization by using a sealed sample vial. Extraction of the samples was performed according to the EPA 3820 method [23]. About 10 g of wet soil sample was mixed with a reagent in a centrifuge tube. Then, it was capped and shaken vigorously for 1 min. The sample was then centrifuged, and the supernatant water was placed into a volumetric flask for TPH analysis. Then, TPH was measured according to the US EPA 8015B method [24]. One of the methods for hydrocarbon measurement is gas chromatography (GC), thus, it was used in this study. Then, 15 g of sample were extracted with acetone and a retention time window standard solution. Sample extracts were centrifuged to remove fine particles. The clear extracts were washed twice with 100 mL of water. The organic layer was collected and dried with sodium sulfate. An Agilent Intuvo 9000 Series Gas Chromatograph was used for the quantitative analysis of total petroleum hydrocarbon contamination in soil samples.

2.9.2. pH Analysis

For pH analysis, EPA's 9045D method was used [25]. In this test, 20 g of soil sample was weighed in a beaker and 20 mL of distilled water was added. Then, the solution was mixed with a glass rod for 5 min and the beaker was left undisturbed for 1 h to allow suspended particles to settle. The liquid phase at the top of the beaker was separated with a pipette and transferred to 50 mL centrifuge tubes. These tubes were centrifuged at 9000 rpm for 10 min to separate the supernatant fraction from the solution. The supernatant fraction was collected in 100 mL beakers and the pH was measured with a previously calibrated pH meter.

2.9.3. Moisture Content

Collected samples were placed in an oven at 105 °C for 1 night. After removing the samples, they were left until their temperature had reached room temperature and then were weighed immediately. The samples were placed in the oven again for a few hours and weighed again until there was no difference between the measured weights of the samples [26,27].

2.9.4. Organic Matter

Organic matter in soil affects the water retaining ability, biological activity, and water/air infiltration rates. ASTM D 2974—standard test methods for organic matter of organic soils [28] was used to measure the organic content of the soil samples. A porcelain dish containing the soil sample was placed in a furnace, temperature of the furnace was increased to 440 °C, and the sample was left in the furnace overnight. Then, the organic fraction of the soil was determined by subtracting the mass of the burned soil (ash) from the mass of dry soil [29].

2.9.5. Organic Carbon

The quantity of organic carbon was determined by treating dried soil samples with phosphoric acid. Organic carbon was determined in the soil samples dried at 105 °C using a carbon analyzer. Prepared soil samples were combusted at 1350 °C in an oxygen atmosphere and carbon was oxidized to form CO₂ [30].

2.9.6. Nutrients

Total nitrogen for the soil samples was determined according to the EN 13654 method [31]. This method is called wet acidic digestion (H₂SO₄) of nitrogen-containing soil samples. There are three steps involved in this method; digestion, distillation, and titration. The wet acidic digestion takes place in a digestion flask, causing transformation of nitrogen to NH₄⁺ ions. In the distillation step, excess base was added to the acid digestion mixture to transform NH₄⁺ to NH₃. By titration, the amount of NH₃ in the receiving solution was quantified. The total nitrogen in the sample was then determined from the quantified amount of ammonia ions in the solution. Total phosphorous in soil samples was determined by digesting with perchloric acid and then measuring by colorimetry [32]. The quantity of potassium in soil samples was determined according to the flame atomic emission spectrometry method [33].

2.10. Microbial Analysis

Collected soil samples from the tanks underwent microbiological analysis before and after the study. A fraction of soil sample (1 g) was placed in a bottle for microbial analysis. In this test, 1 g of soil was added to 10 mL of distilled water and vortexed, then sequentially diluted. The microbial density of bacteria was determined as explained by Nakasaki and Hirai [34]. Amphotericin B solution at a concentration of 100 µL/L was added to modified Luria- Bertani (LB) agar medium and incubated for 3 days to measure the growth of bacteria. Optimum growth temperature was seen at 30 to 35 °C. Cell morphology was studied under an Olympus U-pot microscope, using overnight culture of the strain grown on LB agar for gram staining. Colony forming unit (CFU) was determined by using the formula; CFU/g = (number of colonies × dilution factor)/volume of culture plate.

2.11. Kinetic Model

A mass balance in the experimental tanks was used to find a kinetic model for degradation of total petroleum hydrocarbon. The kinetic model can be defined as shown in Equation (1) [35]:

$$-r = -\frac{dC}{dt} = k \cdot C^n \quad (1)$$

where;

r: reaction rate,

k: biodegradation rate,

C: concentration,

t: time,

n: reaction order.

The constants, k and n, are found by plotting concentration vs. time and determining the best suitable line. The half time ($t_{1/2}$) can be calculated as follows (Equation (2)) [36,37]:

$$t_{1/2} = \frac{\ln 2}{k} \quad (2)$$

Moreover, the growth of microorganisms can be determined by using the Monod equation as shown in Equation (3):

$$\mu = \mu_{max} \cdot \frac{C}{K_s + C} \quad (3)$$

where;

μ : specific growth rate,

μ^{max} : maximum specific growth rate,

K_s : TPH value at half-time.

Then, r is shown as follows (Equation (4)):

$$r = \frac{\mu X}{Y} = \frac{\mu_{max}}{Y} \frac{C}{K_s + C} X \quad (4)$$

where X shows the microorganism concentrations and Y is yield that is expressed as biomass formed per mass of substrate used.

The rate of reaction determined numerically was used to obtain μ_{max} and K_s as defined in Equation (5):

$$\frac{X}{r.Y} = \frac{K_s}{\mu_{max}} \left(\frac{1}{C} \right) + \frac{1}{\mu_{max}} \quad (5)$$

3. Results

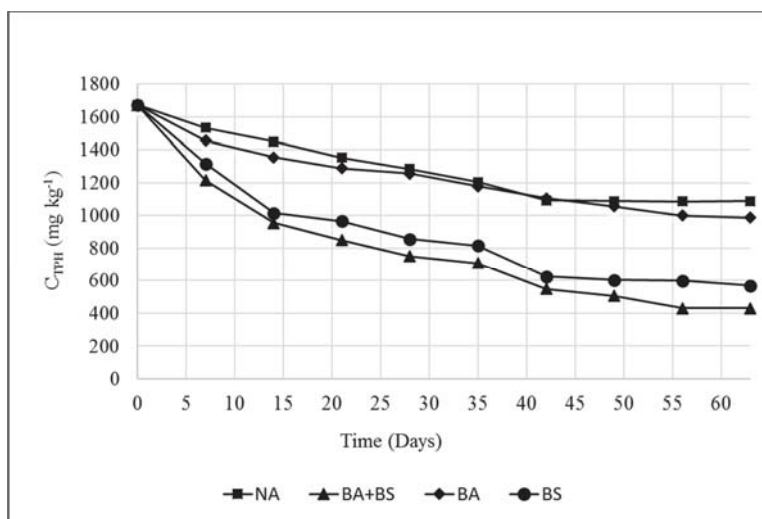
This section summarizes the experimental results, their interpretation, and the discussions that can be drawn.

3.1. Changes in Soil TPH Concentrations

Table 2 shows the chemical characteristics of oil-contaminated soil used in the study. Figure 2 shows the concentrations of TPH for tank 1, tank 2, tank 3, and tank 4 before and after the treatment. TPH concentration in the initial soil for all tanks were $1674 \pm 9.25 \text{ mg.kg}^{-1}$. After 63 days of treatment, TPH concentrations were decreased from $1674 \pm 9.25 \text{ mg.kg}^{-1}$ to $1088 \pm 5.22 \text{ mg.kg}^{-1}$ by the natural attenuation treatment (tank 1), which represents a 35% removal efficiency. TPH was reduced to $430 \pm 2.16 \text{ mg.kg}^{-1}$ in the biostimulation and bioaugmentation treatment (tank 2), which represents a TPH removal efficiency of 74%. The other 2 reactors, tank 3 (BA) and tank 4 (BS), resulted in TPH removal rates of 41% and 66%, respectively. Compared to NA treatment in tank 1 (control), the highest removal rate for TPH was achieved with BA+BS treatment in tank 2 (74%), followed by BS treatment in tank 4 (66%). BA treatment alone was not as effective as BS treatment. The efficiency of biodegradation was the highest when the BS and BA processes were combined. Initial nutrient levels in the contaminated soil were not sufficient based on the selected C:N:P ratio of 100:5:1. This indicated that addition of nutrients to the contaminated soil would be beneficial. Biodegradation in each tank was not hampered by carbon content, pH, or moisture levels [38–40]. Microbial analysis showed that an active microbial population of $1 \times 10^5 (1.0E+05) \text{ CFU.g}^{-1}$ was initially present in the soils prior to treatment. Therefore, bioaugmentation did not accelerate the rate of biodegradation over biostimulation.

Table 2. Chemical characteristics of oil-contaminated soil used in the study.

Parameters	Unit	Values
pH		7.8 ± 0.11
Total Petroleum Hydrocarbon	mg/kg	1674 ± 9.25
Organic matter content of soil (f_{oc})	%	3 ± 0.31
Organic matter	g/kg	3.20 ± 0.25
Organic carbon	g/kg	1.86 ± 0.15
Total Nitrogen	mg/kg	0.002 ± 0.0
C/N ratio (adjusted)		20 ± 0.36
Total phosphorous	mg/kg	0.0005 ± 0.0
Potassium	mg/kg	0.0005 ± 0.0
Moisture content	%	10 ± 0.12

**Figure 2.** Changes in Total petroleum hydrocarbon (TPH) concentrations in the treatment tanks.

3.2. Microbial Analysis

The total number of bacteria (microbial inoculum) added to bioaugmentation and biostimulation tank (tank 2) and bioaugmentation tank (tank 3) was determined. The colonies were counted and defined as the total colony forming units (CFU) g^{-1} dry powder product (microbial inoculum) [41]. As a result of microbial analysis, a bacterium belonging to genus, *Alcanivorax*, and a sub class of Proteobacteria was isolated from the sample, with a cell frequency unit (CFU) of 3×10^7 ($3.E+07$) per gram of microbial inoculum sample (Figure 3). The strain was found to possess a cell-bound granule of glycolipids. Cells appeared to be granular, non-spore-forming, and Gram-negative rods. Colonies were small, non-pigmented, and slightly raised in the center. Optimum growth temperature was observed at 30 to 35 °C. The optimum NaCl required for growth was 4–7% NaCl.

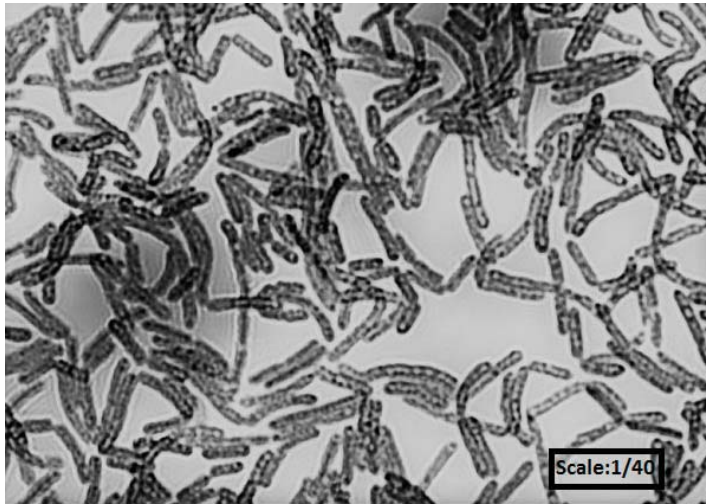


Figure 3. Olympus U-pot microscope picture of the microbial inoculum at 40× magnification.

The initial microbial population in the tanks was 1×10^5 (1.E+05) CFU g^{-1} . Figure 4 shows the variations of microbial population in the treatment tanks during 63 days of operation. The number of total TPH degrader bacteria were measured by taking weekly samples. Continuous rise in microorganism population indicates that the number of microorganisms increased significantly by degrading TPH. This increase in the population was due to the available quantity of TPH, N, and P in the tanks. As the carbon source for microorganisms started to diminish, the microbial population reached a steady-state value at the end of the study. Compared to tank 1, a remarkable increase in TPH degrader bacteria was observed within 63 days in soil samples collected from tank 2 (BA+BS). Significantly higher number of degrader microbial counts was observed in the other two tanks, tank 3 (BA) and tank 4 (BS), compared to tank 1 (NA). At the end of the study, the hydrocarbon degrading bacteria numbers in BA+BS soils were two orders of magnitude higher than in control soils (NA).

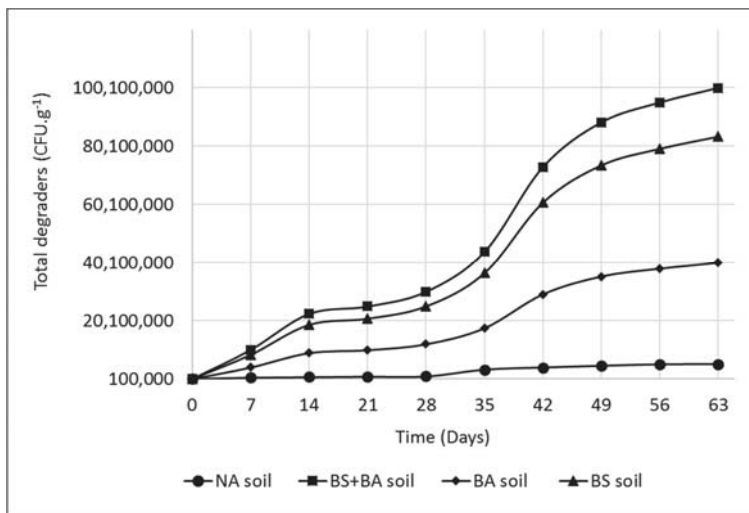


Figure 4. Total degrader bacteria numbers in soil samples over 63 days.

3.3. Bioremediation Kinetics

It has been reported by several investigators that first-order kinetics and Michaelis–Menten kinetic can be used for petroleum-hydrocarbon degradation [36,42–44]. The data obtained from the treatment tanks were applied to the first-order rate model and the Monod model. The yield values (Y), which define the microorganism concentrations in CFU per mg of TPH biodegraded, were determined from the values of CFU and TPH. The Y values for NA, BA+BS, BS, and BA processes were determined as 8530, 80,300, 58,200, and 78,300 CFU g^{-1} TPH, respectively. Figure 5 shows fits of the first-order and the Monod models to data from the NA, BS + BA, BS, and BA treatment processes. It is clearly seen from Figure 5 that the Monod model represents the data better than the first-order reaction rate model, which is validated by the R^2 values. The reaction rate coefficient (k), maximum specific growth rate (μ_{max}), half-reaction time ($t_{1/2}$), and TPH value at half-time (K_s) were determined from the curves in Figure 5 and are summarized in Table 3 for each treatment process.

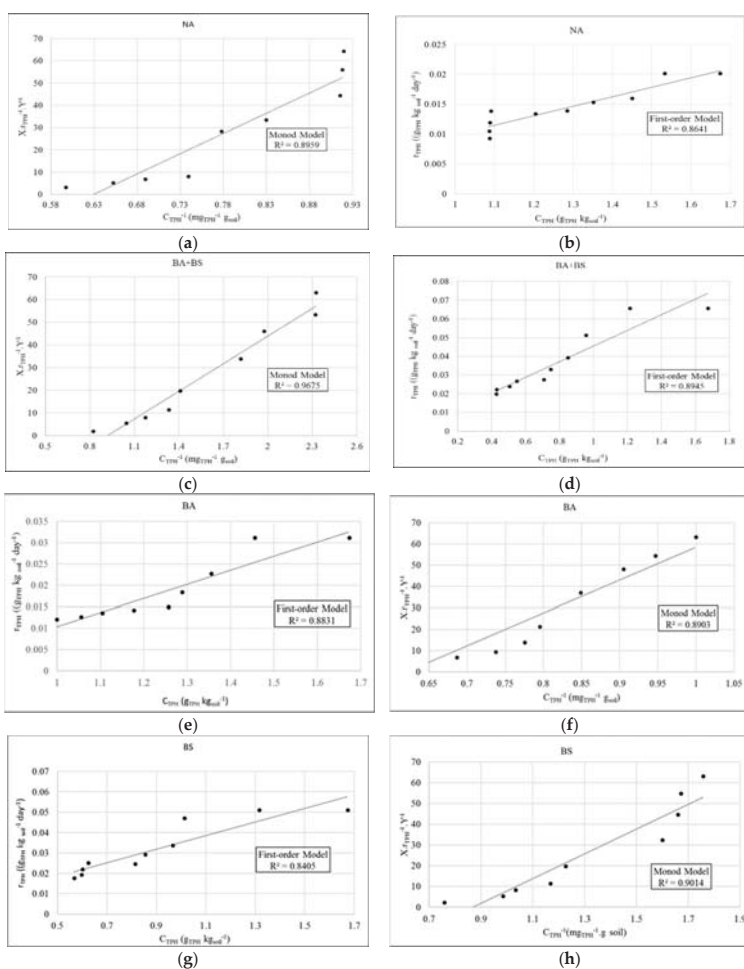


Figure 5. Reaction rate data for the treatment modes. (a) The first-order model for NA, (b) the Monod model for NA, (c) the first-order model for BA+BS, (d) the Monod model for BA+BS, (e) the first-order model for BA, (f) the Monod model for BA, (g) the first-order model for BS, (h) the Monod model for BS.

Table 3. Calculated reaction rate factors for the first-order and the Monod models.

Treatment Type	First Order Model $r=k C$	Monod Model $r=\frac{\mu_{max}}{Y} \left(\frac{C}{K_s+C} \right) X$
NA	k:0.0159 d ⁻¹ t _{1/2} :43.6 d R ² :0.86	μ_{max} :0.00875 d ⁻¹ K _s :1114 mg kg ⁻¹ R ² :0.90
BA+BS	k:0.0419 d ⁻¹ t _{1/2} :16.54 d R ² :0.89	μ_{max} :0.02675 d ⁻¹ K _s :918 mg kg ⁻¹ R ² :0.97
BA	k:0.033 d ⁻¹ t _{1/2} :21.0 d R ² :0.88	μ_{max} :0.0104 d ⁻¹ K _s :1289 mg kg ⁻¹ R ² :0.89
BS	k:0.0333 d ⁻¹ t _{1/2} :20.8 d R ² :0.84	μ_{max} :0.0193 d ⁻¹ K _s :965 mg kg ⁻¹ R ² :0.90

4. Discussion

The results obtained from this study showed that microorganisms can successfully biodegrade TPH, particularly when combined BS and BA processes are used. Results of this study also showed that BS has a higher effect on biodegradation efficiency than BA process. Adding nitrogen and phosphorus, along with microbial inoculation and aeration can create an optimum condition for microorganisms to degrade TPH.

Analysis of the contaminated soil indicated that the C:N:P ratio was 10,000:0.0107:0.0027. This ratio is considered high for C as the suggested C:N:P ratio for bioremediation varies between 100:10:1 and 100:5:1, which corresponds to the nutrients needed for microorganisms [19,45]. In addition, the initial soil contained low numbers of TPH biodegraders. Therefore, adding optimum amount of nutrients and introducing TPH degraders (addition of microbial inoculum) apparently increased the microbial populations in the contaminated soil, providing more efficient TPH biodegradation.

Earlier studies showed that bioremediation was a useful method for decomposing TPH in soils contaminated with weathered oil [46,47]. However, there are limited studies for quick bioremediation of TPH and population density of microbial community in freshly oil-contaminated soils. This study assessed the effectiveness of bioaugmentation combined with biostimulation process on a freshly oil-contaminated soil. The results of this work justified that the bioaugmentation and biostimulation combined provided the accelerated biodegradation of TPH from the contaminated soil through increased microbial biomass. Wu, Dick [17] reported that bioremediation of TPH was achieved between 34 and 60% in a local freshly petroleum contaminated soil after 10 weeks of treatment. However, weathered hydrocarbon contaminants were not readily available to biodegrading microorganisms [48]. This study revealed similar results to those previous works pointing out that biostimulation was more effective than bioaugmentation [1,13,14]. Moreover, several studies showed that the most efficient biodegradation method for TPH removal is a combination of bioaugmentation and biostimulation processes [10,46,47].

Several different bacterial species would be needed to effectively biodegrade hydrocarbons [11]. Single microbial species do not have the capacity to biodegrade more than two different compounds that are usually present in crude oil. Conventionally, the higher the hydrocarbon degrading microbial population, the more hydrocarbon biodegradation takes place [11,49]. It was shown in this work that the number of microorganisms were higher in BS tank than in BA tank, and contaminant removal was 66% for BS tank and 41% for BA tank. Thus, it can be stressed that there is a linear relationship between microbial population and TPH biodegradation.

The coefficients calculated from the first-order kinetics and the Michaelis–Menten kinetic models clearly showed that the Monod model fits better for the BS+BA process than the other treatment processes. For instance, the first-order reaction rate (k) in the BS+BA process was higher compared to NA, BA, and BS processes. The half-reaction time determined from the reaction rate (k) in the BA+BS

process was thus smaller than in the other processes. In both models, maximum specific growth rate (μ^{\max}) was higher and TPH value at half-time (K_s) was lower in the BA+BS process, which indicates that BA+BS process had a faster reaction rate. The results of these both model applications indicated that BS and BA together achieved the best TPH removal efficiency.

5. Conclusions

Petroleum hydrocarbons remaining in soil for a long time after contamination along with costly treatment methods have made them one of the most important environmental pollutants. This study confirmed that it is possible to enhance the biodegradation of TPH in soil by using different treatment methods such as bioaugmentation and biostimulation alone or in combination. Analysis of TPH, microbial population, and kinetic models indicated that bioremediation of oil contaminated soil is very successful especially when BS and BA treatment are used together.

In this pilot study, the TPH degradation in the crude oil contaminated soil was improved by bioaugmentation with genus *Alcanivorax* and biostimulation with nitrogen and phosphorus. The study also showed that bioaugmentation and biostimulation resulted in effective TPH removal and effective recovery of soil's fertility properties within 63 days of treatment. The study highlighted the importance of ex situ soil treatment combined with bioaugmentation and biostimulation as a suitable strategy.

Funding: This research was funded by Imam Abdulrahman bin Faisal University (IAU) project No. (2019-037-Eng) throughout the Deanship of Scientific Research (DSR).

Acknowledgments: The author would like to thank Abdulrahman bin Faisal University for academic support.

Conflicts of Interest: The author declares no conflict of interest.

References

1. Abed, R.M.; Al-Sabahi, J.; Al-Maqrashi, F.; Al-Habsi, A.; Al-Hinai, M. Characterization of hydrocarbon-degrading bacteria isolated from oil-contaminated sediments in the sultanate of Oman and evaluation of bioaugmentation and biostimulation approaches in microcosm experiments. *Int. Biodeterior. Biodegrad.* **2014**, *89*, 58–66. [[CrossRef](#)]
2. Cerqueira, V.S.; Peralba, M.D.C.R.; Camargo, F.A.D.O.; Bento, F.M. Comparison of bioremediation strategies for soil impacted with petrochemical oily sludge. *Int. Biodeterior. Biodegrad.* **2014**, *95*, 338–345. [[CrossRef](#)]
3. Polyak, Y.M.; Bakina, L.G.; Chugunova, M.V.; Mayachkina, N.V.; Gerasimov, A.O.; Bure, V. Effect of remediation strategies on biological activity of oil-contaminated soil—A field study. *Int. Biodeterior. Biodegrad.* **2018**, *126*, 57–68. [[CrossRef](#)]
4. Jiang, Y.; Brassington, K.J.; Prpich, G.; Paton, G.I.; Semple, K.T.; Pollard, S.J.; Coulon, F. Insights into the biodegradation of weathered hydrocarbons in contaminated soils by bioaugmentation and nutrient stimulation. *Chemosphere* **2016**, *161*, 300–307. [[CrossRef](#)]
5. Ramadass, K.; Megharaj, M.; Venkateswarlu, K.; Naidu, R. Bioavailability of weathered hydrocarbons in engine oil-contaminated soil: Impact of bioaugmentation mediated by pseudomonas spp. on bioremediation. *Sci. Total. Environ.* **2018**, *636*, 968–974. [[CrossRef](#)]
6. Safdari, M.-S.; Kariminia, H.-R.; Rahmati, M.; Fazlollahi, F.; Polasko, A.; Mahendra, S.; Wilding, W.V.; Fletcher, T.H. Development of bioreactors for comparative Study of natural attenuation, biostimulation, and bioaugmentation of petroleum-hydrocarbon contaminated Soil. *J. Hazard Mater.* **2018**, *342*, 270–278. [[CrossRef](#)] [[PubMed](#)]
7. Hechmi, N.; Bosso, L.; El-Bassi, L.; Scelza, R.; Testa, A.; Jedidi, N.A.; Rao, M. Depletion of pentachlorophenol in soil microcosms with *Byssoschlamys nivea* and *Scopulariopsis brumptii* as detoxification agents. *Chemosphere* **2016**, *165*, 547–554. [[CrossRef](#)]
8. Tian, H.; Yan, M.; Treu, L.; Angelidaki, I.; Fotidis, I.A. Hydrogenotrophic methanogens are the key for a successful bioaugmentation to alleviate ammonia inhibition in thermophilic anaerobic Digesters. *Bioresour. Technol.* **2019**, *293*, 122070. [[CrossRef](#)]

9. Łebkowska, M.; Zborowska, E.; Karwowska, E.; Miaśkiewicz-Peska, E.; Muszyński, A.; Tabernačka, A.; Naumczyk, J.; Jęczalik, M. Bioremediation of soil polluted with fuels by sequential multiple injection of native microorganisms: Field-scale processes in Poland. *Ecol. Eng.* **2011**, *37*, 1895–1900. [[CrossRef](#)]
10. Taccari, M.; Milanovic, V.; Comitini, F.; Casucci, C.; Ciani, M. Effects of biostimulation and bioaugmentation on diesel removal and bacterial community. *Int. Biodeterior. Biodegrad.* **2012**, *66*, 39–46. [[CrossRef](#)]
11. Wu, M.; Chen, L.; Tian, Y.; Ding, Y.; Dick, W.A. Degradation of polycyclic aromatic hydrocarbons by microbial consortia enriched from three soils using two different culture media. *Environ. Pollut.* **2013**, *178*, 152–158. [[CrossRef](#)] [[PubMed](#)]
12. Yu, K.; Wong, A.; Yau, K.; Wong, Y.; Tam, N.F. Natural attenuation, biostimulation and bioaugmentation on biodegradation of polycyclic aromatic hydrocarbons (PAHs) in mangrove sediments. *Mar. Pollut. Bull.* **2005**, *51*, 1071–1077. [[CrossRef](#)] [[PubMed](#)]
13. Kauppi, S.; Sinkkonen, A.; Romantschuk, M. Enhancing bioremediation of diesel-fuel-contaminated soil in a boreal climate: Comparison of biostimulation and bioaugmentation. *Int. Biodeterior. Biodegrad.* **2011**, *65*, 359–368. [[CrossRef](#)]
14. Sayara, T.; Borràs, E.; Caminal, G.; Sarrà, M.; Sánchez, A. Bioremediation of PAHs-contaminated soil through composting: Influence of bioaugmentation and biostimulation on contaminant biodegradation. *Int. Biodeterior. Biodegrad.* **2011**, *65*, 859–865. [[CrossRef](#)]
15. Balba, M.; Al-Awadhi, N.; Al-Daher, R. Bioremediation of oil-contaminated soil: Microbiological methods for feasibility assessment and field evaluation. *J. Microbiol. Methods* **1998**, *32*, 155–164. [[CrossRef](#)]
16. Wu, M.; Ye, X.; Chen, K.; Li, W.; Yuan, J.; Jiang, X. Bacterial community shift and hydrocarbon transformation during bioremediation of short-term petroleum-contaminated soil. *Environ. Pollut.* **2017**, *223*, 657–664. [[CrossRef](#)]
17. Wu, M.; Dick, W.A.; Li, W.; Wang, X.C.; Yang, Q.; Wang, T.; Xu, L.; Zhang, M.; Chen, L. Bioaugmentation and biostimulation of hydrocarbon degradation and the microbial community in a petroleum-contaminated soil. *Int. Biodeterior. Biodegrad.* **2016**, *107*, 158–164. [[CrossRef](#)]
18. Nwankwegu, A.S.; Onwosi, C.O. Bioremediation of gasoline contaminated agricultural soil by bioaugmentation. *Environ. Technol. Innov.* **2017**, *7*, 1–11. [[CrossRef](#)]
19. Alexander, M. *Biodegradation and Bioremediation*; Academic Press: San Diego, CA, USA, 1999.
20. Zhang, X.-X.; Cheng, S.; Zhu, C.-J.; Sun, S.-L. Microbial PAH-degradation in soil: Degradation pathways and contributing factors. *Pedosphere* **2006**, *16*, 555–565. [[CrossRef](#)]
21. Alavi, N.; Mesdaghinia, A.; Naddafi, K.; Mohebbi, G.; Daraei, H.; Maleki, A.; Alaei, L. Biodegradation of petroleum hydrocarbons in a soil polluted sample by oil-based drilling cuttings. *Soil Sediment Contam. Int. J.* **2014**, *23*, 586–597. [[CrossRef](#)]
22. USEPA. *Test Methods for Evaluating Solid Waste, Physical/Chemical Methods SW-846*; EPA Publication: Washington, DC, USA, 2015.
23. USEPA. *Hexadecane Extraction and Screening of Purgeable Organics*; USEPA: Washington, DC, USA, 1986.
24. USEPA. *Method 8015B Nonhalogenated Organics Using GC/FID*; USEPA: Washington, DC, USA, 2007.
25. USEPA. *Method 9045D Soil and Waste pH*; USEPA: Washington, DC, USA, 2004.
26. Shin, H.; Yu, J.; Wang, L.; Jeong, Y.; Kim, J. Spectral interference of heavy metal contamination on spectral signals of moisture content for heavy metal contaminated soils. *IEEE Trans. Geosci. Remote. Sens.* **2020**, *58*, 2266–2275. [[CrossRef](#)]
27. Bosso, L.; Scelza, R.; Testa, A.; Cristinzio, G.; Rao, M. Depletion of pentachlorophenol contamination in an agricultural soil treated with *Byssochlamys nivea*, *Scopulariopsis brumptii* and urban waste compost: A laboratory microcosm study. *Water Air Soil Pollut.* **2015**, *226*, 183. [[CrossRef](#)]
28. ASTM. *ASTM D2974-14 Standard Test Methods for Moisture, Ash, and Organic Matter of Peat and Other Organic Soils*; ASTM International: West Conshohocken, PA, USA, 2014.
29. Xue, W.; Peng, Z.; Huang, D.-L.; Zeng, G.; Wan, J.; Xu, R.; Cheng, M.; Zhang, C.; Jiang, D.; Hu, Z. Nanoremediation of cadmium contaminated river sediments: Microbial response and organic carbon changes. *J. Hazard Mater.* **2018**, *359*, 290–299. [[CrossRef](#)] [[PubMed](#)]
30. Bernard, B.B.; Bernard, H.; Brooks, J.M. *Determination of TC, TOC, and TIC in Sediments*; TDI Brooks International: College Station, TX, USA, 2004.
31. Van Reeuwijk, L.P. *Procedures for Soil Analysis*; ISRIC: Wageningen, The Netherlands, 2002.

32. Li, J.; Gong, J.; Fu, B.; Huang, Z.; Huang, Y.; Gui, L. Effect of land use conversion on soil organic carbon sequestration in the loess hilly area, loess plateau of China. *Ecol. Res.* **2006**, *22*, 641–648.
33. Klačič, P.M.A.; Nunes, A.M.; Moreira, A.D.S.; Vendruscolo, C.; Ribeiro, A.S. Determination of Na, K, Ca and Mg in Xanthan gum: Sample treatment by acid digestion. *Carbohydr. Polym.* **2011**, *83*, 1895–1900. [[CrossRef](#)]
34. Nakasaki, K.; Hirai, H. Temperature control strategy to enhance the activity of yeast inoculated into compost raw material for accelerated composting. *Waste Manag.* **2017**, *65*, 29–36. [[CrossRef](#)]
35. Komilis, D.; Vrohidou, A.-E.K.; Voudrias, E.A. Kinetics of aerobic bioremediation of a diesel-contaminated sandy soil: Effect of nitrogen addition. *Water Air Soil Pollut.* **2009**, *208*, 193–208. [[CrossRef](#)]
36. Chemlal, R.; Tassist, A.; Drouiche, M.; Lounici, H.; Mameri, N.; Drouiche, N. Microbiological aspects study of bioremediation of diesel-contaminated soils by biopile technique. *Int. Biodeterior. Biodegrad.* **2012**, *75*, 201–206. [[CrossRef](#)]
37. Tellez, G.T.; Nirmalakhandan, N.; Gardeatorresdey, J.L. Evaluation of biokinetic coefficients in degradation of oil-field produced water under varying salt concentrations. *Water Res.* **1995**, *29*, 1711–1718. [[CrossRef](#)]
38. Eweis, J.B.; Ergas, S.J.; Chang, D.P.Y.; Schroeder, E.D. *Bioremediation Principles*; McGraw-Hill Book Company Europe: Maidenhead, UK, 1998; p. 296.
39. Coulon, F.; Brassington, K.J.; Bazin, R.; Linnet, P.E.; Thomas, K.A.; Mitchell, T.R.; Lethbridge, G.; Smith, J.W.N.; Pollard, S.J. Effect of fertilizer formulation and bioaugmentation on biodegradation and leaching of crude oils and refined products in soils. *Environ. Technol.* **2012**, *33*, 1879–1893. [[CrossRef](#)]
40. Wu, G.; Kechavarzi, C.; Li, X.; Sui, H.; Pollard, S.J.; Coulon, F. Influence of mature compost amendment on total and bioavailable polycyclic aromatic hydrocarbons in contaminated soils. *Chemosphere* **2013**, *90*, 2240–2246. [[CrossRef](#)] [[PubMed](#)]
41. Shahsavari, E.; Adetutu, E.M.; Anderson, P.; Ball, A.S. Necrophytoremediation of phenanthrene and pyrene in contaminated soil. *J. Environ. Manag.* **2013**, *122*, 105–112. [[CrossRef](#)] [[PubMed](#)]
42. Brook, T.R.; Stiver, W.H.; Zytner, R.G. Biodegradation of diesel fuel in soil under various nitrogen addition regimes. *Soil Sediment Contam. Int. J.* **2001**, *10*, 539–553. [[CrossRef](#)]
43. Shewfelt, K.; Lee, H.; Zytner, R.G. Optimization of Nitrogen for Bioventing of Gasoline Contaminated Soil. *J. Environ. Eng. Sci.* **2005**, *4*, 29–42. [[CrossRef](#)]
44. Rončević, S.; Dalmacija, B.; Ivancev-Tumbas, I.; Tričković, J.; Petrović, O.; Klasnja, M.; Agbaba, J. Kinetics of degradation of hydrocarbons in the contaminated soil layer. *Arch. Environ. Contam. Toxicol.* **2005**, *49*, 27–36. [[CrossRef](#)]
45. Li, H.; Zhang, Y.; Kravchenko, I.; Xu, H.; Zhang, C.-G. Dynamic changes in microbial activity and community structure during biodegradation of petroleum compounds: A Laboratory experiment. *J. Environ. Sci.* **2007**, *19*, 1003–1013. [[CrossRef](#)]
46. Mancera-López, M.; Esparza-García, F.; Chávez-Gómez, B.; Rodríguez-Vázquez, R.; Saucedo-Castañeda, G.; Barrera-Cortés, J. Bioremediation of an aged hydrocarbon-contaminated soil by a combined System of biostimulation–bioaugmentation with filamentous fungi. *Int. Biodeterior. Biodegrad.* **2008**, *61*, 151–160. [[CrossRef](#)]
47. Suja, F.; Rahim, F.; Taha, M.R.; Hambali, N.; Razali, M.R.; Khalid, A.; Hamzah, A. Effects of local microbial bioaugmentation and biostimulation on the bioremediation of total petroleum hydrocarbons (TPH) in crude oil contaminated soil based on laboratory and field observations. *Int. Biodeterior. Biodegrad.* **2014**, *90*, 115–122. [[CrossRef](#)]
48. Smith, M.J.; Lethbridge, G.; Burns, R.G. Fate of phenanthrene, pyrene and benzo[a]pyrene during biodegradation of crude oil added to two soils. *FEMS Microbiol. Lett.* **1999**, *173*, 445–452. [[CrossRef](#)]
49. Krutz, L.J.; Beyrouy, C.A.; Gentry, T.J.; Wolf, D.C.; Reynolds, C.M. Selective enrichment of a pyrene degrader population and enhanced pyrene degradation in Bermuda grass rhizosphere. *Biol. Fertil. Soils* **2005**, *41*, 359–364. [[CrossRef](#)]



Article

Identification of Copper in Stems and Roots of *Jatropha curcas* L. by Hyperspectral Imaging

Juan Francisco García-Martín ^{1,*}, Amanda Teixeira Badaró ^{2,3}, Douglas Fernandes Barbin ^{2,*} and Paloma Álvarez-Mateos ¹

¹ Departamento de Ingeniería Química, Facultad de Química, Universidad de Sevilla, 41012 Seville, Spain; palvarez@us.es

² Department of Food Engineering, University of Campinas (UNICAMP), 13083-862 Campinas, Brazil; tbadaro.amanda@gmail.com

³ Departamento de Tecnología de Alimentos, Universitat Politècnica de València, Camino de Vera s/n, 46022 Valencia, Spain

* Correspondence: jfgarmar@us.es (J.F.G.-M.); dfbarbin@unicamp.br (D.F.B.)

Received: 9 June 2020; Accepted: 10 July 2020; Published: 12 July 2020

Abstract: The in situ determination of metals in plants used for phytoremediation is still a challenge that must be overcome to control the plant stress over time due to metals uptake as well as to quantify the concentration of these metals in the biomass for further potential applications. In this exploratory study, we acquired hyperspectral images in the visible/near infrared regions of dried and ground stems and roots of *Jatropha curcas* L. to which different amounts of copper (Cu) were added. The spectral information was extracted from the images to build classification models based on the concentration of Cu. Optimum wavelengths were selected from the peaks and valleys showed in the loadings plots resulting from principal component analysis, thus reducing the number of spectral variables. Linear discriminant analysis was subsequently performed using these optimum wavelengths. It was possible to differentiate samples without addition of copper from samples with low (0.5–1% wt.) and high (5% wt.) amounts of copper (83.93% accuracy, >0.70 sensitivity and specificity). This technique could be used after enhancing prediction models with a higher amount of samples and after determining the potential interference of other compounds present in plants.

Keywords: copper; heavy metals; *Jatropha curcas*; near infrared hyperspectral imaging; phytoremediation

1. Introduction

Mining and mineral processing results in soils containing all sorts of waste materials. These mining operations are one of the main anthropogenic sources of heavy metals in soils [1]. The high concentration of heavy metals in mining soils leads to unbalanced textural class, absence or low presence of soil structure, anomalous chemical properties, decrease in the content of essential nutrients, disruption of biogeochemical cycles, difficulty in rooting, low water retention and presence of toxic compounds [2]. Furthermore, these heavy metals represent serious problems for the development of vegetation cover.

One of the alternatives for the restoration of these soils is the use of plants degrading or immobilizing contaminants. *Jatropha curcas* L., a shrub that belongs to the Euphorbiaceae family grown in tropical and subtropical regions, is used to phytoremediate soils because it has high capacity of bioaccumulation and phytotranslocation [3,4]. In addition to the beneficial effects on the soil, the biomass obtained after phytoremediation (stems, leaves and even roots) can be used as a potential source of energy or for the production of catalytic biochars [3].

Heavy metals in plants grown in contaminated soils have a great impact on the combustion quality of the residual biomass. Therefore, the determination of heavy metals in different parts of the plants is mandatory to assess the capacity for phytoremediation and the quality of the biofuel

that can be obtained from its biomass. The in situ measurement of metals in plants is still a challenge. This measurement would allow controlling metal concentration in plants during phytoremediation and thus removing plants from contaminated soils before reaching critical metal levels. There are several methods based on chemical analysis, such as ICP-OES (Inductively Coupled Plasma—Optical Emission Spectrometry), to measure metals in plants, but they require destructive experimental sampling, and are time consuming and laborious for final quantification. Moreover, they do not provide information on the spatial distribution of metal concentrations in plants. Thus, it is necessary to develop faster, more economical and more environmentally friendly non-destructive methods for the in situ determination and quantification of metals. Visible and near-infrared (vis-NIR) spectroscopy and hyperspectral imaging (HSI) technology have been applied to several agricultural products [5–7], and could provide a reliable alternative to traditional methods to assess plant phytoremediation levels.

HSI is an emerging technique that is able to record both spectral and spatial information of samples. Contrary to other spectral techniques, which usually provide a single spectrum, HSI has as a response a hypercube, which is a three-dimensional image, composed of two spatial dimensions and one spectral dimension. In other words, with this technique, it is possible to obtain an image at each wavelength of a spectral region and a spectrum at each pixel of the image, according to the physical and chemical information of the sample to be analyzed. The chemical information identified in the NIR region is related to overtones and combinations of vibrations of molecules of C, N, O and S linked to a hydrogen atom, allowing to identify and quantify the constituents of that sample [8].

Copper (Cu) is the most abundant metal in the mining area of Andalusia (Spain). Metals do not absorb energy in the near infrared region; therefore, Cu does not show bands directly associated to it [9]. Notwithstanding, this metal is able to associate to organic groups, which are detectable in the NIR region [9]. Moreover, absorption features have been observed in metals with an unfilled *d* shell, such as Cu, Ni, Co and Cr at concentrations in soils higher to 0.4% wt. [10]. On the other hand, absorbance of plants is mainly influenced by chlorophyll content, water content and cell structure. Spectral variations in plants growing in heavy-metal-contaminated soils are particularly associated with increases in chlorophyll hydrolysis and destruction of cellular structure. Both can be investigated by vegetation indices and red edge position shift [2,11,12]. Then, the development of calibration models for Cu determination in plants by Vis-NIR HSI or, to cut costs, NIR HIS becomes possible.

The objective of this research was to use NIR HSI as a reliable and fast method to identify Cu in roots and stems of the *J. curcas* L. plant. This could represent a first step for the development of a technique, based on NIR HSI, for in situ determination of metals contained in plants being used for soils remediation and restoration purposes over phytoremediation period.

2. Materials and Methods

2.1. Raw Material

A *Jatropha curcas* L. plant that was germinated from seeds sown in vermiculite in a climate chamber, as described elsewhere [3], was transplanted to peat moss in a garden and let grow there. After roughly four years, the 2.2-meter-tall plant was planted in a 50-cm pot and placed in the rooftop of the Faculty of Chemistry of the University of Seville for 90 days to serve as control plant in a phytoremediation research [4]. Afterwards, the plant was cut, separating roots, stems and leaves.

2.2. Metal Content Analysis

Each separate part (root, stem and leaves) was weighed and dried in an oven at 60 °C for approximately 72 h, until constant weight, to remove all moisture. Once all the moisture from the different parts was extracted separately, they were chopped and ground in a hammer mill (Culatti DFH48), and subsequently sieved using a 1-mm mesh. The powder of each sample was stored in Eppendorf tubes until used.

For the analysis of metals, both stems and roots were digested at 220 °C with concentrated HNO₃ in an Ethos One microwave digester (Milestone Srl, Sorisole, Italy). After digestion, the concentrations of Fe, Cr, Cu, Mn, Ni, Pb, Zn, As, Au and Sb were quantified by using a Spectroblue TI ICP-OES (Spectro Analytical Instruments GmbH, Kleve, Germany). The analysis was performed in duplicate and the average metal concentrations are shown in Table 1.

Table 1. Metal concentrations in *Jatropha curcas* L. stems and roots.

Sample (mg/kg)	Fe	Cr	Cu	Mn	Ni	Pb	Zn	As	Au	Sb
Stem	35.17	2.99	2.99	9.95	0.83	≤0.4	10.29	≤0.8	≤0.2	≤0.2
RSD	0.57	1.24	5.76	0.22	1.37	-	0.50	-	-	-
Root	261.87	12.20	4.39	13.66	5.86	≤0.2	9.27	≤0.8	≤0.2	≤0.2
RSD	0.59	0.72	8.10	0.41	0.61	-	0.42	-	-	-

RSD: Relative standard deviation.

2.3. Sample Preparation and Image Acquisition

Copper was selected because it is the most abundant metal in the mining area of Andalusia (Spain). Fine Cu powder (particle size < 63 µm, purity ≥ 99%) from Merck España (28006 Madrid, Spain) was used for sample preparation. The experimental procedure consisted of preparing four stem samples and four root samples with different known concentrations of copper (0%; 0.5%; 1%; 5% wt.). The dried stems and roots without Cu addition were considered as the samples with 0% wt., since their Cu content was less than 0.0005% wt. (Table 1). Ten samples of each percentage were prepared for stems and roots, totalizing 80 samples. The samples were spread in 3-cm-diameter Petri dishes for image acquisition.

Hyperspectral images were acquired from each image in both sets of experiments in reflectance mode using a SWIR camera (Headwall Photonics SWIR M series, Fitchburg, MA, USA), in the range of 900–2500 nm, with an illuminator of 75 W and a scanning speed of 14.7 mm/s. The program automatically subtracted the white (~99% reflectance) and dark (0% reflectance) references from the acquired images.

2.4. Spectra Extraction and Multivariate Analysis

Image segmentation and spectrum extraction were performed using a code developed by the research group using the open software Python (version 3.7.0; Python Software Foundation License). The reflectance spectra were normalized, smoothed (Savitzky-Golay) and mean centered before multivariate data analysis. Pre-treatments such as Standard Normal Variate (SNV), Multiplicative Scatter Correction (MSC), first derivative (Savitsky-Golay smoothing, 11 points window, second order polynomial), second derivative (Savitsky-Golay smoothing, 11 points window, second order polynomial) and a combination of MSC + second derivative, and SNV + first derivative, were applied in the dataset to test prior qualitative and quantitative analysis (Principal Component Analysis and Linear Discriminant Analysis). All the multivariate data analysis, including PCA and LDA, was performed using The Unscrambler X 10.4 software (CAMO Software AS, Oslo, Norway).

2.5. Principal Components Analysis (PCA)

Principal Components Analysis was applied to data to have an overview of samples behavior and identify outliers. PCA reduces the information in a large amount of variables to Principal Components (PCs), which are new variables resulted from linear combinations of the original ones [13]. Calibration (70% of the samples) and validation (30% of the samples) sets were selected using PCA scores and Kennard-Stone algorithm. Optimum wavelengths were established manually selecting peaks and valleys in the PCA loadings.

2.6. Linear Discriminant Analysis (LDA)

Linear discriminant analysis (LDA) was performed in all pre-treated data using the optimum wavelengths selected in the loadings plot of PCA. LDA was performed with a leave-one-out cross-validation method and an external validation was carried out with the independent dataset. Models performance was measured in terms of sensitivity, specificity (of validation set) and accuracy of calibration model. Values of sensitivity and selectivity close or equal to 1.00 and accuracy of 100% show good discriminative power.

3. Results and Discussion

3.1. Spectral Analysis

Spectra of stems and roots with the same percentage of copper were averaged according to the added copper content (Figure 1). The smoothed spectra (Figure 1a) showed very similar shape for all samples, only differing in the intensity of reflectance across the spectral region. Overall, samples with higher amount of copper had higher reflectance. The smoothed spectra and the pre-treated with SNV and MSC were very similar (Figure 1a,b,e, respectively), showing peaks around 1214, 1728, 1918 and 2100 nm, which correspond to stretching vibrations of C-H in the first and second overtone, a stretching vibration of C=O in the second overtone of amides and a combination of O-H deformation and C-O stretching vibration, associated to starch, respectively. The spectra also had a valley at 1306 nm denoting stretching vibration of C-H or a combination of deformation.

The first derivative pre-treatment and a combination of SNV + first derivative spectra (Figure 1c,f) showed peaks and valleys around 1147, 1290, 1414, 1614, 1690, 1956, 2051 and 2166 nm, most attributed to stretching vibrations of C-H or a combination of the first and second overtones, and symmetric and asymmetric modes of N-H group. The intense valley around 1785 nm and the two peaks around 1900 and 2251 nm were also observed in these samples spectra, matching stretching vibrations of C-H in the first overtone in cellulose, stretching vibration of C=O in the second overtone, and a combination of vibrations of O-H stretching and O-H deformation, associated to starch. Moreover, peaks and valleys were noticed around 1100, 1252, 1366, 1566, 1660, 1747, 1842, 1909, 1994, 2089 and 2204 nm for data pre-treated with the second derivative and a combination of MSC + second derivative (Figure 1d,g), most due to stretching vibration of N-H, C-H, S-H and O-H in the first overtone or a combination of deformation [14].

As earlier mentioned, metals, such as copper, do not absorb energy in the near infrared region; therefore, they do not show bands directly associated to them [9]. Figure 2 shows the behavior of smoothed spectra of pure samples, and the difference between NIR spectra of stems and roots and the NIR spectrum of pure copper is clear. Notwithstanding, the indirect determination of inorganic Cu is possible, as demonstrated in the following sections, probably due to the balance between organic and inorganic components. This was the main objective of the current study. However, future studies should investigate the influence of chromogenic ligands and fluorescence probes, iron oxides, clay minerals and organic matter, present in plants, and how they might affect the identification of the components by optical methods.

3.2. Principal Components Analysis (PCA)

Considering the concept of pairwise classifications, samples of stems and roots added of copper were evaluated in three strategies: 1—Four classes: Class 1—0% copper, Class 2—1% copper, Class 3—0.5% copper and Class 4—5% copper; 2—Three classes: Class 1—“No copper” (0% of copper), Class 2—“Low content” (0.5–1% of copper) and Class 3—“High content” (5% of copper); and 3—Three classes: Class 1—“Low content” (0–0.5% of copper), Class 2—“Intermediate content” (1% of copper) and Class 3—“High content” (5% of copper). PCA was performed in spectra data with all pre-treatments and the outcome was evaluated in terms of the three groups of classes. Figure 3 describes the PCA scores and loadings of samples data. The pre-treatments that better succeeded in separating samples

according to their groups were the first derivative, a combination of SNV + first derivative and the second derivative (Figure 3a–c, respectively).

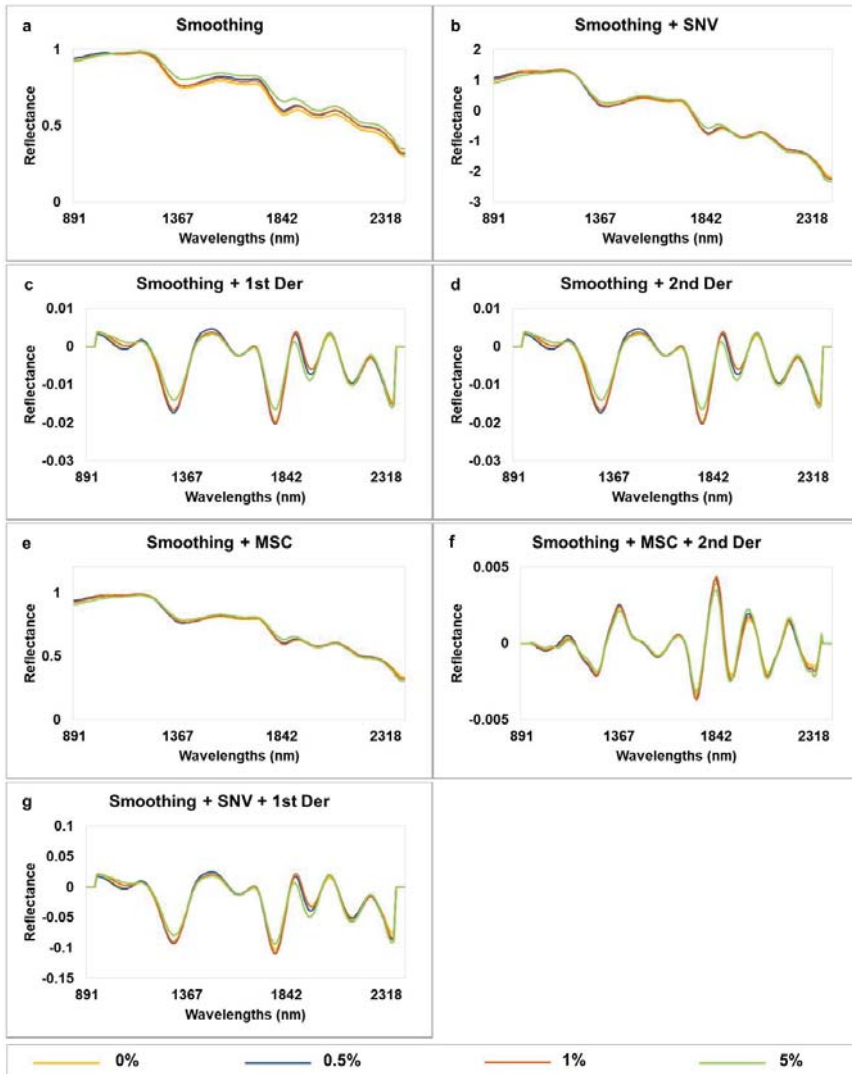


Figure 1. Spectra of stems and roots and copper pre-treated with: (a) Smoothing, (b) Smoothing + Standard Normal Variate (SNV), (c) Smoothing + first derivative, (d) Smoothing + second derivative, (e) Smoothing + Multiplicative Scatter Correction (MSC), (f) Smoothing + MSC + second derivative, (g) Smoothing + SNV + first derivative.

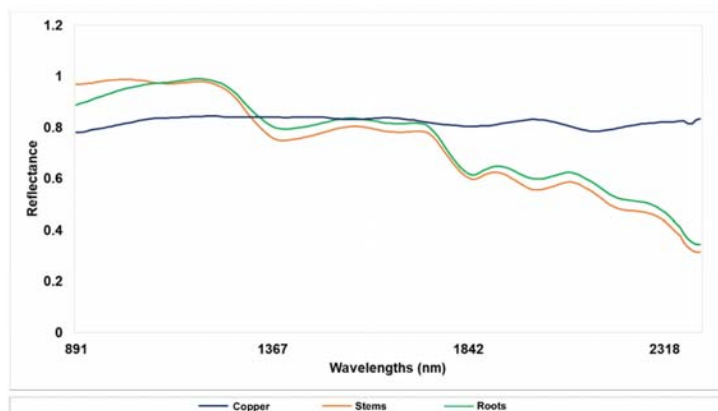


Figure 2. Smoothed spectra of pure samples: Copper (blue), Stems (orange) and Roots (green).

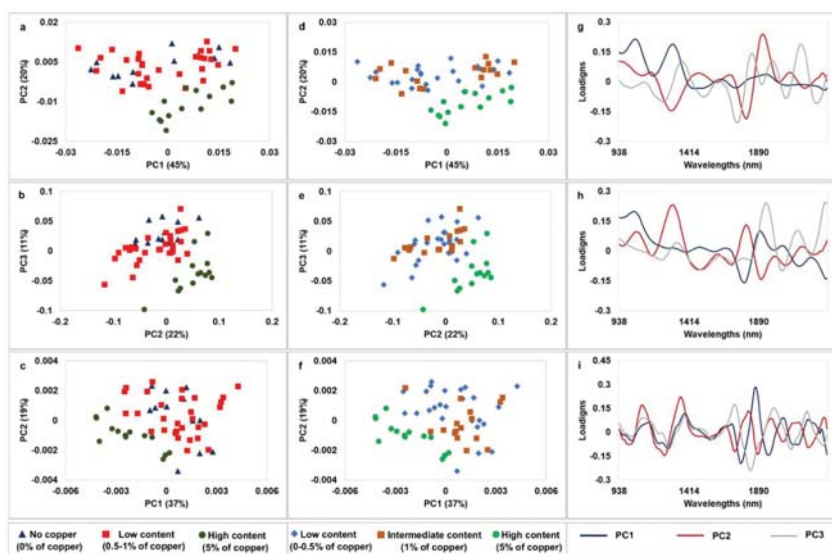


Figure 3. PCA scores and loadings of stems and roots and copper pre-treated with: (a,d,g) Smoothing + first derivative, (b,e,h) Smoothing + SNV + first derivative, (c,f,i) Smoothing + second derivative.

Figure 3a,d show the score plots after 1st derivate pre-treatment, considering strategies 2 and 3, respectively. PC1 and PC2 explained 65% of the total variance among samples in both cases. In strategy 2, samples with “No copper” and “Low content” showed some overlap, whereas samples with “High content” were grouped in a separate cluster in the right part of PC1 and negative side of PC2. In strategy 3, samples with “Low content” and “Intermediate” also had some overlap, whereas samples with “High content” were grouped in a separate cluster in the right part of PC1 and negative side of PC2.

Figure 3b,e displays PC2 and PC3 of data pre-treated with SNV + first derivative combined, showing similar behavior. That means, overlapping of Classes 1 and 2 and a separate cluster in the right part of PC1 and negative side of PC2 with samples belonging to Class 3. Figure 3c,f show that data with the second derivative had 56% of the total variance explained by PC1 and PC2. In this case, samples of Class 3 are displayed in the negative part of PC and PC3, while samples of Classes 1 and 2 are disperse in the positive side.

Figure 3g–i show the loadings plot of PC1, PC2 and PC3. The peaks and valleys on these plots were selected as optimum wavelengths and a new PCA was calculated with these reduced spectra (Figure 4). Except for the second derivative PCA, which now displays samples belonging to Class 3 in the positive side of PC1 and PC3, the recalculated PCA with the two other pre-treatments had similar behavior as with full spectra. However, variable selection seems to have reduced the dispersibility among those samples belonging to the same classes. Then, these wavelengths were used as input for the development of LDA models. Selecting few wavelengths helps reducing the number of predictors and sometimes reduces noise, thus providing better separation among samples for classification models [6,15].

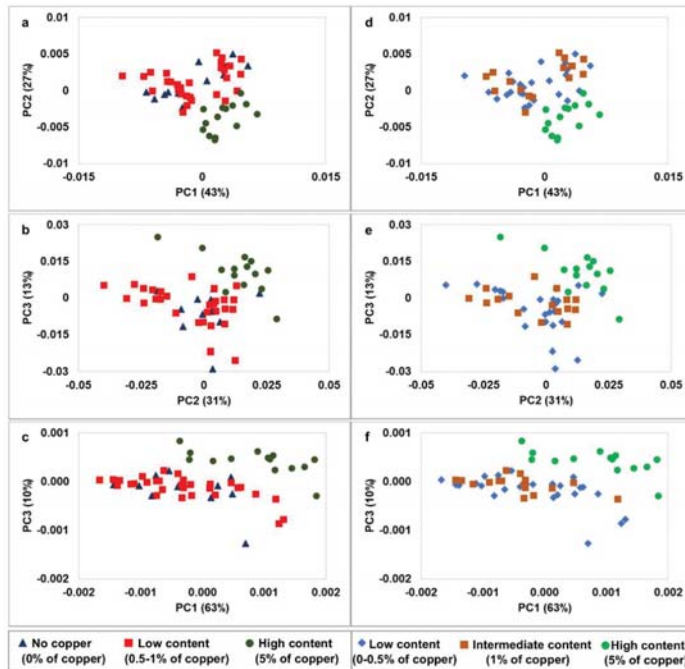


Figure 4. PCA scores of stems and roots and copper after variable selection pre-treated with: (a,d) Smoothing + first derivative, (b,e) Smoothing + SNV + first derivative, (c,f) Smoothing + second derivative.

3.3. Linear Discriminant Analysis (LDA)

Table 2 shows the models performance of LDA models for qualitative analysis of copper in stems and roots. The classifications were based in the three strategies mentioned in PCA analysis. As in PCA of the first strategy (data not shown), the results were not suitable. Even though some of the calibration models have shown good accuracy, the prediction ability for some of the classes was very low, with values of sensitivity close or equal to 0. On the other hand, the second strategy provided good accuracy for all the calibration models, ranging from 76.79–85.71%. In general, the values of sensitivity and specificity were above 0.40 and 0.56, respectively. The first derivative had the best accuracy for the calibration model (85.71%), followed by the second derivative and a combination of SNV + first derivative (83.93%). However, this last had the highest values of sensitivity and specificity (>0.70) in the external validation. Therefore, this was considered the best model for this strategy of classification, since it showed good results for all three parameters at the same time.

Table 2. Models performance of LDA for qualitative analysis of copper in stems and roots.

STRATEGY 1: C1—0% Copper, C2—1% Copper, C3—0.5% Copper, and C4—5% Copper												
Pre-Treatment	Wavelengths	Sensitivity (Validation)				Specificity (Validation)				Accuracy—Calibration Model (%)		
		C1	C2	C3	C4	C1	C2	C3	C4	Model (%)		
Smoothing	1271, 1376, 1737, 1899, 2013, 2089	0.38	0.67	0.14	1.00	0.88	0.71	0.76	1.00	69.64		
Smoothing + SNV	1147, 1376, 1737, 1851, 1928, 2013, 2118, 2223	0.38	0.67	0.43	0.83	0.69	0.86	0.82	1.00	76.79		
Smoothing + first Derivative	1042, 1166, 1309, 1366, 1480, 1709, 1747, 1813, 1918, 1975, 2061, 2185	0.50	0.67	0.14	1.00	0.94	0.67	0.82	1.00	85.71		
Smoothing + second Derivative	1138, 1271, 1376, 1556, 1709, 1775, 1871, 1947, 2051, 2137, 2232	0.38	0.33	0.14	1.00	0.69	0.86	0.71	1.00	75.00		
Smoothing + MSC	1147, 1376, 1699, 1861, 2013, 2223	0.38	0.67	0.43	0.83	0.81	0.76	0.82	1.00	69.64		
Smoothing + MSC + second Derivative	1081, 1271, 1376, 1556, 1633, 1756, 1851, 1947, 2032, 2108, 2213	0.25	0.33	0.43	0.67	0.75	0.67	0.82	1.00	71.43		
Smoothing + SNV + first Derivative	1042, 1166, 1309, 1480, 1671, 1747, 1899, 2061, 2166	0.50	0.67	0.00	0.83	0.88	0.62	0.82	1.00	85.71		
STRATEGY 2: C1—“No Copper” (0%), C2—“Low Content” (0.5–1%) and C3—“High Content” (5%)												
Pre-Treatment	Wavelengths	Sensitivity (Validation)				Specificity (Validation)				Accuracy—Calibration Model (%)		
		C1	C2	C3	C4	C1	C2	C3	C4	Model (%)		
Smoothing	1271, 1376, 1737, 1899, 2013, 2089	0.63	0.70	1.00	0.81	0.81	0.79	1.00	1.00	78.57		
Smoothing + SNV	1147, 1376, 1737, 1851, 1928, 2013, 2118, 2223	0.63	0.40	0.83	0.56	0.56	0.79	1.00	1.00	76.79		
Smoothing + first Derivative	1042, 1166, 1309, 1366, 1480, 1709, 1747, 1813, 1918, 1975, 2061, 2185	0.63	0.70	1.00	0.81	0.81	0.79	1.00	1.00	85.71		
Smoothing + second Derivative	1138, 1271, 1376, 1556, 1709, 1775, 1871, 1947, 2051, 2137, 2232	0.75	0.40	1.00	0.63	0.63	0.86	1.00	1.00	83.93		
Smoothing + MSC	1147, 1376, 1699, 1861, 2013, 2223	0.50	0.50	0.83	0.63	0.63	0.71	1.00	1.00	76.79		
Smoothing + MSC + second Derivative	1081, 1271, 1376, 1556, 1633, 1756, 1851, 1947, 2032, 2108, 2213	0.50	0.50	0.67	0.63	0.63	0.64	1.00	1.00	82.14		
Smoothing + SNV + first Derivative	1042, 1166, 1309, 1480, 1671, 1747, 1899, 2061, 2166	0.75	0.70	1.00	0.81	0.81	0.86	1.00	1.00	83.93		
STRATEGY 3: C1—“Low Content” (0–0.5%), C2—“Intermediate Content” (1%) and C3—“High Content” (5%)												
Pre-Treatment	Wavelengths	Sensitivity (Validation)				Specificity (Validation)				Accuracy—Calibration Model (%)		
		C1	C2	C3	C4	C1	C2	C3	C4	Model (%)		
Smoothing	1271, 1376, 1737, 1899, 2013, 2089	0.33	0.33	1.00	0.78	0.78	0.52	1.00	1.00	69.64		
Smoothing + SNV	1147, 1376, 1737, 1851, 1928, 2013, 2118, 2223	0.67	0.67	0.83	0.78	0.78	0.76	1.00	1.00	78.57		
Smoothing + first Derivative	1042, 1166, 1309, 1366, 1480, 1709, 1747, 1813, 1918, 1975, 2061, 2185	0.40	1.00	1.00	1.00	0.89	0.57	1.00	1.00	82.14		
Smoothing + second Derivative	1138, 1271, 1376, 1556, 1709, 1775, 1871, 1947, 2051, 2137, 2232	0.67	0.67	1.00	0.89	0.76	0.76	1.00	1.00	78.57		
Smoothing + MSC	1147, 1376, 1699, 1861, 2013, 2223	0.40	0.67	0.83	0.78	0.78	0.57	1.00	1.00	75.00		
Smoothing + MSC + second Derivative	1081, 1271, 1376, 1556, 1633, 1756, 1851, 1947, 2032, 2108, 2213	0.53	0.33	0.67	0.78	0.78	0.57	1.00	1.00	80.36		
Smoothing + SNV + first Derivative	1042, 1166, 1309, 1480, 1671, 1747, 1899, 2061, 2166	0.47	0.67	1.00	0.89	0.89	0.62	1.00	1.00	85.71		

Values of sensitivity and specificity for validation models above 0.8 are adequate for classification models with screening purposes. For instance, values of 0.8 or higher in the identification of different types of barley have been achieved [7]. Depending on the composition of samples analyzed and the type of feature to be identified, classification models may range between different levels of sensitivity, specificity, accuracy or other figures of merit used to assess models performance [16]. This approach could be used for screening purposes, identifying heavy-metal contaminated plants that could be subsequently used in different industrial processes [17].

The LDA models accuracy considering the third strategy achieved acceptable results, ranging from 69.64% to 85.71%. The model developed with SNV + first derivative had the best model accuracy (85.71%), followed by the first derivative (82.14%), and a combination of MSC + second derivative (80.36%). However, at least one class in each classification had values of sensitivity lower than 0.50. Although the accuracy of the second derivative and SNV models (78.57%) was lower than the first three, the ability to predict the samples into their classes was better in these models. The values of sensitivity and specificity were above 0.67 and 0.76, respectively. The proposed approach demonstrated feasibility to differentiate samples with different amounts of added copper by NIR-HSI. Further studies should consider the interference of other components in the sample, and how they could affect the spectral information in the near-infrared range.

4. Conclusions

Despite the inherent difficulty of quantify the concentration of metals such as Cu by their NIR absorbance, the results illustrate that NIR-HSI can differentiate plants (roots or stems) samples with different Cu concentrations.

From the PCA plots, it could be observed that, among the spectral pre-treatments assayed, those that better succeeded in separating samples according to their groups were the first derivative, a combination of SNV + first derivative and the second derivative. Samples from classes 1 and 2 had more misclassified samples while the results of the sensitivity and specificity in class 3 were always close or equal to one.

Based on LDA results, the second strategy was considered the most suitable for differentiate stem and root samples with different Cu concentrations. This strategy achieved good accuracy (76.79–85.71%) for all the calibration models, where the first derivative was the spectral pre-treatment that provided the best accuracy. Notwithstanding, the second derivative and a combination of SNV + first derivative showed the highest values of sensitivity and specificity (>0.70) in the external validation along with a good accuracy in the calibration model (83.93%).

Further research on the determination of other highly contaminating heavy metals by NIR-HSI are required to prove that this technology can be used for the in situ determination of the actual level of metals in plants over phytoremediation period. Moreover, the potential interferences due to the presence of chromogenic ligands and fluorescence probes, iron oxides, clay minerals and organic matter should be investigated.

Author Contributions: Conceptualization, D.F.B. and J.F.G.-M.; methodology, D.F.B.; software, D.F.B. and A.T.B.; formal analysis, D.F.B. and A.T.B.; resources, P.Á.-M.; writing—original draft preparation, J.F.G.-M. and D.F.B.; writing—review and editing, J.F.G.-M. and D.F.B.; project administration, P.Á.-M.; funding acquisition, P.Á.-M. All authors have read and agreed to the published version of the manuscript.

Funding: Hyperspectral images acquisition and analysis were performed in the Research, Technology and Innovation Centre (CITIUS) of the University of Seville through a grant for the use of its equipment (VIPIT-2019-I.5) within the “VI Plan Propio de Investigación y Transferencia” of the University of Seville.

Acknowledgments: Douglas Fernandes Barbin would like to acknowledge the University of Seville for the mobility grant (VIPIT-2019-I.3) awarded under the “VI Plan Propio de Investigación y Transferencia” of the University of Seville. Amanda Teixeira Badaró would like to thank the São Paulo Research Foundation (FAPESP) for the grants, numbers 2017/17628-3 and 2019/06842-0.

Conflicts of Interest: The authors declare no conflict of interest.

References

1. Jiménez-Moraza, C.; Iglesias, N.; Palencia, I. Application of sugar foam to a pyrite-contaminated soil. *Miner. Eng.* **2006**, *19*, 399–406. [CrossRef]
2. Shi, T.; Chen, Y.; Liu, Y.; Wu, G. Visible and near-infrared reflectance spectroscopy-An alternative for monitoring soil contamination by heavy metals. *J. Hazard. Mater.* **2014**, *265*, 166–176. [CrossRef] [PubMed]
3. Álvarez-Mateos, P.; Alés-Álvarez, F.J.; García-Martín, J.F. Phytoremediation of highly contaminated mining soils by *Jatropha curcas* L. and production of catalytic carbons from the generated biomass. *J. Environ. Manag.* **2019**, *231*, 886–895. [CrossRef] [PubMed]
4. García Martín, J.F.; del González Caro, M.C.; del López Barrera, M.C.; Torres García, M.; Barbin, D.; Álvarez-Mateos, P. Metal accumulation by *Jatropha curcas* L. adult plants grown on heavy metal-contaminated soil. *Plants* **2020**, *9*, 418. [CrossRef] [PubMed]
5. Badaró, A.T.; García-Martín, J.F.; del López-Barrera, M.C.; Barbin, D.F.; Alvarez-Mateos, P. Determination of pectin content in orange peels by near infrared hyperspectral imaging. *Food Chem.* **2020**, *323*, 126861. [CrossRef] [PubMed]
6. García Martín, J.F. Optical path length and wavelength selection using Vis/NIR spectroscopy for olive oil's free acidity determination. *Int. J. Food Sci. Technol.* **2015**, *50*, 1461–1467. [CrossRef]
7. Lopes, J.F.; Ludwig, L.; Barbin, D.F.; Grossmann, M.V.E.; Barbon, S. Computer vision classification of barley flour based on spatial pyramid partition ensemble. *Sensors* **2019**, *19*, 2953. [CrossRef] [PubMed]
8. Chandrasekaran, I.; Panigrahi, S.S.; Ravikanth, L.; Singh, C.B. Potential of near-infrared (NIR) spectroscopy and hyperspectral imaging for quality and safety assessment of fruits: An overview. *Food Anal. Methods* **2019**, *12*, 2438–2458. [CrossRef]
9. Moros, J.; De Vallejuelo, S.F.O.; Gredilla, A.; De Diego, A.; Madariaga, J.M.; Garrigues, S.; De La Guardia, M. Use of reflectance infrared spectroscopy for monitoring the metal content of the estuarine sediments of the Nerbioi-Ibaizabal River (Metropolitan Bilbao, Bay of Biscay, Basque Country). *Environ. Sci. Technol.* **2009**, *43*, 9314–9320. [CrossRef] [PubMed]
10. Wu, Y.; Chen, J.; Ji, J.; Gong, P.; Liao, Q.; Tian, Q.; Ma, H. A Mechanism study of reflectance spectroscopy for investigating heavy metals in soils. *Soil Sci. Soc. Am. J.* **2007**, *71*, 918–926. [CrossRef]
11. Rathod, P.H.; Rossiter, D.G.; Noomen, M.F.; van der Meer, F.D. Proximal spectral sensing to monitor phytoremediation of metal-contaminated soils. *Int. J. Phytoremediat.* **2013**, *15*, 405–426. [CrossRef] [PubMed]
12. Manios, T.; Stentiford, E.I.; Millner, P.A. The effect of heavy metals accumulation on the chlorophyll concentration of *Typha latifolia* plants, growing in a substrate containing sewage sludge compost and watered with metaliferus water. *Ecol. Eng.* **2003**, *20*, 65–74. [CrossRef]
13. Verdú, S.; Vázquez, F.; Ivorra, E.; Sánchez, A.J.; Barat, J.M.; Grau, R. Hyperspectral image control of the heat-treatment process of oat flour to model composite bread properties. *J. Food Eng.* **2017**, *192*, 45–52. [CrossRef]
14. Osborn, B.G.; Fearn, T.; Hindle, P.H. Theory of near infrared spectroscopy. In *Practical NIR Spectroscopy with Applications in Food and Beverage Analysis*; Longman Singapore Publishers (Pte) Ltd.: London, UK, 1993; pp. 13–35.
15. Barbin, D.F.; Badaró, A.T.; Honorato, D.C.B.; Ida, E.Y.; Shimokomaki, M. Identification of Turkey meat and processed products using near infrared spectroscopy. *Food Control* **2020**, *107*, 106816. [CrossRef]
16. Nolasco-Perez, I.M.; Rocco, L.A.C.M.; Cruz-Tirado, J.P.; Pollonio, M.A.R.; Barbon, S.; Barbon, A.P.A.C.; Barbin, D.F. Comparison of rapid techniques for classification of ground meat. *Biosyst. Eng.* **2019**, *183*, 151–159. [CrossRef]
17. Garcia-Martín, J.F.; Alés-Álvarez, F.J.; Torres-García, M.; Feng, C.-H.H.; Álvarez-Mateos, P. Production of oxygenated fuel additives from residual glycerine using biocatalysts obtained from heavy-metal-contaminated *Jatropha curcas* L. roots. *Energies* **2019**, *12*, 740. [CrossRef]



© 2020 by the authors. Licensee MDPI, Basel, Switzerland. This article is an open access article distributed under the terms and conditions of the Creative Commons Attribution (CC BY) license (<http://creativecommons.org/licenses/by/4.0/>).

Article

A Novel Approach in Crude Enzyme Laccase Production and Application in Emerging Contaminant Bioremediation

Luong N. Nguyen ^{1,*}, Minh T. Vu ¹, Md Abu Hasan Johir ¹, Nirenkumar Pathak ¹, Jakub Zdarta ², Teofil Jesionowski ², Galilee U. Semblante ³, Faisal I. Hai ⁴, Hong Khanh Dieu Nguyen ⁵ and Long D. Nghiem ¹

¹ Centre for Technology in Water and Wastewater, School of Civil and Environmental Engineering, University of Technology Sydney, Ultimo, NSW 2220, Australia; truongminh.vu@student.uts.edu.au (M.T.V.); Mohammed.johir@uts.edu.au (M.A.H.J.); Nirenkumar.pathak@uts.edu.au (N.P.); duclong.ngkiem@uts.edu.au (L.D.N.)

² Faculty of Chemical Technology, Institute of Chemical Technology and Engineering, Poznan University of Technology, Berdychowo 4, 60965 Poznan, Poland; jakub.zdarta@put.poznan.pl (J.Z.); teofil.jesionowski@put.poznan.pl (T.J.)

³ Technical Services, Western Sydney University, Kingswood, NSW 2747, Australia; g.semlante@westernsydney.edu.au

⁴ Strategic Water Infrastructure Lab, School of Civil, Mining and Environmental Engineering, University of Wollongong, Wollongong, NSW 2522, Australia; Faisal@uow.edu.au

⁵ School of Chemical Engineering, Ha Noi University of Science and Technology, Ha Noi 100000, Vietnam; hong.nguyenkhanhdieu@hust.edu.vn

* Correspondence: luongngoc.nguyen@uts.edu.au; Tel.: +61-0468-863-865

Received: 8 May 2020; Accepted: 27 May 2020; Published: 29 May 2020

Abstract: Laccase enzyme from white-rot fungi is a potential biocatalyst for the oxidation of emerging contaminants (ECs), such as pesticides, pharmaceuticals and steroid hormones. This study aims to develop a three-step platform to treat ECs: (i) enzyme production, (ii) enzyme concentration and (iii) enzyme application. In the first step, solid culture and liquid culture were compared. The solid culture produced significantly more laccase than the liquid culture (447 vs. 74 $\mu\text{M}/\text{min}$ after eight days), demonstrating that white rot fungi thrived on a solid medium. In the second step, the enzyme was concentrated 6.6 times using an ultrafiltration (UF) process, resulting in laccase activity of 2980 $\mu\text{M}/\text{min}$. No enzymatic loss due to filtration and membrane adsorption was observed, suggesting the feasibility of the UF membrane for enzyme concentration. In the third step, concentrated crude enzyme was applied in an enzymatic membrane reactor (EMR) to remove a diverse set of ECs (31 compounds in six groups). The EMR effectively removed of steroid hormones, phytoestrogen, ultraviolet (UV) filters and industrial chemical (above 90%). However, it had low removal of pesticides and pharmaceuticals.

Keywords: crude enzyme laccase; white-rot fungi; membrane filtration; emerging contaminants; enzymatic degradation; enzymatic membrane reactor

1. Introduction

The occurrence of emerging contaminants (ECs) in water and wastewater has been identified as a critical environmental and health issue. The EC concentration in water bodies varies from a few nanograms to several micrograms per liter [1–3]. Although ECs occur only at trace level [3], there is compelling evidence that biologically active compounds such as pesticides, steroid hormones, pharmaceuticals, industrial chemicals, phytoestrogens can cause endocrine disruption as well as inhibiting the sexual and reproductive growth of wildlife [3,4]. This portends a potential impact to

greater ecology as well as human health. Thus, the remediation of ECs has been of great interest in recent years. Research efforts have led to innovations in remediation methods (e.g., membrane filtration, advanced oxidation process, membrane bioreactor, and activated carbon adsorption). These methods are based on physical, chemical and biological mechanisms. The membrane filtration process (i.e., nanofiltration and reverse osmosis) can effectively separate ECs with validated data from pilot and full-scale studies [5–7]. However, the treatment of nanofiltration (NF) and reverse osmosis (RO) concentrate is required since it contains a high level of ECs. Advanced oxidation process and activated carbon adsorption have also gained attention for their effectiveness in EC removal [4,8]. These methods have been used in a secondary or tertiary treatment because of the influence of high bulk organic content or high turbidity, which require high UV or ozone and activated carbon dosage. Membrane bioreactor (MBR) technology has been developed as an alternative to the conventional activated sludge process. The research data showed that MBR effectively removes hydrophobic (i.e., adsorption on sludge) and readily biodegradable materials by the bacteria community, and, less effectively, the hydrophilic and biologically persistent ECs [9,10]. Recent development in the enzymatic transformation of ECs that are persistent to bacterial degradation is a promising eco-friendly concept [11].

Lignin modifying enzymes, such as laccase from white-rot fungi, are potential biological agents for the oxidation of ECs. Laccase is one of the lignin modifying enzymes produced extracellularly by white-rot fungi when they degrade plant materials for growth. Since their discovery, enzymes have been applied for detoxifying and decolorizing in the pulp industry. Recently, laccase has been used to biodegrade contaminants due to its oxidation capacity in phenolic and some non-phenolic compounds [11,12]. Enzyme laccase in both crude and purified forms has been demonstrated to biodegrade ECs in batch and continuous experiments [11,13]. However, the high cost and loss of enzyme during the continuous application are two major roadblocks for the widespread application of this promising biotechnology.

Because ECs present in aqueous solutions, previous studies aimed to culture white-rot fungi using solid-free media. This approach is challenged by the low-volume production and high cost [14]. Solid-state culture can increase laccase production because white-rot fungi naturally prefer moist conditions. However, the solid state culture entails extraction and purification steps before its application [14,15]. Applying a membrane process to prevent enzyme washout in the enzyme application process is advantageous [13,16]. A few studies have showed promising results in enzyme retention as well EC removal using membranes [13,16,17]. However, regular enzyme addition is necessary due to enzyme denaturation, suggesting that an enzyme source that provides high amounts of enzyme is needed for this approach to be successful.

This study aims to develop an end-to-end enzyme-based platform that delivers a complete functional solution for EC treatment. The platform has three steps: enzyme production, enzyme concentration, and enzyme application. The enzyme production in liquid and solid culture was compared side by side to determine yield and efficiency. Crude enzyme from both cultures was concentrated in an ultrafiltration (UF) membrane. Finally, the concentrated crude enzyme solution was used to assess the removal efficiency of 31 ECs in an enzymatic membrane reactor (EMR). This study will pave the way for the future development in the enzymatic degradation of pollutants.

2. Materials and Methods

2.1. Liquid and Solid Culture of White-Rot Fungi (WRF) for Enzyme Production

Stock pure cultures (i.e., 1 g pellet) of *Pleurotus ostreatus* (ATCC 34675) were purchased from the American Type Culture Collection, Manassas, VA, USA. The stock was sub-cultured on malt extract agar (41 g/L) Petri dishes in an incubator at 28 °C and 60% humidity. The resultant cultures were then stored at 4 °C for future experiments.

Malt extract broth (Merck, Darmstadt, Germany) was used to develop liquid culture at a concentration of 5 g/L for crude enzyme production. The culture medium (100 mL) was added in an Erlenmeyer flask and adjusted to pH 6.2. The flask was covered with aluminum foils. The culture medium was autoclaved using the Tuttnauer 28 L Bench Top Autoclave (Lab Gear, Brisbane, Australia) at 121 °C for 15 min. One mycelial plug of the stock culture (1 × 1 cm) was transferred from the malt extract agar plate to the flask. The liquid culture was maintained at a temperature and mixing rate of 28 °C and 70 rpm, respectively, for eight days. The medium containing laccase enzyme was harvested and stored at 4 °C in a sterilized bottle. Enzymatic activity of this solution was measured from day 4 of the culture period according to the enzymatic activity assay in Section 2.5.1.

Malt extract agar (Merck, Darmstadt, Germany) was used to develop the solid culture for crude enzyme production. The culture medium was prepared in the same fashion as the liquid culture (i.e., at a concentration of 5 g/L). After the autoclave step, the medium cooled and solidified on the flask. One piece of the stock culture (1 × 1 cm) was transferred from the malt extract agar plate to the flask. The flask was incubated in an incubator at 28 °C and 60% humidity. On day 4 of the incubation period, mycelium developed to cover the agar surface. Autoclaved Milli-Q water (100 mL) was added into the flask. The produced enzyme laccase from the agar dissolved into the water at the bottom, while the agar with mycelium floated on the top. Enzymatic activity was measured from every day from day 4 to day 8. At the end of day 8, the liquid was decanted into a sterile container and stored at 4 °C.

2.2. Emerging Contaminants

A set of emerging contaminants (i.e., 31 compounds) categorized into six groups, such as pharmaceuticals, personal care products (i.e., UV filters), pesticides, industrial chemicals, natural phytoestrogens, steroid hormones was selected as model compounds. These compounds have different chemical properties, such as phenolic or non-phenolic bearing molecular structures [2]. They have also been reported to occur in wastewater and contaminated water bodies around the world [3].

All compounds were analytical grade (>99% purity, Sigma Aldrich, Sydney, Australia). A stock solution containing 31 ECs at 1 g/L each in methanol was prepared and kept in −18 °C conditions. This stock solution was used within a month to avoid any degradation. This stock solution was added in Milli-Q water to achieve 5 µg/L concentration of each compound in the feed.

2.3. Membrane Setup for Enzyme Concentration

A laboratory scale membrane filtration unit consisted of a Tangential Flow Filters (TFF) cartridge (Millipore, Burlington, MA, USA), a pressure gauge and a master flex pump was employed in this study. The TFF cartridge was made of regenerated cellulose. The molecular weight cut off and surface area of the cartridge was 3 kDa and 0.09 m², respectively. The cartridge was operated at a recirculation flow rate and pressure of 4 L/min and 1 bar, respectively (Figure 1).

Crude enzyme extract from liquid and solid culture was used for the enzyme concentration experiment. For this experiment, 2 L of crude enzyme extract was pumped through the cartridge in the upflow configuration at 1 L/min to remove all air bubbles. Then, the flow rate was increased to 4 L/min while the back-pressure valve was gently closed to increase the pressure to 1 bar. Under this condition, the permeate flow rate was 10 mL/min. The crude enzyme extract was concentrated to 1 and 0.3 L volume. Enzymatic activity in the crude enzyme extract and permeate was measured.

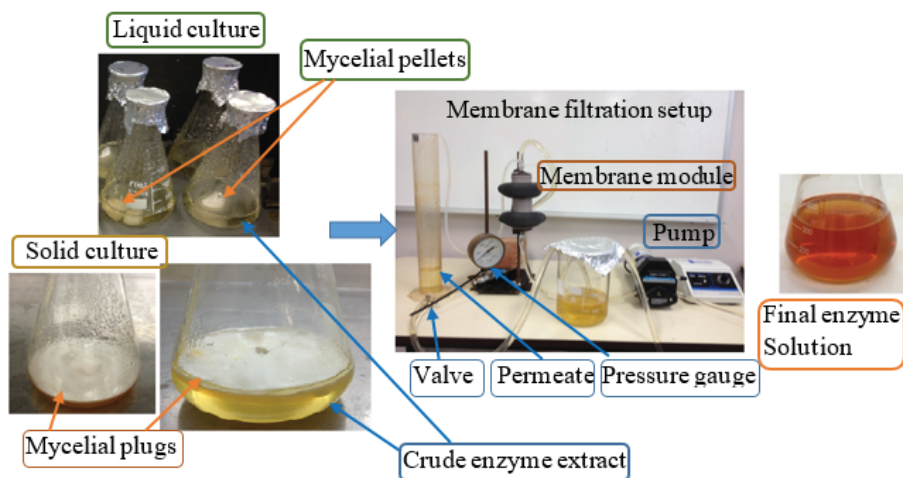
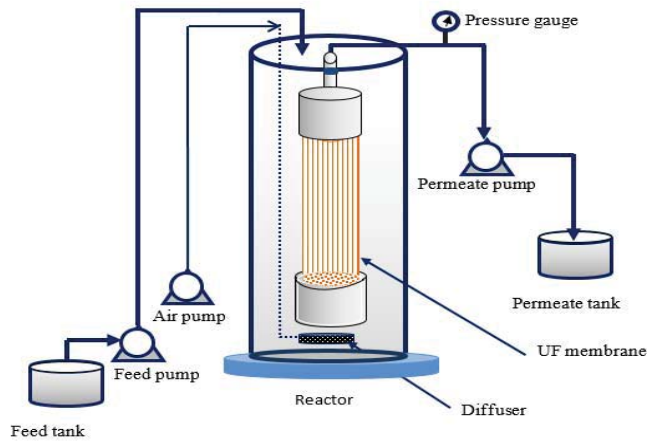


Figure 1. Mycelial pellets and mycelial plugs formation in the liquid and solid culture and the membrane filtration set up to concentrate crude enzyme extract solution.

2.4. Set Up and Operational Protocol of Enzymatic Membrane Reactor

The laboratory-scale EMR unit consisted of a Microza UF membrane (Pall Corporation, Melbourne, Australia), a 1 L glass reactor, two peristaltic pumps (Masterflex L/S, Cole-Parmer, Chicago, IL, USA), and two magnetic stir, a pressure gauge (SPER scientific 840064, Extech equipment Pty. Ltd., Victoria, Australia), a personal computer, an air pump and an air diffuser (Figure 2). The membrane was made of polyacrylonitrile with molecular weight cut off (MWCO) 6 kDa, surface area 0.19 m² and clean water flux 10 L/h·bar. The MWCO of this membrane was expected to retain completely laccase enzyme in the EMR experiment.

The EMR system was initiated by adding 1 L of Milli-Q water into the reactor. Then, a 60 mL concentrated crude enzyme extract was added, resulting in the laccase activity of 50 $\mu\text{M}_{(\text{DMP})}/\text{min}$. The UF membrane was operated in dead-end configuration. One peristaltic pump (i.e., permeate pump) was set up to get the membrane water flux of 1.1 L/m²·h. This permeate pump was run on an 8:1 min on:off cycle. The one min off was designed to provide relaxation time (i.e., without filtration) to the membrane. The permeate was collected in a stainless-steel container. The feed solution containing ECs was pumped continuously into the reactor at flow rate of 2.1 mL/min. The reactor solution (enzyme, ECs and water) was aerated via an air pump and air diffuser to get the dissolved oxygen above 3 mg/L. Air was provided in the reactor because the reaction of laccase required dissolved oxygen molecular as electron acceptor. Without any adjustment, pH of the reactor solution was 6.8 ± 0.2 during the experimental period. The potential membrane fouling was noted by recording the change of transmembrane pressure every 5 min on a data logger. In the course of the EMR operation, membrane fouling was negligible. This may be due to the operation of the UF membrane at its significant water flux. Enzymatic activity in the reactor was measured regularly. The enzyme solution (60 mL laccase/L reactor volume) was manually added (every 12 h) in the EMR to maintain laccase activity of 25 to 50 $\mu\text{M}/\text{min}$. The hydraulic retention time (i.e., how long laccase react with ECs in the reactor) was maintained at 8 h. The EMR was operated continuously for 105 h.



(a)



(b)

Figure 2. A schematic diagram (a) and a photograph of laboratory scale enzymatic membrane reactor (b).

2.5. Analytical Methods

2.5.1. Enzymatic Activity

White rot fungi *Pleurotus ostreatus* (ATCC 34675) secreted mainly laccase in the liquid and solid culture in this study. Laccase activity was measured using the method described in our previous study [18]. In brief, the assay chemicals included 800 μL of 10 mM dimethoxyl phenol (DMP) at pH 4.5 (i.e., buffered by sodium citrate), 1200 μL of 100 mM sodium citrate and 1000 μL laccase solution. The reaction was kept at room temperature (23–24 $^{\circ}\text{C}$) in two min. The resultant solution was subjected to UV absorbent measurement at 468 nm by a Shimadzu spectrophotometer (UV 6000, Shimadzu, Kyoto, Japan). The molar extinction coefficient $\epsilon = 49.6/(\text{mM}\cdot\text{cm})$ was used to calculate final laccase activity in the solution. The laccase activity can vary depending on the used substrate. In this study, laccase activity was expressed in $\mu\text{M}_{(\text{DMP})}/\text{min}$.

2.5.2. Emerging Contaminants Measurement

The EC concentration was measured by a Shimadzu GC/MS QP5000 (Kyoto, Japan) system equipped with a Shimadzu AOC 20i auto sampler (Kyoto, Japan) and a capillary gas chromatography column (i.e., A Phenomenex Zebron ZB-5 (5% diphenyl, 95% dimethylpolysiloxane). This column had 30 m length, 0.25 mm ID and $df = 0.25 \mu\text{m}$).

Samples (500 mL) of feed and permeate were collected and subjected to a solid phase extraction method before GC/MS analysis. The solid phase extraction method included a few steps. In step 1, samples were adjusted to pH 2.5 using 0.25 M H_2SO_4 . In step 2, a 6 mL 200 mg Oasis HLB cartridge was pre-conditioned consequently with the following solution (7 mL) dichloromethane and methanol (1:1 *v/v*), 7 mL methanol and 7 mL Milli-Q water. In step 3, the sample was filtered at 15 mL/min through the cartridges, allowing the absorption of ECs on the cartridges. In step 4, the cartridges were dried under nitrogen gas stream.

The absorbed ECs on the cartridge were eluted using 7 mL methanol and 7 mL mixture of methanol and dichloromethane (1:1 *v/v*). The resultant solution in 5 mL amber bottle was evaporated at 40 °C in a water bath with a gentle flow of nitrogen gas until dryness. Then, 200 μL of pure methanol was added into the bottle to dissolve the ECs. Bisphenol A-d16 (5 μg) was added into the bottle as the internal standard. The resultant solution was evaporated to dryness one more time under same conditions as above. Finally, 100 μL of N,O-Bis(trimethylsilyl)trifluoroacetamide (1% trimethylchlorosilane) plus 100 μL of pyridine was added in the bottle. The final solution was subjected to the GC-MS analysis. The GC-MS set up method for the detection of ECs was described in our previous study [2]. Our method has a quantitative detection limit in the range of 1 to 20 ng/L depending on compounds.

The removal efficiency of ECs by the EMR was calculated as:

$$R = 100 \times \left(1 - \frac{C_{Eff}}{C_{Inf}} \right)$$

where R = removal efficiency, C_{Inf} = EC concentration in influent and C_{Eff} = EC concentration in the permeate.

3. Results and Discussion

3.1. Liquid vs. Solid Culture

The solid culture produced greater enzyme than the liquid culture (Figure 3) because white rot fungi naturally grow on moist solid materials. In the past, fungal cultivation in free-flowing water was researched as a means to develop fungal bioreactors [19]. This approach enabled the direct utilization of enzymes for wastewater treatment and eliminated the need for enzyme purification. However, cultivating fungi in liquid failed to maximize the fungal biomass's potential to produce powerful enzymes. The marginal increase in enzyme production of solid culture was significantly higher than that of the liquid culture (Figure 3). This clearly indicates that fungi thrive better in solid than liquid state.

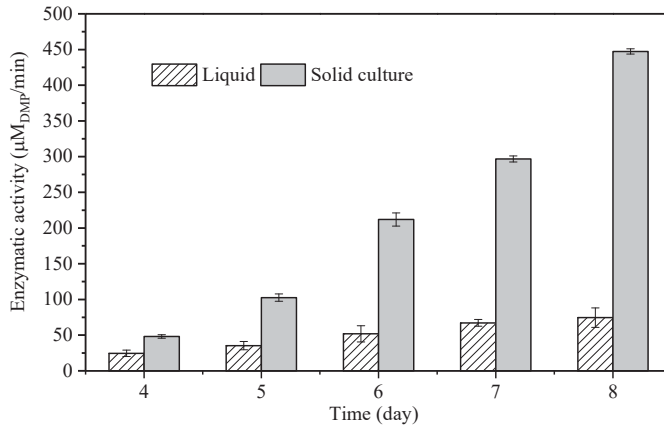


Figure 3. Enzymatic activity in the crude solution from liquid and solid culture. Note, 100 mL of Milli-Q water was added in the solid culture from day 4. The data were the average and standard deviation of five cultures.

3.2. Enhance Enzymatic Activity by Membrane Process

Crude enzyme laccase from liquid and solid culture can be effectively concentrated using the membrane configuration in this study (Figure 4). The initial crude enzyme (2 L) was concentrated to 1 and 0.3 L, resulting in 6.6 folds increment in enzymatic activity. Initial laccase activity of the crude from liquid culture was increased from 74 to 496 µM_(DMP)/min, while that of solid culture increased from 447 to 2980 µM_(DMP)/min. The high laccase activity in the concentrated crude enzyme solution will facilitate the operation of the EMR (Section 3.3), since periodical addition of enzyme is necessary. It is also anticipated that high laccase activity can be achieved if the solution volume continuous to decrease. In a previous study, an UF membrane (10 kDa) provided 20-fold concentration of crude laccase solution from a white-rot fungi *Trametes versicolor* [20]. The authors achieved the recovery of 97.5% of the activity in 50 mL volume from 1 L crude solution. The UF filtration process relies solely on size exclusion. The utilized UF membrane has molecular weight cut off significantly lower than that of the enzyme. Our results are in agreement with peer literature review studies on enzyme concentration (e.g., laccase, manganese peroxidase and lignin peroxidase) [21,22].

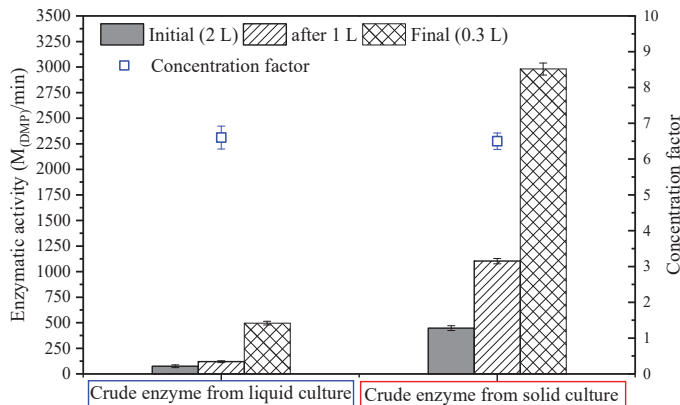


Figure 4. Laccase activity profiles at different solutions. The concentration factor was the ratio of the final over initial laccase activity. The data were the average and standard deviation of three measurements.

Laccase activity loss in this membrane filtration was negligible. The laccase activity in the final solution was proportional to the reduction in the volume (i.e., from 2 to 0.3 L). This observation indicated that no enzyme was lost during the concentration. We observed no laccase activity in the permeate (data not shown). The potential enzyme adsorption on the membrane was not measured; however, the observation of laccase activity in the final solution indicated that adsorption of enzyme on the membrane was negligible. Thus, the membrane process was suitable for the concentration of crude enzyme laccase.

3.3. Performance of Produced Enzyme on Emerging Contaminants Removal

3.3.1. Enzymatic Retention by the UF Membrane

The EMR's UF membrane completely retained *P. ostreatus* laccase (Figure 4). Over the operation period of 112 h, no trace of laccase was detected in the permeate given that the UF membrane's MWCO (6 kDa) was far smaller than the molecular weight of laccase (i.e., 67 kDa) [23]. Previous studies also reported complete enzyme retention by EMRs. Clearly, membrane MWCO and enzyme size are important characteristics that must be considered in EMR design [13,24,25].

3.3.2. Importance of Highly Concentrated Stock Enzyme Solution

The availability of a highly concentrated crude enzyme solution was critical to the smooth operation of the EMR. This was because enzymatic activity inside the EMR decreased over time. The enzymatic activity in the EMR decreased by 50% within the first 16 h operation (54 ± 2.3 to 26 ± 4.5 $\mu\text{M}/\text{min}$) (Figure 5). Hence, regular laccase addition was needed to maintain enzymatic activity and EC removal. This was readily achieved by adding small volumes of concentrated crude enzyme solution. In this study, enzymatic activity was kept within 25 to 55 $\mu\text{M}/\text{min}$ by adding 60 mL of the concentrated crude enzyme into the 1 L reactor every 12 h. Because only small increments of enzyme solution were required, there was minimal impact on reactor water level and hydraulic retention time. This would not have been possible without high output enzyme cultivation via solid culture and the enzyme concentration step.

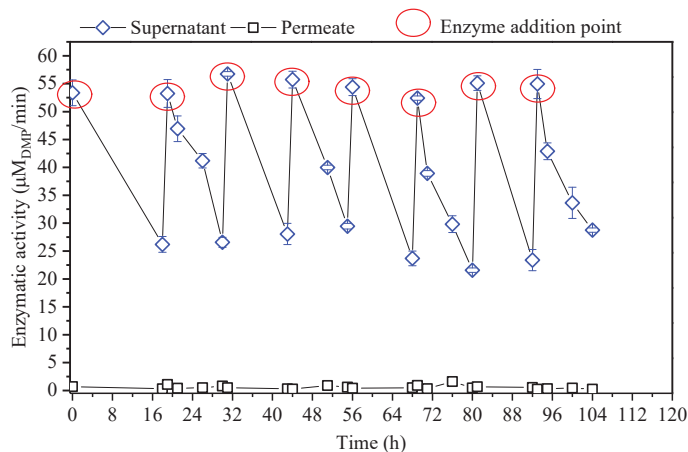


Figure 5. Enzymatic activity in the enzymatic membrane reactor (EMR) supernatant and permeate during the 112 h operation. The data were the average and standard deviation of three measurements.

Enzyme inactivation in continuous reactors is imminent due to several physicochemical and biological factors [25,26]. Operating temperature, shear rate and flow geometry can deform enzyme structure. Adsorption and deposition on membrane surface could reduce the enzyme activity in the

reactor. Chemical reactions between the laccase and pollutants eventually deactivate the enzyme [27]. Free radicals generated during the catalytic conversion of phenols and amines bearing compounds could oxidize the active site of laccase [27,28]. Microbial growth or contamination in the EMR could degrade laccase. The denaturation of laccase in the EMR system could be the combination of these factors. Detailed contributions of each factor to the overall laccase activity loss are not available in the peer-reviewed literature. However, research efforts to enhance the durability of laccase are on this trajectory with a few developed strategies (e.g., immobilization on membrane, addition of preservative chemical) [29].

3.3.3. Removal of ECs in EMR

The EMR removed a broad spectrum of emerging contaminants (i.e., 31 compounds and 6 groups). The removal efficiency depended on EC properties (Figure 6). Industrial chemicals, UV filters, phytoestrogens and steroid hormones were effectively removed (i.e., >90%). Meanwhile, the removal of compounds in the pesticide and pharmaceutical groups varied from 10% to above 90% (Figure 6).

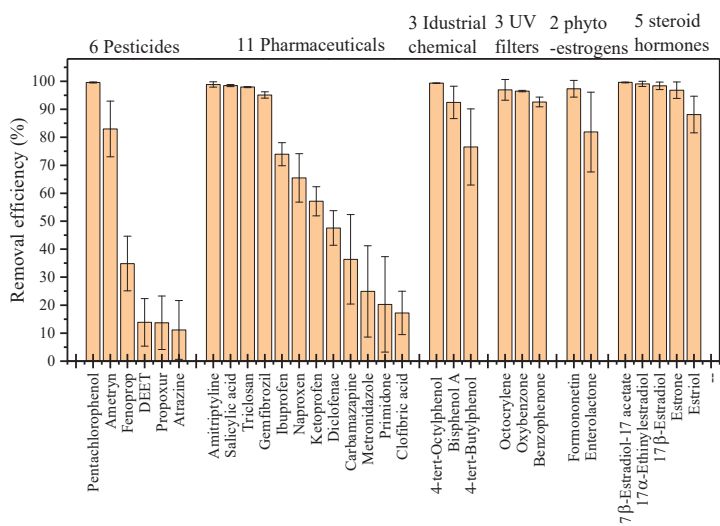


Figure 6. Removal efficiency of 31 emerging contaminants by enzymatic membrane bioreactor with crude enzyme extract from *Pleurotus ostreatus*. The data were the average and standard deviation of six samples. The samples were collected at 22, 44 and 88 h of the EMR operation.

The crude enzyme from *P. ostreatus* efficiently degraded phenolic bearing compounds (Figure 6). The catalytic reaction of laccase with the substrate results in a reductive cleavage of a dioxygen bond. In this reaction, the copper metal atoms within the laccase structure play an important role in the reduction of oxygen to water. There are three copper types in the laccase molecule: one type 1 (Cu 1), one type 2 (Cu 2) and two type 3 (Cu 3). Cu 1 is the most important electron acceptor in the oxidation. Its action governs the catalytic rate. Previous studies have identified that the redox potential of Cu 1 is between 0.42 and 0.79 mV. This redox potential could explain the laccase reaction on phenolic compounds [30]. Mehra et al. [31] also suggested that phenolic substrates have a high affinity to the Cu 1 site of the laccase for electron transfer. The variation in the redox potential of Cu 1 could explain the removal efficiency of phenolic substrates from different studies. Laccase from bacteria, plants and insects is characterized by a low redox potential, whereas white rot fungi laccase is high redox. In our previous EMR study, laccase from *Aspergillus oryzae* (redox potential of 0.28 mV) removed 40% to 60% of

for example salicylic acid, formononetin and pentachlorophenol [2]. In this study, above 95% removal efficiency was achieved for these compounds. The results highlight the importance of laccase selection.

The removal efficiency of pesticide and pharmaceutical compounds by the EMR varied significantly from 10% to 90% due to their different chemical structures. Amongst six pesticides, only one phenolic bearing compound, pentachlorophenol, was removed to 99% (Figure 6). Meanwhile, pharmaceutical compounds such as amitriptyline, salicylic acid, triclosan and gemfibrozil were effectively removed. Amongst these, only salicylic acid and triclosan contains phenolic moiety in their structures. This observation suggests that apart from the oxidation of phenolic moiety, other mechanisms may contribute to the high removal efficiency of these compounds in the EMR system.

The chemical adsorption of EC compounds on the membrane surface and/or on membrane gel layer can contribute to their overall removal. During the filtration process, an enzymatic gel layer can deposit on the membrane surface. This gel layer can perform as an active adsorbent (i.e., adsorb and oxidize). The affinity to the gel layer depends on compound hydrophobicity. In this regard, pentachlorophenol, triclosan, oxybenzone, octocrylene and benzophenone are highly hydrophobic compounds (their log D values higher than 3). This finding is consistent with our previous studies using commercially available laccase [2]. Although the application of concentrated crude enzyme in the EMR can lead to high removal efficiency of emerging contaminants, the low removal efficiency of some compounds (i.e., pesticides and pharmaceuticals) indicates a downstream treatment of EMR permeate is required. It also noted that water matrix (i.e., wastewater containing other pollutants such as metals, organic carbon, organic salts, suspended solid) could affect laccase activity. However, this research is beyond the scope of the current study.

4. Conclusions

This study demonstrated the effectiveness of solid culture over liquid culture of white rot fungi for laccase production. A six fold increment in the enzymatic activity was achieved under the same culture period (i.e., 8 days). The produced crude enzyme was concentrated by UF membrane (3 kDa), providing a new concentrated crude enzyme at laccase activity of 2980 $\mu\text{M}_{(\text{DMP})}/\text{min}$. The concentrated laccase activity was 6.6 times that of the initial value. The results also suggest no loss of enzyme during the concentration process. The concentrated crude enzyme was applied in the EMR for the continuous removal of 31 emerging contaminants. The UF membrane completely retained laccase, but denaturation in laccase activity was observed. An enzyme re-addition strategy was developed by adding 60 mL of crude solution (6% reactor volume) to maintain laccase activity. Under this operation, the EMR effectively removed of phenolic compounds such as steroid hormones, industrial chemical, phytoestrogen and UV filters. However, the removal efficiency of major pesticides and pharmaceuticals was low, indicating the limitation of laccase.

Author Contributions: L.N.N.: conceptualization, data curation, writing—original draft. M.T.V.: data curation, formal analysis. M.A.H.J.: writing—review and editing. N.P.: data curation. J.Z.: writing—review and editing. T.J.: writing—review and editing. G.U.S.: writing—review and editing. F.I.H.: writing—review and editing; supervision. H.K.D.N.: writing—review and editing and L.D.N.: writing—review and editing. All authors have read and agreed to the published version of the manuscript.

Funding: This research received no external funding.

Conflicts of Interest: The authors declare no conflict of interest.

References

- Schwarzenbach, R.P.; Egli, T.; Hofstetter, T.B.; Von Gunten, U.; Wehrli, B. Global Water Pollution and Human Health. *Annu. Rev. Environ. Resour.* **2010**, *35*, 109–136. [[CrossRef](#)]
- Nguyen, L.N.; Hai, F.I.; Price, W.E.; Kang, J.; Leusch, F.D.; Roddick, F.; van de Merwe, J.P.; Magram, S.F.; Nghiem, L.D. Degradation of a broad spectrum of trace organic contaminants by an enzymatic membrane reactor: Complementary role of membrane retention and enzymatic degradation. *Int. Biodeterior. Biodegrad.* **2015**, *99*, 115–122. [[CrossRef](#)]

3. Tran, N.H.; Reinhard, M.; Gin, K.Y. Occurrence and fate of emerging contaminants in municipal wastewater treatment plants from different geographical regions—A review. *Water Res.* **2018**, *133*, 182–207. [[CrossRef](#)] [[PubMed](#)]
4. Bolong, N.; Ismail, A.F.; Salim, M.R.; Matsuura, T. A review of the effects of emerging contaminants in wastewater and options for their removal. *Desalination* **2009**, *239*, 229–246. [[CrossRef](#)]
5. Egea-Corbacho, A.; Ruiz, S.G.; Alonso, J.M. Removal of emerging contaminants from wastewater using nanofiltration for its subsequent reuse: Full-scale pilot plant. *J. Clean. Prod.* **2019**, *214*, 514–523. [[CrossRef](#)]
6. Lopera, A.E.; Ruiz, S.G.; Alonso, J.M. Removal of emerging contaminants from wastewater using reverse osmosis for its subsequent reuse: Pilot plant. *J. Water Process Eng.* **2019**, *29*, 100800. [[CrossRef](#)]
7. Cristóvão, M.B.; Torrejais, J.; Janssens, R.; Luis, P.; Van der Bruggen, B.; Dubey, K.K.; Mandal, M.K.; Bronze, M.R.; Crespo, J.G.; Pereira, V.J. Treatment of anticancer drugs in hospital and wastewater effluents using nanofiltration. *Sep. Purif. Technol.* **2019**, *224*, 273–280. [[CrossRef](#)]
8. Coimbra, R.N.; Escapa, C.; Otero, M. Adsorption separation of analgesic pharmaceuticals from ultrapure and waste water: Batch studies using a polymeric resin and an activated carbon. *Polymers* **2018**, *10*, 958. [[CrossRef](#)]
9. Tadkaew, N.; Hai, F.I.; McDonald, J.A.; Khan, S.J.; Nghiem, L.D. Removal of trace organics by MBR treatment: The role of molecular properties. *Water Res.* **2011**, *45*, 2439–2451. [[CrossRef](#)]
10. Nguyen, L.N.; Hai, F.I.; Kang, J.; Price, W.E.; Nghiem, L.D. Removal of emerging trace organic contaminants by MBR-based hybrid treatment processes. *Int. Biodeterior. Biodegrad.* **2013**, *85*, 474–482. [[CrossRef](#)]
11. Zdart, J.; Jankowska, K.; Wyszowska, M.; Kijeńska-Gawrońska, E.; Zgola-Grzeskowiak, A.; Pinelo, M.; Meyer, A.S.; Moszyński, D.; Jesionowski, T. Robust biodegradation of naproxen and diclofenac by laccase immobilized using electrospun nanofibers with enhanced stability and reusability. *Mater. Sci. Eng. C* **2019**, *103*, 109789.
12. Tran, N.H.; Urase, T.; Kusakabe, O. Biodegradation characteristics of pharmaceutical substances by whole fungal culture *Trametes versicolor* and its laccase. *J. Water Environ. Technol.* **2010**, *8*, 125–140.
13. Nguyen, L.N.; Hai, F.I.; Price, W.E.; Leusch, F.D.; Roddick, F.; McAdam, E.J.; Magram, S.F.; Nghiem, L.D. Continuous biotransformation of bisphenol A and diclofenac by laccase in an enzymatic membrane reactor. *Int. Biodeterior. Biodegrad.* **2014**, *95*, 25–32.
14. Adekunle, A.E.; Zhang, C.; Guo, C.; Liu, C.Z. Laccase Production from *Trametes versicolor* in Solid-State Fermentation of Steam-Exploded Pretreated Cornstalk. *Waste Biomass Valorization* **2017**, *8*, 153–159. [[CrossRef](#)]
15. Galhau, C.; Wagner, H.; Hinterstoisser, B.; Haltrich, D. Increased production of laccase by the wood-degrading basidiomycete *Trametes pubescens*. *Enzym. Microb. Technol.* **2002**, *30*, 529–536. [[CrossRef](#)]
16. Lloret, L.; Eibes, G.; Feijoo, G.; Moreira, M.T.; Lema, J.M. Degradation of estrogens by laccase from *Myceliophthora thermophila* in fed-batch and enzymatic membrane reactors. *J. Hazard. Mater.* **2012**, *213*, 175–183. [[CrossRef](#)]
17. Mendoza, L.; Jonstrup, M.; Hatti-Kaul, R.; Mattiasson, B. Azo dye decolorization by a laccase/mediator system in a membrane reactor: Enzyme and mediator reusability. *Enzym. Microb. Technol.* **2011**, *49*, 478–484. [[CrossRef](#)]
18. Hai, F.I.; Yamamoto, K.; Nakajima, F.; Fukushi, K. Application of a GAC-coated hollow fiber module to couple enzymatic degradation of dye on membrane to whole cell biodegradation within a membrane bioreactor. *J. Membr. Sci.* **2012**, *389*, 67–75.
19. Nguyen, L.N.; Hai, F.I.; Yang, S.; Kang, J.; Leusch, F.D.; Roddick, F.; Price, W.E.; Nghiem, L.D. Removal of trace organic contaminants by an MBR comprising a mixed culture of bacteria and white-rot fungi. *Bioresour. Technol.* **2013**, *148*, 234–241. [[CrossRef](#)]
20. Anteck, A.; Blatkiewicz, M.; Boruta, T.; Górak, A.; Ledakowicz, S. Comparison of downstream processing methods in purification of highly active laccase. *Bioprocess Biosyst. Eng.* **2019**, *42*, 1635–1645. [[CrossRef](#)]
21. Cheng, X.; Jia, R.; Li, P.; Tu, S.; Zhu, Q.; Tang, W.; Li, X. Purification of a new manganese peroxidase of the white-rot fungus *Schizophyllum* sp. F17, and decolorization of azo dyes by the enzyme. *Enzym. Microb. Technol.* **2007**, *41*, 258–264. [[CrossRef](#)]
22. Gottschalk, L.M.; Bon, E.P.; Nobrega, R. Lignin Peroxidase from *Streptomyces viridosporus* T7A: Enzyme Concentration Using Ultrafiltration. In *Biotechnology for Fuels and Chemicals*; Humana Press: Totowa, NJ, USA, 2008.

23. Hublik, G.; Schinner, F. Characterization and immobilization of the laccase from *Pleurotus ostreatus* and its use for the continuous elimination of phenolic pollutants. *Enzym. Microb. Technol.* **2000**, *27*, 330–336. [[CrossRef](#)]
24. Chhabra, M.; Mishra, S.; Sreerishnan, T.R. Laccase/mediator assisted degradation of triarylmethane dyes in a continuous membrane reactor. *J. Biotechnol.* **2009**, *143*, 69–78. [[PubMed](#)]
25. Rios, G.M.; Belleville, M.P.; Paolucci, D.; Sanchez, J. Progress in enzymatic membrane reactors—A review. *J. Membr. Sci.* **2004**, *242*, 189–196.
26. Paolucci-Jeanjean, D.; Belleville, M.P.; Rios, G.M. A comprehensive study of the loss of enzyme activity in a continuous membrane reactor—Application to starch hydrolysis. *J. Chem. Technol. Biotechnol.* **2001**, *76*, 273–278.
27. Arregui, L.; Ayala, M.; Gómez-Gil, X.; Gutiérrez-Soto, G.; Hernández-Luna, C.E.; de los Santos, M.H.; Levin, L.; Rojo-Domínguez, A.; Romero-Martínez, D.; Sapparot, M.C.; et al. Laccases: Structure, function, and potential application in water bioremediation. *Microb. Cell Factories* **2019**, *18*, 200.
28. Kurniawati, S.; Nicell, J.A. A comprehensive kinetic model of laccase-catalyzed oxidation of aqueous phenol. *Biotechnol. Prog.* **2009**, *25*, 763–773.
29. Zdarta, J.; Meyer, A.S.; Jesionowski, T.; Pinelo, M. Developments in support materials for immobilization of oxidoreductases: A comprehensive review. *Adv. Colloid Interface Sci.* **2018**, *258*, 1–20.
30. Jeon, J.R.; Baldrian, P.; Murugesan, K.; Chang, Y.S. Laccase-catalysed oxidations of naturally occurring phenols: From in vivo biosynthetic pathways to green synthetic applications. *Microb. Biotechnol.* **2012**, *5*, 318–332. [[CrossRef](#)]
31. Mehra, R.; Muschiol, J.; Meyer, A.S.; Kepp, K.P. A structural-chemical explanation of fungal laccase activity. *Sci. Rep.* **2018**, *8*, 17285. [[CrossRef](#)]



© 2020 by the authors. Licensee MDPI, Basel, Switzerland. This article is an open access article distributed under the terms and conditions of the Creative Commons Attribution (CC BY) license (<http://creativecommons.org/licenses/by/4.0/>).



Article

Evaluation of Toxicity on *Ctenopharyngodon idella* Due to Tannery Effluent Remediated by Constructed Wetland Technology

Sobia Ashraf ¹, Muhammad Naveed ^{1,*}, Muhammad Afzal ², Sana Ashraf ^{3,4}, Sajid Rashid Ahmad ³, Khadeeja Rehman ², Zahir Ahmad Zahir ¹ and Avelino Núñez-Delgado ⁵

¹ Institute of Soil and Environmental Sciences (ISES), University of Agriculture, Faisalabad 38000, Pakistan; sobiaashraf13@gmail.com (S.A.); zazahir@yahoo.com (Z.A.Z.)

² Soil and Environmental Biotechnology Division (SEBD), National Institute for Biotechnology and Genetic Engineering (NIBGE), Faisalabad 38000, Pakistan; manibge@yahoo.com (M.A.); khadeeja.abc31@gmail.com (K.R.)

³ College of Earth and Environmental Sciences (CEES), University of the Punjab, Lahore 53700, Pakistan; sana.cees@pu.edu.pk (S.A.); sajidpu@yahoo.com (S.R.A.)

⁴ Department of Environmental Sciences, Lahore College for Women University (LCWU), Lahore 54000, Pakistan

⁵ Department Soil Science and Agricultural Chemistry, Engineering Polytechnic School, Campus University Lugo, University of Santiago de Compostela, 27002 Lugo, Spain; avelino.nunez@usc.es

* Correspondence: muhammad.naveed@uaf.edu.pk

Received: 20 April 2020; Accepted: 18 May 2020; Published: 20 May 2020

Abstract: Aquatic pollution caused by industrial effluents is an environmental issue, imposing deleterious impacts on the overall environment, specifically, on humans, by disrupting the balance of the ecosystem. Among all the industries, tanneries are considered some of the most polluting due to heavy use of toxic organic and inorganic compounds during leather processing, most of which find their way into rivers, lakes, and streams, thus exerting adverse effects on aquatic life, particularly on fish. Considering the huge concentrations of pollutants present in tannery effluents, toxicity evaluation is of prime importance. Therefore, bioassays are usually employed to assess the acute toxicity of industrial effluents and efficiency of effluent clean-up technologies as they provide a thorough response of test species to the substances present in the tested media. In the present study, the toxic effects of tannery effluent on common grass carp (*Ctenopharyngodon idella*) were studied for 96 h in laboratory conditions. The effluent was added at different concentrations, before and after treatment by constructed wetlands (CWs). During this period, mortality data was collected to calculate the 96 h-LC50 (lethal concentration inducing 50% mortality) and acute toxicity of *C. idella*. In addition to this, observations on change in morphological, physiological, and behavioural patterns were also made every 24 h. The present toxicity assay revealed that the raw tannery effluent changed the morphology, physiology, and behavioural response of fish. Moreover, fish exposure to raw/untreated effluent caused high acute toxicity and 100% mortality, due to the presence of high concentrations of salts and chromium (Cr) metal. While treatment of tannery effluent by CWs vegetated with different plants (*B. mutica*, *L. fusca*, and *T. domingensis*) significantly reduced its toxicity and fish mortality as well, and inoculation of salt and Cr-tolerant endophytic bacteria (*Enterobacter* sp. HU38, *Microbacterium arborescens* HU33, and *Pantoea stewartii* ASI11) further reduced (up to 90%) its toxicity level. Hence, the use of CWs for tannery effluent treatment can be recommended to favour public health and promote the overall safety of the environment.

Keywords: biotoxicity test; constructed wetlands; treated tannery effluent; morphological changes; behavioural response; *Ctenopharyngodon idella*

1. Introduction

Industrial growth has negatively impacted the environmental quality [1], particularly aquatic life, due to disposal of voluminous amounts of effluents into natural water resources, on a daily basis, all over the world [2–4]. Some chemicals contained in industrial effluents have been reported to be highly toxic, in a variable degree depending on the dose and exposure duration [5,6], having potential to impart serious damage to aquatic life [7,8]. Among the most vulnerable sectors is aquaculture, which is also of main importance, as it constitutes an essential opportunity to meet the global food security challenge [9].

Among all industries, tanneries are considered some of the most polluting, and are a major contributor to aquatic contamination [10]. Tannery effluent is extremely hazardous due to high organic loadings, solids, and metals [11], particularly chromium (Cr), a well-known ubiquitous pollutant considered as a great menace to aquatic environments, and ultimately, human beings [12]. The dark colouration and low oxygen content of tannery effluents indicates the strength of pollution, which ultimately affect the survival of aquatic organisms, especially fish, thus having great ecological relevance [5].

According to Srivastava et al. [13], 1–10% of tannery effluents can kill fish. Almost all types of fish are quite sensitive to polluted environment, and pollutants found in tannery effluent cause significant damage to their physiological and biochemical processes, such as endocrine disruption [14,15]. Huge physiological, histological, haematological, behavioural, genetic, biochemical, and immunological alterations in aquatic organisms have been reported due to Cr exposure [12]. The biological changes in fish caused by pollutants are called biomarkers and can be used for environmental risk assessment [16,17].

Remediation of toxic industrial effluents is crucial for the protection of receiving water bodies [18]. The quality of these obnoxious effluents is most commonly monitored by analysing major pollution parameters such as pH (Pondus Hydrogenii), electrical conductivity (EC), dissolved oxygen (DO), biochemical oxygen demand (BOD₅), chemical oxygen demand (COD), total organic carbon (TOC), total dissolved solids (TDS), total suspended solids (TSS), and metals [19–25]. However, these parameters cannot be used to evaluate toxic effects on receiving waters and subsequent susceptibility of aquatic organisms to these toxic pollutants.

The best way to evaluate effluent toxicity effect is to use biotoxicity tests that provide the complete response of the test organisms to all the pollutants in the surrounding environment [19,26–30]. Different organisms such as fish, algae, bacteria, invertebrates, fungi, etc., are most commonly used in the biotoxicity tests to determine the acceptable and safe level of pollutants in industrial discharge [19,30,31].

Generally, fish have been considered as a useful index for the purity of water, hence they can be used in toxicity assays to detect aquatic hazards [32]. Currently, more attention is being given to acute toxicity testing to detect harmful effects of toxic pollutants present in industrial effluents on aquatic organisms, due to the imposition of stringent environmental laws and regulations on industrial discharge [33,34].

In this context, several studies have reported the harmful effects of industrial effluents on fish, such as that by Martin-Skilton et al. [35], who studied some alterations in hepatic biotransformation enzymes as well as reduced levels of testosterone in juvenile turbot (*Scolophthalmus maximus*) on exposure to fuel oil, which elicits threats to the reproductive system of exposed individuals. In another study by Saborido-Ray et al. [36], tested individuals exhibited reduced growth and feed consumption when exposed to higher concentrations of commercial petroleum fuel. The petroleum fuel also negatively affected the growth and survival of the freshwater fish *Oreochromis niloticus* [37].

Besides the petroleum industry, effluent of textile factories also has damaging effects on fish, such as high lipid peroxide levels in fish, which may cause physiological problems when consumed by humans, as reported by Mahabub-uz-zaman et al. [38]. So, conducting investigations regarding quality of fish sold in local markets are crucial, especially in third world countries. Fish toxicity assays by Bhattacharya et al. [39] revealed a 100% survival rate after 72 h exposure of *Poecilia* sp. in ceramic membrane-treated effluent, as compared to 80% survival rate in untreated effluent. Moreover, high

pollutants concentrations can cause rapid suffocation in fish by destruction of the gill epithelium and inhibition of metabolic activities [40].

Morphological and physiological variations, such as loss of body balance, higher rate of mucus secretion, decrease in breathing rate, haemoglobin percentage, red blood cells (RBC) count, and breakage of deoxyribonucleic acid (DNA) were observed in fish exposed to Cr containing industrial effluents by Bakshi and Panigrahi [12]. Industrial effluents also caused significant histopathological deterioration in gill, kidney, liver, and intestine of test organisms along with significant changes in total glycogen, protein, lipid content in gill, muscle, and liver tissues. In addition to this, physiological disorders, such as hypertension, sporadic fever, renal damage, cramps, and malfunctioning in fish general health conditions due to direct discharge of tannery effluent into water channels, have also been reported by Karthikeyan et al. [41].

Constructed wetlands (CWs) are a contrasted technology, useful for remediation of highly polluted industrial effluents, and can be easily managed with low operation and maintenance cost. These biogeophysical engineered systems consisting of mainly vegetation, soils, and their associated microbial assemblages are constructed in such a way to mimic all the physical, chemical, and biological processes occurring in natural wetlands, but within more controlled environmental conditions that sustain strong plant–substrate–microbe interactions. Many studies have reported its performance for degradation/detoxification of organic and inorganic contaminants present in tannery effluent [42–44], but none of the studies have evaluated the resulting reduction in toxicity level of effluent. The present work is an endeavour to study the effect of tannery effluent (untreated and treated) on the survival of locally available fish *Ctenopharyngodon idella*, commonly known as “grass carp”, which is widely found in natural water bodies in Pakistan. In view of that, this study has a clear novelty, and would allow to obtain new data of environmental relevance.

2. Materials and Methods

2.1. Collection of Fish Samples

Ctenopharyngodon idella, irrespective of sex, were collected from local fish farms at Satiana Road, Faisalabad (Pakistan), in closed polythene bags filled with oxygen and transported to the laboratory. These fish were kept in a large glass aquarium, filled with fresh water, at 26 ± 1 °C, in the fish toxicology laboratory, Soil and Environmental Biotechnology Division, National Institute for Biotechnology and Genetic Engineering (NIBGE), Faisalabad. An aeration pump was used to ensure the continuous supply of oxygen in the aquarium, essential for fish survival. Fish were acclimatized under these conditions for one month, prior to their exposure to tannery effluent. During this period, the fish were fed with commercial fish pellets, and water was renewed on alternate days to remove the remains of feed and faecal matter/metabolic waste.

2.2. Collection of Tannery Effluent after Treatment through CWs

Grab samples of tannery effluent were collected from each CW phytoreactor for toxicity testing, considering three different treatments, viz., CWs vegetated with *Brachiaria mutica*, *Leptochloa fusca*, and *Typha domingensis* plants only (T2), CWs augmented with consortium of salt and Cr-tolerant endophytes (*Enterobacter* sp. HU38, *Microbacterium arborescens* HU33, and *Pantoea stewartii* ASI11) while vegetated with *B. mutica*, *L. fusca*, and *T. domingensis* (T3), and CWs without vegetation or inoculation (T4). Raw tannery effluent (T5) was also collected for its toxicity comparison with treated effluents. Tap water was set as a control (T1).

2.3. Characterization of Treated and Untreated Tannery Effluent

In this research, standard methods to test water and wastewater as described by the American Public Health Association (APHA) were followed, for the physicochemical characterization and for the toxicity assay of tannery effluent on *C. idella* [45]. So, the physicochemical characterization of collected

effluent samples was carried out prior to the toxicity bioassay, to quantify pH, EC, BOD₅, COD, TDS, TSS, and Cr concentration. Results of the analysis of physico-chemical parameters of untreated and treated tannery effluent are given in Table 1.

2.4. Dilution of Tannery Effluent

The dilution of toxic effluents is generally required to perform the bioassays, as it is needed to reduce the effects of inherent toxic substances. Raw tannery effluent sample was diluted at different levels (25%, 50%, 75%, and 100%), using tap water. The same dilution levels were also prepared for effluent samples treated by CWs.

2.5. Experimental Setup

All the collected effluent samples were subjected to the toxicity test at 25%, 50%, 75%, and 100% dilution level (Table 2). So, 28 batches (in triplicates) of ten healthy fish, with average weight 260–270 mg and size 6.5 ± 0.5 cm, were introduced to each effluent sample in glass aquaria of 30 L capacity that were half filled to avoid overcrowding. As the toxicological response of the fish may vary with the body weight, and hence mortality and LC50 values may fluctuate in the same test individuals, fish of equal weight and size were employed for this assay. Four batches of 10 fish were kept in untreated wastewater at the same dilution levels, while one batch of 10 fish was kept in unamended water to be used as a control along with experimental groups. Oxygen was provided with the help of aeration pumps in each test container during the experimental period. All chemicals and reagents were analytical grade, and were provided by Sigma-Aldrich, Burlington, MA, USA and Merck, Darmstadt, Germany.

2.6. Toxicity Evaluation

The experiment was monitored for 96 h (exposure period), and the number of surviving fish was recorded by counting the dead fish at 24, 48, 72, and 96 h to calculate the mortality. The median lethal concentration (LC50) for 96 h, and respective upper and lower limits at 95% confidence level, were calculated as well. Acute toxicity unit (ATU) was also calculated by using the following formula: $ATU = 100/LC50\% (v/v)$.

2.7. Morphological and Behavioural Response Variations

Variations in physical appearance, such as change in body colour, thickening of mucous coating on fish body, etc., were observed during the experimental period. Along with this, the behavioural changes such as swimming movements and responses of the fish to both untreated and treated effluent were observed and compared with the control set.

2.8. Statistical Data Analysis

The results were subjected to statistical evaluation using the Trimmed Spearman–Kärber Method, Version 1.5 (US Environmental Protection Agency, Cincinnati, OH, USA). The data of each concentration was pooled to calculate the mortality, 96 h-LC50 values, and 95% confidence interval with upper and lower limits.

Table 1. Physico-chemical characterization of untreated and treated tannery effluent.

Parameters	Raw Tannery Effluent	Tap Water	Effect of Different Treatments on Pollutant Removal by Constructed Wetlands (CWs)											
			Tannery Effluent Treated by CWs Using <i>Typha domingensis</i>			Tannery Effluent Treated by CWs Using <i>Leptochloa fusca</i>			Tannery Effluent Treated by CWs Using <i>Brachiaria mutica</i>			CWs without Vegetation		
			T1	T2	T3	T2	T3	T3	T2	T3	T2	T3	T4	
Colour	Black	Colourless	Yellow	Yellow	Yellow	Yellow	Yellow	Yellow	Yellow	Yellow	Yellow	Yellow	Brown	
pH	7.9 ± 0.4	7.9 ± 0.4	7.4 ± 0.2	7.8 ± 0.3	7.4 ± 0.2	8.3 ± 0.1	7.8 ± 0.1	8.3 ± 0.1	7.8 ± 0.1	8.2 ± 0.1	7.7 ± 0.3	7.7 ± 0.3	8.5 ± 0.2	
EC (mS/cm)	20.2 ± 1.3	1.37 ± 0.3	2.07 ± 0.1	1.53 ± 0.47	2.07 ± 0.1	1.01 ± 0.01	0.20 ± 0.01	1.30 ± 4.5	0.20 ± 0.01	5.65 ± 0.12	4.64 ± 0.21	4.64 ± 0.21	8.66 ± 0.29	
TDS (mg/L)	12,928 ± 1549	666 ± 27	1715 ± 39	1198 ± 56	1715 ± 39	646 ± 6.23	130 ± 4.5	9 ± 2.1	130 ± 4.5	3619.84 ± 45	2973.44 ± 25	2973.44 ± 25	5542 ± 37	
TSS (mg/L)	4800 ± 230	-	10 ± 1.4	11 ± 0.5	10 ± 1.4	10 ± 3.5	9 ± 2.1	9 ± 2.1	9 ± 2.1	12 ± 0.7	10 ± 2.1	10 ± 2.1	13 ± 4.0	
BOD ₅ (mg/L)	3860 ± 612	-	458 ± 45	190 ± 18	458 ± 45	392 ± 3.4	57 ± 1.2	57 ± 1.2	57 ± 1.2	1003.60 ± 21	810.6 ± 11	810.6 ± 11	1029 ± 25	
COD (mg/L)	6066 ± 1335	-	760 ± 21	432 ± 12.5	760 ± 21	728 ± 23	152 ± 13	152 ± 13	152 ± 13	1819.80 ± 13	1455.84 ± 7.5	1455.84 ± 7.5	1880 ± 41	
Oil & grease (mg/L)	362 ± 2.5	-	66 ± 5.8	48 ± 3	66 ± 5.8	36 ± 2.2	8.3 ± 1.3	8.3 ± 1.3	8.3 ± 1.3	112.22 ± 2.2	97.74 ± 1.3	97.74 ± 1.3	141 ± 6.7	
Cr (mg/L)	247 ± 5.8	0	2.1 ± 0.3	1.3 ± 0.05	2.1 ± 0.3	3.3 ± 0.05	0.9 ± 0.01	0.9 ± 0.01	0.9 ± 0.01	1.7 ± 0.1	1.2 ± 0.11	1.2 ± 0.11	13 ± 1.43	

T2 = Plants; T3 = Plants + bacteria; T4 = Without plants. Each value is mean ± standard deviation and number of replicates for each treatment (n) = 3. EC = Electrical conductivity, TDS = Total dissolved solids, TSS = Total suspended solids, BOD₅ = Five-day biochemical oxygen demand, COD = Chemical oxygen demand, Cr = Chromium, pH = Pondus Hydrogenii.

Table 2. Mortality of *Ctenopharyngodon idella* exposed to different concentrations of both untreated and treated tannery effluent.

Effluent Concentration %	Mortality of <i>C. idella</i> in Untreated and Treated Tannery Effluent after 96 h Exposure Period (%)											
	Treated Effluent by CWs Using <i>T. domingensis</i>				Treated Effluent by CWs Using <i>L. fusca</i>				Treated Effluent by CWs Using <i>B. mutica</i>			
	T2	T3	T4	T5	T2	T3	T4	T5	T2	T3	T4	T5
0 (Control)	0	0	0	0	0	0	0	0	0	0	0	0
25	20	0	40	0	0	40	0	0	20	10	0	40
50	30	0	80	0	10	80	0	80	50	20	80	80
75	50	0	100	20	100	100	100	100	80	40	100	100
100	60	10	100	100	20	100	100	90	90	60	100	100
96 h-LC50		76.61%	-	29.73%	-	29.73%	-	46.53%	46.53%	86.60%	29.73%	29.73%
95% Confidence limit	Lower limit	39.18	-	19.59	-	19.59	-	33.27	33.27	63.13	19.59	19.59
	Upper limit	149.79	-	45.13	-	45.13	-	65.07	65.07	118.68	45.13	45.13
96 h-LC50 as ATU	1.30	-	3.36	-	-	3.36	-	2.14	2.14	1.15	3.36	3.36

T1 = Control; T2 = Plants; T3 = Plants + bacteria; T4 = Without plants; T5 = Mortality in raw tannery effluent at any dilution was 100%. LC = Lethal concentration inducing 50% mortality of *C. idella*, ATU = Acute toxicity unit.

3. Results

Fish were exposed to untreated and treated tannery effluent using different concentrations for a short-term (96 h) exposure period. Characterization of raw effluent in terms of physico-chemical parameters revealed relatively much higher concentrations of pollutants than treated effluent, as shown in Table 1. In addition, general observations on fish morphology, behaviour, mortality, and toxicity were also made.

3.1. Mortality and Toxicity Evaluation

The experimental species, *C. idella*, showed differential toxicity level with varying exposure time. The observed percentage of mortality was recorded for 24, 48, 72, and 96 h, as shown in Figures 1–3.

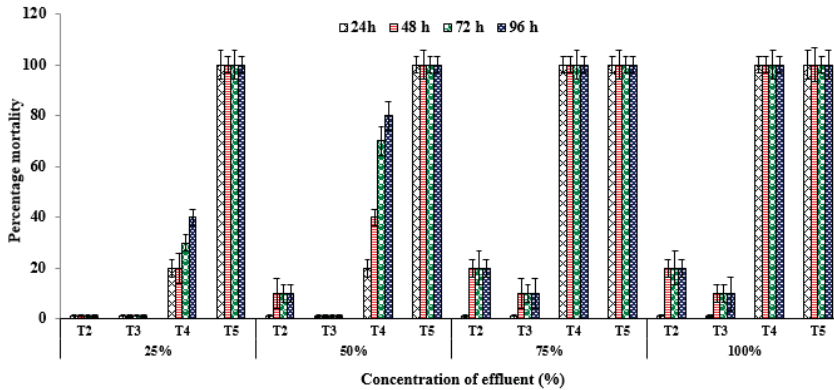


Figure 1. Mortality in fish on exposure to different concentrations of untreated and treated effluent by CWs using *Typha domingensis*. Tannery effluent treated in CWs with only *T. domingensis* (T2), effluent treated in CWs with *T. domingensis* and bacteria (T3), effluent treated in CWs without vegetation (T4), and raw tannery effluent (T5). Each value is mean \pm standard error and number of replicates for each treatment (n) = 3.

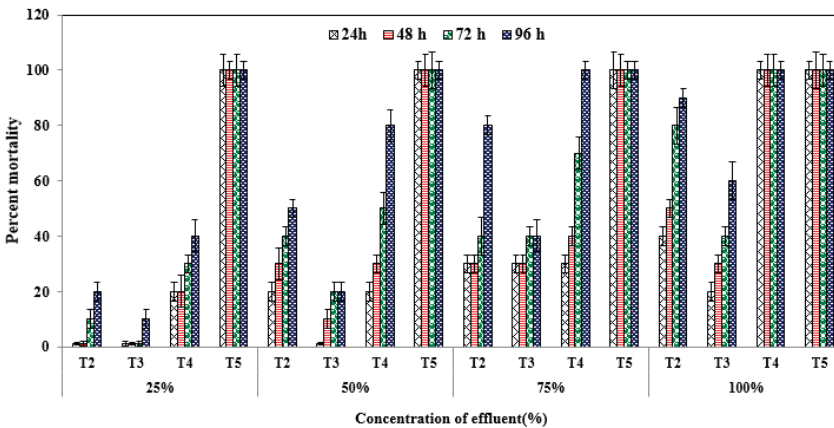


Figure 2. Mortality in fish on exposure to different concentrations of untreated and treated effluent by CWs using *Leptochloa fusca*. Tannery effluent treated in CWs with *L. fusca* only (T2), effluent treated in CWs with *L. fusca* and bacteria (T3), effluent treated in CWs without vegetation (T4), and raw tannery effluent (T5). Each value is mean \pm standard error and number of replicates for each treatment (n) = 3.

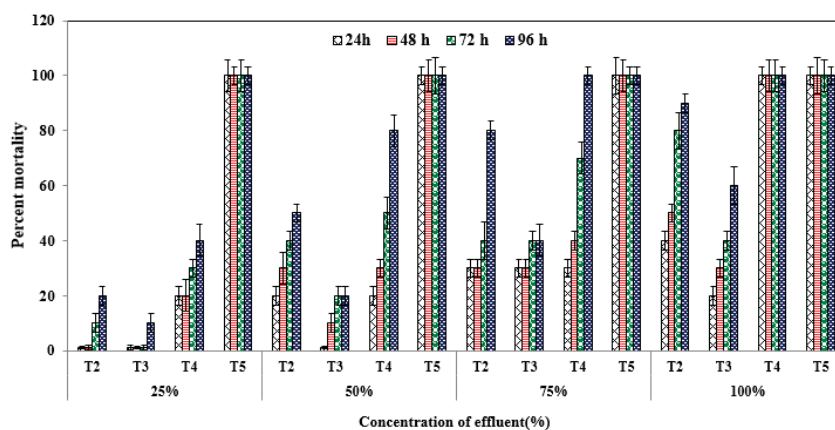


Figure 3. Mortality in fish on exposure to different concentrations of untreated and treated effluent by CWs using *Brachiaria mutica*. Tannery effluent treated in CWs with *B. mutica* only (T2), effluent treated in CWs with *B. mutica* and bacteria (T3), effluent treated in CWs without vegetation (T4), and raw tannery effluent (T5). Each value is mean \pm standard error and number of replicates for each treatment (n) = 3. Stocked in T3 (effluent treatment by combined use of *L. fusca* and bacteria) at 50% effluent concentration, while the maximum percentage mortality observed was only 10% in higher effluent concentrations (100%). Observations for T4 treatment were the same as described above.

3.2. Toxicity of Raw Tannery Effluent

Raw effluent caused high acute toxicity and 100% mortality in exposed fish, even at dilutions up to 25% (Table 2). The fish died immediately after release to raw effluent (T5). In contrast, no mortality of fish was observed in tap water that was set as a positive control (T1).

3.3. Toxicity of Effluent Treated by CWs Using *T. domingensis*

The toxicity study of effluent treated by CWs vegetated with *T. domingensis* only (T2) revealed that the mortality of fish was 30% at the 24 h exposure period and increased to 60% at reaching the 96 h exposure period, while its dilution up to four times decreased fish mortality up to 20%, as shown in Figure 1. Moreover, combined use of plants and bacteria (T3) decreased the mortality of fish up to 10% at the 96 h exposure period, and its two times dilution further decreased this rate to zero. But the effluent treated in CWs in the absence of vegetation (T4) showed high mortality (100%) that decreased to 40% at 1:3 dilutions, while its LC50 value was 30% (v/v), with 19.59 highest and 45.13 lowest limits at 95% confidence level, and ATU was 3.36, revealing high acute toxicity (1–10).

3.4. Toxicity of Effluent Treated by CWs Using *L. fusca*

The toxicity assay conducted on effluent treated in CWs by using *L. fusca* plant and effects of T2, T3, and T4 treatments on percentage mortality of the fish for the 96 h exposure time is shown in Figure 2. As indicated by this figure, T2 (CWs with *L. fusca*) treatment showed 20% mortality at 100% effluent concentration, whereas reduced to 10% at 50% effluent concentration, and no mortality was observed at 25% effluent concentration. Among all the treatments, the lowest mortality was observed on the fish.

3.5. Toxicity of Effluent Treated by CWs Using *B. mutica*

Figure 3 shows the percentage mortality of the fish exposed to effluent treated by CWs vegetated with *B. mutica* (T2), revealing that 40% of fish died after the 24 h exposure period, and at reaching 96 h of exposure, 50% more fish died in this effluent. However, its dilution up to 25% decreased the death

rate, and 80% of fish survived until the 96 h exposure time. While effluent treated by augmenting CWs with bacteria along with *B. mutica* (T3) reduced the mortality percentage from 90% to 60% at 96 h exposure duration and 100% effluent concentration, while its dilution up to 25% decreased the death rate from 60% to 10%. The 96 h-LC50 was also extrapolated to be 46.53% (v/v), with the highest and lowest levels being 33.27 and 65.07 respectively, and 2.14 as ATU for T2 (Table 2). While for T3, 96 h-LC50 was 86.60% (v/v), with 63.13 upper and 118.68 lower limits, and 1.15 as ATU (Table 2). The confidence limit was 95%. Acute toxicity results show a comparatively low mortality level at lower effluent concentrations, while it was higher in concentrated effluent.

3.6. Relative Performance of Different Plant Species in Toxicity Reduction of Tannery Effluent by CWs

Comparative analysis of different plant species to reduce toxicity of tannery effluent by CW technology is presented in Figure 4. The maximum toxicity of effluent was reduced by *L. fusca*, followed by *T. domingensis* and *B. mutica*. Tannery effluent treatment in CWs with vegetation and bacterial augmentation resulted in more reduced toxicity than vegetation alone in CWs.

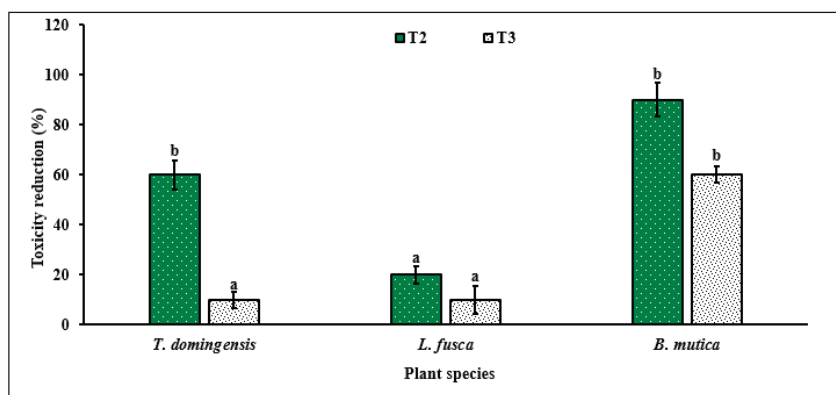


Figure 4. Relative performance of different plant species in toxicity reduction of tannery effluent in constructed wetland systems. Tannery effluent treated in CWs with plants only (T2), and with plants and bacteria (T3). Labels (a) and (b) indicate statistically significant differences ($p < 0.05$) among plant species for toxicity reduction at a 5% level of significance. Each value is mean \pm standard error and number of replicates for each treatment (n) = 3. Different letters on each error bar show significant differences among different treatments.

3.7. Morphological Changes

Morphological change in fish colour was observed on exposure to untreated tannery effluent (T5) and effluent treated by CWs without vegetation (T4), i.e., body of fish became dark, as shown in Figure 5. In addition to this, a thick coat of mucus, spreading all over the body of the fish, was also observed in T4 and T5 treatments, making fish slimier. In effluent treated by CWs with plants only (T2), and with combined use of plants and bacteria (T3), as well as in control (T1), there was apparently no change in body colour, and fish had a normal mucus coating on their body.

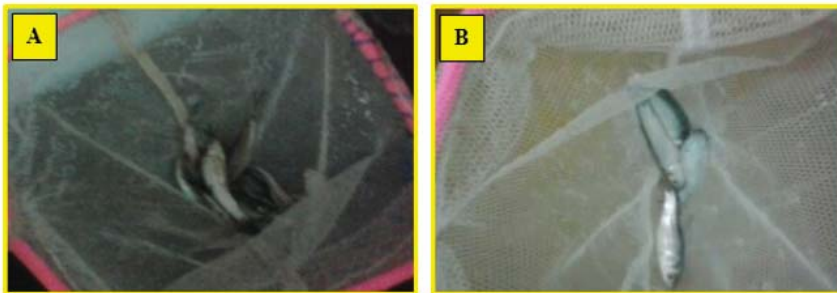


Figure 5. Morphological change in *C. idella* on exposure to tannery effluent before (A) and after treatment (B) by CW technology.

3.8. Variations in Behavioural Response

On the basis of visual observations, data regarding behavioural response of *C. idella* were recorded. As the experiment progressed, fish exhibited irregular zig-zag movements, frequent surfacing, coughing, and opercular movements on exposure to untreated tannery effluent (T5) and effluent treated without vegetation in CWs (T4), in contrast to normal movements and swimming behaviour without any loss of equilibrium in the rest of treated effluent samples and in tap water set as a control (Figure 6).

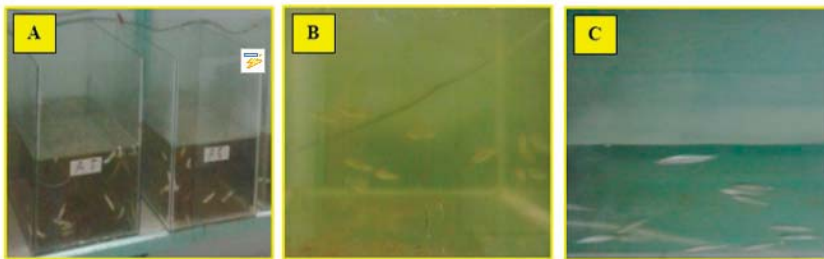


Figure 6. Variation in behavioural response of *C. idella* on exposure to untreated tannery effluent at 50% dilution showing irregular swimming and zig-zag movements (A), and normal movements and swimming behaviour in treated tannery effluent at the same dilution level (B), and in tap water set as control (C).

3.9. Physiological Variations

Untreated tannery effluent was also loaded with oil and grease to the tune of 362 mg/L, in addition to other pollutants. This created respiratory problems in fish by lowering the dissolved oxygen in test media, despite the aeration system. It was observed that fish regularly came to the surface of water for atmospheric oxygen. Such an anomaly was not observed in T2, T3, and the control set, maintained under identical experimental conditions.

4. Discussion

The present investigation evaluated the toxicity of both treated and untreated tannery effluent by measuring mortality, LC50, and acute toxicity in fish for 96 h exposure duration. Along with this, morphological changes and behavioural response of the fish were also observed. In the current study, the mortality of *C. idella* was directly proportional to the exposure period, concentration of pollutants in effluent, and acute toxicity unit, as already observed in previous works [46–48]. At 96 h-LC50 concentration, the ability of natural population of aquatic bodies would be relatively impaired, and an increase in concentration also increased the mortality [49,50].

As indicated in Table 2, from 96 h-LC50 values (29.73–86.60%) at different effluent concentrations, it is clear that the raw tannery effluent exerts high toxicity, while effluent treatment using CWs technology reduced the overall pollution level to a great extent. However, LC50 values still provide information for gross comparison of toxicity of the pollutants to the fishes. The present study revealed that raw and treated effluent by using CWs without vegetation caused more or less similar toxicity, whereas combined use of plants and bacteria in CWs caused a significant reduction in toxicity level of effluent, and among all the tested plants, *L. fusca* was more efficient. The same toxicity results were reported for raw pharmaceutical effluent acting on *Lebistes reticulatus* [51]. The variation in 96 h-LC50 of Cr for different species was previously reported, being 34 mg/L for *Cirrhinus mrigala* [52], 39.4 mg/L for *Labeo rohita* [53], 85.7 mg/L for *Carassius auratus* [54], 87.96 mg/L for *Cyprinus carpio* [55], and 53.08 mg/L for *C. idellus* [50].

In the present study, acute toxicity values were high in concentrated effluents as compared to diluted ones, due to varying amounts of Cr. These toxicity values are organism- and age-specific [12,56]. Here, exposure of *C. idella* to untreated effluent caused death within 24 h, while in treated effluent, most fish survived until 96 h, varying with different treatments and concentration levels of effluent. Similar findings were observed by Arora et al. [31], who assessed toxicity of treated urban wastewater and its reutilization for aquaculture on sucker fishes for 96 h and compared it with untreated wastewater. Fish died within 48 h in untreated wastewater while they survived until 96 h in the treated one. In another investigation, the acute toxicity test revealed about an 80% and 100% survival rate of *Poecilia* sp. in 100% untreated effluent and ceramic membrane-treated effluent respectively, after a 72 h exposure period [39].

Morphological changes in fish occurred in those that were exposed to untreated tannery effluent (T5) and effluent treatment by CWs without vegetation (T4). These changes were darkening of body colour and a thick mucus coating spreading all over the body, due to the presence of toxins in untreated effluent. The same findings were reported by Carpenter [57,58] and Nisha et al. [59]. Thus, these facts are directly reflecting the toxicity level of effluent, because no such morphological change in fish was observed in T2, T3, and the control set (T1). According to Handa and Jindal [50], Cr-contaminated water has the potential to induce morphological and behavioural changes in *C. idellus*. Chromium toxicity also affects the normal survival of fish and produces allergic reactions on skin [60]. It also impairs functioning of the nervous system [61], which causes darkening of body colour due to the reversible response of melanophores [62].

Behavioural responses, the most perceptible indicator of toxicity, are crucial for normal life functions, and ultimately fish survival [63]. The current study revealed that lethal concentrations of tannery effluent caused abnormal changes in the fish, and intensity increased with time. Similar effects were observed on the behaviour of *Mystus vittatus* and *L. reticulatus* on exposure to paper mill and drug industry effluent, respectively [64,65]. Related behavioural changes, such as jerky movements, opening of mouth, erratic swimming, and secretion of mucus, etc., were also observed by Timchalk et al. [66], Bantu and Vakita [67], and Nisha et al. [59].

Exposure of fish to raw tannery effluent proved to be highly unfit for their survival, as fish became inactive immediately after the addition of effluent. Frequent surfacing of fish to gulp the oxygen at initial stages, followed by slow erratic swimming and zig-zag irregular movements, as well as loss of balance, and finally settling at the bottom of the aquarium after a few hours, was an indication of toxicity defects caused on fish due to raw tannery effluent. Similar distressed behavioural observations were also reported earlier [2,59,68–70]. This reduced normal activity could be a consequence of depletion of energy in the body of fish due to impairment of carbohydrate metabolism, wherein organisms that could not tolerate the contaminants enter into a state of coma and subsequent death [47,71]. Cui et al. [72] also noticed a decrease in fish movement leading to cessation of swimming [73] due to the altered carbohydrate metabolism and neurotoxicity induced by Cr metal [74]. According to Roopadevi and Somashekar [47], fish lose their ability to maintain homeostasis on exposure to higher

effluent concentrations for a longer period, and this eventually causes mortality, or some physiological stress may be the reason, which is confirmed by the present results.

Previous investigations also reported similar observations when fish were exposed to toxic industrial effluents, being irregular hyper and hypoactive movements, loss of balance, and increase in surfacing activity that ultimately decrease their tolerance to high pollution load [75–77]. The present findings are also in concordance with earlier studies of fish behavioural response to industrial effluents, revealing normal behaviour and swimming of fish in control, in contrast to the abnormal swimming, loss of equilibrium, coughing, and opercular movements in toxic effluents [2,59,70,78]. According to Sinha and Kumar [79], equilibrium loss and abnormal swimming are caused by damage to the nervous system that regulates all the vital functions.

High organic pollution load of tannery effluent increases its BOD₅ and subsequently reduces its dissolved oxygen level. This oxygen deficiency caused respiratory problems in fish, along with this reduced tolerance capacity of fish towards toxins that caused death. Oyedapo and Akinduyite [80] similarly reported that toxic effluents disrupt the ability of fish to maintain homeostasis and cause physical damages. Another reason for a reduction in oxygen consumption may be malfunctioning of gills due to direct contact with pollutants present in raw tannery effluent. Previous studies support this evidence, indicating that high levels of toxic substances in the test medium cause coagulation of gill mucous in fish that alters their respiratory metabolism [47,49,77,81]. Moreover, accumulation of mucus on the gills of fish and asphyxiation decrease oxygen consumption. A similar kind of observation was also reported by Thorat and Wagh [82], who showed that tanning industry effluent has a strong effect on the oxygen consumption rate of fish, *Channa gachua*, probably due to Cr toxicity.

Toxicity assays play a viable role in monitoring the pollutants' level in industrial effluents and can be used as a promising technology to regulate quality of industrial discharge to receiving reservoirs. As discussed earlier, fish show changed behaviour on exposure to a toxic environment, an indicator of the surrounding pollution level. Such types of variations in behavioural response of fish are an easy way to directly assess the quality of industrial discharges.

Biototoxicity tests are an economical and technical method for direct measurement of toxicity of industrial effluents. In addition to this, the present study showed that toxicity bioassays must be performed to assess the toxicity of treated effluent along with physico-chemical analyses, such as pH, EC, COD, BOD₅, and TSS, to guarantee the aquatic organisms' safety and minimise ecotoxicological issues.

5. Conclusions

Ctenopharyngodon idella were seriously affected by the tested raw tannery effluent, even at very low concentrations, despite making dilutions due to high toxicity of pollutants, in contrast to no adverse effects in treated effluent by CW technology and the control set. Effluent treatment by CWs vegetated with different plants (*B. mutica*, *L. fusca*, and *T. domingensis*) reduced the toxicity causing abnormal changes in morphology and physiology of fish that ultimately lead to mortality, and inoculation of endophytic bacteria (*Enterobacter* sp. HU38, *Microbacterium arborescens* HU33, and *Pantoea stewartii* ASI11) further caused a reduction in its toxicity level up to 90%. In contrast to these treatments, CWs without vegetation could not reduce the toxicity of this effluent. Hence, fish survived for longer periods in effluent treated by CWs vegetated with *L. fusca* plants and augmented with endophytes, wherein pollutants were detoxified by the synergistic effect of plant–microbe interactions. In addition to this, treatment performance of *L. fusca*-planted CWs was more effective than *B. mutica*- and *T. domingensis*-planted CWs. Therefore, this study emphasizes the use of CWs technology to treat tannery effluent, preferably planting *L. fusca* species, along with bacterial augmentation that ultimately results in the reduction of effluent toxicity and aquatic pollution and poisoning. The current bioassay results illustrated that disposal of raw tannery effluent is unsafe to fish, causing mortality, alterations in morphology, physiology, and behaviour, due to its inherent toxicity. Therefore, treatment of tannery effluent by nature-friendly CWs technology is highly recommended prior to its discharge to water

resources (by mixing 50% fresh water) to protect the environment. Moreover, toxicity assays on fish can be practiced economically to ensure safe disposal of industrial discharge.

Author Contributions: Conceptualization, S.A. (Sobia Ashraf), M.A., M.N.; methodology, S.A. (Sobia Ashraf), S.A. (Sana Ashraf), and K.R.; software, S.A. (Sobia Ashraf), and M.A.; validation, M.N., Z.A.Z., A.N.-D., S.R.A., and M.A.; formal analysis, S.A. (Sobia Ashraf), K.R., and M.A.; investigation, S.A. (Sobia Ashraf), M.N., M.A.; resources, M.A., Z.A.Z., A.N.-D., and M.N.; data curation, S.A. (Sobia Ashraf), K.R., S.A. (Sana Ashraf); writing—original draft preparation, S.A. (Sobia Ashraf), and M.A.; writing—review and editing, M.A., Z.A.Z., M.N., S.R.A., and A.N.-D. All authors have read and agreed to the published version of the manuscript.

Funding: This research was conducted under the grant number, No. 20-3854/R&D/HEC/14., of the Higher Education Commission (HEC), Pakistan.

Acknowledgments: The authors are thankful to the Institute of Soil and Environmental Sciences, University of Agriculture, Faisalabad 38000, Pakistan, and the National Institute for Biotechnology and Genetic Engineering (NIBGE), Faisalabad, Pakistan, for providing research facilities.

Conflicts of Interest: The authors declare no conflict of interest.

References

1. Ali, S.H.; De Oliveira, J.A.P. Pollution and economic development: An empirical research review. *Environ. Res. Lett.* **2018**, *13*, 123003. [[CrossRef](#)]
2. Ganeshwade, R.M.; Rokade, P.B.; Sonwane, S.R. Behavioral responses of *Cyprinus carpio* to industrial effluents. *J. Environ. Biol.* **2006**, *27*, 159. [[PubMed](#)]
3. Agrawal, A.; Pandey, R.S.; Sharma, B. Water pollution with special reference to pesticide contamination in India. *J. Water Resour. Protect.* **2010**, *2*, 432–448. [[CrossRef](#)]
4. Edokpayi, J.N.; Odiyo, J.O.; Durowoju, O.S. Impact of wastewater on surface water quality in developing countries: A case study of South Africa. *Water Qual.* **2017**, 401–416.
5. Yusuff, R.O.; Sonibare, J.A. Characterization of textile industries' effluents in Kaduna, Nigeria and pollution implications. *Global Nest: Int. J.* **2004**, *6*, 212–221.
6. Ali, H.; Khan, E.; Ilahi, I. Environmental chemistry and ecotoxicology of hazardous heavy metals: Environmental persistence, toxicity, and bioaccumulation. *J. Chem.* **2019**, *14*, 6730305. [[CrossRef](#)]
7. Vinodhini, R.; Narayanan, M. The impact of toxic heavy metals on the hematological parameters in common carp (*Cyprinus carpio* L.). *Iran. J. Environ. Health Sci. Eng.* **2009**, *6*, 23–28.
8. Mahmood, Q.; Shaheen, S.; Bilal, M.; Tariq, M.; Zeb, B.S.; Ullah, Z.; Ali, A. Chemical pollutants from an industrial estate in Pakistan: A threat to environmental sustainability. *Appl. Water Sci.* **2019**, *9*, 47. [[CrossRef](#)]
9. Brooks, B.W.; Conkle, J.L. Commentary: Perspectives on aquaculture, urbanization and water quality. *Comp. Biochem. Physiol. Part C Toxicol. Pharmacol.* **2019**, *217*, 1–4. [[CrossRef](#)]
10. Chowdhury, M.; Mostafa, M.G.; Biswas, T.K.; Mandal, A.; Saha, A.K. Characterization of the effluents from leather processing industries. *Environ. Process.* **2015**, *2*, 173–187. [[CrossRef](#)]
11. Cooman, K.; Gajardo, M.; Nieto, J.; Bornhardt, C.; Vidal, G. Tannery wastewater characterization and toxicity effects on *Daphnia* spp. *Environ. Toxicol. Int. J.* **2003**, *18*, 45–51. [[CrossRef](#)] [[PubMed](#)]
12. Bakshi, A.; Panigrahi, A.K. A comprehensive review on chromium induced alterations in fresh water fishes. *Toxicol. Rep.* **2018**, *5*, 440–447. [[CrossRef](#)] [[PubMed](#)]
13. Srivastava, S.; Prabhakar, P.; Srivastava, B.C. Toxicity and behaviour of the fish *Labeo rohita* and *Channa punctatus* exposed to pulp paper mill effluent. *J. Ecotoxicol. Environ. Monit.* **2007**, *17*, 241–244.
14. Nemesok, J.; Orban, L.; Vig, E. Accumulation of pesticides in the organs of carp *Cyprinus carpio* at 4 and 20 C. *Bull. Environ. Contamin. Toxicol.* **1987**, *39*, 370–378. [[CrossRef](#)]
15. Hewitt, L.M.; Parrott, J.L.; McMaster, M.E. A decade of research on the environmental impacts of pulp and tannery mill effluents in Canada: Sources and characteristics of bioactive substances. *J. Toxicol. Environ. Health* **2006**, *9*, 341–356. [[CrossRef](#)]
16. Van der Oost, R.; Beyer, J.; Vermeulen, N.P. Fish bioaccumulation and biomarkers in environmental risk assessment: A review. *Environ. Toxicol. Pharmacol.* **2003**, *13*, 57–149. [[CrossRef](#)]
17. Kroon, F.; Streten, C.; Harries, S. A protocol for identifying suitable biomarkers to assess fish health: A systematic review. *PLoS ONE* **2017**, *12*, e0174762. [[CrossRef](#)]

18. Rai, A.; Chauhan, P.S.; Bhattacharya, S. Remediation of Industrial Effluents. In *Water Remediation, Energy, Environment, and Sustainability*; Bhattacharya, S., Ed.; Springer: Deodorant, The Netherland, 2018; pp. 171–187.
19. Movahedian, H.; Bina, B.; Asghari, G.H. Toxicity evaluation of wastewater treatment plant effluents using *Daphnia magna*. *Iran. J. Environ. Health Sci. Engin.* **2005**, *2*, 1–4.
20. Ashraf, S.; Afzal, M.; Naveed, M.; Shahid, M.; Zahir, Z.A. Endophytic bacteria enhance remediation of tannery effluent in constructed wetlands vegetated with *Leptochloa fusca*. *Int. J. Phytoremediation* **2018**, *20*, 121–128. [[CrossRef](#)]
21. Ashraf, S.; Afzal, M.; Rehman, K.; Naveed, M.; Zahir, Z.A. Plant-endophyte synergism in constructed wetlands enhances the remediation of tannery effluent. *Water Sci. Technol.* **2018**, *77*, 1262–1270. [[CrossRef](#)]
22. Ashraf, S.; Afzal, M.; Rehman, K.; Tahseen, R.; Naveed, M.; Zahir, Z.A. Enhanced remediation of tannery effluent in constructed wetlands augmented with endophytic bacteria. *Desalin. Water Treat.* **2018**, *102*, 93–100. [[CrossRef](#)]
23. Ashraf, S.; Naveed, M.; Afzal, M.; Ashraf, S.; Rehman, K.; Hussain, A.; Zahir, Z.A. Bioremediation of tannery effluent by Cr and salt tolerant bacterial strains. *Environ. Monit. Assess.* **2018**, *190*, 716. [[CrossRef](#)] [[PubMed](#)]
24. Ashraf, S.; Naveed, M.; Afzal, M.; Seleiman, M.F.; Al-Suhaibani, N.A.; Zahir, Z.A.; Alotaibi, M. Unveiling the potential of novel macrophytes for the treatment of tannery effluent in vertical flow pilot constructed wetlands. *Water* **2020**, *12*, 549. [[CrossRef](#)]
25. Bhatia, D.; Sharma, N.R.; Kanwar, R.; Singh, J. Physicochemical assessment of industrial textile effluents of Punjab (India). *Appl. Water Sci.* **2018**, *8*, 83. [[CrossRef](#)]
26. Somashekar, R.K.; Gurudev, M.R.; Ramiah, S. Somatic cell abnormalities induced by dye manufacturing industry waste water. *Cytologia* **1985**, *50*, 129–134. [[CrossRef](#)]
27. Tisler, T.; Zagorc-Koncan, J. Toxicity evaluation of water from pharmaceutical industry to aquatic organisms. *Water Sci. Technol.* **1999**, *39*, 71–76. [[CrossRef](#)]
28. Sitre, S.; Dhadse, S.; Satyanarayan, S. Toxicity of herbal pharmaceutical wastewater to a freshwater crustacean *Ceriodaphnia dubia*. *Bull. Environ. Contamin. Toxicol.* **2009**, *82*, 275–279. [[CrossRef](#)]
29. Zhu, X.; Chen, L.; Liu, R.; Liu, C.; Pan, Z. Biototoxicity evaluation of coking wastewater treated with different technologies using Japanese medaka (*Oryzias latipes*). *Environ. Sci. Process. Impact* **2013**, *15*, 1391–1396. [[CrossRef](#)]
30. Terekhova, V.A.; Wadhia, K.; Fedoseeva, E.V.; Uchanov, P.V. Bioassay standardization issues in freshwater ecosystem assessment: Test cultures and test conditions. *Knowl. Manag. Aquat. Ecosyst.* **2018**, *419*, 32. [[CrossRef](#)]
31. Arora, N.; Jaiswal, K.K.; Kumar, V.; Vlaskin, M.S.; Nanda, M.; Pruthi, V.; Chauhan, P.K. Small-scale phyco-mitigation of raw urban wastewater integrated with biodiesel production and its utilization for aquaculture. *Bioresource Technol.* **2020**, *297*, 122489. [[CrossRef](#)]
32. Xia, C.; Fu, L.; Liu, Z.; Liu, H.; Chen, L.; Liu, Y. Aquatic toxic analysis by monitoring fish behavior using computer vision: A recent progress. *J. Toxicol.* **2018**, *11*, 2591924. [[CrossRef](#)]
33. Maleki, A.; Mahvi, A.H.; Vaezi, F.; Nabizadeh, R. Ultrasonic degradation of phenol and determination of the oxidation by-products toxicity. *Iran. J. Environ. Health Sci. Eng.* **2005**, *2*, 201–206.
34. Ebrahimpour, M.; Mosavisefat, M.; Mohabbati, V. Influence of water hardness on acute toxicity of copper and zinc on fish. *Toxicol. Ind. Health* **2010**, *6*, 361–365. [[CrossRef](#)] [[PubMed](#)]
35. Martin-Skilton, R.; Saborido-Rey, F.; Porte, C. Endocrine alteration and other biochemical responses in juvenile turbot exposed to the Prestige fuel oil. *Sci. Total Environ.* **2008**, *404*, 68–76. [[CrossRef](#)] [[PubMed](#)]
36. Saborido-Rey, F.; Dominguez-Petit, R.; Tomas, J.; Morales-Nin, B.; Alonso-Fernandez, A. Growth of juvenile turbot in response to food pellets contaminated by fuel oil from the tanker 'Prestige'. *Marine Ecol. Prog. Ser.* **2007**, *345*, 271–279. [[CrossRef](#)]
37. Safaa, M.S.; Mohsen, A. Eco-physiological Impact of Commercial Petroleum Fuel on Nile Tilapia, *Oreochromis niloticus* (L). In Proceedings of the 9th International Sym. Tilapia in Aquaculture, Shanghai, China, 22–24 April 2011; pp. 31–43.
38. Mahabub-uz-zaman, M.D.; Sarkar, S.; Shahdat, M.D. The effects of industrial effluent discharge on lipid peroxidase levels in punti fish, *Puntius sophore* tissue in comparison with those of freshwater fish. *J. Food Lipids* **2008**, *15*, 198–208. [[CrossRef](#)]
39. Bhattacharya, P.; Ghosh, S.; Swarnakar, S.; Mukhopadhyay, A. Tannery effluent treatment by microfiltration through ceramic membrane for water reuse: Assessment of environmental impacts. *Clean Soil Air Water* **2015**, *43*, 633–644. [[CrossRef](#)]

40. Abdel-Tawwab, M.; El-Sayed, G.O.; Shady, S.H. Acute Toxicity of Water-Born Zinc in Nile Tilapia, *Oreochromis niloticus* (L.) Fingerlings. In Proceedings of the Ninth International Symposium on Tilapia in Aquaculture, Shanghai, China, 22–24 April 2011; p. 44.
41. Karthikeyan, S.; Jambulingam, M.; Sivakumar, P.; Shekhar, A.P.; Krithika, J. Impact of textile effluents on fresh water fish *Mastacembelus armatus* (Cuv. & Val). *J. Chem.* **2006**, *3*, 303–306.
42. Dotro, G.; Larsen, D.; Palazolo, P. Preliminary evaluation of biological and physical–chemical chromium removal mechanisms in gravel media used in constructed wetlands. *Water Air Soil Pollut.* **2011**, *215*, 507–515. [[CrossRef](#)]
43. Calheiros, C.S.; Quiterio, P.V.; Silva, G.; Crispim, L.F.; Brix, H.; Moura, S.C.; Castro, P.M. Use of constructed wetland systems with *Arundo* and *Sarcocornia* for polishing high salinity tannery wastewater. *J. Environ. Manag.* **2012**, *95*, 66–71. [[CrossRef](#)]
44. Saeed, T.; Afrin, R.; Al Muyeed, A.; Sun, G. Treatment of tannery wastewater in a pilot-scale hybrid constructed wetland system in Bangladesh. *Chemosphere* **2012**, *88*, 1065–1073. [[CrossRef](#)] [[PubMed](#)]
45. APHA. *Standard Methods for the Examination of Water and Wastewater*, 20th ed.; American Public Health Association: Washington, DC, USA, 2005.
46. Gabriel, U.U.; Okey, I.B. Effect of aqueous leaf extracts of *lepidagathis alopecuroides* on the behaviours and mortality of hybrid catfish (*Heterobranchus bidorsalis* X *Clarias gariepinus*) fingerlings. *Resour. J. Appl. Sci. Eng. Technol.* **2009**, *1*, 116–120.
47. Roopadevi, H.; Somashekar, R.K. Assessment of the toxicity of waste water from a textile industry to *Cyprinus carpio*. *J. Environ. Biol.* **2012**, *33*, 167–171. [[PubMed](#)]
48. Borgia, V.J.F.; Thattheyus, A.J. Acute toxicity of effluent from electroplating industry to the common carp, *Cyprinus carpio* linn. *Int. J. Zool. Res.* **2015**, *1*, 10–14.
49. Adewoye, S.O.; Fawole, O.O.; Owolabi, O.D.; Omotosho, J.S. Toxicity of cassava wastewater effluents to African catfish: *Clarias gariepinus* (Burchell, 1822). *Ethiop. J. Biol. Sci.* **2005**, *28*, 189–194. [[CrossRef](#)]
50. Handa, K.; Jindal, R.L. Chronic toxicity of hexavalent chromium affects the morphology and behaviour of *Ctenopharyngodon idellus* (Cuvier and Valenciennes). *Int. J. Fish. Aquatic Stud.* **2019**, *7*, 46–51.
51. Vanerkar, A.P.; Satyanarayan, S.; Dharmadhikari, D.M. Toxicity of herbal pharmaceutical wastewater on fish—*Lebistes reticulatus* (Peter). *J. Environ. Sci. Health* **2004**, *39*, 115–123. [[CrossRef](#)]
52. Virk, S.; Sharma, A. Alterations in the biochemical constituents of muscles of *Cirrhinus mrigala* following exposure to and withdrawal from metals. *Bull. Environ. Contam. Toxicol.* **2003**, *70*, 0106–0111. [[CrossRef](#)]
53. Vutukuru, S.S. Acute effects of hexavalent chromium on survival, oxygen consumption, hematological parameters and some biochemical profiles of the Indian major carp, *Labeo rohita*. *Int. J. Environ. Res. Public Health* **2005**, *2*, 456–462. [[CrossRef](#)]
54. Velma, V.; Vutukuru, S.S.; Tchounwou, P.B. Ecotoxicology of hexavalent chromium in freshwater fish: A critical review. *Rev. Environ. Health* **2009**, *24*, 129–146. [[CrossRef](#)]
55. Shaikat, T.; Javed, M. Acute toxicity of chromium for *Ctenopharyngodon idella*, *Cyprinus carpio* and *Tilapia nilotica*. *J. Agric. Biol.* **2013**, *15*, 590–594.
56. Sanyal, T.; Kaviraj, A.; Saha, S. Toxicity and bioaccumulation of chromium in some freshwater fish. *Human Ecol. Risk Assess. An Int. J.* **2017**, *23*, 1655–1667. [[CrossRef](#)]
57. Carpenter, K.E. On the biological factors involved in the destruction of river fisheries by pollution due to lead mining. *Ann. Appl. Biol.* **1924**, *12*, 1–23. [[CrossRef](#)]
58. Carpenter, K.E. The lethal action of soluble metabolic salts on fishes. *J. Exp. Biol.* **1927**, *4*, 378–390.
59. Nisha, J.C.; Sekar, R.R.J.; Chandran, R. Acute effect of chromium toxicity on the behavioral response of zebra fish *Danio rerio*. *Int. J. Plant Animal Environ. Sci.* **2016**, *6*, 6–14.
60. Jomova, K.; Valko, M. Advances in metal-induced oxidative stress and human disease. *Toxicology* **2011**, *283*, 65–87. [[CrossRef](#)]
61. Burton, D. A physiological interpretation of pattern changes in a flatfish. *J. Fish Biol.* **2008**, *73*, 639–649. [[CrossRef](#)]
62. Mills, M.G.; Patterson, L.B. Not just black and white: Pigment pattern development and evolution in vertebrates. *Sem. Cell Dev. Biol.* **2009**, *20*, 72–81. [[CrossRef](#)]
63. Little, E.E.; Flerou, B.A.; Ruzhinskaya, N.N. Behavioural Approaches in Aquatic Toxicology Investigations: A Review. In *Toxic Substances in Aquatic Environment*; Mehrle, P.M., Gray, R.H., Kendall, R.L., Eds.; American Fisheries Society: Bethesda, MD, USA, 1985; pp. 72–98.

64. Deshpande, A.M.; Satyanarayan, S. Toxicity evaluation of through fish bioassay raw bulk drug industry wastewater after electrochemical treatment. *Iran. J. Environ. Health Sci. Eng.* **2011**, *8*, 373–380.
65. Mishra, A.; Tripathi, C.P.M.; Dwivedi, A.K.; Dubey, V.K. Acute toxicity and behavioral response of freshwater fish, *Mystus vittatus* exposed to pulp mill effluent. *J. Environ. Chem. Ecotoxicol.* **2011**, *3*, 167–172.
66. Timchalk, C.; Nolan, R.J.; Mendrala, A.L.; Dittenber, D.A.; Brzak, K.A.; Mattsson, J.L. A physiologically based pharmacokinetic and pharmacodynamic (PBPK/PD) model for the organophosphate insecticide chlorpyrifos in rats and humans. *Toxicol. Sci.* **2002**, *66*, 34–53. [[CrossRef](#)]
67. Bantu, N.; Vakita, V.R. Acute toxicity of chlorantraniliprole to freshwater fish *Channa punctatus* (Bloch). *Adv. Zoology Bot.* **2013**, *1*, 78–82.
68. Anderson, P.D.; Weber, L.J. Toxic response as a quantitative function of body size. *Toxicol. Appl. Pharmacol.* **1975**, *33*, 471–483. [[CrossRef](#)]
69. Durve, V.S.; Jain, S.M. Toxicity of distillery effluent to the cyprinid weed fish *Rasbora daniconius* (Ham). *Acta Hydrochimica* **1980**, *8*, 329–336.
70. Peshine, R.G.; Kurve, S.S. Estimation of LC50 values for *Lebistes reticulatus* with toxicants zinc sulphate and mercuric chloride. *J. Aquatic Biol.* **2000**, *15*, 84–85.
71. Chukwu, L.O.; Okhumale, B.O. Mode of joint action response to binary mixtures of three refined petroleum products by Nile Tilapia *Oreochromis niloticus* fingerlings. *Sci. Res. Essays* **2009**, *4*, 806–811.
72. Cui, Z.; Yang, Z.; Shen, L.; Jiang, H.Z. Complex modal analysis of the movements of swimming fish propelled by body and or caudal fin. *Wave Motion* **2018**, *78*, 83–97. [[CrossRef](#)]
73. Mishra, A.K.; Mohanty, B. Acute toxicity impacts of hexavalent chromium on behavior and histopathology of gill, kidney and liver of the freshwater fish, *Channa punctatus* (Bloch). *Environ. Toxicol. Pharmacol.* **2008**, *26*, 136–141. [[CrossRef](#)]
74. Begum, G.; Venkateswara Rao, J.; Srikanth, K. Oxidative stress and changes in locomotor behavior and gill morphology of *Gambusia affinis* exposed to chromium. *Toxicol. Environ. Chem.* **2006**, *88*, 355–365. [[CrossRef](#)]
75. Konar, S.K.; Ghosh, T.K. Ethology of fish, *Tilapia mosambica* under lindane toxicity. *Geobios* **1982**, *10*, 230–231.
76. Gutierrez, M.F.; Gagneten, A.M.; Parma, M.J. Bioconcentration and trophic transfer of chromium in the *Daphnia magna* (Crustacea: Cladocera)-*Cnesterodon decemmaculatus* (Pisces, Poeciliidae) system. *Fresen. Environ. Bull.* **2008**, *17*, 647–651.
77. Sivakumar, P.; Kanagappan, M.; Sam Manohar Das, S. Toxicity evaluation and behavioural responses of *Danio rerio* exposed to raw tannery effluent. *J. Entomol. Zool. Stud.* **2014**, *2*, 288–291.
78. Dahunsi, S.O.; Oranusi, S.U. Acute toxicity of synhyetic resin effluent to African catfish, *Clarias gariepinus* [BURCHELL, 1822]. *Am. J. Food Nutr.* **2012**, *2*, 42–46. [[CrossRef](#)]
79. Sinha, T.K.P.; Kumar, K. Acute toxicity of mercuric chloride to *Anabas testudineus* (Bloch). *Environ. Ecol.* **1992**, *10*, 720–722.
80. Oyedapo, F.; Akinduyite, V. Acute Toxicity of Aqueous *Morinda lucida* Leaf Extracts to Nile Tilapia, *Oreochromis niloticus* (Linnaeus, 1857). In Proceedings of the Ninth International Symposium on Tilapia in Aquaculture, Shanghai, China, 22–24 April 2011; pp. 52–59.
81. David, A.; Ray, P. Studies on the pollution of the river Daha (N. Bihar) by sugar and distillery wastes. *Environ. Health* **1966**, *8*, 6–35.
82. Thorat, S.S.; Wagh, S.B. Oxygen consumption in fish *Channa gachua* exposed to tannery effluent. *Indian J. Environ. Ecolplan.* **2001**, *5*, 203–206.



© 2020 by the authors. Licensee MDPI, Basel, Switzerland. This article is an open access article distributed under the terms and conditions of the Creative Commons Attribution (CC BY) license (<http://creativecommons.org/licenses/by/4.0/>).

Article

Ability of *Trichoderma hamatum* Isolated from Plastics-Polluted Environments to Attack Petroleum-Based, Synthetic Polymer Films

Kateřina Malachov^{1,*}, enek Novotny^{1,2,*}, Grażyna Adamus³, Nadia Lotti⁴, Zuzana Rybkova¹, Michelina Soccio⁴, Pavlina Šlosarcikova¹, Vincent Verney⁵ and Fabio Fava⁴

¹ Department of Biology and Ecology, Faculty of Science, University of Ostrava, Chittussiho 10, 71000 Ostrava, Czech Republic; zuzana.rybkova@osu.cz (Z.R.); PolinkaS@seznam.cz (P.Š.)

² Laboratory of Environmental Biotechnology, Institute of Microbiology of Czech Acad. Sci., 10000 Prague, Czech Republic

³ Centre of Polymer and Carbon Materials Polish Academy of Sciences, 41-800 Zabrze, Poland; gadamus@cmpw-pan.edu.pl

⁴ Department of Civil, Chemical, Environmental and Materials Engineering, University of Bologna, 40126 Bologna, Italy; nadia.lotti@unibo.it (N.L.); michelina.soccio@unibo.it (M.S.); fabio.fava@unibo.it (F.F.)

⁵ Institut de Chimie de Clermont Ferrand, Universite Blaise Pascal, Ecole Nationale Superieure de Chimie, CNRS UMR6296, 63170 Aubiere, France; vincent.verney@uca.fr

* Correspondence: katerina.malachova@osu.cz (K.M.); novotny@biomed.cas.cz (.N.); Tel.: +420-5970-92315 (K.M.); +420-2964-42767 (.N.)

Received: 31 March 2020; Accepted: 13 April 2020; Published: 16 April 2020

Abstract: Microorganisms colonizing plastic waste material collected in composting-, landfill-, and anaerobic digestion plants were isolated to obtain novel strains maximally adapted to the degradation of plastics due to long-term contact with plastic polymers. Twenty-six bacterial strains were isolated and identified by the 16 S rRNA method, and eighteen strains of yeasts and fungi using 18 S rRNA and the internal transcribed spacer ITS sequencing of the 18 S rRNA gene. In selected strains, the ability to degrade linear low-density polyethylene (LLDPE), low-density polyethylene (LDPE), polystyrene (PS), and polyvinyl chloride (PVC) was tested in aerobic liquid-medium cultures. An oxidative, two-step pretreatment of LLDPE and LDPE using γ - or UV-irradiation followed by a high-temperature treatment was carried out, and the pretreated plastics were also included in the degradation experiments. The respective weight losses after biodegradation by *Trichoderma hamatum* were: virgin and γ /T90-pretreated LLDPE (2.2 ± 1.2 and $3.9 \pm 0.5\%$), virgin and UV/T60-pretreated LDPE (0.5 ± 0.4 and $1.3 \pm 0.4\%$), and virgin PS ($0.9 \pm 0.4\%$). The Fourier transform infrared spectroscopy (FTIR) analysis showed that during the treatment of pretreated LLDPE, *T. hamatum* attacked low molecular weight LLDPE oligomers, reducing the functional groups (carbonyl C = O), which was paralleled by a slight increase of the molar mass of pretreated LLDPE and a decrease of the dispersity index, as demonstrated by gel permeation chromatography (GPC). Thermogravimetric analysis (TGA) highlighted the formation of functional groups on LLDPE due to polymer pretreatment that favored fungal attack at the polymer surface. The results provide insight into microbial consortia that spontaneously colonize the surface of plastics in various environments and their capability to attack plastic polymers.

Keywords: bacteria; fungi; screening; plastic-polymer degradation; *Trichoderma hamatum*

1. Introduction

Research focusing on the biodegradation of recalcitrant plastic polymers brought evidence that many microorganisms are able to attack polymeric chains. However, the degradation efficiency was

mostly low [1,2]. Therefore, there is a need to isolate highly degradative strains of bacteria and fungi and better understand the biochemistry of polymer degradation with the aim to develop efficient degradation technologies [3,4]. Polyethylene (PE) is the most common plastic, accounting for 34% of the total plastics market. It is extremely resistant to biodegradation [1,5]. Its degradability can be enhanced by abiotic photo- and thermooxidative treatments, resulting in the production of carboxyl, hydroxyl, and carbonyl groups that can be oxidized by microbial metabolism [6,7].

PE can be used as the sole carbon source for soil and marine bacteria that generate hydroxyl groups in the polymer [8,9]. Numerous works document the biodegradation potential of fungal organisms towards plastics. The examples include LDPE biodegradation by *Aspergillus* spp. [10,11], *Fusarium* spp. [10,12], and *Penicillium* spp. [13]. An important prerequisite for degradation is an effective contact of the degrading microorganism and its extracellular enzyme machinery with the polymer, ensured by the colonization of the plastic surface with bacterial or fungal biofilms [2,14]. Microorganisms are able to modify the hydrophobicity of their cellular surface to promote hydrophobic interactions with the highly hydrophobic polymer surface [15]. The colonization of the polymer surface and the subsequent degradation can be increased by thermal pretreatment, chemical oxidation, or radiation [16,17].

The biodegradation process includes the introduction of functional groups (hydroxyl -OH and carbonyl C = O) in the polymer molecule and the splitting of the chain by extracellular enzymes to provide small fragments that enter the intracellular metabolism as carbon and energy sources for growth [18]. Peroxidases and laccases are implicated in the degradation of PE, the former reducing the weight average molecular weight and the latter reducing the average molecular weight and average molecular number of the polymer [19,20]. Esterases and lipases are involved in degradation of polyester-type polymers [21,22]. A two-step action of bacterial extracellular hydrolases and of a combination of lipase, esterase, and protease activities was also reported in the degradation of the aliphatic-aromatic co-polyester Ecoflex® [23,24].

Microorganisms that are in prolonged contact with plastic wastes are adapted to these environmental conditions to maximize their degradation potential. The strategy for isolating efficient microbial degraders of plastics is often focused on microorganisms colonizing plastic wastes in soil or other plastics-polluted environments [2,25,26]. In this study, autochthonous microorganisms colonizing surfaces of plastic wastes from composting plants, landfills, and anaerobic digestion plants were used as a source of novel bacterial and fungal strains, presumably well-adapted to the biodeterioration and biodegradation of plastics. A standard isolation method was used, and the strains were taxonomically classified. Virgin LLDPE and LDPE were subjected to an oxidative pretreatment. Subsequently, both virgin and pretreated LLDPE and LDPE, together with virgin PS and polyvinyl chloride (PVC), were tested for degradation in liquid media with the main purpose of obtaining strains with a high potential of degradation of plastic polymers. The weight reduction data obtained by a treatment of LLDPE by *T. hamatum* were supported by FTIR and GPC analyses.

2. Materials and Methods

2.1. Isolation and Taxonomical Identification of Bacteria and Fungi from Plastic-Polluted Environments

Samples of plastic polymers from the following sites were used for the isolation of new bacterial and fungal strains: a compost sample from the municipal composting plant (Grenoble, France), a compost sample from the composting plant (Schendelbeke, Belgium), a sample of black mulching film removed from agricultural soil in Belgium, a plastic sample removed from soil along a highway in Belgium, a sample of sludge from the anaerobic digester at a wastewater treatment plant (Treviso, Italy), and a sample of plastics removed from a landfill (Styron plant, Schkopau, Germany).

The isolation method employed the following media: Nutrient agar (NA), Boyd Kohlmeyer (BK) medium, Malt extract agar (MEA), Malt extract glucose (MEG) medium, Kirk medium [27], and Bushnell Haas (BH) medium. The media were used for the isolation of bacteria and fungi at 28 °C

from the above environmental samples to obtain monoclonal isolates [28]. When fungi were isolated, the medium was supplemented with a penicillin/streptomycin/neomycin solution (Sigma Aldrich, Czech Republic, respective final antibiotic concentrations of 50 units, 0.05 mg·mL⁻¹, and 0.1 mg·mL⁻¹) to inhibit the growth of bacteria. The subsequent prescreening of strains was based on the degradation of persistent Azure B dye (100 mg·L⁻¹), which is a method of choice for the rapid evaluation of the capacity of microorganisms to degrade xenobiotics [29–31].

The screened fungi were identified using a sequence analysis of partial 18 S rRNA and of complete ITS regions of the 18 S rRNA gene. The bacteria were identified using the partial 16 S rRNA gene. An amount of 0.5 g of the samples was used for the isolation of total DNA (soil DNA extraction kit, Sigma-Aldrich, St. Louis, USA), in agreement with the manufacturer's instructions [32]. DNA was analyzed with Nanophotometer P300 (Implen, Munchen, Germany). The amplification of DNA samples was carried out using a bacterial 16 S primer set [33], universal 18 S rDNA primer set [34], and fungal specific ITS1/ITS4 primer [35]. The PCR-amplified products were purified and ligated with a pGEM-T easy cloning vector system (Promega, USA) and transformed into OneShot *E. coli* cells (Invitrogen, Carlsbad, CA, USA) [31,36]. The transformed cells were used for plasmid isolation and purification (Millipore plasmid isolation kit, Millipore, Bedford, USA) [31]. Macrogen Inc. (Amsterdam, Netherlands) sequenced the plasmids. The BLASTN bioinformatics tool was used to obtain the phylogenetic analysis [32]. Alternatively, bacterial isolates were also identified using the BIOLOG system (BIOLOG, Hayward, USA) [37].

2.2. Plastic Polymers and Their Pretreatment

LLDPE and LDPE films (density at 20 °C: 0.88–0.96 g·mL⁻¹; thickness: 70 and 40 µm for LLDPE and LDPE, respectively) as well as PS (containing traces of a decolorant agent and about 2000 ppm of a release agent) were produced by Versalis S.p.A., Italy. PVC (containing plasticizers whose formulation is confidential) was produced by Gruppo Fabbri Spa., Italy. All plastic polymers were delivered by the Department of Civil, Chemical, Environmental, and Materials Engineering, University of Bologna, Italy. PE films were prepared as a neat formulation of the polymer films, avoiding the use of stabilizers and additives.

The Centre National de la Recherche Scientifique, Clermont-Ferrand, France, performed the pretreatment of LLDPE and LDPE. The materials were submitted to an oxidative pretreatment. The goal of this process was to enhance the hydrophilic character of the studied plastics through hydroxyl and carbonyl chemical groups fixation due to radical oxidation reactions. To ensure going far enough in the oxidative degradation mechanism, new unusual treatments have been set up by cycling different oxidative steps. All these treatments and their conditions have been extensively described in a previous paper [31]. After the treatments, the materials were characterized by FTIR and by melt viscoelasticity to assess the molecular weight evolution [31].

2.3. Biodegradation Tests

Aerobic liquid-medium cultures were used to test the capability of microorganisms to degrade plastic polymers. Virgin LLDPE, LDPE, PS, and PVC, as well as pretreated LLDPE and LDPE films, were used in the experiments [38]. The protocol used in the biodegradation experiments with fungal and bacterial strains was the same as that described by Novotny et al. [31]. Small pieces (20–30 mg) of polymer films were used. First, grease was removed from their surface by immersion in 70% ethanol (10 min., 120 rpm) which also sterilized the polymers. Then, the plastic films were washed with sterile water, dried, and pre-weighed under sterile conditions to be able to determine the weight reduction at the end of the experiment. The sterilization of all media was made by autoclaving (120 °C, 20 min) (Systec VX-5, Systec GmbH, Germany).

The biodegradation by fungal strains was carried out aseptically in liquid Czapek Dox medium pH 6.8. After inoculation, the cultures were incubated at 28 °C and aerated by air diffusion. The fungal static cultures were stirred manually every other day. Fungal cultures grown for seven days in MEG

medium (5 g·L⁻¹ malt extract, 10 g·L⁻¹ glucose, pH 4.5) were homogenized (Ultra Turrax T25, IKA Labortechnik, Staufen im Breisgau, Germany) and used as 5% (V/V) inoculum for the above Czapek Dox cultures.

The biodegradation by *Bacillus amyloliquefaciens* occurred under aseptic conditions in liquid BH medium pH 7.0 (Fluka, Germany), to which 1 g·L⁻¹ glucose was added. The medium itself did not contain any carbon source and, thus, it was adjusted by adding a small amount of glucose to support the cometabolic process and maintain the bacterial culture viable and active during biodegradation. The aeration was ensured by shaking at 120 rpm using an orbital shaker (ELMI orbital shaker DOS-20 L, ELMI Ltd., Riga, Latvia). The bacterial inoculum (5%, V/V) was grown overnight (shaken culture, 28 °C, BK medium pH 6.8).

When the biodegradation experiment was terminated, the plastic films were washed (2% SDS solution, 2 h) to get rid of the attached microbes. Then, they were washed with ethanol (70% V/V) and deionized water. The degradation was measured as the weight reduction of the dry samples. The samples were measured in triplicates, always including an abiotic control.

2.4. Physicochemical Analyses

2.4.1. FTIR Analysis

The recording of the infrared spectra of the polymer film samples was as described in [31].

The ATR FTIR spectra of virgin and pretreated LLDPE films obtained before and after the fungal degradation were measured at room temperature [31].

2.4.2. TGA Analysis

The analysis conditions are described in detail by Novotny et al. (2018) [31]. The temperature calibration of the equipment followed the protocol suggested by the producer.

2.4.3. GPC Analysis

The number average molecular mass (M_n) and molecular mass distribution index (M_w/M_n) were measured in 1,2,4-trichlorobenzene containing Santanox-R stabilizer (conditions: 135 °C, flow rate 1 mL·min⁻¹, Alliance GPCV 2000 chromatograph, HT (39,500–30,000) and HT6E (5000–1,000,000) columns, refractive index- and viscometer detectors), as described by Novotny et al. (2018) [31]. Polystyrene standards with a mass range of 580–3,790,000 were used to obtain the calibration curve. $K = 0.0004$ and $\alpha = 0.74$ were used in the calculation [31].

2.4.4. Scanning Electron Microscopy (SEM)

The samples (thin slices of a plastic film) were cut into 5 × 5 mm² sections with scissors. After slitting, the samples were mounted onto aluminum stubs and gold-coated (Automatic Sputter Coater JEOL JFC-1300, JEOL USA, Inc., coating time 20 s). The samples were scanned using a JEOL JSM-6610LV (Japan) in a high vacuum mode and SEI (secondary electron image). The working distance (WD) was 15 mm, accelerating voltage 12 kV, and spot size 30 for all scanned samples. The magnifications used were 500×, 2000×, and 5000×.

3. Results and Discussion

3.1. Isolation and Identification of Microorganisms

New bacterial and fungal strains capable of growth and survival on plastic polymers were isolated from the surface of plastic polymer wastes collected at six environmentally different sites. A total of 26 bacterial strains were identified using the 16 S rRNA eubacterial primer set (Table 1). Similarly, 18 fungal strains were identified using 18 S rRNA and the ITS sequencing of 18 S rRNA (Table 2). Bacteria of the genus *Bacillus* dominated in the compost-, anaerobic sludge- and landfill samples,

whereas no similar predominance by a single genus could be observed among the isolated fungal organisms. The prescreening with Azure B based on the strains' decolorization efficiency, evaluated visually on dye-containing agar media (NA) and in liquid medium (BK), was used to select the following strains: the fungal strains *Trichoderma hamatum* (University of Ostrava collection no. HF4, GenBank accession no. FR87271), *Trichaptum abietinum* (University of Ostrava collection no. CA, GenBank accession no. J768676), *Byssoschlamys nivea* (University of Ostrava collection no. FK1, GenBank accession no. M83256.1), *Byssoschlamys nivea* (University of Ostrava collection no. JM5, GenBank accession no. GU733368.1), and the bacterial strain *B. amyloliquefaciens* (University of Ostrava collection no. JB4, GenBank accession no. KT185076). Those strains provided the most efficient and rapid decolorization response and were further tested for the capability to degrade virgin and pretreated LLDPE, LDPE, PS, and PVC. The results obtained with *B. amyloliquefaciens* JB4 are reported in a parallel paper [31].

Table 1. Bacterial strains isolated from various environments. The strains were identified using BLASTN search with 16 S rRNA gene sequences, and their GenBank accession nos. of the closest relative are given in brackets.

Environmental Origin	Strain Identity (GenBank Accession No.)	Q-Coverage, % (Error Value)
Compost (Grenoble, France)	<i>Vibrio</i> sp. (DQ146981.1)	99 (0)
	<i>Clostridium roseum</i> (KM999946.1)	71 (0)
	<i>Bacillus</i> sp. (JX202600.1)	100 (0)
	<i>Bacillus</i> sp. (KJ162135)	100 (0)
Mulching Film From Soil (Belgium)	<i>Pseudomonas poe</i> (JN897284)	100 (0)
Plastics From Soil Along Highway (Belgium)	<i>Delftia</i> sp. (KF896097)	100 (0)
	<i>Uncultured Klebsiella</i> sp. (JN873189)	100 (0)
Compost (Schendelbeke, Belgium)	<i>Achromobacter</i> sp. (KP670417.1)	100 (1.00 × 10 ⁻¹¹²)
	<i>Vibrio</i> sp. (DQ146981.1)	99 (0)
	<i>Bacillus licheniformis</i> (KM226937.1)	97 (0)
	<i>Bacillus amyloliquefaciens</i> JB4 (KT185076) ¹	100 (0)
	<i>Bacillus amyloliquefaciens</i> (KJ469792.1)	100 (0)
	<i>Bacillus amyloliquefaciens</i> (KJ545589)	100 (0)
	<i>Bacillus amyloliquefaciens</i> (CP006890)	100 (0)
	<i>Bacillus amyloliquefaciens</i> (CP010556.1)	99 (0)
	<i>Bacillus pumilus</i> (DQ275671.1)	97 (0)
	<i>Bacillus subtilis</i> (KJ865584.1)	100 (0)
<i>Bacterium ZI-9</i> (JQ342232.1)	99 (0)	
Sludge From Anaerobic Digester (Treviso, Italy)	<i>Bacillus</i> sp. (CP009938.1)	100 (0)
	<i>Bacillus</i> sp. (EF582419)	100 (0)
	<i>Bacillus amyloliquefaciens</i> (KJ545589)	100 (0)
Plastics From Landfill (Styron, Germany)	<i>Bacillus cereus</i> (KF805048)	100 (3.00 × 10 ⁻¹⁶⁴)
	<i>Bacillus</i> sp. (FJ596521.1)	100 (0)
	<i>Bacillus subtilis</i> (KJ604979.1)	100 (0)
	<i>Klebsiella oxytoca</i> (CP003218)	100 (0)
	<i>Alcaligenaceae</i> sp. (AB847924.1)	99 (0)

¹ The strain written in bold was further tested for the capability to degrade various plastic polymers, and the results are reported in a parallel paper [31].

Table 2. Fungal strains isolated from various environmental samples. The strains were identified using a BLASTN search with the rRNA gene (18 S sequence, ITS sequence), and their GenBank accession nos. of the closest relative are in brackets.

Environmental Origin	18 S Sequence		ITS Sequence	
	Strain Identity (GenBank Access. No.)	Q-Coverage, % (Error Value)	Strain Identity (GenBank Access. No.)	Q-Coverage, % (Error Value)
Compost Sample (Grenoble, France)	-	-	<i>Filobasidium floriforme</i> (KF971359)	100 (0)
Mulching Film from Soil (Belgium)	<i>Fusarium oxysporum</i> (KF562839)	100 (0)	<i>Fusarium oxysporum</i> (JF776163)	100 (0)
	<i>Mucor circinelloides</i> (JQ014009)	100 (0)	<i>Mucor circinelloides</i> (HQ285608)	99 (0)
	<i>Fusarium oxysporum</i> (KF562839)	100 (0)	<i>Fusarium oxysporum</i> (KC202938)	100 (0)
	<i>Trametes</i> sp. (FJ515315)	99 (0)	Uncultured Fungus (KF800596)	100 (0)
Plastics from Soil Along Highway (Belgium)	Uncultured fungus (AB534505)	100 (0)	<i>Fusarium</i> sp. (JQ388248)	100 (0)
	<i>Hypocrea nuroiana</i> (JN941682)	100 (0)	<i>Trichoderma hamatum</i> HF4 ¹ (FR872741)	100 (0)
	Uncultured fungus (GU306002)	99 (0)	<i>Thanatephorus cucumeris</i> (FR670341)	100 (0)
	-	-	<i>Galactomyces geotrichum</i> (DQ683112)	100 (0)
Plastic Samples from Composting Plant (Belgium)	<i>Trichaptum abietinum</i> CA ¹ (FJ768676)	100 (0)	Uncultured fungus (JF721422)	100 (0)
	<i>Byssosclamyces nivea</i> FK1 ¹ (M83256.1)	100 (0)	-	-
	<i>Pseudallescheria</i> sp. (FN666094.1)	99 (0)	<i>Pseudallescheria</i> sp. (AY939802.1)	99 (0)
	-	-	<i>Pseudallescheria boydii</i> (AY213683.1)	99 (0)
	-	-	<i>Trametes suaveolens</i> (KE573015)	99 (0)
	<i>Trametes</i> sp. (FJ51531)	99 (0)	<i>Trametes gibbosa</i> (KC525203)	100 (0)
	<i>Pseudallescheria ellipsoidea</i> (U43911)	100 (0)	<i>Scedosporium apiospermum</i> (JN207446)	100 (0)
	<i>Graphium</i> sp. (FJ176832)	100 (0)	-	-
Sludge (Treviso, Italy)	<i>Byssosclamyces nivea</i> JM5 ¹ (GU733368.1)	99 (0)	-	-

¹ The strains written in bold were further tested for the capability to degrade various plastic polymers (cf. Table 3).

Table 3. Plastic polymer weight reductions obtained with preselected isolates of fungi in two-month biodegradation tests in liquid medium cultures using various synthetic polymers.

Plastic Polymers	Character of Polymers	Microorganism	Weight Loss (%)	Abiotic Control (%)
LLDPE	Virgin	<i>Trichoderma hamatum</i> HF4	2.2 ± 1.2	1.3 ± 0.8
	Pretreated γ/T90 ¹	<i>Trichoderma hamatum</i> HF4	3.9 ± 0.5	0.3 ± 0.1
LDPE	Virgin	<i>Trichoderma hamatum</i> HF4	0.5 ± 0.4	0.2 ± 0.1
	Pretreated γ/T150 ¹	<i>Trichoderma hamatum</i> HF4	0.9 ± 0.1	0.2 ± 0.1
PS	Virgin	<i>Trichoderma hamatum</i> HF4	1.3 ± 0.4	0.4 ± 0.1
		<i>Trichoderma hamatum</i> HF4	20.0 ± 0.5	
PVC	Virgin	<i>Byssosclamyces nivea</i> FK1	18.4 ± 0.7	9.9 ± 2.9
		<i>Trichaptum abietinum</i> CA	17.5 ± 0.7	
		<i>Byssosclamyces nivea</i> JM5	15.5 ± 0.9	

¹ The plastic polymers were pretreated as follows: LLDPE γ/T90, γ-irradiation (200 kGy)/temperature 90 °C; LDPE γ/T150, γ-irradiation (50 kGy)/temperature 150 °C; UV/T60, UV irradiation 7 days/temperature 60 °C.

3.2. Biodegradation of Polymer Plastic Films Measured by Gravimetric Analysis

The results of the gravimetric analysis after the degradation experiments are shown in Table 3. *T. hamatum* exhibited a weight reduction rate of about 4% (w/w) with the pretreated LLDPE after two months. The weight reduction obtained in the abiotic control was ten times lower. In the case of virgin and pretreated LDPE, the weight losses obtained with *T. hamatum* were 0.5%–1.3% (w/w), slightly exceeding the values obtained in the abiotic controls. Compared to the degradation rates obtained with virgin LLDPE and LDPE, the improvement of the biodegradability by the pretreatment of LLDPE and LDPE was rather low (Table 3). The biotic weight losses observed were similar to those reported after a 90-day degradation of γ -irradiated LDPE by fungal strains of *Paecilomyces*, *Aspergillus*, and *Lasiodiplodia* [38,39]. Similarly, Briassoulis et al. [6] reported weight reductions of 0.7% and 6.7% (w/w) of prooxidants-containing LLDPE-P1 mulching films that were exposed to soil conditions for 19 months. On the other hand, wood- and litter-saprotrophic fungi isolated from lake-floating plastic debris were reported not to be able to degrade PE in the form of PE powder in mineral agar medium [40].

PS was highly resistant to biodegradation by *T. hamatum*, the degradation rate after two months being only 0.9% (w/w) (Table 3). The extremely low degradability of PS is in agreement with the reports of other authors [41].

By far, the highest degradation rates were obtained with PVC (Table 3). Four different microorganisms were tested, and the weight reductions were in the range of 15% to 20% (w/w), whereas the abiotic control showed a weight loss of 9.9% (w/w). PVC polymer usually contains additives such as stabilizers, plasticizers, and lubricants, sometimes in large quantities of up to 30% in weight.

The predominant plasticizers used in PVC are phthalic acid esters that are well biodegradable by bacteria and fungi [42,43]. In keeping with other studies documenting that these additives are primarily attacked by microorganisms [44] and that their removal is responsible for the weight reduction observed in biodegradation experiments [45], we concluded that the weight reductions observed after the exposure to the fungi shown in Table 3 were probably caused by the removal of the additives. The weight reduction values obtained in our experiments with PVC films (Table 3) were comparable to those measured with PVC cables in landfill simulation experiments [45].

The SEM observations showed that the fungal degradation of PVC by *T. abietinum* and *T. hamatum* representing a weight loss of 17.5% to 20% (W/W) (Table 3) resulted in a smooth surface comparable to that of the abiotic control films (9.9% weight loss) (Figure 1a,c,d). In comparison, the bacterial degradation by *B. amyloliquefaciens* (18.3% weight loss) described by Novotny et al. (2018) [31] produced an uneven surface of the PVC films with intertwined fibrils (Figure 1b). The bacterial and fungal attacks thus seem to have a different character. The cracks in the film after the degradation by *T. abietinum* indicated that the PVC film became brittle after degradation, suggesting a possible glass transition [44], and its outer layer seemed to peel off as a result of the fungal attack (Figure 1c).

Higher standard deviation values in some degradation experiments (Table 3) probably resulted from small amounts of microbial biofilms that remained attached to the polymer surface after washing. Another factor that also contributed to large standard deviation values was the fragmentation of some plastic polymer films, namely the pretreated LDPE, PS, and PVC, into small pieces during biodegradation. Briassoulis et al. [6] mentioned a similar problem in soil experiments.

3.3. Biodegradation of Polymer Plastic Films by *T. Hamatum* Measured by Physicochemical Methods

3.3.1. FTIR Analysis

The pretreated LLDPE film samples obtained by degradation with *T. hamatum* were analyzed by ATR Fourier transform infrared spectroscopy, and then those spectra were compared, respectively, with the pretreated- and virgin LLDPE that were not subjected to the microorganisms' actions. A relatively strong band with a maximum at 1715 cm^{-1} corresponding to the stretching vibrations of C = O groups was observed in the spectrum of the pretreated LLDPE (Figure 2, line A). It is known that the

appearance of the carbonyl band in the FTIR spectrum of the pretreated LLDPE sample is associated with the presence of carboxylic acid, aldehyde, ketone, ether, or ester groups which arose during the pretreatment of virgin LLDPE by exposing it to γ -irradiation (200 KGy doses)/thermal treatment at 90 °C (Figure 2, line A). A further comparison of the FTIR spectra of the pretreated LLDPE film samples before (line A) and after a two-month degradation by *T. hamatum* (line C) showed noticeable changes in the structure of the samples studied, visualized by a slight decrease in the intensity of the carbonyl band in the spectrum C (Figure 2, line C). In order to express the decrease of the concentration of carbonyl compounds measured by FTIR in the case of the pretreated LLDPE sample after a two-month exposure to *T. hamatum* (Figure 2, line C), the carbonyl index was used, calculated as a ratio between the area of the signal at 1715 cm^{-1} (related to the C = O groups' absorbance region) and the signal at 1470 cm^{-1} (which was ascribed to the methylene absorption band -CH₂).

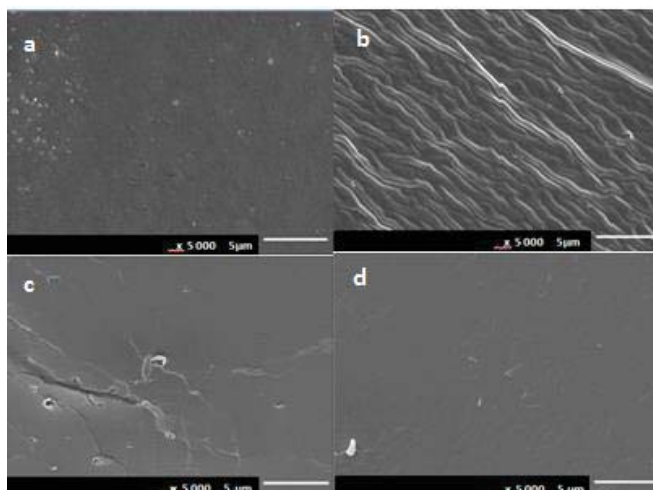


Figure 1. SEM of the PVC surface after a two-month degradation (magnification 5000 \times): (a) Abiotic control; (b) *B. amyloliquefaciens*; (c) *T. abietinum*; and (d) *T. hamatum*.

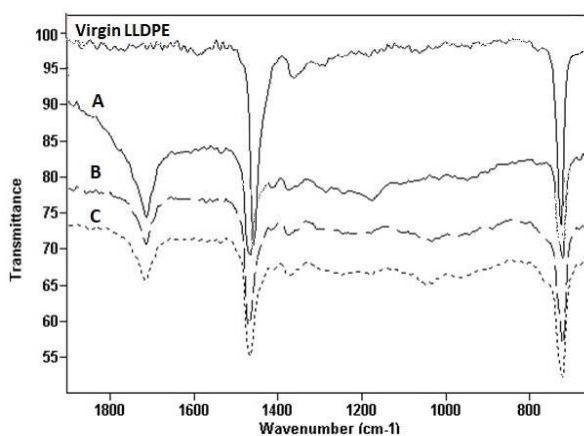


Figure 2. FTIR spectra of pretreated LLDPE after a two-month biodegradation with *T. hamatum* in liquid medium: Top, virgin LLDPE; (line A), No exposure; (line B), abiotic control (two months); (line C), two-month biodegradation. Pretreatment conditions: γ -irradiation (200 KGy dose)/thermal treatment 90 °C, seven days.

The results indicated a slight decrease of the intensity of the C = O band in the case of the LLDPE sample analyzed after a two-month exposure to *T. hamatum* (Figure 2, line C) in comparison to the sample collected after the pretreatment (Figure 2, line A) and to the abiotic control (Figure 2, line B). This observation indicated a slight decrease of the quantity of LLDPE oligomers functionalized with carbonyl groups in the sample measured after a two-month exposure to *T. hamatum* (Figure 2, line C). This effect might be caused by the ability of the fungus to attack and assimilate the C = O-functionalized, low-molecular-weight LLDPE oligomers, which led to a decrease of the quantity of such oligomers on the film surface of the LLDPE sample studied. A similar effect was observed when the pretreated LLDPE was exposed to *B. amyloliquefaciens* [31]. A decrease of the carbonyl index was also reported after a 19-month soil burial of pretreated LLDPE-P1 films [6] or after a 2- to 6-week exposure of aged, oxo-biodegradable, pro-oxidant-containing LDPE to *Pseudomonas aeruginosa* [46].

In the case of the biodegradation of pretreated LDPE (data not shown), the structural differences between the pretreated sample and the sample after a two-month treatment by *T. hamatum* were almost invisible, which indicated a very poor biodegradation ability of this polymer by the microorganism.

3.3.2. GPC Analysis

The FTIR results suggesting a microbial attack on functionalized, low-molecular-weight LLDPE oligomers (Figure 2) are in agreement with the measurements of the changes of the average molar masses of pretreated LLDPE samples before and after a two-month biodegradation. The GPC measurements showed that the average molar mass of the virgin LLDPE sample decreased after the γ -irradiation (200 KGy doses)/thermal treatment of the sample (Table 4, entries 1 and 2). Additionally, the observed higher dispersity index M_w/M_n indicated the formation of polymer chains that differed in their lengths, including low-molar-mass oligomers.

Table 4. GPC analysis of virgin- and pretreated LLDPE films exposed or not exposed to *T. hamatum*.

Polymer	Treatment Conditions	M_n (g·mol ⁻¹)	M_w (g·mol ⁻¹)	M_w/M_n
Virgin LLDPE	No exposure	75,500	163,400	2.16
Pretreated LLDPE	No exposure	1900	32,200	16.9
Pretreated LLDPE	Abiotic control	2700	38,500	14.25
Pretreated LLDPE	60-day exposure	2700	38,000	14.07

M_n , number average molecular weight; M_w , weight average molecular weight; M_w/M_n , polydispersity index. The abiotic control was not exposed to *T. hamatum* but was incubated for two months in the biodegradation medium under similar conditions.

The molar masses of both the pretreated LLDPE sample after biodegradation and the LLDPE abiotic control sample slightly increased, together with the reduction of the dispersity index (Table 4, entries 3 and 4). Such results can be explained by a migration of water-soluble, low-molar-mass, C = O-functionalized LLDPE oligomers into the medium or water. Moreover, it is worth emphasizing that in the case of LLDPE samples, after 60 days of exposure to *T. hamatum*, the dispersity index decreased in comparison with the abiotic control sample. Such a phenomenon can be explained as follows. Due to the presence of the oxygen functional groups (e.g., carbonyl groups) on the surface of the LLDPE film samples, *T. hamatum* could attack this surface and progressively enhance the biodegradation by the further cleavage of the LLDPE polymer chains and by the formation of an additional amount of low-molar-mass LLDPE oligomers. Both the initial functionalization and the biodegradation process were mostly limited to the surface of the LLDPE film samples. Therefore, O-functional oligomers with a low molar mass, formed both as a result of γ -irradiation and of the additional two-month action of *T. hamatum* (due to their greater polarity and greater affinity for the culture medium), could easily be released from the LLDPE film samples into the liquid medium, and could also be assimilated by microorganisms. The migration and/or assimilation of oligomers from the tested LLDPE samples resulted in the loss of low-molecular-weight polymer chains, which

caused an increase of the molecular homogeneity of the sample, a decrease of the dispersion index (M_w/M_n), and an increase of the average molar mass of the LLDPE film obtained by the two-month exposure to *T. hamatum*, as confirmed by the GPC analysis (Table 4, entry 4).

3.3.3. TGA Analysis

Figure 3 shows the TGA curves of the pretreated LLDPE films incubated for 20, 40, and 60 days with *T. hamatum* and the corresponding abiotic controls. For comparison, the curves of the virgin and pretreated LLDPE films are also shown. The pretreatment of LLDPE that included a combined effect of γ irradiation and a high temperature caused a huge decrease of the LLDPE thermal stability, which can be ascribed to the formation of functional groups (hydroxylic, carboxylic, etc.), as also evidenced by the FTIR analysis (Figure 3; also cf. Novotný et al. [37]), which accelerated the thermal deterioration. Nevertheless, the formation of functional groups was limited to the LLDPE surface and probably produced low-molecular-weight, polar segments that solubilized in the culture medium. This is evidenced by the abiotic control curves obtained after a 60-day exposure to the culture medium in the absence of *T. hamatum*, which were very similar to the virgin LLDPE curves. The trend was somewhat different in the presence of the fungus, where the pretreated LLDPE sample incubated for 20 days was the least thermally stable of all the samples. This suggested that the oxidized groups produced by irradiation were preferentially attacked by the fungus, with a further cleavage of polymer chains. This effect was, however, limited to the LLDPE film surface, since the thermal stability of the samples incubated with *T. hamatum* was progressively enhanced with time as the functional groups produced by irradiation were consumed by the fungus.

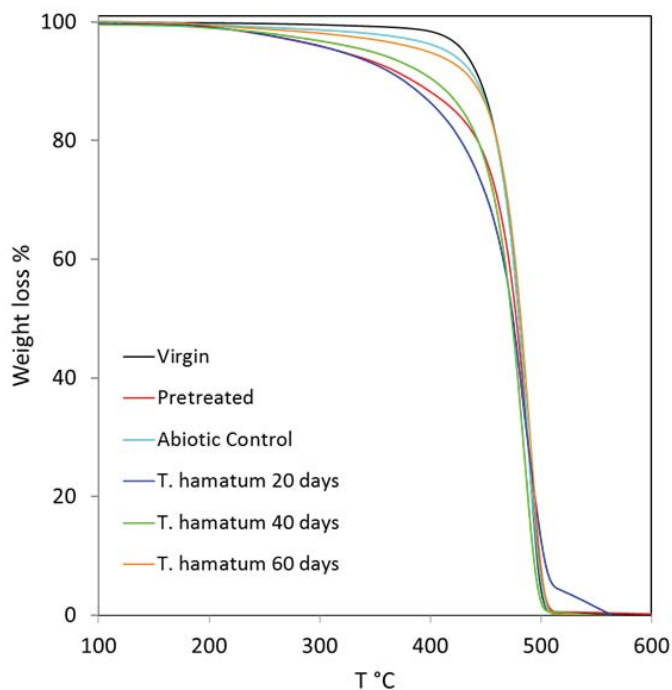


Figure 3. TGA curves of the γ -irradiation (200 kGy)/temperature 90 °C pretreated LLDPE exposed to biodegradation by *T. hamatum* for 20, 40, and 60 days, measured under nitrogen atmosphere (10 °C·min⁻¹). Virgin LLDPE (black), pretreated LLDPE (red), pretreated LLDPE exposed to biodegradation by *T. hamatum* for 20 (blue), 40 (green), and 60 days (orange), abiotic control (cyan).

Figure 4 shows the TGA curves of the pretreated LDPE films incubated for 60 day with *T. hamatum* and the corresponding abiotic control. The curves of the virgin and pretreated LDPE films are also shown for comparison. Those latter curves demonstrate that the main effect of the pretreatment was a lowering of the thermal stability of LDPE. This effect was probably due to the production of oxidized groups and cleavage reactions on the polymer chains. However, in contrast to the pretreated LLDPE (Figure 3), the 60-day incubation in the growth medium, either in the presence of the fungus or in its absence (abiotic control), did not increase the thermal stability of the LDPE films. This finding suggested that the UV irradiation did not generate polymer segments small enough to solubilize in the aqueous culture medium, nor did it generate functional groups enhancing the fungal attack.

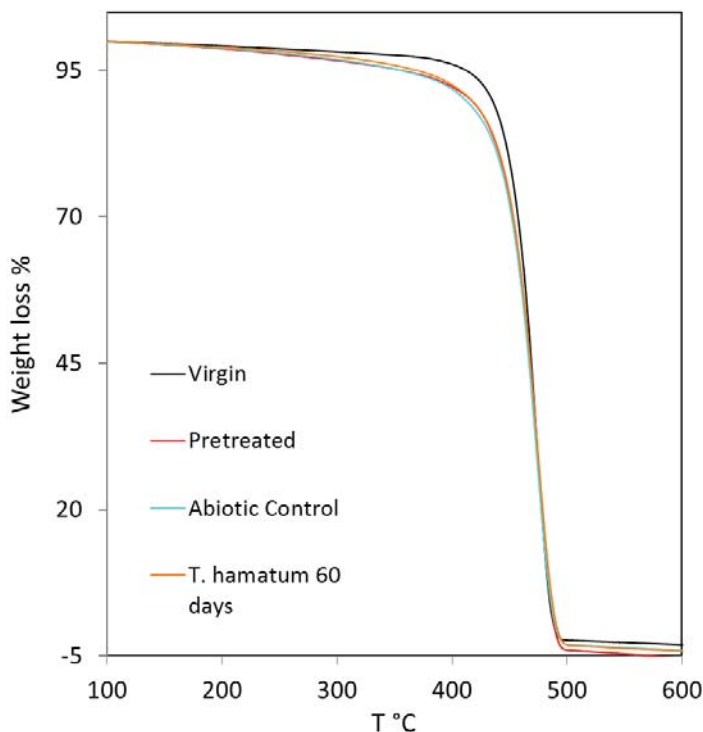


Figure 4. TGA curves of the UV irradiation (seven days)/temperature 60 °C pretreated LDPE exposed to biodegradation by *T. hamatum* for 60 days, measured under nitrogen atmosphere (10 °C·min⁻¹). Virgin LDPE (black), pretreated LDPE (red), pretreated LDPE exposed to biodegradation by *T. hamatum* for 60 days (orange), abiotic control (cyan).

4. Conclusions

A total of 26 and 18 bacterial and fungal strains colonizing weathered plastics in the environment were isolated, from which the fungus *T. hamatum* exhibited the largest weight loss-based biodegradation activities, which were confirmed, in the case of the pretreated LLDPE, by physicochemical analyses. However, even long-term contact with the plastics microenvironment resulting from the colonization of their surface, which was expected to lead to an all-round adaptation to these environmental conditions, provided strains with a generally low plastic-polymer degradation capacity, which documented the strong resistance of plastic polymers to biodegradation. The pretreatment of LLDPE and LDPE resulting in the formation of functional groups on the PE surface was able to slightly increase the degradability.

Author Contributions: Conceptualization, K.M., Č.N., V.V.; Methodology, N.L., G.A., K.M., V.V., Č.N.; Investigation, Z.R., P.Š., M.S., G.A.; Resources, Z.R., P.Š.; Writing—Original draft preparation, Č.N., K.M.; Writing—Review and editing, G.A., N.L., V.V.; Project administration, F.F., K.M.; Funding acquisition, F.F., K.M. All authors have read and agreed to the published version of the manuscript.

Funding: This research was funded by EU programmes BIOCLEAN project No. 312100 and OPVK CZ.1.07/2.3.00/30.0019, by Institutional Research Concept RVO 61388971 provided by Ministry of Education, Youth and Sports of the Czech Republic, and by ERDF Institute of Environmental Technology—Excellent Research No. CZ.02.1.01/0.0/0.0/16_019/0000853.

Acknowledgments: The provision of plastic polymers by Versalis S.p.A. and Gruppo Fabbri Spa., Italy is gratefully acknowledged.

Conflicts of Interest: The authors declare no conflict of interest.

References

- Kale, S.K.; Deshmukh, A.G.; Dudhare, M.S.; Patil, V.B. Microbial degradation of plastic: A review. *J. Biochem. Tech.* **2015**, *6*, 952–961.
- Sivan, A. New perspectives in plastic biodegradation. *Curr. Opin. Biotechnol.* **2011**, *22*, 422–426. [[CrossRef](#)] [[PubMed](#)]
- Ahmed, T.; Shahid, M.; Azeem, F.; Rasul, I.; Shah, A.A.; Noman, M.; Hameed, A.; Manzoor, N.; Manzoor, I.; Muhammad, S. Biodegradation of plastics: Current scenario and future prospects for environmental safety. *Environ. Sci. Pollut. Res.* **2018**, *25*, 7287–7298. [[CrossRef](#)] [[PubMed](#)]
- Ali, M.I.; Ahmed, S.; Robson, G.; Javed, I.; Ali, N.; Atiq, N.; Hameed, A. Isolation and molecular characterization of polyvinyl chloride (PVC) plastic degrading fungal isolates. *J. Basic Microbiol.* **2014**, *54*, 18–27. [[CrossRef](#)] [[PubMed](#)]
- Geyer, R.; Jambeck, J.R.; Law, K.L. Production, use, and fate of all plastics ever made. *Sci. Adv.* **2017**, *3*, e1700782. [[CrossRef](#)] [[PubMed](#)]
- Briassoulis, D.; Babou, E.; Hiskakis, M.; Kyrikou, I. Degradation in soil behavior of artificially aged polyethylene films with pro-oxidants. *J. Appl. Polym. Sci.* **2015**, *132*, 42289. [[CrossRef](#)]
- Fontanella, S.; Bonhomme, S.; Koutny, M.; Husarova, L.; Brusson, J.M.; Courdavault, J.P.; Pitteri, S.; Samuel, G.; Pichon, G.; Lemaire, J.; et al. Comparison of the biodegradability of various polyethylene films containing pro-oxidant additives. *Polym. Degrad. Stab.* **2010**, *95*, 1011–1021. [[CrossRef](#)]
- Restrepo-Flórez, J.M.; Bassi, A.; Thompson, M.R. Microbial degradation and deterioration of polyethylene—A review. *Int. Biodeter. Biodegr.* **2014**, *88*, 83–90. [[CrossRef](#)]
- Watanabe, T.; Ohtake, Y.; Asabe, H.; Murakami, N.; Furukawa, M. Biodegradability and degrading microbes of low-density polyethylene. *J. Appl. Polym. Sci.* **2009**, *111*, 551–559. [[CrossRef](#)]
- Das, M.P.; Kumar, S. Microbial deterioration of low density polyethylene by *Aspergillus* and *Fusarium* sp. *Int. J. Chem. Tech. Res.* **2014**, *6*, 299–305.
- Sindujaa, P.; Padmapriya, M.; Pramila, R.; Vijaya Ramesh, K. Bio-degradation of low density polyethylene (LDPE) by fungi isolated from marine water. *Res. J. Biol. Sci.* **2011**, *6*, 141–145.
- Singh, J.; Gupta, K.C. Screening and identification of low density polyethylene (LDPE) degrading soil fungi isolated from polythene polluted sites around Gwalior city (M.P.). *Int. J. Curr. Microbiol. App. Sci.* **2014**, *3*, 443–448.
- Singh, V.; Dubey, M.; Bhadauria, S. Microbial degradation of polyethylene (low density) by *Aspergillus fumigatus* and *Penicillium* sp. *Asian J. Exp. Biol. Sci.* **2012**, *3*, 498–503.
- Nowak, B.; Pajak, J.; Drozd-Bratkowicz, M.; Rymarz, G. Microorganisms participating in the biodegradation of modified polyethylene films in different soils under laboratory conditions. *Int. Biodeter. Biodegr.* **2011**, *65*, 757–767. [[CrossRef](#)]
- Czaczyk, K.; Bialas, W.; Myszka, K. Cell surface hydrophobicity of *Bacillus* spp. as a function of nutrient supply and lipopeptides biosynthesis and its role in adhesion. *Pol. J. Microbiol.* **2008**, *57*, 313–319.
- Motta, O.; Proto, A.; De Carlo, F.; De Caro, F.; Santoro, E.; Brunetti, L.; Capunzo, M. Utilization of chemically oxidized polystyrene as co-substrate by filamentous fungi. *Int. J. Hyg. Environ. Health* **2009**, *212*, 61–66. [[CrossRef](#)]
- Weiland, M.; Daro, A.; David, C. Biodegradation of thermally oxidized polyethylene. *Polym. Degrad. Stab.* **1995**, *48*, 275–289. [[CrossRef](#)]

18. Arutchelvi, J.; Sudhakar, M.; Arkatkar, A.; Doble, M.; Bhaduri, S.; Uppara, P.V. Biodegradation of polyethylene and polypropylene. *Indian J. Biotechnol.* **2008**, *7*, 9–22.
19. Iiyoshi, Y.; Tsutsumi, Y.; Nishida, T. Polyethylene degradation by lignin-degrading fungi and manganese peroxidase. *J. Wood Sci.* **1998**, *44*, 222–229. [[CrossRef](#)]
20. Santo, M.; Weitsman, R.; Sivan, A. The role of the copper-binding enzyme—Laccase—In the biodegradation of polyethylene by the actinomycete *Rhodococcus ruber*. *Int. Biodeter. Biodegr.* **2013**, *84*, 204–210. [[CrossRef](#)]
21. Khan, I.; Ray Dutta, J.; Ganesan, R. *Lactobacillus* sps. lipase mediated poly (ϵ -caprolactone) degradation. *Int. J. Biol. Macromol.* **2017**, *95*, 126–131. [[CrossRef](#)] [[PubMed](#)]
22. Park, C.; Kim, E.Y.; Yoo, Y.T.; Im, S.S. Effect of hydrophilicity on the biodegradability of polyesteramides. *J. Appl. Polym. Sci.* **2003**, *90*, 2708–2714. [[CrossRef](#)]
23. Cerdà-Cuéllar, M.; Kint, D.P.R.; Muñoz-Guerra, S.; Marqués-Calvo, M.S. Biodegradability of aromatic building blocks for poly (ethylene terephthalate) copolyesters. *Polym. Degrad. Stab.* **2004**, *85*, 865–871. [[CrossRef](#)]
24. Kleeberg, I.; Welzel, K.; VandenHeuvel, J.; Müller, R.J.; Deckwer, W.D. Characterization of a new extracellular hydrolase from *Thermobifida fusca* degrading aliphatic-aromatic copolyesters. *Biomacromolecules* **2005**, *6*, 262–270. [[CrossRef](#)]
25. Corti, A.; Muniyasamy, S.; Vitali, M.; Imam, S.H.; Chiellini, E. Oxidation and biodegradation of polyethylene films containing pro-oxidant additives: Synergistic effects of sunlight exposure, thermal aging and fungal biodegradation. *Polym. Degrad. Stab.* **2010**, *95*, 1106–1114. [[CrossRef](#)]
26. Tourova, T.P.; Sokolova, D.S.; Nazina, T.N.; Gruzdev, D.S.; Laptev, A.B. Phylogenetic diversity of microbial communities from the surface of polyethylene terephthalate materials exposed to different water environments. *Microbiology* **2020**, *89*, 96–106. [[CrossRef](#)]
27. Tien, M.; Kirk, T.K. Lignin peroxidase of *Phanerochaete chrysosporium*. *Method. Enzymol.* **1988**, *161*, 238–249.
28. Mabrouk, A.M.; Kheiralla, Z.H.; Hamed, E.R.; Yousry, A.A.; Abd, A.A.A. Screening of some marine-derived fungal isolates for lignin degrading enzymes (LDEs) production. *Agric. Biol. J. N. Am.* **2010**, *1*, 591–599.
29. Archibald, F.S. A new assay for lignin-type peroxidases employing the dye Azure, B. *Appl. Environ. Microbiol.* **1992**, *58*, 3110–3116. [[CrossRef](#)]
30. Kelley, J.; Yaghmaie, P.A. Screening of fungal strains employed in the testing of plastics materials. *Int. Biodeterior. Biodegr.* **2001**, *48*, 84–93. [[CrossRef](#)]
31. Novotný, Č.; Malachová, K.; Adamus, G.; Kwiecień, M.; Lotti, N.; Soccio, M.; Verney, V.; Fava, F. Deterioration of irradiation/high-temperature pretreated, linear low-density polyethylene (LLDPE) by *Bacillus amyloliquefaciens*. *Int. Biodeter. Biodegrad.* **2018**, *132*, 259–267. [[CrossRef](#)]
32. Altschul, S.F.; Gish, W.; Miller, W.; Myers, E.W.; Lipman, D.J. Basic local alignment search tool. *J. Mol. Biol.* **1990**, *215*, 403–410. [[CrossRef](#)]
33. Wani, A.A.; Surakasi, V.P.; Siddharth, J.; Raghavan, R.G.; Patole, M.S.; Ranade, D.; Shouche, Y.S. Molecular analyses of microbial diversity associated with the Lonar soda lake in India: An impact crater in a basalt area. *Res. Microbiol.* **2006**, *157*, 928–937. [[CrossRef](#)] [[PubMed](#)]
34. White, T.J.; Bruns, T.D.; Lee, S.B.; Taylor, J.W. Amplification and direct sequencing of fungal ribosomal RNA genes for phylogenetics. In *PCR Protocols: A Guide to Methods and Applications*; Innis, M.A., Gelfand, D.H., Sninsky, J.J., White, T.J., Eds.; Academic Press: New York, NY, USA, 1990; pp. 315–322.
35. Gardes, M.; Bruns, T.D. ITS primers with enhanced specificity for basidiomycetes—Application to the identification of mycorrhizae and rusts. *Mol. Ecol.* **1993**, *2*, 113–118. [[CrossRef](#)]
36. Mezei, L.M.; Storts, D.R. *Purification of PCR Products in PCR Technology: Current Innovations*; Griffin, H.G., Griffin, A.M., Eds.; CRC Press: Boca Raton, FL, USA, 1994; p. 21.
37. Bochner, B. “Breathprints” at the microbial level. *ASM News* **1989**, *55*, 536–539.
38. Lee, B.; Pometto, A.L.; Fratzke, A.; Bailey, T.B. Biodegradation of degradable plastic polyethylene by *Phanerochaete* and *Streptomyces* species. *Appl. Environ. Microbiol.* **1991**, *57*, 678–685. [[CrossRef](#)]
39. Sheik, S.; Chandrashekar, K.R.; Swaroop, K.; Somashekarappa, H.M. Biodegradation of gamma irradiated low density polyethylene and polypropylene by endophytic fungi. *Int. Biodeter. Biodegr.* **2015**, *105*, 21–29. [[CrossRef](#)]
40. Brunner, I.; Fischer, M.; Rüthi, J.; Stierli, B.; Frey, B. Ability of fungi isolated from plastic debris floating in the shoreline of a lake to degrade plastics. *PLoS ONE* **2018**, *13*, e0202047. [[CrossRef](#)]

41. Syranidou, E.; Karkanorachaki, K.; Amorotti, F.; Franchini, M.; Repouskou, E.; Kaliva, M.; Vamvakaki, M.; Kolvenbach, B.; Fava, F.; Corvini, P.F.-X.; et al. Biodegradation of weathered polystyrene films in seawater microcosms. *Sci. Rep.* **2017**, *7*, 17991. [[CrossRef](#)]
42. European Commission DGXI.E.3. The Behaviour of PVC in Landfill, Final Report February 2000, ARGUS in Association with University Rostock-Prof. Spillmann, Carl Bro als and Sigma Plan, S.A. Available online: <http://ec.europa.eu/environment/waste/studies/pvc/landfill.pdf> (accessed on 4 January 2017).
43. Liang, D.W.; Zhang, T.; Fang, H.H.P.; He, J. Phthalates biodegradation in the environment. *Appl. Microbiol. Biotechnol.* **2008**, *80*, 183–198. [[CrossRef](#)]
44. Giacomucci, L.; Raddadi, N.; Soccio, M.; Lotti, N.; Fava, F. Polyvinyl chloride biodegradation by *Pseudomonas citronellolis* and *Bacillus flexus*. *New Biotechnol.* **2019**, *52*, 35–41. [[CrossRef](#)] [[PubMed](#)]
45. Mersiowski, I.; Weller, M.; Ejlertsson, J. Fate of plasticised PVC products under landfill conditions: A laboratory-scale landfill simulation reactor study. *Water Res.* **2001**, *35*, 3063–3070. [[CrossRef](#)]
46. Reddy, M.M.; Deighton, M.; Gupta, R.K.; Bhattacharya, S.N.; Parthasarathy, R. Biodegradation of oxo-biodegradable polyethylene. *J. Appl. Polym. Sci.* **2009**, *111*, 1426–1432. [[CrossRef](#)]



© 2020 by the authors. Licensee MDPI, Basel, Switzerland. This article is an open access article distributed under the terms and conditions of the Creative Commons Attribution (CC BY) license (<http://creativecommons.org/licenses/by/4.0/>).

Article

Modification of the Bacterial Cell Wall—Is the Bioavailability Important in Creosote Biodegradation?

Wojciech Smulek *, Amanda Pacholak * and Ewa Kaczorek *

Institute of Chemical Technology and Engineering, Poznan University of Technology, Berdychowo 4, 60-695 Poznan, Poland

* Correspondence: wojciech.smulek@put.poznan.pl (W.S.); amanda.d.pacholak@doctorate.put.poznan.pl (A.P.); ewa.kaczorek@put.poznan.pl (E.K.)

Received: 31 December 2019; Accepted: 21 January 2020; Published: 23 January 2020

Abstract: Creosote oil, widely used as a wood preservative, is a complex mixture of different polycyclic aromatic compounds. The soil contamination result in the presence of a specific microcosm. The presented study focuses on the most active strains involved in bioremediation of long-term creosote-contaminated soil. In three soil samples from different boreholes, two *Sphingomonas maltophilia* (*S. maltophilia*) and one *Paenibacillus ulginis* (*P. ulginis*) strain were isolated. The conducted experiments showed the differences and similarities between the bacteria strains capable of degrading creosote from the same contaminated area. Both *S. maltophilia* strains exhibit higher biodegradation efficiency (over 50% after 28 days) and greater increase in glutathione S-transferase activity than *P. ulginis* ODW 5.9. However, *S. maltophilia* ODW 3.7 and *P. ulginis* ODW 5.9 were different from the third of the tested strains. The growth of the former two on creosote resulted in an increase in cell adhesion to Congo red and in the total membrane permeability. Nevertheless, all three strains have shown a decrease in the permeability of the inner cell membrane. That suggests the complex relationship between the cell surface modifications and bioavailability of the creosote to microorganisms. The conducted research allowed us to broaden the current knowledge about the creosote bioremediation and the properties of microorganisms involved in the process.

Keywords: bacteria; bioavailability; biodegradation; creosote; PAHs

1. Introduction

Creosote is a complex mixture of carbonaceous substances obtained from the distillation of tar. The two main types of creosote are wood-tar creosote and coal-tar creosote. The latter has been widely used for over 150 years as a wood preservative and water-proofing agent, in railroad and utilities industries, construction (roofing), bridge and pier decking, fencing or equipment for children' playgrounds [1–3]. Creosote oil is characterized by a yellowish to dark brown/black color and a characteristic strong odor. It is slightly soluble in water and well soluble in organic solvents. The chemical compositions of the coal-tar creosotes are usually inconsistent and depend on the origin of the coal used and the nature of the distilling process. Despite the fact that average creosote oil contains several hundreds of chemicals, only less than 20% are present in the amounts greater than 1% [4]. However, the dominant classes of the compounds found in creosote oil may be distinguished as follows:

- Aromatic hydrocarbons, including polycyclic aromatic hydrocarbons (PAHs), alkylated PAHs (up to 90%) and benzene-toluene-ethylbenzene-xylene (BTEX) pollutants group,
- Phenolic compounds, such as cresols, phenols and xylenols,
- Heterocycles containing nitrogen, sulfur or oxygen (e.g., pyridines, quinolones, benzotriophenes, dibenzofurans and their derivatives),

- Aromatic amines, such as aniline, aminonaphtalens or diphenylamines [1,4,5].

Due to the wide applications of creosote oil, the substances contained in it can easily enter all environmental compartments. Among them, sediments, soil and groundwater are believed to be the most contaminated. However, the transport and distribution of creosote within the environment depend on the physicochemical properties of its constituents [6–8]. In light of these facts, the chemicals in creosote can be transferred into animals and plants tissues posing a serious threat for humans [9–12] and implementation of new, environmentally friendly strategies of its removal is extremely important.

When the effectiveness of the biodegradation of hydrophobic impurities is considered, the role of bioavailability in this process is increasingly pointed out [13]. The low solubility of PAHs in water as well as their high sorption to soil particles affect the bioaccumulation of these compounds in the environment. Moreover, the bacterial cells that show increased affinity to aromatic hydrocarbons can easier use these compounds as a source of carbon and energy [14,15]. The surface properties of cells are determined by the hydrophobicity of their outer layers. Van der Waals interactions and electrostatic forces largely depend on the chemical nature of the functional groups of compounds that build the outside of the cell wall [16]. On the one hand, the cell wall modification may lead to an increase of cell hydrophobicity and, in consequence, enhances the bioavailability of hydrophobic compounds. On the other hand the cells can modify their surface properties to decrease their affinity to pollutant, which allows us to minimize the contaminant's toxic impact on cells [13]. However, it should be emphasized that the hydrophobicity of cell surfaces is not the only key factor in the efficiency of biodegradation processes. It has been reported that the transport across the membrane of a biodegradable compound also determines the rate of its assimilation [17,18]. However, increased cell membrane permeability means not only increased carbon source transport, but also increased cell exposure to toxic xenobiotics. This negative impact may eventually lead to the death of biomass [19]. Nevertheless, the changes in cell membrane permeability are the way that cells can use to regulate the interaction with pollutants. The compromise between a more efficient transport and lower exposure to toxic contaminant is one of the key factors regulating the biodegradation efficiency. Ultimately, bioavailability is the result of many mechanisms and only a simultaneous measurement of several parameters describing them can provide a broader view of its role.

Hence, the aim of the study was to determine the role of surface modification of environmental strains cells in their biodegradation by creosote. For this purpose, environmental strains were isolated from soil samples contaminated with PAHs, and the biodegradation efficiency was established and bound with the measured parameters describing the cell surface properties. Finally, the results obtained became the basis for verification of the research hypothesis that bioavailability is a factor of significant importance in biodegradation of the hydrocarbons present in creosote oil.

2. Materials and Methods

2.1. Chemicals

All chemicals used in the research were of analytical grade. The mineral medium for microorganisms cultivation as well as other aqueous solutions were prepared using ultra-pure MilliQ water (18.2 MΩ cm). The creosote (type B) was purchased from Centrala Obrotu Towarami Masowymi DAW-BYTOM Sp. z o.o. (Bytom, Poland).

2.2. Bacteria Strains Isolation

Samples of soil were collected from the area of a railway sleeper treatment plant in Koźmin Wielkopolski (Central Poland; 51°50'09.1"N, 17°26'20.1"E) in order to isolate bacterial strains. This area has been subjected to permanent contamination with creosote oil for more than 40 years. The samples were collected in triplicates from three different boreholes (from a depth of 0.5–4.0 m) with the use of a mechanical drill.

The most active strains that displayed the ability to degrade creosote hydrocarbons were isolated in accordance with the following procedure. Approximately 10 g of each soil sample was suspended in a sterile culture medium [20] and 2 mL of a 20% sodium succinate solution was added to each suspension. The systems were incubated at 22 °C for 24 h, then 10 mL of the suspension was introduced into 90 mL of a fresh sterile culture medium, which was supplemented with 1.5 mL of the 20% sodium succinate solution as well as 50 µL of creosote. This step was repeated every 7 days, however the subsequent cultures included only 50 µL of creosote as the sole carbon source. After 28 days, approximately 0.1 mL of the final culture was used to inoculate agar plates (bioMerieux, Warsaw, Poland). The plates were incubated (24 h, 22 °C) and then used to isolate colonies of individual bacterial strains. The isolates were subjected to identification based on their 16S rRNA gene sequence 8F 5'AGTTTGATCATCGCTCAG 3' and 1492R 5'GGTACCTTGTACGACTT3'. Furthermore, Vitek 2 Compact (bioMerieux, Warsaw, Poland) kits were used to determine the biochemical profiles of the isolates [21]. Finally, a hemolysis test was carried out for each isolated strain in accordance with the procedure described by Hassanshahian [22].

2.3. Creosote Biodegradation Test

The following procedure was employed in order to determine the biodegradation efficiency of selected bacterial isolates. Liquid cultures were prepared 100-mL glass bottles, which contained 20 mL of the culture medium and 1 mL of a 20% sodium succinate solution. The bottles were inoculated with a full loop of cells collected from an agar plate used to store the corresponding bacterial strain. After incubation (24 h, 22 °C) the biomass was separated by centrifugation (4500× g, 5 min), rinsed and re-suspended in the mineral medium. Afterwards, 18 mL of the medium that contained the cells was introduced into sterile 100-mL glass bottles, then 2 mL of the described cell suspension ($OD_{600} = 1.0$) from the inoculum was added, followed by 50 µL of creosote. After incubation for 28 days (22 °C in the dark) the residual hydrocarbons were extracted using 8 mL of hexane and subjected to a quantitative analysis using a Pegasus 4D GCxGC-TOFMS (LECO, St. Joseph, MI, USA) equipped with a BPX-5 column (28 m, 250 µm, 0.25 µm). Helium was used as a carrier gas (1 mL min⁻¹) and the following temperature program was employed: 40 °C for the first 2 min and increased to 300 °C at 15 °C min⁻¹ (the final temperature was kept for 15 min). The quantity of the residual hydrocarbons was established using a calibration curve and the final content was corrected based on the values determined for control and abiotic samples.

2.4. Cell Wall Properties

The changes of cell wall properties were evaluated using bacterial cells collected from 7-day cultures, which were prepared in accordance with the procedure used for creosote biodegradation tests. The cells were rinsed twice and then re-suspended in sterile mineral medium in order to obtain an OD_{600} value equal to 1.0. Two different series of cultures were prepared for all studied strains: the first included creosote, while the second included 20% sodium succinate solution.

The hydrophobic–hydrophilic properties of the cells were analyzed based on the adsorption of Congo red dye on the surface of microbial cells (CR assay), as previously described by Ambalam et al. [23]. Additionally, inner membrane permeability was analyzed based on the o-nitrophenyl-β-D-galactoside assay (ONPG), which is based on the measurement of the concentration of β-galactosidase, which is released into the solution after hydrolysis of ONPG [24]. The total membrane permeability was analyzed based on crystal violet uptake (CV assay) by microbial cells using colorimetric measurements [25].

2.5. Glutathione S-Transferase Activity

In order to investigate the impact of creosote on microbial activity of glutathione S-transferases (GST), the bacterial cultures of *Stenotrophomonas maltophilia* ODW 2.4.2, *Stenotrophomonas maltophilia* ODW 3.7 and *Paenibacillus ulginis* ODW 5.9 were established in the same manner as those prepared for cell wall properties measurements. The 7-day, washed bacterial cells were lysed using the CellLytic™

B Plus Kit purchased from Sigma-Aldrich, according to the manufacturer's protocol. The bacterial lysates were used to measure total GST using a Glutathione S-Transferase Assay Kit (Sigma Aldrich, MO, USA), which utilizes 1-Chloro-2,4-dinitrobenzene (CDNB). Upon conjugation of the thiol group of glutathione to the CDNB substrate, there was an increase in the absorbance at 340 nm, which was measured using a Multiskan Sky Microplate Spectrophotometer (Thermo Fisher Scientific, Agawam, MA, USA). Later on, the content of proteins was established using a Pierce™ BCA Protein Assay (Thermo Fisher Scientific, Agawam, MA, USA). The activity of GST was calculated and expressed as the activity of an enzyme per milligram of total protein (Sigma-Aldrich, St. Louis, MO, USA).

2.6. Statistical Analysis

The results presented in the study were calculated as an average value from at least three independent experiments. One-way analysis of variance (ANOVA) with Tukey's range test applied as a post-hoc analysis was applied in order to determine the statistical significance of differences between the average values. The differences were considered as statistically significant at $p < 0.05$. The statistical analysis was carried out using Statistica v13 (StatSoft, Cracow, Poland).

3. Results and discussion

3.1. Bacterial strains

As a result of selective cultures, one of the most active bacterial strains, which showed the ability to degrade creosote oil as the only source of carbon and energy, was isolated from each soil sample. Table 1 contains the strains names and the most important information characterizing them.

Table 1. Bacteria strains isolated from the creosote-contaminated soil samples.

Soil Sample	Strain	GenBank (NCBI) Number	Hemolysis Test
O10	<i>Stenotrophomonas maltophilia</i> ODW 2.4.2	MK503432.1	alpha
O6	<i>Stenotrophomonas maltophilia</i> ODW 3.7	MK503436.1	alpha
O8	<i>Paenibacillus ulginis</i> ODW 5.9	MK503429.1	beta

In the soil samples taken from the creosote-contaminated area, the most active bacterial strains capable of degrading PAHs represented two species of microorganisms. In soil samples O10 and O6 Gram-negative *Stenotrophomonas maltophilia* strains were found, and Gram-positive *Paenibacillus ulginis* in sample O8, respectively. What is more, the *S. maltophilia* strains were characterized by alpha hemolysis. In contrast, the *P. ulginis* cell showed beta hemolysis. Several previous studies have shown that the most common PAH-degrading strains are those belonging to the genera *Pseudomonas*, *Sphingomonas* and *Sphingobium*, slightly less often *Rhodococcus*, *Ochrobactrum* or *Acinetobacter* [26]. However, bacteria of the genus *Paenibacillus* were also observed among them, which is confirmed by studies carried out by Daane et al. [27]. Furthermore, Mesbaiah et al. [28], by studying PAH-degrading strains, isolated strain of the genus *Paenibacillus*, as well, and found its ability to produce extracellular biosurfactant. This corresponds to the observations made for the strain *Paenibacillus ulginis* ODW 5.9, which show a beta hemolysis characteristic of microorganisms producing surfactant compounds [29]. The literature also contains reports on the ability of strains belonging to the species *Stenotrophomonas maltophilia* to degrade pyrene [30] and anthracene, phenanthrene, naphthalene or fluorene [31].

3.2. Creosote Biodegradation

Long-term contact of microorganisms with highly toxic PAHs present in the soil affects the biodiversity of bacteria found there. Three microbial consortia were isolated from the contaminated soil and then in selective cultures, the bacteria with high biodegradability potential in relation to hydrocarbons present in creosote oil were isolated. The highest creosote oil biodegradation was

observed for microorganisms isolated from sample O6 ($51\% \pm 9\%$). This microbial consortia effectively biodegraded dibenzofuran (81%), and anthracene and acenaphthene in approximately 70%. The most active strain isolated from this sample was *S. maltophilia* ODW 2.4.2, for which a similar level of creosote oil biodegradation ($50\% \pm 4\%$) after seven days of the process was obtained (Figure 1). Moreover, high biodegradation of naphthalene (95%), fluorene (82%) and acenaphthene (74%) was noticed (Figure 1). What is more, from sample O6 also a strain belonging to the species *S. maltophilia* ODW 3.7 was isolated, for which a similar level of creosote oil biodegradation was observed (51%). However, this strain was characterized by different biodegradable activity in relation to different creosote oil components. Unlike sample O10, microbial community of O8 sample removed only 35% of creosote. The most active strain was identified as *P. ulginis* ODW 5.9. Nevertheless, the biodegradation efficiency of creosote and creosote components by this strain was the lowest from among the tested bacteria strains. The effectiveness of biodegradation depends on the chemical structure of creosote components, their concentration, as well as on the age of the contaminant [2]. Low molecular weight PAHs (consisting of two and three rings) are faster removed than the compounds of high molecular weight [32–34]. Naphthalene, a two-ringed PAH, is degraded relatively easily [35]. It has been observed that with increasing size of a PAH molecule, the hydrophobicity and electrochemical stability increase [36] and slow down the rates of biodegradation. This high hydrophobicity of the compounds present in creosote and related low water solubility influence their low bioavailability for microorganisms and therefore biodegradation efficiency [37]. Different species of bacteria show great biodegradation potential of polycyclic aromatic hydrocarbons [38]. Muangchinda et al. [39] have demonstrated high potential of *Actinobacteria* in PAH degradation in river sediments. Subashchandrabose et al. [40] have observed high biodegradation of phenanthrene by *Rhodococcus wratislaviensis* strain 9. This strain degraded also pyrene and benzo[a]pyrene. Our results indicated high biodegradation potential of *Stenotrophomonas maltophilia*, which could be used in the degradation of even aged PAHs.

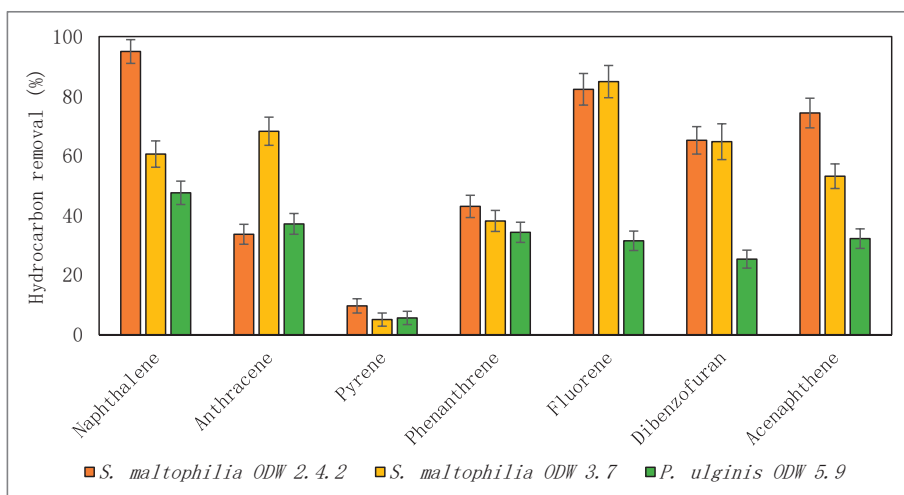


Figure 1. Removal of selected PAH present in creosote by selected strains after 28 days.

3.3. Enzymatic Activity in the Presence of Creosote

The glutathione S-transferase (GST) activity was tested in three bacterial strains. Each strain was cultivated for seven days with the addition of creosote oil (marked as CREO) and without the addition of this component (control samples, marked as CTRL). Each culture was established in three biological repetitions and three technical repetitions of each culture were subjected to analysis. The final results presented in the graph (Figure 2) stand for the average values of these measurements.

Regarding control samples of all strains tested, the highest activity of GST was measured in the strain *S. maltophilia* ODW 3.7 and the lowest value was noted for *P. ulginis* ODW 5.9. Similar directions of changes were observed for bacterial cells exposed to creosote oil. What can be clearly seen in the figure was a significant increase in GST activity in bacterial cells of the strains *S. maltophilia* ODW 2.4.2 and *S. maltophilia* ODW 3.7 exposed to creosote in comparison to control samples. In the cell extract of *P. ulginis* ODW 5.9 bacterial strain, the activity of GST measured in CREO sample was slightly higher (when compared to *P. ulginis* ODW 5.9 CTRL), however, the modifications were not statistically significant. In general, GST is an enzyme involved, among others, in detoxification of a wide range of xenobiotics. It works via nucleophilic conjugation of glutathione with electrophilic substrates. Although, the latter is described as a major detoxification mechanism in mammals [41,42], the activity of GST in bacterial strains was postulated as well. GST is believed to play an important role in biological degradation of xenobiotic compounds by bacteria, what was described by Allocati et al. (2009) [43] and Zablutowicz et al. (1995) [44]. The results of our research confirm the results of these researchers since the higher activity was measured in samples containing toxic, hazardous compounds for bacteria and the cells (especially those of *S. maltophilia* ODW 2.4.2 and *S. maltophilia* ODW 3.7 strains) might have initiated the reaction of biological degradation through GST enzymes.

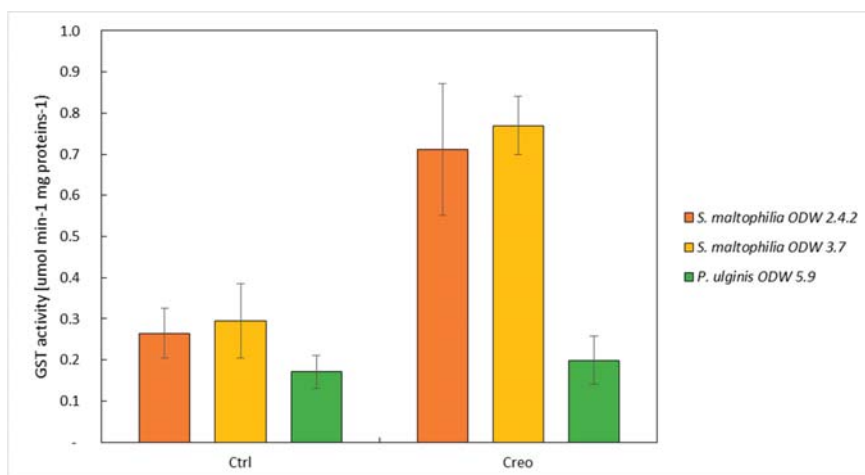


Figure 2. Activity of GST enzymes tested in three bacterial strains in control cultures (Ctrl) and the cultures with the addition of creosote oil (Creo).

3.4. Cell Wall Properties

The next stage of the research has been devoted to the analysis of cell adaptation processes to degradation of hydrophobic hydrocarbons, which consisted of modification of cell wall properties. Such adaptations are a very important parameter, which determines the bioavailability of compounds with low water solubility such as PAH to a high extent [13]. Table 2 includes the results of measurements of Congo red adsorption on the cell surface as well as membrane permeability analyzes. Congo red adsorption studies indicate that all strains were characterized by slight dye adhesion. In addition, the ambiguous response of cells to contact with creosote oil should be emphasized. Strain *S. maltophilia* ODW 2.4.2 in the culture with an easily digestible sodium succinate exhibited an adsorption of 7%, whereas in the case of creosote culture this value was lower than 2%. The *S. maltophilia* ODW 3.7 strain, which belongs to the same species, behaved differently. In this case, a slight increase in dye adsorption was observed after comparing the cells from the culture with creosote and succinate. An analogous but much more pronounced increase (from 3.4% to 13.6%) was observed for *P. ulginis* ODW 5.9 cells.

This is coherent with the previous studies, such as these reported by Ghosh and Mukherji [45] or Obuekwe [46], which established that the biodegradation of PAHs is associated with the increase of cell hydrophobicity. Moreover, Bezza and Chirwa [47] associated the increase of the hydrophobicity of cells during the biodegradation of pyrene with the interaction of biosurfactant produced by the bacteria.

Table 2. Bacteria cell wall properties described by the Congo red adsorption assay (CR), the inner and total membrane permeability tests (ONPG and CV, respectively).

Strain	Carbon Source	CR (%)	ONPG ($\mu\text{M min}^{-1}$)	CV (%)
<i>Stenotrophomonas maltophilia</i>	succinate	7.0 ± 0.8	0.28 ± 0.01	37 ± 3
ODW 2.4.2	creosote	1.8 ± 0.6	0.15 ± 0.01	24 ± 2
<i>Stenotrophomonas maltophilia</i>	succinate	4.2 ± 0.1	0.51 ± 0.06	40 ± 3
ODW 3.7	creosote	5.1 ± 0.5	0.44 ± 0.09	59 ± 4
<i>Paenibacillus ulginis</i>	succinate	3.4 ± 0.8	1.24 ± 0.21	16 ± 2
ODW 5.9	creosote	13.6 ± 0.9	0.13 ± 0.06	36 ± 3

The differences between the two tested strains of *S. maltophilia* were also evident during the analysis of total membrane permeability measured by the degree of penetration of crystal violet. *S. maltophilia* ODW 2.4.2 exhibited a clear decrease (from 3.7% to 24%) of membrane permeability of cells cultured using creosote, while *S. maltophilia* ODW 3.7 cells increased their membrane permeability after the comparison of samples from creosote-supplemented cultures with those from cultures with sodium succinate. Additionally, in the case of strain *P. ulginis* ODW 5.9, the presence of aromatic hydrocarbons resulted in an increased membrane permeability. The influence of the contact of the tested strains with creosote on the permeability of the inner cell membrane was relatively unambiguous and analogous. In all cases, the rate of *o*-nitrophenol formation resulting from the reaction catalyzed with intracellular galactosidase decreased in cultures with a mixture of PAHs. In the case of *P. ulginis* ODW 5.9, there was a significant ten-fold decrease of the measured parameter (from 1.24 to 0.13 $\mu\text{M min}^{-1}$). However, it should be emphasized that the measured value could be affected by both the permeability of the internal membrane and the amount of enzyme produced by the cell. Jiang et al. [48] underlined that the xenobiotic can be a factor that enhances the biodegradation by altering the permeability of bacterial cell membrane. Additionally, the study of Kuyukina et al. [49] suggests that organic solvents primarily affect bacterial membranes. This results in the loss of membrane integrity, but the cells may remain viable. However, the decrease in membrane permeability may be a cellular defense response to the presence of a toxic compound [50]. These two mentioned mechanisms can affect the measured membrane permeability to a different degree, which explains the observed differences in the membrane permeability of the strains studied in the framework of this study. Moreover, it can be assumed that the very low inner membrane permeability and relatively higher Congo red adsorption ratio is associated with lower bioavailability of creosote to bacterial cells, which may explain the low biodegradation of the mixture of these PAHs by *P. ulginis* ODW 5.9 in comparison with *S. maltophilia* strains.

4. Conclusions

The conducted experiments showed the differences and similarities between strains capable of degrading creosote from the same contaminated area. The *S. maltophilia* strains exhibited higher biodegradation efficiency and the more significant increase in glutathione S-transferase than *P. ulginis*. It can suggest the higher adaptation potential of the strains from this genus than the *P. ulginis* strain. High level of the S-transferase activity indicates activation of the metabolic pathways involved in biotransformation of the creosote hydrocarbons. Moreover, it can be presumed that the *P. ulginis* strain uses other enzymes to degrade the pollutant. However, studies of cell surface properties show differences between *S. maltophilia* strains. *S. maltophilia* ODW 3.7 and *P. ulginis* ODW 5.9 distinguished from the third of the tested strains in that the growth on creosote resulted in an increase in both cases in cell adhesion to Congo red, as well as the total membrane permeability. However, all three strains

shown decreased in inner membrane permeability. To summarize, the obtained results brought new valuable information on the variety of characteristics and properties of microorganisms involved in the bioremediation processes of creosote oil in contaminated soil.

Author Contributions: Conceptualization, E.K. and W.S.; methodology, A.P. and W.S.; validation, A.P.; writing—original draft preparation, W.S, A.P. and E.K. All authors have read and agreed to the published version of the manuscript.

Funding: This research was financed as a part of the project “Modern technology for bioremediation soil contaminated with creosote oil on the premises of Sleeper Treating Plant Spółka Akcyjna in Koźmin Wielkopolski”, no. POIR.04.01.02-00-0057/17-00 implemented under sub-measure 4.1.2 “Regional Science and Research Agendas”, co-financed by the European Regional Development Fund.

Conflicts of Interest: The authors declare no conflict of interest.

References

1. Hicknell, B.N.; Mumford, K.G.; Kueper, B.H. Laboratory study of creosote removal from sand at elevated temperatures. *J. Contam. Hydrol.* **2018**, *219*, 40–49. [[CrossRef](#)]
2. Madrid, F.; Rubio-Bellido, M.; Villaverde, J.; Peña, A.; Morillo, E. Natural and assisted dissipation of polycyclic aromatic hydrocarbons in a long-term co-contaminated soil with creosote and potentially toxic elements. *Sci. Total Environ.* **2019**, *660*, 705–714. [[CrossRef](#)]
3. Webb, D.A. Creosote, its biodegradation and environmental effects. *Amer. Wood-Preserv. Assoc.* **1980**, *76*, 65–69.
4. Melber, C.; Kielhorn, J.; Mangelsdorf, I. *Concise International Chemical Assessment Document 62. Coal Tar Creosote*; World Health Organization: Geneva, Switzerland, 2004.
5. Ye, Y.-F.; Ma, F.-Y.; Wu, M.; Wei, X.-Y.; Liu, J.-M. Increase of acenaphthene content in creosote oil by hydrodynamic cavitation. *Chem. Eng. Process.* **2016**, *104*, 66–74. [[CrossRef](#)]
6. Blum, P.; Sagner, A.; Tiehm, A.; Martus, P.; Wendel, T.; Grathwohl, P. Importance of heterocyclic aromatic compounds in monitored natural attenuation for coal tar contaminated aquifers: A review. *J. Contam. Hydrol.* **2011**, *126*, 181–194. [[CrossRef](#)] [[PubMed](#)]
7. Mueller, J.G.; Chapman, P.J.; Pritchard, P.H. Creosote-contaminated sites. Their potential for bioremediation. *Environ. Sci. Technol.* **1989**, *23*, 1197–1201. [[CrossRef](#)]
8. Vähäoja, P.; Piltonen, P.; Hyvönen, A.; Niinimäki, J.; Jalonen, J.; Kuokkanen, T. Biodegradability Studies of Certain Wood Preservatives in Groundwater as Determined by the Respirimetric Bod Oxitop Method. *Water Air Soil Pollut.* **2005**, *165*, 313–324. [[CrossRef](#)]
9. Carlsten, C.; Hunt, S.C.; Kaufman, J.D. Squamous Cell Carcinoma of the Skin and Coal Tar Creosote Exposure in a Railroad Worker. *Environ. Health Perspect.* **2005**, *113*, 96–97. [[CrossRef](#)]
10. Clapp, R.W.; Jacobs, M.M.; Loechler, E.L. Environmental and Occupational Causes of Cancer: New Evidence 2005-2007. *Rev. Environ. Health* **2008**, *23*, 1–38. [[CrossRef](#)]
11. Hu, J.; Mao, Y.; White, K. Renal cell carcinoma and occupational exposure to chemicals in Canada. *Occup. Med.* **2002**, *52*, 157–164. [[CrossRef](#)]
12. Krzyśko-Łupicka, T.; Cybulska, K.; Kołosowski, P.; Telesiński, A.; Sudoł, A. Influence of environmental pollution with creosote oil or its vapors on biomass and selected physiological groups of microorganisms. *E3S Web Conf.* **2017**, *22*, 00092. [[CrossRef](#)]
13. Kaczorek, E.; Pacholak, A.; Zdarta, A.; Smulek, W. The Impact of Biosurfactants on Microbial Cell Properties Leading to Hydrocarbon Bioavailability Increase. *Colloids Interfaces* **2018**, *2*, 35. [[CrossRef](#)]
14. Ren, X.; Zeng, G.; Tang, L.; Wang, J.; Wan, J.; Liu, Y.; Yu, J.; Yi, H.; Ye, S.; Deng, R. Sorption, transport and biodegradation—An insight into bioavailability of persistent organic pollutants in soil. *Sci. Total Environ.* **2018**, *610*, 1154–1163. [[CrossRef](#)] [[PubMed](#)]
15. Zeng, Z.; Liu, Y.; Zhong, H.; Xiao, R.; Zeng, G.; Liu, Z.; Cheng, M.; Lai, C.; Zhang, C.; Liu, G.; et al. Mechanisms for rhamnolipids-mediated biodegradation of hydrophobic organic compounds. *Sci. Total Environ.* **2018**, *634*, 1–11. [[CrossRef](#)]
16. Xing, S.-F.; Sun, X.-F.; Taylor, A.A.; Walker, S.L.; Wang, Y.-F.; Wang, S.-G. D-Amino acids inhibit initial bacterial Adhesion: Thermodynamic evidence. *Biotechnol. Bioeng.* **2015**, *112*, 696–704. [[CrossRef](#)] [[PubMed](#)]

17. Hearn, E.M.; Patel, D.R.; van den Berg, B. Outer-membrane transport of aromatic hydrocarbons as a first step in biodegradation. *Proc. Natl. Acad. Sci. USA* **2008**, *105*, 8601–8606. [[CrossRef](#)]
18. Hua, F.; Wang, H.Q. Uptake and trans-membrane transport of petroleum hydrocarbons by microorganisms. *Biotechnol. Biotechnol. Equip.* **2014**, *28*, 165–175. [[CrossRef](#)]
19. Sikkema, J.; de Bont, J.A.; Poolman, B. Mechanisms of membrane toxicity of hydrocarbons. *Microbiol. Rev.* **1995**, *59*(2), 201–222. [[CrossRef](#)]
20. Kaczorek, E.; Urbanowicz, M.; Olszanowski, A. The influence of surfactants on cell surface properties of *Aeromonas hydrophila* during diesel oil biodegradation. *Colloids Surf. B* **2010**, *81*, 363–368. [[CrossRef](#)]
21. Kaczorek, E.; Salek, K.; Guzik, U.; Jesionowski, T.; Cybulski, Z. Biodegradation of alkyl derivatives of aromatic hydrocarbons and cell surface properties of a strain of *Pseudomonas stutzeri*. *Chemosphere* **2013**, *90*, 471–478. [[CrossRef](#)]
22. Hassanshahian, M. Isolation and characterization of biosurfactant producing bacteria from Persian Gulf (Bushehr provenance). *Mar. Pollut. Bull.* **2014**, *86*, 361–366. [[CrossRef](#)] [[PubMed](#)]
23. Ambalam, P.; Kondepudi, K.K.; Nilsson, L.; Wadström, T.; Ljungh, Å. Bile stimulates cell surface hydrophobicity, Congo red binding and biofilm formation of *Lactobacillus* strains. *FEMS Microbiol. Lett.* **2012**, *333*, 10–19. [[CrossRef](#)] [[PubMed](#)]
24. Pacholak, A.; Simlat, J.; Zgoła-Grzeškowiak, A.; Kaczorek, E. Biodegradation of clotrimazole and modification of cell properties after metabolic stress and upon addition of saponins. *Ecotoxicol. Environ. Saf.* **2018**, *161*, 676–682. [[CrossRef](#)] [[PubMed](#)]
25. Devi, K.P.; Sakthivel, R.; Nisha, S.A.; Suganthy, N.; Pandian, S.K. Eugenol alters the integrity of cell membrane and acts against the nosocomial pathogen *Proteus mirabilis*. *Arch. Pharmacol. Res.* **2013**, *36*, 282–292. [[CrossRef](#)] [[PubMed](#)]
26. Ghosal, D.; Ghosh, S.; Dutta, T.K.; Ahn, Y. Current State of Knowledge in Microbial Degradation of Polycyclic Aromatic Hydrocarbons (PAHs): A Review. *Front. Microbiol.* **2016**, *7*, 1369. [[CrossRef](#)]
27. Daane, L.L.; Harjono, I.; Barns, S.M.; Launen, L.A.; Palleron, N.J.; Häggblom, M.M. PAH-degradation by *Paenibacillus* spp. and description of *Paenibacillus naphthalenovorans* sp. nov., a naphthalene-degrading bacterium from the rhizosphere of salt marsh plants. *Int. J. Syst. Evol. Microbiol.* **2002**, *52*, 131–139. [[CrossRef](#)]
28. Mesbahia, F.Z.; Eddouaouda, K.; Badis, A.; Chebbi, A.; Hentati, D.; Sayadi, S.; Chamkha, M. Preliminary characterization of biosurfactant produced by a PAH-degrading *Paenibacillus* sp. under thermophilic conditions. *Environ. Sci. Pollut. Res.* **2016**, *23*, 14221–14230. [[CrossRef](#)]
29. Tripathi, V.; Gaur, V.K.; Dhiman, N.; Gautam, K.; Manickam, N. Characterization and properties of the biosurfactant produced by PAH-degrading bacteria isolated from contaminated oily sludge environment. *Environ. Sci. Pollut. Res.* **2019**. [Epub ahead of print]. [[CrossRef](#)]
30. Singh, A.; Kumar, K.; Pandey, A.K.; Sharma, A.; Singh, S.B.; Kumar, K.; Arora, A.; Nain, L. Pyrene Degradation by Biosurfactant Producing Bacterium *Stenotrophomonas maltophilia*. *Agric. Res.* **2015**, *4*, 42–47. [[CrossRef](#)]
31. Arulazhagan, P.; Al-Shekri, K.; Huda, Q.; Godon, J.J.; Basahi, J.M.; Jeyakumar, D. Biodegradation of polycyclic aromatic hydrocarbons by an acidophilic *Stenotrophomonas maltophilia* strain AJH1 isolated from a mineral mining site in Saudi Arabia. *Extremophiles* **2017**, *21*, 163–174. [[CrossRef](#)]
32. Bacosa, H.P.; Inoue, C. Polycyclic aromatic hydrocarbons (PAHs) biodegradation potential and diversity of microbial consortia enriched from tsunami sediments in Miyagi, Japan. *J. Hazard. Mater.* **2015**, *283*, 689–697. [[CrossRef](#)] [[PubMed](#)]
33. Valderrama, C.; Alessandri, R.; Aunola, T.; Cortina, J.L.; Gamisans, X.; Tuhkanen, T. Oxidation by Fenton as reagent combined with biological treatment applied to a creosote-contaminated soil. *J. Hazard. Mater.* **2009**, *166*, 594–602. [[CrossRef](#)] [[PubMed](#)]
34. Jurys, A.; Gailiūte, I.; Aikaitė-Stanaitienė, J.; Grigiškis, S.; Maruška, A.; Stankevičius, M.; Levišauskas, D. Review of creosote pollution toxicity and possibilities of bioremediation. *Environ. Technol. Resour.* **2013**, *1*, 34–38. [[CrossRef](#)]
35. Grant, R.J.; Muckian, L.M.; Clipson, N.J.W.; Doyle, E.M. Microbial community changes during the bioremediation of creosote-contaminated soil. *Let. Appl. Microbiol.* **2007**, *44*, 293–300. [[CrossRef](#)] [[PubMed](#)]
36. Widada, J.; Nojiri, H.; Kasuga, K.; Yoshida, T.; Habe, H.; Omori, T. Molecular detection and diversity of polycyclic aromatic hydrocarbon-degrading bacteria isolated from geographically diverse sites. *Appl. Microbiol. Biotechnol.* **2002**, *58*, 202–209. [[CrossRef](#)] [[PubMed](#)]

37. Shor, L.M.; Liang, W.; Rockne, K.J.; Young, L.Y.; Taghon, G.L.; Kosson, D.S. Intraaggregate mass transport-limited bioavailability of polycyclic aromatic hydrocarbons to *Mycobacterium* strain PC01. *Environ. Sci. Technol.* **2003**, *37*, 1545–1552. [CrossRef] [PubMed]
38. Kanaly, R.A.; Harayama, S. Biodegradation of high-molecular-weight polycyclic aromatic hydrocarbons by bacteria. *J. Bacteriol.* **2000**, *182*(8), 2059–2067. [CrossRef]
39. Muangchinda, C.; Yamazoe, A.; Polrit, D.; Thoetkiattikul, H.; Mhuantong, W.; Champreda, V.; Pinyakong, O. Biodegradation of high concentrations of mixed polycyclic aromatic hydrocarbons by indigenous bacteria from a river sediment: a microcosm study and bacterial community analysis. *Environ. Sci. Pollut. Res.* **2017**, *24*, 4591–4602. [CrossRef]
40. Subashchandrabose, S.R.; Venkateswarlub, K.; Naidua, R.; Meghara, M. Biodegradation of high-molecular weight PAHs by *Rhodococcus wratislaviensis* strain 9: Overexpression of amidohydrolase induced by pyrene and BaP. *Sci. Total Environ.* **2019**, *651*, 813–821. [CrossRef]
41. Monostori, P.; Wittmann, G.; Karg, E.; Túri, S. Determination of glutathione and glutathione disulfide in biological samples: An in-depth review. *J. Chrom. B.* **2009**, *877*, 3331–3346. [CrossRef]
42. Pour, L.M.; Farahnak, A.; Rad, M.M.; Golmohamadi, T.; Eshraghian, M. Activity Assay of Glutathione S-Transferase (GSTs) Enzyme as a Diagnostic Biomarker for Liver Hydatid Cyst in Vitro. *Iran J. Public Health.* **2014**, *43*, 994.
43. Allocati, N.; Federici, L.; Masulli, M.; di Ilio, C. Glutathione transferases in bacteria: Bacterial. *FEBS J.* **2009**, *276*, 58–75. [CrossRef] [PubMed]
44. Zablutowicz, R.M.; Hoagland, R.E.; Locke, M.A.; Hickey, W.J. Glutathione-S-Transferase Activity and Metabolism of Glutathione Conjugates by Rhizosphere Bacteria. *Appl. Environ. Microbiol.* **1995**, *61*, 1054–1060. [CrossRef] [PubMed]
45. Ghosh, I.; Mukherji, S. Diverse effect of surfactants on pyrene biodegradation by a *Pseudomonas* strain utilizing pyrene by cell surface hydrophobicity induction. *Int. Biodeter. Biodegrad.* **2016**, *108*, 67–75. [CrossRef]
46. Obuekwe, C.O.; Al-Jadi, Z.K.; Al-Saleh, E.S. Hydrocarbon degradation in relation to cell-surface hydrophobicity among bacterial hydrocarbon degraders from petroleum-contaminated Kuwait desert environment. *Int. Biodeter. Biodegrad.* **2009**, *63*, 273–279. [CrossRef]
47. Bezza, F.A.; Chirwa, E.M.N. Pyrene biodegradation enhancement potential of lipopeptide biosurfactant produced by *Paenibacillus dendritiformis* CN5 strain. *J. Hazard. Mater.* **2017**, *321*, 218–227. [CrossRef]
48. Jiang, Z.; Chen, J.; Li, J.; Cao, B.; Chen, Y.; Liu, D.; Wang, X.; Zhang, Y. Exogenous Zn²⁺ enhance the biodegradation of atrazine by regulating the chlorohydrolase gene trzN transcription and membrane permeability of the degrader *Arthrobacter* sp. DNS10. *Chemosphere* **2020**, *238*, 124594. [CrossRef]
49. Kuyukina, M.S.; Ivshina, I.B.; Korshunova, I.O.; Rubtsova, E.V. Assessment of bacterial resistance to organic solvents using a combined confocal laser scanning and atomic force microscopy (CLSM/AFM). *J. Microbiol. Methods* **2014**, *107*, 23–29. [CrossRef]
50. Dam, S.; Pagès, J.-M.; Masi, M. Stress responses, outer membrane permeability control and antimicrobial resistance in Enterobacteriaceae. *Microbiology* **2018**, *164*, 260–267. [CrossRef]



© 2020 by the authors. Licensee MDPI, Basel, Switzerland. This article is an open access article distributed under the terms and conditions of the Creative Commons Attribution (CC BY) license (<http://creativecommons.org/licenses/by/4.0/>).

Article

Preparation of KOH and H₃PO₄ Modified Biochar and Its Application in Methylene Blue Removal from Aqueous Solution

Li Liu ¹, Yang Li ² and Shisuo Fan ^{3,*}

¹ School of Physics and Electronic Engineering, Fuyang Normal University, Fuyang 236037, China; wenfan1986@163.com

² School of Environmental Science and Engineering, Guangdong University of Technology, Guangzhou 510006, China; linziyi_ly@163.com

³ School of Resources and Environment, Anhui Agricultural University, Hefei 230036, China

* Correspondence: fanshisuo@ahau.edu.cn; Tel./Fax: +86-551-6578-6311

Received: 29 October 2019; Accepted: 25 November 2019; Published: 1 December 2019

Abstract: Improperly treated or directly discharged into the environment, wastewater containing dyes can destroy the quality of water bodies and pollute the ecological environment. The removal of dye wastewater is urgent and essential. In this study, corn stalk was pyrolyzed to pristine biochar (CSBC) in a limited oxygen atmosphere and modified using KOH and H₃PO₄ (KOH-CSBC, H₃PO₄-CSBC, respectively). The biochars were characterized by surface area and pore size, X-ray diffraction (XRD), Fourier transform infrared (FTIR) spectroscopy, X-ray photoelectron spectroscopy (XPS), as well as their behavior in adsorbing methylene blue (MB). Results indicated that the pore structure of CSBC became more developed after modification by KOH. Meanwhile, H₃PO₄-CSBC contained more functional groups after activation treatment. The pseudo-second-order kinetic and the Langmuir adsorption isotherm represented the adsorption process well. The maximum MB adsorption capacity of CSBC, KOH-CSBC, and H₃PO₄-CSBC was 43.14 mg g⁻¹, 406.43 mg g⁻¹ and 230.39 mg g⁻¹, respectively. Chemical modification significantly enhanced the adsorption of MB onto biochar, especially for KOH-CSBC. The adsorption mechanism between MB and biochar involved physical interaction, electrostatic interaction, hydrogen bonding and π - π interaction. Hence, modified CSBC (especially KOH-CSBC) has the potential for use as an adsorbent to remove dye from textile wastewater.

Keywords: corn stalk biochar; KOH modification; H₃PO₄ modification; Methylene blue; Adsorption

1. Introduction

Wastewater from the textile industry typically contains dyes and has a high content of organic toxicants, high color, and strong resistance to biodegradation, photolysis and oxidation, and is potentially carcinogenic. If improperly treated or directly discharged into the environment, wastewater containing dyes can destroy the quality of water bodies and pollute the ecological environment [1]. Methylene blue (MB) is an important synthetic dye and was widely used in the field of chemical indicators, dyes, biological dyes and drugs. Wastewater containing MB can enter a water body through different pathways and cause serious harm to environmental and human health [2]. Therefore, the need is urgent to develop an effective, low cost, easily operated technology for MB wastewater treatment. Adsorption has been an important technology to remove MB from wastewater. The correct choice and preparation of an efficient adsorbent is the priority for effective application of adsorption technology.

Currently, biochar is attracting great attention due to the important function it provides in greenhouse gas emission reduction, soil carbon sequestration, pollutant control and solid waste

reclamation [3,4]. Biochar is the solid residue of an organic material that is pyrolyzed in the absence of oxygen or in a limited oxygen atmosphere. Because biochar can be made from a wide variety of raw materials, has a good adsorption capacity, and has large surface area, pore volume and abundant functional groups, many investigations have assessed the use of biochar as an adsorbent for removing pollutants from aqueous solution [5–9].

Compared with that of commercially available activated carbon, the adsorption effect of biochar needs to be improved. Techniques for achieving this improvement have become an area of intense research activity. Activated or modified biochar has been prepared and applied to remove specific contaminants [10–12]. Activation methods include physical and chemical pathways. Physical activation can increase the surface area and improve the pore structure of biochar. Likewise, chemical activation can enrich the functional types of biochar and provide more binding sites for pollutant removal [13–16]. The preparation of highly effective adsorbents can provide a new option for the utilization of corn residues.

Research has shown that KOH and H_3PO_4 are commonly used biochar activators. Luo et al. [17] investigated the sorption of norfloxacin, sulfamerazine and oxytetracycline by KOH-modified biochar (from cassava waste). Bashir et al. [18] studied Cd removal by KOH-modified biochar (from rice straw). Huang et al. [19] reported removal of tetracycline by KOH-modified biochar (from poplar sawdust). Meanwhile, Chen et al. [20] revealed tetracycline removal by H_3PO_4 -modified biochar (from rice straw and swine manure). Peng et al. [21] indicated that adsorption of Cu(II) and Cd(II) was enhanced by H_3PO_4 -modified biochars (from pine sawdust). Zhao et al. [22] confirmed that Cr(VI) and organic contaminants could be co-removed by H_3PO_4 -modified biochars. All of this research has shown that modification of biochar using KOH and H_3PO_4 is effective and feasible. However, comparison of the modification effect of KOH-biochar and H_3PO_4 -biochar to facilitate pollutant removal has rarely been reported.

More than 250 million metric tons of corn (i.e., maize) residues are generated annually in China [23]. The utilization pathways for these residues include industrial materials, animal feed, fuel products and biomass energy [24]. However, some corn residue is disposed of by open-air burning, which not only pollutes the environment, but also wastes a valuable biomass resource. Hence, it is urgent to explore new ways to utilize these residues.

In this study, corn residue (specifically corn stalks) was chosen as the research object and was pyrolyzed to prepare pristine biochar. KOH and H_3PO_4 were used to modify the pristine biochar. Then, the pristine and modified biochars were applied to remove MB from wastewater. The research was expected to provide a basis for corn residue utilization and removal of MB dye from wastewater.

2. Materials and Methods

2.1. Materials and Reagents

Corn stalk was collected from the Anhui agricultural university's experimental farm. Analytically pure reagents (MB, KOH, HCl, NaOH and H_3PO_4) were purchased from Sinopharm Chemical Reagent Co. Ltd. (Shanghai, China) for use in the experiments.

2.2. Preparation of Biochar and Modified Biochar

First, the corn stalk was washed with deionized water and dried in an oven. After drying, the stalk was crushed and passed through a 100 mesh sieve and then stored for future experimentation. Last, the crushed corn stalk was pyrolyzed to pristine biochar at 500 °C in a muffle furnace under limited oxygen atmosphere. After washing several times with pure water, the biochar was dried in an oven (80 °C for 24 h). This procedure produced pristine corn stalk biochar (CSBC).

A weight of 6.0 g CSBC was put into each of two centrifuge tubes. A weight of 6.0 g KOH and 20 mL pure water was added to one tube. An amount of 6 mL H_3PO_4 and 20 mL ultrapure was added to the other tube. Then, the two tubes were placed on a shaker to fully oscillate for 24 h, after which

the tubes were removed and the biochars dried at 80 °C for 48 h. Then, each of the treated biochars was placed in an individual ceramic crucible, covered with a lid, and placed in a muffle furnace to activate the biochars. The activation temperature was 700 °C (generally, the biochar was prepared under 700 °C, and thus the activation temperature was chosen as 700 °C), which was attained at a heating rate of 10 °C/min and maintained for 2 h. Then, the crucibles were cooled to room temperature and the modified biochars were removed. Deionized water was used to remove impurities from the biochars by washing them several times until the pH of eluent reached neutrality. The washed biochars were dried in an oven for characterization and use in experiments. Hereafter, the KOH-treated and H₃PO₄-treated biochars are referred to as KOH-CSBC and H₃PO₄-CSBC, respectively.

2.3. Characterization

The pristine and modified biochars were characterized using various techniques. The surface area and pore sized of the biochars were measured using an automatic specific surface area and pore analyzer (Tristar II 3020M, Micromeritics Instrument Corporation, Norcross, GA, USA). The surface morphology of biochars was analyzed using scanning electron microscopy (SEM, S-4800, Hitachi, Japan). Fourier transform infrared spectroscopy (FTIR) was used with the KBr pellet technique to characterize the functional groups of biochars (FTIR, Nicolette is50, Thermo Fisher Scientific, Waltham, MA, USA). The minerals in biochars were detected by X-ray diffraction (XRD, D8 Advance, BrukerAXS GmbH, Karlsruhe, Germany). The surface elements, speciation and relative distribution of elements within the biochars were determined by X-ray photoelectron spectroscopy (XPS, ESCALAB 250, Thermo Scientific-VG Scientific, Waltham, MA, USA).

2.4. Adsorption Experiments

2.4.1. Influence of Solid-to-Liquid Ratio on Methylene Blue (MB) Adsorption

MB solution (30 mL) with a concentration of 50 mg L⁻¹ was placed in 50 mL centrifuge tubes. A certain mass of pristine or modified biochar was weighed and added into the tubes to adjust the solid-to-liquid ratio at 0.5, 1.0, 2.0, 3.0 and 4.0 g L⁻¹. Then, the tubes were placed in a constant temperature shaker with a speed of 150 rpm for 24 h at 25 °C. The tubes were centrifuged for 10 min at a speed of 4000 rpm. The resulting supernatant was filtered through a 0.45 µm membrane, and the absorbance of the supernatant at the wavelength of 665 nm was measured using a spectrophotometer.

2.4.2. Influence of Initial pH of Solution on MB Adsorption

MB solution (30 mL) with a concentration of 100 mg L⁻¹ was placed in 50 mL centrifuge tubes. The pH of the solutions was adjusted to 3.0, 5.0, 7.0, 9.0 and 11.0 using either 0.1M HCl or NaOH. A certain mass of pristine or modified biochar was added to the tubes to adjust the solid-to-liquid ratio at 0.5 g L⁻¹. The tubes were then processed as described in Section 2.4.1 (i.e., oscillation, centrifugation, filtration and absorbance determination).

2.4.3. Adsorption Kinetics

MB solution (100 mL) at a concentration of 50 mg·L⁻¹, 100 mg·L⁻¹ or 200 mg·L⁻¹ was added to each of three beakers. Then, 0.1 g CSBC, 0.1 g KOH-CSBC and 0.1 g H₃PO₄-CSBC was added separately to each beaker. Each beaker was placed on a magnetic stirrer and the temperature held constant at 25 °C. Samples were collected at various times and filtered through a 0.45 µm membrane, after which the absorbance at 665 nm was detected. The concentration of MB was set at 50 mg L⁻¹ and 100 mg L⁻¹ for CSBC, and 100 mg L⁻¹ and 200 mg L⁻¹ for both KOH-CSBC and H₃PO₄-CSBC.

2.4.4. Adsorption Isotherm

To develop adsorption isotherms, 30 mL of MB solution was placed in a 50 mL centrifuge tube. The concentration of MB was adjusted in the range 100–500 mg·L⁻¹. Then, 0.015 g of CSBC, KOH-CSBC

and H₃PO₄-CSBC was added separately to individual tubes. The tubes were placed in a constant temperature shaker with a speed of 150 rpm for 24 h at 25 °C. Then, the tubes were centrifuged for 10 min at a speed of 4000 rpm. The resulting supernatant was filtered through a 0.45 µm membrane. The absorbance of the supernatant at the wavelength of 665 nm was measured using a spectrophotometer.

2.4.5. Data Analysis

The amount of MB adsorbed by biochar was calculated using Equation (1).

$$q_t = (C_0 - C_t)V/m \quad (1)$$

In Equation (1) q_t (mg g⁻¹) is the adsorption capacity of MB at time t , C_0 (mg·L⁻¹) is the initial MB concentration, and C_t (mg·L⁻¹) is the equilibrium concentration of MB at time t . V is the volume of dye solution, L. The m is the weight of adsorbent used, g.

The kinetic adsorption data were described (fitted) using a pseudo-first-order model and a pseudo-second-order model.

The pseudo-first-order model [25] is described by Equation (2):

$$\ln(q_e - q_t) = \ln(q_e) - k_1 t \quad (2)$$

and the pseudo-second-order model [26] is described by Equation (3):

$$q_t = k_2 \cdot q_e^2 t / (1 + k_2 q_e^2 t) \quad (3)$$

In Equations (2) and (3), q_t and q_e (mg g⁻¹) are the adsorption capacity of MB on biochar at time t and at equilibrium time, respectively; and k_1 (min⁻¹) and k_2 (g mg⁻¹ min⁻¹) are the rate constants of the pseudo-first-order and pseudo-second-order kinetic reactions, respectively.

The adsorption isotherm data were fitted using the Langmuir and Freundlich models.

The Langmuir model [27] is described by Equation (4):

$$q_e = q_m K_L C_e / (1 + K_L C_e) \quad (4)$$

The Freundlich model [28] is described by Equation (5):

$$q_e = K_f C_e^{1/n} \quad (5)$$

In Equations (4) and (5), C_e (mg L⁻¹) is the equilibrium concentration of the solution; q_e (mg g⁻¹) is the equilibrium adsorption capacity; K_L is a constant for the Langmuir model; q_m (mg g⁻¹) is the maximum adsorption capacity; K_f (L mg⁻¹) is a constant for the Freundlich model; and $1/n$ is the adsorption affinity constant.

3. Results and Discussion

3.1. Characterization of Biochars

The scanning electron microscopy (SEM) micrographs of CSBC, KOH-CSBC and H₃PO₄-CSBC are shown in Figure 1. The morphology of corn stalk remained in the CSBC. Some fragments that appeared in the CSBC were mainly from the thermal decomposition of cellulose and hemicelluloses. The pyrolysis temperature for CSBC was 500 °C. Thermal decomposition of cellulose, hemicellulose and lignin occurs at 220–315 °C, 315–400 °C and 160–900 °C, respectively [29]. After KOH modification, the biochar pore structure became more developed, and more fragments were observed on the surface of the KOH-CSBC. Some crystal particles also appeared on the surface of KOH-CSBC. The mineral components were formed from the thermal decomposition of KOH. Meanwhile, the modification of CSBC by KOH promoted the formation of a more microporous structure. The modification of biochar

using H_3PO_4 resulted in different characteristics than those resulting from KOH modification. More fragments in biochar bonded together after H_3PO_4 modification, and the surface of H_3PO_4 -modified CSBC exhibited a smooth and gelatinous appearance, and the fragments of CSBC bonded together, inhibiting the formation of a microporous structure.

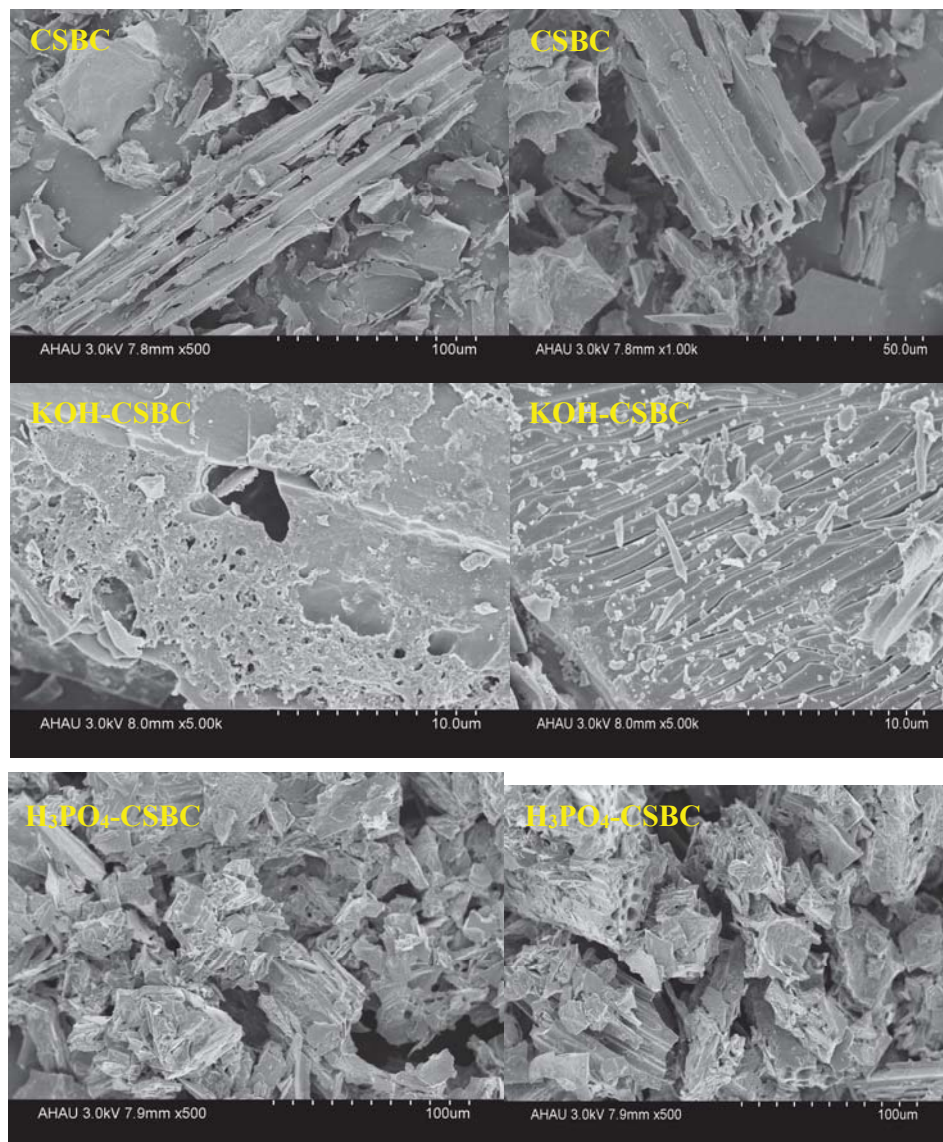


Figure 1. Scanning electron microscope (SEM) micrographs of corn stalk biochar (CSBC), KOH-CSBC and H_3PO_4 -CSBC.

The surface area, pore volume and pore size of biochars are displayed in Table 1. After KOH modification, the surface area of biochar significantly increased from 24.2543 to 473.6432 $m^2 \cdot g^{-1}$. The surface area increased approximately 20 times after KOH activation. The pore volume of KOH-CSBC

also increased and pore size decreased. However, after H_3PO_4 modification, the surface area of biochar decreased from 24.2543 to 2.8404 m^2g^{-1} . The pore volume of H_3PO_4 -CSBC also decreased and pore size increased. Thus, the measurements of surface area, pore volume and pore size were consistent with the observations of SEM images. KOH modification obviously influenced the surface structure of biochar, which suggested the treatment could affect the removal of MB from the solution.

Table 1. Surface area, pore volume and pore size of biochars.

Samples	Surface Area (m^2g^{-1})	Pore Volume (cm^3g^{-1})	Pore Size (\AA)
corn stalk biochar (CSBC)	24	0.021	34.0
KOH-CSBC	474	0.24	20.4
H_3PO_4 -CSBC	3	0.0025	35.1

Surface area: Brunauer–Emmett–Teller (BET- N_2) method; Total pore volume of pores; Adsorption average pore width.

The XRD spectra of CSBC, KOH-CSBC and H_3PO_4 -CSBC are shown in Figure 2. Amorphous carbon peaks were obvious in spectra from the CSBC. Some minerals also were detected in the CSBC, including CaCO_3 and KCl. After KOH modification, K and K_2O were observed in the biochar, suggesting that KOH had reacted with the carbonaceous components in CSBC. Only amorphous carbon was detected in H_3PO_4 -CSBC, indicating that H_3PO_4 modification mainly affected the organic components of CSBC.

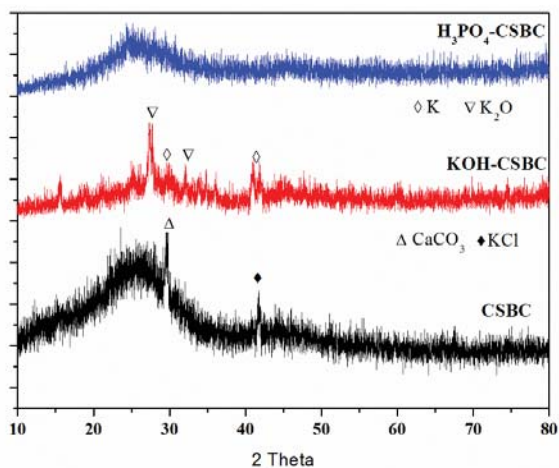


Figure 2. X-ray diffraction (XRD) spectra of tested adsorbents.

The FTIR spectra of CSBC, KOH-CSBC and H_3PO_4 -CSBC are presented in Figure 3. The functional groups of CSBC, KOH-CSBC and H_3PO_4 -CSBC differed significantly. The specific functional groups for the different types of biochar are shown in Table 2. The main groups in CSBC included OH, aliphatic C, C=O and C=C, carboxyl anions (affected by C=O stretching), Si–O and C–H [30]. The main groups in KOH-CSBC included OH, C=O and C=C, substances in the phenolic O–H band, alkenes (affected by C–H bending), cellulosic ethers (affected by C–O–C stretching), aromatic C–H, and CH–of alkenes and alkane [31]. The modification of KOH led to the disappearance of aliphatic C and carboxyl anions due to the high pyrolytic temperature (700 °C). The appearance of the phenolic O–H band, C–H bending of alkenes, and C–O–C stretching indicated the formation of olefin compounds. The existence of aromatic C–H and aromatic C–O stretching suggested the further enhancement of the CSBC's aromatic structure.

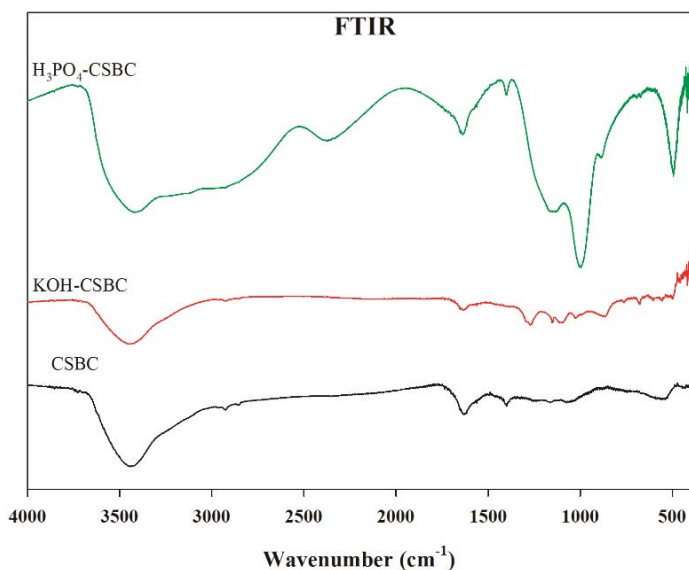


Figure 3. Fourier transform infrared (FTIR) spectra of tested adsorbents.

Table 2. The main functional groups of CSBC, KOH-CSBC and H₃PO₄-CSBC.

CSBC		KOH-CSBC		H ₃ PO ₄ -CSBC	
Wavenumber (cm ⁻¹)	Assignment	Wavenumber (cm ⁻¹)	Assignment	Wavenumber (cm ⁻¹)	Assignment
3443	–OH	3450	–OH	3425	–OH
2925	aliphatic C			2372	C–O vibrations
1633	C=O and C=C	1637	C=O and C=C	1637	C=O and C=C
1560	C=O stretching	1271	aromatic C–O stretching	1401	–COOH or O–H bending
1075	Si–O stretching vibrations	1151	phenolic O–H band	1145	amino phosphonic acid functional group
539	aromatic C–H stretching	1103	C–H bending of alkenes	998	P–OH bond
		1025	C–O–C stretch	495	Si–O–Si
		867	Aromatic C–H		
		676	CH-of alkenes and alkanes		

The functional groups in H₃PO₄-CSBC included –OH, substances exhibiting C–O vibration, C=O and C=C, –COOH, substances exhibiting O–H bending deformation, amino phosphonic acid functional group, P–OH bonded substances and Si–O–Si [20–22]. The modification of H₃PO₄ caused the disappearance of aliphatic C and carboxyl anions owing to the high pyrolytic temperature (700 °C). Meanwhile, the observation of C–O, –COOH and O–H bending deformation illustrated the enhancement of the CSBC's aromatic structure. Furthermore, the presence of the amino phosphonic acid functional group and P–OH bonds in H₃PO₄-CSBC demonstrated that a reaction happened between H₃PO₄ and the carbonaceous components in biochar. The introduction of phosphorous-containing functional groups on biochar may play an important role for MB removal.

The XPS spectra of CSBC, KOH-CSBC and H₃PO₄-CSBC are shown in Figure 4. C, O, N and P were detected in all biochars, but C and O were dominant. The relative content of P increased and the relative content of N decreased after KOH modification. The relative content of C decreased and the relative content of O and P decreased after H₃PO₄ modification.

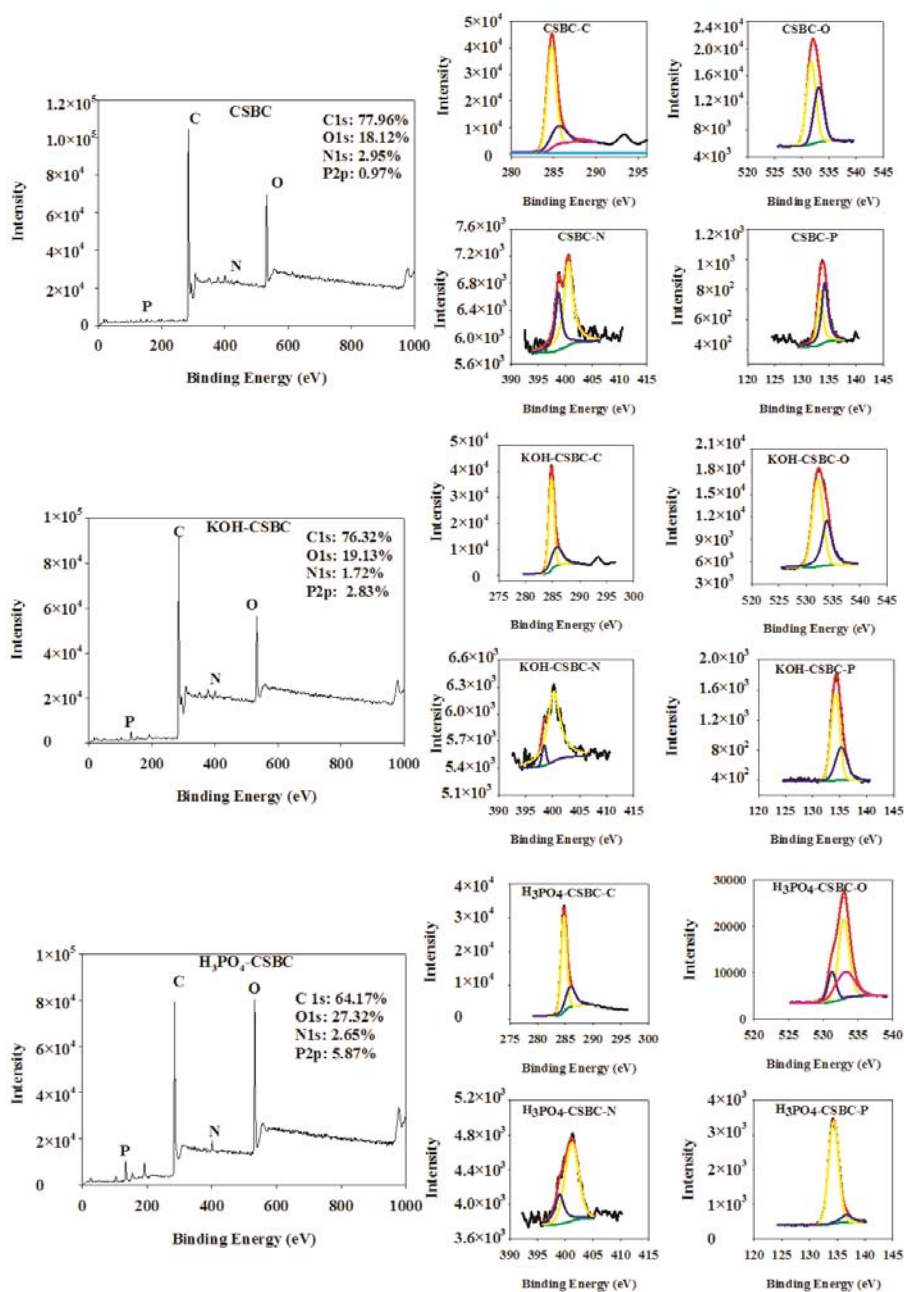


Figure 4. X-ray photoelectron spectroscopy (XPS) spectra of tested adsorbents.

Results from the XPS peak-differentiating analysis for CSBC, KOH-CSBC and H₃PO₄-CSBC are displayed in Table 3. The C-1s XPS spectra of biochar exhibited three peaks at 284.77, 285.58 and 288.34 eV, corresponding to the carbon-based functional groups C–C/C–H, C–O and O=C–O, respectively [32–34]. The carbon functional groups in CSBC included C–C/C–H, C–O and O=C–O.

The carbon-based functional groups in KOH-CSBC and H₃PO₄-CSBC included C–C/C–H and C–O. The O=C–O functional group could not be detected in either KOH-CSBC or H₃PO₄-CSBC due to the thermal decomposition of carbonaceous components. The relative content of C–C/C–H decreased and the relative content of C–O increased in both KOH-CSBC and H₃PO₄-CSBC on account of the introduction of the activating agents.

Table 3. Functional groups and peak fitting of tested adsorbents based on XPS studies.

Functional Groups	CSBC	KOH-CSBC	H ₃ PO ₄ -CSBC	
C	C–C/C–H	284.77 ^a 72.55% ^b	284.78 66.57%	284.78 68.70%
	C–O	285.58 24.23%	285.74 33.43%	286.07 31.30%
	O=C–O	288.34 3.22%		
O	C–O	531.73 58.23%	532.19 61.00%	531.23 (C=O/O=P) 15.77%
	C=O–OH	533.12 41.77%	533.88 39.00%	533.10 30.19%
	O–C/COH/C–O–C/P–O			532.91 54.04%
N	Pyrimidine nitrogen	398.72 33.39%	398.41 6.27%	398.99 25.83%
	Pyrrole nitrogen/ pyridine nitrogen	400.57 66.61%	400.19 93.73%	401.16 74.17%
P	C–PO ₃ /C ₂ –PO ₂	133.38 41.90%		
	C–O–PO ₃	134.22 58.10%	134.23 65.48%	134.33 88.94%
	P ₂ O ₅		135.33 34.52%	136.60 11.06%

^a Binding energy, eV; ^b The relative percentage of functional groups, %.

The O-1s XPS spectra of pristine biochar exhibited three peaks at 531.73, 533.12 and 532.91 eV, corresponding to C–O, C=O–OH and C=O/O=P/O–C/COH/C–O–C/P–O, respectively [35,36]. The oxygen-based functional groups included C–O and C=O–OH in CSBC. The main oxygen-based functional groups were C–O and C=O–OH in KOH-CSBC. The group C=O/O=P/O–C/C–OH/C–O–C/P–O was observed in biochar after H₃PO₄ modification. Thus, H₃PO₄ modification obviously affected the types and relative content of oxygen-containing groups, indicating that this change could influence the removal of MB from solution.

The N-1s XPS spectra of biochar exhibited two peaks at 398.72 eV and 400.57 eV, corresponding to pyrimidine and pyridine/pyrrole, respectively [37]. The main nitrogen-containing groups were pyrimidine and pyridine/pyrrole in CSBC. The main group was pyridine/pyrrole in KOH-CSBC. The relative content of pyrimidine decreased after KOH modification. The relative content of pyridine/pyrrole increased slightly after H₃PO₄ modification.

The P-2p XPS spectra of biochar exhibited three peaks at 133.38 eV, 134.22 eV and 135.33 eV corresponding to C–PO₃/C₂–PO₂, C–O–PO₃ and P₂O₅, respectively [38–41]. The phosphorous-based functional groups were C–PO₃/C₂–PO₂ and C–O–PO₃ in CSBC. After KOH modification, C–O–PO₃ and P₂O₅ were the main phosphorous-containing groups in KOH-CSBC. Meanwhile, C–O–PO₃ was the dominant phosphorous-containing group in H₃PO₄-CSBC. P₂O₅ also was found in H₃PO₄-CSBC. The XPS analysis confirmed that H₃PO₄ reacted with the carbonaceous components in biochar and that H₃PO₄ itself occurred in thermal decomposition. H₃PO₄ modification enriched the functional groups in biochar, indicating that more binding sites would be available to remove MB from solution.

3.2. Effect of Solid-to-Liquid Ratio and Initial pH on MB Removal

The effect of solid-to-liquid ratio on MB removal by CSBC, KOH-CSBC and H_3PO_4 -CSBC is shown in Figure 5a. When the solid-to-liquid ratio increased from 0.5 g L^{-1} to 4 g L^{-1} , the efficiency of removing MB by CSBC, KOH-CSBC and H_3PO_4 -CSBC increased from 13% to 59%, from 99.6% to 100%, and from 93% to 100%, respectively. Higher solid-liquid ratio means a larger amount of adsorbent and a larger number of binding sites for the removal of MB. Compared with pristine biochar (CSBC), the biochar modified by KOH and H_3PO_4 significantly increased the removal of MB at any given solid-to-liquid ratio. Thus, the modification of biochar using these two activation agents was effective. The efficiency of removing MB by KOH-CSBC and H_3PO_4 -CSBC was nearly 100% when the solid-to-liquid ratio was equivalent to 1.0 g L^{-1} .

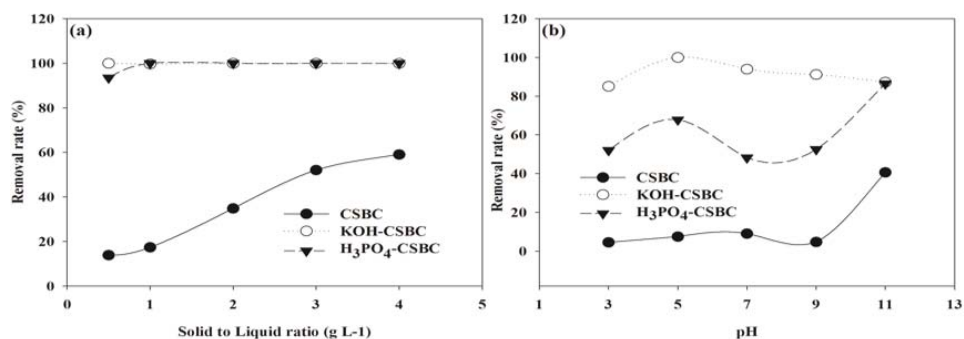


Figure 5. Effect of (a) Solid to Liquid ratio and (b) pH on methylene blue (MB) removal.

The effect of initial pH on MB removal by CSBC, KOH-CSBC and H_3PO_4 -CSBC is shown in Figure 5b. The efficiency of removing MB by CSBC, KOH-CSBC and H_3PO_4 -CSBC was 41%, 87% and 86% at pH 11.0, respectively. However, the maximum MB removal efficiency achieved by KOH-CSBC was nearly 100% at pH 5.0.

As pH increased, the efficiency of removing MB by CSBC first increased and then tended to stabilize. The removal of MB by CSBC was more favorable under alkaline conditions because MB is a cationic dye. The removal of MB by KOH-CSBC as pH increased first increased and then slightly decreased. The overall removal rate was more than 85% at pH 3.0–11.0. The reduced MB removal rate of KOH-CSBC at higher pH (7.0–11.0) may be related to the loss of binding sites under alkaline conditions. The efficiency of removing MB by H_3PO_4 -CSBC at pH first increased, then slightly decreased and finally exhibited a slight increase. These changes in removal efficiency may have been caused by the protonation or deprotonation of phosphorus-containing groups in H_3PO_4 -CSBC at different pH [42].

3.3. Adsorption Kinetics of MB on Biochars

The adsorption kinetics of MB and theoretical fitted curves for CSBC, KOH-CSBC and H_3PO_4 -CSBC are presented in Figure 6. As reaction time increased, the amount of MB adsorbed on CSBC, KOH-CSBC and H_3PO_4 -CSBC first increased quickly and then tended to stabilize. Thus, the adsorption process could be divided into a fast stage and a slow stage. In the initial phase of adsorption (fast stage), the MB molecules rapidly occupied the vacant sites on the surface of biochar. After 30 min (i.e., the end of the fast stage and beginning of the slow stage), the decreased number of vacant adsorption sites on the surface of biochar led to the saturation of adsorption capacity. The adsorption process gradually reached equilibrium after approximately 60 min.

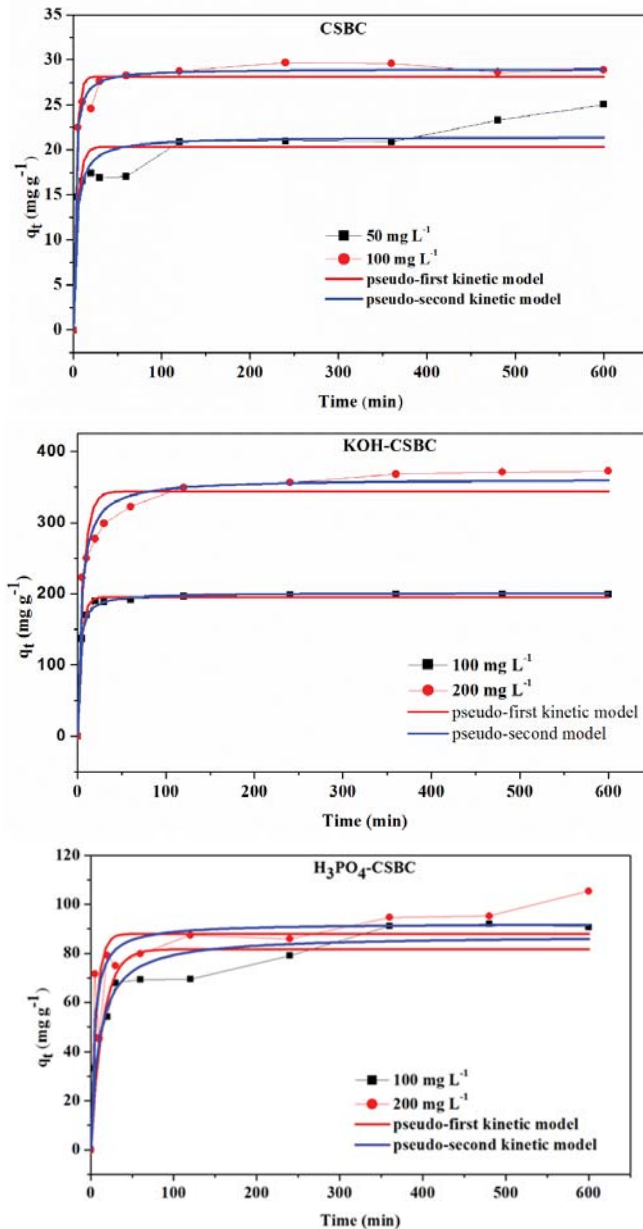


Figure 6. Adsorption kinetics and theoretical fitting curves of MB on tested adsorbents.

The amount of MB adsorbed from the more highly concentrated solution by biochars was larger than that adsorbed from the less highly concentrated solution. When the concentration of MB increased from 50 mg L⁻¹ to 100 mg L⁻¹, the amount of MB adsorbed on CSBC increased from 25.0 mg g⁻¹ to 28.8 mg g⁻¹. Likewise, when the concentration of MB increased from 100 mg L⁻¹ to 200 mg L⁻¹, the amount of MB adsorbed on KOH-CSBC and H₃PO₄-CSBC increased from 199.8 to 372.3 mg g⁻¹, and from 91 to 105 mg g⁻¹, respectively. A higher initial concentration of MB can provide a higher driving

force to overcome the mass transfer resistance of dye molecules between the solid phase and the liquid phase, resulting in more contact between dye molecules and the active sites on an adsorbent [43,44]. This phenomenon likely explains the data shown in Figure 6.

The parameters used to model the adsorption kinetics of MB on CSBC, KOH-CSBC and H₃PO₄-CSBC are shown in Table 4. Compared with predictions using the pseudo-first-order model, the pseudo-second-order model provided a better description of the MB adsorption process, suggesting the adsorption of MB molecules on biochars contained multiple steps (including external liquid film diffusion, surface adsorption and particle diffusion) [45]. Furthermore, chemical interaction played an important role during the MB adsorption process [46].

Table 4. Pseudo-first-order and pseudo-second-order kinetic models adsorption parameters.

Samples	Pseudo-First-Order			Pseudo-Second-Order		
	k_1 (min ⁻¹)	q_e (mg g ⁻¹)	R ²	k_2 (g mg ⁻¹ .min ⁻¹)	q_e (mg g ⁻¹)	R ²
CSBC-50	0.21345	20.32061	0.83583	0.01439	21.47248	0.90152
CSBC-100	0.29512	28.16607	0.96912	0.02148	29.00599	0.98949
KOH-CSBC-100	0.22694	195.77074	0.99472	0.00238	201.40582	0.99655
KOH-CSBC-200	0.14885	343.79494	0.91663	6.55037×10^{-4}	361.7548	0.97949
H ₃ PO ₄ -CSBC-100	0.06862	81.7322	0.89829	0.00112	87.36304	0.95485
H ₃ PO ₄ -CSBC-200	0.14954	87.97926	0.76541	0.00273	92.28821	0.84763

3.4. Adsorption Isotherms

The adsorption isotherms and fitted prediction curves describing adsorption of MB on CSBC, KOH-CSBC and H₃PO₄-CSBC are displayed in Figure 7. As the MB concentration increased, the amount of MB adsorbed on CSBC, KOH-CSBC and H₃PO₄-CSBC first increased and then tended to stabilize. A higher initial MB concentration resulted in higher adsorption, which followed the order KOH-CSBC > H₃PO₄-CSBC > CSBC.

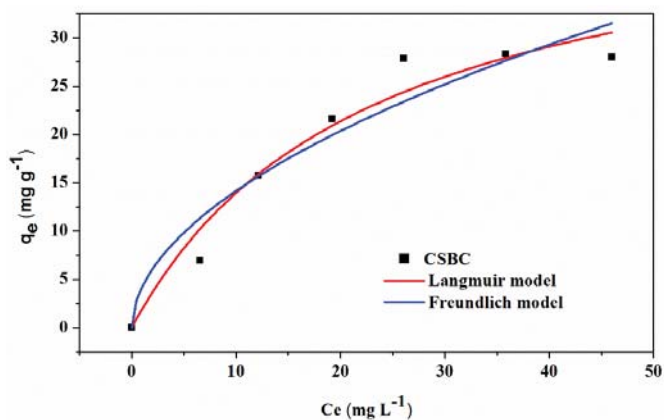


Figure 7. Cont.

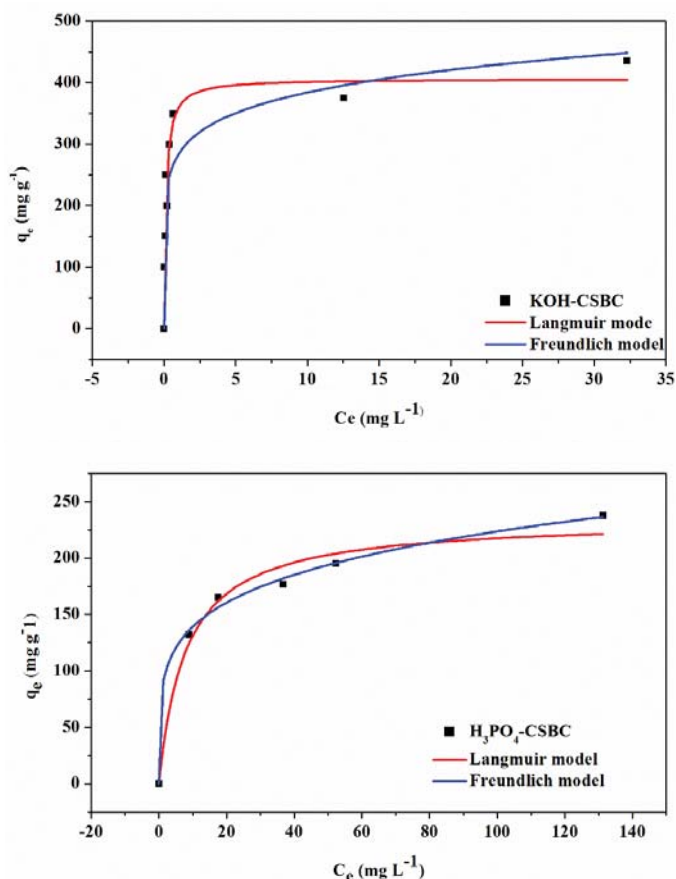


Figure 7. Adsorption isotherm and fitting curves of MB on tested adsorbents.

The parameters used to model the adsorption isotherm of MB on CSBC, KOH-CSBC, H_3PO_4 -CSBC are shown in Table 5. Both the Langmuir and Freundlich models described the adsorption process of MB on biochars well, as indicated by correlation coefficients that exceeded 0.85. The Langmuir isotherm better fit the adsorption process of MB on CSBC and KOH-CSBC (with correlation coefficients in the range 0.87–0.95). Technically, the Freundlich model described the adsorption process of MB on H_3PO_4 -CSBC better, exhibiting a correlation coefficient of 0.99 compared to that (0.97) for the Langmuir model.

Table 5. Fitting parameters of adsorption isotherms.

Samples	Langmuir			Freundlich		
	q_m ($\text{mg}\cdot\text{g}^{-1}$)	K_L ($\text{L}\cdot\text{mg}^{-1}$)	R^2	K_F	$1/n$	R^2
CSBC	45.58	0.04415	0.9535	4.232	0.5245	0.9145
KOH-CSBC	406.43	7.553	0.9084	283.21	0.1321	0.8665
H_3PO_4 -CSBC	234.75	0.1267	0.9746	86.67	0.2058	0.9955

Based on the fitted Langmuir model, the maximum adsorption capacity of CSBC, KOH-CSBC and H_3PO_4 -CSBC for MB was $45.58 \text{ mg}\cdot\text{g}^{-1}$, $406.43 \text{ mg}\cdot\text{g}^{-1}$ and $234.75 \text{ mg}\cdot\text{g}^{-1}$, respectively. The adsorption

capacities of KOH-CSBC and H₃PO₄-CSBC were 9.4 and 5.3 times higher than CSBC, respectively. Thus, KOH and H₃PO₄ modification significantly enhanced the adsorption capacity of biochar for MB, with KOH modification producing nearly twice the increase achieved by H₃PO₄.

The parameter K_L (Equation (4)) reflected the adsorption affinity between biochar and MB molecules [47]. In this study, the K_L associated with KOH-CSBC was larger than that for both H₃PO₄-CSBC and CSBC, indicating that KOH-CSBC had a higher affinity for MB than CSBC and H₃PO₄-CSBC. Similarly, the parameter 1/n derived for the Freundlich model reflected the difficulty of MB adsorption. Generally, when 1/n is less than 0.5, an adsorbent is easily adsorbed, and when 1/n exceeds 2, the adsorbent is hardly adsorbed [48]. In this research, the value of 1/n for KOH-CSBC and H₃PO₄-CSBC was less than 0.5, suggesting the adsorption of MB proceeded easily. Meanwhile, the value of 1/n for CSCB was 0.52448, illustrating that adsorption MB could occur, albeit with slightly more difficulty than for KOH-CSBC and H₃PO₄-CSBC.

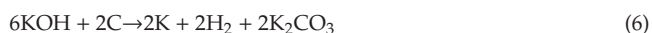
3.5. Discussion of Activation Mechanism and Adsorption Mechanism

3.5.1. Activation Mechanism

In this study, modification (activation) of corn stalk biochar using KOH and H₃PO₄ greatly improved the removal of MB from solution.

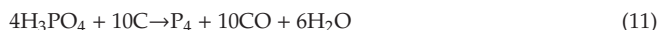
KOH activation was an effective method through which to create a porous structure in biochar. Previous studies [49–53] found that the activation mechanism of KOH is as follows. First, KOH melted at 360 °C and then was involved in a reduction reaction with carbon precursors that formed K₂CO₃ at nearly 400 °C. KOH was gradually consumed at 600 °C and converted entirely to K₂CO₃. K₂CO₃ decomposed into CO₂ and K₂O when the temperature exceeded 700 °C and disappeared completely at 800 °C. Additionally, the generated CO₂ reacted with other sources of C to form CO at high temperature. Meanwhile, potassium compounds were reduced to metallic potassium by carbon at high temperatures. When the alkaline metal became a highly diffused vapor, it was easily inserted into the carbon lattice and thus generated a more well-developed porous structure in the biochar. The reaction process is described in Equations (6)–(10).

The influence of KOH activation on CSBC was easily observed through surface area analysis and by SEM, XRD, FTIR and XPS characterization. Based on surface area measurements and SEM images, the biochar exhibited a larger surface area and better developed pore structure after KOH modification. XRD analysis detected the existence of K and K₂O. FTIR and XPS analysis confirmed that biochar had a more developed aromatic structure after KOH high-temperature activation. The structural characteristic of KOH-CSCB resulted in a high ability to remove MB from aqueous solution.



The function of H₃PO₄ is to first act as an acid catalyst to promote bond-cracking reactions. A chain structure is formed by the reaction of ring and condensation in biochar. Second, the reaction with organic components forms phosphate and polyphosphate bridged and crosslinked biopolymer fragments, which promote the formation of pores [41]. As reported in the literature [41,54], H₃PO₄ activation

proceeded as follows. First, in the pyrolysis process, the oxygen-containing functional group of biochar reacted with H_3PO_4 to generate water vapor, which further reacted with the carbonaceous components in biochar to form the inner pore structure, as indicated in the following reaction (Equation (11)).



Second, the catalysis of H_3PO_4 led to the oxidation and fixation of oxygen-containing functional groups on the pore walls, which led to the reduction of pore size or the transformation of mesopores into micropores. Third, H_3PO_4 promoted the formation of $-COOH$, $-OH$, $C=C$ and an aromatic structure, and enhanced the formation of P-O or P-OOH functional groups.

H_3PO_4 modification of biochar promoted the formation of phosphorus-containing functional groups, $-COOH$, $-OH$ and a highly aromatic structure, as confirmed by FTIR and XPS analysis. However, surface area and pore analyses showed that H_3PO_4 modification did not facilitate the formation of a porous structure of biochar, but instead reduced the specific surface area and pore volume. According to SEM images, the pore structure of biochar was agglomerated and fused, an effect that may be related to the material composition, pyrolysis preparation conditions, or the activation process of H_3PO_4 . Mandal et al. [55] showed that the H_3PO_4 treatment of rice straw biochar reduced both surface area and pore volume, and concluded these changes might be due to the increase in functional groups inside the pores following H_3PO_4 treatment. Consequently, the improvement of MB adsorption capacity by H_3PO_4 treatment of CSBC was independent of the specific surface area and pore structure; rather, other mechanisms determined the high MB adsorption capacity of H_3PO_4 -CSBC. FTIR and XPS analyses showed that H_3PO_4 modification obviously affected the oxygen- and phosphorus-containing functional groups of biochar. Torrellas et al. also found that more functional groups existed on the activated carbon after H_3PO_4 activation [56]. The participation of these functional groups was an important reason for the high MB adsorption capacity of H_3PO_4 -CSBC.

3.5.2. Removal Mechanism of Methylene Blue by Biochar

The main mechanisms for MB removal by adsorbent or biochar involve physical interaction, ion exchange, electrostatic interaction, π - π stacking, hydrogen bonding and pore filling [48,57–65]. The dominant mechanisms depend on the physicochemical properties of biochar and specific environmental conditions in the solution.

In this study, corn stalk biochar was prepared at 500 °C. Cellulose and hemicellulose in the corn stalk gradually decomposed thermally at temperatures less than 500 °C. Meanwhile, the carbohydrate, protein and fat compounds also gradually decomposed. Then, the specific surface area became larger and a pore structure gradually formed, both of which would play an important role in MB removal. Furthermore, the aromatic structure of the biochar was gradually improved. The aromatic structure of the biochar could combine with the benzene ring in MB molecules via π - π stacking. CSBC contained abundant functional groups among which $-OH$ and $-COOH$ could bind with nitrogen molecules in MB through hydrogen bonding. The pH experiment indicated that electrostatic interaction also could affect the combination between CSBC and MB. Therefore, the adsorption mechanism between CSBC and MB was the result of electrostatic interaction, hydrogen bonding, π - π stacking and physical interaction (surface contact and pore diffusion).

After KOH modification, the surface area and pore volume of biochar significantly increased. The capacity of KOH-CSBC to absorb MB was greatly increased compared to that of pristine CSBC. Thus, the specific surface area and pore volume of KOH-CSBC played a key role in MB adsorption. The variety of functional groups in KOH-CSBC was limited, especially for oxygen-containing groups. Organic groups in KOH-CSBC disappeared at the pyrolytic temperature of 700 °C, resulting in weak hydrogen bonds and weak electrostatic interaction between KOH-CSBC and MB. However, the aromatic structure and the degree of graphitization of KOH-CSBC became stronger compared to pristine CSBC, and the contribution of π - π stacking to MB removal was relatively more important. Therefore, the main MB

removal mechanism of KOH-CSBC involved π - π stacking and physical interaction (surface area and pore diffusion).

After H_3PO_4 modification, the surface area and pore volume of biochar decreased relative to that of pristine CSBC. However, the capacity of H_3PO_4 -CSBC to adsorb MB apparently increased, indicating that surface area and pore volume did not play a major role in MB removal by this biochar. FTIR analysis showed that H_3PO_4 -CSBC contained abundant functional groups, including -OH, -COOH, amino phosphonic acid functional group, and P-OH bond. Hydrogen bonding and electrostatic interaction were critical for MB removal by H_3PO_4 -CSBC. Meanwhile, the aromatic structure and the graphitization degree of biochar were enhanced after H_3PO_4 modification. Thus, the main MB removal mechanism of H_3PO_4 -CSBC included electrostatic interaction, hydrogen bonding, and π - π stacking.

The MB removal mechanisms by CSBC, KOH-CSBC and H_3PO_4 -CSBC are summarized in Figure 8.

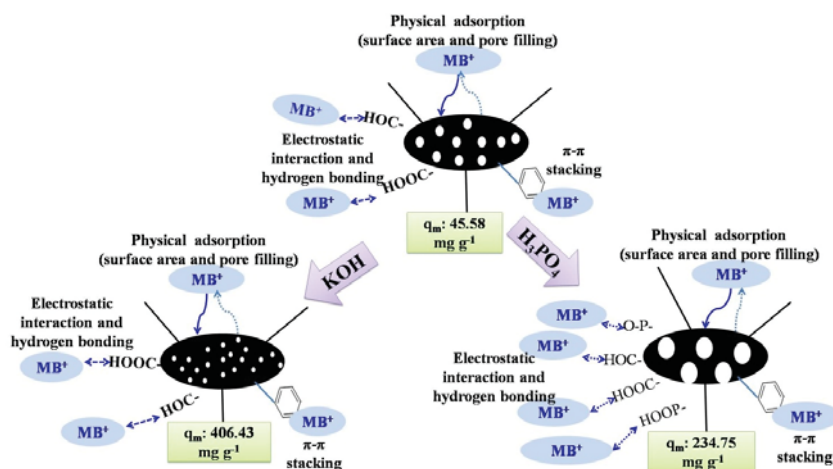


Figure 8. Schematic diagram of removal mechanism between CSBC, KOH-CSBC, H_3PO_4 -CSBC and MB.

4. Conclusions

Biochar was prepared from corn stalk and was modified using KOH and H_3PO_4 . KOH modification of corn stalk biochar significantly increases the surface area and pore volume of the biochar. H_3PO_4 modification enriches the functional groups of biochar. As a result of both types of biochar modification, the maximum adsorption capacity for MB increases approximately 5–10 times (in this study from 43.14 mg g^{-1} for CSBC to 406.43 mg g^{-1} for KOH-CSBC and to 230.39 mg g^{-1} for H_3PO_4 -CSBC). The modification of corn stalk biochar by KOH and H_3PO_4 also affects the MB adsorption mechanism. Therefore, corn stalk is an ideal natural raw material for preparation of biochar, and biochar production represents an effective way to utilize corn residues. Corn stalk biochar, especially if modified by KOH or to a lesser extent by H_3PO_4 , can be applied to remove MB-based dye from wastewater.

Author Contributions: Conceptualization and methodology, L.L. and S.F.; writing—original draft preparation, L.L. and S.F.; writing—review and editing, L.L., Y.L. and S.F.; supervision, Y.L. and S.F.

Funding: This study was funded by National Natural Science Foundation of China, grant number 51809001; Natural Science Foundation of the Education Department of Anhui Province, grant number KJ2018A0125, KJ2018A0347; Fuyang Normal University Youth Fund Project, grant number No. 204008134, 2018FSKJ07ZD.

Conflicts of Interest: The authors have declared no conflict of interest.

Statement of Novelty: KOH and H_3PO_4 were used to modify corn stalk biochar. The order of adsorption capacity was KOH-CSBC > H_3PO_4 -CSBC > CSBC. The interaction mechanism between biochars and methylene blue were different.

References

- Rajoriya, S.; Bargole, S.; George, S.; Saharan, V.K. Treatment of textile dyeing industry effluent using hydrodynamic cavitation in combination with advanced oxidation reagents. *J. Hazard. Mater.* **2018**, *344*, 1109–1115. [[CrossRef](#)] [[PubMed](#)]
- Hui, M.; Shengyan, P.; Yaqi, H.; Rongxin, Z.; Anatoly, Z.; Wei, C. A highly efficient magnetic chitosan “fluid” adsorbent with a high capacity and fast adsorption kinetics for dyeing wastewater purification. *Chem. Eng. J.* **2018**, *345*, 556–565. [[CrossRef](#)]
- Lehmann, J.; Rillig, M.C.; Thies, J.; Masiello, C.A.; Hockaday, W.C.; Crowley, D. Biochar effects on soil biota—A review. *Soil Biol. Biochem.* **2011**, *43*, 1812–1836. [[CrossRef](#)]
- Xiao, X.; Chen, B.; Chen, Z.; Zhu, L.; Schnoor, J.L. Insight into Multiple and Multilevel Structures of Biochars and Their Potential Environmental Applications: A Critical Review. *Environ. Sci. Technol.* **2018**, *52*, 5027–5047. [[CrossRef](#)] [[PubMed](#)]
- Ahmad, M.; Rajapaksha, A.U.; Lim, J.E.; Zhang, M.; Bolan, N.; Mohan, D.; Vithanage, M.; Lee, S.S.; Ok, Y.S. Biochar as a sorbent for contaminant management in soil and water: A review. *Chemosphere* **2014**, *99*, 19–33. [[CrossRef](#)] [[PubMed](#)]
- Gao, B.; Yao, Y.; Xue, Y.; Zimmerman, A.; Mosa, A.; Pullammanappallil, P.; Ok, Y.S.; Cao, X. A review of biochar as a low-cost adsorbent for aqueous heavy metal removal AU—Inyang, Mandu I. *Crit. Rev. Environ. Sci. Technol.* **2016**, *46*, 406–433.
- Mohan, D.; Sarswat, A.; Ok, Y.S.; Pittman, C.U. Organic and inorganic contaminants removal from water with biochar, a renewable, low cost and sustainable adsorbent—A critical review. *Bioresour. Technol.* **2014**, *160*, 191–202. [[CrossRef](#)]
- Trinh, B.-S.; Le, T.K.P.; Werner, D.; Phuong, H.N.; Luu, L.T. Rice Husk Biochars Modified with Magnetized Iron Oxides and Nano Zero Valent Iron for Decolorization of Dyeing Wastewater. *Processes* **2019**, *7*, 660. [[CrossRef](#)]
- Zhang, Y.; Lou, Z.; Wang, C.; Wang, W.; Cai, J. Synthesis of Porous Fe/C Bio-Char Adsorbent for Rhodamine B from Waste Wood: Characterization, Kinetics and Thermodynamics. *Processes* **2019**, *7*, 150. [[CrossRef](#)]
- Liu, W.-J.; Jiang, H.; Yu, H.-Q. Development of Biochar-Based Functional Materials: Toward a Sustainable Platform Carbon Material. *Chem. Rev.* **2015**, *115*, 12251–12285. [[CrossRef](#)]
- Li, H.; Dong, X.; da Silva, E.B.; de Oliveira, L.M.; Chen, Y.; Ma, L.Q. Mechanisms of metal sorption by biochars: Biochar characteristics and modifications. *Chemosphere* **2017**, *178*, 466–478. [[CrossRef](#)] [[PubMed](#)]
- Rajapaksha, A.U.; Chen, S.S.; Tsang, D.C.W.; Zhang, M.; Vithanage, M.; Mandal, S.; Gao, B.; Bolan, N.S.; Ok, Y.S. Engineered/designer biochar for contaminant removal/immobilization from soil and water: Potential and implication of biochar modification. *Chemosphere* **2016**, *148*, 276–291. [[CrossRef](#)] [[PubMed](#)]
- Tan, X.-F.; Liu, S.-B.; Liu, Y.-G.; Gu, Y.-L.; Zeng, G.-M.; Hu, X.-J.; Wang, X.; Liu, S.-H.; Jiang, L.-H. Biochar as potential sustainable precursors for activated carbon production: Multiple applications in environmental protection and energy storage. *Bioresour. Technol.* **2017**, *227*, 359–372. [[CrossRef](#)] [[PubMed](#)]
- Park, J.; Hung, I.; Gan, Z.; Rojas, O.J.; Lim, K.H.; Park, S. Activated carbon from biochar: Influence of its physicochemical properties on the sorption characteristics of phenanthrene. *Bioresour. Technol.* **2013**, *149*, 383–389. [[CrossRef](#)] [[PubMed](#)]
- Dehkhoda, A.M.; Ellis, N.; Gyenge, E. Effect of activated biochar porous structure on the capacitive deionization of NaCl and ZnCl₂ solutions. *Microporous Mesoporous Mater.* **2016**, *224*, 217–228. [[CrossRef](#)]
- Liu, D.; Hao, Z.; Zhao, X.; Su, R.; Feng, W.; Li, S.; Jia, B. Effect of Physical and Mechanical Activation on the Physicochemical Structure of Coal-Based Activated Carbons for SO₂ Adsorption. *Processes* **2019**, *7*, 707. [[CrossRef](#)]
- Luo, J.; Li, X.; Ge, C.; Müller, K.; Yu, H.; Huang, P.; Li, J.; Tsang, D.C.W.; Bolan, N.S.; Rinklebe, J. Sorption of norfloxacin, sulfamerazine and oxytetracycline by KOH-modified biochar under single and ternary systems. *Bioresour. Technol.* **2018**, *263*, 385. [[CrossRef](#)]
- Bashir, S.; Zhu, J.; Fu, Q.; Hu, H. Comparing the adsorption mechanism of Cd by rice straw pristine and KOH-modified biochar. *Environ. Sci. Pollut. Res.* **2018**, *25*, 11875–11883. [[CrossRef](#)]
- Huang, H.; Tang, J.; Gao, K.; He, R.; Zhao, H.; Werner, D. Characterization of KOH modified biochars from different pyrolysis temperatures and enhanced adsorption of antibiotics. *RSC Adv.* **2017**, *7*, 14640–14648. [[CrossRef](#)]

20. Chen, T.; Luo, L.; Deng, S.; Shi, G.; Zhang, S.; Zhang, Y.; Deng, O.; Wang, L.; Zhang, J.; Wei, L. Sorption of tetracycline on H₃PO₄ modified biochar derived from rice straw and swine manure. *Bioresour. Technol.* **2018**, *267*, 431–437. [[CrossRef](#)]
21. Peng, H.; Gao, P.; Chu, G.; Pan, B.; Peng, J.; Xing, B. Enhanced adsorption of Cu(II) and Cd(II) by phosphoric acid-modified biochars. *Environ. Pollut.* **2017**, *229*, 846–853. [[CrossRef](#)] [[PubMed](#)]
22. Zhao, N.; Zhao, C.; Lv, Y.; Zhang, W.; Du, Y.; Hao, Z.; Zhang, J. Adsorption and coadsorption mechanisms of Cr(VI) and organic contaminants on H₃PO₄ treated biochar. *Chemosphere* **2017**, *186*, 422–429. [[CrossRef](#)] [[PubMed](#)]
23. Hong, J.; Ren, L.; Hong, J.; Xu, C. Environmental impact assessment of corn straw utilization in China. *J. Clean. Prod.* **2016**, *112*, 1700–1708. [[CrossRef](#)]
24. Meng, R.; Chen, T.; Zhang, Y.; Lu, W.; Liu, Y.; Lu, T.; Liu, Y.; Wang, H. Development, modification, and application of low-cost and available biochar derived from corn straw for the removal of vanadium(v) from aqueous solution and real contaminated groundwater. *RSC Adv.* **2018**, *8*, 21480–21494. [[CrossRef](#)]
25. Lagergren, S. About the Theory of So-Called Adsorption of Solution Substances. *K. Sven. Vetensk. Handl.* **1898**, *24*, 1–39.
26. Blanchard, G.; Maunay, M.; Martin, G. Removal of heavy metals from waters by means of natural zeolites. *Water Res.* **1984**, *18*, 1501–1507. [[CrossRef](#)]
27. Langmuir, I. The adsorption of gases on plane surfaces of glass, mica and platinum. *J. Am. Chem. Soc.* **1918**, *40*, 1361–1403. [[CrossRef](#)]
28. Freundlich, H. Über die adsorption in lösungen. *Z. Phys. Chem.* **1907**, *57*, 385–470. [[CrossRef](#)]
29. Yang, H.; Rong, Y.; Chen, H.; Dong, H.L.; Zheng, C. Characteristics of hemicellulose, cellulose and lignin pyrolysis. *Fuel* **2007**, *86*, 1781–1788. [[CrossRef](#)]
30. Zhang, G.; Zhang, Q.; Sun, K.; Liu, X.; Zheng, W.; Zhao, Y. Sorption of simazine to corn straw biochars prepared at different pyrolytic temperatures. *Environ. Pollut.* **2011**, *159*, 2594–2601. [[CrossRef](#)]
31. Zhu, L.; Zhao, N.; Tong, L.; Lv, Y. Structural and adsorption characteristics of potassium carbonate activated biochar. *RSC Adv.* **2018**, *8*, 21012–21019. [[CrossRef](#)]
32. Yang, F.; Sun, L.; Zhang, W.; Zhang, Y. One-pot synthesis of porous carbon foam derived from corn straw: Atrazine adsorption equilibrium and kinetics. *Environ. Sci.* **2017**, *4*, 625–635. [[CrossRef](#)]
33. Han, M.; Jiang, K.; Jiao, P.; Ji, Y.; Zhou, J.; Zhuang, W.; Chen, Y.; Liu, D.; Zhu, C.; Chen, X.; et al. Bio-butanol sorption performance on novel porous-carbon adsorbents from corncob prepared via hydrothermal carbonization and post-pyrolysis method. *Sci. Rep.* **2017**, *7*, 11753. [[CrossRef](#)] [[PubMed](#)]
34. Li, H.; Ye, X.; Geng, Z.; Zhou, H.; Guo, X.; Zhang, Y.; Zhao, H.; Wang, G. The influence of biochar type on long-term stabilization for Cd and Cu in contaminated paddy soils. *J. Hazard. Mater.* **2016**, *304*, 40–48. [[CrossRef](#)] [[PubMed](#)]
35. Wen, T.; Wang, J.; Yu, S.; Chen, Z.; Hayat, T.; Wang, X. Magnetic Porous Carbonaceous Material Produced from Tea Waste for Efficient Removal of As(V), Cr(VI), Humic Acid, and Dyes. *ACS Sustain. Chem. Eng.* **2017**, *5*, 4371–4380. [[CrossRef](#)]
36. Srinivasan, P.; Sarmah, A.K. Characterisation of agricultural waste-derived biochars and their sorption potential for sulfamethoxazole in pasture soil: A spectroscopic investigation. *Sci. Total Environ.* **2015**, *502*, 471–480. [[CrossRef](#)]
37. Lian, F.; Cui, G.; Liu, Z.; Duo, L.; Zhang, G.; Xing, B. One-step synthesis of a novel N-doped microporous biochar derived from crop straws with high dye adsorption capacity. *J. Environ. Manag.* **2016**, *176*, 61–68. [[CrossRef](#)]
38. Rosas, J.M.; Ruiz-Rosas, R.; Rodríguez-Mirasol, J.; Cordero, T. Kinetic study of the oxidation resistance of phosphorus-containing activated carbons. *Carbon* **2012**, *50*, 1523–1537. [[CrossRef](#)]
39. Rosas, J.M.; Bedia, J.; Rodríguez-Mirasol, J.; Cordero, T. HEMP-derived activated carbon fibers by chemical activation with phosphoric acid. *Fuel* **2009**, *88*, 19–26. [[CrossRef](#)]
40. Puziy, A.M.; Poddubnaya, O.I.; Ziatdinov, A.M. On the chemical structure of phosphorus compounds in phosphoric acid-activated carbon. *Appl. Surf. Sci.* **2006**, *252*, 8036–8038. [[CrossRef](#)]
41. Sun, K.; Huang, Q.; Meng, X.; Chi, Y.; Yan, J. Catalytic Pyrolysis of Waste Polyethylene into Aromatics by H₃PO₄-Activated Carbon. *Energy Fuels* **2018**, *32*, 9772–9781. [[CrossRef](#)]
42. Puziy, A.M.; Poddubnaya, O.I.; Martínez-Alonso, A.; Suárez-García, F.; Tascón, J.M.D. Surface chemistry of phosphorus-containing carbons of lignocellulosic origin. *Carbon* **2005**, *43*, 2857–2868. [[CrossRef](#)]

43. Lee, L.Y.; Gan, S.; Tan, M.S.Y.; Lim, S.S.; Lee, X.J.; Lam, Y.F. Effective removal of Acid Blue 113 dye using overripe Cucumis sativus peel as an eco-friendly biosorbent from agricultural residue. *J. Clean. Prod.* **2016**, *113*, 194–203. [[CrossRef](#)]
44. Alizadeh, B.; Ghorbani, M.; Salehi, M.A. Application of polyrhodanine modified multi-walled carbon nanotubes for high efficiency removal of Pb (II) from aqueous solution. *J. Mol. Liq.* **2016**, *220*, 142–149. [[CrossRef](#)]
45. Vadivelan, V.; Kumar, K.V. Equilibrium, kinetics, mechanism, and process design for the sorption of methylene blue onto rice husk. *J. Colloid Interface Sci.* **2005**, *286*, 90–100. [[CrossRef](#)]
46. Ho, Y.S.; McKay, G. Pseudo-second order model for sorption processes. *Process. Biochem.* **1999**, *34*, 451–465. [[CrossRef](#)]
47. Hu, Q.; Liu, Y.; Feng, C.; Zhang, Z.; Lei, Z.; Shimizu, K. Predicting equilibrium time by adsorption kinetic equations and modifying Langmuir isotherm by fractal-like approach. *J. Mol. Liq.* **2018**, *268*, 728–733. [[CrossRef](#)]
48. Shi, L.; Zhang, G.; Wei, D.; Yan, T.; Xue, X.; Shi, S.; Wei, Q. Preparation and utilization of anaerobic granular sludge-based biochar for the adsorption of methylene blue from aqueous solutions. *J. Mol. Liq.* **2014**, *198*, 334–340. [[CrossRef](#)]
49. Raymundo-Piñero, E.; Azañs, P.; Cacciaguerra, T.; Cazorla-Amorós, D.; Linares-Solano, A.; Béguin, F. KOH and NaOH activation mechanisms of multiwalled carbon nanotubes with different structural organisation. *Carbon* **2005**, *43*, 786–795. [[CrossRef](#)]
50. Lozano-Castelló, D.; Calo, J.M.; Cazorla-Amorós, D.; Linares-Solano, A. Carbon activation with KOH as explored by temperature programmed techniques, and the effects of hydrogen. *Carbon* **2007**, *45*, 2529–2536. [[CrossRef](#)]
51. Zhou, J.; Li, Z.; Xing, W.; Shen, H.; Bi, X.; Zhu, T.; Qiu, Z.; Zhuo, S. A New Approach to Tuning Carbon Ultramicropore Size at Sub-Angstrom Level for Maximizing Specific Capacitance and CO₂ Uptake. *Adv. Funct. Mater.* **2016**, *26*, 7955–7964. [[CrossRef](#)]
52. Wang, J.; Kaskel, S. KOH activation of carbon-based materials for energy storage. *J. Mater. Chem.* **2012**, *22*, 23710–23725. [[CrossRef](#)]
53. Dehkhoda, A.M.; Gyenge, E.; Ellis, N. A novel method to tailor the porous structure of KOH-activated biochar and its application in capacitive deionization and energy storage. *Biomass Bioenergy* **2016**, *87*, 107–121. [[CrossRef](#)]
54. Jagtoyen, M.; Derbyshire, F. Activated carbons from yellow poplar and white oak by H₃PO₄ activation. *Carbon* **1998**, *36*, 1085–1097. [[CrossRef](#)]
55. Mandal, A.; Singh, N.; Purakayastha, T.J. Characterization of pesticide sorption behaviour of slow pyrolysis biochars as low cost adsorbent for atrazine and imidacloprid removal. *Sci. Total Environ.* **2017**, *577*, 376–385. [[CrossRef](#)]
56. Torrellas, S.Á.; Lovera, R.G.; Escalona, N.; Sepúlveda, C.; Sotelo, J.L.; García, J. Chemical-activated carbons from peach stones for the adsorption of emerging contaminants in aqueous solutions. *Chem. Eng. J.* **2015**, *279*, 788–798. [[CrossRef](#)]
57. Fu, J.; Chen, Z.; Wang, M.; Liu, S.; Zhang, J.; Zhang, J.; Han, R.; Xu, Q. Adsorption of methylene blue by a high-efficiency adsorbent (polydopamine microspheres): Kinetics, isotherm, thermodynamics and mechanism analysis. *Chem. Eng. J.* **2015**, *259*, 53–61. [[CrossRef](#)]
58. Gong, J.; Liu, J.; Chen, X.; Jiang, Z.; Wen, X.; Mijowska, E.; Tang, T. Converting real-world mixed waste plastics into porous carbon nanosheets with excellent performance in the adsorption of an organic dye from wastewater. *J. Mater. Chem. A* **2015**, *3*, 341–351. [[CrossRef](#)]
59. Ai, L.; Zhang, C.; Liao, F.; Wang, Y.; Li, M.; Meng, L.; Jiang, J. Removal of methylene blue from aqueous solution with magnetite loaded multi-wall carbon nanotube: Kinetic, isotherm and mechanism analysis. *J. Hazard. Mater.* **2011**, *198*, 282–290. [[CrossRef](#)]
60. Fan, S.; Wang, Y.; Wang, Z.; Tang, J.; Tang, J.; Li, X. Removal of methylene blue from aqueous solution by sewage sludge-derived biochar: Adsorption kinetics, equilibrium, thermodynamics and mechanism. *J. Environ. Chem. Eng.* **2017**, *5*, 601–611. [[CrossRef](#)]
61. Fan, S.; Tang, J.; Wang, Y.; Li, H.; Zhang, H.; Tang, J.; Wang, Z.; Li, X. Biochar prepared from co-pyrolysis of municipal sewage sludge and tea waste for the adsorption of methylene blue from aqueous solutions: Kinetics, isotherm, thermodynamic and mechanism. *J. Mol. Liq.* **2016**, *220*, 432–441. [[CrossRef](#)]

62. Leng, L.; Yuan, X.; Huang, H.; Shao, J.; Wang, H.; Chen, X.; Zeng, G. Bio-char derived from sewage sludge by liquefaction: Characterization and application for dye adsorption. *Appl. Surf. Sci.* **2015**, *346*, 223–231. [[CrossRef](#)]
63. Du, X.-D.; Wang, C.-C.; Liu, J.-G.; Zhao, X.-D.; Zhong, J.; Li, Y.-X.; Li, J.; Wang, P. Extensive and selective adsorption of ZIF-67 towards organic dyes: Performance and mechanism. *J. Colloid Interface Sci.* **2017**, *506*, 437–441. [[CrossRef](#)] [[PubMed](#)]
64. Gong, J.; Liu, J.; Jiang, Z.; Wen, X.; Mijowska, E.; Tang, T.; Chen, X. A facile approach to prepare porous cup-stacked carbon nanotube with high performance in adsorption of methylene blue. *J. Colloid Interface Sci.* **2015**, *445*, 195–204. [[CrossRef](#)] [[PubMed](#)]
65. Fan, S.; Wang, Y.; Li, Y.; Tang, J.; Wang, Z.; Tang, J.; Li, X.; Hu, K. Facile synthesis of tea waste/Fe₃O₄ nanoparticle composite for hexavalent chromium removal from aqueous solution. *RSC Adv.* **2017**, *7*, 7576–7590. [[CrossRef](#)]



© 2019 by the authors. Licensee MDPI, Basel, Switzerland. This article is an open access article distributed under the terms and conditions of the Creative Commons Attribution (CC BY) license (<http://creativecommons.org/licenses/by/4.0/>).

Review

Use of Nanotechnology for the Bioremediation of Contaminants: A Review

Edgar Vázquez-Núñez ^{1,*}, Carlos Eduardo Molina-Guerrero ¹, Julián Mario Peña-Castro ², Fabián Fernández-Luqueño ³ and Ma. Guadalupe de la Rosa-Álvarez ¹

¹ Departamento de Ingenierías Química, Electrónica y Biomédica, División de Ciencias e Ingenierías, Campus León, Universidad de Guanajuato, Lomas del Bosque 103, Lomas del Campestre, León, Guanajuato C.P. 37150, Mexico; cmolina@fisica.ugto.mx (C.E.M.-G.); delarosa@ugto.mx (M.G.d.l.R.-Á.)

² Laboratorio de Biotecnología Vegetal, Instituto de Biotecnología, Universidad del Papaloapan, Tuxtepec, Oaxaca C.P. 68333, Mexico; julianpc@unpa.edu.mx

³ Programas en Sustentabilidad de los Recursos Naturales y Energía, Cinvestav Saltillo Industrial, Parque Industrial, Ramos Arizpe, Coahuila C.P. 25900, Mexico; fabian.fernandez@cinvestav.edu.mx

* Correspondence: edgarvqznz@fisica.ugto.mx

Received: 22 May 2020; Accepted: 8 July 2020; Published: 13 July 2020

Abstract: Contaminants, organic or inorganic, represent a threat for the environment and human health and in recent years their presence and persistence has increased rapidly. For this reason, several technologies including bioremediation in combination with nanotechnology have been explored to identify more systemic approaches for their removal from environmental matrices. Understanding the interaction between the contaminant, the microorganism, and the nanomaterials (NMs) is of crucial importance since positive and negative effects may be produced. For example, some nanomaterials are stimulants for microorganisms, while others are toxic. Thus, proper selection is of paramount importance. The main objective of this review was to analyze the principles of bioremediation assisted by nanomaterials, nanoparticles (NPs) included, and their interaction with environmental matrices. It also analyzed the response of living organisms employed to remediate the contaminants in the presence of nanomaterials. Besides, we discuss the international regulatory frame applicable to these technologies and how they might contribute to sustainability.

Keywords: contaminants; nanomaterial; bioremediation; sustainability

1. Introduction

The industrial revolution has promoted economic prosperity, along with releasing a variety of pollutants into the environment [1]. During recent years, new technologies have been developed to increase the efficiency of the removal of pollutants, among them, bioremediation techniques have been proven to be a new and effective method for cleaning up pollutants in a variety of environments and a quite flexible management option to be implemented, also at a large scale [2].

Stimulation of the growth of indigenous microorganisms (biostimulation) or inoculation of non-native oil-degrading bacteria (bioaugmentation) were recognized as effective measures for accelerating the detoxification of a polluted site with a minimal impact on the ecological system [3]. Although bioremediation provides an excellent and flexible recovery strategy for different pollutants, it is poorly effective when dealing with high concentrations of the pollutants and xenobiotics or refractory compounds, causing unsustainable treatment efficiencies and recovery time [4].

In this context, the development of nanotechnology and the integration of the use of nanomaterials—defined as the particles with sizes of 100 nm or less in at least one dimension—and particularly nanoparticles—particles with two or three dimensions greater than 1 nm—represents an innovative

strategy to move the bioremediation forward beyond its limitations. This combined approach can include a wider range of potential applications with reduced costs and minimum negative impacts on the environment [5] for treating pollutants in groundwater and wastewater [6], sediments polluted with heavy metals and hydrocarbons [7], and either organic or inorganic compounds in soil [8].

Besides their positive effect on the removal of these contaminants, NMs could interact with biotic and abiotic elements, both in positive and negative ways; this is why many efforts have been conducted in order to evaluate the synergistic effect of the combined use of NMs and bioremediation practices and elucidate their physical, chemical and biological interactions either in soil or water [9].

So far, there are no consistent conclusions about whether the combined technologies are beneficial to improve pollutant removal efficiency and the combination of bioremediation technologies and nanomaterials to remove pollutants has not been widely reported, hence the main objective of this review is to examine bioremediation processes where nanomaterials are applied in order to enhance the removal of contaminants and describe their interactions with biotic and abiotic components during remediation processes and finally, some considerations regarding the international regulatory frame and world markets are mentioned.

2. Principles of Nanobioremediation Technologies

Every year around 10 million tons of toxic chemical compounds are released by industry [10–13]. After release, these compounds may further react to form chemicals, for instance, polychlorinated dibenzo-p-dioxins or polychlorinated dibenzofurans, which are by-products of certain chemical processes involving chlorine.

There is high variability in the physical and chemical properties of these chemical compounds, and their cytotoxicity and multiple interactions with biotic and abiotic environmental factors, i.e., microorganisms, plants, animals, water, minerals, organic matter, wind, etc., have complicated the successful implementation of remediation technologies [14–16]. The combined use of NMs and NPs with biotechnologies could offer a step-change in remediation capabilities, avoiding process intermediates, and increasing the speed of degradation [17,18].

Besides physical and chemical technologies to remediate polluted sites, biological treatments have become relevant due to their low cost and wide range of applications [19]. Bioremediation includes biosorption, bioaccumulation, biotransformation, and biological stabilization, among others [20,21]. These technologies use plants and some microorganisms including bacteria and fungus, as well as combinations of them.

During recent years, NMs have been integrated with biological processes to accelerate and promote the removal of toxic compounds from the environment [22]. Cecchin et al. [23] use the term nanobioremediation for processes where NPs and microorganisms or plants are used to remove contaminants. Moreover, El-Ramady et al. [24] named these types of practices according to the nature of the organism utilized for the remediation of contaminants. Thus, they were more specific and named the techniques as phyto-nanoremediation, microbial nanoremediation, and zoo-nanoremediation.

In any case, since bioremediation uses living organisms to remediate contaminated environments, a proper interaction between nanoparticles (NPs) and living organisms is essential. In this context, some aspects are of paramount importance. For example, it is known that nanotoxicity, NPs size, and nanonutrition may affect the living organisms and this in turn may affect the whole bioremediation process.

Tan et al. [25] reported that the physical and chemical interactions between NMs, biota and contaminants depend on a variety of parameters including NMs size and shape, surface coating, chemical nature of the NMs and contaminant, type of organism, media, pH, and temperature, among others; these interactions are represented in Figure 1. Given the number of potential parameters influencing such interactions, these phenomena become complex. For example, pH media as well as temperature play an essential role in the proper development of living organisms. These parameters in turn, may influence the stability of the NMs as well as that of the contaminant. For example, Wang et al. [26] proved that Au

NPs were stable in MilliO water and a buffer; however, this stability was lost at pHs of 4, 7, 8 and 10. In addition, Tan et al. [27] proved that different synthetic methods influenced the thermal stability of Cu NPs. To the best of our knowledge, no comprehensive studies exist in the literature regarding the influence of the parameters shown above on the nanobioremediation of contaminants. Proper experimental designs should be applied to determine, for example, to what extent temperature and pH affect the synergistic effect of NMs and living organisms for the remediation of contaminants.

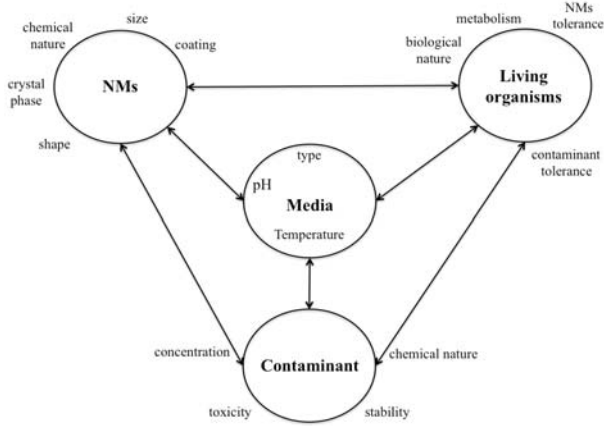


Figure 1. Different parameters influence the interaction of nanomaterials (NMs) and living organisms with the contaminants. Two-way arrows represent interactions.

Figure 2 displays some of the expected effects of the physicochemical interactions of NMs, contaminants, and biota. Once NPs and biota interact, different events may occur including dissolution, absorption, and biotransformation [28]. All events previously mentioned may participate in the degradation of the contaminants. In this case, metabolism is also involved. NPs may be either toxic or stimulant to living organisms and this results in a biocidal effect or a biostimulant effect, which may affect the performance of the organisms involved in the remediation process. Thus, the advantage of using both, NPs and living organisms, is the potential synergistic effect.

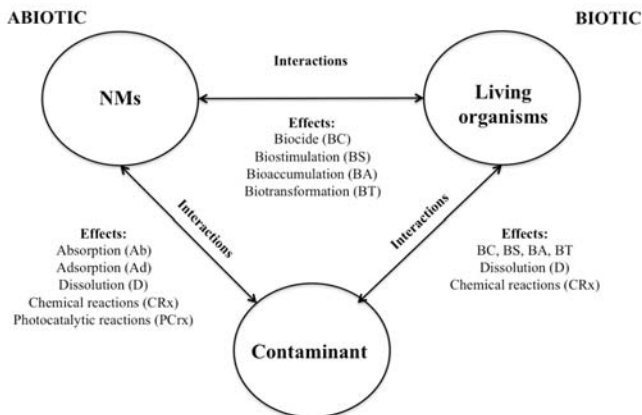


Figure 2. Different phenomena occur as a result of the physical, chemical, and biochemical interactions of NMs, living organisms, and contaminants during nanobioremediation processes.

In nanobioremediation, sorption processes are essential. Sorption involves adsorption and absorption. In the first one, the interaction between the pollutant and the sorbent occurs at a surface level. Conversely, in the second one, the pollutant penetrates deeper layers of the sorbent to form a solution [29]. Moreover, a further distinction can be made. Chemisorption and physisorption are distinguished because, in the first one, a chemical reaction occurs, while in the second case only physical forces are involved. Whatever the case, in sorption, the contaminants may be immobilized, sequestered, and concentrated [29].

A significant amount of research has been performed to understand the nature of the adsorption processes using NMs [30–32]. Thus, mechanistic, thermodynamic, and kinetic studies are essential for describing the behavior of the nanomaterial when this material enters into contact with the contaminants. Some authors explicate several models that describe the behavior of including the biological matrix in remediation processes, i.e., the Freundlich and Temkin Isotherms, and the Langmuir and Dubinin–Radushkevich models [33–36].

Depending on the nature of the NMs, contaminants may be degraded by photocatalytic processes. The resultant products may be further biotransformed by the biotic systems and reduce the pollutant concentration in the media. In addition, some enzymes produced by living organisms may degrade a variety of contaminants [37].

Due to their size, NPs may even enter contaminated zones where other entities are not able to do so. Therefore, nanobioremediation technologies may extend their application fields [38]. This aspect represents an advantage over other remediation techniques. However, other considerations are necessary, for example, the standardization of protocols to evaluate the toxicity of nanoparticles and nanomaterials in soil and water, elucidation of their interactions with biotic and abiotic elements, and the applicable regulatory frame where these materials could be applied [39]. In conclusion, the selection of the NPs and the living organism represents a challenge and is an area of opportunity for further research in terms of the medium and long-term effects of the synergistic use of nanomaterials and biotechnologies, the collateral effects of NMs and NPs on microorganisms, and the trophic transfer of NMs in the food chain and the effects on human health.

3. Nanomaterials and Nanoparticles Used in Bioremediation

As it was mentioned, several NMs have been successfully used for the bioremediation of contaminated systems and to remove several contaminants under different conditions. Herein, we present a summary of the types of NMs with the best efficiencies during the degradation of pollutants (Table 1); in the table are also mentioned the organisms or biological systems used in the experiments. The removal performance of these NMs was measured under laboratory conditions due to the current restrictions for applying these treatments in the field; some remarks regarding the regulatory frame for their field application are done in Section 6.

Table 1. Removal of pollutants mediated by nanoparticles and bio-based treatments.

Type of Nanomaterial	Organisms or Biological Systems Used	Chemical Presentation	System Where It Was Used	Pollutants Degraded	Removal Efficiency	Reference
Nanocrystals	Enzymatic degradation by bacterially overexpressed organophosphorus hydrolase	Zinc sulfide (ZnS)	Water	P-nitrophenol and acid orange 7	>80%	[40]
Nanoparticles	<i>Sphingomonas</i> sp.	Nanoscale zero-valent iron (nZVI); Ti, Mn, Ag, Au	Water	Decarboxinated diphenyl ether; chlorinated hydrocarbons, pathogens	67% for diphenyl ether; >76.8% for chlorinated hydrocarbons	[41]
Nanopowders	Soil microorganisms	Iron oxide nanopowder	Water	Azo dye direct red 23.	98%	[42]
Nanomembranes	A biological extract of <i>Cynorhizum cocineum</i> L.	Thin film composite polyamide	Industrial wastewater	Cyanide compounds	~20%	[32]
Nanocomposites	<i>Arthrobacter globiformis</i> D47	Microorganism-immobilized nanocellulose composites	Water	Herbicide (diuron)	>90%	[43]
Nanotubes	enzyme organophosphate hydrolase-MWNT paper	Unzipped carbon nanotube (CNT), single-walled CNT, and multi-walled CNT	Water and Soil	Organophosphates and heavy metals	~22%	[44,45]
Nano sponge	two organo-clays (Dellite 67G and Dellite 43 B)	Cyclodextrin-based, highly cross-linked polymers	Soil	Triclopyr (3,5,6-Trichloro-2-pyridinyloxyacetic acid)	92%	[46]

Different NMs have been tested to determine their potential in reducing contaminants with the aid of living organisms. Further criteria may be applied for more specificity such as (a) nano iron and its derivatives; (b) dendrimers; (c) carbon-based NMs; (d) single-enzyme NPs; (e) engineered polymeric; (f) biogenic uraninite; and (g) metals other than iron [5]. The selection of the type of NM would depend upon the nature of the contaminant. For example, magnetite, a nano iron material is used to separate heavy metals in soils or water through its magnetic properties. Besides, carbon-based NMs are used to trap organic pollutants or heavy metals from water, soil or air.

As previously mentioned, the type of organism is also important. Plants display certain advantages over microbial organisms. For example, they produce several molecules that are involved in the transformation of pollutants. These include glutathione [47], flavonoids [48], reactive oxygen species [49] and bioactive molecules that act as a response under stress [50]. Besides, plants are easier to cultivate and handle than other organisms that need continuous nutrient supply as well as more controlled conditions.

It is important to take into consideration that NPs not only aid in the remediation process. They also serve for the detection of contaminants and, in consequence, for pollution prevention.

4. Biological Response during the Combined Application of Nanomaterials and Bioremediation

Bioremediation studies have demonstrated that bacteria and plants are capable of immobilizing metals and transforming both organic and inorganic contaminants. During recent years, there have been promising positive results of the combined use of NMs and bioremediation technologies to eliminate contaminants from the environment.

Table 2 shows relevant experiments where this novel approach was used.

Table 2. Successful cases of bioremediation based on nanobiotechnologies.

Treatment	Brief Description of the Achievement	Reference
Hybrid treatment method using nZVI- <i>Sphingomonas</i> sp. PH-07	Effective for degradation of PBDEs through reductive debromination followed by biological oxidation. This method may lead to a remediation strategy for highly halogenated environmental pollutants.	[41]
<i>Rhodococcus rhodochlorus</i> DSM6263 and Fe ₃ O ₄ NP	Given the much easier separation by a magnetic field and high degradation efficiency, this study provided a promising technique for improving biocatalysts for chlorophenols in wastewater.	[51]
nZVI, and nZVI combination with a second metal or microorganisms	There is a high remediation efficiency (78–99%) of PCB with rapid reaction time.	[52]
Bimetallic iron-based NPs and tobacco plants.	27% of the total hexabromocyclododecane (HBCD) was removed from polluted soil.	[53]
Polyvinylpyrrolidone (PVP)-coated iron oxide NPs and <i>Halomonas</i> sp.	The combined approach improved metal removal and shortened metal remediation times (approx. 100% removal of Pb after 24 h, of Cd after 48 h).	[54]

It is important to mention that living organisms respond in a different way, according to the environmental conditions, type of contaminant and NM used. The application of NMs in bioremediation processes can be executed simultaneously or in a separated way, for instance, Kim et al. [41] evaluated the effect of a sequential nano-bio treatment using nZVI and diphenyl ether in combinations with bacteria *Sphingomonas* sp. PH-07 in the degradation of polybrominated diphenyl ethers (PBDEs). They found that PH-07 was able to grow in nZVI concentrations up to a high concentration of 5 g L⁻¹ and participate in the biodegradation of PBDEs and other prospective metabolites. Moreover, the combination of nZVI nanomaterials with electrokinetic remediation, chemical oxidation, and bioremediation has been helpful in the remediation of heavily polluted sites [55]. They discussed a two-step treatment

consisting of nZVI-aided dechlorination followed by biosurfactant-enhanced soil washing technology to remove polychlorinated biphenyls (PCBs) from soil contaminated by a transformer oil. It was found that besides direct dechlorination, nZVI greatly enhanced the soil washing efficiency by reducing the interfacial tension between the oil and soil phases, and 90% of PCBs were removed. The combination of surfactants, electrokinetic treatments, or nZVI has been used as pretreatment in the bioremediation of nitrate anions, heavy metals, pesticides, polychlorinated biphenyls (PCBs), chlorinated volatile organic compounds (cVOCs), and radionuclides [56,57]. However, natural organic matter (NOM) such as fulvic and humic acids affect nZVI reactivity towards pollutants because of the competition between NOM and pollutants for the surface reactive sites on nZVI where the reaction occurs.

Other toxic compounds, such as polychlorinated biphenyls (PCBs), represent a global environmental problem because of their persistence, long-range atmospheric transport, difficult and slow degradation, and bioaccumulation. NPs catalyzed Fenton or Fenton-like, and persulfate activation can provide some useful technologies for the nanobioremediation of PCB-polluted soils. Le et al. [58] developed a nano/bio treatment for the dehalogenation of Aroclor 1248 using the bimetallic nanoparticles Pd/nFe and *Burkholderia xenovorans* LB400. The dehalogenation efficiencies of tri-, tetra-, penta-, and hexachlorinated biphenyls were 99%, 92%, 84%, and 28%, respectively. Therefore, the toxicity of the residual PCBs in terms of toxic equivalent values decreased from 33.8×10^{-5} to 9.5×10^{-5} $\mu\text{g/g}$ after the integrated remediation system. These degradation rates are similar to those reported by other authors [52,55]. However, it has been stated that NMs do not provide any benefit in the context of bioaugmentation, since they inhibit the microbial population in polluted environments [59,60]. It has to be stated that NMs could decrease the diversity and abundance of microbial communities in soil or water but, after some days, these characteristics are recovered. Besides, NMs could also reduce the concentration of enzymes involved in ecological processes, but these increased again after the first days of the experiments. It suggests that NMs have a priming effect at the onset of the studies, but the ecological balance comes back again after some days due to their resilience.

Nevertheless, new evidences are emerging using carbon nanotubes (CNT) and *Arthrobacter* sp. to degrade PCBs. Pereira et al. [61] conducted a natural dye decolorisation, using CNT as redox mediators on anaerobic dye reduction. It was demonstrated that the batch reactor with CNT had the highest biodegradation rate as compared to other carbon nanomaterials.

However, it has been stated that high CNT concentrations reduced the biodegradation rate by inhibiting bacterial growth and microbial activity, while low CNT concentrations increased the biodegradation rate by stimulating bacterial growth and the overexpression of degradation genes [62]. The use of NM could mitigate the limitations regarding immobilization and entrapment of microorganisms during bioaugmentation strategies because of the large surface area [59]. Hou et al. [51] tested the biodegradation of chlorophenol in a 100-mL batch reactor using *Rhodococcus rhodochrous* immobilized in magnetic NPs. The cells were immobilized by using k-carrageenan and Fe_3O_4 NPs and it was proved that they were able to degrade 2-chlorophenol, 4-chlorophenol, 2,3-dichlorophenol and their mixture; these cells performed 30% higher removal efficiency compared to free cells. Although the use of NM for bioaugmentation purposes is still in an early stage, the above-reviewed research mostly based on laboratory scale highlights the potential of nanotechnology for this technique. On the other hand, it should be noted that most of the NM utilized for enhanced adsorption are metals that may pose human or environmental health risks in the long run [63].

The combined effect of phyto- and nanoremediation was tested by Le et al. [53] when comparing the removal efficiency of hexabromocyclododecane in both soil and water. Bimetallic iron-based nanoparticles were used to evaluate their degradative action on HBCF. The effect on humic acids (HAs) and tobacco plants was determined as well.

It was observed that the 99% of the total HBCD (15 mM) was transformed by Pd/nFe (1 g/L) within 9 h of treatment; when HAs were added to the aqueous solution, the removal of the contaminant was increased. In the soil system, the treatments consisted of plant only, plant with HAs, plant with

NPs and, plant with HAs and NPs, obtaining 13%, 15%, 41% and 27% HBCD removal, respectively, compared to the HBCD removal in an unplanted soil.

The 221–298 ng/g of HBCD were detected inside the plant after treatment and the authors concluded that HAs influenced the bioaccumulation in plants; according to Tejada et al., the HAs can accelerate the degradation of organic pollutants by increasing their solubility and enhancing their diffusive mass transfer, promoting their bioavailability to microorganisms. HAs can also act as an electron transfer mediator in the chemical reduction of organic pollutants [64], therefore the humic acids would be a good supplement for bioremediation of polluted soils.

In a seminal work, Cao et al. [54] demonstrated that polyvinylpyrrolidone-coated iron oxide NPs were beneficial for the removal of metals i.e., Cd (II) and Pb (II) by interaction with the Gram-negative bacteria *Halomonas* sp. The treatments consisted in a combined approach involving bacteria and NPs, bacteria only, and NPs only.

The results showed that for the combined approach, 100% of the Cd originally aggregated was removed after 24 h and the same percentage of Cd was eliminated after 48 h. For the treatments with Ns only, the removal of 60% and 80% for Cd and Pb, respectively, was observed. When the metal removal in the presence of *Halomonas* sp. only was estimated, the removal of Cd increased to 80%, contrarily to the same treatment for Pb, where the same removal as that for NPs was observed i.e., 80%.

Cd, Pb and Fe (from NPs) were analyzed in the following bacterial components: extra polymeric substances (EPS), and it was observed that EPS was most important in metal removal, and that there was a significant promotion of Cd intracellular transportation, but not Pb, by NPs. A reduced Pb internalization was identified that may have resulted from EPS acting as an uptake barrier coupled with an effective efflux system of *Halomonas* sp. as a resistance mechanism. Besides the beneficial effects of this combined approach, the authors suggested further and more pointed investigation.

Kumari and Singh [22] demonstrated that NMs are useful as facilitators in the bioremediation of pollutants either by enhancing microbial growth, immobilizing remediating agents or through induced production of remediating microbial enzymes. In a similar study it was demonstrated that NMs induced the production of microbial biosurfactants, improving contaminant solubility and thereby generating a conducive environment for the bioremediation of these compounds [65]. These NMs–biosurfactant interactions could be used through biostimulation techniques i.e., nanobiostimulation techniques. It has to be stated that biostimulation techniques have the potential to efficiently dissipate pollutants from soil or water under eco-friendly, fast, and inexpensive procedures.

Besides, iron oxide NPs coated with polyvinylpyrrolidone (PVP) were used in the bioremediation of sediments from a contaminated river using bacteria of the genus *Halomonas* [66]. They also demonstrated that PVP was effective in transforming labile Cd and Pb to stable fractions, with the decrease of the mobility of metals. Besides, urease and catalase activities were enhanced showing certain degrees of recovery in sediment metabolic functions.

Torres-Martínez et al. [40] explained four steps in the mechanisms of degradation of p-nitrophenol (pNP) using ZnS nanocrystals in water. The first part is the excitation of the glutathione (GSH)- or L-cysteine (Cys)-ZnS nanocrystals with bandgap energy irradiation leading to charge separation, the promotion of electrons into the conduction band, and the formation of positive holes in the valence band. The second step involves the migration of electron–hole pairs to the surface of the nanocrystals, which is facilitated by the small particle size. The third step is the formation of highly reactive hydroxyl radicals in aqueous medium. The fourth and last part is the ring-opening caused by a nonspecific reaction of the hydroxyl radicals with the double-bond structures of pNP.

Hou et al. [51] described the mechanisms involved in the degradation of chlorophenols in a batch reactor using *R. rhodochrous* DSM6263 immobilized in k-carrageenan with magnetic NPs. The first step was the hydroxylation at the ortho positions of the chlorophenolic rings, which formed chlorocatechols. DSM6263 strain biodegraded CPs via the constitutively expressed enzymes [51], and degraded aniline and phenol to catechol via the β -ketoacid pathway. However, no further metabolization of cis, cis-muconic acid occurred. It has been proven that different microbial strains can naturally degrade the

same pollutants through different ways, such as *Rhodococcus* sp. AN-22 by using the phenol metabolic pathway, integrated by CatA (catechol 1,2-dioxygenase), CatB (cis, cis-muconate cycloisomerase) and CatC (muconolactone isomerase) to degrade aniline [67].

Pereira et al. [61] performed experiments where the effect of carbon-based materials (CBM) as a redox mediator on dye biodegradation was evaluated. CNT were used to evaluate the biodegradation kinetics of the anaerobic discoloration of different classes of azo dyes including acid (AO10), mordant (MY10), and reactive (RR120). It is worth mentioning that the anaerobic color removal rate is related to the number of azo bonds in the dye molecule, while the reduction rates are affected by changes in electron density in the azo group region. Therefore, the substitution of electron-withdrawing groups ($-\text{SO}_3\text{H}$, $-\text{SO}_2\text{NH}_2$) in the para position of the phenyl ring concerning the azo bond, improves the reduction rate. On the other hand, electron-withdrawing groups ($-\text{OH}$ and $-\text{NH}_2$) decrease the electron density close to the azo bond, making possible the reduction process. Besides, hydrogen bonding has a significant effect on the rate of reduction in the region of the azo bond [68]. Color removal was associated with the azo bond cleavage. The final products were sulfanilic acid (SA) and 5-aminosalicylic acid (5-ASA), as witnessed by high-performance liquid chromatography (HPLC). These compounds were biodegraded under aerobic conditions via the enrichment cultures during the batch experiment [69].

Various types of NPs are being used to increase the microbial degradation of pollutants [22]. However, avoiding the unintentional release of NPs in the environment is very crucial for maintaining a sustainable ecosystem. Further research on bioaccumulators and toxicokinetics of NP must be executed to prevent adverse effects on flora and fauna [22].

5. Current and Future Development of Environmental Nanoapplications Based on Molecular Biotechnology

In addition to the mentioned nanotechnology applications in environmental biotechnology, innovations may emerge from other fields of nanotechnology that move at a faster pace, for example, medical nanotechnology.

Nanostructure functionalization with biomolecules is an area worth exploring. This approach has been tested with state-of-the-art experimental designs inspired by natural molecular phenomena. For example, in [70] were designed membranes harboring amyloid proteins and activated porous carbon for heavy-metals removal/recovery. Inspired by the detrimental amyloid protein formation in neurons, these authors changed the tertiary structure of milk proteins to create amyloid fibrils capable of capturing different ions by the cysteine moieties. This research highlighted the importance of finding a cheap source of biomolecules as a key to this type of development. Additionally, natural proteins display several advantages. For example, they can be produced through well-established recombinant technologies in a cost-effective manner and can harbor 20 different amino acids that provide a large combinatorial capacity to interact with other molecules, as well as create new catalytic surfaces and structures [71].

Biotechnology can also help to provide ecofriendly methodologies for NPs functionalization. Gao et al. [72] have recently introduced the bacteria *Komagataeibacter sucrofermentans* in the biological toolbox to produce novel cellulose-like polymers functionalized with custom moieties. These bacteria are cultured with traditional bioreactor methodologies and fed with glucose monomers ornamented with the desired chemical modifications resulting in their biological incorporation in the polymer. This strategy bypasses the use of complex solvents, stoichiometry, and the production of environmentally dangerous residues. The optimization of this biosystem by classic and next-generation biotechnological modifications (mutagenesis, protein engineering or gene editing) holds a great potential to simplify the synthesis of a large amount of cellulose-based NMs with several applications [73].

Recent developments in the field of RNA-based fungicides indicate that it is a feasible technology for substituting traditional biochemical fungicides. Double-strand RNAs, designed to hybridize with vital mRNAs of fungal pathogens, are sprayed on leaves or fruits and induce expression silencing in

the pathogen [74]. However, the short mean-life of naked RNAs in the environment is an obstacle to overcome [74]. Traditional clay nanosheets were tested as protectants of double-strand RNA and probed to enhance the mean-life of the biomolecules and extend the biocidal actions against the fungal pathogen [75]. Although this technology was created for the protection of aerial plant organs, it has recently been applied in root protection. Chariou et al. [76] tested several nanoscale encapsulated architectures that ranged from traditional silica particles to recombinant or plant-produced virus capsules. The proof-of-concept was carried out with a nematicide and the biologically derived capsules proved superior in soil penetration and cargo release. These bionanoparticles are biodegradable and leave behind no organic pollution, truly earning the label of ecofriendly. It is expected that this field will highly benefit from next-generation NPs biofunctionalization.

The 3D construction of DNA structures through DNA hybridization constitutes a frontier research area largely unexplored in environmental biotechnology. The relatively simple, yet malleable, rules of recognition between nucleotides of different strands of DNA can be applied to build several geometric arrangements (“molecular origami”), from simple crossover tiles up to polyhedral meshes [77]. These architectures provide a new toolbox for functionalization, as illustrated by the work of DNA nanorobots that can be loaded with intractable molecules (other DNAs/RNAs or proteins) that serve as cargo, fasteners or springs. In [78] is described the design of DNA sheets that interact with the protein thrombin that becomes compartmentalized when other DNA molecules seal the nanosheet, acting as fasteners. The DNA origami, now turned into a nanotube, will only open when a key is found, in this case a tumor-produced protein named nucleolin, releasing the thrombin cargo and inducing coagulation and necrosis of the tumor. This development demonstrated the programmable and complex mechanics that biomolecular-based biorobots could achieve. Although this is a development aimed at biomedicine, it provides an outstanding example of biomolecular interactions that can be extended to environmental applications like next-generation pesticides or the elimination of antibiotic-resistant super-bacteria.

A concern of DNA origami arrangements is cost. Recently, in [77] were reviewed biotechnological options to reach the economic feasibility of DNA/RNA production such as chip synthesis, recombinant bacteria and naturally occurring bacteria able to export RNAs.

Another example of sophisticated codification of nanotechnology to obtain remote information is the work of Koman et al. [79], where a decision diagram was chemically coded with inorganic molecules to detect and irreversibly inform the presence of analytes in the air, such as soot, ammonia and triethylamine. Other inorganic sensors have been developed to trace abiotic particles, like nanoplastics [80]; this concept can be extended to incorporate biomolecules to follow the path of cells in wastewater facilities, or immunedetectable pollutants, tasks currently performed by costly and complicated assays like DNA sequencing and HPLC. Inorganic sensors can also code their self-precipitation through photoinduction and ion changes in their environment [81]; in biology, several proteins have more versatile photoresponsive characteristics that provide materials with novel capabilities, for example, CarH bacterial transcription factor [82] or plant/fungal LOV domains [83].

Molecular biotechnology has also been proposed for large-scale applications such as water desalination. More than a decade ago, Kumar et al. [84] tested the incorporation of the bacterial protein aquaporin Z into polymeric membranes and demonstrated that it could exclude salt and yield purified water. With modern protein modeling algorithms and molecular biology techniques, this approach was optimized to produce porin proteins with enhanced exclusion activities for both organic and inorganic water solutes [85]. An emerging field is the technological use of oxygen-sensitive proteins present in humans and plants to develop O₂ biosensors and inducible genetic circuits; originally thought to be for in vivo applications, they can be adapted to prepare functional NMs able to stoichiometrically respond to O₂ levels [86]. These concepts, explored with proteins, have also been demonstrated with DNA molecules able to exclude complex analytes such as proteins and open a wide area of sensing and purification opportunities [87]. Recently, Ryu et al. [88] and Álvarez et al. [89] reviewed the field of transmembrane proteins incorporated into membranes and their coupling to different transducers and applications in gas monitoring, pesticide detection, microarrays, and energy harvesting.

In the future, enzymes may be incorporated in the above-discussed arrangements to monitor more complex pollutants or their combinations. This concept is used in healthcare monitoring where biosensors have been fixed in a plethora of materials like patches, temporary tattoos or wrists, among others [90]. It should be noticed that the large economic market of diabetes management drives these innovations. However, the protection of workers doing dangerous tasks in radioactive, potentially toxic, or enclosed areas can benefit from the development of real-time monitoring bionanotechnologies.

6. International Markets and Regulations of Nanotechnologies Applied in Bioremediation

Nanotechnologies used in bioremediation processes are expected to drive the technological evolution for the improvement of the environmental quality in developed and emerging countries [91,92]. A significant amount of research has been performed to determine the mechanisms of decontamination and remediation [93].

As it has been discussed previously, the biosafety related to the use and application of nanomaterials is a high concern due to the lack of knowledge and validated protocols to measure the impact of these materials on human health, loss of biodiversity [94] and bioaccumulation [95], and transport of NMs in trophic chains [96]. Diverse international institutions such as USEPA, European Observatory for Nanomaterials (EON), the OECD Working Party on Manufactured Nanomaterials (WPMN) and ISO Technical Committee TC 229 “Nanotechnologies” have established international cooperation in order to increase the application of available regulations [97,98].

Furthermore, nanotechnology and bioremediation world markets are expected to continue growing and developing new niches to improve not only environmental aspects but also human lifestyle [99].

The global nanotechnology market is expected to exceed US\$125 billion by 2024; this sector continues to have an impact on other markets, fundamentally in electronics, energy, biomedical, cosmetics, defense, energy and agriculture [100] and, according to the US-EPA it is estimated that bioremediation and phytoremediation technologies could have an annual growth of US\$1.5 billion per year [101]. The development of new methodologies and incorporation of nanotechnologies will expand new opportunities for treating sewage, lakes, rivers, and ponds, among others, creating new consumers and strengthening world trade [102].

7. Conclusions

The synergy between NPs and microorganisms for the degradation of some contaminants has been proven in batch experiments, however, there is still a lack of knowledge about the synergetic effect of nanoparticles and biotechnologies during a nanobioremediation process and how these combined technologies respond to contaminants of a diverse nature. It should be noted that, to the best of our knowledge, no safety data on the long-term use of NPs with microorganisms has been provided. Bionanoparticles present various advantages over metallic NPs, such as their biodegradability producing less impact on the environment. Current nanotechnologies could be used in remediation processes for decontaminating soil, air, or water, but, more cost-effective methods of production should arise.

An important issue concerning the use of these types of materials is the regulatory framework. Scientists could contribute to the understanding of the interactions of NMs and bio-based technologies during remediation processes under variable environmental conditions and, as a consequence, offer arguments for better regulation.

Finally, nanobioremediation might enormously contribute to sustainability because it offers environmental advantages and is cheap when compared to other technologies; even more the range of applications of NMs, coupled with biological treatments, has demonstrated high effectivity in the degradation of contaminants, which provides new possibilities to face environmental challenges.

Author Contributions: All authors contributed to planning and writing the paper. All authors have read and agreed to the published version of the manuscript.

Funding: J.M.P.-C. thanks CONACYT-CB for financially supporting this research (Grant 287137).

Acknowledgments: E.V.-N. and C.E.M.-G. thank the Universidad de Guanajuato for all the support and facilities to develop this work. E.V.-N. thanks especially the support of BVF for her patient technical support during the preparation of this manuscript.

Conflicts of Interest: The authors declare no conflict of interest.

References

1. Wuana, R.A.; Okieimen, F.E. Heavy Metals in Contaminated Soils: A Review of Sources, Chemistry, Risks and Best Available Strategies for Remediation. *ISRN Ecol.* **2011**, *1*, 1–20. [[CrossRef](#)]
2. Azubuike, C.C.; Chikere, C.B.; Okpokwasili, G.C. Bioremediation techniques—classification based on site of application: Principles, advantages, limitations and prospects. *World J. Microbiol. Biotechnol.* **2016**, *32*, 180. [[CrossRef](#)] [[PubMed](#)]
3. Tanzadeh, J.; Ghasemi, M.F.; Anvari, M.; Issazadeh, K. Biological removal of crude oil with the use of native bacterial consortia isolated from the shorelines of the Caspian Sea. *Biotechnol. Biotechnol. Equip.* **2020**, *34*, 361–374. [[CrossRef](#)]
4. Mapelli, F.; Scoma, A.; Michoud, G.; Aulenta, F.; Boon, N.; Borin, S.; Kalogerakis, N.; Daffonchio, D. Biotechnologies for Marine Oil Spill Cleanup: Indissoluble Ties with Microorganisms. *Trends Biotechnol.* **2017**, *35*, 860–870. [[CrossRef](#)] [[PubMed](#)]
5. Rizwan, M.D.; Singh, M.; Mitra, C.K.; Morve, R.K. Ecofriendly Application of Nanomaterials: Nanobioremediation. *J. Nanopart.* **2014**, *1*, 1–7. [[CrossRef](#)]
6. Yogalakshmi, K.N.; Das, A.; Rani, G.; Jaswal, V.; Randhawa, J.S. Nano-bioremediation: A New Age Technology for the Treatment of Dyes in Textile Effluents. In *Bioremediation of Industrial Waste for Environmental Safety*; Springer: Singapore, 2020.
7. De Gisi, S.; Minetto, D.; Lofrano, G.; Libralato, G.; Conte, B.; Todaro, F.; Notarnicola, M. Nano-scale Zero Valent Iron (nZVI) treatment of marine sediments slightly polluted by heavy metals. *Chem. Eng. Trans.* **2017**, *60*, 139–144.
8. Bharagava, R.N.; Saxena, G.; Mulla, S.I. Introduction to Industrial Wastes Containing Organic and Inorganic Pollutants and Bioremediation Approaches for Environmental Management. In *Bioremediation of Industrial Waste for Environmental Safety*; Springer: Singapore, 2020.
9. Cecchin, I.; Reddy, K.R.; Thomé, A.; Tessaro, E.F.; Schnaid, F. Nanobioremediation: Integration of nanoparticles and bioremediation for sustainable remediation of chlorinated organic contaminants in soils. *Int. Biodeterior. Biodegrad.* **2017**, *119*, 419–428. [[CrossRef](#)]
10. Avio, C.G.; Gorbí, S.; Regoli, F. Plastics and microplastics in the oceans: From emerging pollutants to emerged threat. *Mar. Environ. Res.* **2017**, *128*, 2–11. [[CrossRef](#)]
11. Alimi, O.S.; Farner Budarz, J.; Hernandez, L.M.; Tufenkji, N. Microplastics and nanoplastics in aquatic environments: Aggregation, deposition, and enhanced contaminant transport. *Environ. Sci. Technol.* **2018**, *52*, 1704–1724. [[CrossRef](#)]
12. Sousa, J.C.G.; Ribeiro, A.R.; Barbosa, M.O.; Pereira, M.F.R.; Silva, A.M.T. A review on environmental monitoring of water organic pollutants identified by EU guidelines. *J. Hazard. Mater.* **2018**, *344*, 146–162. [[CrossRef](#)]
13. Thompson, L.A.; Darwish, W.S. Environmental chemical contaminants in food: Review of a global problem. *J. Toxicol.* **2019**. [[CrossRef](#)] [[PubMed](#)]
14. Jeon, J.R.; Murugesan, K.; Baldrian, P.; Schmidt, S.; Chang, Y.S. Aerobic bacterial catabolism of persistent organic pollutants—Potential impact of biotic and abiotic interaction. *Curr. Opin. Biotech.* **2016**, *38*, 71–78. [[CrossRef](#)] [[PubMed](#)]
15. Zhu, X.; Chen, B.; Zhu, L.; Xing, B. Effects and mechanisms of biochar-microbe interactions in soil improvement and pollution remediation: A review. *Environ. Pollut.* **2017**, *227*, 98–115. [[CrossRef](#)] [[PubMed](#)]
16. Hurtado, C.; Montano-Chávez, Y.N.; Domínguez, C.; Bayona, J.M. Degradation of emerging organic contaminants in an agricultural soil: Decoupling biotic and abiotic processes. *Water Air Soil Pollut.* **2017**, *228*, 243. [[CrossRef](#)]
17. Kang, J.W. Removing environmental organic pollutants with bioremediation and phytoremediation. *Biotechnol. Lett.* **2014**, *36*, 1129–1139. [[CrossRef](#)]

18. Fulekar, M.H.; Pathak, B. *Environmental Nanotechnology*, 1st ed.; CRC Press: Boca Raton, FL, USA, 2017; pp. 140–157.
19. Kuppusamy, S.; Thavamani, P.; Venkateswarlu, K.; Lee, Y.B.; Naidu, R.; Megharaj, M. Remediation approaches for polycyclic aromatic hydrocarbons (PAHs) contaminated soils: Technological constraints, emerging trends and future directions. *Chemosphere* **2017**, *168*, 944–968. [[CrossRef](#)]
20. Srivastava, S.; Shukla, A. Emerging aspects of bioremediation of arsenic. In *Green Technologies and Environmental Sustainability*, 1st ed.; Singh, R., Kumar, S., Eds.; Springer: Cham, Switzerland, 2017; Volume 1, pp. 395–407.
21. Fernández, P.M.; Viñarta, S.C.; Bernal, A.R.; Cruz, E.L.; Figueroa, L.I.C. Bioremediation strategies for chromium removal: Current research, scale-up approach and future perspectives. *Chemosphere* **2018**, *208*, 139–148. [[CrossRef](#)]
22. Kumari, B.; Singh, D.P. A review on multifaceted application of nanoparticles in the field of bioremediation of petroleum hydrocarbons. *Ecol. Eng.* **2016**, *97*, 98–105. [[CrossRef](#)]
23. Koul, B.; Taak, P. Chemical methods for soil remediation. In *Biotechnological Strategies for Effective Remediation of Polluted Soils*, 1st ed.; Koul, B., Taak, P., Eds.; Springer: Singapore, 2018; Volume 1, pp. 77–84.
24. El-Ramady, H.; Alshaal, T.; Abowaly, M.; Abdalla, N.; Taha, H.S.; Al-Saeedi, A.H.; Shalaby, T.; Amer, M.; Fári, M.; Domokos-Szabolcsy, É.; et al. Nanoremediation for Sustainable Crop Production. In *Nanoscience in Food and agriculture*, 1st ed.; Ranjan, S., Dasgupta, N., Lichtfouse, E., Eds.; Springer: Singapore, 2017; Volume 1, pp. 335–363.
25. Tan, W.; Peralta-Videa, J.R.; Gardea-Torresdey, J.L. Interaction of titanium dioxide nanoparticles with soil components and plants: Current knowledge and future research needs—a critical review. *Environ. Sci. Nano* **2018**, *5*, 257–278. [[CrossRef](#)]
26. Wang, A.; Ng, H.P.; Xu, Y.; Li, Y.; Zheng, Y.; Yu, J.; Han, F.; Peng, F.; Fu, L. Gold nanoparticles: Synthesis, stability test, and application for the rice growth. *J. Nanomater.* **2014**, *1*, 1–6. [[CrossRef](#)]
27. Tang, H.; Chen, X.; Niu, Y.W.; Luo, X.; Wang, Z.; Chen, M.; Shi, G. Thermal stability characteristics of in situ nano-particles formed in metal melt. *Mater. Lett.* **2016**, *162*, 261–264. [[CrossRef](#)]
28. Taylor, A.; Wilson, K.M.; Murray, P.; Fernig, D.G.; Lévy, R. Long-term tracking of cells using inorganic nanoparticles as contrast agents: Are we there yet? *Chem. Soc. Rev.* **2012**, *41*, 2707–2717. [[CrossRef](#)] [[PubMed](#)]
29. Vieira, R.H.S.F.; Volesky, B. Biosorption: A solution to pollution? *Int. Microbiol.* **2000**, *3*, 17–24.
30. Hu, Z.G.; Zhang, J.; Chan, W.L.; Szeto, Y.S. The sorption of acid dye onto chitosan nanoparticles. *Polymer* **2006**, *47*, 5338–5842. [[CrossRef](#)]
31. Wang, Y.; Morin, G.; Ona-Nguema, G.; Juillot, F.; Calas, G.; Brown, G.E. Distinctive arsenic(V) trapping modes by magnetite nanoparticles induced by different sorption processes. *Environ. Sci. Technol.* **2011**, *45*, 7258–7266. [[CrossRef](#)]
32. Sebeia, N.; Jabli, M.; Ghith, A.; Saleh, T.A. Eco-friendly synthesis of *Cynomorium coccineum* extract for controlled production of copper nanoparticles for sorption of methylene blue dye. *Arab. J. Chem.* **2019**, *13*, 4263–4274. [[CrossRef](#)]
33. Pathak, P.D.; Mandavgane, S.A.; Kulkarni, B.D. Fruit peel waste as a novel low-cost bio adsorbent. *Rev. Chem. Eng.* **2015**. [[CrossRef](#)]
34. Matouq, M.; Jildeh, N.; Qtaishat, M.; Hindiyeh, M.; Al Syouf, M.Q. The adsorption kinetics and modeling for heavy metals removal from wastewater by Moringa pods. *J. Environ. Chem. Eng.* **2015**, *31*, 361–381. [[CrossRef](#)]
35. Dada, A.O.; Ojediran, J.O.; Olalekan, A.P. Sorption of Pb²⁺ from aqueous solution onto modified rice husk: Isotherms studies. *Adv. Phys. Chem.* **2013**, *1*, 1–6. [[CrossRef](#)]
36. Olalekan, A.P.; Dada, A.O.; Okewale, A.O. Comparative adsorption isotherm study of the removal of Pb²⁺ and Zn²⁺ onto agricultural waste. *Res. J. Chem. Environ. Sci.* **2013**, *1*, 22–7. [[CrossRef](#)]
37. Peixoto, R.S.; Vermelho, A.B.; Rosado, A.S. Petroleum-degrading enzymes: Bioremediation and new prospects. *Enzyme Res.* **2011**, *1*, 1–7. [[CrossRef](#)]
38. Sohail, M.I.; Waris, A.A.; Ayub, M.A.; Usman, M.; Zia ur Rehman, M.; Sabir, M.; Faiz, T. Environmental application of nanomaterials: A promise to sustainable future. In *Engineered Nanomaterials and Phytotechnology: Challenges for Plant Sustainability*, 1st ed.; Kumar, V.S., Kumar, D.A., Eds.; Elsevier: Cambridge, MA, USA, 2019; Volume 1, pp. 1–53.

39. Ramírez-García, R.; Gohil, N.; Singh, V. Recent Advances, Challenges, and Opportunities in Bioremediation of Hazardous Materials. In *Phytomanagement of Polluted Sites*, 1st ed.; Chandra, P.V., Baue, K., Eds.; Elsevier: Cambridge, MA, USA, 2019; Volume 1, pp. 517–568.
40. Torres-Martínez, C.L.; Kho, R.; Mian, O.I.; Mehra, R.K. Efficient photocatalytic degradation of environmental pollutants with mass-produced ZnS nanocrystals. *J. Colloid Interface Sci.* **2001**. [[CrossRef](#)] [[PubMed](#)]
41. Kim, Y.M.; Murugesan, K.; Chang, Y.Y.; Kim, E.J.; Chang, Y.S. Degradation of polybrominated diphenyl ethers by a sequential treatment with nanoscale zero valent iron and aerobic biodegradation. *J. Chem. Technol. Biotechnol.* **2012**, *240*, 525–532. [[CrossRef](#)]
42. Kos, L.; Sójka-Ledakowicz, J.; Michalska, K.; Perkowski, J. Decomposition of azo dye C.I. Direct Yellow 86 by the fenton process in the presence of nanoparticles of iron oxides. *Fibres Text. East. Eur.* **2014**, *5*, 114–120.
43. Liu, J.; Morales-Narváez, E.; Vicent, T.; Merkoçi, A.; Zhong, G.H. Microorganism-decorated nanocellulose for efficient diuron removal. *Chem. Eng. J.* **2018**, *354*, 1083–1091. [[CrossRef](#)]
44. Mechrez, G.; Krepker, M.A.; Harel, Y.; Lellouche, J.P.; Segal, E. Biocatalytic carbon nanotube paper: A “one-pot” route for fabrication of enzyme-immobilized membranes for organophosphate bioremediation. *J. Mater. Chem. B* **2014**, *2*, 915–922. [[CrossRef](#)]
45. Fosso-Kankeu, E.; Mulaba-Bafubandi, A.F.; Mishra, A.K. Prospects for Immobilization of Microbial Sorbents on Carbon Nanotubes for Biosorption: Bioremediation of Heavy Metals Polluted Water. In *Application of Nanotechnology in Water Research*, 1st ed.; Mishra, A.K., Ed.; John Wiley & Sons, Inc.: Hoboken, NJ, USA, 2014; Volume 1, pp. 213–235.
46. Baglieri, A.; Nègre, M.; Trotta, F.; Bracco, P.; Gennari, M. Organo-clays and nanosponges for aquifer bioremediation: Adsorption and degradation of triclopyr. *J. Environ. Sci. Health Part B Pestic. Food Contam. Agric. Wastes* **2013**, *48*, 784–792. [[CrossRef](#)]
47. Szalai, G.; Kellos, T.; Galiba, G.; Kocsy, G. Glutathione as an antioxidant and regulatory molecule in plants under abiotic stress conditions. *J. Plant Growth Regul.* **2009**, *28*, 66–280. [[CrossRef](#)]
48. Mierziak, J.; Kostyn, K.; Kulma, A. Flavonoids as important molecules of plant interactions with the environment. *Molecules* **2014**, *19*, 16240–16265. [[CrossRef](#)]
49. Camejo, D.; Guzmán-Cedeño, Á.; Moreno, A. Reactive oxygen species, essential molecules, during plant-pathogen interactions. *Plant Physiol. Biochem.* **2016**, *103*, 10–23. [[CrossRef](#)]
50. Franzoni, G.; Trivellini, A.; Bulgari, R.; Cocetta, G.; Ferrante, A. Bioactive Molecules as Regulatory Signals in Plant Responses to Abiotic Stresses. In *Plant Signaling Molecules*, 1st ed.; Khan, M.I.R., Reddy, P.S., Ferrante, A., Khan, N., Eds.; Woodhead Publishing: Duxford, UK, 2019; Volume 1, pp. 169–182.
51. Hou, J.; Liu, F.; Wu, N.; Ju, J.; Yu, B. Efficient biodegradation of chlorophenols in aqueous phase by magnetically immobilized aniline-degrading *Rhodococcus rhodochrous* strain. *J. Nanobiotechnol.* **2016**, *14*, 5. [[CrossRef](#)] [[PubMed](#)]
52. Jing, R.; Fusi, S.; Kjellerup, B.V. Remediation of Polychlorinated Biphenyls (PCBs) in contaminated soils and sediment: State of knowledge and perspectives. *Front. Environ. Sci.* **2018**, *6*, 79. [[CrossRef](#)]
53. Le, T.T.; Yoon, H.; Son, M.H.; Kang, Y.G.; Chang, Y.S. Treatability of hexabromocyclododecane using Pd/Fe nanoparticles in the soil-plant system: Effects of humic acids. *Sci. Total Environ.* **2019**, *689*, 444–450. [[CrossRef](#)] [[PubMed](#)]
54. Cao, X.; Alabresm, A.; Chen, Y.P.; Decho, A.W.; Lead, J. Improved metal remediation using a combined bacterial and nanoscience approach. *Sci. Total Environ.* **2020**, *704*, 135378. [[CrossRef](#)]
55. Fan, G.; Wang, Y.; Fang, G.; Zhu, X.; Zhou, D. Review of chemical and electrokinetic remediation of PCBs contaminated soils and sediments. *Environ. Sci. Process. Impacts* **2016**, *18*, 1140–1156. [[CrossRef](#)] [[PubMed](#)]
56. Bhattacharya, K.; Mukherjee, S.P.; Gallud, A.; Burkert, S.C.; Bistarelli, S.; Bellucci, S.; Bottini, M.; Star, A.; Fadeel, B. Biological interactions of carbon-based nanomaterials: From coronation to degradation. *Nanomed. Nanotechnol. Biol. Med.* **2016**, *12*, 333–351. [[CrossRef](#)] [[PubMed](#)]
57. De Lima, R.; Seabra, A.B.; Durán, N. Silver nanoparticles: A brief review of cytotoxicity and genotoxicity of chemically and biogenically synthesized nanoparticles. *J. Appl. Toxicol.* **2012**, *32*, 867–879. [[CrossRef](#)] [[PubMed](#)]
58. Le, T.T.; Nguyen, K.H.; Jeon, J.R.; Francis, A.J.; Chang, Y.S. Nano/bio treatment of polychlorinated biphenyls with evaluation of comparative toxicity. *J. Hazard. Mater.* **2015**, *287*, 335–341. [[CrossRef](#)]
59. Nzila, A.; Razzak, S.A.; Zhu, J. Bioaugmentation: An emerging strategy of industrial wastewater treatment for reuse and discharge. *Int. J. Environ. Res. Public Health* **2016**, *13*, 846. [[CrossRef](#)]

60. Amoatey, P.; Baawain, M.S. Effects of pollution on freshwater aquatic organisms. *Water Environ. Res.* **2019**, *91*, 1272–1287. [[CrossRef](#)]
61. Pereira, R.A.; Pereira, M.F.R.; Alves, M.M.; Pereira, L. Carbon based materials as novel redox mediators for dye wastewater biodegradation. *Appl. Catal. B Environ.* **2014**, *393*, 219–226. [[CrossRef](#)]
62. Zhang, C.; Li, M.; Xu, X.; Liu, N. Effects of carbon nanotubes on atrazine biodegradation by *Arthrobacter* sp. *J. Hazard. Mater.* **2015**, *287*, 1–6. [[CrossRef](#)]
63. Fayemiwo, O.M.; Daramola, M.O.; Moothi, K. Btex compounds in water—Future trends and directions for water treatment. *Water SA* **2017**, *43*, 602–613. [[CrossRef](#)]
64. Li, J.; Liu, G.; Zhou, J.; Wang, A.; Wang, J.; Jin, R. Redox activity of lignite and its accelerating effects on the chemical reduction of azo dye by sulfide. *RSC Adv.* **2016**. [[CrossRef](#)]
65. Decesaro, A.; Machado, T.S.; Cappellaro, Â.C.; Reinehr, C.O.; Thomé, A.; Colla, L.M. Biosurfactants during in situ bioremediation: Factors that influence the production and challenges in evaluation. *Environ. Sci. Pollut. Res.* **2017**, *24*, 20831–20843. [[CrossRef](#)] [[PubMed](#)]
66. Xue, W.; Huang, D.; Zeng, G.; Wan, J.; Zhang, C.; Xu, R.; Cheng, M.; Deng, R. Nanoscale zero-valent iron coated with rhamnolipid as an effective stabilizer for immobilization of Cd and Pb in river sediments. *J. Hazard. Mater.* **2018**, *341*, 381–389. [[CrossRef](#)] [[PubMed](#)]
67. Matsumura, E.; Sakai, M.; Hayashi, K.; Murakami, S.; Takenaka, S.; Aoki, K. Constitutive expression of catABC genes in the aniline-assimilating bacterium *Rhodococcus* species AN-22: Production, purification, characterization and gene analysis of CatA, CatB and CatC. *Biochem. J.* **2006**, *393*, 219–226. [[CrossRef](#)] [[PubMed](#)]
68. Beydilli, M.I.; Pavlstathis, S.G.; Tincher, W.C. Biological decolorization of the azo dye reactive red 2 under various oxidation-reduction conditions. *Water Environ. Res.* **2000**, *72*, 698–705. [[CrossRef](#)]
69. Tan, N.C.G.; Prenafeta-Boldú, F.X.; Opsteeg, J.L.; Lettinga, G.; Field, J.A. Biodegradation of azo dyes in cocultures of anaerobic granular sludge with aerobic aromatic amine degrading enrichment cultures. *Appl. Microbiol. Biotechnol.* **1999**, *51*, 865–871. [[CrossRef](#)]
70. Bolisetty, S.; Mezzenga, R. Amyloid-carbon hybrid membranes for universal water purification. *Nat. Nanotechnol.* **2016**, *11*, 365. [[CrossRef](#)]
71. Ljubetič, A.; Lapenta, F.; Gradišar, H.; Drobnak, I.; Aupič, J.; Strmšek, Ž.; Lainšček, D.; Hafner-Bratkovič, I.; Majerle, A.; Krivec, N.; et al. Design of coiled-coil protein-origami cages that self-assemble in vitro and in vivo. *Nat. Biotechnol.* **2017**, *35*, 1094–1101. [[CrossRef](#)] [[PubMed](#)]
72. Gao, M.; Li, J.; Bao, Z.; Hu, M.; Nian, R.; Feng, D.; An, D.; Li, X.; Xian, M.; Zhang, H. A natural in situ fabrication method of functional bacterial cellulose using a microorganism. *Nat. Commun.* **2019**, *10*, 1–10. [[CrossRef](#)]
73. Sharma, A.; Thakur, M.; Bhattacharya, M.; Mandal, T.; Goswami, S. Commercial application of cellulose nano-composites—A review. *Biotechnol. Rep.* **2019**, *21*, e00316. [[CrossRef](#)] [[PubMed](#)]
74. Wang, M.; Weiberg, A.; Lin, F.M.; Thomma, B.P.H.J.; Huang, H.D.; Jin, H. Bidirectional cross-kingdom RNAi and fungal uptake of external RNAs confer plant protection. *Nat. Plants* **2016**, *2*, 1–10. [[CrossRef](#)]
75. Mitter, N.; Worrall, E.A.; Robinson, K.E.; Li, P.; Jain, R.G.; Taochy, C.; Fletcher, S.J.; Carroll, B.J.; Lu, G.Q.; Xu, Z.P. Clay nanosheets for topical delivery of RNAi for sustained protection against plant viruses. *Nat. Plants* **2017**, *3*, 1–10. [[CrossRef](#)] [[PubMed](#)]
76. Chariou, P.L.; Dogan, A.B.; Welsh, A.G.; Sidel, G.M.; Baskaran, H.; Steinmetz, N.F. Soil mobility of synthetic and virus-based model nopenesticides. *Nat. Nanotechnol.* **2019**, *14*, 712–718. [[CrossRef](#)]
77. Li, J.; Green, A.A.; Yan, H.; Fan, C. Engineering nucleic acid structures for programmable molecular circuitry and intracellular biocomputation. *Nat. Chem.* **2017**, *9*, 1056. [[CrossRef](#)] [[PubMed](#)]
78. Li, S.; Jiang, Q.; Liu, S.; Zhang, Y.; Tian, Y.; Song, C.; Wang, J.; Zou, Y.; Anderson, G.J.; Han, J.Y.; et al. A DNA nanorobot functions as a cancer therapeutic in response to a molecular trigger in vivo. *Nat. Biotechnol.* **2018**, *36*, 258. [[CrossRef](#)] [[PubMed](#)]
79. Koman, V.B.; Liu, P.; Kozawa, D.; Liu, A.T.; Cottrill, A.L.; Son, Y.; Lebron, J.A.; Strano, M.S. Colloidal nanoelectronic state machines based on 2D materials for aerosolizable electronics. *Nat. Nanotechnol.* **2018**, *13*, 819–827. [[CrossRef](#)]
80. Mitrano, D.M.; Beltzung, A.; Frehland, S.; Schmiedgruber, M.; Cingolani, A.; Schmidt, F. Synthesis of metal-doped nanoplastics and their utility to investigate fate and behaviour in complex environmental systems. *Nat. Nanotechnol.* **2019**, *14*, 362–368. [[CrossRef](#)] [[PubMed](#)]

81. Brandl, F.; Bertrand, N.; Lima, E.M.; Langer, R. Nanoparticles with photoinduced precipitation for the extraction of pollutants from water and soil. *Nat. Commun.* **2015**, *6*, 1–10. [[CrossRef](#)]
82. Wang, R.; Yang, Z.; Luo, J.; Hsing, I.M.; Sun, F. B12-dependent photoresponsive protein hydrogels for controlled stem cell/protein release. *Proc. Natl. Acad. Sci. USA* **2017**, *114*, 5912–5917. [[CrossRef](#)] [[PubMed](#)]
83. Seifert, S.; Brakmann, S. LOV Domains in the design of photoresponsive enzymes. *ACS Chem. Biol.* **2018**, *13*, 1914–1920. [[CrossRef](#)] [[PubMed](#)]
84. Kumar, M.; Grzelakowski, M.; Zilles, J.; Clark, M.; Meier, W. Highly permeable polymeric membranes based on the incorporation of the functional water channel protein aquaporin Z. *Proc. Natl. Acad. Sci. USA* **2007**, *104*, 20719–20724. [[CrossRef](#)]
85. Chowdhury, R.; Ren, T.; Shankla, M.; Decker, K.; Grisewood, M.; Prabhakar, J.; Baker, C.; Golbeck, J.H.; Aksimentiev, A.; Kumar, M.; et al. PoreDesigner for tuning solute selectivity in a robust and highly permeable outer membrane pore. *Nat. Commun.* **2018**, *9*, 1–10. [[CrossRef](#)]
86. Licausi, F.; Giuntoli, B. Synthetic biology of hypoxia. *New Phytol.* **2020**. [[CrossRef](#)] [[PubMed](#)]
87. Diederichs, T.; Pugh, G.; Dorey, A.; Xing, Y.; Burns, J.R.; Hung Nguyen, Q.; Tornow, M.; Tampé, R.; Howorka, S. Synthetic protein-conductive membrane nanopores built with DNA. *Nat. Commun.* **2019**, *10*, 1–11. [[CrossRef](#)]
88. Ryu, H.; Fuwad, A.; Yoon, S.; Jang, H.; Lee, J.C.; Kim, S.M.; Jeon, T.J. Biomimetic membranes with transmembrane proteins: State-of-the-art in transmembrane protein applications. *Int. J. Mol. Sci.* **2019**, *20*, 1437. [[CrossRef](#)]
89. Alvarez, P.J.J.; Chan, C.K.; Elimelech, M.; Halas, N.J.; Villagrán, D. Emerging opportunities for nanotechnology to enhance water security. *Nat. Nanotechnol.* **2018**, *13*, 634. [[CrossRef](#)]
90. Kim, J.; Campbell, A.S.; de Ávila, B.E.F.; Wang, J. Wearable biosensors for healthcare monitoring. *Nat. Biotechnol.* **2019**, *37*, 389–406. [[CrossRef](#)]
91. Bartke, S.; Hagemann, N.; Harries, N.; Hauck, J.; Bardos, P. Market potential of nanoremediation in Europe—Market drivers and interventions identified in a deliberative scenario approach. *Sci. Total Environ.* **2018**, *619*, 1040–1048. [[CrossRef](#)] [[PubMed](#)]
92. Medina-Pérez, G.; Fernández-Luqueño, F.; Vazquez-Nuñez, E.; López-Valdez, F.; Prieto-Mendez, J.; Madariaga-Navarrete, A.; Miranda-Arámbula, M. Remediating polluted soils using nanotechnologies: Environmental benefits and risks. *Pol. J. Environ. Stud.* **2019**, *28*, 1–18. [[CrossRef](#)]
93. Kumar, S.R.; Gopinath, P. Nano-bioremediation: Applications of nanotechnology for bioremediation. In *Handbook of Advanced Industrial and Hazardous Wastes Management*, 1st ed.; Wang, K.L., Wang, S.M.-H., Hung, Y.-T., Shammas, N.K., Chen, J.P., Eds.; CRC Press: Boca Raton, FL, USA, 2009; Volume 1, pp. 27–48.
94. Sun, Y.; Liang, J.; Tang, L.; Li, H.; Zhu, Y.; Jiang, D.; Song, B.; Chen, M.; Zeng, G. Nano-pesticides: A great challenge for biodiversity? *Nano Today* **2019**, *28*, 100757. [[CrossRef](#)]
95. Lead, J.R.; Batley, G.E.; Alvarez, P.J.J.; Croteau, M.N.; Handy, R.D.; McLaughlin, M.J.; Judy, J.D.; Schirmer, K. Nanomaterials in the environment: Behavior, fate, bioavailability, and effects—An updated review. *Environ. Toxicol. Chem.* **2018**, *37*, 2029–2063. [[CrossRef](#)]
96. Vázquez Núñez, E.; de la Rosa-Álvarez, G. Environmental behavior of engineered nanomaterials in terrestrial ecosystems: Uptake, transformation and trophic transfer. *Curr. Opin. Environ. Sci. Health* **2018**, *6*, 42–46. [[CrossRef](#)]
97. Rasmussen, K.; González, M.; Kearns, P.; Sintés, J.R.; Rossi, F.; Sayre, P. Review of achievements of the OECD Working Party on Manufactured Nanomaterials' Testing and Assessment Programme. From exploratory testing to test guidelines. *Regul. Toxicol. Pharmacol.* **2016**, *74*, 147–160. [[CrossRef](#)]
98. Kica, E.; Wessel, R.A. Transactional arrangements in the governance of emerging technologies: The case of nanotechnology. In *Embedding New Technologies into Society: A Regulatory, Ethical and Societal Perspective*, 1st ed.; Bowman, D.M., Stokes, E., Rip, A., Eds.; CRC Press: Boca Raton, FL, USA, 2017; pp. 219–257.
99. Hess, D.J.; Lamprou, A. Nanotechnology and the environment. In *Nanotechnology and Global Sustainability*, 1st ed.; Maclurcan, D., Radywyl, N., Eds.; CRC Press: Boca Raton, FL, USA, 2011; pp. 50–73.
100. Singh, D.; Wohlleben, W.; De La Torre Roche, R.; White, J.C.; Demokritou, P. Thermal decomposition/incineration of nano-enabled coatings and effects of nanofiller/matrix properties and operational conditions on byproduct release dynamics: Potential environmental health implications. *NanoImpact* **2019**, *13*, 44–55. [[CrossRef](#)]

101. Song, Y.; Hou, D.; Zhang, J.; O'Connor, D.; Li, G.; Gu, Q.; Li, S.; Liu, P. Environmental and socio-economic sustainability appraisal of contaminated land remediation strategies: A case study at a mega-site in China. *Sci. Total Environ.* **2018**, *610*, 391–401. [[CrossRef](#)]
102. Rafique, M.; Tahir, M.B.; Sadaf, I. Nanotechnology: An Innovative Way for Wastewater Treatment and Purification. In *Advanced Research in Nanosciences for Water Technology*; Springer: Cham, Switzerland, 2019.



© 2020 by the authors. Licensee MDPI, Basel, Switzerland. This article is an open access article distributed under the terms and conditions of the Creative Commons Attribution (CC BY) license (<http://creativecommons.org/licenses/by/4.0/>).

Review

Environmental Remediation of Antineoplastic Drugs: Present Status, Challenges, and Future Directions

Abhilash Kumar Tripathi ¹, Aditi David ¹, Tanvi Govil ^{1,2}, Shailabh Rauniyar ¹, Navanietha Krishnaraj Rathinam ^{1,3}, Kian Mau Goh ⁴ and Rajesh Kumar Sani ^{1,2,3,*}

¹ Department of Chemical and Biological Engineering, South Dakota School of Mines and Technology, Rapid City, SD 57701, USA; abhilashkumar.tripathi@mines.sdsmt.edu (A.K.T.); aditi.david@mines.sdsmt.edu (A.D.); tanvi.govil@mines.sdsmt.edu (T.G.); shailabh.rauniyar@mines.sdsmt.edu (S.R.); Navanietha.Rathinam@sdsmt.edu (N.K.R.)

² Composite and Nanocomposite Advanced Manufacturing Centre–Biomaterials, Rapid City, SD 57701, USA

³ BuG ReMeDEE Consortium, South Dakota School of Mines and Technology, Rapid City, SD 57701, USA

⁴ Faculty of Science, Universiti Teknologi Malaysia, Johor 81310, Malaysia; gohkianmau@utm.my

* Correspondence: Rajesh.sani@sdsmt.edu; Tel.: +1-605-394-1240

Received: 27 May 2020; Accepted: 20 June 2020; Published: 27 June 2020

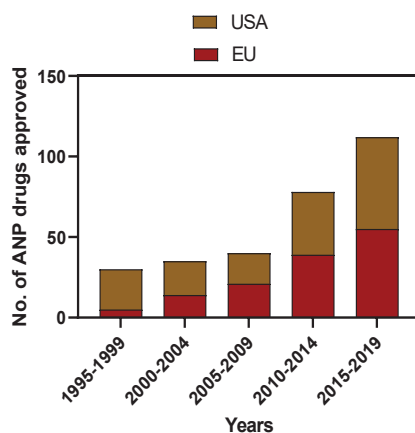
Abstract: The global burden of cancer is on the rise, and as a result, the number of therapeutics administered for chemotherapy is increasing. The occupational exposure, recalcitrant nature and ecotoxicological toxicity of these therapeutics, referred to as antineoplastic (ANP) drugs, have raised concerns about their safe remediation. This review provides an overview of the environmental source of ANPs agents, with emphasis on the currently used remediation approaches. Outpatient excreta, hospital effluents, and waste from pharmaceutical industries are the primary source of ANP waste. The current review describes various biotic and abiotic methods used in the remediation of ANP drugs in the environment. Abiotic methods often generate transformation products (TPs) of unknown toxicity. In this light, obtaining data on the environmental toxicity of ANPs and its TPs is crucial to determine their toxic effect on the ecosystem. We also discuss the biodegradation of ANP drugs using monoculture of fungal and bacterial species, and microbial consortia in sewage treatment plants. The current review effort further explores a safe and sustainable approach for ANP waste treatment to replace existing chemical and oxidation intensive treatment approaches. To conclude, we assess the possibility of integrating biotic and abiotic methods of ANP drug degradation.

Keywords: antineoplastic drug; environment; toxicity; remediation; biodegradation

1. Introduction

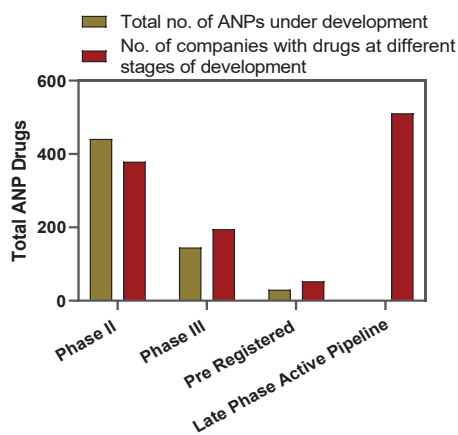
Last few decades have experienced rising concerns over the release of pharmaceutical drugs into the environment. Though pharmaceutical compounds have targeted effects on the human body, the knowledge about the direct impact of their transformation products (TPs) and metabolites on other organisms and indirect effects on human health is scarce. Antineoplastic (ANP) drugs (also known as anticancer or cytostatic) are a specific group of pharmaceutical compounds which prevent, inhibit, or terminate the development of cancer. However, due to their non-specific mode of action, affecting both cancerous and healthy cells, ANP drugs exhibit cytotoxic, genotoxic, mutagenic, carcinogenic and teratogenic effects in all eukaryotic cells [1–3]. Nevertheless, due to their low environmental concentrations (10–100 ng/L or below), there is not enough evidence to accurately assess whether or not ANPs have an impact on the environment [4]. However, since they are designed to disrupt or prevent cellular proliferation, usually by interfering in DNA synthesis, their fate and transport in the environment should be explored.

The World Health Organization estimated the global burden of cancer at 18.1 million new cases and 9.6 million deaths in 2018 [5]. As per an evaluation by the American Cancer Society, 1,806,590 new cancer cases and 606,520 cancer deaths are projected to occur in the United States by 2020 [6]. In compliance with this trend of increasing cancer prevalence, new ANP drugs are also being designed, tested, and manufactured at an increasing rate [7]. Over the past few years, 70 new ANP drugs have been released to treat 20 variants of tumors (cancerous growths), the number of ANP drugs has expanded by more than 60% [8]. More than 500 companies are currently pursuing ANP drug development, with 300 companies having cancer drugs under clinical development stages [8]. Figure 1a,b shows the total number of ANP drugs approved in USA and EU, and total ANP molecules under different phases of development, respectively. In 10 years from 2010 to 2020, ANP drug production is expected to double [9]. The production of novel ANP drugs has varied greatly across countries over the years. For example, in 2004, Canada and Australia consistently produced a higher volume of ANP drugs (51 and 39 for Australia and Canada, respectively) whereas United States and Germany produced significantly lower volume (29 and 17 for Germany and United States, respectively). On the other hand, in 2014, United States and Germany produced higher volume of novel ANP drugs [10]. A comparative global heatmap of some prominent ANP drug producing countries in 2004 and 2014 is shown in Figure 1c. The raw data of Figure 1c is given in Table S1 of Supplementary Information. In addition to the production, it is also crucial to highlight the sites where ANPs are mostly released into the environment. However, there is not enough data to categorize sites in terms of ANP emission into the environment. The number of publications on occurrence of ANP compounds in environment is scarce, and most of studies to date are almost exclusively focused on Europe [11]. Nevertheless, the number of cancer cases in different countries can be a governing factor that dictates the introduction of these compounds in the environment. The country with highest number of cases will consume the most ANP drugs and hence there will be a greater probability of introduction of these compounds into the environment. The global heatmap of the number of cancer cases in different countries per 100,000 people is given in Figure 1d. The raw data was obtained from the GLOBOCAN online database [12], and is provided in Table S2 of the Supplementary Information.

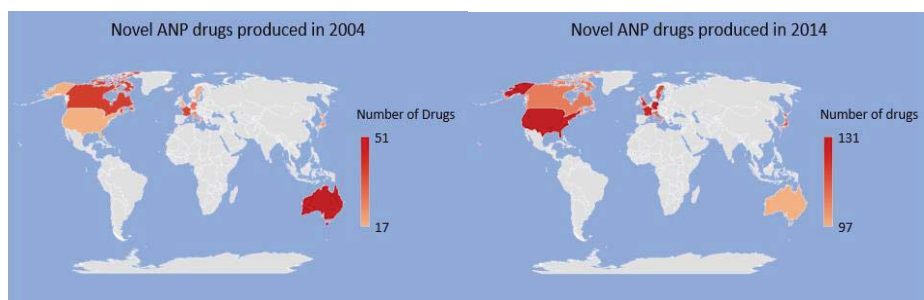


(a)

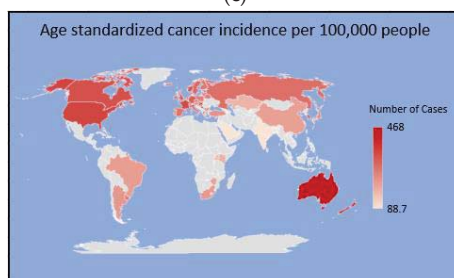
Figure 1. Cont.



(b)



(c)



(d)

Figure 1. (a) Number of antineoplastic (ANP) drugs approved between 1995 and 2019 in USA and European Union (EU) [7,13–15]; (b) The Global Late Phase Oncology Pipeline in 2015 [8]; (c) comparative global heatmap of ANP drug produced in some select countries in 2004 and 2014 [10]; (d) age standardized cancer incidence in select countries in 2018 [12]. (Phase II and Phase III refers to ANP drugs that are at second and third phase of clinical trials, respectively).

ANP drugs are categorized into different groups based on the organ or system on which they act and their therapeutic, pharmacological, and chemical properties [16]. These different categories of ANP drugs differ in their chemical structures and physicochemical properties. The physicochemical properties play an indispensable role in the potential fate of these drugs in the environment [17]. Building a physicochemical profile of ANPs will allow for their partitioning, and help us study the

fate of ANPs within aquatic and terrestrial ecosystems [18]. In total, 102 active antineoplastic drugs have been identified which are environmentally relevant [19]. Section 2 of this review describes the parameters that determine the fate and distribution of ANPs in the environment.

Though used in minimal quantity, ANP drugs persist in the environment [19] and can be harmful even if present under low concentrations [20,21]. All ANP compounds are potent immunosuppressive agents and have a high pharmacological potency that is fatal to aquatic and terrestrial organisms [22]. Significant disadvantages and environmental concerns associated with the usage of ANP drugs include the following: (i) inevitable contamination of natural ecosystems (terrestrial and aquatic) by the drugs themselves and their potentially toxic transformation products (TPs); (ii) scarcity of complete and coherent knowledge on the environmental fate of these drugs, its human metabolites, or TPs; (iii) their biomagnification at various trophic levels which can have adverse effects on the flora and fauna of the contaminated ecosystems.

The aforesaid environmental concerns have made it imperative to develop a safe, economical, and environmentally friendly process to remediate residual ANP drugs in the ecosystem. To date, limited studies have been successful in using a single microbial system or microbial consortia for the complete or partial elimination of ANP wastes [23–26]. The integration of microbial bioremediation systems with abiotic remediation techniques can be beneficial as it will decrease the requirements of harsh chemicals and may also reduce the generation of toxic degradation products [27]. This review presents a case for integrating abiotic and biotic modes of ANP degradation. With our decade-long continuous exploration in the field of extremophilic bioprocessing and bioremediation [28–34], we have identified the scope of thermophilic microbes and thermophilic bioprocessing towards developing sustainable and environment friendly methods of ANP waste degradation.

The primary objectives of this review effort are to (i) outline the parameters that affect the circulation of ANP drugs in an environment; (ii) provide a brief overview of the source, types, and concentration of ANPs in the environment; (iv) compare and contrast the Environmental Risk Assessment (ERA) strategies being implemented in different regions; (iii) compile the information on existing biotic and abiotic methods of remediation of ANP drugs; (iv) discuss the possibility of designing a more energy efficient remediation method through integration of biotic and abiotic methods of treatment.

2. Parameters Determining the Fate and Distribution of ANPs

The decomposition or deactivation of ANP drugs in the waste treatment plants and environment is greatly influenced by the individual physicochemical properties of ANPs and its TPs [4]. The physicochemical properties of some common ANP drugs are listed in Table 1, that include octanol-water partition coefficient/hydrophobicity (K_{ow}), dissociation constant (pK_a), solubility, toxicity, biological half-life, bioconcentration factor (BCF), and organic carbon partition coefficient (K_{oc}).

Table 1. *Contd.*

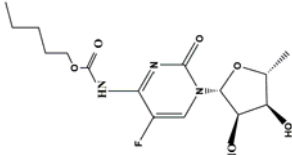
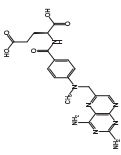
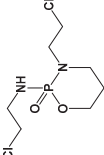
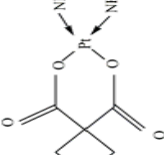
ANP Drug	Chemical Structure	log K _{ow}	pK _a ^f	Solubility in Water (at 25 °C)	Toxicity (LD ₅₀ ^d Value, Oral)	Biological Half-Life ^e	BCF ^c
CPC		0.56	1.9	26 g/L	>2120 mg/kg (women)	45–60 min	NA
MTX		1.85	4.70	2.6 g/L	135 mg/kg (rats)	Low doses: 3–10 h High doses: 8–15 h	3.2
IF		0.86	1.45	3.8 g/L	150–190 mg/kg (rats)	7–15 h	3
CPT		-0.46	6.6	15 g/L	61 mg/kg (rats)	1.1–2 h	NA

Table 1. *Cont.*

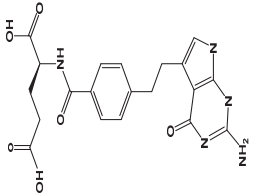
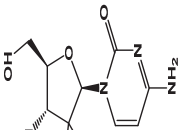
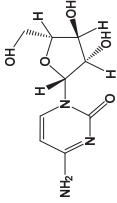
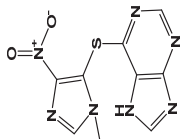
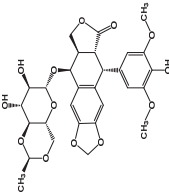
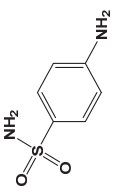
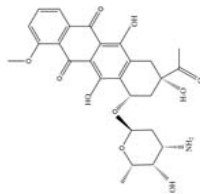
ANP Drug	Chemical Structure	log K _{ow}	pK _a ^f	Solubility in Water (at 25 °C)	Toxicity (LD ₅₀ ^d Value, Oral)	Biological Half-Life ^e	BCF ^c
PEM		0.16	3.6 (pK _{a1}) 4.4 (pK _{a2})	Insoluble	1754 mg/kg (rats)	3.5 h	3.2
GEM		-2.01	3.6	51.3 g/L	500 mg/kg (mice and rats)	Short infusions: 42–94 min Long infusions: 245–638 min	1
CTB		-2.46	4.22	17.6 g/L	3150 mg/kg (mice)	10 min	1
AZT		0.10	7.87	Insoluble	400 mg/kg (rats)	12–15 min	NA

Table 1. *Cont.*

ANP Drug	Chemical Structure	log K _{ow}	pK _a ^f	Solubility in Water (at 25 °C)	Toxicity (LD ₅₀ ^d Value, Oral)	Biological Half-Life ^e	BCF ^c
ETS		0.60	9.8	Sparingly soluble (0.08 g/L)	118 mg/kg (mice)	4–11 h	3
SFL		-0.62	10.6	7.5 g/L	3700 mg/kg (mice)	Dependent on renal function	0.2
DAU		1.83	7.85	30 g/L	1737 mg/kg (mice)	36 ± 13 h	110

Notes: 5-FU: 5-Fluorouracil; CP: Cyclophosphamide; DOX: Doxorubicin; TAM: Tamoxifen; CIP: Ciprofloxacin; CPC: Capecitabine; MTX: Methotrexate; IF: Ifosfamide; CPT: Carboplatin; PEM: Pemetrexed; GEM: Gemcitabine; AZT: Azathioprine; ETS: Etoposide; SFL: Sulfamonomethoxine; DAU: Daunorubicin. Physico-chemical and toxicity value data sources: HSDB—Hazardous Substances Data Bank (<https://toxnet.nlm.nih.gov/cgi-bin/sis/htmlgen?HSDB>), PubChem (<https://pubchem.ncbi.nlm.nih.gov/>), ChEMSPIDER (<http://www.chemspider.com/>). N.A. no data available. ^a Cayman Chemical—MSDS of Ifoxifen (<https://www.caymanchem.com/msds/13258m.pdf>). ^b Pfizer—MSDS of Ciprofloxacin (http://www.pfizer.com/files/products/material_safety_data/PZO1031.pdf). ^c BCF stands for bioconcentration factor which indicates biomagnification (BMG) risk (low BMG risk (< 100); moderate BMG risk (100–1000)); very high BMG risk (> 1000) [21,35]. ^d LD50 is the dosage of a given drug that kills 50% of the test population. ^e Biological half-life is the time required for half of the total drug in a biological system to be degraded by biological process when the rate of removal is nearly exponential (<https://medical-dictionary.thefreedictionary.com/biological+half-life>). ^f pK_a is the acid-base dissociation constant (pK_a affects ionization of weakly basic and weakly acidic ANPs. The ionization of basic drugs for instance is suppressed at pH above their pK_a and is enhanced at a pH below their pK_a [36]; pK_{a1}, pK_{a2}, and pK_{a3} are the dissociation constants for first, second, and third ionization, respectively).

Sorption (absorption and adsorption) which is influenced by these physico-chemical parameters is the key unit operation in remediation of ANPs [37,38]. One of the key factors that determines the fate of ANPs in effluents flown from the treatment facilities is the magnitude of ANPs sorption onto organic matter [39]. In addition, the chemical structure of the ANPs also determines the mechanism and effectiveness of sorption [4]. Sorption of a chemical/organic compound to an organic matter is determined using the octanol/water partition coefficient (K_{ow}) and organic carbon normalized sorption coefficient (K_{oc}) which are derived from n-octanol/water distribution coefficient (D_{ow}) and the solid-water distribution coefficient (K_d), respectively. K_d value dictates both adsorption and absorption of the chemical compound to natural organic matter [39]. The dissemination of a chemical/organic compound between lipids and fats, sorption to biomass and distribution among environmental compartments is indicated by D_{ow} . However, D_{ow} cannot be applied to organic compounds with multiple functional groups because such compounds rapidly ionize at environmental pH levels. D_{ow} is therefore corrected for K_{ow} which considers concentration of non-ionized species only. For undissociated compounds, $\log D_{ow}$ is approximately equal to $\log K_{ow}$. In general, $\log K_{ow} < 1$ indicates that a chemical compound is highly mobile in aquatic and is unlikely to sorb onto organic matter (with the exception of IB ($\log K_{ow} = 3$)) that remains in the water phase and is less likely to undergo sorption. On the other hand, $\log K_{ow} \geq 3$ is indicative of a hydrophobic compound that can undergo rapid sorption. Based on $\log K_{ow}$, it is possible to separate a mixture of ANPs and investigate potential toxicity of the ANPs [22]. From Figure 2 and Table 1, we can see that many ANPs are highly polar with $\log K_{ow}$ values < 1 . This suggests that they will mostly be distributed in the water phase. In fact, in many studies, both cyclophosphamide (CP, $\log K_{ow} = 0.63$), and ifosfamide (IF, $\log K_{ow} = 0.86$), were detected at concentration (w/w) of $< 2 \times 10^{-5}$ mg/gram of sewage sludge, where their concentrations per liter of the sewage treatment plant influent were 10^2 – 10^3 times higher [21,40,41]. Therefore ANPs with $\log K_{ow}$ values < 1 are unlikely to be eliminated by adsorption onto sewage sludge, and if they are not biodegraded, they will pass onto surface waters [25,42]. The $\log K_{ow}$ values, when plotted with half-life of the ANPs (Figure 2), shows that the drugs with higher biological half-life possesses higher hydrophobicity ($\log K_{ow} > 2$). Though, there are some outliers that do not fit the curve (Figure 2), more than 80% of the data demonstrates the expected trend. For hydrophobic ANPs, adsorption to biomass plays an important role in their elimination process and as such hydrophobic ANPs can be removed by using an adsorption based remediation method such as powered activated carbon [43].

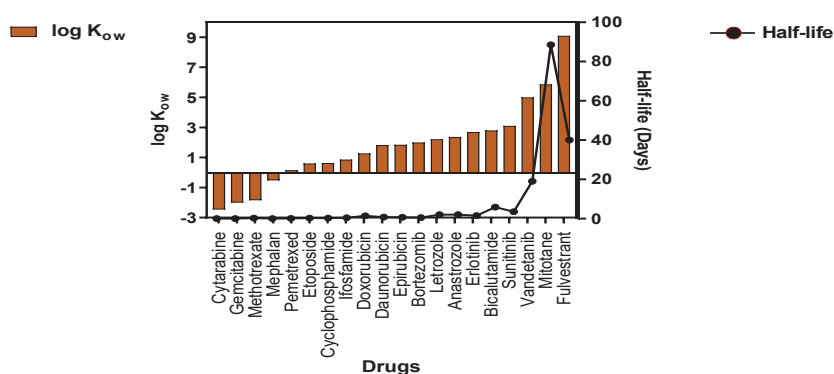


Figure 2. Plot indicating relationship between hydrophobicity and half-life of common ANP drugs. Drugs list obtained from NIOSH List of Antineoplastic and Other Hazardous Drugs in Healthcare Settings, 2016 ([https://www.cdc.gov/niosh/docs/2016/\\$-161/pdfs/2016-161.pdf?id=10.26616/NIOSH-PUB2016161](https://www.cdc.gov/niosh/docs/2016/$-161/pdfs/2016-161.pdf?id=10.26616/NIOSH-PUB2016161)). K_{ow} and half-life values were obtained from PubChem (<https://pubchem.ncbi.nlm.nih.gov/>) and DrugBank (<https://www.drugbank.ca/>).

The acid-base dissociation constant (pKa) is a key physicochemical parameter that describes the extent to which a compound would dissociate at a particular pH. For example, methotrexate (MTX) has a relatively low dissociation constant, and therefore it is more likely to be dissociated in the aquatic ecosystem. MTX therefore has high mobility in the aquatic environment because of its high polarity [22]. The typical range of pKa values that a compound may have is related to the nature and frequency of occurrence of the functional groups that are commonly observed in pharmaceuticals including ANPs. Another important parameter is solubility which varies widely amongst the different classes of ANP drugs. It varies from 0 for some plant alkaloids class of ANPs to as high as 10^4 and 10^5 mg/L for ANP drugs such as capecitabine (CPC), cytarabine (CTB), cyclophosphamide (CP), and 5-fluorouracil (5-FU) as mentioned in Table 1. In fact, due to the combination of low log K_{ow} (hydrophilic) and high water solubility, some ANP drugs such as cisplatin (CPT), carboplatin (CBT), and oxaliplatin (OXT) become highly mobile in the aquatic environment [44]. In the same light, it is also important to mention bioconcentration factor (BCF), which indicates the biomagnification risk. Most cytostatic drugs have BCF between 1 and 4. However, for some other ANPs such as tamoxifen (TAM) and bicalutamide (BLT) BCF is 827, while lapatinib (LTB) has BCF of 2535, mitotane (MTN) 7649, and estramustine (ERT) 13,783, which is indicative of an extremely high potential for bioconcentration in aquatic organisms [43]. It could thus be potentially dangerous to humans as well. These physico-chemical parameters are therefore important factors that should be taken into consideration before designing environmental risk assessment programs, and biotic and abiotic degradation strategies.

3. Sources of ANPs in the Environment

Since the very first detection of ANP drugs in the aquatic environment in 1985 [45], various studies have discovered different classes of ANP drugs in the aquatic environment, with negligible or almost unchanged structural conformation [46]. ANP agents are mostly introduced into the environment through the urine and feces of outpatients who consume the drug at home (oral chemotherapy), or patients who undergo chemotherapy at hospitals [1,40]. Particularly effluents from cancer hospitals or hospital wards specialized in oncology are the key emission source of ANP drugs in the aquatic environment [47,48]. In fact, excretions of patients undergoing chemotherapy at hospitals is the main source of introduction of ANP drugs in the environment [43]. The excretion route (feces or urine) is dependent on the type of drug administered. For example, 70% of bleomycin (in less than 2 h) and 40% of doxorubicin (in 5 days) is excreted in urine, and 50% of irinotecan (ITN) (48 h) in feces [43]. A few more ANP drugs such as MTX and pemetrexed (PEM) have shown high urinary excretion rates ($\approx 90\%$). MTX and PEM are mainly excreted as human metabolites of the parent drug [21,49]. For example, the urinary excretion of 5-FU is only about 15% as parent compound (5-FU), and 80% as its metabolite R-fluoro-alanine [50]. The excretion rate of ANP drugs varies with medication (duration of medication, formulation), mode of application (intra-dermal, intravenous, oral), and metabolic rates among treated patients. Figure 3 shows the possible routes for the introduction of pharmaceutical drugs into the environment. The occurrence and concentration of ANPs in effluents is also dependent on many factors, such as the number of patients, the physico-chemical nature of the drug used, dosing, excretion rates, methods of sampling, storage, and transport, as well as daily water consumption, which can significantly dilute the effluent and affect the detectability of ANP and its TPs [43]. ANPs through effluents can enter the aquatic environment unaltered or as TPs depending on the physicochemical characteristics discussed in Section 2. These drugs or their TPs can have detrimental effects on the environment, aquatic life, and human health [20]. Due to danger that these drugs pose, it is important to gather data on the usage of ANPs in a decentralized way because every patient and hospital do not use the same type ANP drugs. Such decentralized categorization of data would also help in designing efficient environmental risk assessment and remediation strategies.

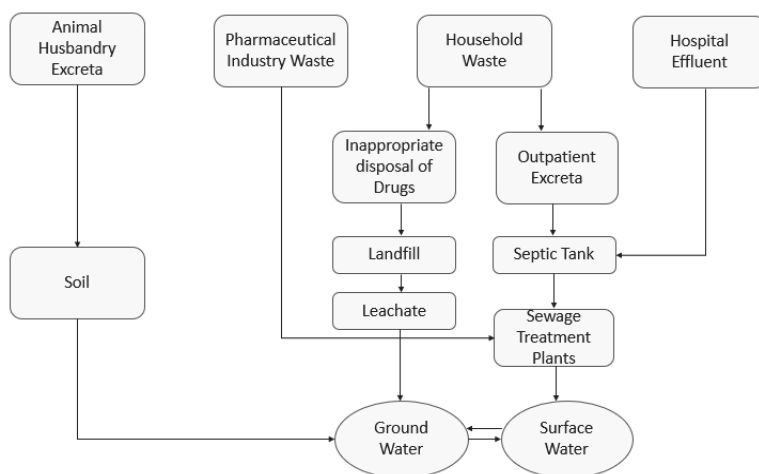


Figure 3. Sources for the introduction of ANP waste into the environment (modified from [51,52]).

4. Environmental Risk Assessment (ERA) of ANPs

Recent years have seen a sharp spike in the number of ANP drugs in the market which has promoted anticancer home treatments [40]. As a result, more ANPs are being increasingly reported in wastewater and natural water bodies [17,20,53]. Due to their increased accumulation and highly hazardous nature, it has become imperative to quantify the concentration of ANPs in the environment and carry out an environmental risk assessment (ERA). The ERA methodology varies in different regions of the world. The European medical agency (EMA) calculates the predicted environmental concentration (PEC) in addition to screening the persistence, bioaccumulation, and toxicity of the drug during phase I assessment [54,55]. The PEC value is calculated using the following Equation (1) [55].

$$PEC_{SW} = (DOSE_{AS} \times F_{PEN}) / (WASTE_{INHAB} \times DILUTION) \quad (1)$$

where, PEC_{SW} predicted environmental concentration for surface water (mg/L); $DOSE_{AS}$ is the maximum daily dose of the active substance consumed per inhabitant (mg/inh-d); F_{PEN} is the fraction of a population receiving the active substance; $WASTE_{INHAB}$ amount of wastewater per inhabitant per day (L/inh-d); $DILUTION$ is the dilution factor.

As per the EMA standard guidelines, if the PEC_{SW} value is <10 ng/L, the pharmaceutical drug is unlikely to represent a risk to the environment [55]. Persistence, bioaccumulation, and other toxicity tests are not required for ANPs that fall under this category. Lipophilic ANPs ($\log K_{ow} > 4.5$) are directly moved to phase II because of their bioaccumulative nature. In contrast, the USA uses different ERA methodology where the drugs are first sorted based on its potency to enter the environment. Various tests such as the water solubility test, dissociation constant test, octanol/water partition coefficient (K_{ow}) test, and vapor pressure is conducted on the sorted drugs. The environment introduction concentration (EIC) is then estimated using the following Equation (2) [55].

$$EIC_{AQ} = A \times B \times C \times D \quad (2)$$

where, EIC_{AQ} : expected introduction concentration of an active moiety into the aquatic environment (ppb); A: amount produced for direct use as active moiety (kg/year); B: inverse of liters per day entering the publicly owned treatment works, (POTWs) (day/L); C: conversion factor (year/365 day); D: conversion factor (109 $\mu\text{g}/\text{kg}$). If the $EIC_{AQ} < 1000$ ng/L, the drug is excluded from further testing. PEC_{SW} is generally lower than EIC_{AQ} due to dilution factor.

When compared to EU and USA, Canada's ERA assesses not only the harmful effects of the substance on human health and environment but also their exposure potential [55]. Canada's ERA considers the lethality, mutagenicity, reproductive effects, and organ toxicity of the drug. This detailed testing weighs the impact of ANPs and is not carried out in the EU or USA. In Canada, PEC is calculated using the following Equation (3) [55].

$$PEC_{SW} = (\text{kg of API/year}) \times (1 \text{ year}/365 \text{ days}) / (\text{Wastewater L/day}\cdot\text{capita}) \times (\text{population}) \quad (3)$$

where, PEC_{SW} : predicted environmental concentration in surface water ($\mu\text{g/L}$); kg of API/year: amount produced per year (kg/year); Wastewater L/day·capita: volume of wastewater generated per day per capita (L/day). The substance tested is designated to be toxic when PEC_{sw} divided by predicted no-effect concentration (PNEC) is ≥ 1 .

One major obstacle in assessing the risk of ANPs in the environment is that the existing ERA procedures differ significantly in the European Union (EU), USA, and Canada. The most notable distinction is that the EU and USA regulate products (drug), whereas Canada regulates substances (active pharmaceutical ingredients (APIs)) [55]. In EU and USA, existing drugs or new drug applications before the introduction of the ERA guidelines are not required for assessment whereas in Canada all substances entering or which may enter the environment are premised to be toxic until evaluation [55]. The EU and USA have implemented a tiered approach in which only the drugs that are suspected to be toxic are transferred onto the next stage of assessment. Canada, on the contrary, has adopted a classification-based approach in which the timing of notification is determined by the type of substances, i.e., polymer, chemical, or biological living systems [55]. However, in Canada, toxic and even non-toxic substances are checked for their accumulation impact to the land and water. The criteria of toxicity testing even after ERA clearance is vital as accumulation or circumstances of exposure to the substance may render the substance toxic. Table 2 gives a comparison of ERA procedures implemented in the USA, EU, and Canada.

Table 2. Characteristics of Environmental Risk Assessment (ERA) regulatory approach implemented in USA, EU, and Canada.

	USA	EU	Canada
Implementing organization	Food and Drug Administration (FDA)	European Medical Agency (EMA)	Health Canada and Environment and Climate Change Canada
Regulated product	All drugs manufactured for sale in EU member states	New Drugs	New Substances
Timing of ERA	When applying for marketing approval	New Drug applications [56]	Before notification
ERA Methodology	Phase-tiered based approach (Phase I; Phase II-Tier A and Tier B)	Tiered based approach (Tier 1, Tier 2, Tier 3)	Classification based approach (polymers, living organisms, chemicals)
Drug exclusion criteria	PEC ^a < 10 ng/L	EIC ^b < 1000 ng/L	PEC < 100 ng/L
Risk Assessment Criteria	PEC/PNEC ^c ≥ 1	EC ^d ₅₀ /MEEC ^e < 10	PEC/PNEC ≥ 1
Strengths	Responsibility lies with government Tiered approach	Responsibility lies with government Tiered approach	Responsibility lies with government Analyzes substances that are presumed to be non-toxic.
Weaknesses	No ERA for existing drugs. Non-consistent ERA procedure between member states	No ERA for existing drugs	Non-tiered approach

Notes: ^a—Predicted environmental concentration (for details see Section 4 of the review); ^b—Environment Introduction Concentration (for details see Section 4 of the review); ^c—Predicted no effect concentration (for details see [55]); ^d—Concentration of a drug that gives half maximal response; ^e—Maximum expected environmental concentration.

Some ERA studies elucidated that ANP drugs that directly interact with DNA do not have any safe threshold concentrations [22,55,57], and as such the stipulated PEC and EIC values may give false positives for certain ANP drugs. For instance, Kidd et al. [58] showed that concentration of breast cancer drug 17 α -ethynylestradiol (in the concentration range 5–6 ng/L) impacted reproductive health in the fish (*Pimephales promelas*), that lead to a decline in its population at a concentration lower than the EMA suggested toxic level (10 ng/L).

One major issue with accurate ERA is the persistence and accumulation of some ANP drugs in the environment over time. The recalcitrant nature of some ANP drugs in activated sludge environment indicates the possibility of these compounds being persistent in river water [19,59]. The analysis of data provided by the German Environmental Agency confirmed that nearly 30% of ANP compounds are persistent in the water phase [19]. This persistence may gradually increase the actual environmental concentration. Rowney et al. [57] showed that alkylating ANP drugs (0–145 ng/L), antimetabolite ANPs (0–27.4 ng/L), and anthracycline ANPs (0–0.7 ng/L) were detected in the Thames catchment in the United Kingdom. Similarly, the data available for the measured environmental concentration of cyclophosphamide in surface water varies from a negligible 0.05 to 64.8 ng/L [40].

Since there are a large number of ANP drugs currently in the market, and several others in the pipeline (Figure 1), it is necessary to categorize ANPs that are widely prescribed and are likely to persist in the environment. In addition to persistence, the current ERA methodologies do not have any guidelines on dealing with the transformation products (TPs) or human metabolites (HMs) of these drugs. It is not possible to design strategies to study the toxicity of TPs beforehand as the generation of TPs depends on the type of remediation methods employed and environmental parameters such as pH, temperature, type of remediation technique, etc. [22]. Some studies have suggested that TPs or HMs, in some cases, may be more toxic than the parent drug [40,60]. Besse et al. [40] reasoned that the metabolites of ANP drug methotrexate could be more toxic than their parent drug. Similarly, the TPs of certain medications can be more active, even more polar, and therefore of higher mobility in aquatic environments than the parent drug [61]. Consequently, it seems plausible to redesign the current ERA methodologies keeping in mind the toxicity of HMs and TPs. Genotoxicity assessments of ANPs and their relevant TPs should be conducted to allow for a better development of biodegradation or a combination of both biotic and abiotic remediation techniques.

5. Overview of Existing Methodologies of ANPs Degradation in Environment

5.1. Biological Treatments

Microbial systems are known to synthesize certain pharmaceutical drugs and harbor efficient molecular mechanisms that make them resistant to these compounds [62]. Various studies have documented the presence of drug-resistant microbes in hospitals, agriculture, and animal husbandry where these drugs have been used to treat microbial infections [63–65]. Microorganisms evolve numerous biochemical mechanisms to counteract the toxicity of pharmaceutical drugs. Some general mechanisms that microbes exploit to resist pharmaceutical drugs are (a) variation of sites where drugs are targeted, (b) alteration of enzymes that inactivate antimicrobials, (c) reduced membrane permeability, and (d) dynamic and active efflux of pharmaceuticals [66].

Some microbial enzymes mimic the mammalian enzymes that perform xenobiotic detoxification and thus can serve as useful models of drug metabolism [67]. For instance, soil microbes, especially *Actinobacteria*, synthesize and secrete molecules that exhibit anticancer activity into their niche [68]. The presence of such anticancer molecules, which are a vital component of ANP drugs, accentuates other soil bacteria to harbor mechanisms to avoid the toxic effects of these drugs in their natural habitat. The use of soil bacteria to detoxify ANPs is a potent and under-investigated strategy to detoxify anticancer drugs.

5.1.1. Fungal and Bacterial Biodegradation of ANPs

Currently, limited numbers of fungal and bacterial species are known to be an excellent degrader or inactivator of ANPs. Such establishment gives the proof of principle that microorganisms can modify or degrade ANPs. The white-rot fungus, *Trametes versicolor*, is known to have a unique capability of removing a wide variety of ANP compounds [69,70]. In one study, Ferrando Climent et al. [70] explored the possibility of eliminating some selected ANPs from sterile and non-sterile hospital wastewater in a 10 L fluidized bed bioreactor inoculated with the fungus *T. versicolor*. Maximum removal (in non-sterile wastewater) was observed for Azathioprine (AZT) (100%), Etoposide (ETS) (100%), and Ciprofloxacin (CIP) (97%), whereas minimum removal was observed with TAM (48%), but no degradation or sorption was recorded for cyclophosphamide (CP) and Ifosfamide (IF). More efficient removal of some ANPs in non-sterile wastewater possibly resulted from positive interactions between the fungi and common fecal bacteria which led to synergistic degradation of the ANP drugs. No biodegradation of IF and CP can be attributed to the halogenated atoms in their molecular structure which probably hindered aerobic biodegradation since halogenated functional groups decrease electron density at the reaction site [71]. For tamoxifen, no conclusive evidence was found for its low biodegradation in non-sterile wastewater.

On the contrary, TAM was degraded more rapidly in sterile wastewater. This increased degradation coincided with increased fungal activity in the absence of other competing microorganisms. However, the most prominent mechanism of TAM removal was attributed to sorption process since the heat-killed experiment showed 94% removal after 9 days. The high sorption of TAM in contrast to IF and CP was because of its high hydrophobicity ($\log K_{ow} = 6.3$). In addition, the presence of electron-donating amino group and the absence of halogenated functional groups in TAM also increased its degradation rate in sterile wastewater. In both sterile and non-sterile hospital wastewater, highest laccase activity was reached at the end of the treatment, indicating that *T. versicolor* was active throughout the experiment.

In another study, the fungus *T. versicolor* was used to biodegrade 10 mgL⁻¹ of sulfonamides sulfapyridine (SPY), and sulfathiazole (SPZ) [72]. Sulfonamides constitute an important class of drugs that show substantial anticancer activity [73]. SPY was completely removed after 24 h whereas the removal of STZ was slower and around 20% of STX was detected even after 72 h. Unlike in the study by Ferrando Climent et al. [70], where TAM was removed by sorption to heat-killed controls, no sorption of SPY and SPZ was observed when heat-killed controls were used in this study. This suggests that the fungus *T. versicolor* utilizes different mechanisms of ANP detoxification/degradation depending on the nature of the drug. The presence of TPs of SPY and SPZ confirmed that the elimination of these drugs was due to biodegradation and not due to sorption. The study indicated that the enzyme laccase played an important role in biodegradation. When cell-free purified laccases with mediators were tested for biodegradation capabilities, elimination ranged from 75% to 98% ($\pm 4\%$) for SPY and 82% to 100% ($\pm 3\%$) for STZ by the end of the experiment.

The use of mediators such as violuric acid and ABTS enhances biodegradation as they favor the oxidation of non-phenolic compounds such as sulfonamides [74]. Though the fungus does not release these mediators, similar molecules with analogous functions may be released during active growth [72]. In addition to laccase, cytochrome P450, an intracellular enzyme complex, was also implicated in biodegradation of STZ. Culture of *T. versicolor* containing inhibitors of cytochrome P450 decelerated biodegradation of STZ whereas the presence of such inhibitors did not show any appreciable effect on the degradation of SPY. These results indicate that cytochrome P450 was involved in the degradation of STZ whereas there was no experimental evidence for its role in the degradation of SPY. The authors concluded that the use of whole fungal cells with active cytochrome P450 resulted in shorter degradation time. In contrast, with the use of purified laccases, significant biodegradation was seen only with longer incubation times (9–16 days) [70,75]. Laccase mediated degradation has also been shown for other ANPs such as naproxen (NPX) [76]. Naproxen is a non-steroidal inflammatory drug shown to exhibit ANP activity [77]. Biodegradation experiments with purified laccase from *T. versicolor* plus mediators showed almost complete degradation of NPX (95%) at a concentration of 55 $\mu\text{g/L}$ [76]. This study on NPX highlighted the importance of adding mediators during biodegradation in the

presence of laccase. Purified laccase (1000 AU/L) without mediators degraded less than 10% of NPX whereas when mediator (1-hydroxybenzotriazole) was added extensive degradation of NPX (>95%) was detected. The study also established that inhibition of cytochrome P450 decreased the active uptake of NPX by *T. versicolor* and that cytochrome P450 plays a crucial role in the degradation of NPX and other ANPs.

In addition, fluorinated ANPs such as 5-FU and Citalopram (CTP) tend to be more recalcitrant in nature due to the strong C-F bond. For biodegradation of fluorinated drugs, the cleavage of C-F bond is required. CTP, a fluorinated drug was degraded entirely after 14 days at a concentration of 1 mg/L using three white-rot fungi: *Bjerkandera* sp. R1, *Bjerkandera adjusta*, and *Phanerochaete chrysosporium* [78]. Biotransformation of many fluorinated compounds such as fluorophenol, fluorobenzene, and fluorobenzoic acid by aerobic microorganisms is reported [79,80]. Many oxidative enzymes are known to oxidize fluorinated derivatives of natural substances. In contrast to CTP5-FU was not readily biodegradable by *T. versicolor* and inoculum from the effluent of STP [78]. In fact, some fluorinated drugs require advanced photo-oxidation treatment for degradation [81]. This is because the position of fluorine on the fluorinated drug impacts its catabolism, and the position of fluorine might result in the formation of non-biodegradable dead-end metabolites [82].

Actinomyces exhibit positive potential in degrading the ANP doxorubicin, which belongs to the anthracycline class of anticancer drugs [83]. *Actinomyces*, a phylum of Gram-positive bacteria, are morphologically similar to fungi because of their elongated cells that branch into filaments or hyphae [84]. Westman et al. [83] examined *Actinomyces* isolates for their resistance against ANP, 67% of these strains were resistant for up to 150 µg/mL doxorubicin (DOX). Interestingly, *Streptomyces* sp. strain WAC04685 could degrade DOX at concentrations higher than 200 µg/mL to a deglycosylated alcohol derivative (7-deoxydoxorubicinol) which is a non-toxic residual. The study also highlighted that the deglycosylation of doxorubicin by strain WAC04685 is mediated by the NADH dehydrogenase component of the respiratory electron transport complex I, and the addition of NADPH to crude extracts improved the degradation of DOX. The study of the purified enzyme NADH dehydrogenase revealed the involvement of three subunits (NuoE, NuoF, and NuoG), among which, only NuoF was predicted to have NADH binding function [85]. Furthermore, strain WAC04685 could catalyze reactive oxygen species that resulted from Doxorubicin by the action of two homologs superoxide dismutases, two catalases, and a glutathione peroxidase. genome. This study on DOX inactivation gives directions to further explore and engineer novel biodegradation strategies involving *Actinomyces*.

In separate research on studying colon cancer models, the bacteria *Mycoplasma hyorhinis* could metabolize the chemotherapeutic drug gemcitabine (GEM) (2',2'-difluorodeoxycytidine) into its inactive form, 2',2'-difluorodeoxyuridine [86]. The inactivation of the GEM was dependent on the enzymatic reaction of cytidine deaminase (CDD_L). Besides *M. hyorhinis*, 13 other *Mycoplasma* species exhibited the ability to inactivate GEM completely. The majority of these species express CDD_L for such purpose indicating the importance of this enzyme in inactivation of GEM.

5.1.2. Biodegradation of Antineoplastic Drugs in Sewage Treatment Plants (STPs)

ANPs residues can be removed from the aqueous phase in STPs either by biotic (biodegradation or biotransformation) or abiotic (sorption, photolysis, hydrolysis) processes [87]. Specifically for ANPs, different values for their removal in wastewater treatment plants were published earlier [40,88,89]. The removal rate can range anywhere between 10% and 90% [89,90]. The removal efficiency at STPs (F_{WWTP}) varies widely because F_{WWTP} is dependent on various factors such as locations of the served population, capacity, configuration, type of treatment, operating parameters, and hydraulic and solid retention times [91]. It is therefore necessary to decentralize data collection procedures at STPs, and whenever possible, specific experimental data of the STP operating in the study area should be used. Furthermore, important physical-chemical parameters such as volatilization, mixing, adsorption, and degradation should be considered to estimate F_{WWTP} as stipulated by the United States Environmental Protection Agency (US-EPA) and European Union System for the Evaluation of

Substances (EUSES) [91]. In addition to the factors already mentioned, the removal rate in STPs greatly varies among different ANP drugs and the efficiency of biodegradation is associated with the drugs and its physicochemical properties (hydrophobicity, solubility etc.) [21]. Elimination rates of some ANPs detected in STPs ranges from 10–88% (CP, ifosfamide (IF), CPC, TAM, and cytarabine (CTB)) to 77–100% (DOX, doxetaxel (DOX), ETS, GEM, ITN, CP, paclitaxel (PAC), megestrol [92], 5-FU, and MTX) clearly indicating that physicochemical properties of the drug impacts biodegradability [93]. Before jumping into the specifics of some STP studies on a few selected ANPs, it is necessary to understand that operation details on the fate and behavior of various ANPs in STPs are not provided in many studies, and as such no concrete conclusions can be drawn regarding this issue [93]. Some of the most commonly used ANP drugs and their removal during conventional biological treatment (STPs) are discussed in the following paragraphs.

Removal of Alkylating Agents in STP

Alkylating agents are a class of ANP drugs that prevent cell division primarily by cross-linking strands of DNA, and thereby inhibiting RNA and protein synthesis [94]. IF and CP are the most widely consumed alkylating agent type of ANPs, and several studies with conflicting results regarding their biodegradation have been published in literature [25,41,95–97]. In one of the early studies conducted in a laboratory scale sewage treatment plant (LSSTP), the result suggested that activated sludge did not appear to acclimatize to the presence of CP in the media and the drug was not efficiently biodegraded in LSSTP [25]. During the 39 days of operation (10 µg/L cyclophosphamide added/day), an average of 83% of undegraded CP was recovered in the effluent [25].

On the other hand, significantly high removal of IF and CP (100%) was recorded in some other studies [93]. IF (between 3 and 2 ng/L) and CP (up to 13.1 µg/L) have been found in the influent streams of STPs in Spain [93]. In the treated effluent streams, their concentration ranged from 0.09 to 71 ng/L for IF and 0.19 to 25 ng/L for CP, respectively [93]. The efficiency of removal is far exceeded to that of the result obtained in a study in Slovenia that merely removed 10% [98]. For IF, a higher removal efficiency of up to 87% in a STP in Switzerland [41], but less than 3% in a Chinese STP [99], whereas the maximum removal of CP was 100% in a Spanish STP [93], and the lowest removal was 10% in a STP study in Slovenia [98]. The varying elimination efficiency of CP and IF can be attributed to their different physicochemical properties (K_{ow} , water solubility, pKa, etc.). Moreover, the microbiota of STPs and concentration of these drugs in sewage varies geographically, and therefore no conclusions can be obtained regarding the efficiencies of these treatment plants. It should also be noted that in some studies these ANPs were detected in the effluent streams but were negligible in the influent streams of the STP process [26,100]. This paradox could be because in influent streams these drugs are present as conjugates (not detected as free drugs in influent streams) whereas in the effluent streams these conjugates are broken down and free drugs are thus detected [101].

Removal of Antimetabolites in STP

Antimetabolites are another class of ANP agents that are structural analogs of natural substances (such as vitamins, nucleosides, or amino acids) that compete with the natural substrate for the active site on an essential enzyme or receptor, thereby interfering with the DNA synthesis [102]. 5-FU, GEM, CTB, and MTX are another widely consumed group of ANP drugs belonging to the class antimetabolites that have been investigated so far [93]. Complete elimination of 5-FU present at an initial concentration of 5 mg/L was observed in Germany [103]. These results were corroborated by other studies where 5-FU was not detected in the influent or the effluent wastewater of four Spanish WWTPs, one Swiss, and one in Baltimore [93]. The absence of 5-FU in the influent stream can probably be explained by the fact that it is swiftly metabolized and produces biologically inactive metabolites [104].

In an STP in Slovenia, 5-FU was detected inside the influent wastewater at very low quantity (<3.1 ng/L) with up to 100% removal efficiency after the biological treatment. The removal of 3.5 ng/L 5-FU in a Spanish WWTP was also 100% [98]. Both findings stated above may indicate that 5-FU is

highly biodegradable at low concentrations. However, at higher levels (20 and 100 mg/L), 5-FU is partially biodegraded, and the TPs produced could be toxic [105]. In contrast to the results mentioned above, Kümmerer and Al-Ahmad [26] and Yu et al. [106] elucidated that 5-FU was persistent to biodegradation. Yu et al. [99] observed incomplete removals of 5-FU, even at lower concentrations (1 and 50 µg/L). Amid these contrasting results, Straub [107] critically evaluated available data regarding 5-FU biodegradability tests and suggested since biodegradability of 5-FU was conducted using different treatment methods in different laboratories it is challenging to compare biodegradation rates [108]. Lutterbeck et al. [81] reasoned that the difference in biodegradability of 5-FU was due to the varying initial bacterial population density. All the tests conducted with higher bacterial densities [105] showed faster elimination of 5-FU; whereas an analysis with lower bacterial densities showed the persistence of 5-FU.

Bioremediation studies for GEM (another antimetabolite) is scarce. The removal of GEM ranged from 25% to 100% during biological treatment [98,109]. Martin et al. [110] detected a higher concentration of GEM in treated effluents (65–88 ng/L) to that of the untreated influents (39–52 ng/L). Higher concentration in the influent stream was because GEM was present in conjugate form in influent streams whereas it was dissociated into free drug in the effluent stream [93].

For CTB, the elimination rates ranged from 24% up to 64%, and it was detected in quite high quantity in both influent and effluent streams [19,110]. For example, in samples taken from four Spanish STPs, the average influent and effluent concentrations were 464 and 190 ng/L, respectively [110]. The higher level in the influent stream was possibly due to conjugated CTB, as explained in detail before. Nevertheless, it should be noted that compared to other ANP drugs, neither cytarabine nor gemcitabine may possess mutagenicity or teratogenicity according to the International agency for research on cancer [93].

Lastly, another antimetabolite ANP that is widely used is MTX. Kosjek et al. [111] described the biotransformation of MTX in an aerobic conventional activated sludge (CAS) type STP. The findings in that study suggested that MTX was readily biodegradable and transformed into several TPs. Methotrexate is consumed faster by the microbes in the presence of nutrients. The high biodegradability of MTX can also be attributed to the fact that this drug is a weak carboxylic acid, and thus it is mostly dissociated at environmental pH. MTX is sufficiently removed by biodegradation in STPs, achieving complete degradation in some studies [96,112]. In general, the influent concentration of MTX ranged from 2.6 to 303 ng/L, while its effluent concentrations from <0.08 to 53 ng/L [93]. Nevertheless, based on the limited data on removal of antimetabolites, no concrete conclusion can be drawn regarding their elimination in STPs, and therefore more conclusive biodegradation studies are required to confirm the biodegradability of such antimetabolites.

Removal of Plant Alkaloids in STP

Plant alkaloids are nitrogen-containing organic compounds obtained from specific plants and used as an ANP agent in the treatment of cancer [113]. These plant alkaloids attack cells at different phases of cell cycle and inhibit cell division. Docetaxel (DOC), ETS, PAC, vincristine (VIN), and ITN are five major plant alkaloids that have been studied regarding their elimination through biological processes. Almost complete removal of DOC ($\log K_{ow} = 2.83$) was observed in a CAS type STP in a study in Spain where its effluent concentration was lower than 3.8 ng/L as compared to its influent concentration (65–219 ng/L) [112]. For ETS, highest removal in a CAS type STP is reported to be between 77% and 100%. The influent concentrations of ETS in these studies were in the range 15–83 ng/L, whereas the effluent concentration was in the range 2.9–3.5 ng/L [95,109,110]. ETS is primarily observed at high concentrations in hospital effluents (≈ 714 ng/L), and it was not detected in the influent or effluent streams of some domestic STPs in Spain and Slovenia [96,98,112]. This is probably because the use of ETS as a chemotherapeutic agent generally requires hospitalization [93]. The occurrence and removal of PAC has only been studied once by Ferrando-Climent et al. [112].

PAC ($\log K_{ow}$: 3.95) was detected (18 ng/L) only in one of three influent streams of a CAS type STP in Spain whereas it was not detected in effluent streams suggesting its complete removal. Complete elimination of another plant alkaloid, ITN, was observed in a CAS type STP with tertiary treatment in Spain with an influent concentration of up to 21.3 ng/L [96]. ITN was also detected in the influent stream (49 ng/L) of a CAS type STP in Slovenia where it was almost completely degraded as the effluent concentration was less than 0.4 ng/L [98]. The biotransformation of the another plant alkaloid vincristine was also recently investigated [114]. The study showed that vincristine was readily biodegradable in CAS. This study observed that the presence of a nutrient-rich medium accelerated biodegradation rate. However, the study cautioned that the biodegradation rates could appreciably slow down if the microbial consortia present is inhibited due to the presence of some other drug which is toxic. Therefore, it is necessary to design systems keeping in mind the presence of other drugs in the system. The high removal efficiency of plant alkaloids observed in all these studies is possibly due to its high sorption to sewage sludge due to hydrophobic (low $\log K_{ow}$ value) and ionic interactions as suggested by Kosjek and Heath [4].

Removal of Antitumor Antibiotics in STP

Antitumor antibiotics are amongst the most important ANP agents administered for chemotherapeutic purposes. They mainly to bind to DNA or RNA through intercalation and stop cancer cells from growing [115]. DOX and epirubicin [116] are the only two antitumor antibiotics that have been investigated until now [93]. Contrasting results have been obtained regarding the removal of DOX in STPs. According to the study by Martin et al. [109] in Spain, DOX was not detected in the influent (concentration below limit of detection) whereas it was detected in the range 20.3–42.4 ng/L in the effluent stream. This was probably because DOX existed in conjugated form in the influent stream. The study by Negreira et al. [96], however, found that DOX was completely eliminated from 12 STPs in Spain as the median concentration of doxorubicin changed from 2.6 ng/L in the influent stream to below limit of detection in the effluent stream. On the other hand, Franquet-Griell et al. [117] noted that DOX remained at 40% of the initial concentration, and in one more study by Martin et al. [110] DOX was detected at higher concentrations in the effluent streams of four Spanish STPs (20.3–42.4 ng/L) probably due to conjugate formation. EPI, another antitumor antibiotic was undetected in the effluent stream of three STPs in Spain while it was detected at very low concentrations (in the range 4.5–6 ng/L) in hospital effluent in the same studies indicating EPI might be degraded or adsorbed to sewage sludge while passing through the STP [109]. This result was corroborated by the another study where EPI was neither detected in the influent or in the effluent streams of two STPs in Canada [97]. The limited and contradictory literature data for doxorubicin DOX shows that its removal from STPs is not properly understood and further investigation is required to get a lucid picture regarding its biodegradability. On the other hand, for epirubicin, it seems that it is completely degraded in a STP, however, more research is needed from different geographic locations to confirm its complete removal in a STP.

Removal of Hormonal ANPs in STP

Hormonal ANPs are another type of chemotherapeutic treatment that interferes with hormone system, in order to slow or stop the growth of cancer cells. Hormonal ANPs are used in the treatment of various hormone-dependent cancers such as breast and prostate cancer [93]. TAM and Megestrol [92] are the two mostly studied hormonal ANPs with regard to their removal from STPs. TAM is one of the most widely used ANP for breast cancer treatment. The removal of TAM was noted to be insufficient (ranging from 18% to 50.6%) from secondary and tertiary biological treatment in STPs. The concentration of TAM in influent stream of STP ranged from 3.5 to 215 ng/L and in the effluent stream the concentration ranged from 5.8 to 13.5 ng/L in various studies [96,98,112,118]. Even when tertiary treatment was applied the removal efficiency of TAM was lower (37% and 30% in STPs in Spain and United Kingdom, respectively) indicating its resistance to biodegradation [96,118]. Another most widely used hormonal ANP is MEG which is the most common progesterone used in medicine. It was

detected in the influent of a Spanish STP at concentration ranging from 3 to 150 ng/L, and achieving a significant removal of 87% through CAS treatment [119]. In the same study, MEG was the only ANP drug detected in a second STP at an influent concentration of 220 ng/L which was completely removed (100% elimination) through biological treatment [119]. In the study by Franquet-Griell et al. [117], MEG was not detected in the effluent stream of STP indicating its complete removal. However, the study was inconclusive as to whether elimination of MEG was due to sorption onto sewage sludge or through biodegradation. When both these hormonal drugs are compared, TAM appears to be poorly biodegradable through secondary and tertiary treatment and therefore would require further investigation regarding its occurrence and toxicity in aqueous and terrestrial environments. On the other hand, MEG appears to be completely removed, however, there are contradictions regarding the mechanism of its removal (biodegradation or sorption). Therefore, further investigations focused on the mechanism of its removal is necessary.

5.1.3. Removal of ANP Drugs Using Membrane Bioreactors

Membrane bioreactors (MBRs) are advanced biological treatment processes that combine the CAS with a membrane filtration process [120]. Previous investigations have shown that pharmaceutical residues are often not completely removed during the activated sludge process, which makes CAS inefficient for some pharmaceuticals [121]. MBRs is a notable system as it can be operated with highly intensified biomass, high sludge retention time, lower sludge production, high effluent quality, and enhanced biotransformation and mineralization of resistant pharmaceutical compounds [93,121]. Though the total operational cost is higher for MBR systems, it is an attractive alternative waste treatment technology as it provides a more environmentally friendly effluent [93]. However, it is necessary to note that the use of MBRs for removal of ANPs at large-scale is not available and as such only pilot scale and bench-scale studies on removal ANPs have been discussed.

Mahnik et al. [48] investigated the biodegradability of four drugs, 5-FU, DOX, EPI, and daunorubicin (DAU), present in the wastewater of an oncogenic ward by elimination using activated sludge and treatment in a 1000 L pilot scale membrane-bio-reactor system. 5-FU was almost completely eliminated within 24 h, and biodegradation was hypothesized to be the most plausible mechanism as 5-FU did not adsorb to suspended solids in wastewater. On the other hand, DOX, EPI, and DAU were eliminated more than 90% from the sewage sludge mainly due to adsorption. The results indicated that all the studied anticancer drugs are eliminated by sewage treatment plants, either by biodegradation or adsorption.

In another study, the removal of cancerostatic platinum compounds (CPC) CPT, CBT, OXT, 5-FU, and anthracyclines DOX, DAU, and EPI were conducted in a pilot-scale MBR system [122]. The CPC compounds were removed at a mean value of 60% due to their adsorption to sewage sludge whereas 5-FU and the three anthracyclines were removed below limit of detection within 24 h mainly due to the adsorption by the MBR system. In addition, the genotoxicity of the CPC compounds was reduced in the effluent. Delgado et al. [123] studied the removal of CP and its principal metabolite 4-ketocyclophosphamide (4-ketoCP) in a laboratory scale MBR. The pharmaceutical removal efficiency for CP remained quite stable at 80%, largely due to adsorption and biodegradation. On the other hand, the concentration of 4-ketoCP was higher in the reactor than in the feed, and its removal efficiency decreased from day 35 to day 66 largely due to the conversion of CP to its metabolite 4-ketoCP indicating further downstream treatment may be required.

In another study, CP was removed up to 80% in a pilot-scale crossflow MBR from urban effluents. However, toxicity was observed in the effluent stream, indicating that further post-treatment is required to eliminate effluent toxicity [124]. On the other hand, insignificant removal of CP ($\approx 20\%$) was observed in the effluents of hospital wastewater treated in a pilot-scale MBR, though, no reason was given for its low removal efficiency [125]. The cause could be due to the fouling of the membranes in MBR as observed during the removal of CP by Avella et al. [126]. The transmembrane pressure increased significantly (3-fold increase) due to fouling of the membrane as CP was added to the urban wastewater.

The increased fouling was possibly due to increased exopolysaccharide or other microbial product synthesis caused by stress due to the presence of CP [127].

In a more recent study, the removal efficiency of eight ANP drugs was investigated in an anaerobic osmotic MBR (AnOMBR) [128]. AnOMBR is an innovative technology that combines biological treatment with forward osmosis (FO) under anaerobic conditions [129]. AnOMBR is highly efficient because of its low energy demand, high organic loading, and methane production [130]. Wang et al. [128] observed high removal rates (>95.6%) for all the eight investigated ANP drugs. A high removal rate was ensured due to the high rejection of the FO membrane combined with the extended organic retention time in the reactor. DOX, EPI, and TAM were almost eliminated through adsorption, while MTX and CP were eliminated by biodegradation and FO rejection, respectively. MTN, AZT, and Flutamide (FLT) were eliminated by both biodegradation and adsorption to anaerobic sludge. However, there are disadvantages associated with AnOMBR as envisaged in the study by Wu et al. [131]. In that study, it was observed that the presence of ANPs caused the inhibition of microbial metabolism. At the same time, marginally changing microbial community's composition, while the extracellular polymeric substances (EPS) concentration was increased. The increased EPS production caused severe biofouling and significantly increased transmembrane pressure.

The level of STP processing (primary, secondary, and tertiary treatment) is not mentioned in many of the studies. Therefore, the removal efficiencies cannot be compared for the different studies reviewed above. The concentrations and the removal rates of these ANPs (specifically the two alkylating agents) vary significantly through the WWTPs worldwide, making it difficult to conclude if these compounds are highly resistant or not to biological treatment. However, most of the available studies so far indicated that the removal rates of these two alkylating agents through conventional processes are lower than 65%, showing that there is a need for subsequent post-treatments.

Furthermore, when compared to STP-CAS systems, higher removal efficiency seems to be observed in MBR systems in a lab- and pilot-scale. However, more studies on a larger scale are required to provide more concrete and reliable finding regarding its efficiency and total operating costs for each setup. In addition, more investigation is needed with regard to MBR effluents toxicity; though the toxicity is expected to be low because of the filtration systems, however, more data is required to confirm this hypothesis [93]. Moreover, it is also necessary to conduct microbial community analysis in the presence of various ANP drugs to understand the influence of such drugs on the composition and function of the microbial community. The removal of some regularly prescribed ANP drugs through conventional biological processes is shown in Table 3.

Table 3. Biological degradation of some widely used ANP drugs.

ANP Drug	Type of Biological Treatment	Mechanism of Bioremediation	Initial Concentration (ng/L)	% Elimination of the Parent Drug	Reference
TAM	Fluidized bed bioreactor (with <i>Trametes versicolor</i>)	Intracellular transformation by cytochrome P-450 system	970	91%	[70]
IF	CAS-STP ^a	N.D.	16.4	45%	[99]
FLT	Biotransformation by <i>Caenorhabditis elegans</i>	Cytochrome P450 mediated oxidation	9×10^7 ^b	50%	[67]
CP	LSSTP ^c	Biodegradation	6–143	>80%	[25]
CPC	STP	Biodegradation	158	100%	[98]
CTB	CAS-STP	N.D.	N.D.	24%	[19]
DOC	CAS-STP	Biodegradation and sorption	65–219	≈100%	[112]

Table 3. Cont.

ANP Drug	Type of Biological Treatment	Mechanism of Bioremediation	Initial Concentration (ng/L)	% Elimination of the Parent Drug	Reference
ETS	CAS-STP	N.D.	15 ng/L	77%	[109]
VNB	CAS-STP	Non-biodegradable	<LOD ^d	0% ^e	[110]
PAC	CAS-STP	Biodegradation and sorption	<LOD-18	100%	[112]
GEM	CAS-STP	Adsorption to sewage sludge	840	40–79%	[132]
BLC	CAS-STP	N.D.	11–19	-	[133]
MTN	AnOMBR ^f	Adsorption and biodegradation	100	100%	[128]
5-FU	eMBR ^g	Biotransformation and sorption	0–1.2 × 10 ⁶ h	>90%	[134]
DOX	CAS-STP	Biodegradation	2.5–2.7	100%	[96]

Notes: Tamoxifen: TAM; Ifosfamide: IF; Flutamide: FLT; Cyclophosphamide: CP; Capecitabine: CPC; Cytarabine: CTB; Docetaxel: DOC; Etoposide: ETS; Vinorelbine: VNB; Paclitaxel: PAC; Gemcitabine: GEM; Bleomycin: BLC; Mitotane: MTN; 5-Fluorouracil: 5-FU; Doxorubicin: DOX. ^a Conventional activated sludge type sewage treatment plant; N.D. not determined in the study; ^b The experiment was conducted in a conical flask (5 mg flutamide dissolved in 50 mL broth and 5 mL culture); ^c Laboratory scale sewage treatment plant; ^d Limit of detection; ^e vinorelbine showed high concentration in effluent wastewater (up to 170 ng/L); ^f Anaerobic osmotic membrane bioreactor; ^g External membrane bioreactor; ^h The concentration in the study was in range 0–1287 µg/L.

6. Removal of ANPs Using Abiotic Methods

As discussed earlier, the elimination of ANP agents by conventional wastewater treatment such as CAS and MBR is often incomplete and inefficient. The reason is that some of these ANP drugs are resistant to biodegradation, have low adsorption efficiency, and tend to generate TPs [21,135]. In addition, some researchers believe that despite excellent removal efficiency (>80%) of biological methods, ANP agents might have adverse effects on all eukaryotic organisms even at deficient concentrations due to their toxicological properties [1,22,40]. Further, due to the possibility of occurrence of ANP drugs in potable water, their complete elimination is of high importance. In this sense, abiotic treatment methods such as chemical, filtration, and other oxidation and advanced oxidation treatments become essential as they can degrade numerous ANPs that are missed in conventional wastewater treatment. Some of these abiotic methods are explained in brief in the following sections.

6.1. Adsorption on Abiotic Surfaces

Various physical and chemical methods have been used for the remediation of ANP drugs. Techniques such as adsorption, membrane filtration, and electrodialysis rely on the differences in physico-chemical properties of ANP drugs [136,137]. Both polar and non-polar ANP agents in aqueous systems such as wastewater effluents can be omitted by using activated carbon in powdered or granulated forms. Chen et al. [138] analyzed the adsorption of three ANP drugs (Irinotecan (IRN), TAM, and CP) on powdered activated carbon (PAC) [139]. They inferred an inverse relationship between the hydrophobicity of the tested drugs and their adsorption on PAC with more hydrophobic drugs (lower log K_{ow}) showing better adsorption (Tamoxifen (log K_{ow} = 6.30) > Irinotecan (log K_{ow} = 3.73) > Cyclophosphamide (log K_{ow} = 0.63)). More hydrophobic compounds exhibited better adsorption.

However, adsorption cannot be chosen as a standalone approach in removing all ANPs because of two reasons. (i) pH influences the hydrophobicity of ANPs due to which some ANPs may become ionized, thereby minimizing their adsorption efficiency [19]. (ii) The calculation of hydrophobicity is inaccurate or not possible in some cases. For instance, it is hard to know the hydrophobicity of

protein-based ANPs; such as antibodies (ATC code L01XC) and recombinant proteins (ATC code L01XE). The distribution equilibrium of macromolecules is also pH-dependent [19]. In general, polar compounds with log K_{ow} values < 1 should not adsorb to organic matters [4]. However, interactions between polar compounds and organic matter by hydrophobic and ionic interactions cannot be neglected. It is therefore recommended that any decontamination technique being developed should consider the pH dependency of the drugs, including its ionizability, and physico-chemical parameters that were stated earlier in Section 2.

6.2. Membrane Based Filtration Technologies

Membrane-based filtration and dialysis techniques such as reverse osmosis (RO), nanofiltration (NF), ultrafiltration (UF), and electrodialysis have also been used for the removal of pharmaceutical drugs from wastewater and have given ambiguous results [21,140–144]. NF was able to efficiently remove (>90%) negatively charged pharmaceuticals while the removal efficiency of non-charged pharmaceuticals varied widely (12% to 99%) [143]. Electrostatic exclusion was the main reason for the removal of charged medicines, while size exclusion was the critical mechanism for the removal of non-charged compounds [143]. Another study on the removal of CP by NF and RO membranes demonstrated that CP was efficiently (>90%) removed when RO membrane was applied; however, only 20–40% removal of CP was observed when NF was operated [145]. The high elimination efficiency of the RO membrane was seen under all operating conditions with no effect of changing trans-membrane pressure, feed concentration, and water matrix on the removal rate. Though membrane-based filtration technologies have shown some success in removal of ANP drugs, they suffer from two significant drawbacks of membrane fouling and high maintenance cost due to the pressure-driven nature of these technologies [21].

Another membrane-based technology tested for degradation of ANP agents is electrodialysis [144,146]. Electrodialysis is a membrane-based process operated under the influence of an electric field in which ions move across a semi-permeable membrane (cation exchange or anion exchange). Electrodialysis can be used for source-based separation of residual drugs in urine in which the concentrated stream contains salts, whereas the diluted stream is rich in pharmaceutical compounds [21]. Pronk et al. [144] conducted electrodialysis experiments and observed that the adsorption of drugs depends on the ionic characteristics (acidic or basic), in addition to the hydrophobicity of the compounds. The results indicated that compounds with greater hydrophobicity are easier to separate through electrodialysis.

Studies on membrane filtration-based removal of ANPs are still insufficient, and no absolute conclusions can be drawn based on the separation of a few pharmaceuticals evaluated under ideal laboratory conditions. This warrants the need for further research in designing new membranes at lower-costs and optimizing the system's operating condition.

6.3. Chemical Treatments

Remediation using chemical treatments has been extensively applied in the past to treat ANP wastes from hospitals but is losing popularity nowadays. Strong oxidizing (potassium permanganate and sodium hypochlorite), and alkylating agents (hydrogen peroxide and Fenton reagent) are commonly utilized chemicals [147–149]. The degradation ability of these chemicals depends mostly on the chemical structure of the drugs, and the concentration of chemicals used. Additionally, the TPs formed by chemical degradation can be mutagenic and toxic from some chemical treatments and benign from others [147,149,150]. Hydrogen peroxide (30%, *v/v*) and Fenton reagent (30%, *v/v*) have been used to degrade various ANP agents (e.g., idarubicin (IDA), DOX, EPI, pirarubicin (PIR), aclarubicin (ACL), DAU, CP, IF, and melphalan (MEL)) [148,149]. DOX and DAU were degraded entirely after an hour when using either sodium hypochlorite or Fenton reagent (a mixture of H_2O_2 and a ferrous salt), and the TPs formed were found to be non-mutagenic. In the same study, treatment with 30% H_2O_2 led to only partial degradation (68%) of DOX whereas complete degradation of daunorubicin was observed

after 48 h of treatment [148]. However, similar studies conducted using Fenton reagent resulted in the generation of mutagenic TPs during the degradation of MEL and DAU [149,151]. Therefore, the mutagenicity of TPs generated by various chemical treatments should be tested irrespective of treatment procedure used since the mutagenicity is mostly dependent on drug type. In addition to the drug type, the drug preparation protocols have also affected the efficiency of chemical treatments in many studies [149,150]. Hansel et al. [63] found that chemical degradation of CP by Fenton oxidation in the presence of 5% Dextrose (D5%) generated mutagenic TPs, whereas in the absence of D5% no mutagenic TPs were created.

Another limitation of chemical treatments is the need to quench and neutralize the pH after reaction for subsequent mutagenicity tests. Furthermore, due to the risk of secondary contamination with toxic chemicals used in ANP treatment, and the associated costs, scaling of these treatment methods is not feasible. Due to this concern, future research efforts should be directed towards minimizing the use of chemical treatment methods and developing an integrated technology that degrades ANP agents and prevents them from causing irreparable damage to the aquatic and terrestrial ecosystem.

6.4. Decontamination Using Oxidation and Advanced Oxidation Methods

6.4.1. Oxidation Methods

Methods such as photolysis, photooxidation, ozonation, UV treatment are the most trending oxidation methods used for degradation of ANPs [2,81,105,152]. Photolysis, i.e., sunlight-mediated photodegradation may occur via direct and indirect pathways: direct photolysis occurs through light absorption by the chemical itself and leads to chemical bond cleavage. Indirect photolysis involves light absorption by dissolved organic matter (DOM) such as nitrates, nitrites, and carbonates in the aqueous environment, producing reactive species that react with target analytes (ANPs) [153].

Generally, natural attenuation under direct solar radiation cannot occur when a substance cannot absorb radiation over 290 nm [154]. For example, results from direct photolysis experiments conducted by Lin et al. [153], demonstrated that CP showed minimal to no absorbance in the 250–350 nm range and did not show any signs of degradation even after 24 h of exposure to sunlight. 5-FU, on the other hand, had a maximum absorbance at ≈ 265 nm and underwent direct photolysis with a half-life of 56 h [153]. During indirect photolysis, in the presence of nitrate (>5 mg/L) and significant amounts of bicarbonate (close to 2 mM), 93% of 5-FU was rapidly removed (within one day) from the sample tested, whereas CP showed minimal degradation. The degree of mineralization was another criterion used in this study to test the efficacy of photolysis. The analysis of the degree of mineralization was done through the determination of total organic carbon (TOC) which would increase if the drug reacts and incorporates with the organic matrix. Further insight into the byproducts from both direct and indirect photolysis of 5-FU revealed that photolytic degradation had transformed 5-FU into other organic substances of unknown toxicity, with no mineralization even after 42 h of reaction time [153]. The high 5-FU degradation and lack of mineralization further implied that photoproducts of 5-FU are likely to be less photolabile. Similar results were observed in other studies, where ANPs and other pharmaceuticals have been found to undergo only photo-transformation (no mineralization), and the TPs generated were less photolabile and more toxic [21,135,154]. These results challenge the validity of the current understanding of sunlight photolysis and prompts us to investigate for other efficient alternatives. Gomez et al. [155] have also shown the complexity of the photodegradation process of 5-FU, where a large number of photo-TPs were identified. This study also did not identify the toxicity of photo-TPs formed. Franquet-Griell et al. [117] studied the UV-C light photolysis of 16 widely used ANP drugs. They found that ANP drugs MEL, ETS, and prednisone (PDN) were completely eliminated by UV-C light photolysis when all of these drugs were previously passed through hydrolysis and a STP plant. The degradation was fast, and after 30 min of treatment none of these compounds were detected. The fast degradation was possibly due to the presence of aromatic groups in these drugs that absorb UV light. Non-aromatic drugs such as MEG and CTB were still present at 18% and 40% of the

initial concentration. IF and CP were the most refractory drugs that showed minimal degradation even after 90 min. This suggests that if UV-C photolysis is the last step in treatment some drugs may not be removed and could be discharged to surface waters.

Some other studies that used electro-Fenton oxidation [156] and photo-Fenton oxidation [157] were able to almost completely remove refractory drug 5-FU. Electro-Fenton oxidation resulted in complete degradation of 5-FU in 7 min. It was also noted that oxidation increased on increasing Fe^{2+} concentration to 0.2 mM. This was possibly because of larger production of OH^{\bullet} radicals at 0.2 mM. Photo-Fenton oxidation achieved 98% degradation of 5-FU in 30 min. All the oxidation methods discussed in this section show that a more advanced and integrated treatment procedure needs to be designed depending on whether the drugs are refractory, or whether they have aromatic side chains or not.

6.4.2. Advanced Oxidation Methods

Advanced oxidation processes (AOPs) can be a suitable alternative, which could result in the satisfactory elimination of ANPs. Some studies have investigated the degradation of ANP agents such as 5-FU [81,105,158]; MTX [108], bortezomib (BRZ) [152] using primarily three different advanced photooxidation processes (AOPs) individually as well in combination: UV/ H_2O_2 , UV/ $\text{Fe}^{2+}/\text{H}_2\text{O}_2$, and UV/ TiO_2 . Results indicated faster elimination of most of the 5-FU and MTX in all the irradiation reactions. Treatment of 5-FU with UV/ $\text{Fe}^{2+}/\text{H}_2\text{O}_2$ and UV/ TiO_2 achieved the highest degree of mineralization, whereas the lowest degree of mineralization was seen after treatment with UV/ H_2O_2 . The low mineralization (with UV/ H_2O_2) was due to the formation of per hydroxyl radicals [81]. The TPs formed during the reactions did not show positive indications for mutagenic effects but were still toxic. However, in another AOP study conducted by Burleson and Chambers [159], the TPs formed by ozonation of CP were more mutagenic than the parent compound. The implications of this and other works, suggests that photolysis and AOPs, like other abiotic treatments, cannot achieve complete ANP drug remediation. A potentially efficient alternative for ANP remediation is the use of chemical and oxidation methodologies in association with biological treatments [160,161]. Biological treatments use natural biological systems for drug degradation and are therefore more environmentally safe. Though the integration of biological and AOP treatments appear encouraging, increasing the biodegradability through either partial oxidation or as a post-treatment for the degradation of persistent compounds [81], gives contradictory results. Biodegradability studies conducted by Lutterbeck et al. [81], showed negligible biodegradation of 5-FU, and thus classified the compound as not readily biodegradable. However, the compounds present in the photolytic mixture (mostly TPs) obtained after UV/ H_2O_2 treatment had a better biodegradability.

As observed in all these abiotic methods, all parent compounds were eliminated (either entirely or partially) but the mixture of TPs formed was toxic and non-biodegradable in many cases (Table 4). Highlights from some more studies on degradation/elimination of ANP drugs using various abiotic methods are listed in Table 4. A schematic view of the existing biotic and abiotic methods of ANP degradation is provided in Figure S1 of the Supplementary Information. The use of harsh chemicals and advanced oxidation is costly and is not environmentally benign, and it may contribute to the formation of other complex products that may be difficult to eliminate. It is therefore necessary to design efficient and sustainable treatment technologies which includes both biotic and abiotic methods, and which is environmentally friendly and is inexpensive. The next section of this review discusses one such idea that incorporates energy generation to reduce total capital cost of remediation.

Table 4. Studies on removal of ANP agents using physico-chemical and oxidation methods.

Treatment Process	Target ANP Drug	% Elimination	No. of TPs Formed	Biodegradability Treated Drug and Its TPs	Change in Toxicity (Drug vs. TPs)	Reference
Advanced (Photo)Oxidation (UV/TiO ₂)	DOX	100% in 30 min	17 TPs	N.D.	Decrease in toxicity in 2 h (3% toxicity reduction)	[162]
Advanced (Photo)Oxidation (UV/H ₂ O ₂)	MTX	>99% in 16 min	6 TPs	Very low biodegradability	40% decrease in toxicity	[108]
UV Photolysis	5-FU	100% elimination in 32 min	3 TPs	Increased biodegradability	45% decrease in toxicity	[2]
Ozonation (O ₃)	CP	69.8% at pH 9 61.2% at pH 5	N.D.	N.D.	Increase in acute toxicity	[163]
Chlorination	ERL	95% in 1 h	16 TPs	N.D.	Increase in toxicity of TPs	[164]
Electron beam irradiation	CPC	73% for 50 mg/L CPC and 36% for 150 mg/L CPC	5 TPs	N.D.	TPs had lower toxicity than parent compound	[165]
Electro-oxidation	MTX	100% in 30 min at CD ^b of 30 mA/cm ²	4 TPs	N.D.	Increase in toxicity	[166]
Photo Fenton oxidation (UV/Vis/H ₂ O ₂ /Fe ²⁺)	5-FU	100% in 1 h	N.D.	N.D.	Decrease in toxicity	[167]
TiO ₂ /H ₂ O ₂ /SSL ^c	CTB	100% in <45 min	4 TPs	N.D.	11% decrease in toxicity	[168]
Advanced (Photo)Oxidation (UV-C/HO ₂)	ETS	100% elimination	N.D.	N.D.	Not tested for toxicity	[169]

Notes: 5-FU: 5-Fluorouracil; CP: Cyclophosphamide; IF: Ifosfamide; CIP: Ciprofloxacin; DOX: Doxorubicin; Erlotinib: ERL; Capecitabine: CPC; Cytarabine: CTB; Etoposide: ETS; TPs: Transformation products; N.D.: Data not determined in the study; ^b Current density; ^c Photochemical degradation by TiO₂ photocatalysis under simulated solar light.

7. Possible Strategies for Improved Remediation of ANP Waste Incorporating Thermophiles

Despite the strategies already undertaken to degrade ANP waste and considering the growing concern on efficacious ANP waste disposal, there is an urgent need of developing a systematic, efficient, and integrated degradation process for complete remediation of ANP waste (including its TPs and human metabolites). The waste treatment technologies should be chosen to take into account the origin and nature of waste, the degree of hazard attrition required, nature of TPs formed, and economics [170]. Many unexplored ideas could be used to degrade ANP waste and their TPs systematically. Some of the strategies that could be of valuable importance and have not yet been used successfully are discussed in brief in this section.

Treatment of high strength aqueous waste containing ANPs by integrating biotic and abiotic treatment methods or a combination of these have been proposed in recent years [170,171]. For example, when abiotic treatment methods such as UV/Ozonation was combined with biological treatment, degradation efficiency of greater than 99% was achieved for CP and IF [27]. Other methods such as source-based separation and treatment of urine [21], combined with an integrated abiotic and biotic treatment downstream can be used to minimize the concentration of ANP waste in aquatic systems. Source-based treatment of urine is separate collection and treatment of urine before discharging it into the wastewater treatment plants [172]. Source-based separation of urine also contributes toward reducing excessive nutrient release into downstream treatment plants thereby abating eutrophication, increasing the treatment efficiency of settled wastewater by 60%, and ultimately increasing the life of downstream treatment plants [21,173,174].

For enhanced biological transformation and mineralization of pharmaceuticals after urine separation, membrane bioreactors (MBR) [27] can be employed that have the inherent ability to process higher organic loading rates. If downstream waste treatment processes incorporating MBRs operate at mesophilic temperatures, it will create a breeding ground for pathogens and other antibiotic-resistant bacteria. To counter this concern, thermophilic decontamination techniques could be employed. Thermophilic conditions have distinct advantages over mesophilic ones, such as high organic loading and rapid removal rate of biodegradable substrates, ability to treat high strength aqueous wastes from industrial facilities containing hazardous compounds constituting ANP agents, and potential for minimal effluent discharge [170,175,176]. The role of thermophiles in ANP drug elimination has not been explored much but owing to the benefits of thermophiles, an efficient integrated abiotic and biotic treatment technology could employ thermophilic MBR systems for treatment of source separated urine from hospital settings.

Apart from thermophilic MBRs, another approach to enhance the biodegradation could be the use of electrochemical techniques. The electrochemical strategies provide clues for harnessing the thermophilic electroactive microorganisms for mediating the detoxification of these ANP drugs. These systems operate by applying external electrical energy for mediating the chemical transformation of these drugs. Application of specific oxidation or reduction potential will aid in microbial oxidation/reduction of these drugs at accelerated rates. Barisci et al. [177] reported an electrooxidation strategy for the degradation of ANP drug carboplatin using differently mixed metal oxide and boron-doped diamond electrodes. Experiments at different pH values showed that Ti/RuO₂ anodes degraded ANP drug carboplatin up to 49% and 75% at pH 9 and 4, respectively. Another study Zhang et al. [178] examined the electrochemical treatment of anticancer drugs wastewater containing 5-Fluoro-2-Methoxypyrimidine (5FMP) using a tubular porous electrode electrocatalytic reactor. They found that increasing the flow rate improved the removal efficiency of the 5FMP. Approximately 96.1% removal of 5FMP was observed after 180 min at a flow rate of 0.31 L/min. This could be attributed to the fact that high flow rate enhanced the mass transfer efficiency of the drug. Such examples of electrochemical methods give a strong background for developing bio-electrochemical process employing thermophilic microorganisms for faster degradation of ANP drugs. Figure 4 shows a possible integrated ANP waste decontamination methodology using the techniques mentioned in this section.

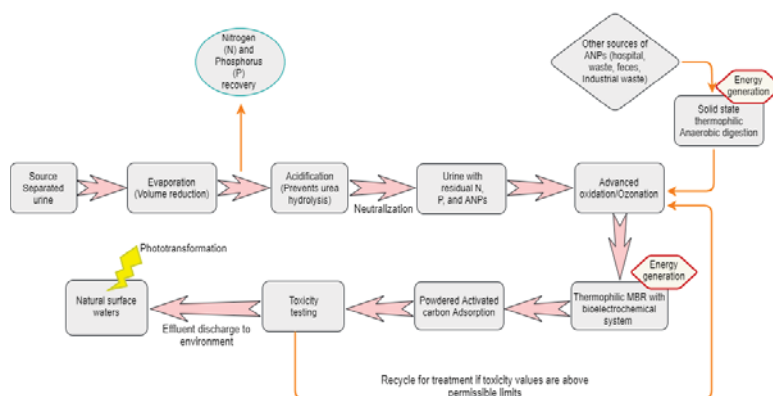


Figure 4. Proposed integrated ANP waste treatment methodology employing thermophiles.

8. Conclusions

This review summarizes the sources and occurrence of ANP drugs in the environment as well as the methods currently being used for their remediation to address the present challenges and future opportunities of these methods. Though these studies have explored the potential of biodegradation of ANPs, however, specific issues related to the generation of TPs and epoxides have come to light recently. For example, fungi in sewage treatment plants (STPs) generate epoxides by oxidizing aromatic hydrocarbons that can have toxic effects on human and animal health [92,179]. The toxicity and mutagenicity of the intermediate and degradation products are not reported in many of ANP biodegradation studies. TPs can be sometimes more toxic than the parent compound, and therefore toxicity studies should be conducted on TPs generated after biodegradation of the parent compound. The need for environmentally safe remediation of ANP drugs has become a paramount concern due to their increased production in the last decade. The highly toxic nature of ANP waste adversely affects the terrestrial and aquatic life. The use of expensive and harsh abiotic techniques is not environmentally friendly and often transforms the parent drug into recalcitrant TPs. Considering this, there is a need to develop an efficient and environmentally friendly remediation method. Integration of biological remediation with the non-biological techniques could be more sustainable and promising alternative for the safe removal of ANP drugs. The use of thermophilic MBRs for treatment of source-separated urine can also aid in safe-remediation of ANP drugs. Future strategies would require thorough techno-economic evaluation before implementation at large scale waste removal plants. Improved ANP degradation strategies will protect ground and surface water which in turn is crucial for the human health and agricultural sector. This will maintain the quality of irrigation products and restrict the entry of ANP waste in food cycle of higher eukaryotes, thus eliminating the chances of ANP biomagnification.

Supplementary Materials: The following are available online at <http://www.mdpi.com/2227-9717/8/7/747/s1>, Table S1: Raw data for global heat map on number of ANP drugs produced in 2004 and 2014 in select countries, Table S2: Raw data on age standardized number of cancer cases per 100,000 people in select countries, Figure S1: Schematic of existing methods of ANP degradation.

Author Contributions: Conceptualization: A.K.T. and R.K.S.; methodology, A.K.T., A.D., T.G. and S.R.; validation, N.K.R. and A.K.T.; formal analysis, A.D., T.G. and S.R.; investigation, A.K.T. and R.S.; resources, A.D., T.G. and S.R.; data curation, A.K.T. and R.S.; writing—A.K.T.; writing—review and editing A.K.T., A.D., T.G., S.R., K.M.G., N.K.R. and R.K.S.; visualization, A.K.T. and A.D.; supervision, R.K.S. and K.M.G. All authors have read and agreed to the published version of the manuscript.

Funding: This research was supported by the National Science Foundation (Award # 1736255, #1849206, and #1920954).

Acknowledgments: The authors gratefully acknowledge the support from National Science Foundation in the form of BuG ReMeDEE initiative (Award # 1736255) and the Department of Chemical and Biological Engineering at the South Dakota School of Mines and Technology.

Conflicts of Interest: The authors declare no conflict of interest.

References

1. Johnson, A.C.; Jürgens, M.D.; Williams, R.J.; Kümmerer, K.; Kortenkamp, A.; Sumpter, J.P. Do cytotoxic chemotherapy drugs discharged into rivers pose a risk to the environment and human health? An overview and UK case study. *J. Hydrol.* **2008**, *348*, 167–175. [CrossRef]
2. Lutterbeck, C.A.; Wilde, M.L.; Baginska, E.; Leder, C.; Machado, Ê.L.; Kümmerer, K. Degradation of cyclophosphamide and 5-fluorouracil by UV and simulated sunlight treatments: Assessment of the enhancement of the biodegradability and toxicity. *Environ. Pollut.* **2016**, *208*, 467–476. [CrossRef] [PubMed]
3. Espinosa, E.; Zamora, P.; Feliu, J.; González Barón, M. Classification of anticancer drugs—A new system based on therapeutic targets. *Cancer Treat. Rev.* **2003**, *29*, 515–523. [CrossRef]
4. Kosjek, T.; Heath, E. Occurrence, fate and determination of cytostatic pharmaceuticals in the environment. *Trends Anal. Chem.* **2011**, *30*, 1065–1087. [CrossRef]
5. Meegan, M.J.; O’Boyle, N.M. Special Issue “Anticancer Drugs”. *Pharmaceuticals* **2019**, *12*, 134. [CrossRef] [PubMed]
6. Siegel, R.L.; Miller, K.D.; Jemal, A. Cancer statistics, 2020. *CA A Cancer J. Clin.* **2020**, *70*, 7–30. [CrossRef] [PubMed]
7. Sun, J.; Wei, Q.; Zhou, Y.; Wang, J.; Liu, Q.; Xu, H. A systematic analysis of FDA-approved anticancer drugs. *BMC Syst. Biol.* **2017**, *11*, 87. [CrossRef] [PubMed]
8. Aitken, M. Global Oncology Trend Report: A Review of 2016 and Outlook to 2020. *IMS Inst. Healthc. Inform.* **2016**, *1*, 1–45.
9. Hoppe-Tichy, T. Current challenges in European oncology pharmacy practice. *J. Oncol. Pharm. Pract.* **2010**, *16*, 9–18. [CrossRef]
10. Salas-Vega, S.; Mossialos, E. Cancer Drugs Provide Positive Value In Nine Countries, But The United States Lags In Health Gains Per Dollar Spent. *Health Aff.* **2016**, *35*, 813–823. [CrossRef]
11. Heath, E.; Isidori, M.; Kosjek, T.; Filipič, M. *Fate and Effects of Anticancer Drugs in the Environment*, 1st ed.; Springer Nature: Cham, Switzerland, 2020. [CrossRef]
12. Bray, F.; Ferlay, J.; Soerjomataram, I.; Siegel, R.; Torre, L.; Jemal, A. Global Cancer Statistics 2018: GLOBOCAN estimates of incidence and mortality worldwide for 36 cancers in 185 countries. *CA Cancer J. Clin.* **2018**, *68*, 394–424. [CrossRef] [PubMed]
13. Hofmarcher, T.; Brådvik, G.; Svedman, C.; Lindgren, P.; Jönsson, B.; Wilking, N. *Comparator Report on Cancer in Europe 2019—Disease Burden, Costs and Access to Medicines*; IHE: Lund, Sweden, 2019.
14. EMA Drugs Approved in 2019. Available online: <https://pharmaboaroom.com/facts/ema-drugs-approved-in-2019/> (accessed on 17 June 2020).
15. 2019 in Review: New Cancer Drug Approvals. Available online: <https://www.cancer.org/latest-news/2019-in-review-new-cancer-drug-approvals.html> (accessed on 17 June 2020).
16. Chen, L.; Zeng, W.-M.; Cai, Y.-D.; Feng, K.-Y.; Chou, K.-C. Predicting Anatomical Therapeutic Chemical (ATC) Classification of Drugs by Integrating Chemical-Chemical Interactions and Similarities. *PLoS ONE* **2012**, *7*, e35254. [CrossRef] [PubMed]
17. Azuma, T. Distribution of Anticancer Drugs in River Waters and Sediments of the Yodo River Basin, Japan. *Appl. Sci.* **2018**, *8*, 2043. [CrossRef]
18. Booker, V.; Halsall, C.; Llewellyn, N.; Johnson, A.; Williams, R. Prioritising anticancer drugs for environmental monitoring and risk assessment purposes. *Sci. Total Environ.* **2014**, *473–474*, 159–170. [CrossRef]
19. Kümmerer, K.; Haiß, A.; Schuster, A.; Hein, A.; Ebert, I. Antineoplastic compounds in the environment—Substances of special concern. *Environ. Sci. Pollut. Res.* **2016**, *23*, 14791–14804. [CrossRef]
20. Heath, E.; Filipič, M.; Kosjek, T.; Isidori, M. Fate and effects of the residues of anticancer drugs in the environment. *Environ. Sci. Pollut. Res.* **2016**, *23*, 14687–14691. [CrossRef]
21. Zhang, J.; Chang, V.W.; Giannis, A.; Wang, J.Y. Removal of cytostatic drugs from aquatic environment: A review. *Sci. Total Environ.* **2013**, *445–446*, 281–298. [CrossRef]

22. Toolaram, A.P.; Kummerer, K.; Schneider, M. Environmental risk assessment of anti-cancer drugs and their transformation products: A focus on their genotoxicity characterization-state of knowledge and short comings. *Mutat. Res. Rev. Mutat. Res.* **2014**, *760*, 18–35. [[CrossRef](#)]
23. Ribeiro, A.R.; Goncalves, V.M.; Maia, A.S.; Carvalho, M.F.; Castro, P.M.; Tiritan, M.E. Microbial degradation of pharmaceuticals followed by a simple HPLC-DAD method. *J. Environ. Sci. Health Part A Toxic/Hazard Subst. Environ. Eng.* **2012**, *47*, 2151–2158. [[CrossRef](#)]
24. Murphy, C.D. Microbial degradation of fluorinated drugs: Biochemical pathways, impacts on the environment and potential applications. *Appl. Microbiol. Biotechnol.* **2016**, *100*, 2617–2627. [[CrossRef](#)]
25. Steger-Hartmann, T.; Kümmerer, K.; Hartmann, A. Biological Degradation of Cyclophosphamide and Its Occurrence in Sewage Water. *Ecotoxicol. Environ. Saf.* **1997**, *36*, 174–179. [[CrossRef](#)] [[PubMed](#)]
26. Kümmerer, K.; Al-Ahmad, A. Biodegradability of the Anti-tumour Agents 5-Fluorouracil, Cytarabine, and Gemcitabine: Impact of the Chemical Structure and Synergistic Toxicity with Hospital Effluent. *Acta Hydrochim. Hydrobiol.* **1997**, *25*, 166–172. [[CrossRef](#)]
27. Česen, M.; Kosjek, T.; Laimou-Geraniou, M.; Kompare, B.; Širok, B.; Lambropoulou, D.; Heath, E. Occurrence of cyclophosphamide and ifosfamide in aqueous environment and their removal by biological and abiotic wastewater treatment processes. *Sci. Total Environ.* **2015**, *527–528*, 465–473. [[CrossRef](#)]
28. Bhalla, A.; Bischoff, K.M.; Sani, R.K. Highly Thermostable Xylanase Production from A Thermophilic *Geobacillus* sp. Strain WSUCF1 Utilizing Lignocellulosic Biomass. *Front. Bioeng. Biotechnol.* **2015**, *3*, 84:1–84:8. [[CrossRef](#)] [[PubMed](#)]
29. Goh, K.M.; Chan, K.-G.; Sani, R.K.; Donati, E.R.; Reysenbach, A.-L. Editorial: Genetics, Genomics and –Omics of Thermophiles. *Front. Microbiol.* **2017**, *8*, 560:1–560:2. [[CrossRef](#)]
30. Carlson, C.; Singh, N.K.; Bibra, M.; Sani, R.K.; Venkateswaran, K. Pervasiveness of UVC254-resistant *Geobacillus* strains in extreme environments. *Appl. Microbiol. Biotechnol.* **2018**, *102*, 1869–1887. [[CrossRef](#)]
31. Rathinam, N.K.; Tripathi, A.K.; Smirnova, A.; Beyenal, H.; Sani, R.K. Engineering rheology of electrolytes using agar for improving the performance of bioelectrochemical systems. *Bioresour. Technol.* **2018**, *263*, 242–249. [[CrossRef](#)]
32. David, A.; Govil, T.; Tripathi, A.; McGeary, J.; Farrar, K.; Sani, R. Thermophilic Anaerobic Digestion: Enhanced and Sustainable Methane Production from Co-Digestion of Food and Lignocellulosic Wastes. *Energies* **2018**, *11*, 2058. [[CrossRef](#)]
33. Tripathi, A.K.; Kumari, M.; Kumar, A.; Kumar, S. Generation of Biogas Using Pine Needles as Substrate in Domestic Biogas Plant. *Int. J. Renew. Energy. Res.* **2015**, *5*, 6.
34. David, A.; Tripathi, A.K.; Sani, R.K. Acetate Production from Cafeteria Wastes and Corn Stover Using a Thermophilic Anaerobic Consortium: A Prelude Study for the Use of Acetate for the Production of Value-Added Products. *Microorganisms* **2020**, *8*, 353. [[CrossRef](#)]
35. Beek, B.; Böhling, S.; Bruckmann, U.; Franke, C.; Jöhncke, U.; Studinger, G. *The Assessment of Bioaccumulation*; Springer: Berlin/Heidelberg, Germany, 2001; Volume 2.
36. Kuntworbe, N.; Alany, R.G.; Brimble, M.; Al-Kassas, R. Determination of pKa and forced degradation of the indoloquinoline antimalarial compound cryptolepine hydrochloride. *Pharm. Dev. Technol.* **2013**, *18*, 866–876. [[CrossRef](#)] [[PubMed](#)]
37. Azuma, T.; Ishiuchi, H.; Inoyama, T.; Teranishi, Y.; Yamaoka, M.; Sato, T.; Mino, Y. Occurrence and fate of selected anticancer, antimicrobial, and psychotropic pharmaceuticals in an urban river in a subcatchment of the Yodo River basin, Japan. *Environ. Sci. Pollut. Res. Int.* **2015**, *22*, 18676–18686. [[CrossRef](#)] [[PubMed](#)]
38. Folens, K.; Abebe, A.; Tang, J.; Ronsse, F.; Du Laing, G. Biosorption of residual cisplatin, carboplatin and oxaliplatin antineoplastic drugs in urine after chemotherapy treatment. *Environ. Chem.* **2018**, *15*, 506–512. [[CrossRef](#)]
39. Scheytt, T.; Mersmann, P.; Lindstadt, R.; Heberer, T. Determination of sorption coefficients of pharmaceutically active substances carbamazepine, diclofenac, and ibuprofen, in sandy sediments. *Chemosphere* **2005**, *60*, 245–253. [[CrossRef](#)] [[PubMed](#)]
40. Besse, J.P.; Latour, J.F.; Garric, J. Anticancer drugs in surface waters: What can we say about the occurrence and environmental significance of cytotoxic, cytostatic and endocrine therapy drugs? *Environ. Int.* **2012**, *39*, 73–86. [[CrossRef](#)] [[PubMed](#)]

41. Buerge, I.J.; Buser, H.-R.; Poiger, T.; Müller, M.D. Occurrence and Fate of the Cytostatic Drugs Cyclophosphamide and Ifosfamide in Wastewater and Surface Waters. *Environ. Sci. Technol.* **2006**, *40*, 7242–7250. [[CrossRef](#)] [[PubMed](#)]
42. Aherne, G.W.; Hardcastle, A.; Nield, A.H. Cytotoxic drugs and the aquatic environment: Estimation of bleomycin in river and water samples. *J. Pharm. Pharmacol.* **1990**, *42*, 741–742. [[CrossRef](#)]
43. Jureczko, M.; Kalka, J. Cytostatic pharmaceuticals as water contaminants. *Eur. J. Pharmacol.* **2020**, *866*, 172816. [[CrossRef](#)]
44. Ghafuria, Y. Environmental risk assessment of platinum cytotoxic drugs: A focus on toxicity characterization of hospital effluents. *Int. J. Environ. Sci. Technol.* **2018**, *15*, 1983–1990. [[CrossRef](#)]
45. Richardson, M.L.; Bowron, J.M. The fate of pharmaceutical chemicals in the aquatic environment. *J. Pharm. Pharm.* **1985**, *37*, 1–12. [[CrossRef](#)]
46. Kümmerer, K. The presence of pharmaceuticals in the environment due to human use—present knowledge and future challenges. *J. Environ. Manag.* **2009**, *90*, 2354–2366. [[CrossRef](#)] [[PubMed](#)]
47. Ort, C.; Lawrence, M.G.; Reungoat, J.; Eaglesham, G.; Carter, S.; Keller, J. Determining the fraction of pharmaceutical residues in wastewater originating from a hospital. *Water Res.* **2010**, *44*, 605–615. [[CrossRef](#)] [[PubMed](#)]
48. Mahnik, S.N.; Lenz, K.; Weissenbacher, N.; Mader, R.M.; Fuerhacker, M. Fate of 5-fluorouracil, doxorubicin, epirubicin, and daunorubicin in hospital wastewater and their elimination by activated sludge and treatment in a membrane-bio-reactor system. *Chemosphere* **2007**, *66*, 30–37. [[CrossRef](#)]
49. Weissbrodt, D.; Kovalova, L.; Ort, C.; Pazhepurackel, V.; Moser, R.; Hollender, J.; Siegrist, H.; McArdell, C.S. Mass Flows of X-ray Contrast Media and Cytostatics in Hospital Wastewater. *Environ. Sci. Technol.* **2009**, *43*, 4810–4817. [[CrossRef](#)] [[PubMed](#)]
50. Judson, I.R.; Beale, P.J.; Trigo, J.M.; Aherne, W.; Crompton, T.; Jones, D.; Bush, E.; Reigner, B. A human capecitabine excretion balance and pharmacokinetic study after administration of a single oral dose of ¹⁴C-labelled drug. *Investig. New Drugs* **1999**, *17*, 49–56. [[CrossRef](#)] [[PubMed](#)]
51. Li, W.C. Occurrence, sources, and fate of pharmaceuticals in aquatic environment and soil. *Environ. Pollut.* **2014**, *187*, 193–201. [[CrossRef](#)]
52. Sui, Q.; Cao, X.; Lu, S.; Zhao, W.; Qiu, Z.; Yu, G. Occurrence, sources and fate of pharmaceuticals and personal care products in the groundwater: A review. *Emerg. Contam.* **2015**, *1*, 14–24. [[CrossRef](#)]
53. Souza, D.M.; Reichert, J.F.; Martins, A.F. A simultaneous determination of anti-cancer drugs in hospital effluent by DLLME HPLC-FLD, together with a risk assessment. *Chemosphere* **2018**, *201*, 178–188. [[CrossRef](#)]
54. Johnson Andrew, C.; Oldenkamp, R.; Dumont, E.; Sumpter John, P. Predicting concentrations of the cytostatic drugs cyclophosphamide, carboplatin, 5-fluorouracil, and capecitabine throughout the sewage effluents and surface waters of Europe. *Environ. Toxicol. Chem.* **2013**, *32*, 1954–1961. [[CrossRef](#)]
55. Lee, D.; Choi, K. Comparison of regulatory frameworks of environmental risk assessments for human pharmaceuticals in EU, USA, and Canada. *Sci. Total Environ.* **2019**, *671*, 1026–1035. [[CrossRef](#)]
56. Dundas, C.M.; Graham, A.J.; Romanovicz, D.K.; Keitz, B.K. Extracellular Electron Transfer by *Shewanella oneidensis* Controls Palladium Nanoparticle Phenotype. *ACS Synth. Biol.* **2018**, *7*, 2726–2736. [[CrossRef](#)] [[PubMed](#)]
57. Rowney, N.C.; Johnson, A.C.; Williams, R.J. Erratum: Cytotoxic drugs in drinking water: A prediction and risk assessment exercise for the Thames catchment in the United Kingdom. *Environ. Toxicol. Chem.* **2011**, *30*, 1729. [[CrossRef](#)]
58. Kidd, K.A.; Blanchfield, P.J.; Mills, K.H.; Palace, V.P.; Evans, R.E.; Lazorchak, J.M.; Flick, R.W. Collapse of a fish population after exposure to a synthetic estrogen. *Proc. Natl. Acad. Sci. USA* **2007**, *104*, 8897–8901. [[CrossRef](#)] [[PubMed](#)]
59. Cristovao, M.B.; Janssens, R.; Yadav, A.; Pandey, S.; Luis, P.; Van der Bruggen, B.; Dubey, K.K.; Mandal, M.K.; Crespo, J.G.; Pereira, V.J. Predicted concentrations of anticancer drugs in the aquatic environment: What should we monitor and where should we treat? *J. Hazard. Mater.* **2020**, *392*, 122330. [[CrossRef](#)] [[PubMed](#)]
60. Ng, C.A.; Scheringer, M.; Fenner, K.; Hungerbühler, K. A framework for evaluating the contribution of transformation products to chemical persistence in the environment. *Environ. Sci. Technol.* **2011**, *45*, 111–117. [[CrossRef](#)] [[PubMed](#)]
61. Escher, B.I.; Fenner, K. Recent Advances in Environmental Risk Assessment of Transformation Products. *Environ. Sci. Technol.* **2011**, *45*, 3835–3847. [[CrossRef](#)] [[PubMed](#)]

62. Ventola, C.L. The antibiotic resistance crisis: Part 1: Causes and threats. *Pharm. Ther.* **2015**, *40*, 277–283.
63. Davies, J.; Davies, D. Origins and Evolution of Antibiotic Resistance. *Microbiol. Mol. Biol. Rev.* **2010**, *74*, 417–433. [[CrossRef](#)]
64. Seruga Music, M.; Hrenovic, J.; Goic-Barisic, I.; Hunjak, B.; Skoric, D.; Ivankovic, T. Emission of extensively-drug-resistant *Acinetobacter baumannii* from hospital settings to the natural environment. *J. Hosp. Infect.* **2017**, *96*, 323–327. [[CrossRef](#)]
65. Economou, V.; Gousia, P. Agriculture and food animals as a source of antimicrobial-resistant bacteria. *Infect. Drug Resist* **2015**, *8*, 49–61. [[CrossRef](#)]
66. Ashraf, M.; Mustafa, B.-E.; Rehman, S.-U.; Bashir, M.K.; Ashraf, M.A. Emergence of Antimicrobial Resistance, Causes, Molecular Mechanisms, and Prevention Strategies: A Bovine Perspective. In *Bovine Science—A Key to Sustainable Development*; InTech Open: London, UK, 2019. [[CrossRef](#)]
67. Amadio, J.; Murphy, C.D. Production of human metabolites of the anti-cancer drug flutamide via biotransformation in *Cunninghamella* species. *Biotechnol. Lett.* **2011**, *33*, 321–326. [[CrossRef](#)] [[PubMed](#)]
68. Busi, S.; Swaraj Pattnaik, S. Chapter 9—Current Status and Applications of Actinobacteria in the Production of Anticancerous Compounds. In *New and Future Developments in Microbial Biotechnology and Bioengineering*; Singh, B.P., Gupta, V.K., Passari, A.K., Eds.; Elsevier: Amsterdam, The Netherlands, 2018; pp. 137–153. [[CrossRef](#)]
69. Cruz-Morato, C.; Ferrando-Climent, L.; Rodriguez-Mozaz, S.; Barcelo, D.; Marco-Urrea, E.; Vicent, T.; Sarra, M. Degradation of pharmaceuticals in non-sterile urban wastewater by *Trametes versicolor* in a fluidized bed bioreactor. *Water Res.* **2013**, *47*, 5200–5210. [[CrossRef](#)] [[PubMed](#)]
70. Ferrando-Climent, L.; Cruz-Morato, C.; Marco-Urrea, E.; Vicent, T.; Sarra, M.; Rodriguez-Mozaz, S.; Barcelo, D. Non conventional biological treatment based on *Trametes versicolor* for the elimination of recalcitrant anticancer drugs in hospital wastewater. *Chemosphere* **2015**, *136*, 9–19. [[CrossRef](#)]
71. Tadkaew, N.; Hai, F.I.; McDonald, J.A.; Khan, S.J.; Nghiem, L.D. Removal of trace organics by MBR treatment: The role of molecular properties. *Water Res.* **2011**, *45*, 2439–2451. [[CrossRef](#)] [[PubMed](#)]
72. Rodriguez-Rodriguez, C.E.; Jesús García-Galán, M.; Blázquez, P.; Díaz-Cruz, M.S.; Barceló, D.; Caminal, G.; Vicent, T. Continuous degradation of a mixture of sulfonamides by *Trametes versicolor* and identification of metabolites from sulfapyridine and sulfathiazole. *J. Hazard. Mater.* **2012**, *213*, 347–354. [[CrossRef](#)]
73. Casini, A.; Scozzafava, A.; Mastrolorenzo, A.; Supuran, L.T. Sulfonamides and sulfonylated derivatives as anticancer agents. *Curr. Cancer Drug Targets* **2002**, *2*, 55–75. [[CrossRef](#)]
74. Bourbonnais, R.; Leech, D.; Paice, M.G. Electrochemical analysis of the interactions of laccase mediators with lignin model compounds. *Biochim. Biophys. Acta. Gen. Subj.* **1998**, *1379*, 381–390. [[CrossRef](#)]
75. Schwarz, J.; Aust, M.-O.; Thiele-Bruhn, S. Metabolites from fungal laccase-catalysed transformation of sulfonamides. *Chemosphere* **2010**, *81*, 1469–1476. [[CrossRef](#)]
76. Marco-Urrea, E.; Perez-Trujillo, M.; Blázquez, P.; Vicent, T.; Caminal, G. Biodegradation of the analgesic naproxen by *Trametes versicolor* and identification of intermediates using HPLC-DAD-MS and NMR. *Bioresour. Technol.* **2010**, *101*, 2159–2166. [[CrossRef](#)]
77. Thun, M.J.; Henley, S.J.; Patrono, C. Nonsteroidal Anti-inflammatory Drugs as Anticancer Agents: Mechanistic, Pharmacologic, and Clinical Issues. *J. Natl. Cancer. Inst.* **2002**, *94*, 252–266. [[CrossRef](#)]
78. Murphy, C.D.; Palmer-Brown, W.; Quinn, L.; Saccomanno, M. 7-Microbial metabolism of fluorinated drugs. In *Fluorine in Life Sciences: Pharmaceuticals, Medicinal Diagnostics, and Agrochemicals*; Haufe, G., Leroux, F.R., Eds.; Academic Press: Cambridge, MA, USA, 2019; pp. 281–299. [[CrossRef](#)]
79. Hidde Boersma, F.G.; Colin McRoberts, W.; Cobb, S.L.; Murphy, C.D. A 19F NMR study of fluorobenzoate biodegradation by *Sphingomonas* sp. HB-1. *Fems. Microbiol. Lett.* **2004**, *237*, 355–361. [[CrossRef](#)]
80. Kim, E.J.; Jeon, J.R.; Kim, Y.M.; Murugesan, K.; Chang, Y.S. Mineralization and transformation of monofluorophenols by *Pseudonocardia benzenivorans*. *Appl. Microbiol. Biotechnol.* **2010**, *87*, 1569–1577. [[CrossRef](#)] [[PubMed](#)]
81. Lutterbeck, C.A.; Wilde, M.L.; Baginska, E.; Leder, C.; Machado, E.L.; Kummerer, K. Degradation of 5-FU by means of advanced (photo)oxidation processes: UV/H₂O₂, UV/Fe²⁺/H₂O₂ and UV/TiO₂—Comparison of transformation products, ready biodegradability and toxicity. *Sci. Total Environ.* **2015**, *527–528*, 232–245. [[CrossRef](#)] [[PubMed](#)]

82. Engesser, K.-H.; Rubio, M.A.; Knackmuss, H.-J. Bacterial metabolism of side-chain-fluorinated aromatics: Unproductive meta-cleavage of 3-trifluoromethylcatechol. *Appl. Microbiol. Biotechnol.* **1990**, *32*, 600–608. [[CrossRef](#)] [[PubMed](#)]
83. Westman, E.L.; Canova, M.J.; Radhi, I.J.; Koteva, K.; Kireeva, I.; Waglechner, N.; Wright, G.D. Bacterial Inactivation of the Anticancer Drug Doxorubicin. *Chem. Biol.* **2012**, *19*, 1255–1264. [[CrossRef](#)]
84. Pepper, I.L.; Gentry, T.J. Chapter 4—Earth Environments. In *Environmental Microbiology*, 3rd ed.; Pepper, I.L., Gerba, C.P., Gentry, T.J., Eds.; Academic Press: San Diego, CA, USA, 2015; pp. 59–88. [[CrossRef](#)]
85. Friedrich, T.; Scheide, D. The respiratory complex I of bacteria, archaea and eukarya and its module common with membrane-bound multisubunit hydrogenases1. *FEBS Lett.* **2000**, *479*, 1–5. [[CrossRef](#)]
86. Geller, L.T.; Barzily-Rokni, M.; Danino, T.; Jonas, O.H.; Shental, N.; Nejman, D.; Gavert, N.; Zwang, Y.; Cooper, Z.A.; Shee, K.; et al. Potential role of intratumor bacteria in mediating tumor resistance to the chemotherapeutic drug gemcitabine. *Science* **2017**, *357*, 1156–1160. [[CrossRef](#)]
87. Radjenović, J.; Petrović, M.; Barceló, D. Fate and distribution of pharmaceuticals in wastewater and sewage sludge of the conventional activated sludge (CAS) and advanced membrane bioreactor (MBR) treatment. *Water Res.* **2009**, *43*, 831–841. [[CrossRef](#)]
88. Chang, H.; Wan, Y.; Wu, S.; Fan, Z.; Hu, J. Occurrence of androgens and progestogens in wastewater treatment plants and receiving river waters: Comparison to estrogens. *Water Res.* **2011**, *45*, 732–740. [[CrossRef](#)]
89. Fan, Z.; Wu, S.; Chang, H.; Hu, J. Behaviors of glucocorticoids, androgens and progestogens in a municipal sewage treatment plant: Comparison to estrogens. *Environ. Sci. Technol.* **2011**, *45*, 2725–2733. [[CrossRef](#)]
90. Ortiz de García, S.; Pinto Pinto, G.; García Encina, P.; Irusta Mata, R. Consumption and occurrence of pharmaceutical and personal care products in the aquatic environment in Spain. *Sci. Total Environ.* **2013**, *444*, 451–465. [[CrossRef](#)]
91. Gómez-Canela, C.; Santos, M.S.F.; Franquet-Griell, H.; Alves, A.; Ventura, F.; Lacorte, S. Predicted Environmental Concentrations: A Useful Tool to Evaluate the Presence of Cytostatics in Surface Waters. In *Fate and Effects of Anticancer Drugs in the Environment*; Heath, E., Isidori, M., Kosjek, T., Filipič, M., Eds.; Springer International Publishing: Cham, Switzerland, 2020; pp. 27–54. [[CrossRef](#)]
92. Aukema, K.G.; Escalante, D.E.; Maltby, M.M.; Bera, A.K.; Aksan, A.; Wackett, L.P. In Silico Identification of Bioremediation Potential: Carbamazepine and Other Recalcitrant Personal Care Products. *Environ. Sci. Technol.* **2017**, *51*, 880–888. [[CrossRef](#)] [[PubMed](#)]
93. Ioannou-Ttofa, L.; Fatta-Kassinos, D. Cytostatic Drug Residues in Wastewater Treatment Plants: Sources, Removal Efficiencies and Current Challenges. In *Fate and Effects of Anticancer Drugs in the Environment*; Heath, E., Isidori, M., Kosjek, T., Filipič, M., Eds.; Springer International Publishing: Cham, Switzerland, 2020; pp. 103–138. [[CrossRef](#)]
94. Chu, C.S.; Rubin, S.C. 17—Basic Principles of Chemotherapy. In *Clinical Gynecologic Oncology*, 9th ed.; DiSaia, P.J., Creasman, W.T., Mannel, R.S., McMeekin, D.S., Mutch, D.G., Eds.; Elsevier: Amsterdam, The Netherlands, 2018; pp. 449–469. [[CrossRef](#)]
95. Ferrando-Climent, L.; Rodriguez-Mozaz, S.; Barcelo, D. Development of a UPLC-MS/MS method for the determination of ten anticancer drugs in hospital and urban wastewaters, and its application for the screening of human metabolites assisted by information-dependent acquisition tool (IDA) in sewage samples. *Anal. Bioanal. Chem.* **2013**, *405*, 5937–5952. [[CrossRef](#)]
96. Negreira, N.; de Alda, M.L.; Barcelo, D. Cytostatic drugs and metabolites in municipal and hospital wastewaters in Spain: Filtration, occurrence, and environmental risk. *Sci. Total Environ.* **2014**, *497*–498, 68–77. [[CrossRef](#)] [[PubMed](#)]
97. Rabii, F.W.; Segura, P.A.; Fayad, P.B.; Sauve, S. Determination of six chemotherapeutic agents in municipal wastewater using online solid-phase extraction coupled to liquid chromatography-tandem mass spectrometry. *Sci. Total Environ.* **2014**, *487*, 792–800. [[CrossRef](#)] [[PubMed](#)]
98. Isidori, M.; Lavorgna, M.; Russo, C.; Kundi, M.; Zegura, B.; Novak, M.; Filipic, M.; Misik, M.; Knasmueller, S.; de Alda, M.L.; et al. Chemical and toxicological characterisation of anticancer drugs in hospital and municipal wastewaters from Slovenia and Spain. *Environ. Pollut.* **2016**, *219*, 275–287. [[CrossRef](#)] [[PubMed](#)]
99. Yin, J.; Shao, B.; Zhang, J.; Li, K. A preliminary study on the occurrence of cytostatic drugs in hospital effluents in Beijing, China. *Bull. Environ. Contam. Toxicol.* **2010**, *84*, 39–45. [[CrossRef](#)]

100. Thomas, K.V.; Dye, C.; Schlabach, M.; Langford, K.H. Source to sink tracking of selected human pharmaceuticals from two Oslo city hospitals and a wastewater treatment works. *J. Environ. Monit.* **2007**, *9*, 1410–1418. [[CrossRef](#)]
101. Michael, C.; Bayona, J.M.; Lambropoulou, D.; Aguera, A.; Fatta-Kassinos, D. Two important limitations relating to the spiking of environmental samples with contaminants of emerging concern: How close to the real analyte concentrations are the reported recovered values? *Environ. Sci. Pollut. Res. Int.* **2017**, *24*, 15202–15205. [[CrossRef](#)]
102. Freres, P.; Jerusalem, G.; Moonen, M. Chapter 2—Categories of Anticancer Treatments. In *Anti-Cancer Treatments and Cardiotoxicity*; Lancellotti, P., Zamorano Gómez, J.L., Galderisi, M., Eds.; Academic Press: Boston, MA, USA, 2017; pp. 7–11. [[CrossRef](#)]
103. Kiffmeyer, T.; Götte, H.-J.; Jursch, M.; Lüders, U. Trace enrichment, chromatographic separation and biodegradation of cytostatic compounds in surface water. *Fresenius J. Anal. Chem.* **1998**, *361*, 185–191. [[CrossRef](#)]
104. Rosano, T.G. Ellenhorn’s Medical Toxicology: Diagnosis and Treatment of Human Poisoning. *Clin. Chem.* **1998**, *44*, 366. [[CrossRef](#)]
105. Kosjek, T.; Perko, S.; Zigon, D.; Heath, E. Fluorouracil in the environment: Analysis, occurrence, degradation and transformation. *J. Chromatogr. A* **2013**, *1290*, 62–72. [[CrossRef](#)] [[PubMed](#)]
106. Yu, J.T.; Bouwer, E.J.; Coelhan, M. Occurrence and biodegradability studies of selected pharmaceuticals and personal care products in sewage effluent. *Agric. Water. Manag.* **2006**, *86*, 72–80. [[CrossRef](#)]
107. Straub, J.O. Combined environmental risk assessment for 5-fluorouracil and capecitabine in Europe. *Integr. Environ. Assess Manag.* **2010**, *6*, 540–566. [[CrossRef](#)] [[PubMed](#)]
108. Lutterbeck, C.A.; Baginska, E.; Machado, E.L.; Kummerer, K. Removal of the anti-cancer drug methotrexate from water by advanced oxidation processes: Aerobic biodegradation and toxicity studies after treatment. *Chemosphere* **2015**, *141*, 290–296. [[CrossRef](#)] [[PubMed](#)]
109. Martin, J.; Camacho-Munoz, D.; Santos, J.L.; Aparicio, I.; Alonso, E. Simultaneous determination of a selected group of cytostatic drugs in water using high-performance liquid chromatography-triple-quadrupole mass spectrometry. *J. Sep. Sci.* **2011**, *34*, 3166–3177. [[CrossRef](#)] [[PubMed](#)]
110. Martín, J.; Camacho-Muñoz, D.; Santos, J.L.; Aparicio, I.; Alonso, E. Occurrence and Ecotoxicological Risk Assessment of 14 Cytostatic Drugs in Wastewater. *Water Air Soil Pollut.* **2014**, *225*, 1896. [[CrossRef](#)]
111. Kosjek, T.; Negreira, N.; de Alda, M.L.; Barcelo, D. Aerobic activated sludge transformation of methotrexate: Identification of biotransformation products. *Chemosphere* **2015**, *119*, S42–S50. [[CrossRef](#)]
112. Ferrando-Climent, L.; Rodriguez-Mozaz, S.; Barcelo, D. Incidence of anticancer drugs in an aquatic urban system: From hospital effluents through urban wastewater to natural environment. *Environ. Pollut.* **2014**, *193*, 216–223. [[CrossRef](#)]
113. Pietsch, J.; Gunther, J.; Henle, T.; Dressler, J. Simultaneous determination of thirteen plant alkaloids in a human specimen by SPE and HPLC. *J. Sep. Sci.* **2008**, *31*, 2410–2416. [[CrossRef](#)]
114. Kosjek, T.; Negreira, N.; Heath, E.; López de Alda, M.; Barceló, D. Aerobic activated sludge transformation of vincristine and identification of the transformation products. *Sci. Total Environ.* **2018**, *610–611*, 892–904. [[CrossRef](#)] [[PubMed](#)]
115. Jeswani, G.; Paul, S.D. Chapter 15—Recent Advances in the Delivery of Chemotherapeutic Agents. In *Nano and Microscale Drug Delivery Systems*; Grumezescu, A.M., Ed.; Elsevier: Amsterdam, The Netherlands, 2017; pp. 281–298. [[CrossRef](#)]
116. Wang, X.; Liu, W.; Xin, C.; Zheng, Y.; Cheng, Y.; Sun, S.; Li, R.; Zhu, X.-G.; Dai, S.Y.; Rentzepis, P.M.; et al. Enhanced limonene production in cyanobacteria reveals photosynthesis limitations. *Proc. Natl. Acad. Sci. USA* **2016**, *113*, 14225. [[CrossRef](#)] [[PubMed](#)]
117. Franquet-Griell, H.; Medina, A.; Sans, C.; Lacorte, S. Biological and photochemical degradation of cytostatic drugs under laboratory conditions. *J. Hazard. Mater.* **2017**, *323*, 319–328. [[CrossRef](#)] [[PubMed](#)]
118. Roberts, P.H.; Thomas, K.V. The occurrence of selected pharmaceuticals in wastewater effluent and surface waters of the lower Tyne catchment. *Sci. Total Environ.* **2006**, *356*, 143–153. [[CrossRef](#)]
119. Gómez-Canela, C.; Ventura, F.; Caixach, J.; Lacorte, S. Occurrence of cytostatic compounds in hospital effluents and wastewaters, determined by liquid chromatography coupled to high-resolution mass spectrometry. *Anal. Bioanal. Chem.* **2014**, *406*, 3801–3814. [[CrossRef](#)] [[PubMed](#)]

120. Melin, T.; Jefferson, B.; Bixio, D.; Thoeye, C.; De Wilde, W.; De Koning, J.; van der Graaf, J.; Wintgens, T. Membrane bioreactor technology for wastewater treatment and reuse. *Desalination* **2006**, *187*, 271–282. [[CrossRef](#)]
121. Gu, Y.; Huang, J.; Zeng, G.; Shi, L.; Shi, Y.; Yi, K. Fate of pharmaceuticals during membrane bioreactor treatment: Status and perspectives. *Bioresour. Technol.* **2018**, *268*, 733–748. [[CrossRef](#)]
122. Lenz, K.; Mahnik, S.N.; Weissenbacher, N.; Mader, R.M.; Krenn, P.; Hann, S.; Koellensperger, G.; Uhl, M.; Knasmüller, S.; Ferik, F.; et al. Monitoring, removal and risk assessment of cytostatic drugs in hospital wastewater. *Water Sci. Technol. J. Int. Assoc. Water Pollut. Res.* **2007**, *56*, 141–149. [[CrossRef](#)]
123. Delgado, L.F.; Dorandeu, C.; Marion, B.; Gonzalez, C.; Faucet-Marquis, V.; Schetrite, S.; Albasi, C. Removal of a cytostatic drug by a membrane bioreactor. *Desalin. Water Treat.* **2009**, *9*, 112–118. [[CrossRef](#)]
124. Delgado, L.F.; Faucet-Marquis, V.; Pfohl-Leszakowicz, A.; Dorandeu, C.; Marion, B.; Schetrite, S.; Albasi, C. Cytotoxicity micropollutant removal in a crossflow membrane bioreactor. *Bioresour. Technol.* **2011**, *102*, 4395–4401. [[CrossRef](#)]
125. Kovalova, L.; Siegrist, H.; Singer, H.; Wittmer, A.; McArdell, C.S. Hospital wastewater treatment by membrane bioreactor: Performance and efficiency for organic micropollutant elimination. *Environ. Sci. Technol.* **2012**, *46*, 1536–1545. [[CrossRef](#)]
126. Avella, A.C.; Delgado, L.F.; Görner, T.; Albasi, C.; Galmiche, M.; de Donato, P. Effect of cytostatic drug presence on extracellular polymeric substances formation in municipal wastewater treated by membrane bioreactor. *Bioresour. Technol.* **2010**, *101*, 518–526. [[CrossRef](#)]
127. Meng, F.; Chae, S.-R.; Drews, A.; Kraume, M.; Shin, H.-S.; Yang, F. Recent advances in membrane bioreactors (MBRs): Membrane fouling and membrane material. *Water Res.* **2009**, *43*, 1489–1512. [[CrossRef](#)]
128. Wang, X.; Zhang, J.; Chang, V.W.C.; She, Q.; Tang, C.Y. Removal of cytostatic drugs from wastewater by an anaerobic osmotic membrane bioreactor. *Chem. Eng. J.* **2018**, *339*, 153–161. [[CrossRef](#)]
129. Gu, Y.; Chen, L.; Ng, J.-W.; Lee, C.; Chang, V.W.C.; Tang, C.Y. Development of anaerobic osmotic membrane bioreactor for low-strength wastewater treatment at mesophilic condition. *J. Membr. Sci.* **2015**, *490*, 197–208. [[CrossRef](#)]
130. Chang, H.-M.; Sun, Y.-C.; Chien, I.C.; Chang, W.-S.; Ray, S.S.; Cao, D.T.N.; Cong Duong, C.; Chen, S.-S. Innovative upflow anaerobic sludge osmotic membrane bioreactor for wastewater treatment. *Bioresour. Technol.* **2019**, *287*, 121466. [[CrossRef](#)] [[PubMed](#)]
131. Wu, Y.; Wang, X.; Tay, M.Q.X.; Oh, S.; Yang, L.; Tang, C.; Cao, B. Metagenomic insights into the influence of salinity and cytostatic drugs on the composition and functional genes of microbial community in forward osmosis anaerobic membrane bioreactors. *Chem. Eng. J.* **2017**, *326*, 462–469. [[CrossRef](#)]
132. Kovalova, L.; McArdell, C.S.; Hollender, J. Challenge of high polarity and low concentrations in analysis of cytostatics and metabolites in wastewater by hydrophilic interaction chromatography/tandem mass spectrometry. *J. Chromatogr. A* **2009**, *1216*, 1100–1108. [[CrossRef](#)] [[PubMed](#)]
133. Halling-Sorensen, B.; Nors Nielsen, S.; Lanzky, P.F.; Ingerslev, F.; Holten Lutzhoft, H.C.; Jørgensen, S.E. Occurrence, fate and effects of pharmaceutical substances in the environment—a review. *Chemosphere* **1998**, *36*, 357–393. [[CrossRef](#)]
134. Hamon, P.; Moulin, P.; Ercolei, L.; Marrot, B. Oncological ward wastewater treatment by membrane bioreactor: Acclimation feasibility and pharmaceuticals removal performances. *J. Water Process Eng.* **2018**, *21*, 9–26. [[CrossRef](#)]
135. Wang, X.-H.; Lin, A.Y.-C. Is the phototransformation of pharmaceuticals a natural purification process that decreases ecological and human health risks? *Environ. Pollut.* **2014**, *186*, 203–215. [[CrossRef](#)]
136. Badia-Fabregat, M.; Oller, I.; Malato, S. Overview on Pilot-Scale Treatments and New and Innovative Technologies for Hospital Effluent. In *Hospital Wastewaters: Characteristics, Management, Treatment and Environmental Risks*; Verlicchi, P., Ed.; Springer International Publishing: Cham, Switzerland, 2018; pp. 209–230. [[CrossRef](#)]
137. Seira, J.; Sablayrolles, C.; Montréjaud-Vignoles, M.; Albasi, C.; Joannis-Cassan, C. Elimination of an anticancer drug (cyclophosphamide) by a membrane bioreactor: Comprehensive study of mechanisms. *Biochem. Eng. J.* **2016**, *114*, 155–163. [[CrossRef](#)]
138. Chen, Z.; Park, G.; Herckes, P.; Westerhoff, P. Physicochemical Treatment of Three Chemotherapy Drugs: Irinotecan, Tamoxifen, and Cyclophosphamide. *J. Adv. Oxid. Technol.* **2008**, *11*, 254–260. [[CrossRef](#)]

139. Paci, A.; Martens, T.; Royer, J. Anodic oxidation of ifosfamide and cyclophosphamide: A biomimetic metabolism model of the oxazaphosphorinane anticancer drugs. *Bioorg. Med. Chem. Lett.* **2001**, *11*, 1347–1349. [[CrossRef](#)]
140. Oh, B.S.; Oh, S.; Kim, S.-J.; Choi, Y.; Hwang, T.-M. Optimization of wastewater reclamation and reuse system using membrane filtration and oxidation processes: Removal of pharmaceuticals. *Desalin. Water Treat.* **2016**, *57*, 10146–10151. [[CrossRef](#)]
141. Shojaee Nasirabadi, P.; Saljoughi, E.; Mousavi, S.M. Membrane processes used for removal of pharmaceuticals, hormones, endocrine disruptors and their metabolites from wastewaters: A review. *Desalin. Water Treat.* **2016**, *57*, 24146–24175. [[CrossRef](#)]
142. Dolar, D.; Košutić, K. Chapter 10—Removal of Pharmaceuticals by Ultrafiltration (UF), Nanofiltration (NF), and Reverse Osmosis (RO). In *Comprehensive Analytical Chemistry*; Petrovic, M., Barcelo, D., Pérez, S., Eds.; Elsevier: Amsterdam, The Netherlands, 2013; Volume 62, pp. 319–344.
143. Kimura, K.; Amy, G.; Drewes, J.E.; Heberer, T.; Kim, T.-U.; Watanabe, Y. Rejection of organic micropollutants (disinfection by-products, endocrine disrupting compounds, and pharmaceutically active compounds) by NF/RO membranes. *J. Membr. Sci.* **2003**, *227*, 113–121. [[CrossRef](#)]
144. Pronk, W.; Biebow, M.; Boller, M. Electrodialysis for Recovering Salts from a Urine Solution Containing Micropollutants. *Environ. Sci. Technol.* **2006**, *40*, 2414–2420. [[CrossRef](#)]
145. Wang, L.; Albasi, C.; Faucet-Marquis, V.; Pfohl-Leszkowicz, A.; Dorandeu, C.; Marion, B.; Causserand, C. Cyclophosphamide removal from water by nanofiltration and reverse osmosis membrane. *Water Res.* **2009**, *43*, 4115–4122. [[CrossRef](#)]
146. Escher, B.I.; Pronk, W.; Suter, M.J.F.; Maurer, M. Monitoring the Removal Efficiency of Pharmaceuticals and Hormones in Different Treatment Processes of Source-Separated Urine with Bioassays. *Environ. Sci. Technol.* **2006**, *40*, 5095–5101. [[CrossRef](#)]
147. Benvenuto, J.A.; Connor, T.H.; Monteith, D.K.; Laidlaw, J.L.; Adams, S.C.; Matney, T.S.; Theiss, J.C. Degradation and Inactivation of Antitumor Drugs. *J. Pharm. Sci.* **1993**, *82*, 988–991. [[CrossRef](#)] [[PubMed](#)]
148. Castegnaro, M.; Sportouch, M.H.; De Meo, M.; Laget, M.; Michelon, J.; Garren, L.; Hansel, S. Chemical degradation of wastes of antineoplastic agents 2-Six Anthracyclines: Idarubicin, doxorubicin, epirubicin, pirarubicin, aclarubicin, and daunorubicin. *Int. Arch. Occup. Environ. Health* **1997**, *70*, 378–384. [[CrossRef](#)] [[PubMed](#)]
149. Hansel, S.; Castegnaro, M.; Sportouch, M.H.; De Meo, M.; Milhavet, J.C.; Laget, M.; Dumenil, G. Chemical degradation of wastes of antineoplastic agents: Cyclophosphamide, ifosfamide, and melphalan. *Int. Arch. Occup. Environ. Health.* **1997**, *69*, 109–114. [[CrossRef](#)] [[PubMed](#)]
150. Lunn, G.; Sansone, E.B.; Andrews, A.W.; Hellwig, L.C. Degradation and disposal of some antineoplastic drugs. *J. Pharm. Sci.* **1989**, *78*, 652–659. [[CrossRef](#)]
151. Macholz, R. Laboratory decontamination and destruction of carcinogens in laboratory wastes: Some antineoplastic agents. International Agency for Research on Cancer. *IARC Sci. Publ.* **1985**, *32*, 1–634.
152. Martignac, M.; Balayssac, S.; Gilard, V.; Benoit-Marquié, F. Photochemical Degradation of the Anticancer Drug Bortezomib by V-UV/UV (185/254 nm) Investigated by 1H NMR Fingerprinting: A Way to Follow Aromaticity Evolution. *J. Phys. Chem. A* **2015**, *119*, 6215–6222. [[CrossRef](#)]
153. Lin, A.Y.-C.; Wang, X.-H.; Lee, W.-N. Phototransformation Determines the Fate of 5-Fluorouracil and Cyclophosphamide in Natural Surface Waters. *Environ. Sci. Technol.* **2013**, *47*, 4104–4112. [[CrossRef](#)]
154. Trawiński, J.; Skibiński, R. Studies on photodegradation process of psychotropic drugs: A review. *Environ. Sci. Pollut. Res. Int.* **2017**, *24*, 1152–1199. [[CrossRef](#)]
155. Gómez-Canela, C.; Bolivar-Subirats, G.; Tauler, R.; Lacorte, S. Powerful combination of analytical and chemometric methods for the photodegradation of 5-Fluorouracil. *J. Pharm. Biomed. Anal.* **2017**, *137*, 33–41. [[CrossRef](#)] [[PubMed](#)]
156. Ganzenko, O.; Oturan, N.; Sirés, I.; Huguenot, D.; van Hullebusch, E.D.; Esposito, G.; Oturan, M.A. Fast and complete removal of the 5-fluorouracil drug from water by electro-Fenton oxidation. *Environ. Chem. Lett.* **2018**, *16*, 281–286. [[CrossRef](#)]
157. Koltsakidou, A.; Antonopoulou, M.; Sykiotou, M.; Evgenidou, E.; Konstantinou, I.; Lambropoulou, D.A. Photo-Fenton and Fenton-like processes for the treatment of the antineoplastic drug 5-fluorouracil under simulated solar radiation. *Environ. Sci. Pollut. Res.* **2017**, *24*, 4791–4800. [[CrossRef](#)] [[PubMed](#)]

158. Anheden, M.; Goswami, D.Y.; Svedberg, G. Photocatalytic Treatment of Wastewater From 5-Fluorouracil Manufacturing. *J. Solar Energy Eng.* **1996**, *118*, 2–8. [[CrossRef](#)]
159. Burleson, G.R.; Chambers, T.M. Effect of ozonation on the mutagenicity of carcinogens in aqueous solution. *Environ. Mutagenesis* **1982**, *4*, 469–476. [[CrossRef](#)] [[PubMed](#)]
160. Gouider, M.; Mlaik, N.; Feki, M.; Sayadi, S. Integrated physicochemical and biological treatment process for fluoride and phosphorus removal from fertilizer plant wastewater. *Water Environ. Res.* **2011**, *83*, 731–738. [[CrossRef](#)] [[PubMed](#)]
161. Feng, F.; Xu, Z.; Li, X.; You, W.; Zhen, Y. Advanced treatment of dyeing wastewater towards reuse by the combined Fenton oxidation and membrane bioreactor process. *J. Environ. Sci.* **2010**, *22*, 1657–1665. [[CrossRef](#)]
162. Calza, P.; Medana, C.; Sarro, M.; Rosato, V.; Aigotti, R.; Baiocchi, C.; Minero, C. Photocatalytic degradation of selected anticancer drugs and identification of their transformation products in water by liquid chromatography–high resolution mass spectrometry. *J. Chromatogr. A* **2014**, *1362*, 135–144. [[CrossRef](#)] [[PubMed](#)]
163. Lin, A.Y.; Hsueh, J.H.; Hong, P.K. Removal of antineoplastic drugs cyclophosphamide, ifosfamide, and 5-fluorouracil and a vasodilator drug pentoxifylline from wastewaters by ozonation. *Environ. Sci. Pollut. Res. Int.* **2015**, *22*, 508–515. [[CrossRef](#)] [[PubMed](#)]
164. Negreira, N.; Regueiro, J.; Lopez de Alda, M.; Barcelo, D. Degradation of the anticancer drug erlotinib during water chlorination: Non-targeted approach for the identification of transformation products. *Water Res.* **2015**, *85*, 103–113. [[CrossRef](#)]
165. Huo, Z.; Wang, S.; Shao, H.; Wang, H.; Xu, G. Radiolytic degradation of anticancer drug capecitabine in aqueous solution: Kinetics, reaction mechanism, and toxicity evaluation. *Environ. Sci. Pollut. Res.* **2020**. [[CrossRef](#)]
166. Barışçı, S.; Turkay, O.; Ulusoy, E.; Şeker, M.G.; Yüksel, E.; Dimoglo, A. Electro-oxidation of cytostatic drugs: Experimental and theoretical identification of by-products and evaluation of ecotoxicological effects. *Chem. Eng. J.* **2018**, *334*, 1820–1827. [[CrossRef](#)]
167. Governo, M.; Santos, M.S.F.; Alves, A.; Madeira, L.M. Degradation of the cytostatic 5-Fluorouracil in water by Fenton and photo-assisted oxidation processes. *Environ. Sci. Pollut. Res.* **2017**, *24*, 844–854. [[CrossRef](#)]
168. Koltsakidou, A.; Antonopoulou, M.; Evgenidou, E.; Konstantinou, I.; Lambropoulou, D.A. Cytarabine degradation by simulated solar assisted photocatalysis using TiO₂. *Chem. Eng. J.* **2017**, *316*, 823–831. [[CrossRef](#)]
169. Janssens, R.; Cristóvão, B.M.; Bronze, M.R.; Crespo, J.G.; Pereira, V.J.; Luis, P. Photocatalysis Using UV-A and UV-C Light Sources for Advanced Oxidation of Anti-Cancer Drugs Spiked in Laboratory-Grade Water and Synthetic Urine. *Ind. Eng. Chem. Res.* **2020**, *59*, 647–653. [[CrossRef](#)]
170. Collivignarelli, M.C.; Abbà, A.; Bertanza, G.; Setti, M.; Barbieri, G.; Frattarola, A. Integrating novel (thermophilic aerobic membrane reactor-TAMR) and conventional (conventional activated sludge-CAS) biological processes for the treatment of high strength aqueous wastes. *Bioresour. Technol.* **2018**, *255*, 213–219. [[CrossRef](#)] [[PubMed](#)]
171. Kårelid, V.; Larsson, G.; Björleinius, B. Pilot-scale removal of pharmaceuticals in municipal wastewater: Comparison of granular and powdered activated carbon treatment at three wastewater treatment plants. *J. Environ. Manag.* **2017**, *193*, 491–502. [[CrossRef](#)]
172. Lienert, J.B.; Bürki, T.; Escher, B.I. Reducing micropollutants with source control: Substance flow analysis of 212 pharmaceuticals in faeces and urine. *Water Sci. Technol.* **2007**, *56*, 87–96. [[CrossRef](#)] [[PubMed](#)]
173. Wilsenach, J.A.; Van Loosdrecht, M.C.M. Effects of Separate Urine Collection on Advanced Nutrient Removal Processes. *Environ. Sci. Technol.* **2004**, *38*, 1208–1215. [[CrossRef](#)]
174. Wilsenach, J.; van Loosdrecht, M. Impact of separate urine collection on wastewater treatment systems. *Water Sci. Technol. J. Int. Assoc. Water Pollut. Res.* **2003**, *48*, 103–110. [[CrossRef](#)]
175. Collivignarelli, M.C.; Abba, A.; Bertanza, G. Treatment of high strength pharmaceutical wastewaters in a Thermophilic Aerobic Membrane Reactor (TAMR). *Water Res.* **2014**, *63*, 190–198. [[CrossRef](#)] [[PubMed](#)]
176. Duncan, J.; Bokhary, A.; Fatehi, P.; Kong, F.; Lin, H.; Liao, B. Thermophilic membrane bioreactors: A review. *Bioresour. Technol.* **2017**, *243*, 1180–1193. [[CrossRef](#)]
177. Barisci, S.; Turkay, O.; Ulusoy, E.; Soydemir, G.; Seker, M.G.; Dimoglo, A. Electrochemical treatment of anti-cancer drug carboplatin on mixed-metal oxides and boron doped diamond electrodes: Density functional theory modelling and toxicity evaluation. *J. Hazard. Mater.* **2017**, *344*, 316–321. [[CrossRef](#)] [[PubMed](#)]

178. Zhang, Y.; Yu, T.; Han, W.; Sun, X.; Li, J.; Shen, J.; Wang, L. Electrochemical treatment of anticancer drugs wastewater containing 5-Fluoro-2-Methoxypyrimidine using a tubular porous electrode electrocatalytic reactor. *Electrochim. Acta.* **2016**, *220*, 211–221. [[CrossRef](#)]
179. Manson, M.M. Epoxides—Is there a human health problem? *Br. J. Ind. Med.* **1980**, *37*, 317–336. [[CrossRef](#)]



© 2020 by the authors. Licensee MDPI, Basel, Switzerland. This article is an open access article distributed under the terms and conditions of the Creative Commons Attribution (CC BY) license (<http://creativecommons.org/licenses/by/4.0/>).

MDPI
St. Alban-Anlage 66
4052 Basel
Switzerland
Tel. +41 61 683 77 34
Fax +41 61 302 89 18
www.mdpi.com

Processes Editorial Office
E-mail: processes@mdpi.com
www.mdpi.com/journal/processes



MDPI
St. Alban-Anlage 66
4052 Basel
Switzerland

Tel: +41 61 683 77 34
Fax: +41 61 302 89 18

www.mdpi.com



ISBN 978-3-0365-2901-1